Combining Tumour-Treating Fields with DNA damage response inhibitors for the improved treatment of glioblastoma

Aurelie Vanderlinden

Academic Unit of Molecular Oncology

Department of Oncology and Metabolism

University of Sheffield

Primary Supervisor: Dr Spencer Collis

Thesis submitted to the University of Sheffield

for the degree of Doctor of Philosophy

March 2023

Abstract

Glioblastoma is the most common and deadliest type of primary brain cancer, taking over 2,500 lives each year in the UK. glioblastoma has a median overall survival of 10-16 months, despite treatment consisting of maximal surgical resection followed by chemo- and radio-therapy. glioblastoma survival rates have seen little improvement over the past 40 years and given this devastating prognosis, new treatment options for the management of glioblastoma are urgently needed. Recently, Tumour Treating Fields (TTFields) has emerged as a novel fourth modality for the treatment of high-grade gliomas following its success in clinical trials, where the addition of TTFields to standard care temozolomide was shown to increase median progression-free survival (6.7 versus 4.0 months) and overall survival (20.9 vs 16.0 months) of newly-diagnosed glioblastoma patients compared to temozolomide alone. TTFields are primarily thought to mediate their anti-cancer effects by disrupting tubulin dimer alignment during mitosis, resulting in abnormal chromosomal segregation and mitotic cell death. In addition, recent data suggests that TTFields affect a number of other cellular processes – 1- cell membrane and blood-brain barrier (BBB) permeability, 2- cell migration and invasion, 3- anti-tumour immunity, 4- autophagy, and 5- replication stress and DNA damage repair, the latter of which will be the focus of this project. TTFields has also been shown to downregulate DNA damage response (DDR) proteins and delay the repair of radiotherapy- and chemotherapy-induced DNA lesions, an effect that is thought to be mediated through reduced homologous recombination repair efficiency and induction of a 'BRCAness' phenotype. Such vulnerabilities within DNA damage repair pathways provides a rational for the use of TTFields in combinational therapeutic approaches that target the DDR.

We therefore aim to assess whether combining TTFields with DDR inhibitors (PARPi, ATMi, ATRi and WEE1i) can enhance the efficacy of TTFields in clinically relevant glioblastoma stem-like cultures (GSCs) using a number of established cell survival assays. Additionally, we aim to investigate the mechanisms by which combination treatments of DDR inhibitors and TTFields affect the DNA damage response. In this thesis we show that combining TTFields with radiation and clinically approved PARP inhibitor therapy leads to significantly increased amounts of DNA damage with concurrent decreased clonogenic survival in GSCs. Furthermore, we have shown similar impressive potency when TTFields treatments are combined with BBB-penetrant ATR inhibitors that are currently being assessed in various global clinical trials for glioblastoma as well as other cancers. Overall, these exciting findings support further assessment of TTFields and DDRi combinations to underpin future clinical trials combining TTFields with clinically approved DDRi to improve outcomes for patients with currently incurable high-grade gliomas.

Acknowledgements

I would first like to thank my supervisor, Dr. Spencer Collis, for guiding me throughout the course of my PhD and for pushing me out of my comfort zone. Thank you for always making time for me when I needed advice or feedback and for trusting me with my work.

Ola – I would not be here without you, thank you for believing in me and making me believe in myself. You are the most inspirational person I have met, thank you for always reminding me the importance of the work we do.

Thank you to everyone from the Collis, Bryant and Thompson labs that has contributed to making this experience so enjoyable. I would particularly like to thank the following people. Katie – Thank you for always being patient with me when I had millions of questions and for helping me in the lab. I look up to you so much, both inside and outside of the lab and I will miss you a lot. Callum – I am so glad you joined the project, thank you for always making me laugh and offering an empathetic ear when I was having a bad day. You really had such a positive impact on my experience in the lab and I am so grateful to you for that. Tom and Tegan - I have told you both this before, but I wish we had had longer in the lab together. Thank you for your friendship and good luck with the remainder of your projects.

Mum and Seb – I could not ask for a more supportive family and I am incredibly lucky to have you both.

Finally, thank you to both The University of Sheffield and Novocure for funding my PhD and making this amazing opportunity a possibility.

Dedication

This thesis is dedicated to my farther, Thierry Vanderlinden.

List of publications and manuscripts

- Vanderlinden A*, Rominiyi O*, Clenton S, Bridgewater B, Al-Tamimi Y & Collis S. Tumour Treating Fields for the treatment of glioblastoma: new advances and future directions. *British Journal of Cancer* (2020). – available in appendix B. *denotes first authors.
- Vanderlinden A, Jones C, Myers K, Rominiyi O and Collis S. DNA damage response inhibitor combinations enhance Tumour Treating Fields potency in glioma stem-like cells. Manuscript in preparation (see appendix A for draft manuscript).
- Carmell N, Rominiyi O, Myers K, McGarrity-Cottrell C, Vanderlinden A, Lad N, Perroux-David E, El-Khamisy S, Fernando M, Finegan K, *et al*. Identification and Validation of ERK5 as a DNA Damage Modulating Drug Target in Glioblastoma. Cancers 2021, 13, 944. https://doi.org/10.3390/cancers13050944
- Rominiyi O, Myers K, Lad N, Dar D, Vanderlinden A, Gomez-Roman N, Jellinek DA, Chalmers AJ, Carroll TA, Chen B, Al-Tamimi Y & Collis SJ. FA pathway-based combinations targeting the DNA damage response to enhance chemotherapy and radiotherapy response in glioblastoma stem cells. Manuscript in preparation.

List of publishes abstracts

- Vanderlinden A, Jones C, Myers K, Rominiyi O and Collis S. DNAR-12. Combining Tumour Treating Fields with therapeutic DNA damage response inhibitors to increase potency in high-grade glioblastomas using clinically relevant ex-vivo glioma stem cell models. *Neuro-Oncology*, Volume 24. https://doi.org/10.1093/neuonc/noac209.344
- Vanderlinden A, Myers K, Carroll T, Al-Tamimi Y, Rominiyi O, and Collis S. F-1187. DNA damage response inhibitor combinations to enhance TTFields potency using clinically relevant ex-vivo glioblastoma models. *Brain Tumor Res Treat.* 2022 Mar. https://doi.org/10.14791/btrt.2022.10.F-1187

List of presentations

- Society for Neuro-Oncology (SNO) 27th Annual Meeting, Tampa, Florida (November 16 - 20, 2022) - Combining Tumour Treating Fields with therapeutic DNA damage response inhibitors to increase potency in high-grade glioblastomas using clinically relevant ex-vivo glioma stem cell models. Poster presentation.
- World Federation of Neuro-Oncology Societies (WFNOS), 6th Quadrennial Meeting, Seoul, Korea (March 24 - 27, 2022) - DNA damage response inhibitor combinations to enhance TTFields potency using clinically relevant ex-vivo glioblastoma models. Poster presentation.
- Inovitro™ Meeting, Haifa, Israel (October 16th, 2021) - Combining Tumour-Treating Fields with DNA damage response inhibitors for the improved treatment of glioblastoma. Oral presentation.

Abbreviations

4EBP1	4E-binding protein 1
5'dRP	5'deoxyribose phosphate
53BP1	Tumor suppressor p53-binding protein 1
9-1-1 complex	RAD9-RAD1-HUS1 complex
Adv DMEM	Advance DMEM
AIM2	Absent in melanoma 2
AKT	Protein kinase B
ALT	Alternative telomere lengthening
AMPK	AMP-dependent kinase
a-NHEJ	Alternative non-homologous end-joining
AP site	Apurinic/apyrimidinic site
APE1	AP endonuclease
APNG	Alkylpurine-DNA-N-glycosylase
A-T	Ataxia-telangiectasia
ATG	Autophagy-related protein
ATM	Ataxia-telangiectasia mutated
ATP	Adenosine triphosphate
ATR	Ataxia telangiectasia and Rad3-related protein
ATRIP	ATR-interacting protein
ATRX	Alpha thalassemia/mental retardation syndrome X-linked
BBB	Blood brain barrier
BER	Base excision repair
BRCA1	Breast cancer type 1 susceptibility protein
BRCA2	Breast cancer type 2 susceptibility protein
BSA	Bovine Serum Albumin
CAR	Chimeric antigen receptor
CD	Catalytic domain
CDC2	Cycle protein 2 homolog
Cdc25A/C	Cell division cycle 25 A/C
CDK	Cyclin-dependent kinase
cGAMP	Cyclic guanosine monophosphate-adenosine monophosphate
cGAS	Cyclic-GMP-AMP synthase

Chk1/2	Checkpoint kinase 1/2
CNS	Central nervous system
CQ	Chloroquine
CSA	Cockayne syndrome, type A
CSC	Cancer stem cell
DBD	DNA-binding domain
ddH2O	Double distilled H2O
DDR	DNA damage response
DDRi	DNA damage response inhibitor
DMEM	Dulbecco's Modified Eagle's Medium
DMG	Diffuse midline glioma
DMSO	Dimethyl sulfoxide
DNA-PK	DNA-dependent protein kinase
DNA-PKcs	DNA-dependent protein kinase catalytic subunit
DNA-SCARS	DNA segments with chromatin alterations reinforcing senescence
DSB	Double-strand break
DSBR	Double strand break repair
DTT	Dithiothreitol
DUB	Deubiquitinating enzymes
EB	Evans blue
EC	Extracellular matrix
EDTA	Ethylenediaminetetraacetic acid
EGF	Epidermal growth factor
EGFR	Epidermal growth factor receptor
EMT	Epithelial-to-mesenchymal transition
ERCC1	DNA excision repair protein
ERK	Extracellular-signal-regulated kinase
EXO1	Exonuclease 1
FA	Fanconi Anaemia
FAAP24	Fanconi anemia-associated protein of 24kDa
FAN1	FANCI Associated Nuclease 1
FANCA	FA Complementation Group A
FANCB	FA Complementation Group B
FANCC	FA Complementation Group C

FANCD2	FA Complementation Group D2
FANCD2-Ub	Mono-ubiquitinated FANCD2
FANCE	FA Complementation Group E
FANCF	FA Complementation Group F
FANCG	FA Complementation Group G
FANCL	FA Complementation Group L
FANCM	FA Complementation Group M
FAPi	FA pathway inhibitor
FDA	Federal Drug Administration
FEN-1	Flap endonuclease-1
FGF	Fibroblast growth factor
GSC	Glioblastoma stem-like cell
H2AX	H2A histone family member X
H3K27M	Methylation of the Lys 27 residue of the H3 histone variants
HAT	Histone acetyltransferases
HDAC	Histone deacetylase
HIF1	Hypoxia-inducible factor 1
HR	Homologous recombination
HRR	Homologous recombination repair
ICER	Incremental cost-effectiveness ratio
ICL	DNA interstrand crosslinks
ID complex	Complex formed by FANCD2 and FANCI proteins
IDH	Isocitrate dehydrogenase
IDLs	Isertion-deletion mismatches
IKK	IκB kinase
IL	Interleukin
iNOS	Inducible Nitric Oxide Synthase
IR	Ionising radiation
JNK	c-Jun N-terminal kinase
kDa	kiloDalton
kHz	kiloHertz
Ku heterodimer	Ku70 and Ku80
LC3-I	Microtubule-associated protein light chain 3
LYG	Life year gain

MAPK	Mitogen-activated protein kinase
MCM	Mini chromosome maintenance
MGMT	O6-methylguanine-DNA-methyltransferase
MMR	Mismatch repair
MOA	Mechanism of action
MRN complex	Complex consisting of Mre11, Rad50 and Nbs1
mRNA	Messenger RNA
MSH2	MutS protein homolog 2
MSH6	MutS protein homolog 6
mTOR	Mammalian target of rapamycin
MUS81	Crossover junction endonuclease MuS81
MutLα	MLH1-PMS2 heterodimer
MutSα	MSH2-MSH6 heterodimer
N3-methylA	N3-methyladenine
N7-methylG	N3-methylguanine
NAD+	Nicotinamide adenine dinucleotide
NADPH	Nicotinamide adenine dinucleotide phosphate
NBS1	Nijmegen breakage syndrome 1
NER	Nucleotide excision repair
NF-kB	Nuclear Factor kappa-light-chain-enhancer of activated B
NHEJ	Non-homologous end joining
NLS	Nuclear localisation signal
NO	Nitric Oxide
NSCLC	Non-small cell lung cancer
O6-BG	O6-benzylguanine
O6-MeG	O6-methylguanine
O6-methylG	O6-methylguanine
OD	Optical density
OS	Overall survival
p53	Tumor protein p53
P70S6K	70 kDa ribosomal protein S6 kinase
PAR	Poly(ADP-ribose
PARG	Poly ADP-ribose glycohydrolase
PARP	poly(ADP-ribose) polymers

PARylation	Poly(ADP-ribosyl)ation
p-ATM	Phosphorylated ATM
PBS	Phosphate-buffered saline
p-Chk2	Phosphorylated Chk2
PCNA	Proliferating cell nuclear antigen
PD-1	Programmed cell death protein 1
PE	Plating efficiency
PenStrep	Penicillin-Streptom
PFS	Progression Free Survival
PI3K	Phosphoinositide 3-kinases
PIKK	Phosphatidyl inositol 3' kinase-related kinases
PLK1	Polo-like kinase 1
Pol β	Polymerase β
PS	Phosphatidylserine
PTEN	Phosphatase and tensin homolog
RAD51	DNA Repair Protein RAD51 Homolog 1
REV1	DNA repair protein REV1
RMS	Root Mean Square
ROS	Reactive oxygen species
RPA	Replication protein A
RT	Radiotherapy
SAC	Spindle-assembly checkpoint
SAR	Specific absorption rate
SASP	Senescence-associated secretory phenotype
SA-β-gal	Senescence-associated beta-galactosidase
SDS-PAGE	Sodium Dodecyl Sulfate–PolyAcrylamide Gel Electrophoresis
SER	Sensitiser enhancement ratios
SF	Surviving Fraction
SMARCAL1	SWI/SNF-related, matrix-associated, actin-dependent, regulator of chromatin, and subfamily A-like 1
SOX2	SRY (sex determining region Y)-box 2
SSB	Single strand break
SSBR	Single strand break repair
ssDNA	Single-stranded DNA

STAT3	Signal transducer and activator of transcription 3
STING	Stimulator of interferon genes
TBP1	Topoisomerase Binding Protein 1
TBS	Tris-buffered saline
TBST	TBS and Tween20
TCGA	The Cancer Genome Atlas
TEER	Transendothelial electrical resistance
TERT	Telomerase reverse transcriptase
TFIIH	Transcription initiation factor IIH
TGF-β	Tumour growth factor-β
TLS	Translesion synthesis
TME	Tumour microenvironment
TMZ	Temozolomide
TNFα	Tumour Necrosis Factor α
TOPBP1	DNA topoisomerase II binding protein 1
TTFields	Tumour-Treating Fields
UAF1	Usp1-associated factor 1
USP1	Ubiquitin specific peptidase 1
UV	Ultraviolet light
VEGF	Vascular endothelial growth factor
Vm	Membrane potential
WHO	World Health Organisation
XLF	XRCC4-like factor
XPA	DNA Damage Recognition And Repair Factor
XRCC4	X-ray repair cross-complementing protein 4
ZO-1	Zonula occludens-1
ZRANB3	Zinc finger, RAN-binding domain containing 3
α-KG	α-Ketoglutaric acid
γH2AX	Phosphorylated H2AX

Table of contents

List of figures

List of tables

CHAPTER 1. INTRODUCTION

1.1 Glioblastoma

1.1.1 Characterisation of adult gliomas

Central nervous system (CNS) cancers comprise any cancer that develops within the CNS, either intracranially or extracranially (e.g. in the spinal cord). The CNS is comprised of neurons and glial cells. Glioma is a type of CNS cancer that originates from glial cells. Glial cells provide physical and chemical support to neurons, which themselves provide the electrical impulses and chemical signals to the whole CNS. There are three types of glial cells: astrocytes, oligodendrocytes and microglial cells. According to The World Health Organization (WHO), adult diffuse gliomas are classified according to grade and additional features of the cancer cells, such as oligodendrocytic or astrocytic phenotypes and the location of the tumour: grade II and grade III astrocytic tumours, grade II and III oligodendrogliomas, and grade IV glioblastomas depending on histological features and astrocytic and oligodendroglial phenotype (figure 1.1) (1). Of these, glioblastoma, which is astrocytic in lineage, is the most aggressive and deadly (2), with most patients succumbing to the disease within 12 months of diagnosis and less than ~25% of patients surviving beyond two years despite aggressive treatment regimens (3).

Glioblastoma is defined into primary glioblastoma, where it arises de novo without the presence of precursor lesions, and secondary glioblastoma, which develops from a pre-existent, lower grade astrocytomas (grade II or III). Primary and secondary glioblastoma present differently, with primary glioblastoma being more common (roughly 90% of cases) (4). Primary glioblastoma often presents at grade IV, progresses more rapidly and the risk of developing this type of glioblastoma increases with age (more common in people over 50 years old). Secondary glioblastoma is usually lower in grade and develops slowly initially before becoming more aggressive (5). Recurrent glioblastoma presents differently to the primary tumour with yet again different molecular alterations (6-10). Brain metastases refers to tumours originating from a different organ but spreading to the brain. Different parts of the tumour exhibit different genetic alterations, making the diagnosis, prognosis and treatment of glioblastoma difficult because different parts of the tumour will respond differently to treatment and glioblastoma recurrence often occurs after treatment (11-13).

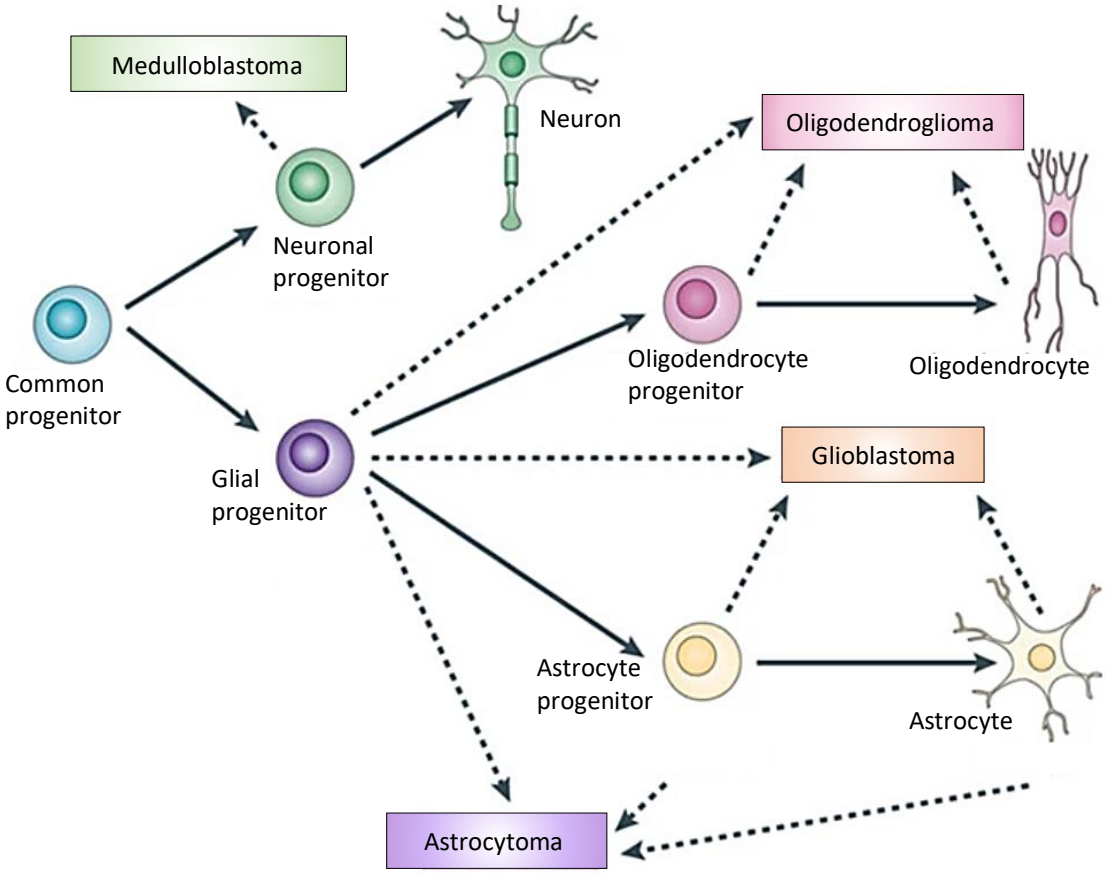

Figure 1.1. Origins of tumours arising in the central nervous system.
Gliomas are defined based on the mature cell of origin they arise from: astrocytomas and glioblastomas arise from astrocytes whilst oligodendroglioma arise from oligodendrocytes. Medulloblastoma is a primary CNS tumour arising from neuronal progenitor cells and occur more commonly in children. Adapted from Huse *et al*. (14).

The Cancer Genome Atlas (TCGA) program initially identified four molecular subtypes of glioblastomas: classical, mesenchymal, neural, and proneural, although the neural subtype has since been removed. Classification into these three subtypes is based on gene expression profiles: the classical subtype is associated with chromosome 7 amplification, loss of chromosome 10, CDKN2A (Cyclin Dependent Kinase Inhibitor 2A) deletion, high levels of EGFR (epidermal growth factor receptor) amplification and TP53 mutations are usually absent; the proneural subtype is associated with IDH1 (isocitrate dehydrogenases 1) point mutations, alterations of PDGFRA (platelet-derived growth factor receptor alpha) and mutations in TP53 (tumor protein 53) are frequently described with this subtype; and, the mesenchymal subtype expresses mesenchymal markers and is associated with mutations in NF1 (Neurofibromatosis 1) (15, 16). Each subtype demonstrates different treatment responses, with the proneural subtype being most treatment resistant (15). Since 2016, the WHO revised the classification of brain tumours to include molecular markers (17). The addition of

molecular markers to histological phenotypes improved prognosis and better predicted treatment response and survival outcomes (1, 18, 19). In 2021, the WHO further updated the classification of adult diffuse gliomas, simplifying the classification into 3 subtypes (as opposed to the 15 different entities from the 2016 classification): astrocytoma (IDH-mutant); oligodendroglioma (IDH-mutant and 1p/19q-codeleted); and Glioblastoma (IDH-wildtype) (figure 1.2).

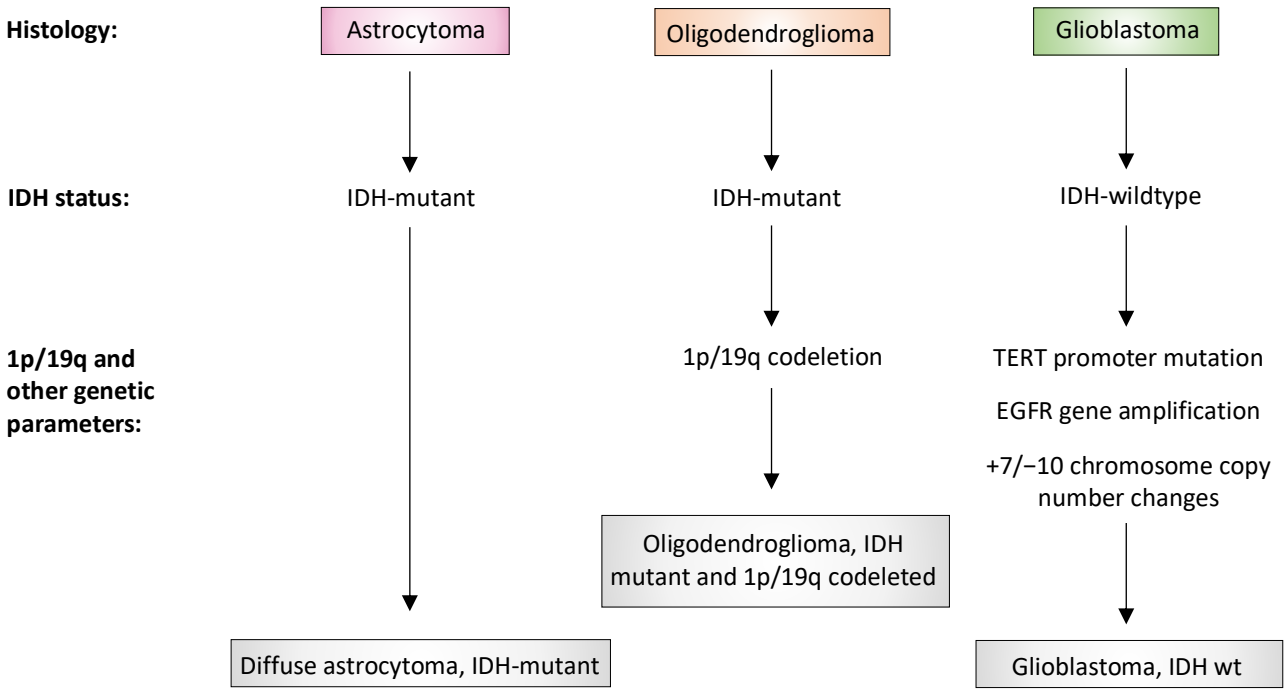

Figure 1.2. Histological and molecular classification of adult diffuse gliomas from the '2021 WHO Classification of Tumours of the Central Nervous System'
In 2021,WHO published an updated classification for tumours of the CNS, which incorporates both histological (astrocytic/oligodendritic) and molecular markers (such as, IDH status and/or evidence of codeletion of chromosome 1p/19q). Gliomas of astrocytic lineage carrying an IDH-mutation are now classified as diffuse astrocytoma, IDH-mutant, and are no longer considered glioblastoma. TERT promoter mutation, EGFR gene amplification, and/or 7 and loss of entire chromosome 10 [+7/−10]) are associated with the glioblastoma, IDH-wildtype entity. Adapted from Louis *et al*. (1).

Isocitrate dehydrogenases (IDH1-3) are enzymes that catalyse the production of α-Ketoglutaric acid (α-KG) from isocitrate. Mutations in IDH1 and IDH2 have been described in glioblastoma and are associated with improved outcomes. Only 5% of glioblastoma patients exhibit mutations in IDH genes at first occurrence, but roughly 80% of secondary glioblastoma patients express IDH mutations. As such, mutations in IDH are considered markers of secondary glioblastoma and IDH status is used in the categorisation of gliomas (20). IDH mutations are often associated with mutations in ATRX and TP53 (21, 22). The most common mutation in IDH1 is a single amino acid substitution at arginine 132 (R132) in IDH1 and arginine 172 (R172) in IDH2 in glioma (23). Mutations result in increased conversion of a-KG into 2-HG (2-Hydroxyglutarate). 2-HG then competes with aKG-dependent dioxygenases, which drive methylation events and gliomagenesis (24).

Co-deletion of the short arm of chromosome 1 (1p) and the long arm of chromosome 19 (19q): 1p/19q co-deletion, together with IDH mutations, make a subtype of glioma know as oligodendroglioma (25). Patients with 1p/19q co-deletion respond better to DNA damaging therapy and predicts improved progression-free and overall survival (26).

ATRX (Alpha thalassemia/mental retardation syndrome X-linked) is a chromatin remodeler that regulates the activity of gene expression and contributes to telomere maintenance. Telomeres are TTAGGG repeats found at the chromosome ends. Telomeres shorten with each cell cycle division until cells eventually lose the ability to divide and activate apoptosis or cellular senescence (27). As such, preservation of telomeres enables tumour cells to survive forever. Mutations in ATRX induce alternative telomere lengthening (ALT) (28, 29), a process that protects telomeres from being degraded with each cell cycle by upregulation of the enzyme telomerase which catalyse the addition TTAGGG at telomere ends (30). ATRX mutations are associated with tumour progression (31) and glioma cells deficient in ATRX are more sensitive to ionising radiation treatment (32).

Methylation of the Lys 27 residue of the H3 histone variants (H3K27M) are associated with gliomas developing from midline structures and is more commonly found in paediatric gliomas but can also been found amongst the adult population (33). H3K27M-mutant diffuse midline glioma (DMG) is predictive of poor prognosis in paediatric patients but does not affect overall survival in older patients (34, 35). H3K27M prevents H3K27 trimethylation (H3K27me3) by the methyltransferase EZH2 (Enhancer of Zeste 2) (36, 37). H3K27me3 is usually responsible for repressing tumour-driving genes such as PDGFRA. H3K27M has been suggested to contribute to gliomagenesis by releasing this repressive state (38).

Telomerase reverse transcriptase (TERT): Mutations in the promoter of TERT have also been associated with poor prognosis. TERT mutations arise in 70% to 80% of all glioblastoma patients and are more

common in older patients (39), with C228T and C250T being the most common mutations. These mutations increased TERT expression and telomerase activity and correlate with reduced survival (40).

O-6-methylguanine-DNA methyltransferase (MGMT) promoter methylation status: Certain chemotherapies, such as TMZ, function by adding methyl groups to DNA, including at O6-methylguanine (O6-MeG). MGMT removes alkyl groups specifically at position O^6 sites on guanine (41). Methylation in the promoter region of the MGMT gene, which occurs in roughly 50% of newly diagnoses glioblastoma patients, results in transcriptional silencing and, in so doing, prevents the repair of O6-MeG lesions (42, 43).

Phosphatase and tensin homolog (PTEN): Loss of the tumour suppressor PTEN (30-40%) is a very common mutation in glioblastoma and is associated with treatment resistance (15, 44, 45). PTEN is a protein that catalyses the dephosphorylation of PIP3 (phosphatidylinositol-3,4,5-trisphosphate) to produce PIP2 (phosphatidylinositol-4,5-bisphosphate), inhibiting activity of the phosphoinositide-3-kinase (PI3K)/protein kinase B (Akt) pathway (46). Loss of PTEN results in increased activation of PI3K/Akt pathway, which has been correlated with tumour grade and with reduced survival outcomes in human gliomas (47).

Epidermal growth factor receptor (EGFR) amplification is found in 40 to 50% of glioblastoma patients and is more common in primary glioblastoma patients (5, 48, 49). The most common mutation is EGFR variant III (EGFRvIII) that arises from the deletion of exon 2-7 (50). EGFR is a transmembrane protein that is involved in the regulation of cell proliferation, survival, differentiation, and migration. EGFR becomes activated upon ligand binding to the extracellular domain, which leads to phosphorylation of its intracellular tyrosine kinase domain (51). The tyrosine kinase activity of EGFRvIII is constitutively active due to truncation in the extracellular domain that imitates the effects of ligand binding (52). EGFRvIII expression enhances tumorigenesis and is correlated with poor prognosis (53, 54). Although, recent studies have contested the use of EGFRviii expression as a prognostic tool (55, 56).

1.1.2 Treatment of glioblastoma

The Stupp protocol, published in 2005, has become the standard-of-care (SoC) for the treatment of glioblastoma patients. It consists of maximal safe surgical resection followed by DNA damaging therapy with adjuvant radiotherapy (daily fractions of 2 Gy given 5 days per week for 6 weeks, for a total of 60 Gy) and concomitant temozolomide (TMZ; 75 mg per square meter of body-surface area per day for the duration of the course of radiotherapy treatment). Chemotherapy is continued at a dose of 150 to 200 mg per square meter following completion of radiation therapy for 6 cycles (temozolomide is taken for 5 days during each 28-day cycle). The addition of TMZ to the standard care for glioblastoma offered a 2.5-month survival increase compared to radiation alone. However, even

with this protocol, the overall survival for glioblastoma patients is still only 14.6 months (57). Several major factors are responsible for the limited treatment efficacy.

Only a subset of glioblastoma patients benefit from additional treatment with TMZ because the MGMT enzyme is expressed in over half of glioblastoma patients and limits the antitumor activity of TMZ (58, 59). Whilst MGMT status predicts which patients will respond to TMZ, all patients receive TMZ irrespective of MGMT status (58, 60). Although glioblastoma rarely metastasises outside of the brain (61), glioblastoma cells are highly invasive and infiltrate into surrounding healthy tissue, which often means the tumour cannot be completely removed during surgery, leaving behind cancer cells that may repopulate the tumour and glioblastoma therefore almost always recurs, often in a more treatment resistant type (62). Additionally, glioblastoma is characterised by extensive intra-tumoral heterogeneity and therefore not all parts of the tumour respond the same way to treatment, with certain subpopulations being particularly resistant (e.g. GSCs, discussed later), which again drives tumour regrowth after treatment. The brain is protected by the blood brain barrier (BBB), which adds an extra layer of complexity to the treatment of glioblastoma because the BBB restricts drug accessibility to the brain from the blood. All these factors have contributed to the failure of many clinical trials over the years and have limited the progression of treatment options for glioblastoma patients.

Recently however, Tumour-Treating Fields (TTFields), which is a non-invasive medical device that delivers low-intensity (1-3 V/cm), intermediate-frequency (100-300 kHz) alternating electric fields has emerged as a first-in-class modality for the treatment of high-grade gliomas, and, following its success in clinical trials was approved by the U.S. Federal Drug Administration (FDA) for treatment of recurrent and newly diagnosed glioblastoma in 2011 and 2015, respectively. The mechanisms of action of TTFields therapy are detailed in the following sections.

1.2 The DNA damage response

The DNA damage response (DDR) refers to the collection of cellular pathways that detect DNA lesions and subsequently coordinates the mechanisms required to repair these lesions and/or determine appropriate cell fate. The DDR comprises of DNA damage tolerance mechanisms, DNA repair and cell-cycle checkpoint pathways as well as signalling pathways involved in cell fate decision (for instance, the induction of programmed cell death pathways where damage cannot be repaired) (66, 67). Several thousand DNA lesions are sustained in our cells every day and the DDR has therefore evolved as a surveillance mechanism to monitor DNA integrity and prevent the generation of potentially harmful genomic insults (68).

DNA damage can be induced exogenously by physical (ionising radiation (IR) and ultraviolet (UV) light) (69, 70) or chemical sources (chemotherapeutic agents, such as alkylating agents and crosslinking agents e.g. temozolomide and mitomycin C, respectively) (71, 72). DNA damage also arises endogenously from by-products of normal cellular metabolism, such as reactive oxygen species (ROS) generated by mitochondria during oxidative respiration (73). Different types of DNA damage elicit activity from different DNA repair pathways (74). For instance, DNA damage from oxidation, deamination and alkylation is repaired via the base excision repair (BER) pathway (see figure 1.7a) (75). Single-strand breaks (SSBs), as the name indicates are discontinuities in one strand of the DNA double helix and are the most common type of DNA damage (76) and are repaired by the single strand break repair pathway (SSBR) (see figure 1.7b). DNA double-strand breaks (DSBs) are breaks in both strands of the DNA double helix and represent the most toxic type of DNA lesion. They are repaired by the homologous recombination repair (HRR) pathway and by non-homologous end-joining (NHEJ) repair pathways (C-NHEJ and alt-NHEJ) (see figure 1.8) (77). The choice of DSBR pathway is primarily determined by the stage of the cell cycle (NHEJ occurs throughout the cell cycle, whilst HHR only takes place during S and G2 phases of the cell cycle as it requires an intact sister chromatid as a template for repair) and the extent of DNA resection at the break (78). Mismatched base-pairs and nucleotide insertions and deletions are corrected by the mismatch repair (MMR) pathway (see figure 1.6) (79). The nucleotide excision repair (NER) pathway (see figure 1.3) is responsible for repairing modified nucleotides that distort the structure of the DNA double helix (80). The Fanconi anaemia repair pathway (see figure 1.4) coordinates the repair of lesions that impede DNA replication, such as inter-strand crosslinks, which are covalently linked adjacent nucleotides on opposite DNA strands (81). Non-canonical functions (non-ICL repair) of FA proteins have also recently been described, such as their involvement in replication fork stabilisation and restart and the repair of non-ICL replication blocking lesions (82). DNA damage tolerance mechanisms, such as transletion synthesis (TLS), mediate lesion bypass so that the DNA replication machinery can replicate past the DNA damage, leaving the damage to be repaired at a later stage (83). Finally, certain types of base damage (e.g. O6-methylguanine, 1-methyladenine, and 3-methylcytosine) can be corrected directly by a single enzymatic reaction (84).

Cell cycle checkpoints coordinate with the DDR to prevent progression through the process of growth and cell division when DNA lesions have been detected. These allow time for DNA lesions to be repaired before the cycle can begin again and are important for the maintenance of genetic stability because they prevent damaged DNA from being passed onto daughter cells (85, 86). There are three commonly accepted cell cycle checkpoints: G1, intra-S and G2/M phase checkpoints that are controlled by several factors within the DDR network. Progression through each stage of the cell cycle

is controlled by fluctuating concentrations of cyclins. Cyclins bind to cyclin-dependent kinases (CDKs) and form activatable complexes (87). Once activated, cyclin-CDK complexes phosphorylate target proteins on specific serine and threonine residues to mediate the events required for progression through respective stages of the cell cycle (88). Inhibition of cyclin-CDK complex activity, as takes place in response to DNA damage, mediates cell cycle arrest at respective stages of the cell cycle (see figure 1.5) (89).

The repair of damage induced by temozolomide and radiation treatment are detailed in the next section.

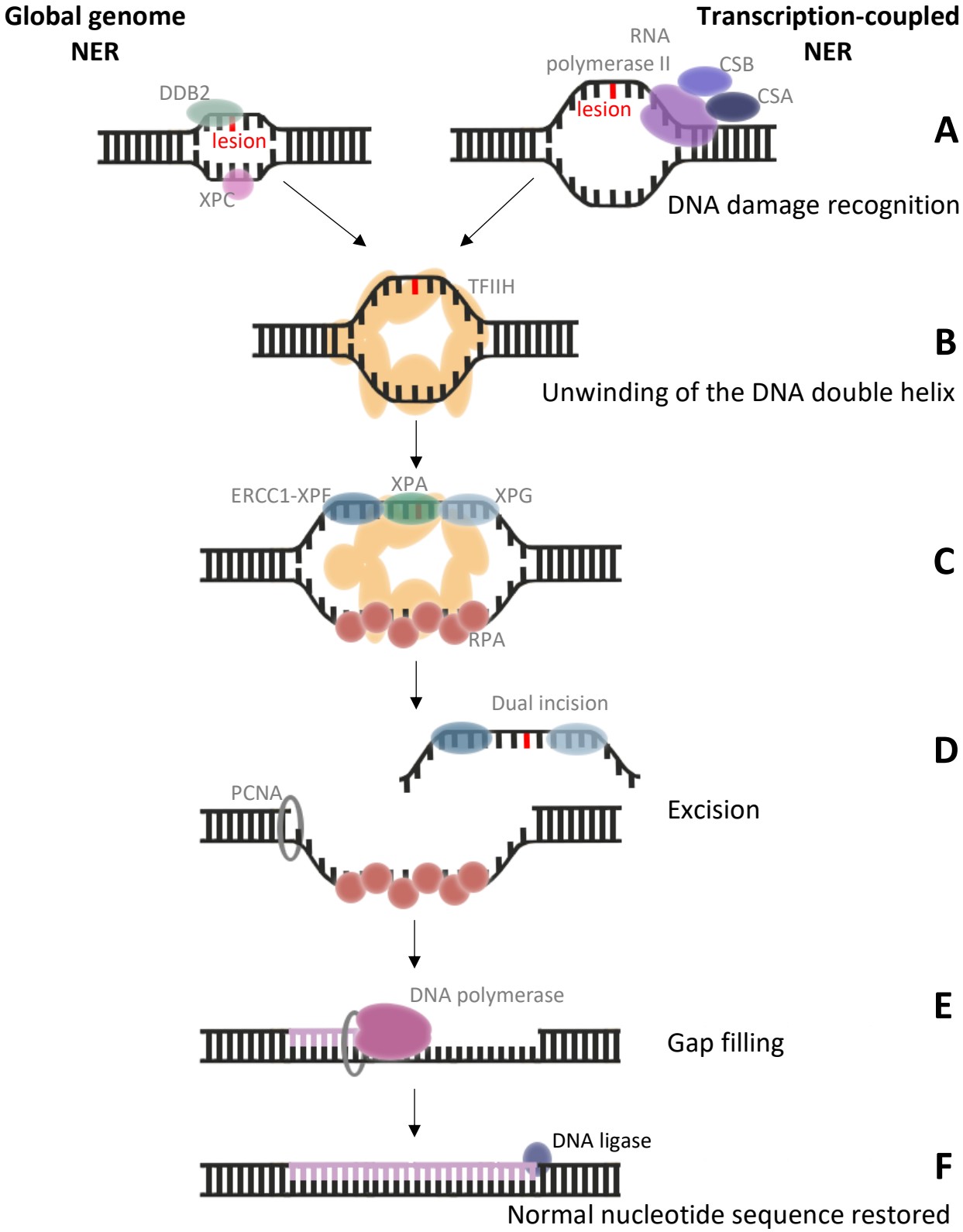

Figure 1.3. Nucleotide excision repair.
A. During global genome NER, XPC or DBD2 recognises the DNA lesions. In contrast, during transcription-coupled NER, RNA polymerase stalls when it encounters the lesions, which triggers recognition by CSA (Cockayne syndrome, type A) or CSB. **B.** Transcription initiation factor IIH (TFIIH) complex unwinds the DNA surrounding the lesion. **C.** ERCC1-XPF, XPA and XPG bind the damaged DNA strand. RPA binds to and stabilises ssDNA on the intact strand. **D.** ERCC1-XPF and XPG cut the DNA strand 5′ and 3′ from the lesion, respectively. **E.** DNA polymerase binds the DNA and mediates DNA synthesis to fill in the gap and restore the normal nucleotide sequence. **F.** DNA ligase seals the gap.

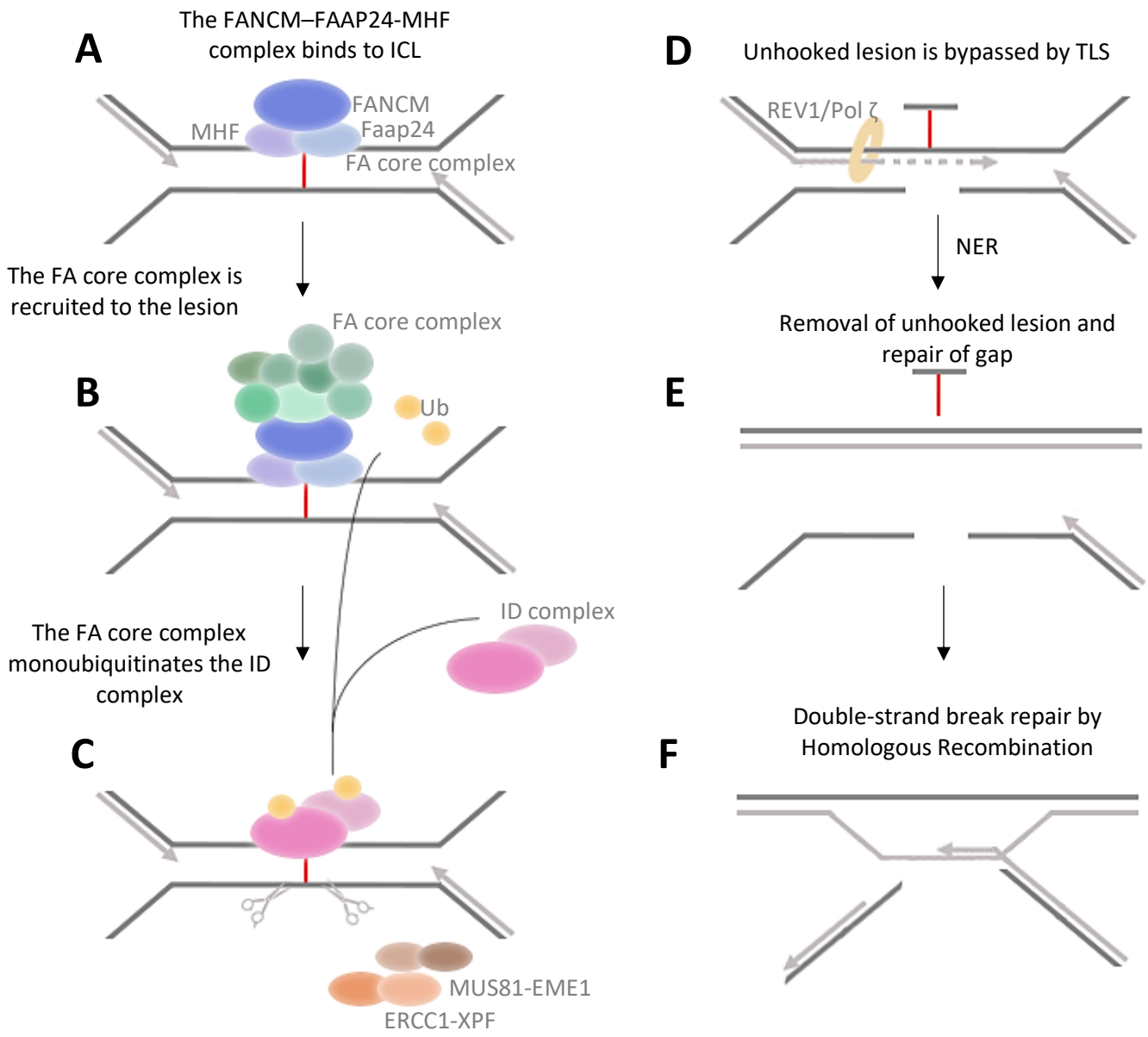

Figure 1.4. Fanconi anaemia repair pathway.
A-B. FANCM forms a heterodimeric complex with FAAP24 and MHF that recognises and binds to the ICL. The FA core complex (formed by the interaction of 8 FA proteins: FANCA/B/C/E/F/G/L/M) is then recruited to the lesion and stabilises the stalled replication fork. **C.** The FA core complex recruits and monoubiquitinates the ID complex (FANCI and FANCD2). Ub-ID2 recruits nucleases (ERCC1–XPF, MUS81–EME1 and/or FAN1) required for nucleolytic incisions either side of the ICL. **D.** The ICL is unhooked, leaving the ICL tethered to the complementary strand and generating a DSB. Specialized TLS polymerases (REV1 and Pol ζ) mediate bypass of the unhooked lesion. **E.** The unhooked lesion is removed and repaired by NER. **F.** The DSB is repaired via HRR. The FA repair pathway is completed when deubiquitinating enzyme (USP1–UAF1 DUB) cleave ubiquitin from the ID complex.

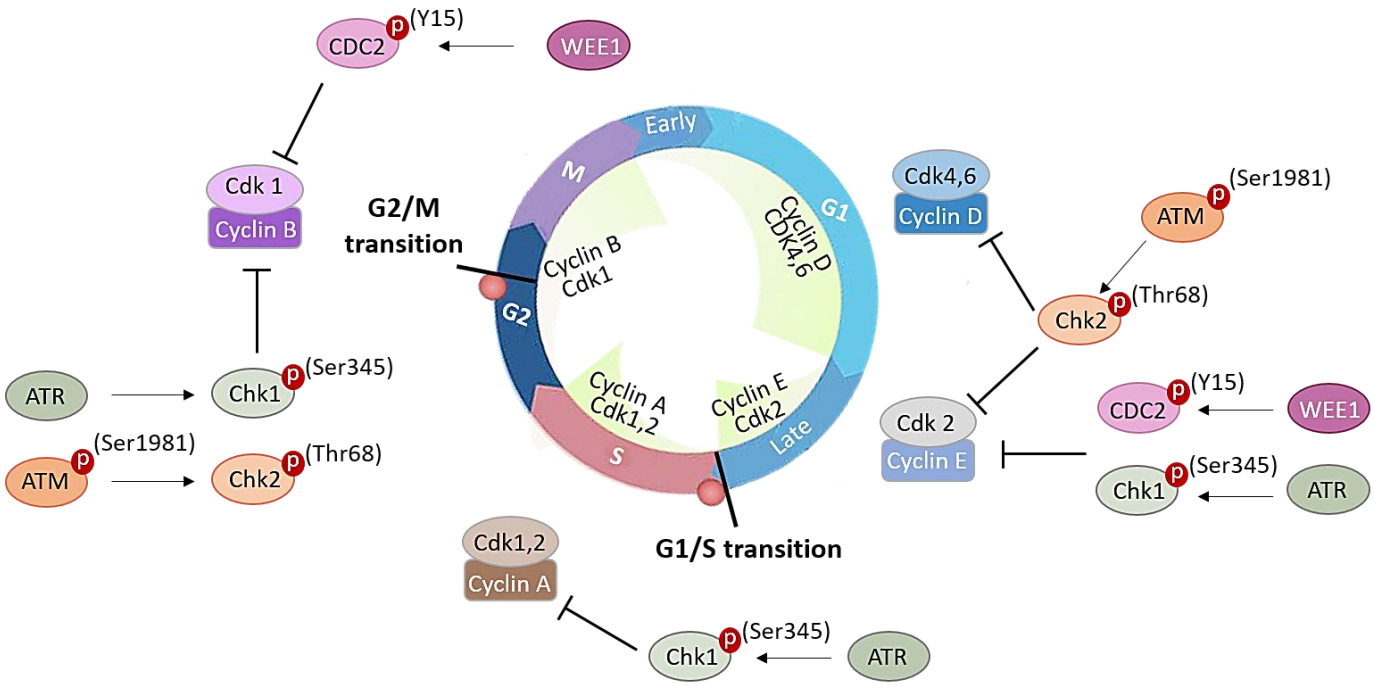

Figure 1.5. DNA damage checkpoint activation.
G1 arrest. ATM mediates G1 checkpoint activation via phosphorylation of p53 on Ser-15. p53 phosphorylation upregulates the expression of p21/WAF1, which inhibits cyclin E/Cdk2 and cyclin D/Cdk4 complexes, which are required for progression into S-phase. Additionally, ATM phosphorylates Chk2 on residue Threonine 68, which in turn phosphorylates p53 on Ser-20 and Cdc25A phosphatase required for CDK complex activation), to inhibit cyclin E/Cdk2 and cyclin D/Cdk4 complexes. ATR phosphorylates Chk1 on residue Serine 345, which in turn prevents CDC25 activity and negatively regulates cycle E-Cdk2 activity. Finally, WEE1 protein kinase regulates Cdk2 activity by inhibitory phosphorylation on tyrosine 15 (Tyr15) and prevents transition from G1 to S phase. **G2-M arrest.** ATM mediates Chk2(Thr68) phosphorylation. P-Chk2 inactivates Cdc25C, which is required for cyclinB1/Cdk1 complex activation. CyclinB1/Cdk1 complex activity mediates G2-M phase transition. ATR phosphorylates and activates Chk1. P-Chk1(Ser345) also inactivates Cdc25C, preventing activation of the cyclinB1/Cdk1 complex and entry into mitosis. Additionally, ATM and ATR both phosphorylate p53 to promote p21 accumulation and inhibit CyclinB1/Cdk1 complex activation. Wee1 phosphorylates Cdk1 on residue Tyr15, inactivating Cdk1 and preventing progression through the G2/M checkpoint.

1.2.1 Direct repair of O6-methylguanine

TMZ is a DNA alkylating agent which adds a methyl group at various positions on the DNA. The most commonly found product of TMZ methylation is product N7-methylguanine (N7-MeG), which accounts for around 70% of the lesions, followed by N3-methyladenine (N3-MeA, ~10%), N3-methylguanine (N3-MeG), and O6-methylguanine (O6-MeG) (90). Whilst methylation on O6-guaning is least common (<8%), O6-MeG is the most cytotoxic lesion induced by TMZ. TMZ-induced O6-MeG lesions are subject to direct removal by the enzyme MGMT (91). Efficacy of TMZ treatment is therefore determined by MGMT status and predicts prognosis in glioblastoma (92, 93). MGMT transfers the methyl group from O6-MeG onto the cytosine residue within its active pocket. Even when MGMT is present, because it is a suicide enzyme, MGMT is targeted for proteasomal degradation following removal of O6-MeG (94, 95). O6-benzylguanine (O6-BG) is an inhibitor of the MGMT enzyme that enhances TMZ toxicity in MGMT-proficient cells *in vitro* (96). However, O6-BG has only demonstrated limited efficacy in the clinic because MGMT levels and activity are restored within 24 hours after removal of O6-BG (97, 98). Resistance to TMZ-induced O6-MeG lesions therefore depends both on MGMT levels and the ability to restore MGMT levels following depletion either by proteasomal degradation or chemical inhibition.

Inactivation of MGMT, for example through promoter methylation (94, 99), results in persistent O6-MeG lesions that mispair with thymine during DNA replication (100). O6-MeG itself is mutagenic, however O6-MeG lesions become lethal when they are converted to DSBs during DNA replication through the MMR pathway. O6meG:T mispairs trigger activation of the MMR pathway (described in figure 1.6) (101, 102). In brief, MutSα and MutLα initiate the MMR pathway by localisation and recognition of the mismatched base. Exonucleases mediate degradation of the mismatched base on the newly synthesised DNA strand. DNA polymerases mediate DNA synthesis and the gap is sealed by DNA ligases (103). However, because the MMR pathway can only remove mismatched bases on the newly synthesised strand (e.g. thymine in this instance), O6-MeG continues to pair with thymine during DNA synthesis, resulting in 'futile cycling' and eventual conversion of these replication-impeding lesions into DSBs. At least two cycles of replication are necessary for the conversion of O6-MeG into DSBs (101). MMR-induced DSBs have also been shown to occur independently of replication. O6-MeG lesions do not directly obstruct DNA synthesis. Simultaneous activation of MMR and BER on opposite DNA strands within close proximity may generate DSBs, for example when N3-MeA or N7-MeG lesions, which activate BER, occur on the complimentary strand in the region that is degraded by exonucleases during MMR (104). Comparison of tumours from matched primary pre-treated glioblastoma patients and recurrent post-treatment glioblastoma patients identified that downregulation of MSH6, a MMR gene, is more commonly detected in post-treatment recurrent

glioblastoma, suggesting that these mutations may arise during treatment and have been suggested to mediate resistance to TMZ (105, 106). The cytotoxicity of TMZ therefore also depends on a functioning MMR pathway and deficiencies in the MMR pathway have been shown to lead to resistance to TMZ and has also been linked to the recurrence of glioblastoma (107).

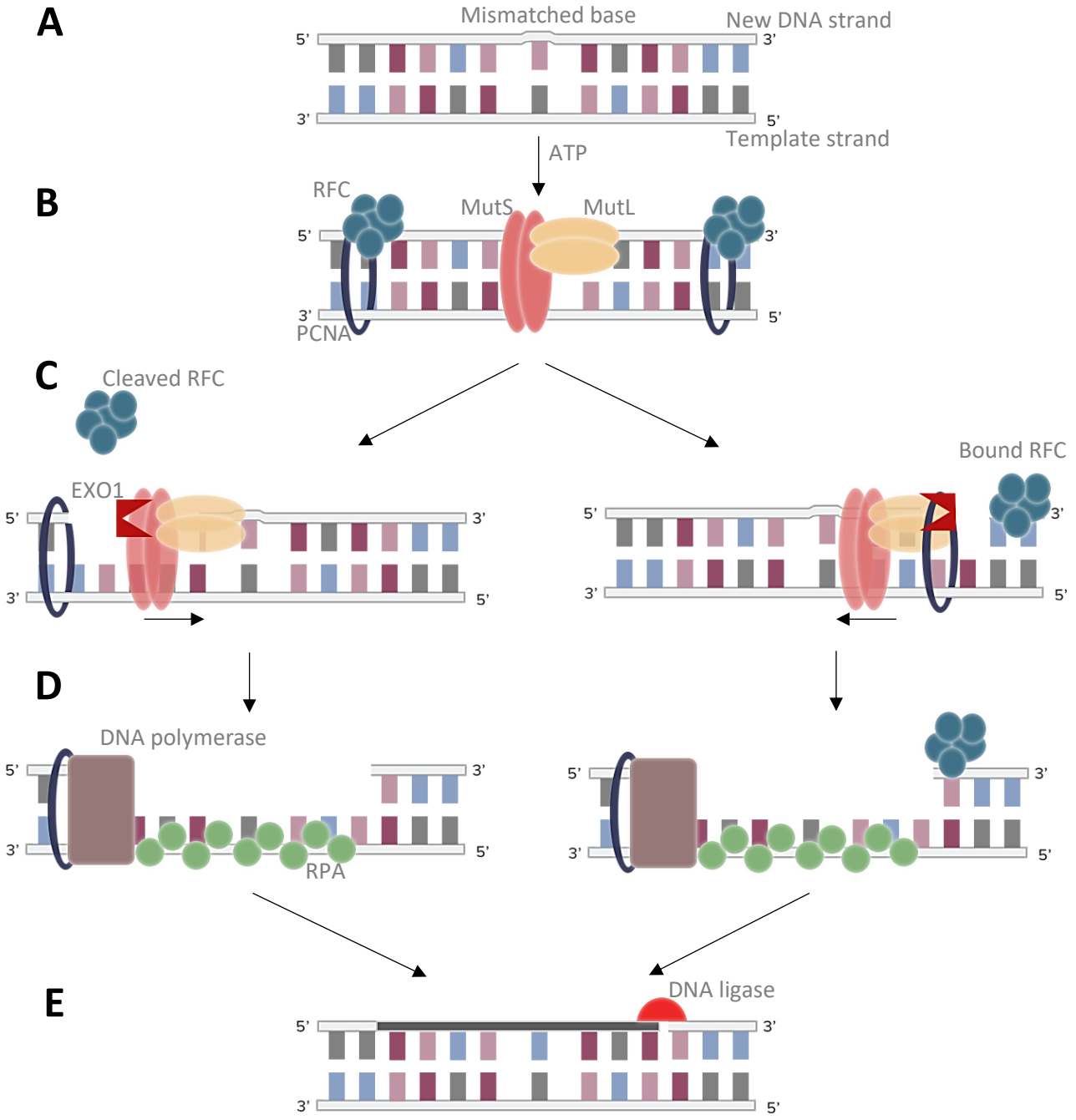

Figure 1.6. Mismatch repair.
MMR can only remove mismatches on the newly synthesised DNA strand. **A.** Mismatched base on newly synthesised DNA strand. **B.** A mismatch is detected in the newly synthesised DNA by MutS heterodimer (comprised of proteins MutS homolog 2 (MSH2) and MutS homolog 6 (MSH6)), which allows recruitment of MutL heterodimer (comprised of proteins MutL homolog 1 (MLH1) and PMS1 homolog 2 (PMS2)). ATP binds MutS/MutL, inducing a conformational change to become a sliding clamp which travels along the DNA. **C.** (*left*) Clamp travels upstream of the mismatch until the 5' nick/replication factor C (RFC) is located and cleaved. EXO1 is loaded onto the DNA to mediate degradation of the newly synthesised strand in the 5'-3' direction, through and beyond the mismatch. (*right*) Alternatively, the sliding clamp travels downstream from the mismatch until the 3' nick/Proliferating cell nuclear antigen (PCNA) is located. EXO1 is loaded onto the DNA strand. Bound RFC promotes degradation by EXO1 in the 3'-5' direction. **D.** RPA binds to ssDNA and stabilises the template strand. The mismatched base and surrounding bases are replaced by DNA polymerase. **E.** DNA ligase seals the gap.

1.2.2 Single strand break repair (SSBR)/Base Excision repair (BER)

SSBs arise directly from various stresses (such as radiation) that disintegrate the sugar backbone (108). Ionising radiation also generates SSBs indirectly by increasing intracellular levels of reactive oxygen species (ROS) from the ionisation of water molecules (radiolysis) within the cell. Oxidative damage induced by ROS is in fact the most common source of SSBs (109). Oxidated bases are processed by the BER pathway (described in figure 1.7a), which indirectly generates a SSB (110). The majority of TMZ-induced lesions (N7-MeG and N3-me-A) are substrates for repair by BER. There is significant overlap between proteins involved in repair of SSBs, irrespective of how they are generated and BER is therefore considered a form of SSBR. SSBs are much more common than DSBs (25:1 ratio) but, unlike DSBs, are not cytotoxic in themselves (111) but can become toxic when they are converted into DSBs, for example during replication stress when the replication fork machinery collides with a SSB and collapses (112). Although these DSBs can be repaired by DSBR pathways (see below), excessive DSB formation may cause these pathways to become saturated (113).

SSBR generally consists of four steps (figure 1.7): SSB detection, DNA end processing, DNA synthesis and finally, DNA ligation. Poly(ADP-ribose) polymerase (PARP) initiates repair by recognising SSBs and recruiting downstream DNA repair proteins. DNA glycosylases (Alkylpurine-DNA-N-glycosylase, APNG) then cut the N-glycosyl bond between the sugar and the base of DNA, generating an abasic site (i.e. apurinic/apyrimidinic (AP) site) (114, 115). The phosphodiester backbone is cleaved either side of the AP site by an AP site-specific endonuclease, such as APE1, generating a SSB intermediate with 3'OH and 5'deoxyribose phosphate (5'dRP) ends (116). DNA polymerases, POLβ or Polδ/ε, respectively, mediate DNA synthesis of either a single nucleotide (short-patch BER) or multiple nucleotides (long-patch BER) (117, 118). DNA ligases seal the gap to complete the process (119).

Although MGMT-mediated repair of O6-MeG lesions is the primary determinant of TMZ sensitivity, some patients that are deficient in MGMT still do not respond to TMZ treatment (120), indicating that other DNA repair mechanisms may dictate TMZ treatment response. Over 80% of TMZ-induced lesions are repaired via the BER pathway. As such, BER has been suggested to mediate resistance to TMZ (121). BER is also the main repair pathway recruited for the repair of IR-induced SSBs (122). Targeting the SSBR pathways therefore constitutes a strategy that is being explored to overcome TMZ and radiation resistance.

PARP activity (discussed in section 4.1) is a central regulator in the repair of SSBs and is upregulated in glioblastoma (123), which makes PARP a therapeutic target for the treatment of glioblastoma. PARP inhibitors enhance sensitivity to DNA damaging agents and have even been shown to overcome TMZ resistance in cells where the MMR pathway is inactive (124). Additionally, a link between APNG

expression and TMZ sensitivity has been suggested. Increased APNG expression mediates resistance to TMZ and is associated with worse overall survival in glioblastoma patients (125). Targeting the BER pathway may provide therapeutic gain in the treatment of glioblastoma.

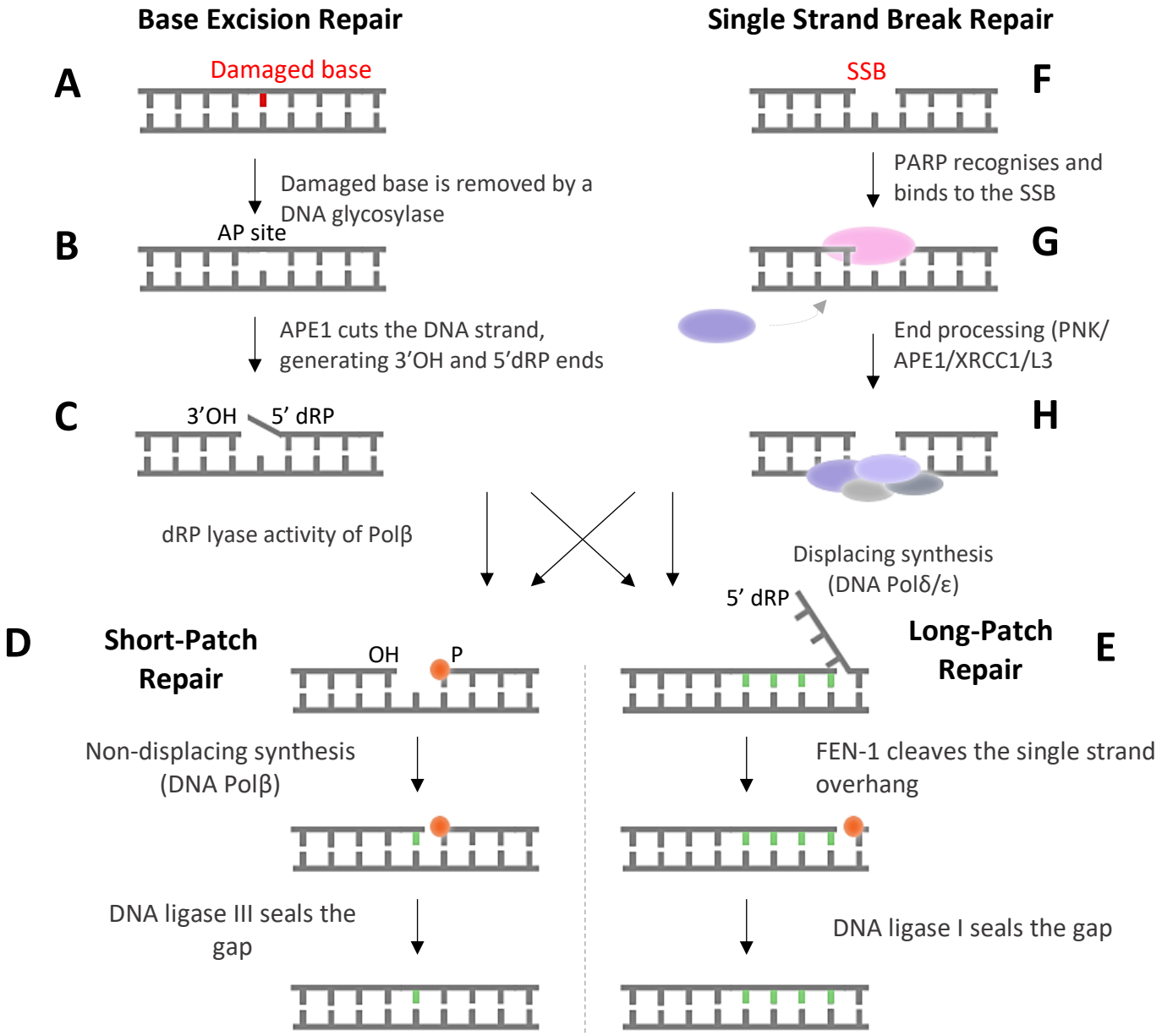

Figure 1.7. Single strand break repair and base excision repair pathways.
Base excision repair. A-B. The DNA glycosylase (APNG) cuts the N-glycosyl bond between the sugar and the base of DNA, generating an abasic site (i.e. apurinic/apyrimidinic (AP) site). **B-C.** The AP endonuclease (Ape1) cuts the DNA strand 5' of the abasic site, resulting in 3'OH and 5'deoxyribose phosphate (5'dRP) ends. DNA polymerases fill the gap with either a single nucleotide (short-patch BER) or multiple nucleotides (long-patch BER). **D.** Short-patch repair: Polβ removes the 5'dRP ends and mediates nucleotide synthesis to fill the gap. The gap is sealed with DNA ligase III. **E.** Long-patch repair: Polδ/ε carries out displacing synthesis. Flap endonuclease-1 (FEN-1) removes 5'dRP ssDNA overhang. DNA ligase I seals the gap. **Single strand break repair. F-G.** PARP1 and XRCC1 detect and bind the SSB. **G-H.** PNK/APE1/XRCC1/L3 mediate end processing of damaged 3'- or 5'-termini at the break. **D-E.** The SSB is then repaired via short-patch or long-patch repair.

1.2.3 Double strand break repair

DSBs are the most toxic types of DNA lesions, and a single unrepaired DSB is enough to induce growth arrest and cell death (126, 127). Ionising radiation directly affects the DNA by inducing single- and double-strand breaks (128). DSBs are not generated directly by TMZ, however, failure to repair damaged bases by BER/SSBR pathways may lead to DSB formation during replication (129, 130). Nonetheless, TMZ has been suggested to activate HRR more potently (~10-fold) than IR (131), and a number of DSBR factors (e.g., NBS1, RAD51 and BRCA2) have been implicated in mediating TMZ sensitivity (132-134).

There are two pathways involved in the repair of DSBs: homologous recombination repair (HHR) and non-homologous end joining, which can be further divided into canonical and alternative NHEJ (figure 1.8). DSBR, irrespective of the pathway, is initiated when the MRE11/RAD50/NBS1 (MRN) complex binds to the DSB and activates the PI3K, ATM (135). ATM phosphorylation then mediates the recruitment of DSBR factors at the DSB, alters chromatin structure at the site of damage allowing access to repair factors and induces checkpoint activation so that the damage can be repaired before progressing onto the next stage of the cell cycle (136-138). The cNHEJ repair pathway is the main repair pathway in mammalian cells and is initiated by binding of the DSB by the DNA-PK complex (Ku70, Ku80 and DNA-PKcs), which protects the DSB from end resection by other repair proteins, and is followed by ligation of blunt DNA ends by the DNA IV complex (XLF and XRCC4) seals the gap (139). ATM-mediated activation of proteins that preserve blunt ends and prevent DNA end resection, such as 53BP1 (140, 141), histone γH2AX (142), and the MRN complex (143, 144), promote activation of cNHEJ. When DSBs are not repaired in time, they are at risk of end processing by nucleases, forming single-stranded 3’ overhangs that are substrates for repair by either HRR or A-NHEJ (145, 146). aNHEJ is limited to short track resection by MRE11 (147) and CtIP (148-150), which is mediated by ATM activation. The single-stranded overhangs produced by end resection are ligated, a process that relies on microhomology (151-153) and results in the loss of genetic information and is therefore associated with increase genetic instability (154). For HRR, initial short track resection by MRE11 and CtIP is extended by EXO1 (143) and BLM (155) to provide longer stretches of single-stranded 3’ overhangs that are required for homology search on the sister chromatid, a process that is dependent on ATM-mediated activation of BRCA1 in late S phase and G2. BRCA1 displaces 53BP1 in order to channel repair through HRR (140, 141, 156, 157). RPA initially binds to ssDNA produced during end resection but is rapidly displaced by RAD51. BRCA2 binds to RAD51-coated ssDNA to mediate homology search (158-161).

DSBR pathway choice is therefore mediated by cell cycle stage and the extent of DNA end resection. BRCA1 and 53BP1, which are both recruited to DSBs by phosphorylation of the histone variant H2AX, compete which each other during end resection. During G1 phase, 53BP1 recruits KU and DNA-PKcs to DSBs which compete with BRCA1 to channel repair through cNHEJ (162). BRCA1 binding is therefore prevented by 53BP1, which in turn prevents CtIP-mediated end resection. 53BP1 therefore limits the extent of end resection and favours repair through NHEJ (163). Despite this, 53BP1 is not considered a core NHEJ factor, rather 53BP1 maintains blunt DNA ends or shorter ssDNA strands by preventing end resection, preventing activation of HRR but promoting activation of cNHEJ (164). In contrast, BRCA1 displaces KU factors in order to channel repair through HRR (165). BRCA-deficient cells allow 53BP1 to bind at DSBs, even in S-G2 phases of the cell cycle, and therefore lose the ability to activate HRR because DNA end resection cannot take place (141). BRCA-deficient cells are therefore associated with enhanced genomic instability and tumorigenesis (166). Loss of 53BP1 is sufficient to restore HRR in BRCA-deficient cells by allowing resection to occur (156). Competition between 53BP1 and BRCA1 couples cell cycle regulation with DSB repair pathway choice. aNHEJ is activated in the absence of cNHEJ, loss of HRR, or by inhibition of EXO1-mediated long track resection (167). NHEJ takes place during all stages of the cell cycle, unlike HRR which requires a sister chromatid as a template for repair and therefore only takes place during late S and G2 phase and is an error-free repair pathway (168). Given that NHEJ is active throughout the cell cycle, NHEJ is considered the main DSBR pathway and has been shown to play a considerable role in the repair of IR-induced DSBs in glioblastoma patients (169, 170).

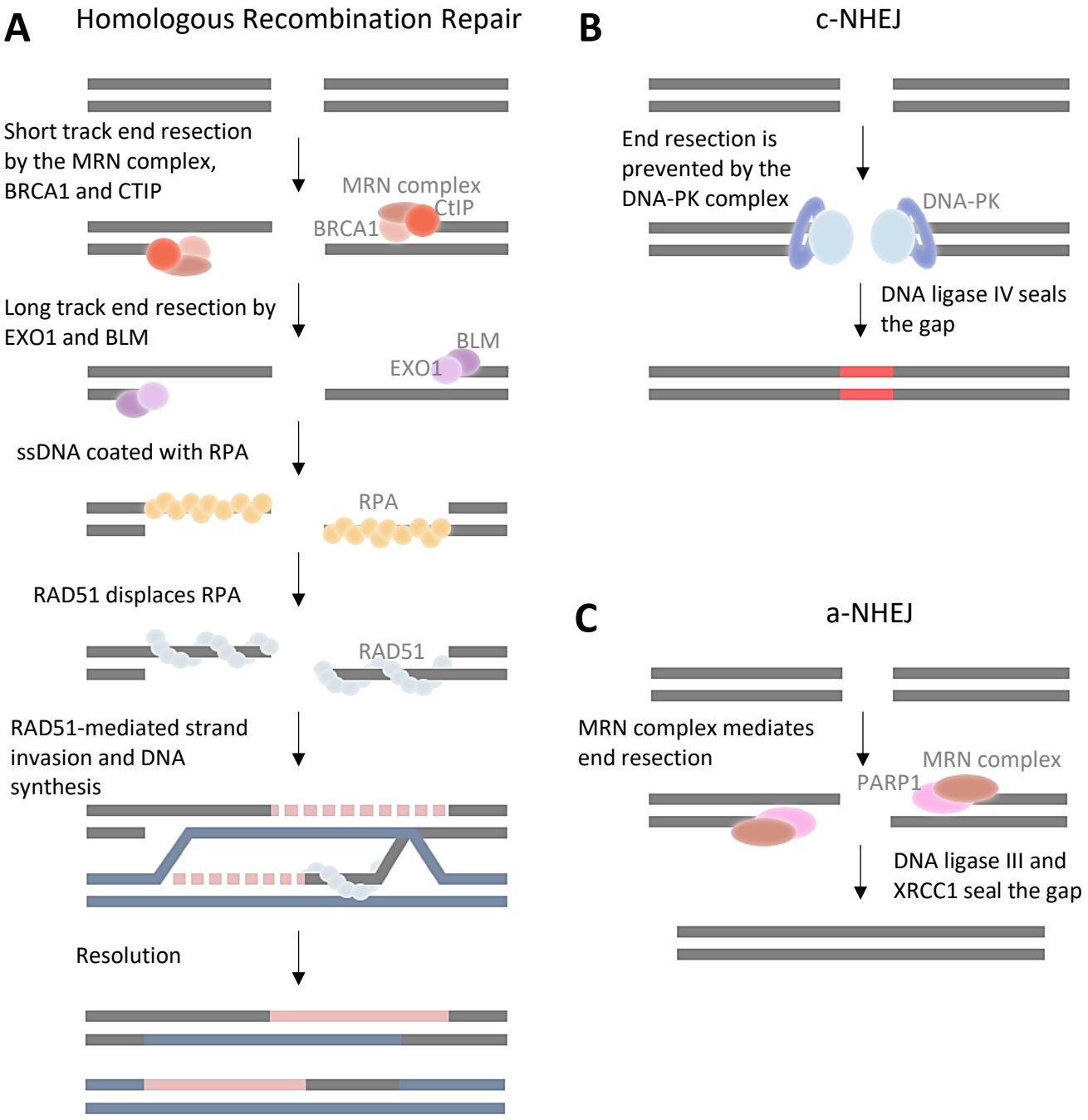

Figure 1.8. Double strand break repair.

A. Homologous Recombination Repair. HRR is active only in the S and G2 phases of the cell cycle. MRN complex (Mre11/Rad50/NBS1), CtIP, and BRCA1 bind to the DSB and mediate initial resection of the 5' ends of both strands of the DSBs to produce 3' single-strands. EXO1 and BLM mediate further resection of 5' ends. RPA binds to and stabilises ssDNA formed during end resection. BRCA2 displaces RPA, allowing RAD51 to bind to ssDNA. RAH51 then mediates strand invasion into the intact sister chromatid. DNA polymerase mediates nucleotide synthesis and DNA ligase seals the gap to resolve the DSB. **Non-Homologous End Joining.** NHEJ is active throughout the cell cycle. **B. Canonical NHEJ.** The DNA-PK complex (Ku70, Ku80 and DNA-PKcs) binds the DSB and protects the DSB from end resection by other repair proteins. Polymerase m and Pol l then mediate nucleotide synthesis and the DNA IV complex (XLF and XRCC4) seals the gap. **C. A-NHEJ.** PARP1 binds to the DSB and recruits the MRN complex, which mediates short-track end resection of the DSB. The resected ends are ligated by DNA ligase III and XRCC1.

Cell cycle stage, the extent of end resection and competition between DNA-PK complex/resection machinery binding will determine whether DSBs are repaired by HRR, canonical NHEJ or A-NHEJ.

1.2.4 Replication stress

Replication stress refers to a change in speed or stalling of replication fork progression. Replication stress occurs both endogenously (from oncogene drivers, errors during DNA replication and transcription, and some DNA lesions) (171-173) and exogenously, from exposure to DNA damaging agents, such as chemo- and radio-therapy (figure 1.9a) (174, 175). DNA lesions, which pose a physical barrier to replication fork progression, are the most common source of replication stress (176). DNA damage tolerance (DDT) pathways use special DNA polymerases that allow replication to continue in the presence of damage and help minimise the deleterious effects of replication fork collapse (177). Lesion bypass generally occurs on the lagging strand, where DNA synthesis is discontinuous and therefore a ssDNA gap can be left for repair after replication (178). Lesions in the lagging strand are therefore generally well tolerated. Prolonged stalling on the leading strand, however, results in uncoupling of the CMG helicase and DNA polymerases and exposure of ssDNA, which can be converted into DSBs. One-ended DSBs are formed when stalled replication forks are cleaved by endonucleases, such as Mre11, DNA2 and Mus81 (179-181). Replication fork collapse or replication fork cleavage convert unligated Okazaki fragments in the lagging strand into DSBs. Alternatively, if a replication fork on the leading strand encounters an unligated Okazaki fragment on the lagging strand, a DSB can be generated (182). Two-ended DSBs can form during replication stress if two separate fork collision events occur either side of the origin (183). These ensuing DSBs are pick up by DSBR pathways and are recognised by ATM and ATR. NHEJ can also repair DSBs induced during replication stress (184). Increased levels of replication stress are therefore associated with DNA damage generation and genomic instability (185).

Replication fork reversal or regression is the first step in the resolution of replication stress. Replication fork reversal refers to a change in direction in replication fork course when the replication fork collides with a DNA lesion (figure 1.9b). During replication fork reversal, a protective four-way junction is formed by annealing of nascent complementary strands (186). Fork reversal facilitates nucleolytic attack because the four-way junction is recognised as a one-ended DSB by nucleases (180, 181). Mre11 is recruited to stalled replication forks by PARP1 (147, 148, 187) and has been implicated in replication fork restart by mediating short track resection of DNA ends behind the replication fork that form substrates for repair by HR, enabling HR-mediated replication fork restart. While end resection is needed for replication fork stabilisation, excessive resection results in chromosomal abnormalities and genomic instability (188, 189). BRCA genes are required to prevent extensive end processing by Mre11 (190). FANCD2, another FA repair pathway protein, also prevents excessive resection by Mre11 (189). The appearance of ssDNA during nuclease resection signals the presence of replication stress. ssDNA gaps can be filled in by HRR, translesion synthesis (which is mediated by specialised translesion

synthesis polymerases) or template switching (where an alternative intact template is employed for synthesis on nascent strands) (figure 1.9c) (191). Firstly, RPA binds to ssDNA. BRCA2 mediates loading of RAD51 onto ssDNA. FA pathway proteins, FANCA and FANCD2, coordinate with BRCA genes to promote RAD51 nucleofilament formation on nascent DNA (189). RAD51 plays a role in fork reversal by mediating invasion of ssDNA into the complementary strand. HRR pathway components, such as RAD51, have been implicated in fork stabilisation, independently to their role in HR-mediated DSBR (192, 193). HR-mediated repair of DSBs occurs differently to HR during replication stress, although the same components are involved (194).

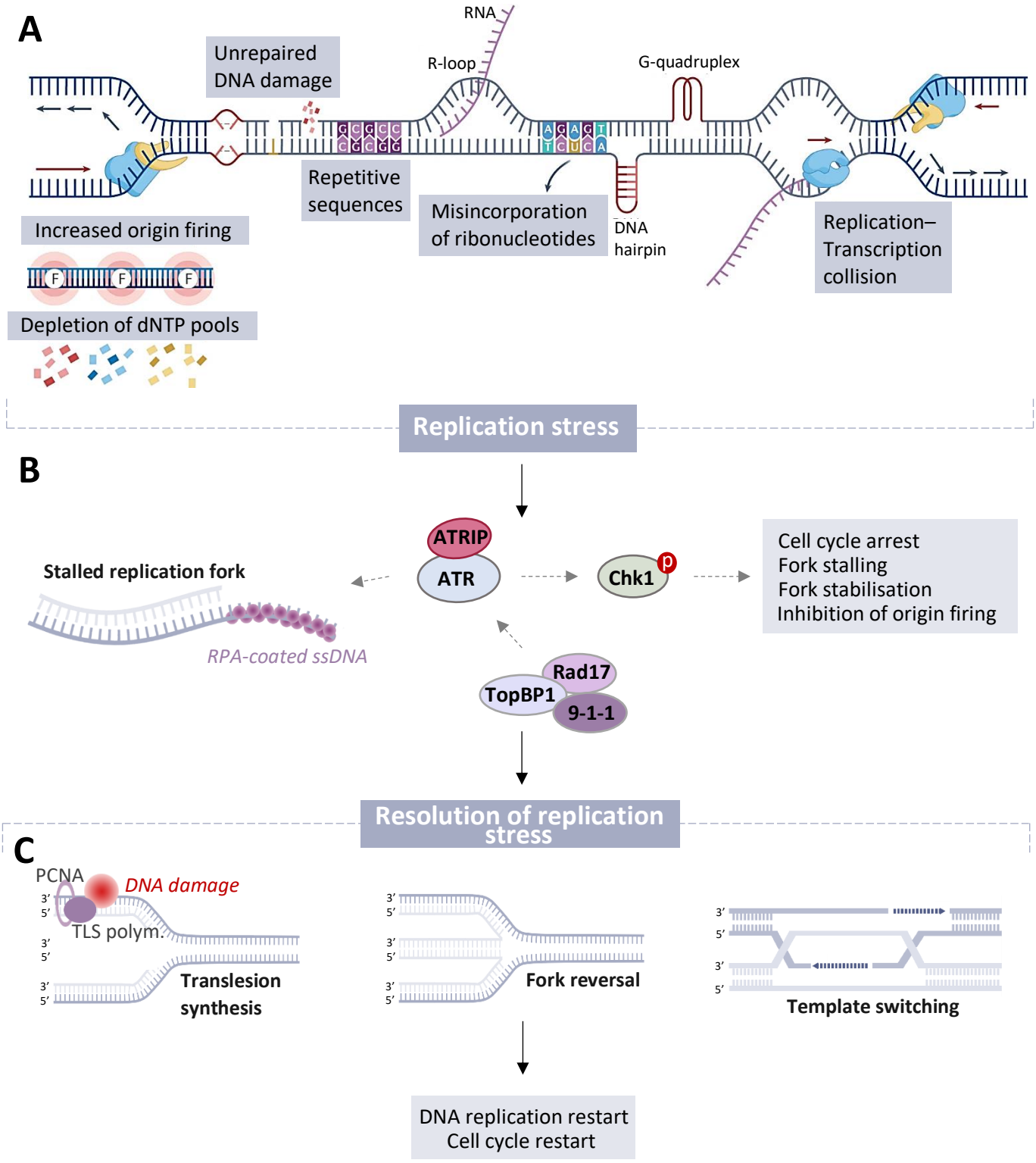

Figure 1.9. Replication stress
A. Sources of replication stress. Replicative stress results from both endogenous or exogenous stresses, examples of which include: depletion of deoxynucleotides (dNTPs) that impairs progression of ongoing DNA replication, sustained DNA damage, repetitive DNA sequence, R-loops, misincorporation of ribonucleotides, secondary DNA structures (hairpins and quadruplexes) and collisions between replication and transcription machinery. Adapted from da Costa *et al.* (1, 2). **B. Activation of ATR.** ssDNA is first bound RPA. ATRIP then binds to RPA and recruits ATR to RPA-coated ssDNA. Interactions between RAD17, the RAD9-RAD1-HUS1 (9-1-1) complex and Topoisomerase Binding Protein 1 (TOPBP1) complete ATR activation. Once activated, ATR phosphorylates several substrates to orchestrate checkpoint activation, DNA repair, and stabilisation of stalled replication forks. **C. Resolution of replication stress.** Different responses take place after replication stress. Translesion synthesis: DNA damage tolerance pathways employ special TLS polymerase to mediate replications past lesions. Fork reversal: the replication fork changes direction, forming a protective four-way junction by annealing of nascent complementary strands. Template switching: an alternative intact template is employed for synthesis on nascent strands to mediate repair.

1.2.4.1 The role of RPA in replication stress

RPA is composed of three subunits, namely RPA1, RPA2 and RPA3 (or RPA70, RPA32 and RPA14, respectively) (195). During normal replication, RPA regulates DNA polymerases (such as DNA Pol α and Pol δ) assembly and activity to promote initiation and elongation of replication and processing of Okazaki fragments on the lagging strand (196-198). During replication stress, RPA firstly protects ssDNA generated during replication stress from excessive nucleolytic attack (199). RPA-coated ssDNA also prevents repair by aNHEJ by preventing spontaneous annealing between microhomologies (200). Annealing of short inverted repeats can generate secondary DNA structures such as hairpins after DNA synthesis and ligation (201, 202). RPA also recruits chromatin remodelers, such as SMARCAL1 (SWI/SNF-related, matrix-associated, actin-dependent, regulator of chromatin, and subfamily A-like 1), ZRANB3 (zinc finger, RAN-binding domain containing 3), and HLTF, which contribute to fork reversal and stabilisation by mediating invasion into the complimentary strand (203). ssDNA-coated RPA recruits ATRIP and ATR (figure 1.13b) (204). Rad17 and 9-1-1 then localise to the break, and together with DNA topoisomerase II binding protein 1 (TOPBP1) mediate activation of ATR to promote repair via HR (205-208). Activated ATR also induces cell cycle arrest by phosphorylation of Chk1, which in turn inhibits cyclin-cdk activity (figure 1.13b) (209). This ensures that replication forks can be stabilised before cell cycle progression is resumed. Chk1 activation also presents origin firing (210). Re-replication occurs when the genome is replicated more than once during the same cell cycle and is a major source of genomic instability. One way in which DSBs can be generated is when two adjacent replication forks collide during re-replication, causing replication fork collapse and formation of a DSB (211-213). In contrast to normal replication forks, replication forks that are established during re-replication are limited in their ability to progress along the DNA (30–35 kb from the origin). As such, re-replication is associated with loss of genomic information and ploidy (214). Regulation of replication initiation is coupled with cell cycle regulation in order to guarantee that origin firing only takes place once per cell cycle. CDK activity inhibits re-replication (215).

Activation of ATR by RPA also mediates phosphorylation of RPA itself. Phosphorylation of RPA is mediate by the phosphoinositide 3-kinase (PI3K)-like protein kinases, ATM, ATR and DNA-PK. RPA2 is the primary site of phosphorylation, with T21 and S33 being the most commonly phosphorylated sites (216). Phosphorylation of RPA alters its structure such that it no longer interacts with DNA polymerases, thereby preventing replication initiation (217). RPA phosphorylation enhances its affinity for ssDNA, however, increased affinity for ssDNA does not necessarily translate to increased RPA activity (218). Phosphorylation of RPA is also carried out by cyclin-Cdk complexes and occurs during S and G2 phases of the normal cell cycle, but also occurs in response to DNA damage (219, 220). RPA phosphorylation is lost after mitosis during normal cell cycle (221). Protein phosphatase 2A (PP2A)-mediated dephosphorylation of RPA is necessary to complete the repair process. Replication fork protection therefore depends on the availability of RPA (222).

In the absence of RPA, or when excessive ssDNA is generated, RPA stores can become depleted, a process known as RPA exhaustion. Any additional ssDNA formed beyond this point results in replication fork collapse and DSB formation (223) and loss of RPA is synthetically lethal (224). RPA binds to ssDNA during replication stress and to ssDNA that form as intermediates during processing by repair pathways (such BER and NER) and RPA-coated ssDNA has been suggested to dictate which pathway is recruited for repair, although how exactly this takes place has not yet been established. ssDNA intermediates vary in length and are accompanied by different proteins and adjacent structures depending on how they were generated, which allows differentiation between ssDNA that arises during replication stress or during DNA damage processing (225).

1.2.5 Parallel targeting of DDR processes

Disruptions in cellular pathways that are enlisted to resolve DNA damage are important for driving cancer development and progression due to increased genomic instability, increased mutation rate and the establishment of a heterogenous cancer cell population (226, 227). Genomic instability is therefore recognised as one of the hallmarks of cancer (228) and germline mutations in essential DDR genes are associated with a predisposition to cancer (66). Consequently, and unsurprisingly, cancer cells often harbour somatic mutations in key DDR genes, such that cancer cells often rely on a reduced subset of functioning DNA damage repair pathways in comparison to normal cells which possess a fully functioning set of DDR pathways (229, 230). Cancer cells are therefore perpetually subjected to increased DNA damage as a result of combined failure to repair DNA damage and continual formation of additional DNA lesions due to increased replicative and oxidative stress, which typically drive genomic instability in cancer (231, 232). These characteristics make cancer cells particularly vulnerable

to treatments that further exacerbate the induction of DNA damage and overwhelm cancer cells with DNA damage, hence the establishment of DNA-damaging agents, such as chemotherapy and radiotherapy, as the mainstay in cancer therapy (233, 234). However, despite efforts to minimise normal tissue toxicity, the cytotoxic effects of radio- and chemo-therapy on normal tissue remain a limiting factor for radiation and chemotherapy doses (235). Additionally, cancers display intrinsic or acquired resistance to these treatment modalities, such that their efficacy and clinical benefit is often limited or short-lived (236).

Because of these deficiencies in key DDR genes, cancer cells are particularly reliant on remaining and unimpaired DDR processes to compensate for such high DNA damage burden, such that activity of these remaining DNA repair pathways is enhanced in cancer cells compared to normal cells (237, 238). This is exemplified in glioblastoma, where increased activity of DNA repair processes is particularly seen in a subpopulation of glioma cells, called glioblastoma stem-like cells (GSCs). These GSCs have been shown to have increased DNA damage repair efficiency compared to glioblastoma bulk cells due to this increased DDR/DNA repair pathway activity (239). As such, GSCs are better able to recover from DNA-damaging agents compared to their bulk counterparts and due to their stem-cell like properties, such as their self-renewal and multi-lineage differentiation capabilities, GSCs likely mediate tumour regrowth and cancer recurrence after treatment (240).

The addition of DNA damage repair inhibitors (DDRi) to DNA-damaging treatment therefore constitutes an obvious and sensible approach in efforts aiming to overcome and mitigate the establishment of resistance to conventional chemoradiation therapy and to improve DNA-damaging agent efficacy (241). Indeed, further inhibition of even one of these remaining and highly active repair pathways should in theory increase the cytotoxic effects and chemo- and radio-therapy treatment. This particularly holds true in cases where cancer cells rely specifically on a single backup repair pathway for survival and where a synthetic lethality relationship between two repairs pathways has been described; a relationship between two or more genes where deficiencies in a single one of these genes does not lead to cell death but where deficiencies arising in these genes simultaneously results in cell death, offering the possibility for single-agent activity (242). In addition, the use of DDRi with DNA-damage inducing agents should expand therapeutic efficacy within cancer cells specifically with minimal cytotoxicity effects on healthy tissue due to healthy cells owning a complete set of function DNA damage repair pathways allowing them to recover from such treatments (243). This approach has proven successful so far, with various DDRi/DNA-damaging agents combinations either currently undergoing investigation in clinical trials (see table 1) or having demonstrated sensitising effects and improvements in survival in cancer patient cohorts (244-246).

However, because of functional redundancy (where backup repair pathways can compensate in the absence of the more favourable repair pathway) and overlapping functions between DNA damage repair processes (247), inhibition of a single DNA damage repair pathway often only offers partial sensitising effects to DNA damaging agents and/or can trigger alternative backup repair pathways to become activated, in turn leading to drug resistance (248, 249). Therefore, in an attempt to maximise efficacy of combination strategies, targeting multiple DDR processes simultaneously has been proposed by reason of complimenting effects between drugs (249, 250). Given that TTFields has been shown to induce conditional vulnerabilities within DDR processes (discussed in the following section) and no additional systemic toxicities have been associated with TTFields treatment, TTFields makes the ideal candidate to form the basis of combinational strategies aimed at the DDR, particularly in resistant GSC populations.

Table 1. DDRi in combination with DNA damaging agents - completed and ongoing clinical trials in glioblastoma.

DDRi clinical trials in GBM - completed and ongoing				
Trial name and Identifier	**Status & Design**	**Number of participants**	**Treatments**	**Conclusions**
A Phase 0 Study of AZD1775 in Recurrent GBM Patients (NCT02207010)	Completed, Single Arm Phase 0 trial	20	Drug: Adavosertib (WEE1i)	Primary outcomes: plasma and intratumoral concentration of AZD1775 Secondary outcomes: measurements of p-CDC2(Tyr15), H3 and γH2AX levels in patient tissue
Adavosertib, Radiation Therapy, and Temozolomide in Treating Patients With Newly Diagnosed or Recurrent Glioblastoma (NCT01849146)	Completed, Phase I Non-Randomised Study	114	Drug: Adavosertib (WEE1i) Radiation: Radiation Therapy Drug: Temozolomide	Primary outcomes: MTD of adavosertib radiotherapy and temozolomide and incidence of toxicities Secondary outcomes: OS and PFS
ABT-888, Radiation Therapy, and Temozolomide in Treating Patients With Newly Diagnosed Glioblastoma Multiforme (NCT00770471)	Completed, Single Arm Phase I/II trial	24	Drug: Veliparib (PARPi) Radiation: Radiation Therapy Drug: Temozolomide	Primary outcomes: MTD of veliparib when administered in combination with radiotherapy and temozolomide and OS Secondary outcomes: determine toxicity and frequency of toxicity

Olaparib and Temozolomide in Treating Patients With Relapsed Glioblastoma (NCT01390571)	Completed, Open Label Phase I trial	34	Drug: Olaparib (PARPi) Drug: Temozolomide	Primary outcomes: determine whether olaparib crosses the BBB and achieves tumor penetration and determine the safety and tolerability of the combination Secondary outcomes: assess the possible anti-tumor activity of the combination
Study of the Safety and Efficacy of MK-4827 Given With Temozolomide in Participants With Advanced Cancer (Including GBM) (NCT01294735)	Completed, Non-Randomised Phase I study	19	Drug: Niraparib (PARPi) Drug: Temozolomide	Primary outcome: number of participants with DLTs Secondary outcomes: Number of participants with an objective response rate of partial or complete response and PFS
Carmustine Plus O(6)-Benzylguanine in Treating Patients With Recurrent or Progressive Gliomas of the Brain (NCT00003348)	Completed, Phase I trial	56	Drug: O6-benzylguanine (MGMT inhibitor) Drug: Carmustine	Objectives: Determine the MTD of carmustine when administered following O6-benzylguanine and characterise the toxic effects
Temozolomide and O6-benzylguanine in Treating Patients	Completed, Phase I trial	20-30	Drug: O6-benzylguanine (O6-BG)	Objectives: Determine the dose of O6-BG effective in producing complete

With Newly Diagnosed, Recurrent, or Progressive Anaplastic Glioma (NCT00006474)			Drug: Temozolomide	suppression of tumor MGMT activity, determine MTD of TMZ administered after O6-BG and determine toxicity and anti-tumour response
O6-Benzylguanine and Carmustine Implants in Treating Patients With Recurrent Malignant Glioma (NCT00004892)	Completed, Phase I trial	14	Drug: O6-benzylguanine Drug: Carmustine implants	Determine the dose of O6-BG that completely suppresses AGT levels and evaluate the safety and tolerance of O6-BG + carmustin implants
A Study to Assess the Safety and Tolerability of AZD1390 Given With Radiation Therapy in Patients With Brain Cancer (NCT03423628)	Active, Single Arm Phase I trial	132	Radiation: Radiation Therapy Drug: AZD1390 (ATMi)	Primary outcomes: incidence of DLTs and AEs Secondary outcomes: EVS, objective response (RANO, RANO-BM and RECIST criteria) and pharmacodynamic properties
BGB-290 and Temozolomide in Treating Patients With Recurrent Gliomas With IDH1/2 Mutations (NCT03914742)	Recruiting, Non-Randomised Single Arm Phase I/II trial	100	Drug: Pamiparib (PARPi) Drug: Temozolomide	Primary outcomes: MTD and percentage of participants with AEs Secondary outcomes: PFS, OS and percentage of participants with serious or life-threatening AEs

AZD1390 in Recurrent Grade IV Glioma Patients (NCT05182905)	Recruiting, Non-Randomised Phase 0/1b trial	21	Drug: AZD1390 (ATMi)	Primary outcomes: pharmacokinetics (PK) of AZD1390 in tumor tissue and PFS. Secondary outcomes: Drug-related toxicity, AEs, OS, PK of AZD1390 in CSF and deaths at 12 months
Olaparib in Treating Patients With Advanced Glioma, Cholangiocarcinoma, or Solid Tumors With IDH1 or IDH2 Mutations (NCT03212274)	Recruiting, Single Arm Phase II trial	145	Drug: Olaparib (PARPi)	Primary outcomes: overall response rates Secondary outcomes: PFS, OS, duration of response and safety and tolerability of olaparib monotherapy
Study of Pamiparib in Newly Diagnosed and rGBM (NCT04614909)	Recruiting, Non-Randomised A Phase 0/2 Clinical Trial	30	Drug: Pamiparib Drug: Olaparib (PARPi) Drug: Temozolomide Radiation: Radiation therapy	Primary outcomes: Systemic plasma PK profile parameters Secondary outcomes: PFS, OS, Drug-related toxicity, AEs, PD of pamiparib and deaths at 24 months
Cediranib Maleate and Olaparib Compared to Bevacizumab in Treating Patients With Recurrent Glioblastoma (NCT02974621)	Active, Randomised Phase 2 Clincial Trial	70	Drug: Bevacizumab Drug: Cediranib Drug: Cediranib Maleate	Primary outcomes: PFS Secondary outcomes: OS, AEs, levels of circulating cytokines involved with angiogenesis, levels of serial circulating

			Drug: Olaparib (PARPi)	biomarkers involved with deoxyribonucleic acid (DNA) repair
Veliparib, Radiation Therapy, and Temozolomide in Treating Patients With Newly Diagnosed Malignant Glioma Without H3 K27M or BRAFV600 Mutations (NCT03581292)	Active, Single Arm Phase 2 Clincial Trial	115	Drug: Veliparib (PARPi) Drug: Temozolomide Radiation: Radiation Therapy	Primary outcomes: Efficacy of Veliparib, TMZ and IR in combination based on H3 K27M, BRAF, and IDH1/2 status of patients with newly-diagnosed high-grade glioma
Talazoparib - Carboplatin for Recurrent High-grade Glioma With DDRd (TAC-GReD)	Recruiting, Single Arm Phase 2 Trial	33	Drug: Talazoparib	Primary outcomes: PFS at 6 months Secondary outcomes: OS, objective response rate and duration of response (RANO criteria)

1.3 Tumour-Treating Fields

Tumour-Treating Fields (TTFields) are an emerging and recently clinically approved non-invasive therapeutic device (Optune, Novocure™) that deliver low-intensity (1-3 V/cm), intermediate-frequency (100-300 kHz), alternating electric fields. The Optune system consists of four transducer arrays (each made up of 9 ceramic disks), a field-generator, and a power source (shown in figure 1.10). For glioblastoma, the four transducers arrays are attached in pairs, orthogonally to the patient's shaved scalp, the optimal positioning of which is determined using NovoTAL™ (Novocure Ltd., Haifa, Israel) simulation software based on tumour location and the size and shape of the patient's head (251). The field-generator delivers the alternating electric fields at a set frequency through the transducer arrays, across the brain and to the tumour site.

Figure 1.10. The Optune System.
Left - The Optune delivery system consisting of four transducer arrays, a field-generator, and a power source. Right – A patient wearing the Optune delivery system. Images taken from Novocure, 2020.

The optimal frequency at which anti-cancer effects are imparted by the Optune system varies between cancer types, which for glioma cells is at a frequency of 200 kHz (252). The patient's head must be shaven consistently to allow optimal contact of the transducer arrays with the scalp and a layer of conductive hydrogel is coated onto the ceramic disks before application. The main adverse event of TTFields is contact dermatitis at the site of transducer array attachment caused by irritation from sweat and/or hydrogel, however, this is usually of low grade (I-II) and can easily be managed by changing the positioning of the arrays or protecting the skin with sterile dressing pads and oral antibiotics may be prescribed if necessary (253).

Important financial considerations are associated with incorporating TTFields therapy into the standard of care for glioblastoma patients. Presently, Novocure, the sole producer of the therapeutic TTFields delivery systems, rents Optune to patients for a total monthly cost of around $21,000 (subject to discounts negotiated by healthcare providers/payers) (254). This cost covers the TTFields delivery system, and includes transducer arrays, array layout planning, patient/physician training and 24-h technical support (255). Additional expenses associated with implementing TTFields might include additional staff and training (251), and costs associated with managing treatment-related morbidities (256).

There have been three major studies estimating the costs associated with adding TTFields to the standard-of-care therapy for glioblastoma, all of which use EF-14 trial data. Bernard-Arnoux *et al*.(257) used interim EF-14 data, while Connock *et al*.(258) and Guzauskas *et al*. (259) used the trial's final results. During economical modelling, the assumptions made by Bernard-Arnoux et al. and Connock *et al*. were based on a French National Health Insurance perspective, while analyses by Guzauskas *et al*. were based on the US healthcare perspective. All three studies relied on the full list price of TTFields therapy and therefore do not incorporate potential discounts negotiated by healthcare payers.

Bernard-Arnoux *et al*. estimated 0.34 life years gained (LYG) from the addition of TTFields to maintenance of TMZ, with an added cost of €185,476, while Connock et al. estimated 0.604 LYG with an added cost of €453,848. These two studies then estimated the incremental cost-effectiveness ratio (ICER, a summary measure that compares the economic value of a particular intervention with another expressed as cost per LYG) to be €549,909 and €510,273, respectively. Both studies analysed survival using statistical models that were unable to account for changing (decreasing) hazard rates as patients live longer. This is an important limitation since epidemiological data suggest that as a patient survives longer, the ongoing probability of death reduces. For example, analysis of the US SEER database

demonstrated patients alive 5 years after diagnosis had a 70.4% probability of surviving to 10 years post diagnosis (260). Therefore, although data from the EF-14 trial suggested that addition of TTFields may increase 5-year OS from 5% to 13%, the studies by Bernard-Arnoux et al. and Connock *et al*. did not fully account for the impact of long-term survivors beyond the trial period. This resulted in reported incremental lifetime survival benefits (the LYG) close to the median OS benefit observed within the trial period. By contrast, Guzauskas *et al*. integrated EF-14 data with external glioblastoma epidemiology data and US life expectancy data to estimate long-term conditional survival (similar integration of oncology trial and epidemiological data to model long-term survival has previously been considered by NICE in its decision to licence ipilimumab for metastatic melanoma (261, 262)). Consequently, the Guzauskas model estimates 1.25 LYG from adding TTFields to TMZ and estimates a corresponding ICER of $150,452.

As such, Japan, Israel and Sweden have included TTFields within their national reimbursement systems following cost-effectiveness evaluations, whilst Germany has approved TTFields for national reimbursement based on a clinical comparative effectiveness review without respect to costs. As noted above, the method of estimating future survival beyond the time observed in the trial is a critical assumption within any model. Healthcare payers that prefer the extrapolated constant hazard rate models of Bernard-Arnoux and Connock might not be willing to adopt the therapy. Adoption by healthcare systems that include considerations of cost-effectiveness as a major driver of decision-making, such as the NHS in the United Kingdom or the Australian and Canadian systems (263, 264), is likely to depend on how those systems choose to model long-term survival.

Although the number of patients receiving TTFields has increased since this approach was first approved for use in glioblastoma patients (2909 patients worldwide in 2019 compared with 605 patients in 2015) (265, 266), it is thought that many more patients with approved indications could benefit from TTFields treatment (on average, 30% of eligible glioblastoma patients currently receive TTFields in countries where the therapy is available) (259, 266). Substantial geographic variation in TTFields availability exists in the clinical usage of Optune, with the majority of patients who receive TTFields residing in the United States (roughly twice as many patients receive TTFields in the United States compared with the rest of the world) (266). As highlighted above, high treatment costs and differences in long-term survival modelling represent major drivers of geographical variation in the usage of TTFields worldwide. Notably, some reluctance to adopt TTFields within the neuro-oncology community also exists; this might be fuelled by a range of factors. Firstly, the high cost of TTFields therapy (discussed above) may represent a barrier to adoption at an individual or national level.

Secondly, valid concerns have been raised that patients in the control group of the EF-14 trial did not receive any placebo treatment (63), such as via a sham TTFields device. However, requiring patients to wear a sham device (ideally > 18 h per day) with no potential for benefit would likely present its own ethical challenges (267), and objective endpoints such as OS (which demonstrated survival benefit with TTFields in the EF-14 trial) are unlikely to be influenced substantially by the lack of placebo or blinding. Thirdly, a perceived burden of patients having to carry and wear the device with high compliance may contribute to reluctance to adopt or prescribe TTFields; nevertheless, objective data suggest that quality of life in these patients is not reduced (65, 268). Critically, much reluctance to adopt TTFields may stem from the fact that the mechanisms of action for TTFields are currently less well-defined relative to more established therapeutic modalities (269). It can be expected that, as technologies continue to evolve and as competing products enter the market, TTFields might become increasingly affordable. Additionally, any enhancement of the therapeutic efficacy of TTFields might also improve the ICER and facilitate TTFields uptake by healthcare systems that currently do not deem the technology to be cost-effective, including the NHS (NICE) (270). To improve the efficacy of TTFields, an improved understanding of the diverse mechanistic effects of this therapy and how these effects can be exploited to increase the therapeutic index of TTFields-based regimens is required.

1.3.1 Existing and novel mechanisms of TTFields

Electric fields have been shown to exert biological effects at various frequency ranges. Low-frequency electric fields (<1kHz) influence cell membrane polarisation and may alter the behaviour of excitable tissue, such as action potential firing in neuronal cells (271). On the other hand, high-frequency fields (>500kHz) cause charged and/or polar molecules inside cells to vibrate. As vibrating molecules come into contact with other vibrating molecules this creates friction and causes kinetic energy to transfer between molecules, which can be radiated out as thermal energy, leading to tissue heating (272). Intermediate-frequency alternating electric fields (100kHz-500kHz), however, do not generate enough thermal energy to cause significant tissue heating and alternate too quickly to trigger action potential firing, and thus, alternating electric fields of intermediate frequency were originally not thought to have any considerable biological effects (273). In the past two decades, however, intermediate-frequency alternating electric fields have been shown to exert effects on many more biological processes than initially thought (figure 1.12) and will be discussed in the following section. Figure 1.11. describes the different properties that characterise electric fields that are required in order to understand the MOAs of TTFields.

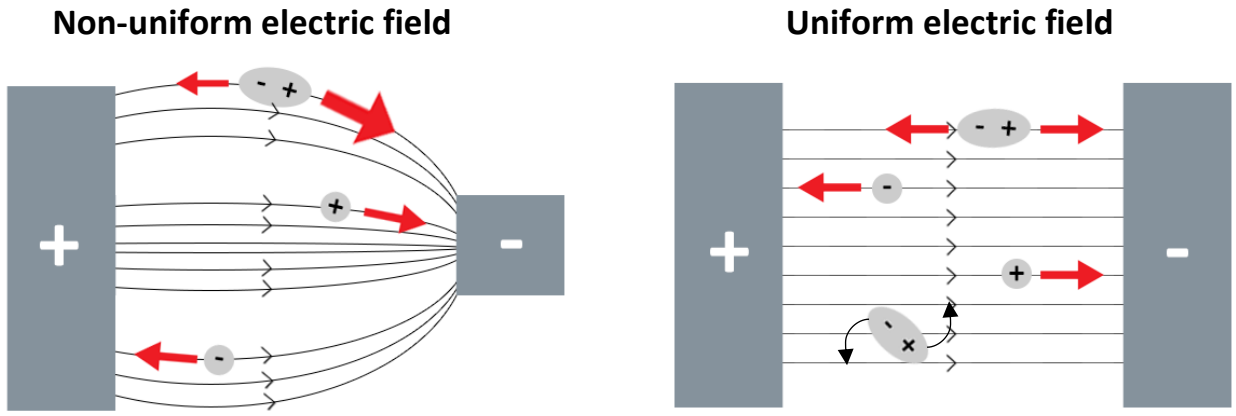

Figure 1.11. Properties of electric fields.
An electric field describes the area around an electric charge in which an electric force is exerted on other surrounding charged particles. Electric fields are represented by arrows, with the arrow direction reflecting the direction in which positive charges travel. The distance between electric field lines represents the field strength. Electric fields can be either uniform or non-uniform. Uniform fields refer to electric fields that generate the same field strength at any point in space (represented by equally distant field lines), whereas the magnitude and/or the direction (converging or diverging) of the field can vary at any point in space with non-uniform fields (represented with narrower field lines where the field intensity is highest and wider spaced lines where the field intensity is lowest). When the field is uniform, the forces exerted on dipole molecules are equal and opposite, therefore dipolar molecules do not travel along the field but simply align with the field instead (right). On the other hand, when the field is non-uniform, dipolar molecules travel toward the point of highest field intensity, resulting in a process known as dielectrophoresis (left). Single charge particles travel to the oppositely charged source when the field is both uniform and non-uniform. Electric fields can also be constant (usually when only one source charge is present), meaning that the field travels in a single direction only toward the source of opposite charge. Alternating electric fields refer to fields that are generated from different sources in time resulting in fields that travel in different directions at different points in time. Therefore, the orientation of dipolar molecules and the direction in which single charged particles (both when the field is uniform and non-uniform) and dipolar molecules (when the field is non-uniform) travel will change as the source of the field alternates.

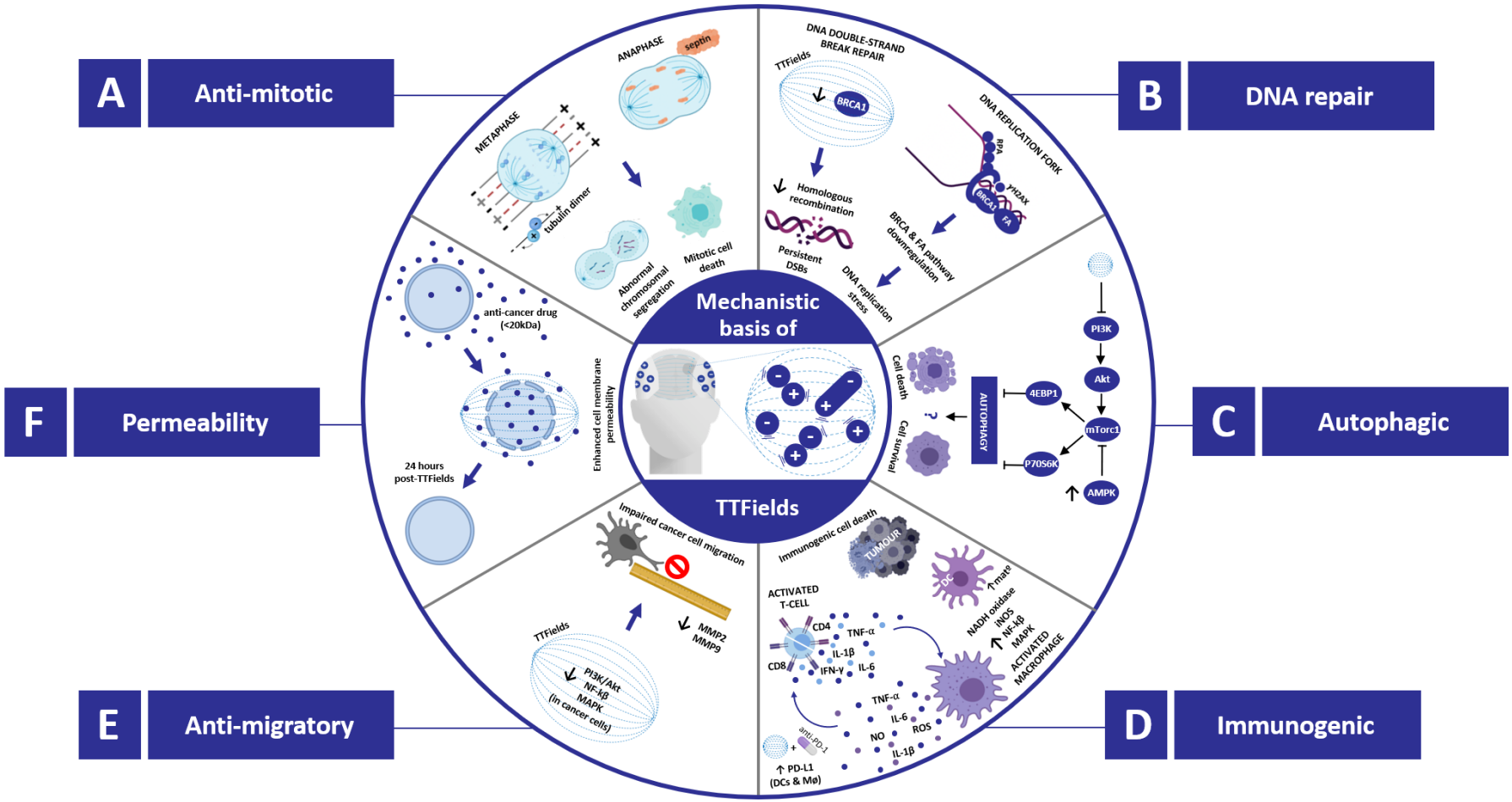

Figure 1.12. Summary of the mechanisms of action (MOAs) of TTFields.

A. *Anti-mitotic effects*. During metaphase, the electric fields are uniform, causing dipolar molecules, such as tubulin, to align with the field. TTFields therefore interferes with tubulin polymerisation and depolymerisation during metaphase. At anaphase, the electric fields are non-uniform, with the fields converging to the cleavage furrow, where the field intensity is highest. As a result, TTFields prevent localisation of Septin proteins to the mitotic spindle and prevent assembly of the Septin complex into a ring structure at the cleavage furrow. These effects result in abnormal chromosome segregation and/or cell death. **B.** *DNA repair*. TTFields have been shown to downregulate genes BRCA and FA proteins. This has been associated with increased replication stress and increased DSB break formation. Additionally, HRR has been shown to be impaired with TTFields. **C.** *Autophagy*. TTFields have been suggested to prevent the inhibitory effects of the mTroc1/PI3K/Akt signalling pathway on autophagy, resulting in increased activation of autophagy with TTFields. The mechanisms which determine whether autophagy is activated as a cell survival or cell death signal in response to TTFields are unknown. **D.** *Cell membrane permeability*. TTFields increase cell membrane permeability possibly by increasing the number and size of holes on the cell membrane. *Blood brain barrier permeability*. TTFields increase BBB permeability by causing the localisation of tight junction proteins, claudin-5 and ZO-1, from the cell membrane of endothelial cells to the cytoplasm. **E.** *Anti-tumour immunity*. TTFields stimulate macrophages to secrete ROS, NO and pro-inflammatory cytokines, such as IL-1β, TNF-α, and IL-6. Additionally, TTFields increase the accumulation of CD4+ and CD8+ T cells at the tumour site. **F.** *Cell migration and invasion.* TTFields has been shown to inhibit cell migration and invasion *in vitro*, which was suggested to take place via downregulation of the expression of pro-angiogenic and pro-metastatic factors, such as VEGF, HIF11 and MMP-2 and -9, and through inhibition of EMT. Figure taken from our published review (3).

The biological effects of low-intensity, intermediate-frequency (100–300 kHz), alternating electric fields, were originally studied in 2004 both *in vitro* in melanoma, glioma, lung, prostate, and breast cancer cell lines, and *in vivo*. Kirson *et al*. (2004) demonstrated that alternating electric fields successfully inhibited cancer cell growth, both *in vitro* and *in vivo*, by interfering with microtubule polymerisation during mitosis (252). These findings led to the first pilot study in glioblastoma patients in 2007 (275) and, eventually, to the development of TTFields as a therapeutic strategy for treating cancer (figure 1.13 and table 2). Indeed, TTFields have since been evaluated in two phase III clinical trials in patients with either primary or recurrent glioblastoma. In 2014, a phase III clinical trial concluded that although TTFields (200kHz) as a single agent did not offer additional benefits in terms of overall survival (OS) or progression-free survival (PFS) compared to 'physician's best choice' chemotherapy in patients with recurrent glioblastoma, TTFields efficacy was at least comparable with the added benefit of having fewer toxicities (65). In patients with newly diagnosed glioblastoma, a phase III clinical trial showed that the addition of TTFields to maintenance TMZ chemotherapy offered significant improvements in PFS (7.1 months vs 4.0 months in TMZ alone group) and OS (20.5 months vs 15.6 months in TMZ alone group) compared to TMZ monotherapy, again with no additional systemic adverse effects (63). On the basis of these positive clinical trial results, TTFields received approval from the FDA for the treatment of both recurrent and primary glioblastoma in 2011 and 2015, respectively. In addition, preliminary data suggest that glioblastoma patients should benefit from TTFields treatment irrespective of MGMT status (276). However, despite its apparent success in clinical trials, scepticism surrounding TTFields technology, stemming from the unblinded nature/lack of sham-control group in clinical trials to date, high costs and from a lack of understanding of the underlying mechanisms of action (MOAs) of the technology against tumour cells, has hindered its acceptance amongst clinicians and patients (269, 277).

Additionally, despite improvements in OS and PFS for newly diagnosed glioblastoma following the addition of TTFields therapy to standard care TMZ, over half of glioblastoma patients still do not survive beyond 2 years, indicating a requirement for further advances in the management of glioblastoma, even for patients receiving TTFields treatment (267). Whilst the anti-mitotic effects of TTFields remain the main MOA mediating its anti-cancer effects, which formed the basis of much of the preclinical studies that ultimately led to its approval as a novel strategy for the treatment of glioblastoma, since its establishment as a fourth modality for glioblastoma treatment, TTFields have been shown to affect a number of other cellular processes: (1) cell membrane and blood-brain barrier (BBB) permeability, (2) cell migration and invasion, (3) anti-tumour immunity, (4) autophagy, and (5) replication stress and DNA damage repair. In addition to alleviating some of the concerns surrounding

the TTFields technology, new insights into the MOAs of TTFields have highlighted potential TTFields-induced vulnerabilities that could be exploited for the basis of future combinational approaches in the management of glioblastoma.

Given the TTFields effects on DNA damage induction and repair, combining TTFields with inhibitors directed at the DNA damage response (DDR) is one such strategy that is being explored in efforts aiming to enhance TTFields efficacy. This is a particularly attractive strategy in the treatment of glioblastoma due to the role of DNA damage repair in mediating IR- and chemo- resistance, especially amongst the GSC population (239, 278). TTFields may elicit conditional vulnerabilities in cancer cells that make them more susceptible to additional treatment with DDR inhibitors (DDRi), especially in combination with DNA-damaging agents. In addition, the lack of systemic toxicities seen in the clinic following the addition of TTFields to standard care chemotherapy (64) make TTFields an ideal candidate for strategies exploring combinational approaches in the management of glioblastoma.

In the following sections, the various mechanisms of action through which TTFields have been demonstrated to mediate their anti-cancer effects will be examined. Additionally, how the various DNA damage checkpoint and repair proteins previously introduced can be exploited for use in a combinational therapeutic approach to enhance TTFields efficacy will be highlighted.

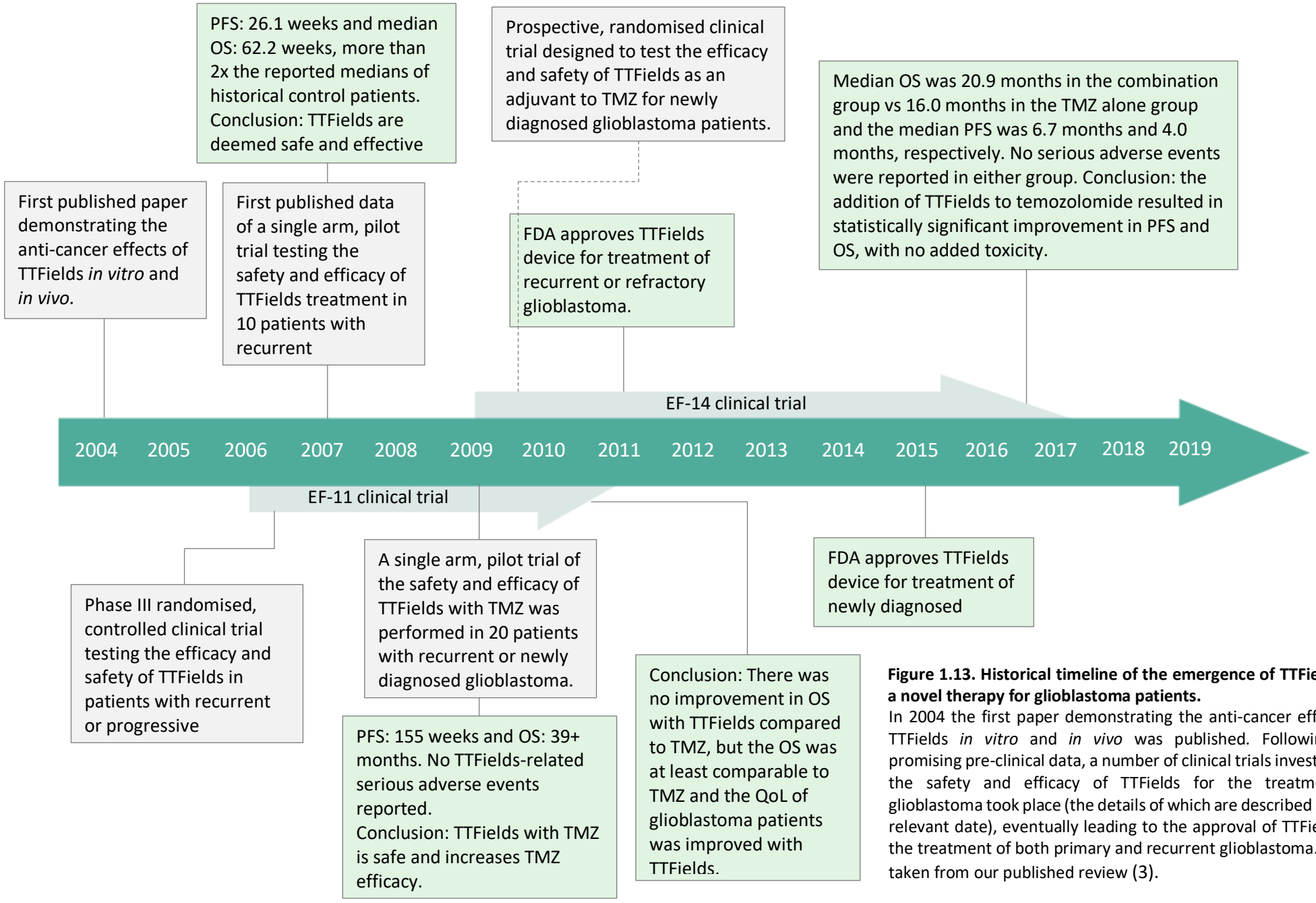

Figure 1.13. Historical timeline of the emergence of TTFields as a novel therapy for glioblastoma patients.
In 2004 the first paper demonstrating the anti-cancer effects of TTFields *in vitro* and *in vivo* was published. Following the promising pre-clinical data, a number of clinical trials investigating the safety and efficacy of TTFields for the treatment of glioblastoma took place (the details of which are described at each relevant date), eventually leading to the approval of TTFields for the treatment of both primary and recurrent glioblastoma. Figure taken from our published review (3).

Table 2 Key TTFields clinical trials - completed and ongoing

Intracranial tumours				
Indication & Trial	**Status & Design**	**Number of participants**	**Treatments**	**Outcomes**
EF-11 Trial (NCT00379470): Effect of NovoTTF-100A in Recurrent Glioblastoma Multiforme (glioblastoma).	COMPLETE, Phase III Randomised	237 patients	TTFields alone (120) TMZ alone (117)	OS: 6.6m (TTFields) vs 6.0m (TMZ) PFS: 2.2m (TTFields) vs 2.1m (TMZ) BOS at 1-year: 20% in both groups Toxicity: 6% (TTFields) vs 16% (TMZ)
EF-14 Trial (NCT00916409): Effect of NovoTTF-100A Together with Temozolomide in Newly Diagnosed Glioblastoma Multiforme (glioblastoma).	COMPLETE, Phase III Randomised	695 patients	TTFields + TMZ (466) TMZ alone (229)	PFS: 6.7m (TTFields+TMZ) vs 4.0m (p<0.2006-09001) OS: 20.9m (TTFields+TMZ) vs 16m (p<0.001). Toxicity: 48% (TTFields+TMZ) vs 44%
METIS Trial (NCT02831959): Effect of TTFields (150 kHz) in Non-small Cell Lung Cancer (NSCLC) Patients With 1-10 Brain Metastases Following Radiosurgery.	Ongoing (Recruiting) Phase III Randomised	260 patients – planned	TTFields after SRS (130 planned) SRS only (130 planned)	Primary endpoint: Time to 1st intracranial progression Secondary endpoint: OS. Toxicity, QoL, Radiological response (RANO-BM & RECIST V1.1), Neurocognitive failure.
Extracranial tumours				
Indication & Trial	**Status & Design**	**Number of participants**	**Treatments**	**Outcomes**
STELLAR (NCT02397928): Safety and Efficacy of TTFields (150 kHz) Concomitant with Pemetrexed and Cisplatin or Carboplatin in Malignant Pleural Mesothelioma.	COMPLETE Phase II Single arm	80 patients	TTFields + chemo (pemetrexed with cisplatin or carboplatin)	OS: 18.2m PFS: 7.6m Toxicity: 36% AEs(G3-4) + 3 (4%) chemo-related deaths – TTFields-related AEs = 5% (all grade 3 skin). Radiological response (mRECIST): 40% partial response, 57% stable disease at first F/U scan (6 weeks).

NovoTTF-100L in Combination with Pemetrexed (Alimta®) for Advanced Non-small Cell Lung Cancer. (NCT00749346)	COMPLETE Phase I/II Single arm	42 patients	TTFields + chemo (pemetrexed)	Time to local progression: 28w) PFS: 22 weeks. OS: 13.8m (57% survival at 1 year) Radiological response: 15% partial response, 49% stable disease. Toxicity: no TTFields-related SAEs.
LUNAR (NCT02973789): Effect of Tumor Treating Fields (TTFields) (150 kHz) Concurrent with Standard of Care Therapies for Treatment of Stage 4 Non-small Cell Lung Cancer (NSCLC) Following Platinum Failure.	Ongoing (Active) Phase III Randomised	534 patients – planned	TTFields + ICI or DOCE ICI or DOCE	OS (TTFields+ICI/DOCE vs ICI/DOCE alone) OS (TTFields+ICI vs ICI) and OS (TTFields+DOCE vs DOCE). PFS, Toxicity, Radiological response, QoL, Exploratory non-inferiority analysis of TTFields+DOCE vs ICI
PANOVA (NCT01971281): Safety Feasibility and Effect of TTFields (150 kHz) Concomitant with Gemcitabine or Concomitant With Gemcitabine Plus Nab-paclitaxel for Front-line Therapy of Advanced Pancreatic Adenocarcinoma.	COMPLETE Phase II Non-randomised	40 patients	TTFields + GEM TTFields + GEM & nab-P	Toxicity (SAEs): TTFields+GEM = 85% TTFields+GEM+nab-P = 85% G3 TTFields-related skin toxicities = 18% OS: 14.9m (TTFields+GEM) & median OS not reached (>15m) (TTFields+GEM+nab-P). PFS: 8.3m (TTFields+GEM) & 12.7m (TTFields+GEM+nab-P)
PANOVA-3 (NCT03377491): Effect of Tumor Treating Fields (TTFields, 150 kHz) as Front-Line Treatment of Locally-advanced Pancreatic Adenocarcinoma Concomitant With Gemcitabine and Nab-paclitaxel.	Ongoing (Recruiting) Phase III Randomised	556 patients – planned	TTFields + GEM & nab-P GEM & nab-P	OS, PFS, Toxicity (Aes), Radiological response, Resectability rate and QoL.

INNOVATE (EF-22) (NCT02244502): Safety, Feasibility and Effect of TTFields (200 kHz) Concomitant With Weekly Paclitaxel in Recurrent Ovarian Carcinoma	COMPLETE Phase II Single arm	31 patients	TTFields + PAC	Toxicity: G3-4 AEs 55% patients G3 TTFields-related skin toxicities = 6% OS: median not reached (>21m). PFS: 8.9m. Response rate: 25% partial response, 46% stable disease.
INNOVATE-3 (NCT03940196): Effect of Tumor Treating Fields (TTFields, 200 kHz) Concomitant With Weekly Paclitaxel for the Treatment of Recurrent Ovarian Cancer.	Ongoing (Active) Phase III Randomised	540 patients – planned	TTFields + PAC PAC	OS,PFS, Toxicity (AEs), Radiological response rate and QoL (EORTC QLQC30).
HEPANOVA (NCT03606590): Effect of Tumor Treating Fields (TTFields, 150kHz) Concomitant With Sorafenib For Advanced Hepatocellular Carcinoma (HCC).	COMPLETE Phase II Single arm	27 patients	TTFields + sorafenib	Overall response rate (ORR): TTFields/sorafenib (9.5%) vs. historical controls (4.5%). OS rate at 1 year TTFields + Sorafenib: 30% PFS rate at 12 months TTFields + Sorafenib: 23% 70% of patients experienced TTFields-related skin AEs (none serious).
Gastric cancer (NCT04281576): Effect of Tumor Treating Fields (TTFields, 150 kHz) Concomitant With Chemotherapy as First Line Treatment of Unresectable Gastroesophageal Junction or Gastric Adenocarcinoma.	COMPLETE Phase II Single arm	28 patients – planned	TTFields + XELOX (+ Trastuzumab if HER-2 positive)	Overall response rate, OS, PFS, disease control rate, time to progression, duration of response, 12-month OS rate and toxicity (AEs)

1.3.1.1 Anti-mitotic effects of TTFields.

The main mechanism of action through which TTFields application is thought to mediate its therapeutic effects are anti-mitotic. Alternating electric fields at frequencies between 100-300 kilohertz (kHz) can generate electric fields within cells and this has been hypothesised to disrupt interactions within dipolar molecules (those containing equal and oppositely charged poles) (252). During chromosome segregation, chromosomes align at the metaphase plate and sister chromatids are separated and pulled to opposite poles of the cell by the mitotic spindle. The mitotic spindle is formed of a bipolar array of microtubules, which are made up of tubulin polymers (279). Electric fields are uniform during metaphase, therefore when TTFields are applied, tubulin dimers align with the electric field, preventing its accumulation at the growing end of the microtubule and interfering with microtubule polymerisation-depolymerisation during mitosis. This in turn results in abnormal spindle formation and failure of the spindle assembly checkpoint (SAC) (280-282), a mitotic checkpoint that ensures that all chromosomes are properly attached to the mitotic spindle before proceeding through to anaphase and ensures correct chromosome segregation (283). TTFields have been shown to disrupt normal spindle assembly, leading to aberrant metaphase exit, abnormal chromosome segregation, multinucleation and cell death (280, 284). Because these effects require cells to be actively replicating, TTFields has been suggested to selectivity target cancer cells (284-286).

Additionally, whist the electric field is uniform in non-replicating cells, the electric field is non-uniform in dividing cells because of the 'hourglass' structure dividing cells assume after anaphase. Non-uniform electric fields generate forces that cause dielectrophoresis, whilst uniform fields lead to dipole alignment. During anaphase, the electric fields converge to the cleavage furrow, where the field intensity is highest, causing dipolar molecules to accumulate at the furrow (275). During cytokinesis, the mitotic Septin complex (comprised of Septin 2, 6 and 7) is normally recruited to the spindle midline and cleavage furrow (a hollowing of the cell's surface which initiates the cleavage process) at anaphase and assembles into a ring structure, where it stabilises microtubule structure and sets the partition for cleavage furrow contractility that limits contraction to the equatorial plane and restricts determinants to separate cortical domains (287, 288). The Septin complex is also involved in cross-linking actin, non-muscle myosin II and RhoA, easing actin-based myosin contraction which directs cleavage furrow ingression and provides the contractile forces required to physically separate the forming daughter cells from each other (288-290). TTFields has been shown to interfere with the assembly of the mitotic Septin complex at anaphase due to TTFields-induced dielectrophoresis. This

again caused abnormal chromosomal segregation, extended duration in mitosis and induced morphological changes in the membrane of cells that are characteristic of post-mitotic apoptotic cell death, such as cell membrane rupture and membrane blebbing (284). However, due to the faster microtubule polymerisation dynamics, the effects of TTFields on microtubule assembly are expected to mostly account for the anti-mitotic effects of TTFields (291). Only about 25% of cells rupture at the cleavage site and Li *et al*. suggested that the duration of telophase may influence the ability of TTFields to induce cell death his way because they found that it took up to 40 minutes for molecules to accumulate at the cleavage furrow during telophase.

Others have however claimed that the forces exerted by TTFields would not be sufficient to induce such cytoskeletal disruptions, challenging the theory that TTFields interferes with the mitotic spindles (292-294). Li *et al*. (293) proposed that, alternatively, TTFields affect the membrane potential (Vm) of cancer cells, specifically. The Vm is cells is important to cell homeostasis, it maintains the intracellular ionic concentration and regulates processes, such as cell metabolism and proliferation (295, 296). Changes in Vm may as a result lead to cell death (297). They postulated that this effects was specific to cancer cells because tumour cells have a different resting Vm relative to healthy cells (−70 mV to −90 mV), with the Vm of tumour cells being more depolarised (−26.7 mV) (293, 298). Additionally, the Vm of cells changes throughout proliferation therefore the effects of TTFields may still preferentially act on dividing cells. Changes in Vm correlate with changes in expression and/or activation of ion channels. TTFields has been shown to activate the CaV1.2 channels of glioblastoma cells (299). Activation of calcium channels results in a rapid diffusion of calcium ions into the cytoplasm because the extracellular concentration of Ca2+ is much higher than the concentration within the cytoplasm (300). Ca2+ influx into the cytoplasm has been shown to decrease microtubule polymerisation (301). TTFields-induced changes in Vm may then not only induce changes in ion channel activity but could also interfere with microtubule polymerisation as has previously been shown.

Alternatively, Berkelmann *et al*. (302) suggested that TTFields-incudes cell death was a result of localised tissue heating at the cleavage furrow. Whilst the frequencies applied during TTFields treatment are generally considered not to be within a range known to induce significant tissue heating, increases in temperatures can still occur due to the Joule effect (which describes the phenomenon where electric energy is converted into thermal energy when a current passes through an object or a tissue) (303, 304). This is particularly expected with sustained exposure to an electric field as is recommended for the optimal anticancer effects of TTFields (>18h). Berkelmann *et al*. (302) predicted that the specific absorption rate (SAR), a measure of power absorption that describes the amount of energy that is converted into heat per unit time, was increased in dividing cells at the

cleavage furrow during cytokinesis specifically with TTFields treatment (100kHz) and proposed that this was responsible for the anti-proliferative effects of TTFields. The increased SAR during cytokinesis may result in local heating of the cells and interfere with cell proliferation and induce cell death (305). The SAR measured within cells at different stages during cell division was normalised to the SAR in the surrounding medium. At this frequency, the effects were not likely to be due to heating of the external medium because TTFields did not enhance the temperature of the medium the cells were cultured in. As has been suggested by previous studies, they concurred that the maximal effects of TTFields on proliferation were exerted on cells that were dividing parallel to the field direction and claimed that this was because the SAR at the cleavage furrow reduces as the angle between the axis of cell division and the field increases rather than the effects on Septin localisation. However, how exactly SAR measurements are reflected as a temperature change is not obvious and depends on different factors: thermal conduction, blood perfusion, and other thermoregulation processes are all factors that would affect the SAR (306), which were not considered in their model and therefore their measurement for SAR is not likely to translate with what would be seen in patients. Berkelmann *et al*.'s model only accounted for membrane capacitance based on membrane thickness and permittivity and measured the SAR with TTFields delivered at a frequency of 100kHz. Additionally, they showed that SAR measurements were frequency-dependent but did not assess the effects on SAR at the only approved frequency for glioblastoma (200kHz). Temperature calculations are likely to be more informative than SAR measurements because there is a more direct relationship between temperature changes and biological changes. Hyperthermia has been used as a treatment for cancer by exposing cancer cells to temperatures within the range of 39°C to 43°C to induce a heat shock response, which in turn leads to cancer cell death, induces DNA damage, inhibits DNA repair and cell cycle progression (307-310). Gentilal *et al*. (311) established a model based on different properties that contribute to tissue temperature (such as metabolism, conduction, blood perfusion etc.) to predict the effect of TTFields on tissue heating at the tumour site. They also took into account the fact that the Optune system is programmed to shutdown automatically when the temperature sensors within the transducer arrays detect temperatures of 41 ℃ at the site of array attachment, and the Optune system consequentially shuts down roughly every 2.5 minutes for 2 to 4 seconds at a time, which is the time required for the transducer arrays to cool. Based on this model, they showed that the expected temperature at the tumour site does not surpass 37.1 ℃ and therefore concluded that the effects of TTFields are not likely to be due to induced hyperthermia.

1.3.1.2 Effects of TTFields on the DNA damage response

A couple of studies have reported that TTFields sensitise glioma cell lines to radiotherapy (RT) (312, 313). TTFields have been suggested to radiosensitise cancer cells by delaying the repair of radiation-induced DNA damage, promoting mitotic catastrophe and cell death. Indeed, although TTFields treatment alone has been shown to induce DNA damage, when combined with RT treatment, DNA damage induction was enhanced, as measured by a significant increase in γH2AX foci (an established marker of DNA damage) and 53BP1 foci (an established double strand break marker) after combination treatment compared to either treatment alone, and this was accompanied by a synergistic effect on cancer cell killing in the combination group (312); similar effects were observed in the studies presented in this thesis. Importantly, TTFields has been suggested to induce DSBs specifically in cancer cells. Jo *et* al. measured an increase in H2AX stain and an increase in tail length by alkaline comet assay with TTFields treatment in cancer cells but not in normal cells (285). In addition, because cells receiving combination treatment sustained more γH2AX and 53BP1 foci 24-hours following treatment compared to cells receiving either treatment alone, TTFields was suggested to interfere with DNA damage repair efficiency (312-314). Together, these results suggest that the increased sensitivity to RT seen with TTFields application could be mediated through both an increase in DNA damage and/or a persistence of this DNA damage over time in TTFields-treated cells due to impaired DNA repair kinetics. In addition, TTFields treatment both prior to and after RT treatment was shown to radiosensitise various cancer cell lines (312-314), therefore, these findings could have implications for the scheduling of TTFields application in future pre-clinical and clinical studies, with TTFields application prior to or immediately after radiotherapy likely to enhance therapeutic efficacy the most.

Differential gene expression analysis revealed that the expression of BRCA1 DNA-damage response genes (BRCA1, ATRIP, MLH1, MRE11A) and FA repair pathway genes (FANCM and FANCD2) (i.e. genes involved in the repair of RT-induced DNA damage) were significantly downregulated in TTFields-treated non-small cell lung carcinoma (NSCLC) cell lines and in malignant pleural mesothelioma cell lines compared to baseline expression levels (314, 315). Interestingly, this downregulation was more pronounced in TTFields-sensitive cell lines compared to cell lines that are more resistant to TTFields (42), further supporting the notion that TTFields treatment could interfere with DNA damage repair efficiency (314). BRCA1 plays a central role in homologous recombination repair (HRR). During HRR, BRCA1, along with BRCA2, recruits RAD51 filaments at sites of DNA damage (160, 316, 317). RAD51 mediates sequence homology search, strand invasion into the sister chromatid and prevents replication fork degradation (318). RAD51 foci can be used to monitor HRR efficiency, with cells that retain RAD51 foci for 24 hours following RT being associated with persistent double strand breaks

(DSBs) and eventual cell death. Giladi *et al*. (2017) showed an increase in RAD51 foci formation 24 hour following combination treatment (RT + TTFields) compared to either treatment alone, suggesting that the reduced repair efficiency previously reported with TTFields could be the result of impaired HRR following TTFields application, especially considering non-homologous end joining repair (an alternative DSB repair pathway) kinetics were not affected by TTFields treatment (312). In addition to their role in HRR, BRCA genes cooperate with FA pathway proteins to maintain replication fork stabilisation (319). Karanam *et al.* (2019) showed that replication stress was increased with TTFields and that replication fork dynamics were impaired (320). Measuring the incorporation of labelled nucleotides onto newly synthesised DNA strands during DNA replication serves as a robust readout for replication stress and replication fork dynamics (321). Karanam *et al.* (2019) showed that DNA fibre length was shorter in H157 and H1299 cells treated with TTFields compared to untreated cells, and that the difference in DNA fibre length between groups increased over time, indicating that TTFields interferes with replication fork progression and induces replication stress. In addition, they showed the presence of other replication stress markers following TTFields treatments (320); such as increased RPA foci (322) and increased R-loop formation (3-stranded nucleic acid that form when a replication fork collides with the transcription machinery, these are produced at a higher rate during replication stress) (323). Finally, they also showed reduced expression of the Mini-Chromosome Maintenance (MCM) complex genes, MCM6 and MCM10 (a DNA helicase that is crucial for replication initiation and replication fork assembly) (320). Together, these data suggest that downregulation of BRCA genes and FA pathway proteins with TTFields treatment results in an increase in replication stress induced DSBs and reduced double strand break repair efficiency due to impaired HRR kinetics.

1.3.1.3 Effects of TTFields on autophagy.

The role of autophagy in cancer is diverse. During the early phases of cancer initiation, upregulation of autophagy carries out tumour suppressive functions, whilst at later stages of cancer development autophagy can be activated to promote cancer cell survival and treatment resistance (324). Previous studies have demonstrated that TTFields-treated cells display features that are characteristic of autophagy, such as increased cell volume and granularity, and the formation of double-membraned autophagosomes (284, 325, 326). When cells undergo autophagy, microtubule-associated protein light chain 3 (LC3-I) is converted to LC3-II through lipidation by autophagy-related protein 7 (ATG7), permitting its recruitment to the autophagic vesicle membrane, where it activates ATG5 (involved in autophagic vesicle formation) (327). As such, LC3 is often used as a marker for monitoring autophagy (328). Shteingauz *et al.* (2018) recently showed an increase in the LC3-II protein in cancer cells in response to TTFields application (325). However, increased levels of LC3-II do not always correlate

with increased autophagy, they can also signify reduced autophagosome turnover due to defects in autophagosome transport and fusion of the autophagosome with the lysosome (329), therefore autophagic flux, which describes the entire process of autophagy (autophagosome formation, maturation, fusion with lysosomes, and lysosomal degradation of cytoplasmic constituents) must be measured to determine the degree of autophagy. Measuring the difference in LC3-II levels in the presence and absence of a lysosome inhibitor, such as Chloroquine (CQ, inhibits autophagosome-lysosome fusion), allows the determination of how much LC3-II is degraded in a lysosome-dependent manner because it stops autophagic flux before lysosomal degradation can take place and therefore indicates the extent of degradation that would have taken place during the treatment, reflecting the degree of autophagy (330). Combining CQ with TTFields was shown to significantly increase LC3-II levels in cells relative to control and relative to TTFields-treated cells in the absence of CQ, indicating that TTFields increases autophagic flux and activates autophagy (325).

TTFields has also been shown to induce abnormal chromosomal segregation (280) and aberrant mitotic events have been linked to increased activation of autophagy (331). TTFields-treated cells that underwent aberrant mitosis (identified as cells displaying abnormal numbers of chromosomes or abnormal cell morphology) were shown to be more likely to activate autophagy in comparison to cells that had not divided over the course of the experiment or cells that underwent normal cell division (325), suggesting that TTFields-induced aberrant mitotic events could be driving activation of autophagy.

The PI3K/protein kinase B (Akt)/mTOR signalling pathway is known to suppress activation of autophagy (332). Kim *et al.* (2019) found that the expression of Akt2 and downstream targets of mTORC1 (4E-binding protein 1 (4EBP1) and 70 kDa ribosomal protein S6 kinase (p70S6K)) were downregulated in glioma cells upon TTFields application, and that phosphorylation of mTOR at Ser2448 was reduced. Re-expressing Akt2 prevented the TTFields-mediated induction of autophagy, indicating that Akt2 pathway signalling regulates autophagy in TTFields-treated cells and that TTFields activates autophagy by suppressing the inhibitory action of the PI3K/Akt/mTOR pathway on autophagy (326). Additionally, mTORC1 function is inhibited under various types of stress in the cell. For example, AMPK (AMP-dependent kinase) is activated by low energy (ATP) levels. AMPK phosphorylates and inhibits mTORC1, thus suppressing the inhibitory effects of mTORC1 on autophagy (333). Shteingauz and Porat *et al*. (2018) demonstrated that TTFields reduced intracellular ATP levels in surviving daughter cells. They showed that siRNA-mediated knockdown of AMPK prevented TTFields-mediated upregulation of autophagy and concluded that activation of AMPK was required

for increased activation of autophagy in TTFields-treated cells (325). Together these data suggest that activation of autophagy in TTFields-treated glioblastoma cells is mediated via regulation of the mTOR/PI3K/Akt signalling pathway.

Whether activation of autophagy with TTFields serves as a cell survival or a cell death signal is still unclear. Some studies have shown that inhibition of autophagy enhances cell killing of cancer cells with TTFields, suggesting that upregulation of autophagy may act as a mechanism resistance to TTFields and thus highlighting the potential use of autophagy inhibition as strategies to enhance the therapeutic effects of TTFields (325). Others have reported that autophagy inhibition reduces the cell killing of cancer cells with TTFields (326). For example, Silginer *et al.* (2017) reported that TTFields-mediated cell death took place in a caspase-independent manner and that autophagy played an important role in TTFields-mediated cell death (334). However, TTFields-mediated cell death has been shown to occur through both caspase-dependent (characteristic of apoptotic cell death) and caspase-independent pathway (280, 284, 334), suggesting that the type of cell death activated upon TTFields application may vary between cell lines. Identifying the regulatory mechanism directing autophagy to act as a pro-survival or a pro-death signal with TTFields warrants further study and will facilitate the identification of a population of patients that may benefit from additional inhibition of autophagy.

1.3.1.4 TTFields to enhance immunogenic cell death.

Glioblastoma possesses an immunosuppressive tumour microenvironment (TME) associated with lack of cytotoxic T cell infiltration and upregulation of regulatory T cells (Tregs) which release of immunosuppressive cytokines (335). TTFields has been suggested to activate an immune response in glioblastoma and could be exploited to switch the TME of glioblastoma patients from an immunosuppressive TME to an immune active one.

Macrophages play a central role in governing the nature of the immune response. Macrophages can assume one of two phenotypes. M1 macrophages are proinflammatory macrophages and secrete proinflammatory cytokines, such as interleukin-1β (IL-1β), IL-12, tumour necrosis factor-α (TNF-α). M1 macrophages initiate the immune response. M2 macrophages are anti-inflammatory and release anti-inflammatory cytokines, such as IL-10 and tumour growth factor-β (TGF-β). M2 macrophages are involved in the resolution of inflammation. Macrophages are also themselves stimulated by cytokines (336, 337). Inflammatory cytokines stimulate macrophages to produce Nitric Oxide (NO). NO induces toxic reactions against invading pathogens and regulates the function of host immune cells. NO is converted from L-arginine by the inducible NO synthase (iNOS) during inflammation, and the

expression of iNOS is regulated by both pro-inflammatory and anti-inflammatory cytokines. The pro-inflammatory cytokines TNF-α, IL-1β and IL-6 participate in upregulation of iNOS by activating the transcription factor, nuclear factor kappa-light-chain-enhancer of activated B cells (NF-kB), and the mitogen-activated protein kinase (MAPK) proteins p38, extracellular-signal-regulated kinases (ERK) Erk1/2 and c-Jun N-terminal kinases (JNK). Additionally, when NO is present at low concentrations when macrophages are first activated by cytokines, NO can stimulate the NF-kB signalling pathway to upregulate iNOS expression in a positive feedback loop (338).

The mRNA expression levels of IL-1β and TNF-α were significantly increased in RAW 264.7 cells (a macrophage-like cell line) following TTFields treatment. TTFields-treated RAW 264.7 cells were also shown to upregulate messenger RNA (mRNA) and protein expression of iNOS and increased NO production (339). Park *et al*. (2019) showed that an increase in IL-1β, TNF-α, and IL-6 secreted into the medium of RAW 264.7 co-cultured with 4T1 cancer cells was detected in the TTFields-treated group. These data indicate that TTFields promotes activation of proinflammatory macrophages and the expression of proinflammatory cytokines. Additionally, 4T1 cells that were exposed to the culture media from TTFields-treated RAW 264.7 cells displayed a reduction in cell viability compared to 4T1 cells that were exposed to the culture media of RAW 264.7 untreated cells, suggesting that TTFields-mediated activation of macrophages promotes anti-tumour immunity (339). Gene expression analysis of glioblastoma patient tumour prior and after TTFields treatment revealed that the expression of immune-related genes switched from pro-tumoral to anti-tumoral with TTFields treatment (340).

Reactive Oxygen Species (ROS) are also produced by macrophages via the NAPDH oxidase. ROS is a secondary messenger that activates both NF-kB and MAPK signalling pathways (341). Interestingly, ROS secretion was also increased in RAW 264.7 cells following TTFields treatment. Under normal circumstances, the inhibitor of kappa B (IκB-α) protein is bound to and inhibits NF-κB, sequestering NF-κB to the cytoplasm. Both ROS and TNFα can activate IκB kinase (IKK). IKK phosphorylates IκB-α, which results in polyubiquitination and subsequent proteasomal degradation of IκB-α, releasing the transcriptional subunit of NF-κB, NF-kappa-B p65 subunit, which can subsequently translocate to the nucleus and regulate transcription of target genes, including transcription of pro-inflammatory cytokines (342). TTFields-treated RAW 264.7 cells showed increased phosphorylation of IκB-α and the NF-kappa-B p65 subunit (339). This could be due to increased activation of the cyclic-GMP-AMP synthase/stimulator of interferon genes (cGAS/STING) signalling pathway with TTFields treatment (343). cGAS recognises cytosolic DNA, such as extra-nuclear micronuclei formation from DSBs (344), which was shown to be increased by exposure to TTFields (345). cGAS produces cyclic guanosine

monophosphate-adenosine monophosphate (cGAMP) upon detection of cytosolic DNA and activates dimerisation of STING. TANK-binding kinase 1, an IKK-related serine/threonine kinase, associates with STING and mediates NF-κB signalling in the presence of cytosolic DNA though inhibitory phosphorylation of IκB-α (346). The sensing of cytosolic double-stranded DNA can also be detected by the DNA sensor absent in melanoma 2 (AIM2), which activates caspase-1 and promotes maturation of proinflammatory cytokines (IL-1β and IL-18) (347). TTFields was also shown to stimulate this process (343). Phosphorylation on both threonine and tyrosine residues within a TxY motif is required for full activation of MAPK proteins (348). Additionally, TTFields-treated RAW 264.7 cells displayed increased phosphorylation of the MAPK protein, p38 (339). Sorafenib-mediated inhibition of signal transducer and activator of transcription 3 (STAT3) enhanced cancer cell killing by TTFields in vitro and delayed tumour growth in vivo. Re-expressing STAT3 in glioblastoma cells prevented sorefanib-mediated sensitisation to TTFields, suggesting that this effect was mediated by STAT3 only and not through other targets of kinase activity (serine/threonine kinases, receptor tyrosine kinases and MAPK/ERK pathway), which are known to be inhibited by sorafenib (349). These data suggest that TTFields mediates its anti-tumour immunity effects via regulation of NF-κB/MAPK signalling pathways in RAW 264.7 macrophages.

Patients that benefited most from TTFields treatment had higher blood T cell counts (350). T helper cells, or CD4+ cells, stimulate B cells to secrete antibodies and macrophages against the invading organism and activate cytotoxic T cells (CD8+ cells). Using rabbit models of lung cancer, Kirson *et al*. (2009) showed that TTFields significantly increased the expression of CD45, CD4 and CD8 T-cells inside the tumour compared to sham controls, suggesting that TTFields can also stimulate anti-tumour immunity *in vivo* (351). TTFields may interfere with T cell functions that depend on cytoskeletal changes or on vesicular transport, such as secretion, degranulation, and surface molecule presentation. Importantly, TTFields was shown not alter T cell functions, such as IFN-γ secretion, cytotoxic degranulation, and PD1 upregulation. TTFields-treated chimeric antigen receptor (CAR)-T cells were just as cytotoxic as untreated CAR-T cells toward their CAR targets. Although, TTFields did reduce the viability of proliferating T cells, therefore a balance must be achieved between selecting a frequency and intensity of treatment that permits efficient cancer cell killing whilst minimising the anti-proliferative effects on T cells (340). Programmed cell death protein 1 (PD-1) functions by preventing CD28-mediated co-stimulation during T-cell activation. By disrupting TCR/CD28 signalling, PD-1 prevents cytokine production and therefore prevents activation of the immune response (352). Such negative regulatory signals are essential to prevent hyperactivation of the immune system which can result in autoimmune disorders (e.g. rheumatoid arthritis and multiple sclerosis), however, cancer

cells can exploit this mechanism to evade immune response mediated cell death (353). Finally, Voloshin *et al*. (2017) showed that combining TTFields with a PD-1 inhibitor reduced the tumour volume of lung tumour-bearing mice with TTFields compared to sham control and compared to mice treated with the inhibitor alone (354), suggesting that PD-1 inhibition may further promote the anti-tumour immune response elicited by TTFields treatment.

1.3.1.5 TTFields suppresses cancer cell migration

Glioblastoma is characterised by highly infiltrative growth, which limits the extent of surgical resection that is safely possible and therefore contributes to the aggressiveness of the disease and disease recurrence (355). Kirson *et al*. (2009) previously showed that TTFields treatment reduced metastasis of solid tumours to the lungs in mice models (351).

Metastasis is a multi-step process that requires migration and invasion of cancer cells from a primary tumour site to a secondary site where a new tumour is initiated (356). Wound healing and trans-well assays demonstrated that TTFields treatment significantly reduced cell migration and invasion of established glioma cell lines compared to untreated cells (334, 357). More importantly, these effects were reproduced in the glioblastoma stem cell (GSC) population, a population of cells thought to be of particular significance in terms of driving tumour recurrence and cancer progression (334). Epithelial-to-mesenchymal transition (EMT) is an essential step that drives the establishment of a highly migratory and invasive cell population and promotes metastasis (358, 359). EMT is accompanied by the loss of epithelial cell markers, such as the cell-cell adhesion protein E-cadherin, in favour of mesenchymal markers, such as vimentin. TTFields treatment was shown to increase expression of the epithelial marker E-cadherin whilst decreasing the expression of the mesenchymal marker vimentin, suggesting that TTFields could potentially inhibit EMT and prevent the establishment of a more migratory and invasive cell population (357). TTFields downregulated the expression of Snail and Twist, transcription factors associated with EMT (360).

Cell migration is especially important during invasion, the initial step of metastasis. Cancer cell migration is facilitated by focal adhesions, which are structures that connect the cell cytoskeleton to the extracellular matrix (EC) through integrins. Integrin molecules are transmembrane receptors that control cytoskeletal organisation (by mediating actin polymerisation and depolymerisation) and link the actin cytoskeleton to the extracellular matrix, a process regulated by Rho GTPases and ROCK (361) (362). Focal adhesion strength determines the ability to form attachments with the EC. Strong

adhesions are required to form connections with the EC at the leading edge so as to provide the forces required to pull the cell body forward, whilst weaker focal adhesions are required to enable to release the cell from the EC at the trailing edge. Too weak focal adhesions at the leading edge means the cell cannot be pulled forward, whilst increasing strength of focal adhesions at the trailing edge prevents release of the cell (363, 364). The size of the focal adhesion has been shown to be proportional to its strength (365). TTFields increased the number of focal adhesions formed and increased their size relative to untreated cells, such that cells formed stronger adhesions (366). Actin polymerisation and clustering of integrin molecules is required to provide the mechanical forces that pull the cell forward, whilst disassembly of integrins and actin depolymerisation is required to mediate detachment (367). As might be expected, TTFields affects microtubule and actin organisation during cell migration and was shown to activate the GEF-H1/RhoA/ROCK signalling pathway (366). The effects of TTFields are more pronounced on tumour cells that migrate in the direction that is perpendicular relative to the field. TTFields also affects the directionality of microtubule assembly (366).

In addition, Kim *et al*. (2016) demonstrated via a Matrigel-based tube formation assay that TTFields reduced tube formation of glioma cell lines, effects that were accompanied by a reduction in expression of the angiogenic factors, hypoxia-inducible factor 1 (HIF1) and vascular endothelial growth factor (VEGF). Therefore, in addition to preventing cell invasion and migration, TTFields appear to inhibit angiogenesis, another essential factor that drives cancer metastasis (368). Finally, matrix metalloproteinases 2 and 9, which are proteins that degrade components of the extracellular matrix and basement membrane and are therefore required for both angiogenesis and cell invasion (369, 370), were also downregulated by TTFields treatment, which was suggested to be due to inhibition of NF-κB, MAPK and PI3K/AKT signalling pathways (357, 360). However, given the role the tumour microenvironment plays in driving angiogenesis and cancer cell migration and invasion, *in vivo* investigations will help consolidate the effects of TTFields on cell migration and invasion.

1.3.1.6 TTFields to enhance BBB permeability, cell membrane permeability and intra-cellular drug delivery

The blood brain barrier (BBB) characterises the collection of micro vessels of the central nervous system, which closely control the exchange of substances between the blood and brain tissues. Whilst the BBB helps to maintain correct neuronal function and keeps the brain safe of toxins and pathogens, the BBB also restricts access into the brain (and therefore at the tumour site) to a lot of drugs, some of which have shown some hopeful preclinical data for the treatment of glioblastoma (371). The BBB

is formed by a tightly packed monolayer of endothelial cells connected by tight junctions, a cell-cell junction that is impermeable to most molecules either side of the epithelium. Two of the main constituents of tight junctions are claudins, which limit paracellular diffusion of molecules, and occludin proteins, which provide structural integrity to the tight junction (372).

Kessler *et al.* (2019) recently showed that TTFields application interfered with BBB integrity by causing tight junction proteins, Claudin 5 and Zonula occludens-1 (ZO-1), to localise from the membrane of endothelial cells to the cytoplasm, with most prominent effect seen at a frequency of 100 kHz and with prolonged exposure to TTFields (72 hours). After 48 hours following cessation of TTFields treatment, cell morphology started to return to normal and had fully recovered by 96 hours post-TTFields exposure indicating that the effects of TTFields on the BBB are reversible (373). Evans Blue (EB) dye extravasation is the most common method used to measure BBB permeability *in vivo*. EB does not normally pass through thee BBB, therefore detection of EB within brain tissue is indicative of changes in BBB permeability (374). Kessler *et al*. (2018) showed that TTFields significantly increased EB build-up in the brain of rats, indicating an increase in BBB permeability with TTFields, making the barrier leakier and more permissive to therapeutics. TTFields was also shown to reduce transendothelial electrical resistance (TEER), indicative of reduced membrane integrity and increased permeability (375). These effects have been suggested to be mediated through disruption of BBB integrity via delocalisation of tight junction proteins, Claudin 5 and ZO-1 (373). GEF-H1/Rho/Rho kinase activity, which has been shown to be elevated by TTFields treatment, disrupts the association between claudin-5 and ZO-1. TTFields-induced activation of ROCK activity could also lead to changes in microtubule organisation that resulted in delocalisation of claudin-5. Preventing activation of ROCK using the inhibitor fasudil prevented TTFields-mediated delocalisation of claudin-5 (375).

In addition to increasing BBB permeability, TTFields has also been shown to increase cell membrane permeability (376). Whilst integral membrane proteins mediate the transport of large polar molecules and ions across the membrane by passive or active transport, small ions and molecules can simply diffuse across the cell membrane through small holes that punctuate the surface of the cell membrane (377). Electroporation is a technique that applies short electric field pulses to induce temporary and reversible pores in the membrane of cells. Electroporation significantly modifies the transmembrane potential around the cell and once a certain threshold is reached, the membrane is destabilised in such way that aqueous pores form on the cell membrane (and activate ion channels) (378). As previously described, TTFields has been suggested to induce changes in the Vm of cancer cells (293) and has been shown to activate Cav2+ channels (299). Scanning Electron Microscopy showed that TTFields increased both the number and the size of holes in the membrane of glioma cells, with the

average hole size of TTFields-treated cells being 240.6 ± 91.7 nm^2 compared to 129.8 ± 31.9 nm^2 in untreated cells. Parameters such as electric field intensity, electric field frequency, and duration of exposure contribute to the extent of electroporation that can be achieved (379), and TTFields may therefore not be able to induce electroporation to same degree as standard electroporation techniques. For example, standard electroporation techniques usually employ short electric fields pulses at a frequency much higher than what would be expected with TTFields. Interestingly and importantly, these changes were specific to cancer cells as they did not see any changes in membrane structure of healthy human fibroblast cells with TTFields, possibly because cancer cells have varied ion channel expression and membrane potential relative to healthy cells and the resting membrane potential is important for the threshold for permeabilization (380). Additionally, they showed a significant increase in the uptake of membrane-associating drugs of up to a size of 20 kDa (kilodalton), and no larger than 50 kDa, into glioma cells with TTFields. These changes were reversible and returned to normal by 24 hours after stopping TTFields treatment (376).

These findings could explain the reported increase in sensitivity to chemotherapeutic drugs with TTFields and might even explain the EF-14 trial results demonstrating a significant improvement in survival when combining TTFields with TMZ compared to TMZ alone (63). If indeed TTFields renders cell membranes more permeant to chemotherapeutics and increases drug uptake across the BBB, TTFields should in theory improve therapeutic efficacy of current chemotherapeutic agents, such as TMZ, having important implications for the rational design of TTFields-chemotherapy combinations and drug scheduling. Additionally, the use of TTFields could potentially widen the options of drugs that can be used to treat glioblastoma, as it could not only potentially allow delivery of drugs into the brain that were previously unable to cross the BBB but could also potentially increase intracellular concentrations of these drug once inside the brain.

1.3.2 TTFields-based combinational approaches

Even with the addition of TTFields therapy to standard care TMZ, over half of glioblastoma patients still do not survive beyond 2 years (267), and therefore improved treatment options are urgently needed for the management of glioblastoma. Combination approaches directed at the DDR are being explored as strategies for the treatment of glioblastoma, however considering that distinct DNA damage response pathways share common functions and functional redundancy is observed within the DDR, targeting separate DDR processes in parallel is likely to offer optimal therapeutic responses and overcome treatment resistance. TTFields is associated with no additional systemic toxicities in combination with DNA-damaging agents and has been shown to induce vulnerabilities within DNA

damage repair processes making it the ideal candidate to form the basis of combinational strategies directed at the DDR. However, whilst TTFields is gaining attention in glioblastoma research, there have been to date no studies extensively exploring the therapeutic potential and scope of TTFields in combination with DDRi for the treatment of glioblastoma. As highlighted above, PARP1, FAP proteins, WEE1, ATM and ATR each play a notable role in the response to DNA damage induction, therefore providing a strong preclinical, and potentially clinical rational for the use of inhibitors towards these proteins in combination with TTFields.

1.4 Hypothesis and Project Aims

1.4.1 Hypothesis

Combining TTFields with therapeutic DDR inhibitors will enhance TTFields potency in glioma cells alone or in combination with current standard care chemo-/radio-therapy.

1.4.2 Aims

1. To determine the most effective combination of therapeutic DDRi with TTFields using a range of glioma cell models (including those representing residual tumour following surgical resection and tumour heterogeneity).

2. To assess the mechanistic basis of interaction of TTFields/DDRi-based combinations.

3. To develop and optimise a clinically relevant ex-vivo 3D scaffold-based TTFields culture system for the assessment of treatment effects in primary, patient-derived glioblastoma cancer stem cell cultures.

CHAPTER 2. MATERIALS AND METHODS

2.1 Materials

2.1.1 General laboratory equipment

Table 3. General laboratory equipment.

Item	Company
Centrifuge (5430)	Eppendorf
Centrifuge (Heraeus MegaFuge 16)	Thermo Fisher Scientific
Dri-Block® (DB-2D)	Techne
Electric Pipet Controller	FisherBrand™
Electrophoretic Transfer Cell	Bio-Rad
Film Processor (Mibolta SRX101A)	Konica
Fluorescent Microscope (Eclipse TE200)	Nikon
Haemocytometer (Improved Neubauer AC1000)	Hawksley
Incubator (Tissue Culture)	Sanyo
Incubator with Integrated Cooling System (CCL-170 – dedicated TTFields Tissue Culture)	ESCO
Inovitro™ Tumour Treating Fields Delivery System	Novocure
Mini Gel Tank (Invitrogen)	Thermo Fisher Scientific
Mini Gyro-rocker	Stuart®
Mini-Cell Electrophoresis System (XCell SureLock™)	Thermo Fisher Scientific
Mini-PROTEAN tetra cell	Bio-Rad
Multi-channel Pipettes – P10, P20, P1000	Gilson
pH Meter (Model 3510)	Jenway
Pipettes – P2, P10, P20, P200, P1000	Gilson
PowerPac™ Basic Power Supply	Bio-Rad
Repetman™ Electronic Pipette	Gilson
Scanner (Expression 1680 Pro)	Epson
Vortex	Fisons Scientific Equipment
Water Bath (JB Aqua 18 Plus)	Grant Instruments

2.1.2 Consumables

Table 4. Consumables

Item	Company
Cell Scraper – 25cm	Sartedt
Centrifuge Tubes – 15ml	Corning
Centrifuge Tubes – 50ml	FisherBrand™
Coverglass – 22 x 22mm	Menzel-Glazer
Cryovials (CryoPure White) – 1.8ml	Sarstedt
Disposable Serological Pipettes – 5ml, 10ml & 25ml	FisherBrand™
Eppendorfs – 0.2ml, 0.5ml, 1.5ml & 2ml	Sarstedt
Filter Tips – 0.1-10µl, 2-20µl, 2-200µl, 1001000µl	Biosphere®
Filter Tips – 0.1-10µl, 2-20µl, 2-200µl, 1001000µl	Starlab
Gel Loading Tips	Starlab
Glass Bottles	Fisher Scientific
Microlance Needles	Becton Dickinson
Optical Adhesive Film (MicroAmp™)	Thermo Fisher Scientific (4311971)
Pipette Tips – 2-200µl, 100-1000µl	Sarstedt
Reagent Reservoir – 50ml	Corning
Repetman™ Sterile Pipet Tips – 1.25ml, 5ml, 12.5ml	Gilson
Round Tissue Culture Dishes – 10cm	Cellstar
Sterile Syringes – 1ml, 5ml, 10ml (Plastipak™)	BD Biosciences
Tissue Culture Flasks (Nunclon™ Delta Surface EasYFlask™) – 25cm2, 75cm2	Fisher Scientific
Tissue Culture Treated Plates – 24 well	Corning
Tissue Culture Treated Plates – 6 well	Costar
X-Ray Film (Fuji Medical Super RX)	Fujifilm

2.1.3 Sterilisation

Solutions requiring sterilisation, such as PBS, were autoclaved. Autoclaving was performed at a pressure of 15 pounds per square inch (psi) and temperature of 120°C for 15 mins.

Stock solutions of chemotherapeutic agents or DDR inhibitors were filter sterilised using a 5ml syringe and a Millex GP filter unit (0.22µm pore size).

2.1.4 Purified water

Type 1 ultra-pure deionised water (ddH2O) was produced using a Triple Red System.

2.1.5 Reagents

Table 5. Reagents

Item	Company (Product code)
1,4-dithiothreitol (DTT)	Sigma (DTT-RO)
30% Acrylamide Mix	Geneflow (A2-0084)
4',6-diamidino-2-phenylindole (DAPI)	Merck (D9542-10MG)
Accutase™ StemPro™ Cell Dissociation Reagent	Invitrogen (A11105-01)
Advanced DMEM/F-12 (Dulbecco's Modified Eagle Medium/Ham's F-12)	Invitrogen (12634028)
Ammonium Persulfate (APS)	Thermo Fisher Scientific (17874)
Amphotericin B (Fungizone)	Gibco (15290)
Annexin V	BD Biosciences (# 556419)
B-27 Supplement (50x) Serum Free	Invitrogen (17504-044)
Benzonase Nuclease	Novagen (70664-3)
Bovine Serum Albumin (BSA)	Sigma (A2153)
Dimethyl Sulfoxide (DMSO)	Fisher Scientific (D/4120/PB08)
EGF Recombinant Human Protein	Invitrogen (PHG0313)
Ethanol	Fisher Scientific (AC615090010)
Ethylenediaminetetraacetic acid (EDTA)	Sigma (1233508)
Goat Calf Serum	Sigma (G6767)
FGF Recombinant Human Protein	Invitrogen (PHG0263)
HiMark™ Pre-stained Protein Standard (Ladder)	Thermo Fisher Scientific (LC5699)
Hydrochloric acid (HCL) 37%	Fisher Scientific (A144-500LB)

Industrial methylated spirit (IMS)	Fisher Scientific
L-Glutamine-200mM (100x)	Invitrogen (25030081)
LMagrose	R&D Systems (4250-050-02)
Matrigel® Growth Factor Reduced (GFR) Basment Membrane Matrix LDEV-Free (Corning®)	BD Biosciences (354230)
Methanol	Fisher Scientific (A452SK-4)
Methylene blue	Sigma-Aldrich (M9140)
Milk Powder	Marvel
N-2 Supplement (100x) Serum Free	Invitrogen (17502-048)
Nitrocellulose Membrane (Protran®	VWR (10600010)
NuPAGE™ 4-12% Bis-Tris Protein Gels –1.5 mm, 10 well	Thermo Fisher Scientific (NP0335BOX)
NuPAGE™ LDS Sample Buffer (4X)	Thermo Fisher Scientific (NP0007)
NuPAGE™ MOPS SDS Running Buffer (20X)	Thermo Fisher Scientific (NP0001)
NuPAGE™ Transfer Buffer (20X)	Thermo Fisher Scientific (NP0006)
NuPAGE™ Tris-Acetate SDS Running Buffer (20X)	Thermo Fisher Scientific (LA0041)
Oxoid PBS Tablet	Thermo Fisher Scientific (BR0014)
Paraformaldehyde (PFA) – 4% solution in PBS	Santa Cruz Biotechnology (SC-281692)
Penicillin-Streptomycin (10,000U/ml)	Invitrogen (15140122)
Phosphatase Inhibitor Tablets (PhosSTOP™)	Sigma (4906845001)
PierceECL Western Blotting Substrate	Thermo Fisher Scientific (32106)
Propidium iodide	Sigma (P4864)
Protease Inhibitor Cocktail (cOmplete™ ULTRA Tablets Mini EASYpack)	Sigma (5892970001)
Protein Assay Dye Reagent Concentrate	Bio-Rad (500-0006)
SeeBluePlus2 Prestained Standard (Ladder)	Thermo Fisher Scientific (LC5925)
Sodium chloride	Sigma (S7653)
Sodium Dodecyl Sulphate (SDS)	Sigma (L3771-500G)
Sodium Hydroxide (NaOH) Pellets	Sigma (S5881)
Sucrose	Sigma (S7903)

SYBR® Gold Nucleic Acid Gel Stain	Thermo Fisher Scientific (S11494)
Tris Base	Sigma (TRIS-RO)
Tris Hydrochloride	Sigma (10812846001)
Triton™ X-100	Sigma-Aldrich
TWEEN® 20	Sigma (P1379)
Visualiser™ Western Blot Detection Kit	Thermo Fisher Scientific (10553414)

2.1.6 DNA damaging agents and DDR inhibitors

Table 6. DNA damaging agents and DDR inhibitors

Item	Description	Solvent	Company
AZD0156	Selective inhibitor of ATM	DMSO	Selleckchem (S8375)
AZD1390	Selective inhibitor of ATM	DMSO	Selleckchem (S8680)
AZD1775	WEE1 inhibitor	DMSO	Selleckchem (S1525)
AZD6738	Selective ATR inhibitor	DMSO	Selleckchem (S7693)
Olaparib (Lynparza; AZD2281)	PARP inhibitor	DMSO	Adooq Bioscience (A10111)
Temozolomide	Alkylating agent	DMSO	Sigma (T2577)

2.1.7 Antibodies

Table 7. Antibodies

Antibody	Host	Dilution	Product code
PARP1	Mouse	1:1000 (WB)	Santa Cruz (sc-8007)
αPAR	Rabbit	1:1000 (WB)	Millipore (MABE1016)
FANCD2	Mouse	1:1000 (WB)	Santa Cruz (sc-20022)
CDC2	Rabbit	1:1000 (WB)	Cell signaling (# 77055S)
p-CDC2(Y15)	Rabbit	1:1000 (WB)	Cell signaling

			(# 9111S)
Chk1	Mouse	1:1000 (WB)	Cell signaling (# 2360S)
p-Chk1(Ser345)	Rabbit	1:500 (WB)	Cell signaling (#2341)
ATR	Goat	1:250 (WB)	R&D Systems (#AF4717)
ATR	Mouse	1:250 (WB)	Santa Cruz (sc-515173)
Chk2	Rabbit	1:1000 (WB)	Cell signaling (# 2662S)
p-Chk2(Thr68)	Rabbit	1:500 (WB)	Cell Signaling (# 2197S)
ATM	Mouse	1:1000 (WB)	Abcam (ab78)
p-ATM(Ser1981)	Rabbit	1:500 (WB)	Cell signaling # 13050S
KAP1	Rabbit	1:1000 (WB)	ThermoFisher # A300-274A
p-KAP1(S284)	Rabbit	1:1000 (WB)	ThermoFisher # A300-767A-M
BRCA1	Rabbit	1:200 (WB)	Santa Cruz (sc-642)
P53	Rabbit	1:1000 (WB)	Bethyl (A300-247A)
Caspase-3	Rabbit	1:1000 (WB)	Cell signaling # 9662S
LC3-B	Rabbit	1:1000 (WB)	Cell signaling # 3868S
β-actin	Mouse	1:5000 (WB)	Santa Cruz (sc-47778)
GAPDH	Mouse	1:5000 (WB)	Antibodies
Anti-rabbit	Swine	1:1000 (WB)	DAKO

			(P0399)
Anti-rabbit	Goat	1:1000 (WB)	Cell signaling (7074S)
Anti-goat	Rabbit	1:1000 (WB)	DAKO (P0449)
Anti-mouse	Goat	1:1000 (WB)	DAKO (P0447)
Anti-mouse	Horse	1:2000 (WB)	Cell signalling (7076S)
53BP1	Rabbit	1:500 (IF)	Abcam (ab21083)
γH2AX	Mouse	1:500 (IF)	Millipore (05-636)
p-RPA2(T21)	Rabbit	1:500 (IF)	Abcam (ab61065)
Alexa Fluor® 594 Anti-Mouse	Goat	1:500 (IF)	Invitrogen (A-11005)
Alexa Fluor® 594 Goat Anti-Rabbit	Goat	1:500 (IF)	Invitrogen (A-11012)
Alexa Fluor® 488 Anti-Rabbit	Goat	1:500 (IF)	Invitrogen (A-11010)

2.1.8 Standard solutions

Table 8. Standard solutions

Standard solutions
1.0M Tris pH 8.0: 131.14 g tris base was dissolved in 500mL ddH2O. HCl was used to pH the solution. Once a pH of 8.0 was reached, the solution was topped up with ddH2O to 1000mL.
10% APS: 1g APS dissolved in 10mL ddH2O.
10% SDS: 50g SDS dissolved in 500mL ddH2O.
10X TBS: 24.2g Tris-Base and 80g NaCl dissolved in 500mL ddH2O. HCl was used to pH the solution. Once a pH of 7.6 was reached, the solution was topped up with ddH2O to 1000mL.
1X TBS: 100mL 1x TBS dissolved in 900mL ddH2O.
1M DTT: 1.54g DTT dissolved in 10mL ddH2O.
5% BSA: 25g BSA dissolved in 500mL PBS.
5% Marvel Milk: 5g Marvel milk powder dissolved in 100mL PBS-T.

500mM EDTA: 146.12g EDTA dissolved in 1000mL ddH2O.
5M NaCl: 146g NaCl dissolved in 500mL ddH2O.
70% Ethanol: 700mL ethanol and 300mL ddH2O.
70% Methanol: 700mL methanol and 300mL ddH2O.
Alkaline Unwinding Solution: 4g NaOH pellets and 2.5ml 20mM EDTA (R&D Systems cat. # 4250-050-04, included in comet assay kit) made up to 500ml with ddH2O.
Alkaline Electrophoresis Solution for Comet Assay: 8g NaOH pellets and 2ml 500mM EDTA made up to1000ml with ddH2O.
Methylene Blue (0.4%): 2g methylene blue dissolved in 500mL 70% or 100% methanol.
NuPage MOPS SDS Running Buffer: 50mL NuPage MOPS SDS Running Buffer (20X) in 950mL ddH2O.
NuPage Transfer Buffer: 50mL NuPage Transfer Buffer (20X), 750ml ddH2O and 200ml methanol.
PBS-T: 500µL TWEEN 20 dissolved in 500ml PBS.
PBS: 1 Oxoid PBS tablet dissolved in 100mL ddH2O and sterilised by autoclaving.
TBS-T: 500µL TWEEN 20 dissolved in 500mL 1X TBS.
TE buffer pH 7.5: 10mM TRIS HCl pH 7.5 with 1mM EDTA.

2.2 Methods

2.2.1 Cell lines

G1 and G7 primary, patient-derived glioblastoma stem cells (GSCs) were kindly gifted by Professor Colin Watts (University of Birmingham, Brain Cancer Programme Chair) and Professor Anthony Chalmers (University of Glasgow, Chair of Clinical Oncology). These cell lines were initially derived from freshly resected glioblastoma specimens by Professor Watts' former laboratory in Cambridge (381-383). Preliminary work using additional Sheffield derived primary glioma cell lines, including residual surgical resected and tumour heterogeneity models, such as OX5-core and edge stem cell models (figure 2.1), are also presented in this thesis. These models are described in the recently submitted PhD thesis of Mr. Ola Rominiyi.

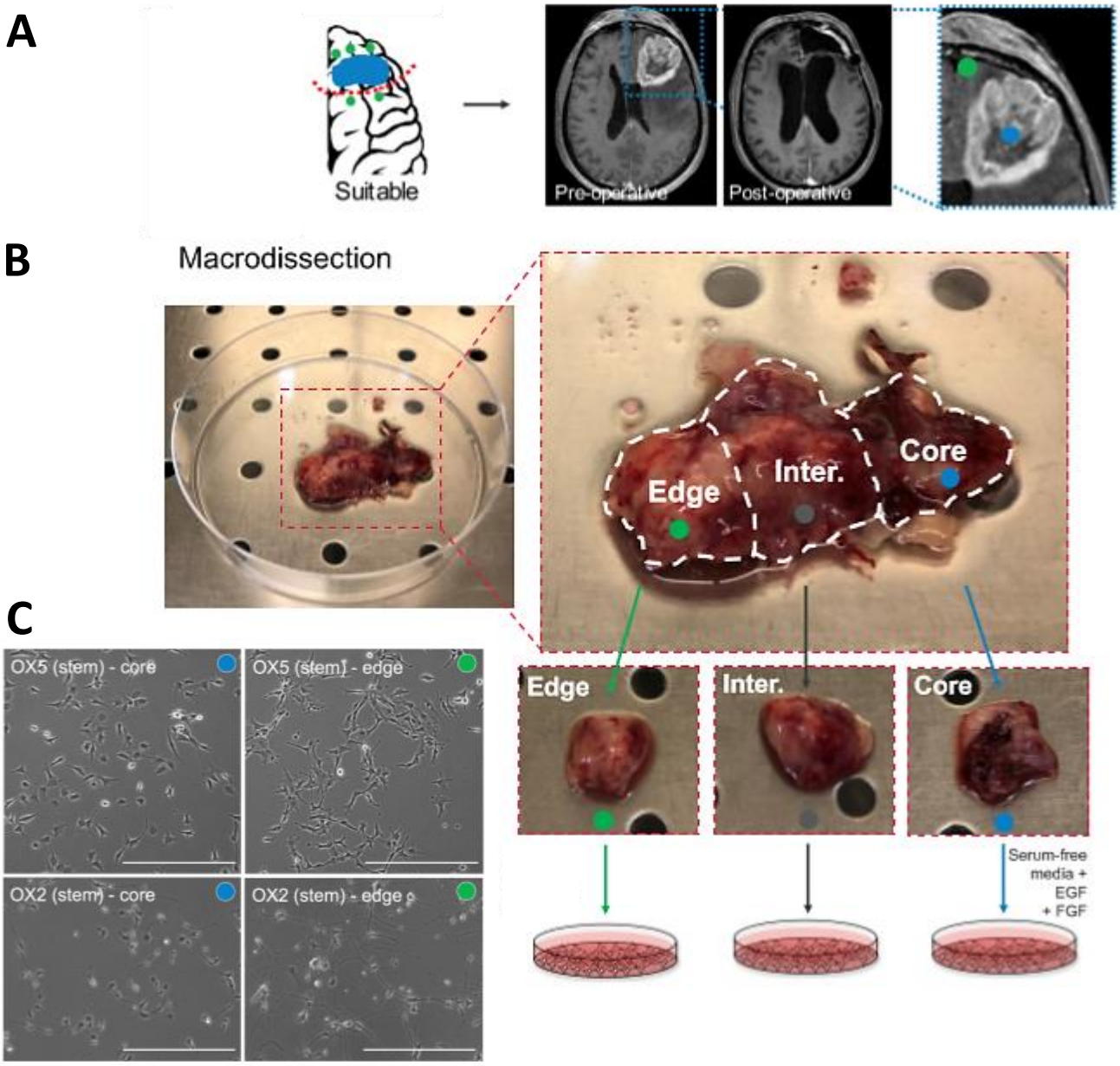

Figure 2.1. Derivation of parallel Sheffield GSC lines to model intra-tumoural heterogeneity.
A. Pre- and post-operative MRI scans following intravenous contrast. The blue dot indicates the tumour core, whilst the green dot indicates healthy, adjacent brain tissue infiltrated by the tumour edge. **B.** Tumour sample retrieved from the Royal Hallamshire Hospital both prior to dissection (left) and after microdissection (right) into core, infiltrative edge, and intermediate (inter.) components for parallel GSC line derivation. **C.** Brightfield light microscopy images (20x magnification) of Sheffield OX-5 and OX-2 core and edge GSC monolayers. Scale bars = 500µm. Glioma tumour heterogeneity models have also been generated from multiple sampling within a single tumour (data not shown). Cell lines and figure courtesy of Mr. Ola Rominiyi.

2.2.2 Growth conditions

All glioblastoma stem cell lines were propagated as adherent monolayers on matrigel-coated T75 flasks with 10mL advanced DMEM supplemented with L-glutamine, B27, N2, Penicillin-Streptom, Heparin, amphotericin B, EGF (2uL EGF (100µg/mL) per 10mL media) and FGF (1uL FGF (100µg/mL) per 10mL media) in a humidified incubator at: 37°C, 5% CO2 and 21% O2. Cells were passaged roughly every 5-7 days (once cells had reached ~70-80% confluency), the frequency of passaging varying between cell lines.

2.2.3 Matrigel preparation

Ice-cold (to prevent solidification) liquid Matrigel™ was diluted 1:40 with Adv DMEM (without additives or growth factors). Diluted matrigel (1:40) was then coated onto tissue culture flasks and plates (1.5mL/T25 flask, 2.5mL/T75 flask, 0.5mL in each well of 6-well and 12-well plates). Once coated with matrigel, plates and flasks were incubated for 45-60mins at 37°C to allow matrigel solidification. Excess matrigel was aspirated off. Matrigel-coated plates and flasks were either used immediately or stored for later use at -2°C (stored for up to two weeks).

2.2.4 Serial passaging of cells

GSCs were passaged once they were roughly 70-80% confluent, based on microscopic appearance. Old culture media was discarded, and cells were then washed twice with PBS to remove any remaining culture media and to remove dead cells and cell debris. 500 µL Accutase was then added to cell monolayers and cells were placed in the incubator until the cells had detached. Cells were re-suspended with 4.5mL culture media was (enough to inactivate the Accutase). A fraction of this cell suspension (usually 1:10) was then used to re-seed the cells onto a new matrigel-coated T75 flask containing fresh culture media (advance DMEM with additives and growth factors). Cells were passaged up to 25 times before cells were discarded and fresh cells were thawed.

2.2.5 Counting cells

GSCs were detached from monolayers using 0.5 mL Accutase and were then re-suspended with 4.5mL Adv DMEM with additives and growth factors (stem media) to form a single cell suspension. 10µL of this single cell suspension was pipetted into each chamber of a haemocytometer, between the haemocytometer and the cover glass using a P-20 micropipette. The number of cells in each of eight outer squares (four squares/chamber) were counted. The mean number of cells counted was

determined by dividing the sum of the cells counted in each square by eight. The number of cells per mL is equal to the mean cell count x 10^4.

2.2.6 Cryopreservation

GSCs were detached from the flask using Accutase (0.5mL) and re-suspended in 4.5 mL Adv DMEM media (without additives or growth factors). The cell suspension was transferred to 15 mL centrifuge tubes and the cell suspension was centrifuged at 1000 rpm for 3 minutes. The media was then discarded, and cell pellets were resuspended in 2-3 mL (depending on cell confluence) of Adv DMEM media with 10% DMSO. 1ml aliquots were placed in labelled cryovials. Cryovials were either stored at -80°C for short-term storage or were transferred to liquid nitrogen for long-term storage, after being stored at -80°C overnight.

2.2.7 Thawing cells

Cryovials were recovered from liquid nitrogen storage/-80°C freezer and were warmed in a 37°C water bath to form a liquid cell suspension. Once thawed, the cell suspension was immediately transferred to a T25 matrigel-coated flask containing 10ml stem media. Cells were left to adhere overnight. Old media was discarded and replaced with new media the following day. Cells were transferred to T75 matrigel-coated flasks once cells had reached a confluence of 70-80%.

2.2.8 Survival assays

2.2.8.1 Cell counting

Following TTFields treatment, the number of GSCs in each dish (including control dishes) was counted to assess how the viability of TTFields-treated GSCs compared to control cells (untreated). Old media was discarded and 500uL Accutase was added to each dish. Each dish was covered with sterile parafilm and placed in the incubator for ~4 mins to allow cells to detach. Cells were then re-suspended in 1.5ml stem media. Cell suspensions were transferred to centrifuge tubes and mixed thoroughly. Cells were counted using a haemocytometer as described above. The average number of cells counted using the haemocytometer (in cells/ml) was multiplied by 2 to give the total number of cells per dish.

2.2.8.2 Clonogenic assay

Clonogenic assays were used in GSCs cultured in stem media to determine the effects of TTFields on cell survival. Following TTFields treatment, G1 and G7 stem cells were plated in 6-well tissue culture plates coated in Matrigel at varying densities (300, 500 and 1000 cells/well). Cells were then incubated

for 21 days at 37°C. At the end of the incubation, the media was discarded, and cells were stained by addition of ~2mLs/well methylene blue in 70% methanol for ~30 minutes. Methylene blue was then removed, and plates were then washed by slowly dipping each plate twice in warm water to remove any excess methylene blue. Plates were left overnight to dry, and colonies were then counted (a colony = a group of 50 cells or more). Once counted, the plating efficiency (PE) was determined for the untreated control of each cell line using the following equation:

$$Plating\ efficiency\ (PE) = \frac{number\ of\ colonies\ formed}{number\ of\ colonies\ seeded}$$

The surviving fraction (SF) for each experimental condition was calculated relative to the untreated control, using the following formula:

$$Surviving\ Fraction\ (SF) = \frac{number\ of\ colonie\ formed\ after\ treatment}{number\ of\ cells\ seeded\ x\ PE}$$

Where applicable, individual sensitiser enhancement ratios (SER) were assessed. SERs are conventionally used to describe the ratio of radiation dosage (D) that is required to provide the same reduction in survival with and without a sensitiser:

$$Sensitiser\ Enhacement\ ratio\ (SER) = \frac{D_1(survival\ fraction\ without\ sensitiser)}{D_2(survival\ fraction\ with\ sensitiser)}$$

2.2.9 Western blotting

2.2.9.1 Protein extraction

2D inhibitor optimisations – At the end of the treatment, 6-well plates were washed three times with ice cold PBS. Plates were kept at -80°C if not proceeding immediately. 100µl lysis buffer (table 9.) was added to each well and cells were harvested from each well using a cell scraper and transferred into labelled Eppendorf's. Cells were left to lyse for 30 minutes on ice and were vortexed every 15 minutes. Cells were then centrifuged at 15,000G for 15 minutes at 4°C and the supernatants were transferred into fresh Eppendorf tubes.

3D inhibitor optimisations – At the end of the treatment, 6-well plates were washed three times with ice cold PBS. Plates were kept at -80°C if not proceeding immediately. 100µl lysis buffer (table 9.) was added to each well and incubated on ice for 15 minutes. Plates were then transferred to a rotating

platform for 10 minutes at ~ 200rpm. Cell solution was then transferred to labelled Eppendorf tubes and were left to lyse for 30 minutes on ice and were vortexed every 15 minutes. Cells were then centrifuged at 15,000G for 15 minutes at 4°C and the supernatants were transferred into fresh Eppendorf tubes.

TTFields-treated samples – At the end of the treatment, media was discarded and cells were lifted with Accutase. Cells were resuspended in media and centrifuged for 3-minutes. Media was discarded and cells were resuspended in ice cold PBS and transferred to Eppendorf tubes. Cells were centrifuged at 15,000G for 3 minutes at 4°C before discarding the PBS. Cell pellets were stored at -80°C if not proceeding immediately. Cells were resuspended in 100µl lysis buffer. Cells were left to lyse for 30 minutes on ice and were vortexed every 15 minutes. Cells were then centrifuged at 15,000G for 15 minutes at 4°C and the supernatants were transferred into fresh Eppendorf tubes.

Table 9. Lysis buffer

Reagent	Stock	Amount for 5 mL
Tris pH 8.0	1M	250 µl
NaCl	5M	200 µL
Triton X-100	100%	50 µL
DTT	1M	5 µL
EDTA	500mM	10 µL
Benzonase	25U/ml	250 µL
Protease inhibitor cocktail	-	2.5 mL
ddH2O	-	1.98 mL

2.2.9.2 Protein quantification

The protein content of each lysate was then quantified if the following manner. 39µl of ddH2O and 1µl of protein lysate were pipetted into a 96-well plate in triplicate. 200µL Protein Assay Dye Reagent Concentrate (BioRad), diluted 1:5 with ddH2O, was then added to each well. The Optical Density (OD) was read at 595nm on a Multiskan FC, Thermo Scientific spectrophotometer, relative to distilled water. Protein standard curves were generated from known concentrations of protein using bovine serum albumin (BSA). Protein standard curves were used to quantify protein concentration by solving the linear quadratic equation y = mx + c (with m = slope gradient, c = y-intercept and where solving for x gives the protein concentration of the lysate). Once quantified, 25uL of 4X NuPage LDS Loading Buffer and 5mM DTT mix (10uL 5mM DTT/1mL loading buffer) was added to each lysate. Samples were then vortexed and boiled for 5 minutes at 95°C and stored at -80°C until required.

SDS-PAGE and western Blotting - 10-well NuPAGE 4-12% Bis-Tris gradient gels and 10-well NuPAGE 3-8% Tris-Acetate gradient gels were used for western blotting. Between 25-50µg of protein and 4X NuPage LDS Loading Buffer mix (depending on protein content of samples) were loaded onto the gels. 1X SeeBluePlus2 Pre-stained Standard was also loaded on either side of the protein samples, acting as a molecular weight reference. Empty wells were loaded with 5µl of 4X NuPage LDS Loading Buffer. The samples were electrophoresed in NuPAGE SureLock Mini Cell Gel Tank or ThermoFisher Mini Gel Tank (when blotting for FANCD2), with 1X NuPage MOPS SDS (20X stock) Running Buffer or 1X NuPage Tris-Acetate Running Buffer (20X stock), respectively, at 140-150V for ~90 minutes. Protein from the gels was transferred to nitrocellulose membranes at 100V for 120 minutes in Mini PROTEAN Tetra Cells, using 1X NuPAGE transfer buffer (20X stock) diluted with pure methanol and ddH2O. Membranes were blocked for 60 minutes in 5% milk with PBS-T or 5% BSA with TBS-T, when blotting for p-Chk1(Ser345). Primary antibodies were made up in 5% milk with PBS-T or 5% BSA with TBS-T, again when blotting for p-Chk1. Membranes were incubated with primary antibodies overnight at 4°C. Membranes were washed 3x with PBS-T, each wash lasting 10 minutes. Membranes were then incubated with secondary antibodies conjugated to HRP made up with 5% milk with PBS-T at a concentration of 1:1000 for 1 hour. Membranes were washed 3 times in PBS-T. Membranes were visualised using Pierce ECL western blotting substrate and developed using medical x-ray film and a Konica SRX 101A Processor.

2.2.10 Immunofluorescence

2.2.10.1 Seeding cells and treatments

Cells were seeded onto sterile Matrigel-coated coverslips in 12-well plates at a density of 3 x 10^4 cells/well and cells were then incubated overnight. The following day, cells were pre-treated with inhibitor treatment (as specified in the results) in the 12-well plates. 1-hour post inhibitor treatment, cells were irradiated (2Gy) and cover slips were then transferred out of the 12-well plates into the respective Inovitro™ dish containing either DMSO/media or drug/media. TTFields (48 hours, 1.33 V/cm RMS, 200kHz) treatment was initiated as soon as possible following irradiation and once all cover slips had been transferred into dishes.

2.2.10.2 Immunostaining

H2AX/51BP1 – Following TTFields treatment, cover slips were transferred back into 12-well plates and cells were then washed twice with cold PBS. Cells were fixed with 4% PFA for ten minutes and subsequently washed with PBS twice. Cell were permeabilised with 0.5% Triton X-100 in PBS for ten

minutes. Once permeabilised, cells were washed three times with PBS and blocked for 1 hour with 3% BSA in PBS. Cells were then incubated overnight at 4℃ with primary antibodies at the required concentration (see table 7) in 1% BSA PBS. Following incubation with primary antibodies, cells were washed three times with PBS. Cells were then incubated with secondary antibodies (M595 1:500 and R488 1:500) and DAPI (1:500) made up in PBS with 1% BSA at room temperature for 1-hour in the dark (wrapped in foil). Finally, cells were washed three times and cover slips were mounted onto microscope slides using Shandon Immu-Mount medium (Thermo Fisher Scientific). Slides were left to dry overnight at room temperature in the dark.

p-RPA(T21) – Following TTFields treatment, cover slips were transferred back into 12-well plates and cells were then washed twice with cold PBS. Cells were pre-extracted with 300mM sucrose, 0.2% Triton-X in PBS on ice for 5 minutes. Cells were then fixed with 4% PFA for ten minutes and subsequently washed with PBS twice. Cell were permeabilised with 0.5% Triton X-100 in PBS for ten minutes. Once permeabilised, cells were washed three times with PBS and blocked for 1 hour with 5% Goat serum in PBS. Cells were then incubated overnight at 4℃ with primary antibodies at the required concentration (see table 7) in 3% Goat serum in PBS. Following incubation with primary antibodies, cells were washed three times with PBS. Cells were then incubated with secondary antibodies (M595 1:500 and R488 1:500) and DAPI (1:500) made up in PBS with 3% Goat serum at room temperature for 1-hour in the dark (wrapped in foil). Finally, cells were washed three times and cover slips were mounted onto microscope slides using Shandon Immu-Mount medium (Thermo Fisher Scientific). Slides were left to dry overnight at room temperature in the dark.

2.2.10.3 Immunofluorescence microscopy and foci quantification

Microscopy was carried out on a Nikon Eclipse T200 inverted microscope (Melville), equipped with a Hamamatsu Orca ER camera and a 200W metal arc lamp (Prior Scientific) using a 100x objective lens. Images were analysed using ImageJ software. Individual 53BP1 foci in each cell nucleus were counted and cells were scored as either positive (≥5 foci) or negative (<5 foci) for γH2AX stain. A minimum of 100 cells were analysed for each experimental condition.

2.2.11 Alkaline Comet Assay

2.2.11.1 Alkaline comet assay procedure

Cells were plated on cover slips in 12-well plates at a density if 3 x 10^4 and incubated at 37°C overnight. Cells were treated as details in the results and then processed immediately following treatment. The Trevigen comet assay kit was used to process samples. LMagarose was pre-warmed in the microwave and kept at 37℃ in the water bath. Media was discarded from dishes and cells were detached with

500µL Accutase. Cells were resuspended in warm PBS and transferred to centrifuge tubes. Cells were pelleted at 1000rpm for 3mins and washed twice with warm PBS. Cell pellets were then resuspended in 1mL warm PBS and cells were counted using a haemocytometer. A final cell suspension of 1 x 10^5 cells/mL in PBS for each sample was produced. 112.5µl of LMagarose was pipetted into pre-labelled Eppendorf's stored on a heat block set to 37℃ (to prevent the LMagarose solidification). 12.5µL cell suspension was then mixed with the LMagarose (1:10 dilution). 100µL LMagarose/cell mix was pipetted onto the sample area of Trevigen comet slides. Cells were stored flat at 4℃ in the dark for 30 mins to promote adherence. Cells were then lysed with Comet Lysis Solution at 4℃ for 30 mins in the dark. Following lysis, cells were exposed to Alkaline Unwinding Buffer for 20 mins at room temperature. Electrophoresis was carried out at ~21V, with a constant current of 300mA (achieved by adjusting the volume of electrophoresis buffer) for 30 mins at 4℃. Slides were rinsed with H2O twice and were then immersed in 70% ethanol for 5 minutes. Samples were dried overnight at room temperature. To stain cells, 100µl SYBR Gold in TE buffer (1:30,000) was pipetted onto each sample area and left to stain for 30 mins in the dark. Excess SYBR Gold solution was removed by gently tapping the slides and dipping them in H2O. Slides were allowed to dry before imaging.

2.2.11.2 Image acquisition and analysis

A least 50 cells per condition per experiment were imaged using the FITC channel and 20x lens on a Nikon Eclipse TE200 Fluorescent Microscope. Images were analysed using TriTek Comet Score software (AMSBiotechnology, 2010). The tail moment (Mt) was used as a measure of DNA damage.

$$Tail\ moment\ (Mt) = \%\ DNA\ in\ comet\ tail\ x\ comet\ tail\ length$$

2.2.12 Flow Cytometry – Annexin V/PI stain

2.2.12.1 Sample preparation and PI staining

Cells were plated in 12-well plates on cover slips, treated, and collected at various time points as specified in the results. Following treatment, media from each dish was collected and transferred to a labelled centrifuge tube. Cells were detached using Accutase and cells were transferred to the corresponding centrifuge tube. Cells were pelleted at 1000rpm for 3 mins and cells were washed twice with cold PBS. The supernatant was discarded, and cells were resuspended in 100µL Binding Buffer. 5µL Annexin V and 5µL PI were added to each sample and cells were incubated at room temp for 15mins in the dark. A further 200µL Binding Buffer was added to each tube and the cell suspension was then transferred into labelled FACS tube and analysed by BD LSR II Flow Cytometer.

2.2.12.2 LSRII flow cytometric analysis

10,000 cells/sample were analysed on the LSRII and the data was analysed using FlowJo software. Analysis of the Annexin V channel (Comp-Blue 530_30A) versus the PI channel (Comp-Blue 695_40A) was used to gate double negative (DN) cells (no stain) in untreated cells. Analysis of the Side Scatter (SS) versus the Forward Sactter (FS) on the DN fraction was used to exclude any debris. Using the Annexin V channel versus the PI channel, four quadrants were drawn ($AnnexinV^-PI^-$, $AnnexinV^+PI^-$, $AnnexinV^+PI^+$ and $AnnexinV^-PI^+$) and the percentage of cells in each quadrant were produced. The quadrants were set on untreated cells and applied to all other conditions.

2.2.13 Cell counting for growth curves

G1 and G7 cells were seeded onto 6-well matrigel-coated plates at a density of 2.5 x 10^4 cells/well. Plates were kept in the incubator for the duration of the experiment. Cells were counted on the indicated days (3-wells/day). When counting cells, media was discarded and 500 µL Accutase was added to the desired wells and returned to the incubator until cells had detached. Cells were re-suspended with 1.5ml stem media and transferred to centrifuge tubes. The cell suspension was mixed well, and cells were counted using a haemocytometer (as above). The cell count obtained using the haemocytometer was doubled to give the total number of cells/well. Results were plotted on a log-linear scale using GraphPad to give the cell growth curve. Cell growth curves were used to determine the cell doubling time of G1 and G7 stem cells.

Growth curves typically follow a sigmoid pattern and are characterised by four phases: a lag phase (where cells do not divide as they adapt to the culture conditions), a logarithmic (log) growth phase (during which cells are proliferating and cell number increases exponentially), a plateau phase (where cell proliferation begins to slow down as cells reach confluence and cell number stabilises) and a decline phase (where cells begin to die). The Log Growth Phase of the curve is used to determine cell doubling time using the following equation (384):

$$Doubling\ time = \frac{duration * \log(2)}{\log(Final\ concentration) - \log(Initional\ concentration)}$$

The initial concentration refers to the number of the cells present at the start of the log phase and the final concentration refers to the number of the cells present at the end of the log phase. The duration is time elapsed between initial and final concentration.

2.2.14 Treatments

2.2.14.1 DDR inhibitor drugs

G1 and G7 stem cells were seeded onto 6-well matrigel-coated plates at a density of 25 x 10^4 cells/well. Cells were then incubated overnight in order to allow cell adhesion to the plates prior to starting the treatment. All DDRi (AZD1390 and AZD0156 (ATMi), AZD6738 (ATRi), AZD1775 (WEEi) or Olaparib (PARPi)) were diluted with DMSO to make 10mM stocks and were stored at-20°C. Cells were treated with one of DDRi at the indicated concentrations or with vehicle control only (DMSO). DMSO and all DDRi were diluted in stem media to the final intended concentrations and 2mL of the drug/DMSO dilutions was added to the desired wells. DMSO at concentrations equivalent to the drug solutions were used as the vehicle control in all experiments. One hour following DDRi treatment, cells were treated with a DNA damaging agent.

2.2.14.2 DNA damaging agents

Irradiation - Cells were irradiated in a Caesium-137 Blood Irradiator. Either a dose of 2 or 5 Gy (as indicated) was used. In all experiments, irradiation was administered 1 hour following the inhibitor treatment. Control plates (not to be irradiated) were taken out of the incubator for the same duration as the treatment plates to minimise experimental variation and act as a 'sham' radiation control such that control plates were subjected to comparable environmental changes as experienced by cells during the irradiation process. One hour following IR treatment, drug media was discarded, and cells were washed 3x with ice cold PBS and stored at -80 °C unless proceeding immediately.

Temozolomide - A 50 mM stock dilution (diluted in DMSO) was further diluted with stem media to 20x the intended final concentration (100uM) and 100 µL of the 20x drug solution was added to the desired wells 1 hour following DDRi treatment. DMSO was also diluted with stem media to form a dilution of 20x the intended final concentration and 100 µL of the DMSO dilution was added to control wells. Four hours following TMZ treatment, drug media was discarded, and cells were washed 3x with ice cold PBS and stored at -80 °C unless proceeding immediately.

2.2.14.3 TTFields treatment

The Inovitro™ system consists of a generator, which delivers the electric fields; a base plate, which is connected to the generator via a flat cable; and ceramic dishes, which connect to the base plates (see figure 2.2a-b). This system permits the transfer of the electric fields from the generator to and across the ceramic dishes where the cells are found. The delivery and scheduling of TTFields/DDRi-based combinations were carried out as described below.

G1 stem cells were seeded onto sterile, matrigel-coated glass coverslips in 12-well plates at a density of 10 x 10^4 cells/well. Following seeding, cells were incubated overnight to allow for cell adhesion to the coverslips. The following day, the matrigel-coated coverslips with attached cells were transferred into Inovitro™ dishes (one coverslip/dish). 2mL of Advanced DMEM with additives and growth factors was added to each dish and each dish was then covered with sterilised parafilm. Control dishes were placed in a humidified incubator at: 37°C, 5% CO_2 and 21% O_2 for the duration of the treatment. Dishes to receive TTFields treatment were slotted onto an Inovitro™ base plate and placed in a refrigerated incubator (set at a temperature of 18°C, with 5% CO_2 and 21% O_2) to maintain the temperature of each dish at 37°C, as the delivery of electric fields generates heat within the dish. The temperature of the refrigerated incubator will determine the intensity at which the electric fields can be delivered (see table 10.). In these studies, the ambient incubator temperature was ~20-22℃ (depending on room temperature), equating to intensities ranging between 1.19-1.48 V/cm RMS (385). The frequency of alternating electric fields to be delivered to each dish (200kHz) and the temperature to be maintained within each dish (37°C) were set using the Inovitro™ software on the computer and the treatment was initiated.

The treatment schedule for the full combination treatment (i.e. TTFields/DDRi/IR) was as follows (see figure 2.2c): both G1 and G7 stem cells were pre-treated with DMSO or DDRi for 1-hour (to allow time for the inhibitor to take effect) prior to irradiation in 12-well plates. Immediately after irradiation, cover slips were transferred into Inovitro dishes containing either DMSO/media or DDRi/media and the TTFields treatment was initiated as soon as possible. Cells were treated for a duration of 48 hours (roughly equal to one cell doubling time of G1 and G7 stem as determined by cell growth assays).

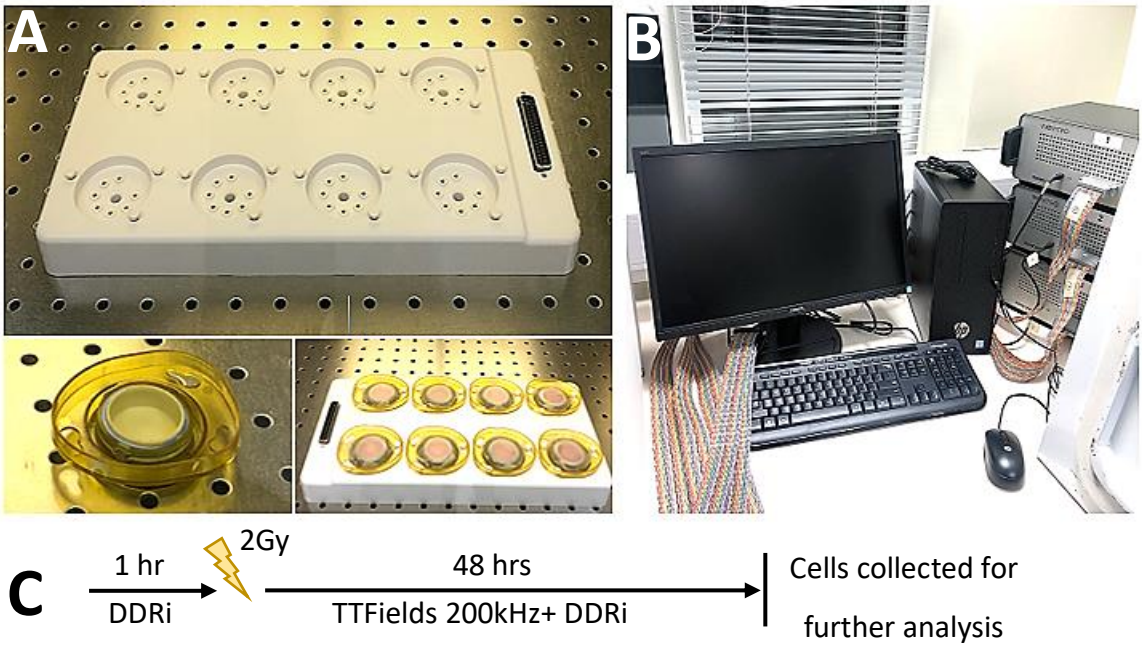

Figure 2.2. The Inovitro™ system.
A. Invitro™ system base plate (top) with a single ceramic dish shown in the lower left panel and a full set of ceramic dishes slotted onto the base plate after seeding cells shown in the lower right panel. **B.** TTFields generators, which deliver the electric fields to the base plates via flat cables. Frequency of the electric fields is set using the Inovitro™ software on a dedicated desktop computer. **C.** Treatment scheduling for DDRi and TTFields-based combinations.

Table 10. Incubator ambient temperature and expected TTFields intensities inside the Inovitro™ system ceramic dish, taken from (385).

Incubator ambient temperature (°C)	Expected TTFields intensities (V/cm RMS)
18	1.62
19	1.55
20	1.48
21	1.41
22	1.33
23	1.26
24	1.19
25	1.12
26	1.04
27	0.97
28	0.9
29	0.83
30	0.76

2.2.15 Statistical analysis

Statistical analysis was carried out using GraphPad Prism. Standard deviation of the mean was calculated for values taken from multiple replicates. Standard error of the mean was calculated when comparing means. The one way ANOVA test was used to compare means between conditions. $p<0.05$ = *, $p<0.01$ = **, $p<0.001$ = ***, $p<0.0001$ = **** and no significant difference = ns.

CHAPTER 3. TARGETING PARP1 IN COMBINATION WITH TTFIELDS AND STANDARD-OF-CARE TREATMENT

3.1 Introduction

Poly (ADP-ribose) polymerases (PARPs) form a family of enzymes that are defined by their ability to catalyse the transfer of ADP-ribose units from NAD+ to form chains of negatively charged poly(ADP-ribose) (PAR) on itself and on target proteins, a process known as Poly(ADP-ribosyl)ation (PARylation) (386). PARPs produce branched and unbranched chains of up to 200 units in length (387), with PAR chains forming scaffolds that recruit PAR-binding proteins and regulate signal transduction (386). PARPs are involved in numerous processes, such as DNA repair, transcription, replication and regulating chromatin structure. There are altogether 18 related PARP enzymes, sharing homology in a conserved catalytic domain, however, PARP1, PARP2 and PARP3 are the main PARP enzymes involved in regulating DNA repair processes (388). PARP1 is estimated to be responsible for 80-90% of the PARylation activity triggered in response to DNA damage (389). However, whilst embryonic knockout of both PARP1 and PARP2 simultaneously is embryonically lethal, knockout of either PARP1 or PARP2 alone is viable, suggesting that PARP1 and PARP2 exhibit some functional redundancy (390). Such PARylation is a brief response to the detection of DNA damage (388), and therefore the removal of PAR by PAR-degrading enzymes, such as PARG (poly ADP-ribose glycohydrolase), is equally important (391). DePARylation ensures the DDR occurs in an orderly manner by allowing the release of early DNA damage responders from the DNA in order to make way for other downstream repair factors required for subsequent steps in the DDR (392). This also ensures PARP1 recruitment and activation is possible in the event of any future DNA damage threat. Overactivation of PARP1 exhausts NAD+ and ATP stores and triggers the release of apoptosis-inducing factor (AIF) from mitochondria, activating cell death pathways (393, 394).

A summary of PARP1 function within the DDR is shown below in Figure 3.1.

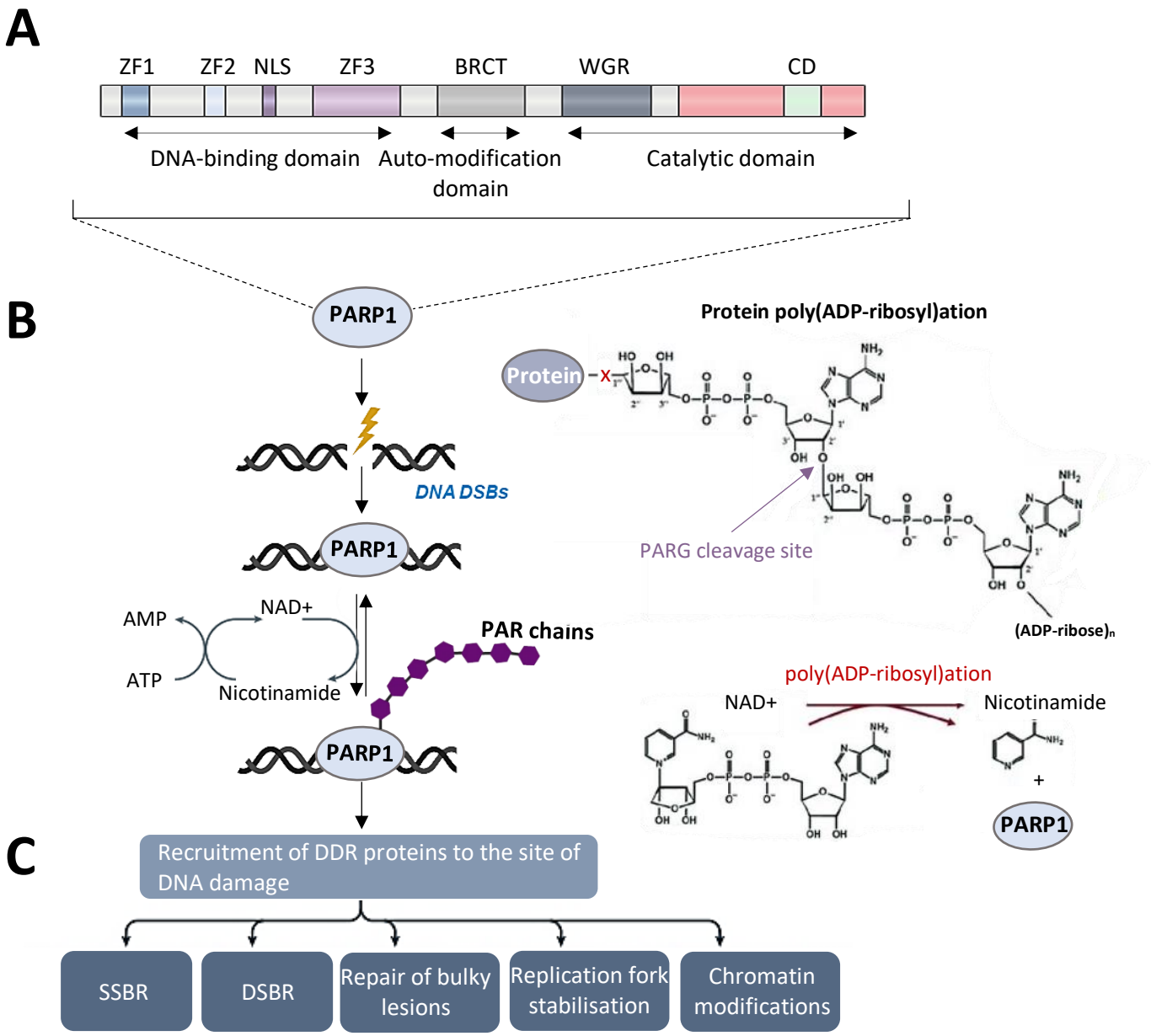

Figure 3.1. Multi-functional role of PARP1 in the DNA damage response.
A. PARP1 domains. PARP1 carries three different domains: the DNA-binding domain (DBD), consisting of three zinc finger motifs (ZF1–3) and a nuclear localisation signal (NLS); an auto-modification domain, which consists of an interaction motif (BRCA1 C terminus, or BRCT) domain; and a conserved catalytic domain (CD), which carries the active site, that binds to NAD+, and the Trp-Gly-Arg (WGR) domain. **B. PARP1 signalling.** DNA lesions are detected via the DBD domain. PARP1 synthesis PAR chains on itself and target proteins, using NAD+ as a substrate. Nicotinamide is utilised to replenish NAD+ stores, which is ATP-dependent. PARG rapidly mediates removal of PAR chains. **C. PARP1 function in DNA repair.** PARylation of PARP1 and target proteins enables the recruitment of DNA damage repair proteins to site of DNA damage to facilitate resolution of the DNA damage. Figure adapted from Chaudhuri *et al.* (2017) and Sukhanova *et al*. (4).

3.1.1 Roles of PARP1 in DDR

3.1.1.1 Role in DNA repair

PARP1 is a DNA damage sensor that interacts with various types of DNA damage, such as SSBs, DSBs and bulky adducts, through its DNA binding domain. Binding of PARP1 to DNA breaks results in conformational change and activation of its catalytic domain and catalyses the formation of PAR on itself and other proteins (396, 397). PARylation occurs at or close to the site of damage and mediates the recruitment of PAR-binding DNA repair factors (388). PARP1 has mainly been described for its role in the repair of bulky adducts during BER (figure 1.7, section 1.2) (398). PARP1 is recruited to SSBs intermediates that are generated indirectly during BER following the activity of AP endonucleases, APE1, which cuts the DNA backbone 5' of the AP site (399). PARP1 then becomes activated and mediates the recruitment of PAR-binding proteins like XRCC1, DNA polymerase β and DNA ligase III at damaged DNA sites (400-402). In addition, PARP1 has also been shown to mediate repair of SSB intermediates that form following excision of modified nucleotides during NER (403). PARP1 can however also detect SSBs that have occurred directly (404), although its role in SSBR is not essential because SSBs can still be repaired even in the absence of PARP1 (405, 406). PARP1 also localises to DBSs and recruits DSBR proteins ATM, Mre11 and Nijmegen breakage syndrome 1 (NBS1) to facilitate repair through either HR or a-NHEJ, PARP1 therefore mediates DSBR pathway choice (187, 407-409). PARP1 has also been shown to bind to and PARylate MGMT and promote repair of the O^6-MeG lesions caused by TMZ treatment. PARylation of MGMT by PARP1 has also been proposed to be required for its localisation on chromatin, where MGMT exerts its effects (410). Once the damage is repaired, the negatively charged PAR chains on PARP1 trigger detachment of PARP1 from the DNA to finalise the DNA repair process (411). In addition to its role in DNA repair, PARP1 has also been shown to regulate cell cycle progression by activating Chk1 in the absence of stimulation by ATR (412).

3.1.1.2 Role in replication stress

PARP1 has been implicated in replication fork stabilisation during replication stress (413). Replication fork stabilisation consists of three main processes: fork reversal, fork protection and fork restart (186). PARP1 binds to sites of stalled replication forks and once activated, maintains reversed forks by antagonising the activity of RECQ1 DNA helicase (414). PARP1 then recruits MRE11, a nuclease involved in the DNA end resection at stalled forks, producing short strands of ssDNA (187). PARP1 along with BRCA genes constrain the extent of DNA end resection carried out by MRE11 (188, 415, 416), with extensive end resection leading to replication fork cleavage and collapse and subsequent generation of DSBs (111, 416). RPA is initially localised to the exposed ssDNA produced by end resection (417) but is rapidly displaced by RAD51 (418, 419), a process that is mediated by both PARP1

and BRCA2 (420, 421), further contributing to replication fork protection. This also primes stalled forks for replication fork restart, with RAD51 promoting homology search into the sister chromatid to resolve the damage by recruiting factors involved in HR repair (111, 192, 422, 423).

RECQ1 is also responsible for initiating replication fork restart at stalled replication forks following repair. PARP1 through PARylation of RECQ1 prevents premature reactivation of RECQ1 so that DNA damage beyond the stalled fork can be removed prior to fork restart. If RECQ1 activity is permitted too soon, SSBs can be converted to DSBs (414). This is because the replication fork machinery 'falls off' the DNA when it collides with ssDNA gaps, a process known as replication run-off (424). Once repaired, normal PCNA-mediated replication by polymerases δ/ε can be resumed (425). PARP1 therefore promotes replication fork stabilisation and replication fork restart after processing of any lesion impeding DNA replication fork progression and PARP activity is therefore necessary to promote cell survival following replication stress (426).

3.1.1.3 Role in chromatin modifications

Chromatin structure dictates a wide range of processes, including DNA replication, transcription, and DNA repair, by either restricting or facilitating accessibility to DNA in its compact form (referred to as heterochromatin) or relaxed form (euchromatin), respectively. For example, upon DNA damage detection, chromatin decondensation is essential in order to allow access to DNA repair factors at the site of damage in order to coordinate DNA damage repair (427). Without this re-structurisation, the damaged DNA may become trapped within the condensed chromatin structure resulting in a failure to repair the damage and genomic instability (428). On the other hand, once the damage has been repaired, chromatin must restore its original condensed structure to complete the process (429), and therefore chromatin remodelling is a highly organised process that must be carefully controlled. This remodelling is generally mediated by chromatin remodelling enzyme complexes, post-translational modifications of DNA and histones, such as acetylation and methylation, and/or by histone exchange (429-433).

PARP is one of the first proteins that is activated at sites of damage to promote changes in chromatin structure. PARP PARylates itself and other chromatin-associated proteins, such as histones, within proximity to the damage. Because both PAR chains and DNA are negatively charged, PARylation may also serve to unwind and disrupt the compact structure of chromatin through charge repulsion, easing the accumulation of DDR factors at the site of damage. PARP-mediated PARylation of histones can cause them to become excluded from chromatin to initiate the relaxation process (434, 435). This then allows chromatin remodelling enzymes to accumulate on the DNA to further enhance the unwinding of the compact chromatin structure. PARP1 also indirectly regulates chromatin structure

by PARylating a range of factors involved in post-translational modifications, including acetylation and methylation of histones. Acetylation and deacetylation of histones is carried out by histone acetyltransferases (HATs) and histone deacetylases (HDACs), respectively. Acetylation has been suggested to neutralise the positively charged lysine residues on histone proteins and, in so doing, weakens the affinity between histones and DNA, which is negatively charged. PARP has been shown to mediate this modification of lysine residues on histone proteins by HATs, promoting electrostatic repulsion between DNA and histones, resulting in the opening of the chromatin structure (430, 431). PARP1 also regulates methylation patterns of histones. PARP1-medeiated PARylation preserves H3K4 trimethylation by blocking KDM5B demethylase enzyme activity (436). Trimethylation of Histone 3 on lysine 4 (H3K4me3) is enriched within euchromatic regions (437). On the other hand, trimethylation of H3K27 accumulates in heterochromatic regions (438, 439). PARP1 PARylates and inactivates EZH2, the methyltransferase responsible for methylation of H3K27, again promoting relaxation of chromatin (440).

In addition to its role in histone modifications, PAR chains recruit additional factors involved in chromatin remodelling. For example, ALC1, which is a nuclease that relaxes chromatin structure around damaged DNA, is recruited to sites of DNA damage by binding to PAR chains through its PAR-binding macrodomain resulting in configurational change and activation (441). ALC1 also prevents the removal of PAR chains by PARG on PARP1 (442). PARP also activates transcriptional repressors to prevent transcription of damaged DNA, allowing time for damage to be repaired before transcription can be resumed and preventing the threat of further genomic insult (443).
PARP1, through its PARylating activity, therefore, promotes both directly and indirectly very rapid decondensation of chromatin to facilitate DNA repair.

3.1.2 PARP inhibitors for glioblastoma treatment

Given the multifaceted role of PARP1 in the DDR, PARP1 constitutes an attractive target that can be exploited for oncology therapeutic purposes. PARP inhibitors are NAD+ analogs and bind competitively to the NAD+ binding domain within the active site on PARP (444). Two mechanisms have been suggested for the use of PARP inhibition for the treatment of cancer.

Firstly, PARP inhibition can be used to enhance the effects of DNA damaging agents by exacerbating the amount of DNA damage experienced by cancer cells by reducing DNA repair capacity. PARP inhibition enhances TMZ sensitivity by preventing the repair of TMZ-induced lesions N^3-methyladenine and N^7-methylguanine, through inhibition of BER, and O^6-MeG lesions by preventing PARylation of MGMT and its localisation on chromatin (410). Additionally, PARP can accumulate at chromatin irrespective of whether it is active or not. Even in the presence of PARP inhibitor, PARP still

localises at sites of damage and replication stress where it becomes trapped on chromatin, which has been suggested to be due to changes in its configuration that strengthen its association with DNA through its N-terminal zinc finger domain (445, 446), although the precise mechanism through which this is achieved have not yet been established. Whilst all PARP inhibitors prevent the formation of PAR chains, different PARP inhibitors are able to trap PARP on DNA to varying degrees irrespective of their activity, with talazoparib exhibiting the highest PARP trapping ability (447, 448). PARP must be released from chromatin so that downstream factors can accumulate on DNA and mediate the next steps in the repair process. Failure to release PARP from chromatin therefore not only interferes with damage repair but trapped PARP can also itself lead to formation of DSBs by interfering with replication fork progression (449). It has even been suggested that trapping of PARP on DNA is more toxic than unrepaired SSBs from PARP inhibition (111). This is due to two reasons. First, PARP is dispensable for SSBR (405, 406) and secondly the DSBs that eventually form from PARP being trapped on DNA are more toxic than SSBs. However, these ensuing DSBs can usually be restored via HR repair.

As such, PARP inhibition can be exploited under the concept of synthetic lethality, whereby cells that are deficient in key HRR proteins have been shown to heavily rely on PARP activity for DNA repair and cell survival, such that further inhibition of PARP results in an inability to compensate and cell death (450). This is because when PARP is inhibited, DNA SSBs, that normally constitute substrates for repair by HR at stalled replication forks, accumulate and, in the absence of a functioning HRR pathway, are converted to DSBs (111). Whilst these DSBs are still subject to repair, this process relies on the error-prone NHEJ DSBR pathway, which contributes to genomic instability and can even be lethal to cells (409). However, these affects alone would not translate in such high toxicity seen with this combination and therefore additional roles of PARP and BRCA are thought to be at play. This discovery led to the first application of synthetic lethality in the clinic, with PARPi being approved for the treatment BRCA1/2 deficient ovarian and breast cancer (451).

Efforts are being made to extend this to a wider range of cancers, including in the neuro-oncology setting, both within and outside of the BRCA1/2 mutant contexts. Gliomas harbouring IDH mutations have been suggested to mimic the phenotype of BRCA deficient cancers. IDH mediates the conversion of isocitrate to α-ketoglutarate by oxidative decarboxylation, a process that is dependent enzymatic activity of nicotinamide adenine dinucleotide phosphate (NADP+). Mutations in IDH alter its function such that α-ketoglutarate is converted to the oncometabolite 2-hydroxyglutarate instead. Mutations in IDH have been linked to defects in HR repair pathway, making this type of tumour particularly sensitive to treatment with PARP inhibitors. This defect in HR repair could also explain why glioblastoma patients harbouring IDH mutations demonstrate improved prognosis in comparison to

patient with WT IDH and are associated with low-grade gliomas (80%) and only 3% of primary glioblastoma patients (452, 453). PTEN mutations, which occur in roughly 36% of glioblastoma patients, have also been implicated in dysregulation of HR, an effect that has been shown to be mediated through transcriptional silencing of RAD51 (454). In both cases, these patients may constitute a subgroup of glioblastoma patient that might particularly benefit from treatment with PARP inhibitors and demonstrates how treatment strategies could be guided by patient specific mutations. Olaparib as a single agent has been investigated in a phase II clinical trial setting (OLAGLI, NCT03561870) for recurrent glioblastoma patients with IDH mutations and has been shown to be well tolerated by patients (455).

The trapping ability of PARP inhibitors mediates single-agent efficacy (456), and therefore the use of PARP inhibitors could demonstrate therapeutic gain even in cancers without deficiencies in HR repair. PARP1 activity is enhanced in GSCs relative to their bulk counterparts and has even been proposed as a marker for glioblastoma because its expression is consistently high across glioblastoma tumours but is not active in healthy brain tissue (123, 382). A study by Lesueur et al. showed that PARP inhibitor treatment radiosensitised GSCs to a greater extent than bulk cells (457), which supports the theory that increased DNA repair activity might be to blame for the increased resistance conferred by GSCs to DNA damaging treatment. Therefore, PARP inhibitors constitute a promising pharmacological tool for the treatment of gliomas.

3.1.3 Rational for use in combination with TTFields

A few factors limit the potential widespread application of PARP inhibitors for the treatment of glioblastoma. Overtime, PARP inhibitor resistance develops. Several processes have been suggested to be responsible for this, such as reverse mutations in BRRCA1/2 proteins that cause reactivation of BRCA genes (458, 459), or reactivation of repair through HR independently of BRCA genes (for example, mutations in NHEJ factors, such as 53BP1, allow sufficient DNA end resection to occur, channelling repair of DSBs through HR even in the absence of BRCA genes) (460-462) or reinstatement of replication fork stability (190). Additionally, point mutations within PARP domains which prevents PARPi-mediated trapping of PARP1 on DNA have also been shown to contribute to PARPi resistance (463). Downregulation of PARG is another mechanism thought to drive PARP inhibitor resistance because PARG-deficient cells have been shown to sustain sufficient PARylation levels on target proteins such that DNA repair can still occur (464). One promising strategy in which resistance to PARP inhibitors can be overcome is through combination treatment. Given that TTFields has been suggested to induce a state of BRCAness (314), PARP inhibition could potentially enhance TTFields efficacy, and

could extend the application of PARP inhibitors to patients without mutations that predispose them to being sensitive to PARP inhibitor treatment.

Although the OPARATIC clinical trial demonstrated that Olaparib could in fact cross the BBB and that concentrations of Olaparib ranging from 100-1000 nM could be detected within the tumour core and margins, glioblastoma is known for its extensive infiltration into the surrounding healthy tissue some distance away from the tumour margins where it may escape the effects of PARP inhibitor (465). Given that TTFields has been shown to enhance BBB permeability (373, 375, 466), this could increase delivery of PARP inhibitor to the tumour site. Additionally, the TMZ-induced haematological toxicities are aggravated by PARP inhibitor treatment, requiring that PARP inhibitor be delivered intermittently when given with TMZ (465). Enhancement of PARP inhibitor delivery to the tumour by TTFields means that a lower dose of the drug could be given to patients for the same therapeutic effect, which would in turn reduce systemic toxicities. No systemic toxicities have been reported with TTFields treatment and therefore toxicities should not be exacerbated by TTFields treatment.

Whilst the effects of this combination have not yet been explored in glioma cells, Karanam *et al.* (2019) demonstrated that PARP inhibition (Olaparib, 10 μM) enhanced cell killing of NSCLC cell lines when combined with TTFields compared to either treatment alone (314), and Mulvey *et al.* showed that PARP inhibitor, niraparib, sensitised ovarian cancer cell lines to TTFields treatment (467). As such, further exploration of the potential of combining therapeutically approved PARPi and TTFields for the treatment of glioblastoma is warranted.

3.2 Results

3.2.1 Optimisation of PARPi for use in glioma stem cells

Olaparib (Lynparza) is the most developed and clinically approved PARP inhibitor, receiving FDA approval in 2014 for the treatment of BRCA1/2 mutant ovarian cancers and becoming the first cancer treatment directed against an inherited genetic mutation to receive approval (468).

Western blot analysis was used to determine the effects of Olaparib on PARP activity in G1 and G7 GSC models using a PARP1 antibody together with a pan-PAR antibody, which recognises both mono- and poly-ADPr units. Although Olaparib inhibits PARP1- and PARP-2, PARP1 is responsible for ~90% of PARylation in response to DNA damage, therefore, changes in PARylation levels with and without the inhibitor are likely to mostly reflect changes in PARP1 activity. Baseline levels of PARP1 activity were high in both G1 and G7 stem cells as a strong PARylation band was detected in the DMSO control for both cell lines. Olaparib strongly inhibited PARylation of PARP1 in both cell lines at all doses tested, indicating inhibition of PARP1 activity (figure 3.2). As 0.5µM Olaparib demonstrated strong inhibition of PARP1 activity in GSCs, this dose was chosen for subsequent experiments to reduce inherently cytotoxicity as much as possible.

Importantly, this a clinically relevant dose. Indeed, one of the exploratory endpoints of the Oparatic clinical trial (NCT01390571) aimed to assess the concentrations of Olaparib achieved within the tumour core and margins of recurrent glioblastoma patients who had received Olaparib (100mg, 150mg and 200mg) prior to surgery. They determined that the concentrations of Olaparib in resected tumour specimens to be within the range of 100-1000nM, with mean concentrations of 500nm and 588nM in the tumour margins and core, respectively. Olaparib concentrations detected in the tumour samples did not vary significantly based on the different doses of Olaparib administered (465, 469).

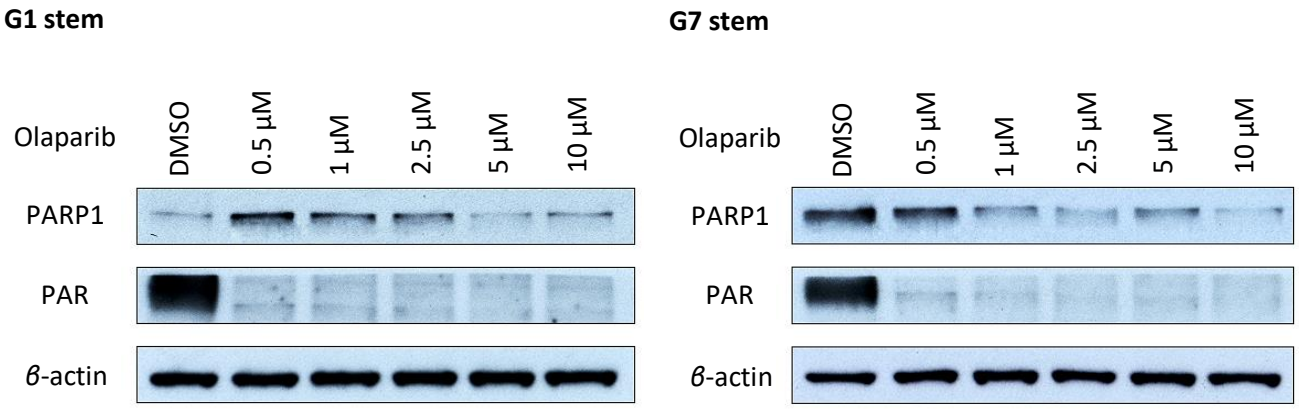

Figure 3.2. Inhibition of PARP1 activity in GSC using a PARPi.
G1 and G7 GSCs were treated overnight with either DMSO control or PARPi (Olaparib) at doses ranging between 0.5µM and 10µM. At the end of the 16-hour treatment, cells were harvested and protein samples were analysed by western blot. G1 and G7 exhibit high basal PARP activity and therefore PARP activity did not require stimulation by radiation treatment. Olaparib strongly inhibited PARylation of PARP1 at all doses tested in both G1 and G7 cells. *β*-actin was used as a loading control. It is unlikely that the total PARP1 levels seen in the DMSO control in G1 stem cells would be so low given the high levels of PARylation levels seen in this condition. Rather, the faint band seen in this condition may be due to problems in the transfer of the protein from the gel onto the membrane. Alternatively, insufficient incubation times or uneven distribution of antibodies and/or ECL reagents may also contribute to uneven staining of the membrane. Even PARP1 staining is demonstrated in further western blots presented in this thesis. n=1

3.2.2 Effects of PARP inhibition with radiation on TTFields response

Firstly, because TTFields has been shown to downregulate the BRCA1 gene and protein in both NSCLC and mesothelioma cell lines (314, 315), and that downregulation of HRR confers sensitivity to PARPi treatment, BRCA1 expression was assessed in G1 and G7 GSCs. TTFields downregulated expression of BRCA1 protein in G1 and G7 GSCs (figure 3.3a). Interestingly, preliminary data suggests that TTFields-mediated downregulation of BRCA1 could persist for up to 8-hours following removal of the TTFields treatment (figure 3.4.).

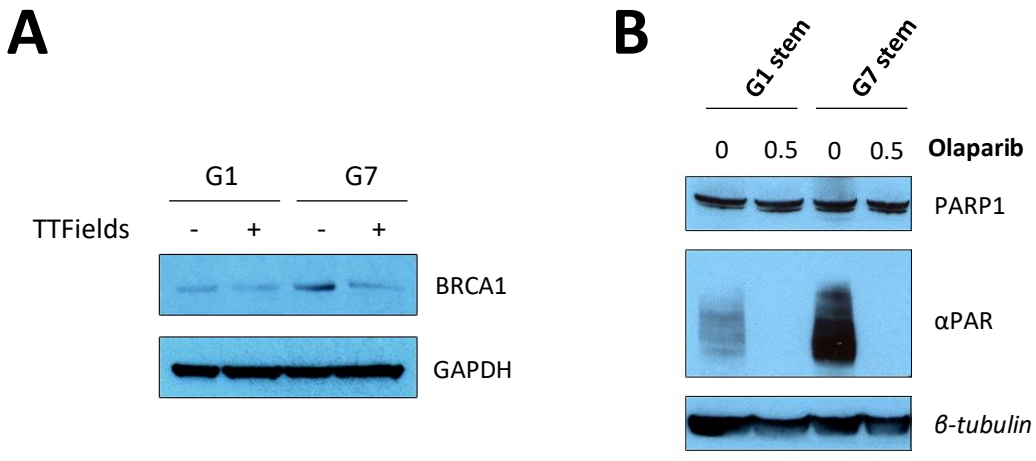

Figure 3.3. Baseline PARP activity of various glioma stem cell lines.
A. BRCA1 expression of G1 and G7 GSCs following TTFields treatment. GSCs were treated with or without TTFields and cells were harvested. BRCA1 expression was assessed via western blot. **B. Baseline PARP activity of G1 and G7 GSCs.** GSCs were treated with or without PARPi (500nM) overnight. Following PARPi treatment, cells were harvested and PARP activity of was assessed via western blot. Baseline PARP activity varies amongst GSC lines.n=1

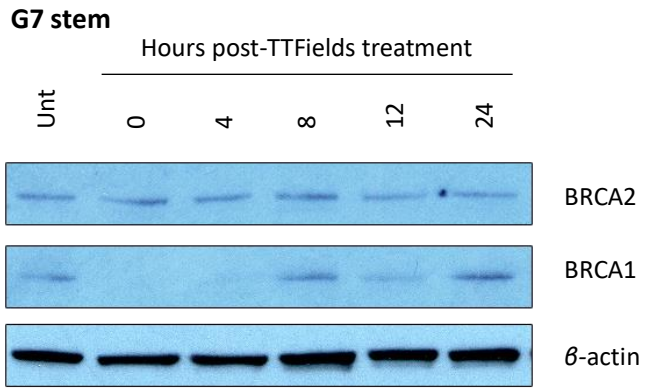

Figure 3.4. BRCA expression following TTFields treatment in G7 GSCs.
G7 stem cells were treated with and without TTFields. Cells were harvested at the indicated times post-TTFields treatment and expression BRCA proteins was assessed via western blot. BRCA1, but not BRCA2, protein levels were downregulated by TTFields. Downregulation of BRCA1 protein persisted for up to 4 hours and returned to baseline levels by 8 hours post-TTFields treatment. n=1

G1 and G7 stem cell lines were then treated with either radiation (2Gy – this is the fractionation dose given in the clinic), Olaparib (500nM), TTFields (200kHz – this is the only frequency that is clinically approved for the treatment of glioblastoma), or various combinations of these treatment as described in the methods section. The TTFields treatment was left to run for 48 hours. The duration of the treatment was determined based on the cell doubling time of G1 and G7 stem cells (1.3 and 1.6 days, respectively) (see figure 3.5.). Seeing as the most established effects of TTFields treatment are thought to be on mitosis, the recommended treatment duration is equated to one cell doubling time, based on the assumption that all cells should have attempted to go through at least one cycle of cell division, and would therefore have been susceptible to effects of TTFields treatment.

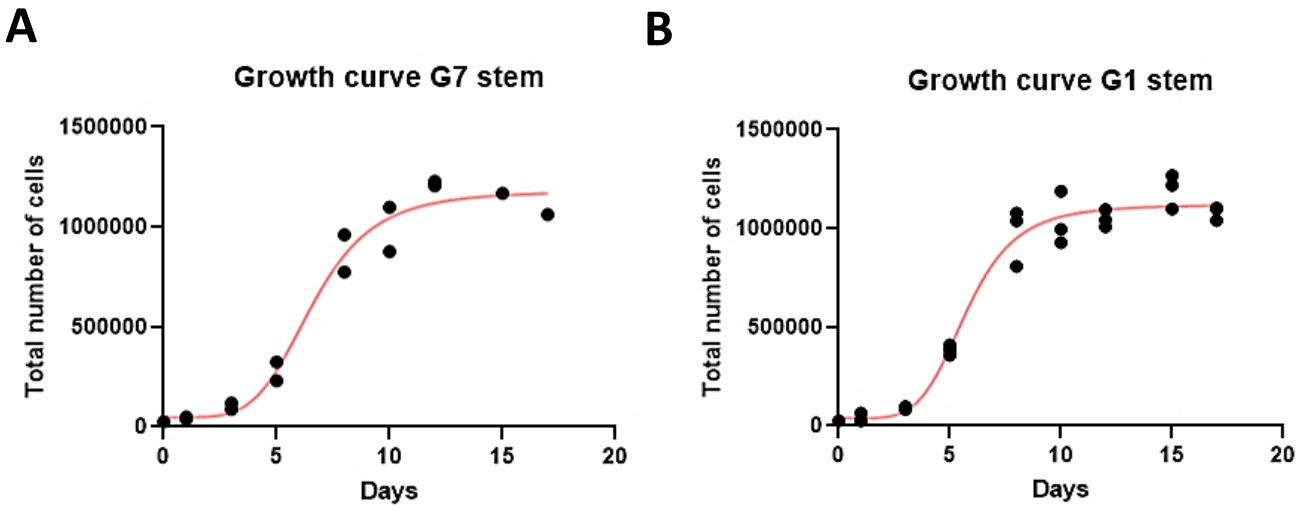

Figure 3.5. Cell doubling time of G1 and G7 stem cells.
G1 and G7 stem cells were plated at a density of $2.5x10^4$ cells/well and counted on the indicated days. Data points are from two independent repeats in **A.** Data points represent replicates of a single experiment in **B.** Data points were plotted in GraphPad and the line of best fit was drawn using 4 Parameter Logistic Regression model. The cell doubling time was calculated from the growth phase of the curve, using the equation presented in the methods. G7 stem cells have a cell doubling time of 1.6 days and G1 stem cells have a cell doubling time of 1.3 days. n≥2

At the end of treatment, G1 and G7 stem cells were lifted and counted for replating into 6-well Matrigel-coated plates and subjected to clonogenic survival assay. For subsequent clonogenic survival assays, all cells were grown in normal media (Adv. DMEM with supplements and growth factors) without DMSO or PARP inhibitor for the duration of the assay. The resulting clonogenic surviving fractions are shown in figure 3.6.

TTFields treatment alone significantly reduced clonogenic potential in G1 stem cells (30% reduction in surviving fraction) but not in G7 stem cells (only an 8% reduction in surviving fraction) (figure 3.6). This corroborates with what has previously been shown in the literature, with different cell lines displaying differential sensitivity to TTFields treatment. As expected, PARPi radiosensitised both G1 and G7 stem cells. However, this effect was not significant when compared with the IR-alone treated samples (significance not shown on graph). PARP inhibitor with TTFields only induced a modest decrease in survival fraction relative to the TTFields treatment alone in both cell lines (10% and 14% reduction in G7 and G1 stem cells, respectively). However, the addition of TTFields to PARP inhibitor enhanced the effects PARPi as a single agent on the surviving fraction of both cell lines (~30% reduction in survival in both cells lines).

Pre-treatment with radiation alone prior to TTFields exposure had a much more pronounced effect on reducing surviving fraction compared to pre-treatment with PARPi alone. However, relative to their matched controls (TTFields+IR vs IR and TTFields+Olap vs Olap), the sensitisation by radiation and PARP inhibitor alone to TTFields treatment was in fact comparable in both G1 and G7 stem cells. The most pronounced reduction in surviving fraction in G1 and G7 stem cells was seen when cells were pre-treated with both PARPi and radiation followed by TTFields treatment. However, the difference in surviving fraction did not reach significance when compared with the TTFields+IR group in both cell lines.

The full combination did significantly reduce the surviving fraction of G7 stem cells compared to cells treated with either the PARPi+2Gy combination, TTFields alone or compared to cells pre-treated with PARPi only before TTFields exposure. Interestingly, despite the difference in sensitivity to TTFields treatment, pre-treatment with PARPi and radiation together prior to TTFields treatment reduced the fraction of surviving cells by roughly the same amount in both cell lines compared to TTFields alone, with a ~64% and ~73% reduction in G1 and G7 stem cells, respectively. In fact, G7 stem cells, despite seemingly being more resistant to treatment in general, were sensitised slightly more by PARPi and radiation pre-treatment relative to the more sensitive G1 cell line, highlighting the benefit of using combination therapy in overcoming resistance. Nonetheless, G7 stem cells exhibited a smaller reduction in surviving fraction overall with TTFields+IR+Olap combination treatment compared to G1

stem cells (20% vs 6% surviving fraction, respectively) (figure 3.6). G7 GSCs also demonstrated increased PARP activity relative to G1 GSCs (figure 3.6b), which might explain the difference in sensitivity seen between these two cell lines to PARPi-based combinations.

Whilst the clonogenic survival assay measures the ability of a single cell to form a colony, changes in colony formation can be accounted for by commitment to different cell fates. For examples failure to form a colony could be due to the cells dying, or due to cells activating more cytostatic processes such as quiescent or senescent states. The follow-up experiments set out to assess the mechanisms driving these changes in colony formation abilities with the various treatments.

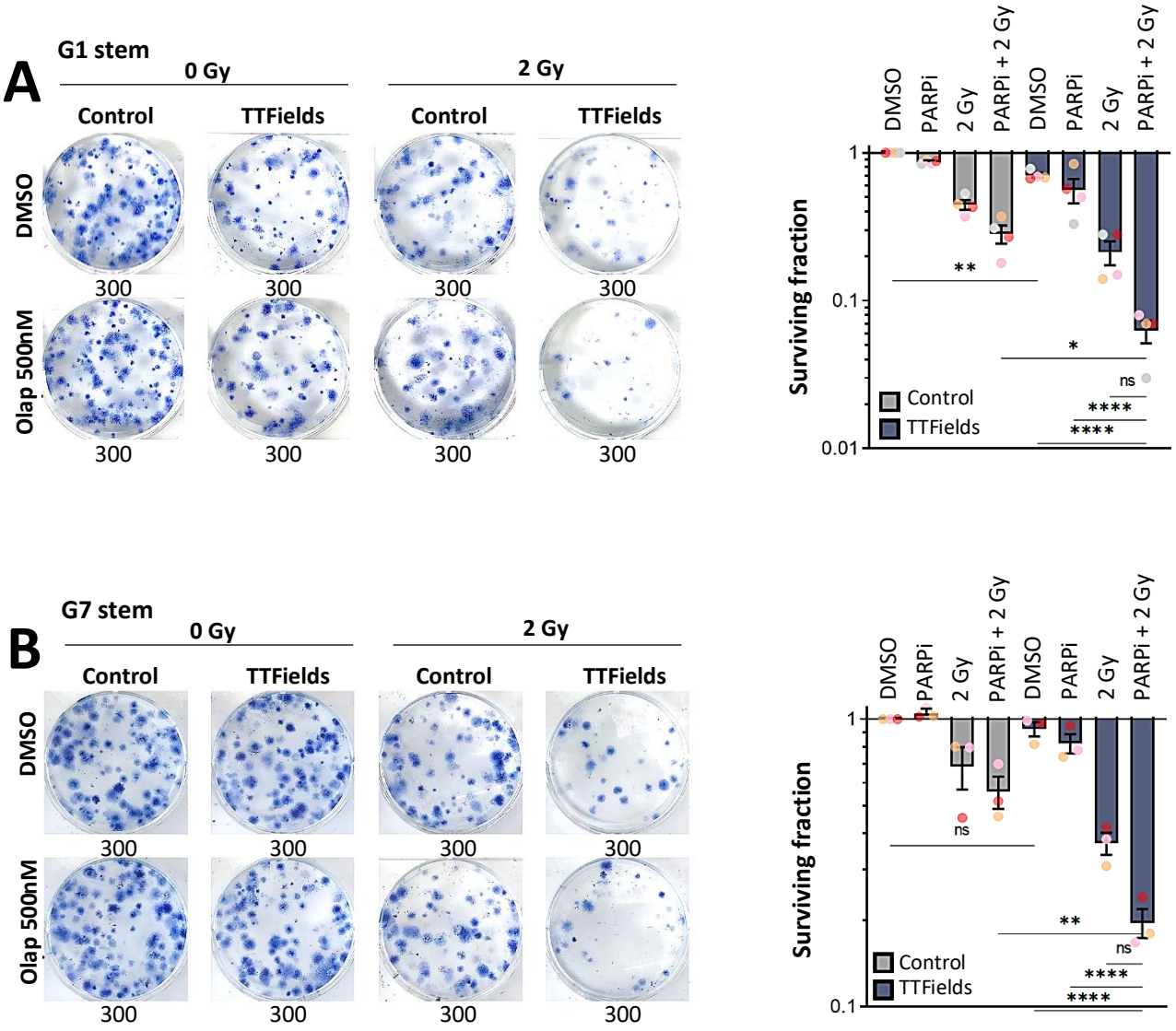

Figure 3.6. Clonogenic survival of G1 and G7 stem cells pre-treated with PARPi and radiation is reduced by TTFields. At the end of TTFields treatment, cells were replated in 6-well plates and the effects of the combination treatment on toxicity were assessed by clonogenic survival assay in G1 (**A.**) and G7 (**B.**) stem cells. Left – Representative images of the clonogenic survival in G1 and G7 stem cells. Right – Summary of the surviving fraction for each condition. Graph bars represent the mean of experimental replicates and individual dots representing each replicate. Error bars represent the standard error of the mean. n≥3

3.2.3 Cell death mechanisms

Given that the cells are replated at the end of treatment for the clonogenic survival assay, the effects of treatment on the induction of cell death pathways at the time of replating were assessed by Annexin V/PI stain and caspase-3/LC3B activation in order to determine whether immediate changes in the fraction of live to dead cells could account for the reduced clonogenicity previously seen.

When cells are healthy, there is an asymmetry between the components that make up the inner and outer leaflet of the cell membrane, with certain constituents being restricted to the inner leaflet, such as phosphatidylserine (PS). As cells undergo apoptosis, this asymmetry is lost, and PS presents itself on the outer leaflet. Whereas Annexin V cannot bind to PS restricted to inner leaflet, Annexin V binds to PS on the outer membrane of apoptotic cells and therefore demarks the apoptotic population. Healthy cells with intact cell membranes are impermeable to PI, but as cells become necrotic, cell membrane integrity is lost, rendering cells permeable to PI. PI-stained cells therefore represent the necrotic population. Cells devoid of Annexin V and PI stains mark the live cells (470). In both G1 and G7 stems cells there was no difference in the proportion of live, apoptotic and necrotic cells between all conditions as measured by Annexin V/PI stain (see figure 3.7). The same was seen 24 hours post-treatment (see supp figure 3.17). Caspase-3 cleavage denotes commitment to the apoptotic process and therefore serve as a marker of apoptosis (471). There was no difference in uncleaved caspase-3 (apoptotic marker) levels (see figure 3.8), corroborating the Annexin V data. Based on this data, there appears to be no induction of apoptosis across all treatment combinations.

In the absence of apoptosis and given that autophagy as a cell death pathway has been reported to be activated with TTFields treatment, the levels of LC3B protein, a marker of autophagy, were also assessed by western blot. During autophagy, LC3-I is converted to LC3-II and is recruited to the autophagic vesicle membrane. Changes in LC3-II levels can therefore be used to track the autophagic process. Again, there was no difference in LC3 signal via western blot across all conditions (see figure 3.8), suggesting that autophagy is not activated by these treatments. Together these data suggest that the cells are not dead or dying (by apoptosis or autophagy at least) at the time of replating and therefore unlikely to account for the treatment-induced changes in clonogenic potential.

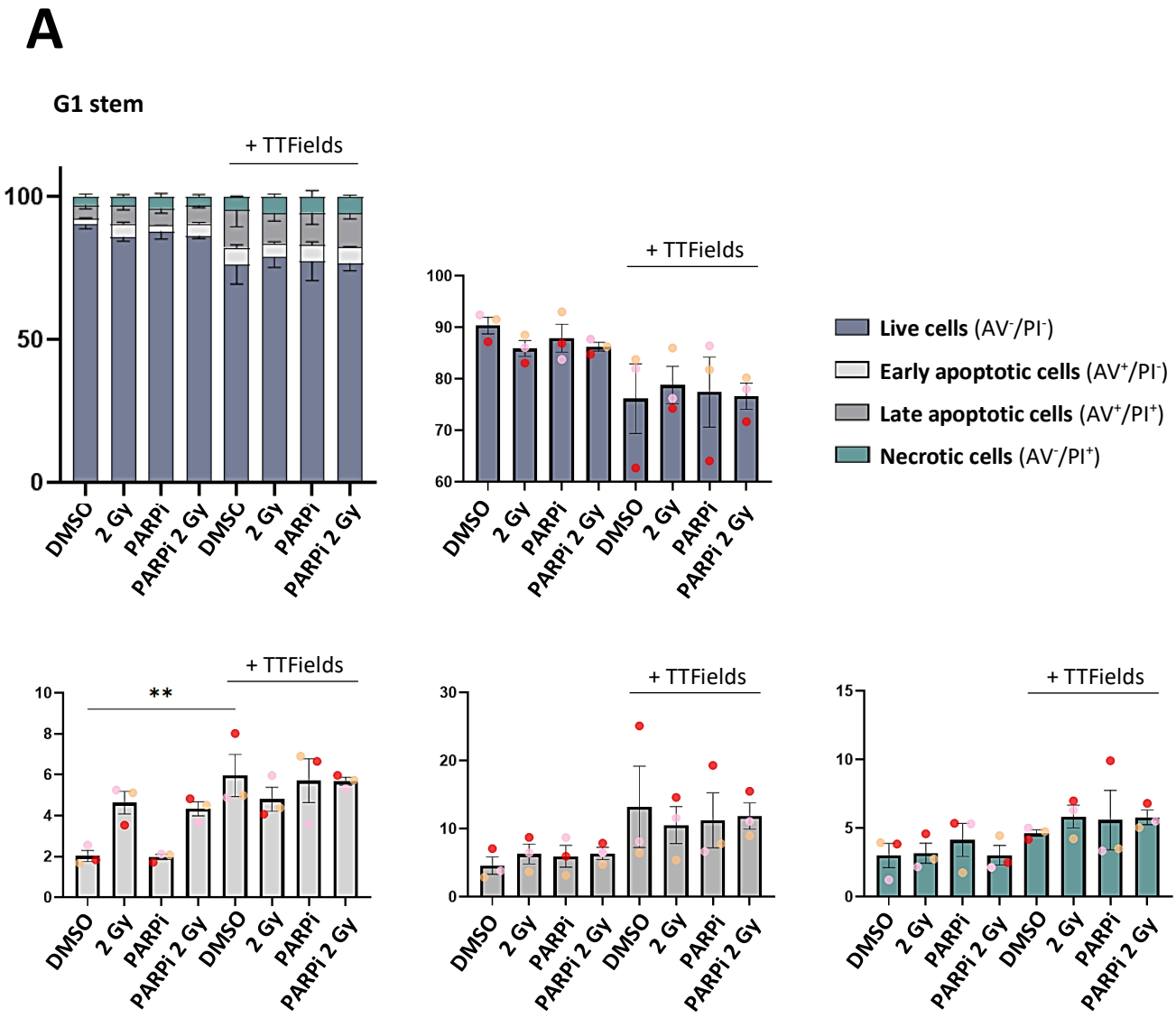
A
G1 stem
+ TTFields
100
50
0
DMSO
2 Gy
PARPi
PARPi 2 Gy
DMSO
2 Gy
PARPi
PARPi 2 Gy
+ TTFields
100
90
80
70
60
DMSO
2 Gy
PARPi
PARPi 2 Gy
DMSO
2 Gy
PARPi
PARPi 2 Gy
Live cells (AV-/PI-)
Early apoptotic cells (AV+/PI-)
Late apoptotic cells (AV+/PI+)
Necrotic cells (AV-/PI+)
+ TTFields
**
10
8
6
4
2
0
DMSO
2 Gy
PARPi
PARPi 2 Gy
DMSO
2 Gy
PARPi
PARPi 2 Gy
+ TTFields
30
20
10
0
DMSO
2 Gy
PARPi
PARPi 2 Gy
DMSO
2 Gy
PARPi
PARPi 2 Gy
+ TTFields
15
10
5
0
DMSO
2 Gy
PARPi
PARPi 2 Gy
DMSO
2 Gy
PARPi
PARPi 2 Gy

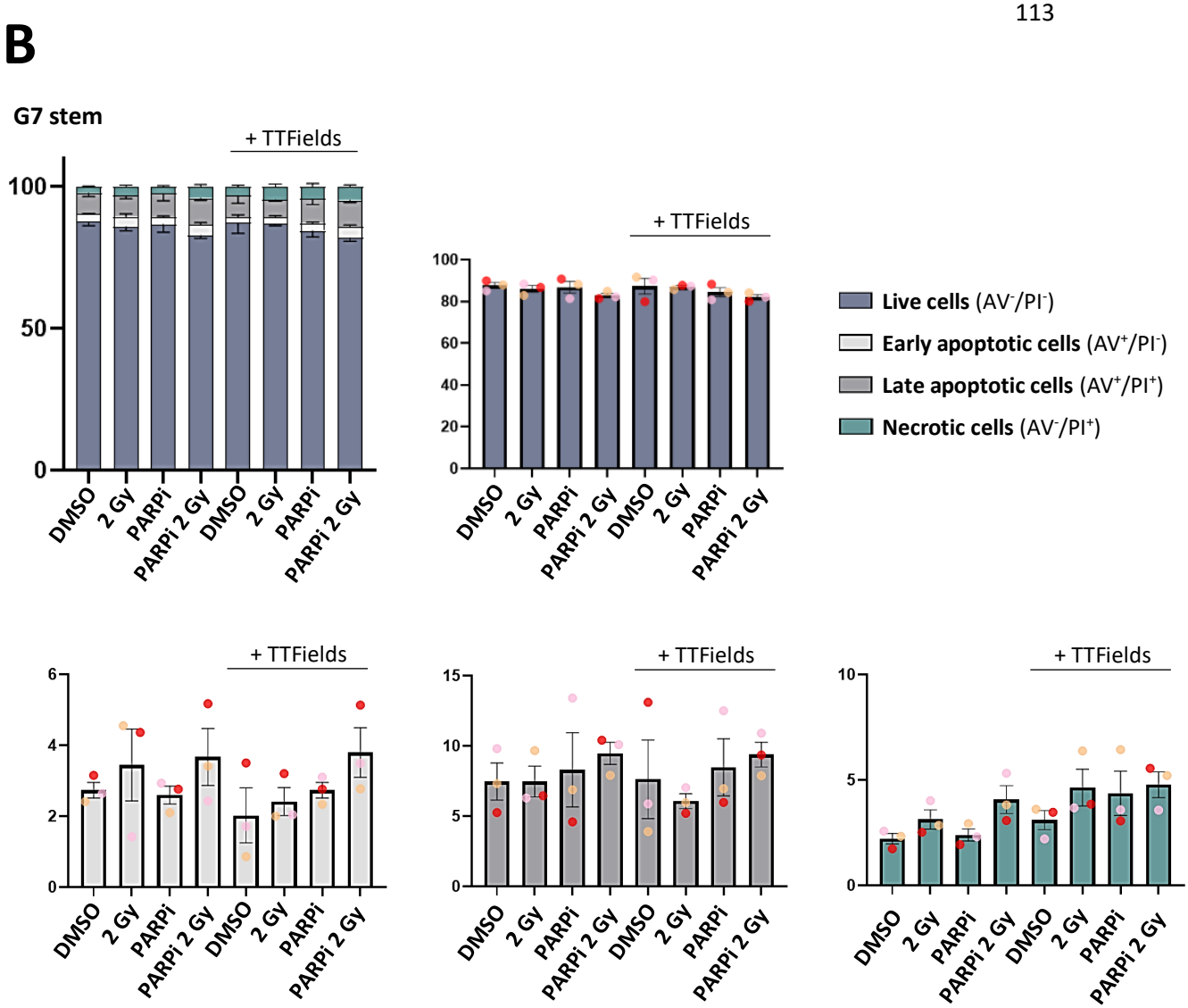

Figure 3.7. Treatment with PARPi, IR and TTFields either alone or in combination does not induce activation of apoptosis.

Following treatment, G1 (**A.**) and G7 (**B.**) stem cells were collected and analysed for Annexin V/PI staining via flow cytometry to assess the effects of treatment on the induction of apoptosis. There was no significant difference in induction of apoptosis across all conditions in both cell lines immediately after treatment completion. Error bars represent the standard deviation of the mean, with individual repeats represented as differently coloured dots. n=3

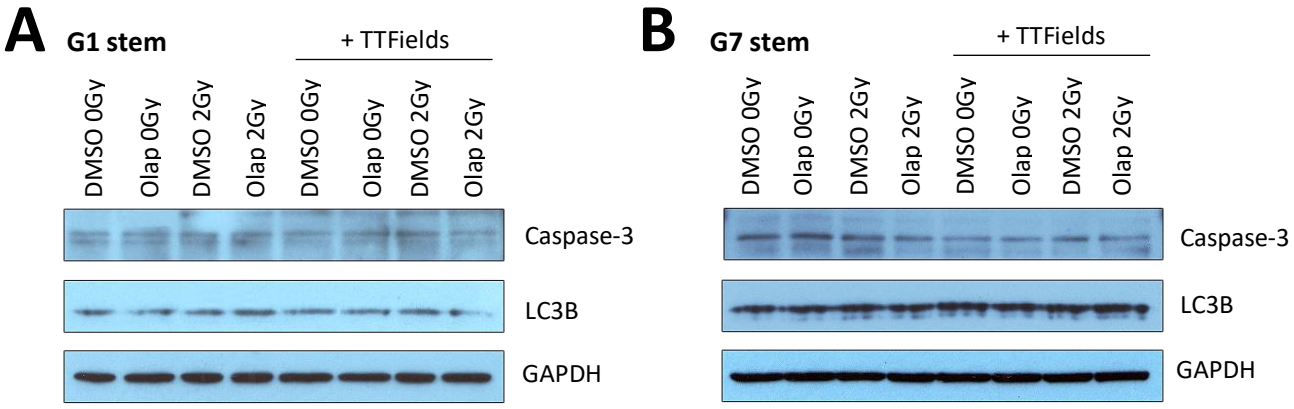

Figure 3.8. Treatment with PARPi, IR and TTFields either alone or in combination does not induce activation of autophagy.

Following treatment, G1 (**A.**) and G7 (**B.**) stem cells were collected and probed for caspase-3 and LC3B via western blot to assess the effects of treatment on the induction of apoptosis and autophagy, respectively. There were no changes in caspase-3 and LC3B across all conditions in both G1 and G7 stem cells. n=2

3.2.4 Effects of PARP inhibition in combination with radiation and TTFields on DNA damage induction

Next, the effects of treatment on DNA damage induction were assessed indirectly by γH2AX, a global DNA damage marker, and 53BP1, a DSB marker, foci formation via immunofluorescence and directly by the alkaline comet assay.

Upon DNA damage induction, the histone variant H2AX becomes rapidly phosphorylated at S139 (γH2AX) near the site of damage and serves to unwind the compact chromatin structure and acts as a scaffold for the recruitment of repair factors required for the resolution of the damage. H2AX phosphorylation extends several megabases and forms discreet foci that can be visualised and quantified by immunofluorescence (472). H2AX is phosphorylated by the PI3K family of enzymes and therefore serves as a marker for all types of DNA damage (473-475). 53BP1 on the other hand is exclusively recruited to DSBs via its Tudor domain by a DSB-specific histone code (including H4K20me1 and H4K20me2 and γH2AX itself) and therefore is a marker for DSBs specifically (476-478). 53BP1 is mainly involved in DSBR pathway choice, but 53BP1 has also been suggested to amplify ATM signalling and recruit proteins involved in the repair of DSBs (479-481).

TTFields treatment alone did not significantly induce either γH2AX- or 53BP1-foci formation in both G1 stem and G7 stem cells (figure 3.9), suggesting that TTFields treatment alone does not significantly induce DNA lesions in these cell lines. In G7 stem cells, TTFields treatment significantly enhanced both γH2AX- or 53BP1-foci formation in cells pre-treated with PARPi and IR together compared to cells receiving PARPi and IR treatment only (48.7% positive γH2AX cells vs 23%, and 2.5 53BP1 foci/cell vs 3.8). γH2AX- or 53BP1-foci formation were also increased in the full combination group relative to all other TTFields-treated combinations (TTF alone, TTFields+IR and TTFields+Olap) (figure 3.7b).

TTFields did not significantly enhance 53BP1 foci formation following pre-treatment with Olaparib and IR in combination in G1 stem cells compared to cells not receiving TTFields treatment, although there was a significant increase in the percentage of cells with positive γH2AX staining (54% vs 26.6%) (figure 3.9a). Whilst foci formation was significantly enhanced for 53BP1 with the full combination treatment compared to all other TTFields-treated combinations, this was not the case for γH2AX foci, which only achieved significance when compared with the TTFields monotherapy group (figure 3.9a).

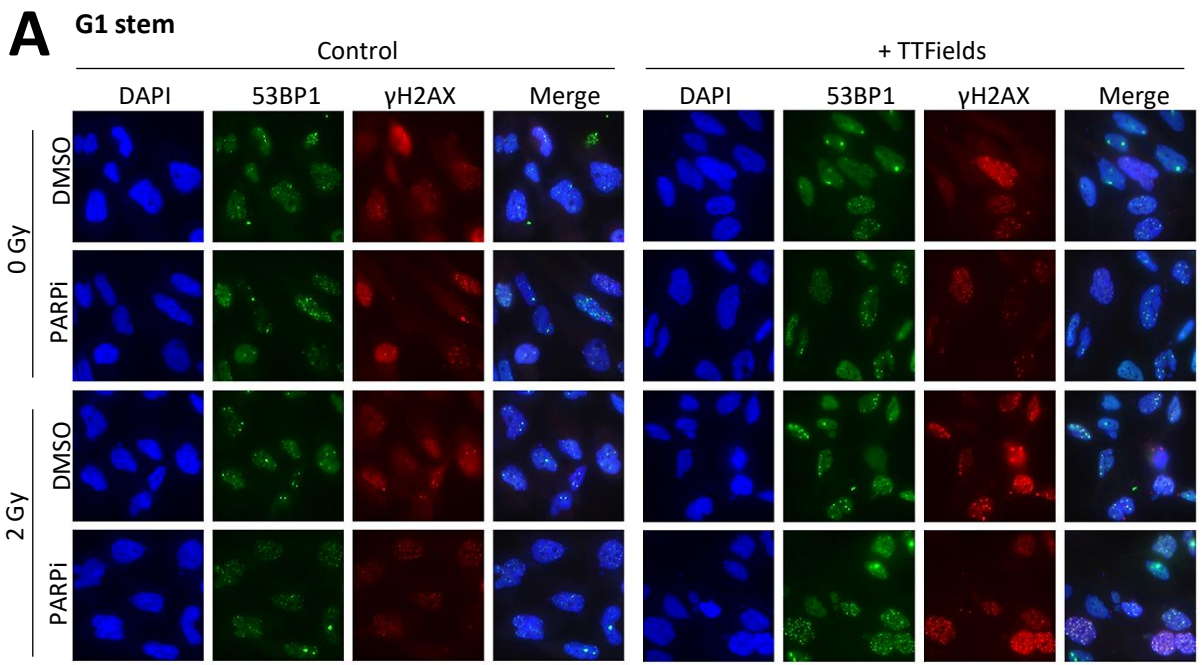
A
G1 stem
Control
+ TTFields
DAPI
53BP1
γH2AX
Merge
0 Gy
2 Gy
DMSO
PARPi

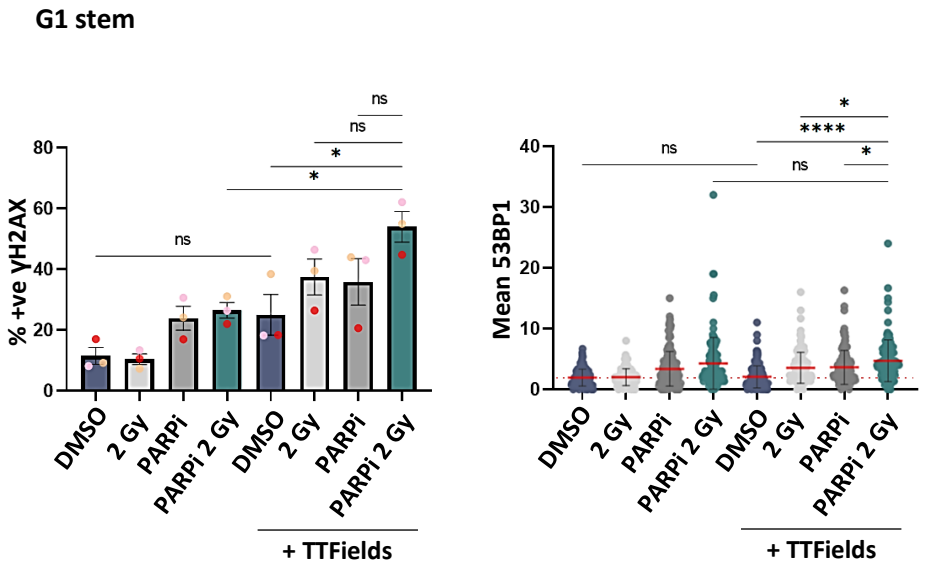
G1 stem
% +ve γH2AX
Mean 53BP1
DMSO
2 Gy
PARPi
PARPi 2 Gy
+ TTFields
ns

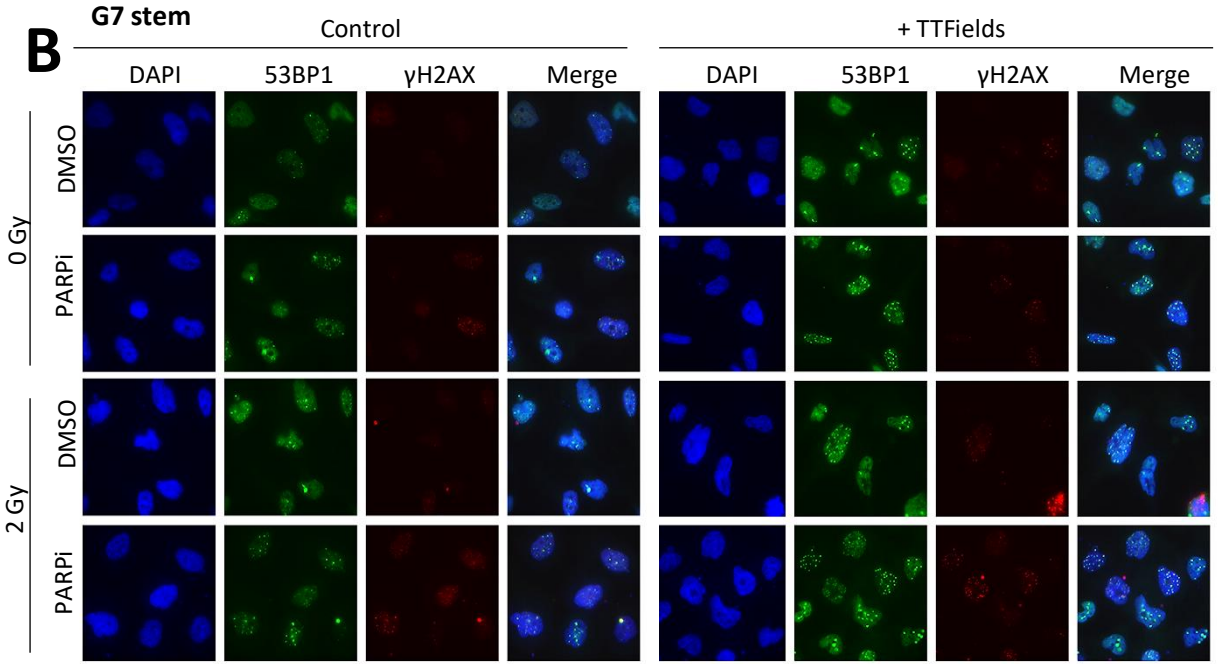
B
G7 stem
Control
+ TTFields
DAPI
53BP1
γH2AX
Merge
0 Gy
2 Gy
DMSO
PARPi

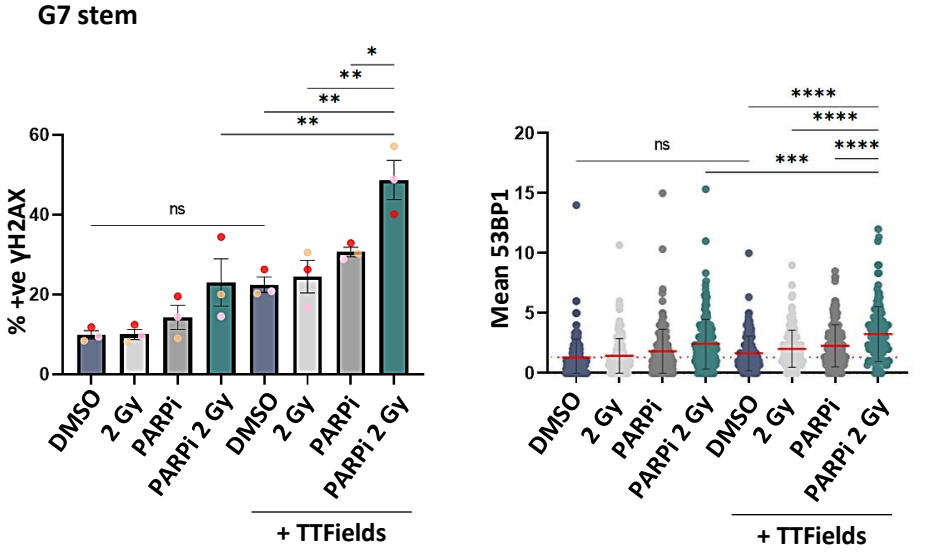
G7 stem
% +ve γH2AX
Mean 53BP1
DMSO
2 Gy
PARPi
PARPi 2 Gy
+ TTFields
ns

Figure 3.9. The effects of treatment with PARPi, IR and TTFields either alone or in combination on DNA damage induction in G1 and G7 stem cells.
The effects of treatment on DNA damage induction were assessed via γH2AX- and 53BP1-foci quantification using immunofluorescence in both G1 (**A.**) and G7 (**B.**) stem cells. Left – Representative images. Right – Bar charts showing the percentage of cells showing positive γH2AX staining (≥5foci/cell), where graph bars represent the mean of experimental replicates and individual dots representing each replicate. The error bars from the bar charts represent the standard error of the mean (SEM). Dot plots demonstrate the number of 53BP1 foci/cell, where each dot represents an individual cell, and the red line represents the mean +- standard deviation (SD). n=3

The alkaline comet assay operates on the basis that DNA is negatively charged and can be pulled out of the nucleus when a current is applied. When the DNA is intact in healthy cells, the DNA is supercoiled and cannot migrate far out of the nucleus and remains in the 'head' of the comet. When the DNA is damaged, broken fragments of uncoiled DNA are pulled out of the nucleus, producing what appears as a 'tail' protruding out of the 'head'. The length of the tail is proportional to amount of damage. However, there is limit to how much the tail can run. Any additional damage beyond this limit is reflected by changes in the intensity of the tail. The tail moment accounts for both the tail length and the tail intensity (=% DNA in tail). The alkaline comet assay detects all types of SSBs, including those that form as intermediates in the BER and NER repair processes and those formed from alkali-labile sites under alkaline conditions. The alkaline comet assay can detect DSBs but is considered more sensitive to the detection of SSBs (482). SSBs are the most common type of damage induced by IR, therefore the alkaline Comet assay was chosen to give a holistic readout of DNA damage within the combination treated cells.

Whilst there was no difference in tail moment of control and TTFields-treated G7 stem cells in the alkaline comet assay (figure 3.10b), the tail moment of G1 stem cells were significantly increased by TTFields treatment which, in contrast to the immunofluorescence data, would indicate that TTFields induces DNA damage in G1 stem cells (figure 3.10a). The average tail moment of G1 stem cells pre-treated with PARPi and IR together followed by exposure to TTFields was enhanced compared with cells pre-treated with either Olap or IR alone, but there was no significant increase when compared with cells receiving TTFields treatment only (figure 3.10a). In G7 stem cells, full combination treatment significantly enhanced the tail moment of cells when compared with TTFields alone treatment, but not when compared with TTFields + Olap or IR or compared to treatment with PARP inhibitor with IR but without TTFields (figure 3.10b).

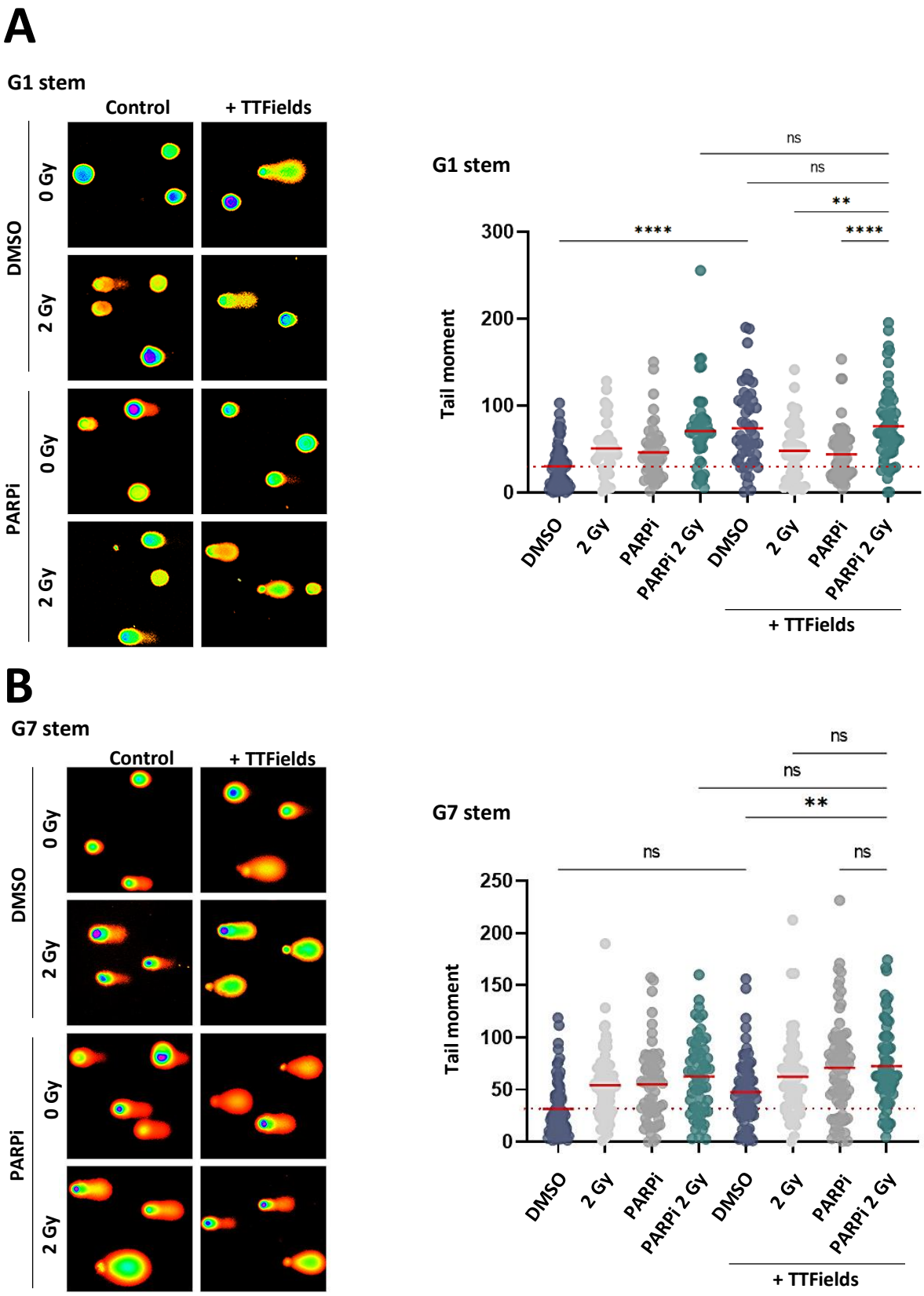

Figure 3.10. The effects of treatment with PARPi, IR and TTFields either alone or in combination on DNA damage induction in G1 and G7 stem cells.

The effects of treatment on DNA damage induction were assessed via alkaline comet assay in both G1 (**A.**) and G7 (**B.**) stem cells. Representative images for the alkaline comet assay. Right – Dot plots showing the tail moment of individual cells, with the red line showing the mean for each condition. n=3

3.2.5 Effects of PARP inhibition in combination with radiation and TTFields on replication stress

Given that TTFields has been shown to enhance replication stress by downregulation of BRCA and FA repair pathway genes and that PARP1 is important for replication fork stabilisation during replication stress (discussed in section 1.2.4), the effects of treatment on replication stress were assessed. RPA rapidly binds to exposed ssDNA formed during replication stress or during various DNA repair processes. RPA is then phosphorylated at several sites by DNA repair proteins to mediate the repair process. For example, RPA32 is phosphorylated at T21 by ATR during replication stress, activating cell cycle checkpoints and promoting DNA repair through the recruitment of DDR factors (483). RPA form foci that can be visualised with immunofluorescent imaging and RPA foci quantification is commonly used as a measure of replication stress.

Exposure to TTFields enhance the formation of p-RPA32(T21) foci in G1 stem cells compared to the untreated control (9.2 vs 3.7 foci/cell, respectively), suggesting that TTFields enhances levels of replication stress in these cells (figure 3.11a). TTFields treatment with either PARPi or radiation alone induced comparable levels of replication stress (11.3 vs 12.9 foci/cell, respectively). G1 stem cells treated with PARPi and radiation in combination enhanced levels of replication stress relative to control (5.8 foci/cell), but this was further increased when followed with TTFields treatment (17.5 foci/cell). Surprisingly, there was no significant change in p-RPA32(T21) foci formation with the various treatment combination in G7 stem cells (figure 3.11b).

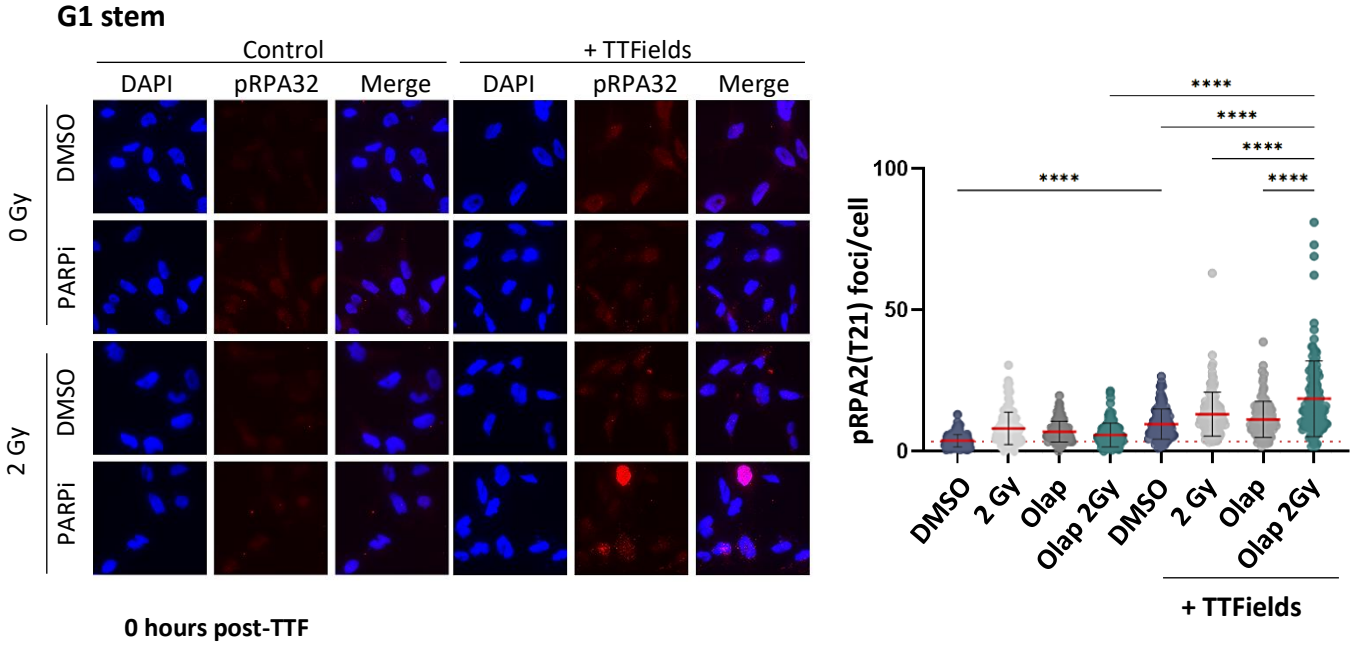

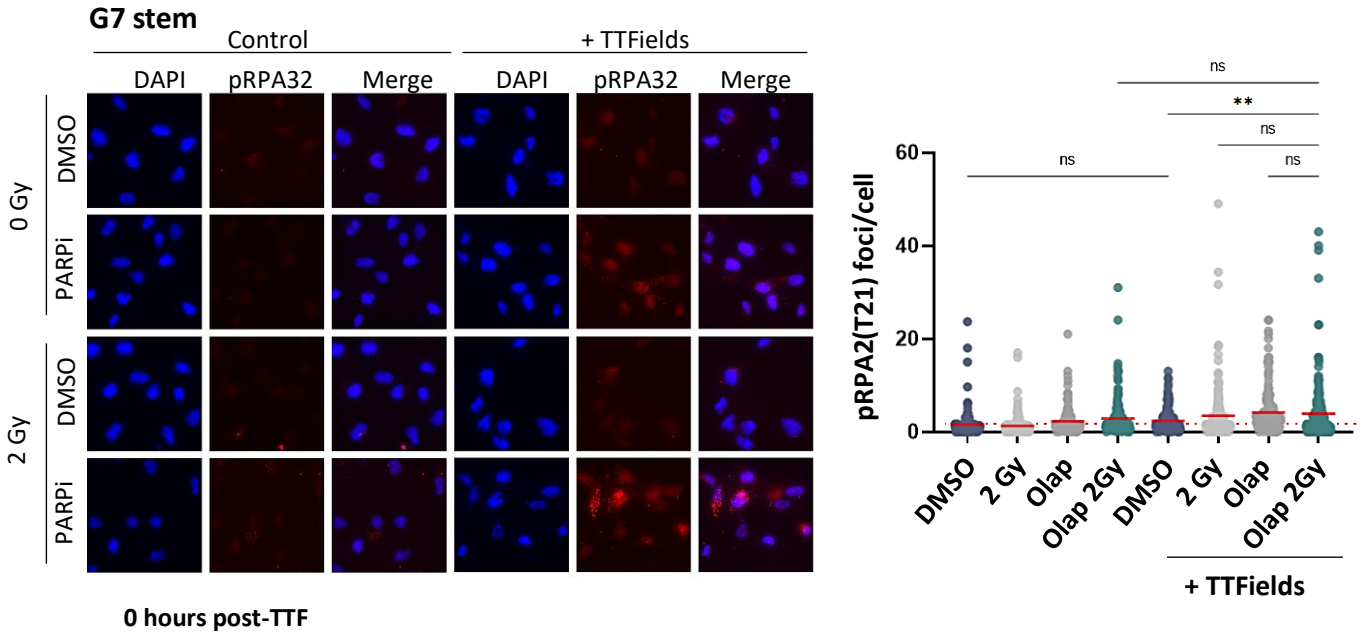

Figure 3.11. The effects of treatment with PARPi, radiation and TTFields either alone or in combination on pRPA32(T21) levels.
G1 and G7 stem cells were stained for p-RPA32(21) foci and quantified by immunofluorescence. Left shows representative images and right shows dot plots demonstrating the number of p-RPA32(T21) foci/cell, where each dot represents an individual cell and the red line = mean +- SD. n=3

3.2.6 Combination treatment with PARP inhibitor, radiation and TTFields impedes DNA damage repair.

To determine the downstream effects of the combination treatments on the DDR, the repair of induced DNA damage was assessed by tracking γH2AX and 53BP1 foci over a period of 24 hours (samples were collected at 0-, 4- and 24-hours post-treatment completion; figure 3.12-13). Persistent foci overtime indicates either continual DNA damage induction and/or failure to repair DNA damage.

The percentage of cells demonstrating positive γH2AX staining and the number of 53BP1 foci per cell peaked 4 hours post-treatment in G7 stem cells exposed to TTFields following pre-treatment with PARPi and IR in combination (figure 3.12b), jumping from 46.8% up to 57% H2AX positive cells and 2.7 up to 5.3 53BP1 foci per cell at 0- and 4-hours post-treatment, respectively (figure 3.13b). From 4 hours onwards, G7 stem cells started repairing damage as measured by a drop in the percentage of γH2AX positive cells (43.1%) and the number of 53BP1 foci per cell (4.8) at 24 hours post-treatment completion. G7 stem cells treated with PARPi, IR and TTFields sustained the highest amount of γH2AX- and 53BP1-foci 24 hours post-treatment compared to other treatment conditions, indicating persistent DNA damage burden and impaired repair kinetics.

G1 stem cells pre-treated with PARPi and radiation in combination prior to TTFields treatment sustained more 53BP1- and γH2AX-foci 24-hours post TTFields treatment, with 47.5% γH2AX-postive cells (comparable to G7 stem cells) remaining and a mean 9 53BP1 foci per cell (almost double that of

G7 stem cells) (figure 3.12a and figure 3.13a). G1 stem cells sustained more DSBs in comparison to G7 stem cells and carried more DSBs under basal conditions compared to G7 stem cells (4.1 vs 2 53BP1 foci per cell, respectively), which might explain why they are more sensitive to treatment.

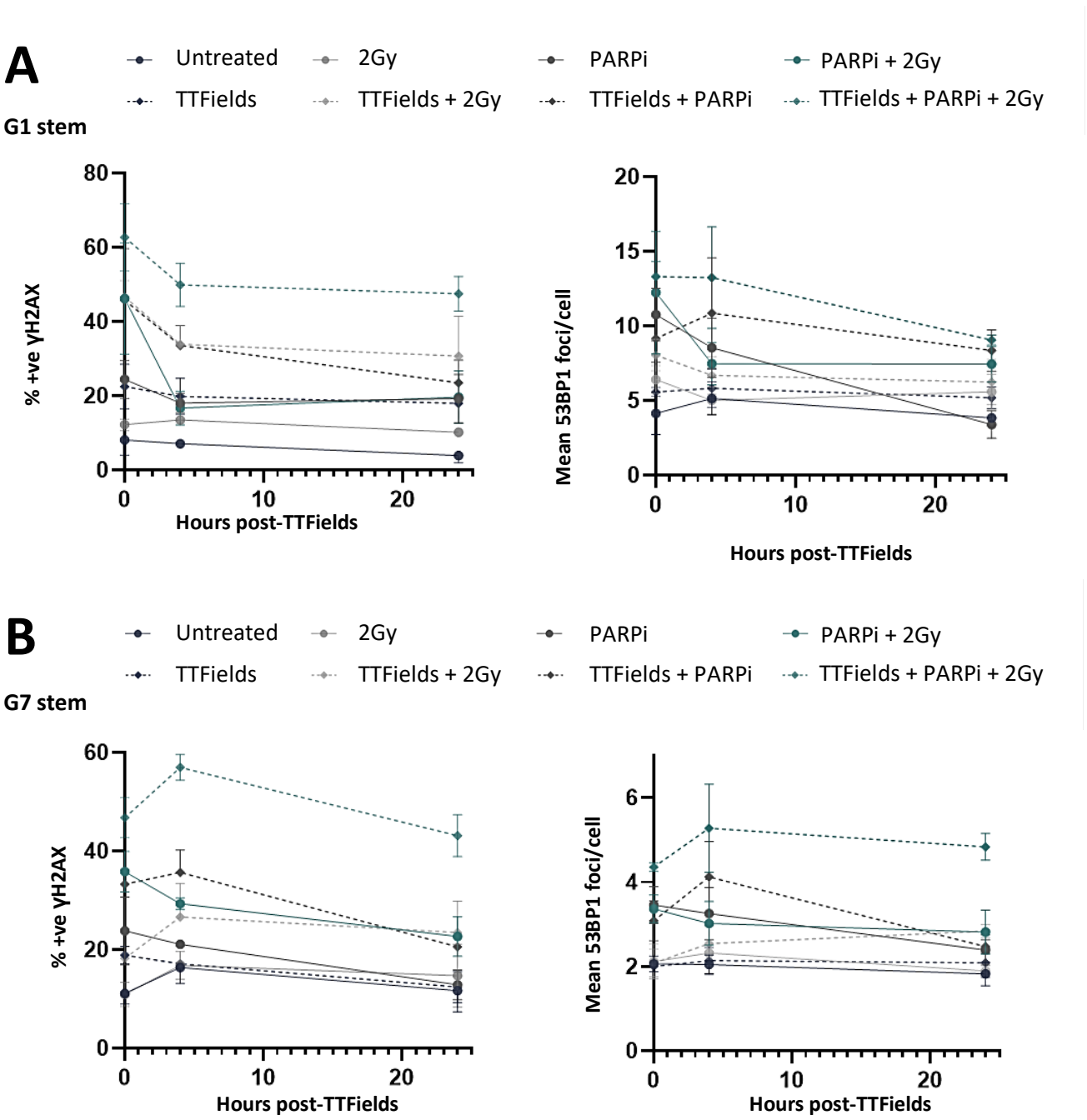

Figure 3.12. The effects of PARPi, IR and TTFields either alone or in combination on the resolution of γH2AX- and 53BP1-foci formation.
The effects of combination treatment with TTFields/Olap/IR on DNA damage repair were assessed in G1 (**A.**) and G7 (**B.**) stem cells. Cells were fixed at 0-, 4- and 24-hours following completion of TTFields treatment. Cells were subsequently stained for γH2AX and 53BP1. Figures shows the summary line graph for γH2AX and 53BP1 for the timecourse experiment in G1 and G7 stem cells, respectively. n=3

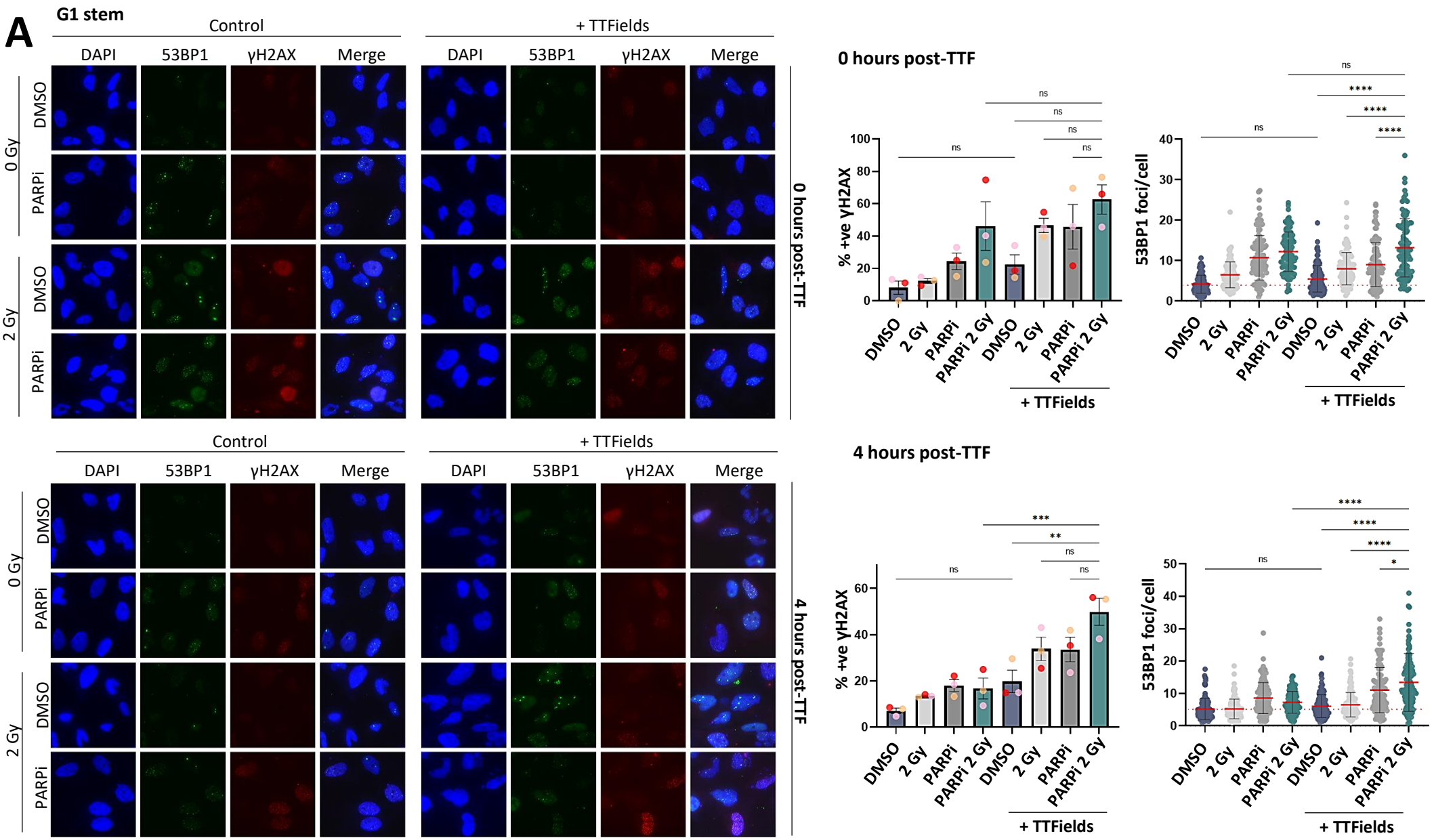
A
G1 stem
Control
+ TTFields
DAPI
53BP1
γH2AX
Merge
0 Gy
2 Gy
DMSO
PARPi
0 hours post-TTF
4 hours post-TTF
0 hours post-TTF
4 hours post-TTF
% +ve γH2AX
53BP1 foci/cell
ns
*
**
***
****
DMSO
2 Gy
PARPi
PARPi 2 Gy
+ TTFields

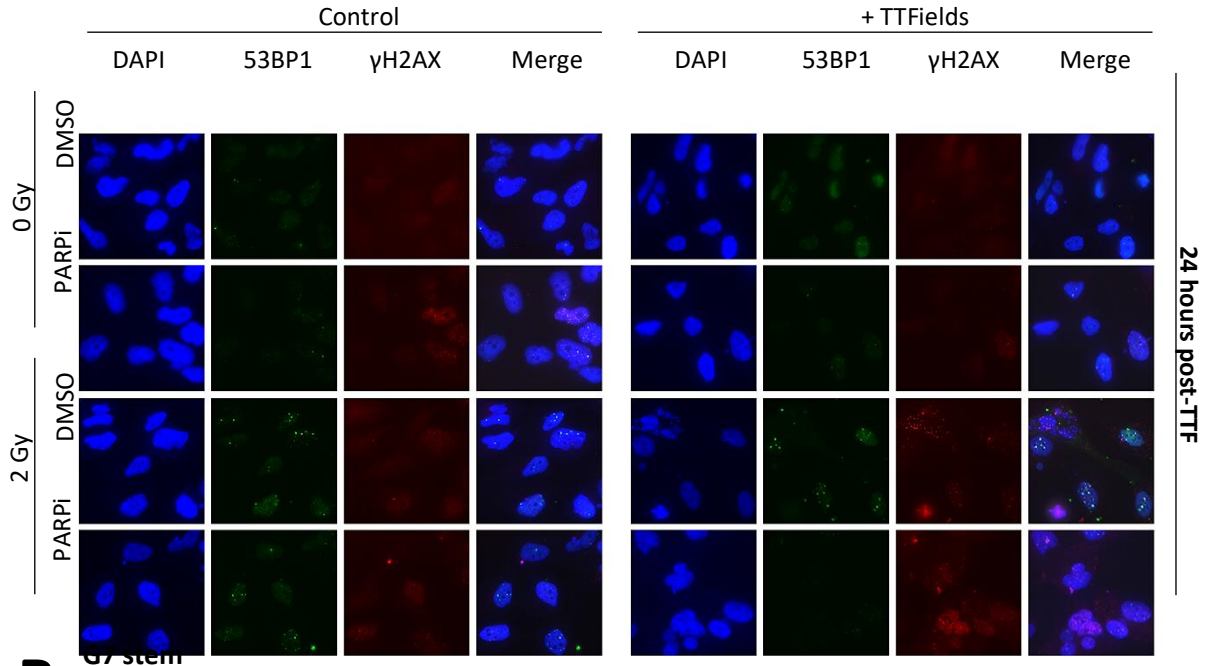
Control
+ TTFields
DAPI
53BP1
γH2AX
Merge
0 Gy
2 Gy
DMSO
PARPi
24 hours post-TTF

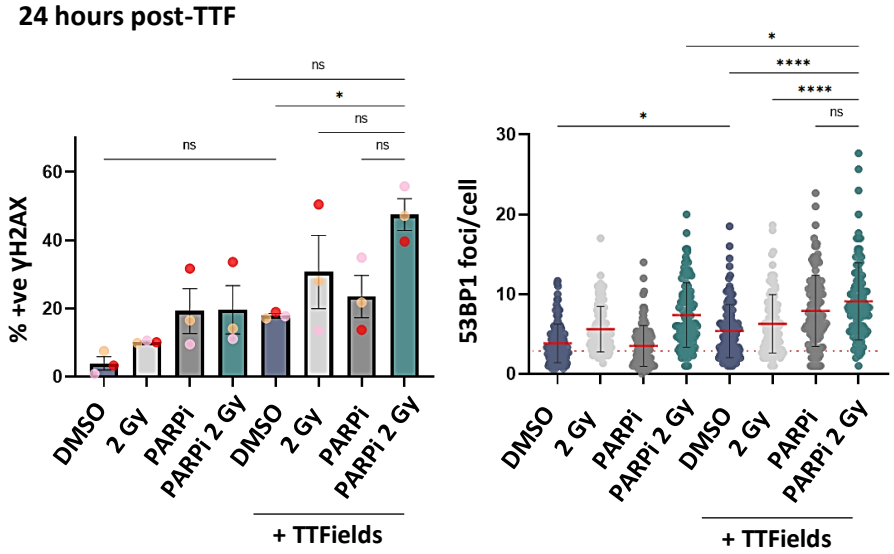
24 hours post-TTF
% +ve γH2AX
53BP1 foci/cell
DMSO
2 Gy
PARPi
PARPi 2 Gy
+ TTFields
ns
*
****

B

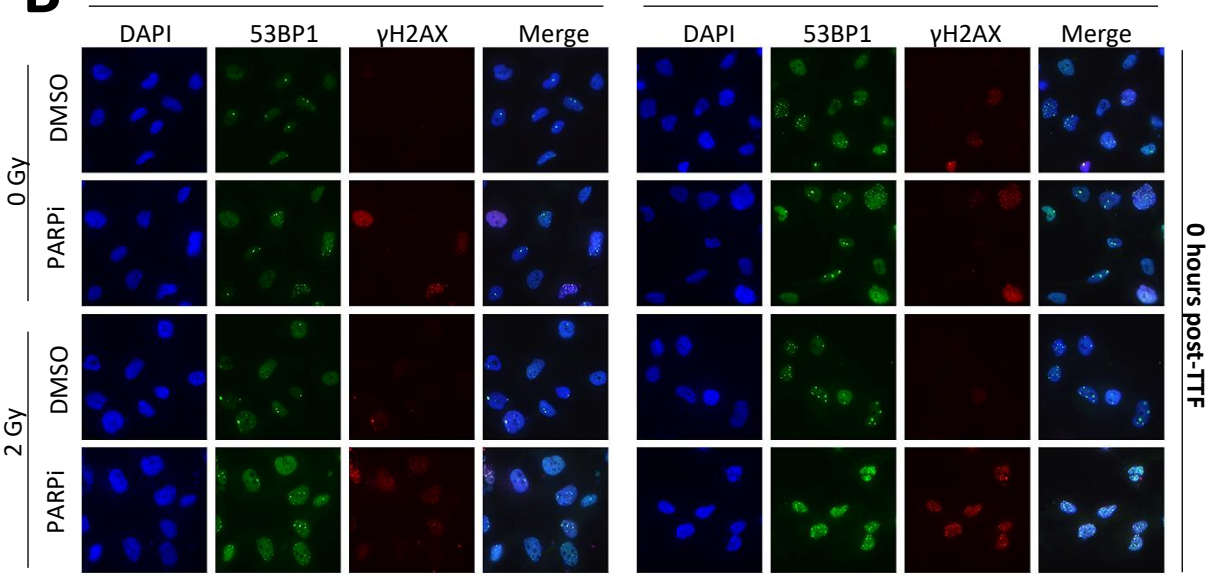
Control
+ TTFields
DAPI
53BP1
γH2AX
Merge
0 Gy
2 Gy
DMSO
PARPi
0 hours post-TTF

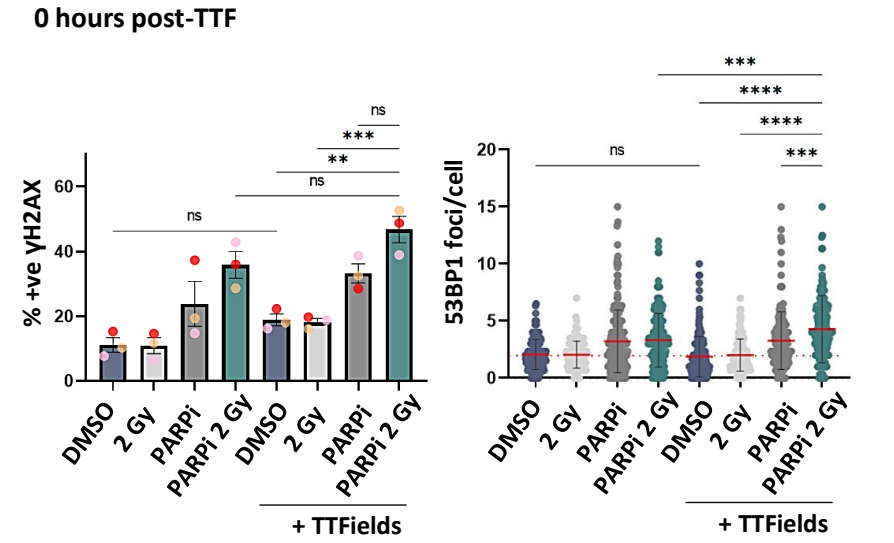
0 hours post-TTF
% +ve γH2AX
53BP1 foci/cell
DMSO
2 Gy
PARPi
PARPi 2 Gy
+ TTFields
ns
***
****

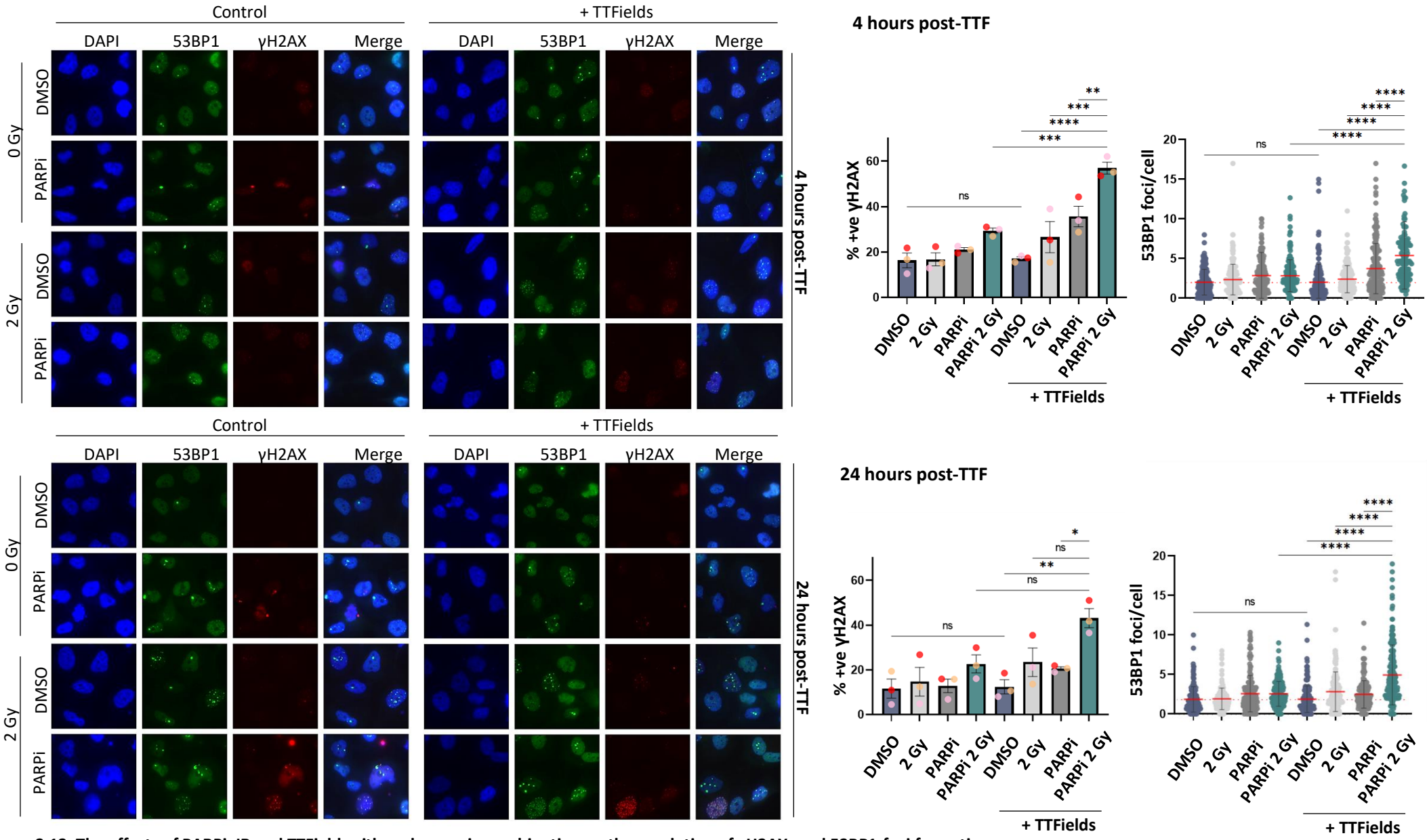

Figure 3.13. The effects of PARPi, IR and TTFields either alone or in combination on the resolution of γH2AX- and 53BP1-foci formation.
The effects of combination treatment with TTFields/Olap/IR on DNA damage repair were assessed in G1 (**A.**) and G7 (**B.**) stem cells. Cells were fixed at 0-, 4- and 24-hours following completion of TTFields treatment. Cells were subsequently stained for γH2AX and 53BP1. **A.** and **C.** Left – Representative images. Right – Bar charts showing the percentage of cells showing positive γH2AX staining (≥5foci/cell) at 0-, 4- and 24-hours post-TTFields treatment. Graph bars represent the mean of experimental replicates +- SESM, and individual dots representing each repeat. Dot plots showing the number of 53BP1 foci/cell at 0-, 4- and 24-hours post-TTFields treatment. Each dot represents an individual cell and the red line = mean +- SD. n=3

3.2.7 Effects of PARP inhibition with temozolomide on TTFields response

Given that temozolomide is the chemotherapeutic agent most frequently used for the treatment of glioblastoma (92, 125), the effects of PARP inhibition with and without radiation on TTFields response in GSCs were assessed. The same treatment scheduling was used as for the IR combinations; however, cells were treated with 5 µM TMZ instead of 2 Gy IR. A dose of 5 µM TMZ was selected because this is the dose that has been shown to reach the tumour in the clinic (484, 485). Effects of the combination treatment on survival of G7 stem cells were assessed by clonogenic survival assay (figure 3.14.). Due to time restrictions, this combination was assessed in G7 stem cells only. PARP inhibitor alone enhanced TMZ sensitivity in G7 stem cells. Additional treatment with TTFields further enhanced PARPi-mediated chemo-sensitisation of G7 stem cells reflected by a ~35% reduction in surviving fraction compared to cells treated with PARPi and TMZ. Cells pre-treated with both PARPi and TMZ followed by TTFields exposure significantly reduced the surviving fraction of G7 stem cells by ~41% and ~33% compared with cells pre-treated with PARPi or TMZ alone, respectively. As previously shown, TTFields alone did not significantly reduce the surviving fraction of G7 stem cells (~11%).

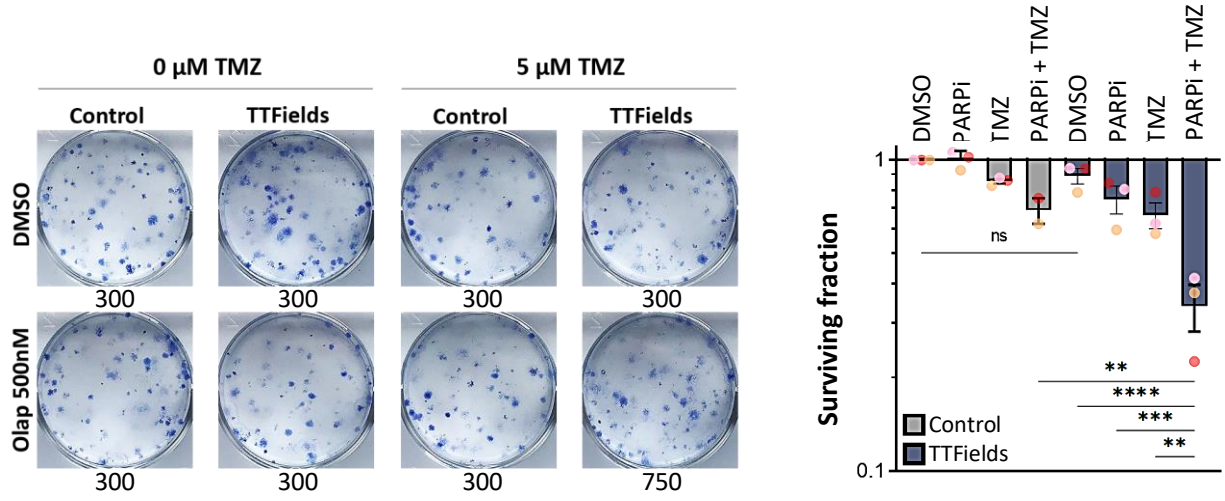

Figure 3.14. Survival of G7 stem cells pre-treated with PARPi and TMZ is further reduced by TTFields treatment. The effects of treatment on survival of G7 stem cells were assessed by clonogenic survival assay. Left – Representative images, with numbers showing the number of cells plates for each condition. Right – Graph bars represent the mean of experimental replicates and individual dots representing each replicate. Error bars represent SEM. n=3

Seeing as MGMT status mediates TMZ sensitivity, MGMT protein levels were assessed via western blot. Based on patient histology, G1 and G7 stem cells were not expected to express MGMT, whereas OX5-core and edge cells were derived from patients known to express MGMT. Therefore, OX5 cells

were used as a positive control. As expected, MGMT protein levels were not detectable in G1 and G7 stem cells, whereas OX5 cells expressed MGMT (figure 3.15).

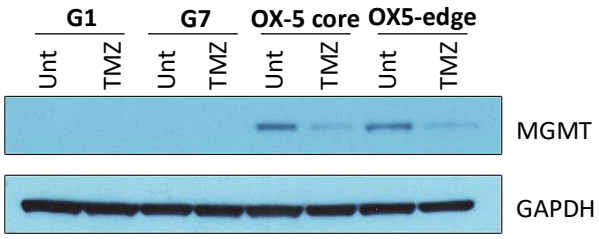

Figure 3.15. MGMT protein expression in GSCs.

MGMT protein expression of various GSCs was assessed via western blot, both following treatment with TMZ and without. TMZ is a known inducer of O^6-MeG lesions which are repaired by the MGMT enzyme. G1 and G7 GSCs do not express MGMT, whilst OX5-core and edge GSCs express MGMT. MGMT is a suicide enzyme, therefore, MGMT expression is reduced in OX5-core and edge GSCs following 4-hour treatment with TMZ, indicative of MGMT repair activity. n=1

3.3 Discussion

PARP is one of the key players in the DDR and acts as a first responder to DNA damage where it binds different types of lesions, including SSBs and DSBs, and mediates recruitment of downstream factors involved in the DDR through its PARylating function. PARP inhibitors have emerged as a valuable tool for the sensitisation to current standard care treatment, especially for those cancers harbouring deficiencies in the HRR pathway. TTFields can recreate this HRR pathway deficiency by downregulation of BRCA genes, and therefore PARP inhibitors constitute an obvious candidate for use in TTFields-based combination strategies.

PARP inhibitor activity was initially confirmed via western blot by assessing PARylation levels with increasing doses of inhibitor. PARP1 activity was high under normal conditions in both cell lines. Western blots are considered a semi-quantitative assay as they do not provide an absolute measurement of protein levels but provide a relative measurement instead. Whereas the levels of DDR proteins in relation to their bulk counterparts were not assessed in this study, G7 bulk and stem cells have been previously characterised (382, 486). They showed that G7 stem cells demonstrated enhanced activity of DDR proteins relative to their bulk counterparts, including increased ATM and ATR activity, and importantly to this study, heightened PARP1 activity. PARylation levels were higher in G7 stem cells compared to G1 stem cells which might predict any differences in treatment response (see figure 3.3b). Doses of PARPi (Olaparib) as low as 500nM reduced PARP activity in both G1 and G7 stem cells and therefore a dose of 500nM Olaparib was selected for following studies. Both G1 and G7 stems were radiosensitised by PARP inhibitor treatment, with G1 cells being more sensitive to both PARP inhibitor or radiotherapy treatment either alone or in combination. PARP-mediated radiosensitisation has been suggested to be mainly directed at cells that are actively replicating, and therefore cells with varied proliferation rates (see figure 3.5.) may show different degrees of sensitisation by PARP inhibitors. PARP-mediated radiosensitisation was amplified by additional TTFields treatment in both cell lines. Despite the differences in sensitivity to TTFields as a single-agent between the two cell lines, additional pre-treatment with PARPi and radiation together equally sensitised both cell lines to TTFields treatment, suggesting that TTFields-based combinations could be beneficial to tumours of different genetic backgrounds.

Annexin V/PI and caspase-3 studies showed that this increased sensitisation was not mediated through activation of cell death pathways. Maybe this is unsurprising given that a previous study has shown that doses as high as 30 Gy were not enough to induced apoptosis in the G7 stem cells (382). One characteristic of cancer cells is their ability to evade cell death mechanisms (382). Different glioma cell lines have shown different responses in terms of induction of apoptosis upon exposure to TTFields-

based treatments (286, 343, 487-489) and TTFields has been shown to induce cell death via caspase-dependent (i.e.) and -independent pathways (282, 284, 334). Given that TTFields has been shown to induce activation of autophagy as a cell death mechanism, the effects of treatment on the induction of autophagy by quantification of LC3 levels via western blot were also assessed. However, autophagy was not activated by any treatment combination in these GSC models. Together, this data suggest that the cells were not dead or dying immediately post-treatment and at the time of replating for clonogenic survival assay. This could either mean that another process is responsible for the reduced colony formation, such as reduced proliferation abilities through activation of a quiescent or senescent state, or that cell death is occurring at a later stage. A cell has three major ways to permanently exit the cell cycle: it can enter a senescent state, or the cell can undergo cell death, via apoptosis or necrosis. Cell cycle checkpoint activation as a response to DNA damage can become irreversible when the DNA damage is particularly abundant or when it is sustained over extended periods of time (490, 491). As might be expected with an anti-mitotic treatment, TTFields has been shown to reduce the proliferation rate of glioma cells and this effect may be further exacerbated by additional treatment (302). Alternatively, the cells may be dying at a later timepoint. Radiotherapy-induced cell death has been suggested to be driven through the accumulation of unrepaired DSBs overtime. The effects of this may not be immediate as the cells must first attempt to repair the damage and only sustained DNA damage upon failing to repair the damage become toxic to cells (492). As such, the effects of treatment on DNA damage induction and repair were assessed by immunofluorescence and alkaline comet assay.

Radiation-induced 53BP1- and H2AX-foci formation was enhanced by TTFields treatment, especially with the full combination treatment (TTFields, PARPi and IR) in G7 stem cell lines, suggesting increased formation of DNA lesions, including DSBs, by combination therapy with TTFields+Olap+IR. In G1 stem cells however, the trend was more complicated. Whilst 53BP1 foci was significantly enhanced by TTFields+Olap+IR compared to all other conditions, this did not match up in terms of H2AX foci, which were only significantly enhanced in comparison to the TTFields alone group. This is surprising because DSBs should be marked by both 53BP1 and H2AX stain and given that H2AX is phosphorylated at all types of DNA damage, you would in fact expect to detect increase H2AX foci formation in comparison with 52BP1. However, direct comparison between γH2AX and 53BP1 data is not possible because γH2AX foci formation data is described as a measure of the percentage of cells with ≥5 foci (= positive cells), whereas the number of foci per cell were scored for 53BP1. Using percentage of positive cells may not depict the true extent of differences because any cell with more than 5 foci will be scored as positive, irrespective of how many foci above the threshold are present, therefore the difference could be either over- or under-estimated depending on the trend of the population. For example, the

difference could be exaggerated if a large portion of the cell population contain exactly 5 or close to 5 foci, but if a large number of cells contain foci counts much higher than 5 foci per cell then the differences might be underestimated. Therefore, the number of foci per cell is more informative. Small differences in foci formation are still likely to have a significant impact at the radiobiological level, because even a single unrepaired DSB can be deadly to cells (493). There is also some debate as to when damage can be considered repaired. Some would consider DSBs as repaired once the DNA ends are re-joined (which would result in the loss of 53BP1 signal), whilst others argue that chromatin must be restored to its original condensed state for the repair process to be considered complete (which would be reflected by a persistence of H2AX signal even in the absence of 53BP1 signal) (472, 494-496). This also explains why differences might be seen between methods that assess DNA damage indirectly, for example through signalling of 53BP1 and H2AX via immunofluorescence, and methods that assess DNA damage directly, such as the comet assay, because signalling can persist even in the absence of damage after the damage has been repaired. Indeed, whilst G7 stem cells showed enhanced signalling through H2AX and 53BP1 with the combination treatment, this did not translate into increased levels of damage as measured by the alkaline comet assay. However, the comet assay also carries its own limitations. Nucleotide and base damage are only detectable by the comet assay following incision of the damage that generates a SSB and prior to the ligation step. Therefore, the levels of DNA damage measured by the alkaline comet assay may vary depending on the stage of the repair process, which may vary from experiment to experiment (482).

Replication stress is a major source of DSB formation. Given that TTFields has been shown to enhance replication stress by downregulation of BRCA and FA repair pathway genes and PARP1 is important for replication fork stabilisation during replication stress, the effects of treatment on replication stress were assessed. p-RPA32(T21) levels were enhanced by full combination treatment compared to all other treatment conditions in G1 stem cells, suggesting that treatment with TTFields enhances replication stress in cells pre-treated with PARPi and radiation. Surprisingly, p-RPA32(T21) foci counts were unchanged by treatment in G7 stem cells. However, this may not necessarily reflect a lack of induction of replication stress. Previous groups have shown that cells depleted in PARP1, either via knockout or inhibitor treatment, displayed reduced RPA foci formation even though assays such as the fibre assay still detected impairments in replication fork dynamics, indicating that replication stress is still occurring. They suggested that PARP recruitment of the nuclease MRE11 to stalled replication forks is required for fork reversal and resection of DNA ends that produce the short strands of ssDNA which are bound by RPA (187, 497). Failure to produce ssDNA would translate in an inability for RPA to bind and loss of RPA detection. However, in the absence of MRE11, the nuclease DNA2 and the WRN helicase have been shown to mediate fork resection at stalled replication forks (180).

Therefore, ssDNA formation is not always abrogated by PARP inhibitor treatment and cell lines with different genetic background may display different responses to PARP inhibitor treatment. Additionally, RPA32 is phosphorylated by ATR at T21 during replication stress, activating cell cycle checkpoints and promoting DNA repair through the recruitment of DDR factors (483). However, RPA dephosphorylation by the phosphatase, PP2A, is also needed for successful repair (222). Timely regulation of this phosphorylation and dephosphorylation of RPA has therefore been suggested to be essential for a successful DDR. When the initial phosphorylation of RPA32 is prevented, cells fail to activate cell cycle checkpoints and progress through the cell cycle with unrepaired DNA damage. Failure to remove this phosphorylation on the other hand negatively affects DNA repair (222). Changes in p-RPA32(T21) levels may therefore not reflect changes in replication stress levels but may reflect changes in PP2A activity instead. As such, RPA foci may not be the most accurate measure of replication stress in this scenario and DNA fibre assays, which directly visualise ongoing and stalled replication forks, might be a more informative assay for replication stress in this setting.

Next, the repair kinetics of the damage induced by the various treatment combinations were evaluated in GSCs. In both G1 and G7 stem cells, H2AX and 53BP1 foci formation were sustained 24-hours after removal of treatment in the TTFields+IR+Olap combination group whereas damage was resolved by 24 hours in other treatment groups. This would suggest that TTFields may delay the repair of damage induced by PARP inhibitor and IR treatment or that damage is still being generated even after treatment completion. So even if there was no increase in DNA damage levels in G7 stem cells, as the comet data would suggest, it seems that at least this damage is less efficiently repaired in the full combination compared to other conditions, which would still be reflected by a bigger reduction in survivability compared to less harsh treatment conditions. Given that TTFields has been shown to downregulate BRCA genes, this could be due to defects in the HRR pathway, however further studies need to be carried out to confirm this. The repair kinetics were assessed following removal of all treatments and it must therefore be considered whether downregulation of BRCA genes is maintained upon removal of TTFields treatment. Preliminary data suggests that downregulation of BRCA genes may be sustained for up to 8 hours after termination of TTFields treatment in G7 stem cells (see figure 3.4.).

Finally, given that temozolomide is the chemotherapeutic agent most frequently used for the treatment of glioblastoma, the effects of PARP inhibition with and without chemotherapy on TTFields response in GSCs were assessed. G7 stem pre-treated with PARP inhibitor and TMZ were further sensitised by TTFields treatment as measured by clonogenic survival assay. A recent study has suggested that PARylation is important in mediating TMZ toxicity and showed that PARP inhibition

could in fact reinstate TMZ sensitivity in glioma cells that express MGMT (410). In line with this, whilst G1 and G7 stem cells are expected to be sensitive to TMZ treatment because they lack MGMT, OX5-core and edge are expected to be more resistant to TMZ because they express MGMT. Combination with TTFields, Olap and TMZ showed comparable efficacy irrespective of MGMT status. TTFields has been shown to sensitise glioblastoma patients in the clinic irrespective of MGMT status and *in vitro* work also supports the application of TTFields for both +/- MGMT expressing patients (64, 276, 286). PARP inhibitors enhance TMZ-induced haematological toxicities, requiring PARP inhibitors to be administered intermittently which limits their efficacy (465). Seeing as TTFields has no systematic toxicities, when used in combination with TTFields, a smaller dose of PARP inhibitor could be employed for the same therapeutic gain, which would hopefully reduce the haematological toxicities otherwise seen when combined with TMZ.

To summarise, inhibition of PARP, a central protein in the DDR, sensitises GSC models to TTFields treatment especially when administered in combination with radiotherapy or chemotherapy. PARP is known to drive resistance to DNA damaging treatment by providing increased DNA repair capacity. Here, we show that PARPi given in combination with TTFields and radiation further enhances DNA damage induction, compared to each treatment given individually, and delays DNA damage repair.

3.4 Supplementary figures

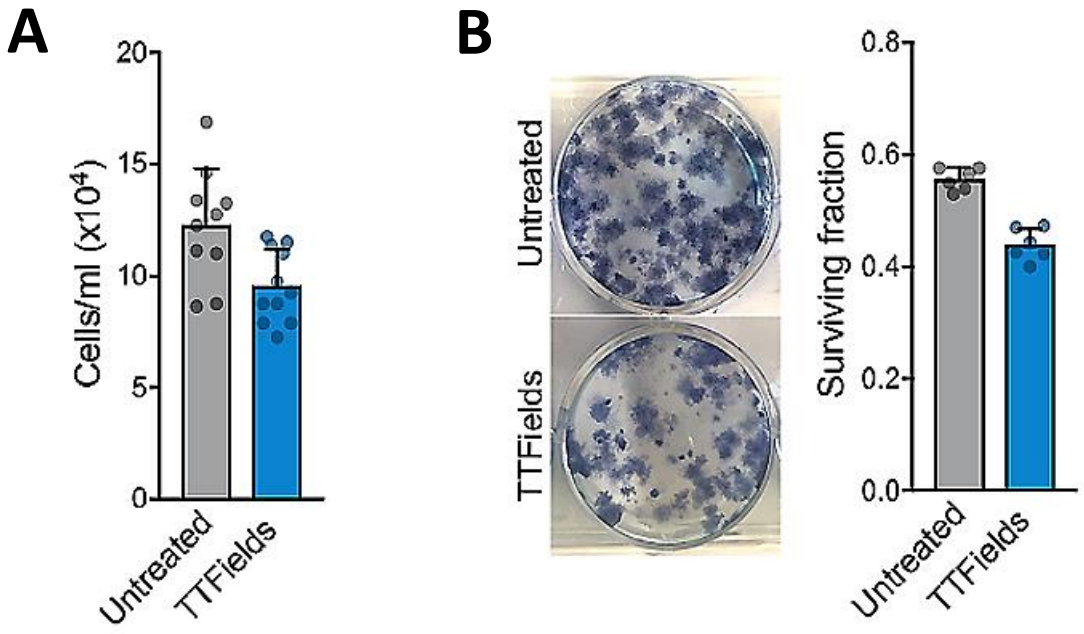

Figure 3.16. Cell survival of G1 stem cells treated with TTFields (200kHz, 48 hours).
Survival of G1 stem cells following 48-hour TTFields treatment (200kHz, 1.6 V/cm RMS) as established by cell counting in (**A.**) and by clonogenic assay in (**B.**). Graph bars represent the mean of experimental replicates and individual dots representing each replicate. Error bars represent the standard deviation of the mean.

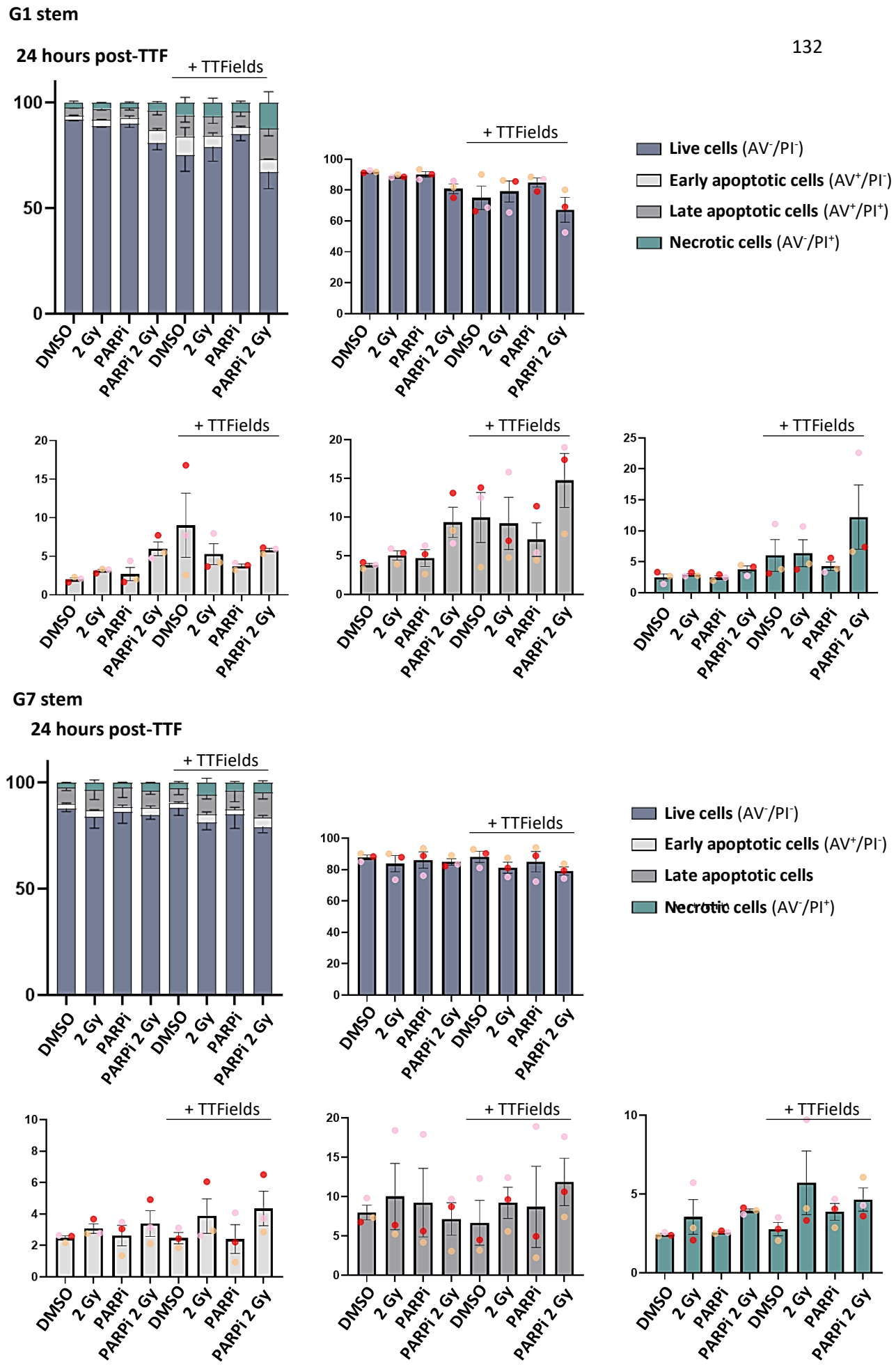

Figure 3.17. Treatment with PARPi, IR and TTFields either alone or in combination does not induce activation of cell death mechanisms.

Following treatment, G1 and G7 stem cells were collected and analysed for Annexin V/PI staining via flow cytometry to assess the effects of treatment on the induction of apoptosis. There was no significant difference in induction of apoptosis across all conditions in both cell lines 24-hours after treatment completion. Error bars represent the standard error of the mean, with individual repeats represented as differently coloured dots. n=3

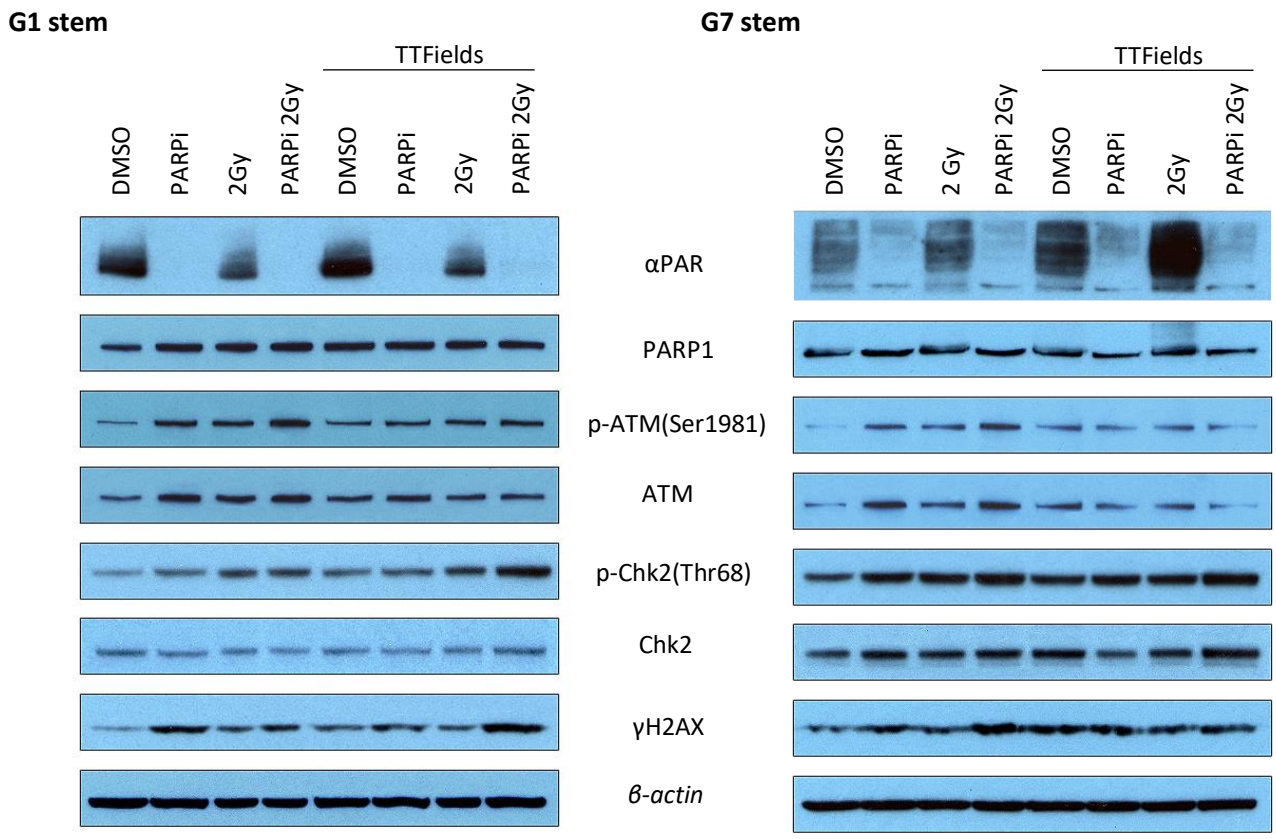

Figure 3.18. Protein expression of DDR proteins following treatment with PARPi, IR and TTFields either alone or in combination.

G1 and G7 stem cells were treated with PARPi (500nM), IR (2 Gy) and TTFields (48 hours at 200kHz) either alone in combination. Following treatment, cells were harvested and protein activity of various DDR factors (PARP1 and ATM) were assessed via western blot. n=1

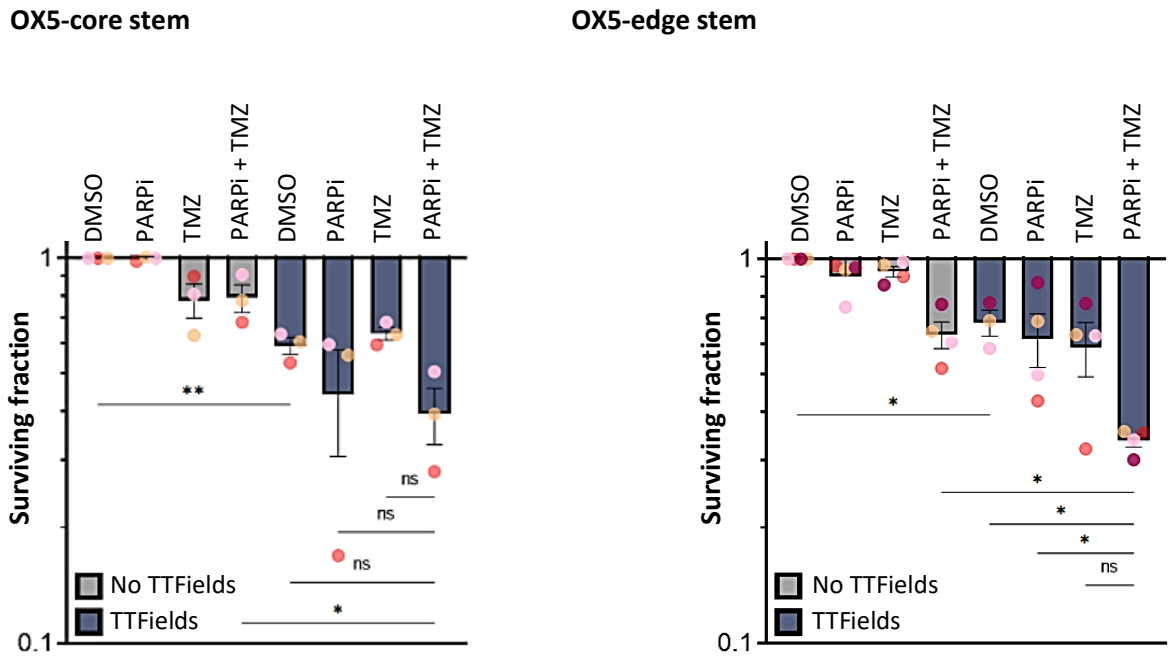

Figure 3.19. Survival of OX5-core and edge stem cells pre-treated with PARPi and TMZ is further reduced by TTFields treatment.

The effects of treatment on survival of OX5-core and -edge stem cells were assessed by clonogenic survival assay. Graph bars represent the mean of experimental replicates and individual dots representing each replicate. Error bars represent the standard deviation of the mean. n=3 Data shown were produced by Dr. Callum Jones.

CHAPTER 4. TARGETING ATR IN COMBINATION WITH TTFIELDS AND STANDARD-OF-CARE TREATMENT

4.1 Introduction

4.1.1 Role of ATR in the DDR

ATR belongs to the phosphoinositide 3-kinases (PI3K) family of kinases and is essential for replication under normal and stressed conditions (figure 1.11b) (498). ATR is essential for survival and its deletion is embryonically lethal (499). ATR is mainly activated at single stranded DNA (ssDNA), but ATR can also by activated by R-loops that form during transcription and at telomere ends (500-502). ssDNA is induced by stalled replication forks, during end processing of DSBs and during processing by NER, MMR and long-patch BER repair pathways, where ssDNA form as intermediates during the repair process (168, 503, 504). ATR is therefore recruited to a range of types of damage. ssDNA is first bound by the ssDNA binding protein RPA. ATR-interacting protein then binds to RPA and recruits ATR to RPA-coated ssDNA (figure 1.9b). Once ATR is loaded onto ssDNA, interactions between RAD17-RCF, the RAD9-RAD1-HUS1 (9-1-1) complex and Topoisomerase Binding Protein 1 (TOPBP1) complete ATR activation (505, 506). 9-1-1 is recruited to ssDNA-dsDNA junctions by the clamp loader RAD17-RFC (507). The RAD9 subunit from the 9-1-1 complex is then phosphorylated on S387, which promotes the TopBP1-ATR interaction and subsequent activation of ATR (508). Once activated, ATR phosphorylates several substrates to orchestrate checkpoint activation, DNA repair, and stabilisation of stalled replication forks during DNA damage or within regions that are difficult to replicate (e.g. fragile sites and microsatellites) (500, 509).

Chk1 is the most established substrate of ATR and is Chk1 is recruited to the DNA lesion and is phosphorylated by ATR on two residues, Ser345 and Ser317 (209, 510). This process is dependent on the protein Claspin, which is recruited to the site of damage by RAD17 and enables interaction between ATR and Chk1 (511, 512). Chk1 in turn signals to a variety of intracellular substrates involved in DNA repair, DNA damage checkpoint activation and replication fork stabilisation (468). For example, Chk1 mediates checkpoint activation during S phase and G2-M transition through inhibitory phosphorylation of Cdc25A and Cdc25C, respectively (513), and activation of WEE1 (514). Chk1 also helps to minimise the extent of replication taking place under conditions of replication stress by slowing the rate of DNA synthesis by preventing replication origin firing (503, 515). Origin firing is also prevented by ATR mediated activation of the FA pathway through phosphorylation of FANCI (516). RPA is the limiting factor for ATR-mediated replication fork stabilisation. The pool of RPA is finite and

when the RPA pool is depleted, known as RPA exhaustion, any additional ssDNA cannot be protected by RPA from nuclease attack and DSBs are generated as a result. ATR prevents excessive ssDNA formation and RPA exhaustion by halting origin firing. In the absence of ATR, stalled replication forks are stable to begin with due to RPA binding but as ssDNA starts to build up from unscheduled origin firing, unprotected replication forks collapse. Increasing RPA levels in ATR deficient cells is sufficient to restore replication stability (223).

Other substrates of ATR activity include members of the FA pathway, FANCD2 and FANCI, and NER pathway, XPA, to mediate inter-strand crosslink and bulky DNA adduct repair, respectively (517, 518). Finally, Chk1 has been shown to recruit and phosphorylate two proteins essential for HRR, RAD51 recombinase and BRCA2 (519).

4.1.2 Rational for targeting ATR in combination with TTFields

Chk1-mediated G2/M checkpoint activation has been suggested to drive resistance to radiotherapy in GSCs (382). ATR inhibition might then overcome radio-resistance by preventing activation of the G2/M checkpoint and forcing cells through the cell cycle with unresolved DNA lesions. Given that glioma stem cells have higher levels of replication stress under basal conditions, glioma stem cells might be expected to reach RPA exhaustion more rapidly than their bulk counterparts upon treatment with an ATRi. However, Ahmed *et al*. showed that whilst preventing G2/M activation, unexpectedly, ATR inhibitor radiosensitised bulk cells to a greater extent that GSCs, suggesting that other mechanisms may restrict Chk1-mediated radiosensitisation. Ahmed *et al*. showed that, whilst GSCs exhibited increased levels of DNA damage relative to their bulk counterparts following treatment with ATRi and IR, these lesions were repaired more rapidly in GSCs compensating for the increased DNA damage burden, restricting the effects of ATR inhibition (382).

Likewise, ATR-Chk1-mediated activation of the G2/M checkpoint was suggested to limit TMZ sensitivity and as such, ATR inhibition has also been shown to sensitise glioma cells to chemotherapy (520). ATR inhibition has been suggested to prevent activation of the G2/M checkpoint, allowing cells to continue replicating when subjected to TMZ treatment and ultimately converting TMZ-induced lesions into DSBs in a replication stress-dependent manner. This process has been suggested to be dependent on MGMT status and MMR pathway activity. In MGMT-deficient cells, O^6-MeG lesions accumulate and are recognised by the MMR pathway. However, because the MMR pathway can only remove mismatched bases on the newly formed DNA strand, the MMR pathway repeatedly attempts to repair the mismatch but fails to do so, eventually forming SSBs that can be converted into DSBs under conditions of prolonged replication stress. Additionally, MMR proteins (MSH2, MSH6) have

been shown to interact with ATR and regulate ATR-mediated phosphorylation of Chk1 and subsequent activation of G2/M checkpoint. MSH2-mediatied activation of ATR also suppresses DNA synthesis during S-phase (521, 522). Loss of MMR proteins prevents ATR activity and inactivation of the MMR pathway has been shown to prevent ATR inhibitor sensitisation to TMZ (523). Together this data supports the use of ATRi for the sensitisation of glioblastoma to current standard treatment.

Mutations in other regulators of G2/M checkpoint activation, such as p53 or ATM, means that cells rely more heavily on ATR activity for G2/M checkpoint activation and may mediate ATR inhibitor sensitivity (524-527). Alternatively, cells that carry defects in other proteins involved in the resolution replication stress, such as XRCC1 or ERCC1, are more sensitive to ATR inhibition (528, 529). Broadly speaking, cells with defects in replication fork proteins, where enhanced levels of replication stress are expected, are likely to be susceptible to ATR inhibition. Because TTFields have been shown to increase replication stress (320), one might expect that inhibition of a protein that is involved in the resolution of replication stress, like ATR, would demonstrate therapeutic efficacy in combination with TTFields (530, 531). The effects of ATR inhibition in combination with TTFields have not yet been explored.

Given that ATR is essential for survival, the effects of ATR inhibition on normal tissue are a concern, especially when combined with DNA damaging treatment. There are currently no clinical trials investigating the effects of AZD6738 in glioblastoma, perhaps because a study by Fròsina *et al.* (2018) showed that, despite the favourable pharmacokinetics properties of AZD6738 (including good BBB penetration), no improvement in over survival was seen in combination with RT, discouraging its use as a radiosensitising agent in glioblastoma (532). The BBB penetrant ATR inhibitor, AZD6738 (532), is currently undergoing investigation in several clinical trials, including in combination with the PARP inhibitor, Olaparib (NCT03428607), and in combination with radiotherapy (NCT02223923), and has been suggested to be well tolerated (533, 534).

4.2 Results

4.2.1 Optimisation of ATR inhibitor for use in glioma stem cells

AZD6738 is the only selective ATR inhibitor that has been demonstrated to penetrate the BBB (532), and was therefore selected to investigate the effects of ATR inhibition on ATR activity. The effects of increasing doses (250nM-5µM) of ATRi (AZD6738) on ATR activity in G1 and G7 GSCs were assessed by western blot, following stimulation by 5 Gy IR. Western blotting showed that a 250nM AZD6738 successfully decreased phosphorylation of Chk1 on residue Ser345 back to baseline levels, indicative of effective and potent inhibition of ATR activity, in G1 and G7 stem cells (figure 4.1) following stimulation with IR. As 250nM AZD6738 showed robust inhibition of ATR activity in both cell lines, this dose was therefore selected for future experiments. Additionally, AZD6738 has been reported to exert a high degree of selectivity to ATR kinases relative to other members of the PI3K family, ATM and DNA-PKcs (IC_{50} >30) (174), therefore off-target effects are not expected at this dose.

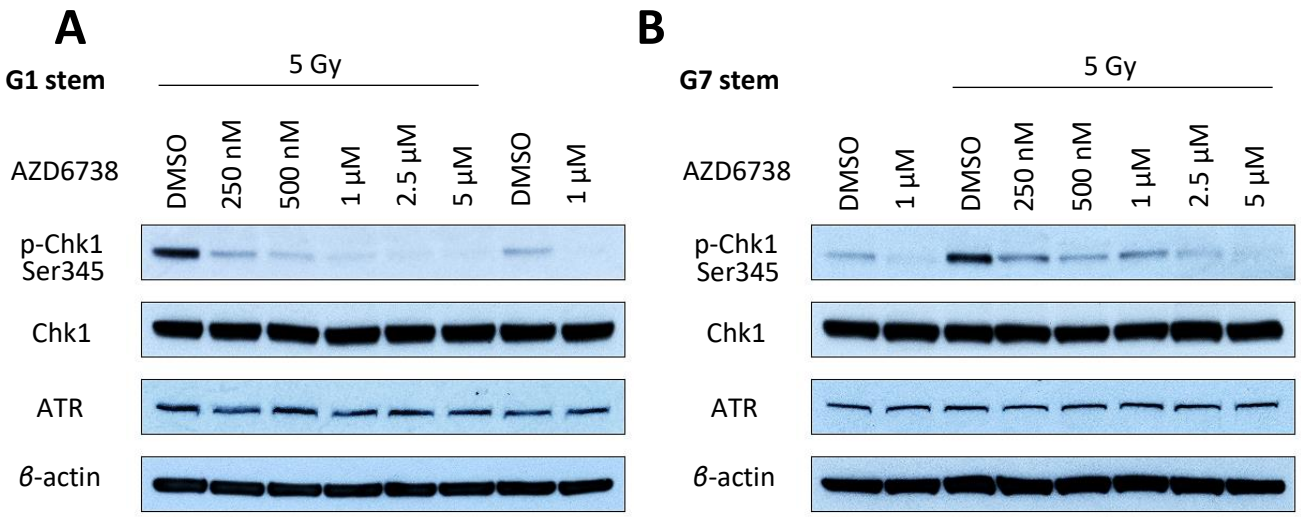

Figure 4.1. Inhibition of ATR activity in GSCs using ATRi.
G1 (**A.**) and G7 (**B.**) GSCs were treated with either DMSO control or varying doses ATRi, AZD6738 (250nM - 5µM). Cells were treated with 5 Gy IR 1-hour post-inhibitor treatment to stimulate kinase activity. 1-hour post-IR treatment, cells were harvested and samples were ran on a western blot. AZD6738 inhibited phosphorylation of Chk1 on residue Ser345 in both G1 and G7 GSCs at all doses tested in combination with IR. *β*-actin was used as a loading control. n=1

4.2.2 The effects of ATR inhibition alone or in combination with radiation on survivals of GSCs with or without TTFields.

G1 and G7 stem cells were pre-treated with ATRi (250nM AZD6738) for 1 hour prior to irradiation with 2 Gy. TTFields treatment (200kHz for 48 hours) was initiated immediately following irradiation. At the end of TTFields treatment, GSCs were replated into 6-well plates and a clonogenic survival assay was

carried out to determine the effects of treatment on survival (figure 4.2). ATRi alone had no effect on the survival of G1 stem cells but reduced survival by 15% in G7 stem cells. Exposure to TTFields following pre-treatment with ATRi further reduced the survival of G7 stem cells by 35% and reduced the survival of G1 stem cells by 54% (surviving fractions of ~50% and 46%, respectively). Pre-treatment with ATRi radiosensitised G1 and G7 with a surviving fraction of ~26% for both cell lines. This radiosensitisation was augmented by TTFields treatment with surviving fractions of 2.8% and 7.1% for G1 and G7 stem cells respectively. Annexin V/PI stain showed that there was no difference in the fraction of apoptotic and necrotic cells between conditions in both cell lines at the end of treatment (figure 4.3).

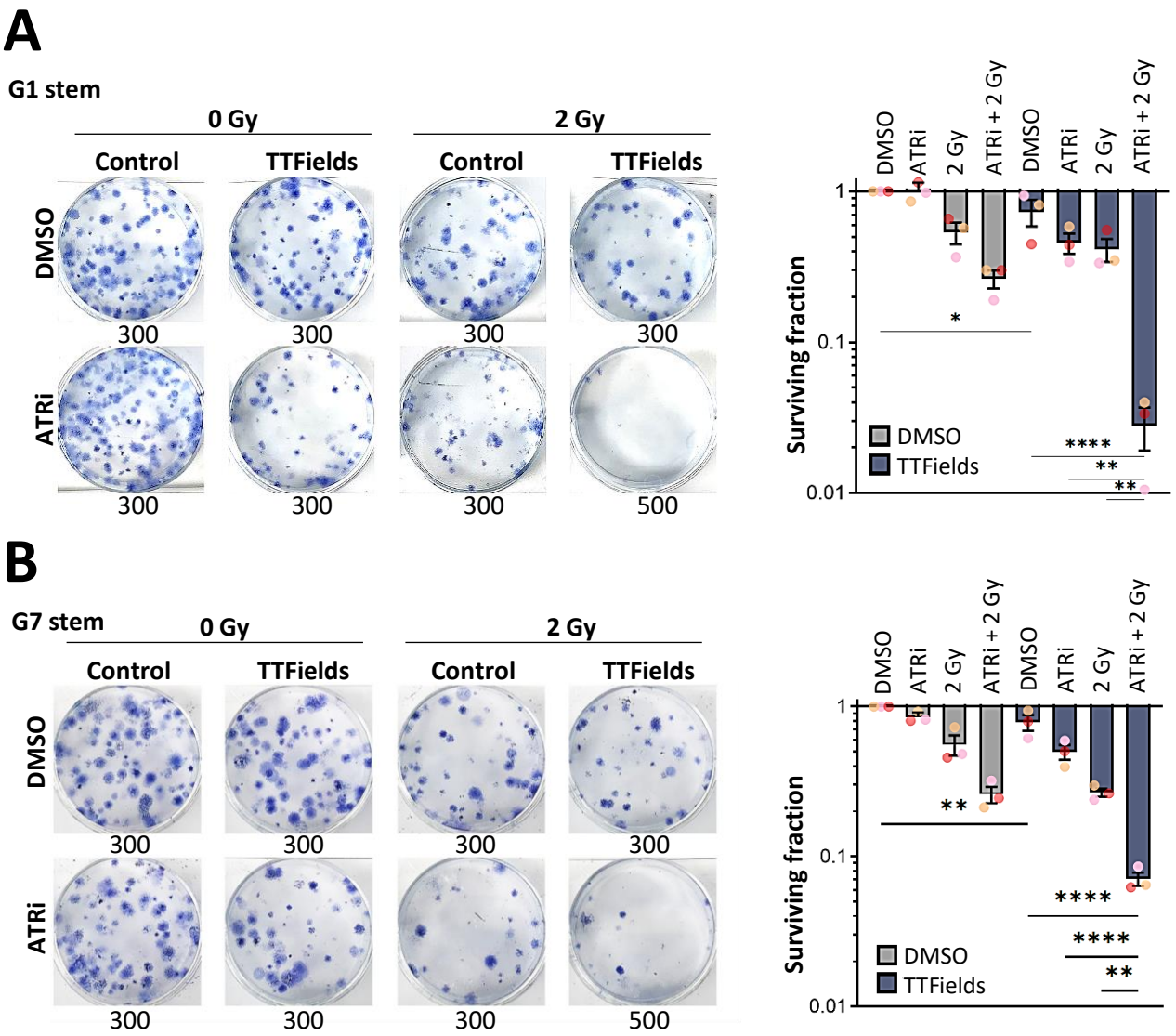

Figure 4.2. The effects of pre-treatment with ATRi and radiation either alone or in combination on survival of GSCs exposed to TTFields treatment.
At the end of TTFields treatment, cells were replated in 6-well plates and the effects of the combination treatment on toxicity were assessed by clonogenic survival assay in G1 (**A.**) and G7 (**B.**) stem cells. Left – Representative images of the clonogenic survival in G1 and G7 stem cells. Right – Summary of the surviving fraction for each condition. Graph bars represent the mean of experimental replicates and individual dots representing each replicate. Error bars represent the standard error of the mean. n=3

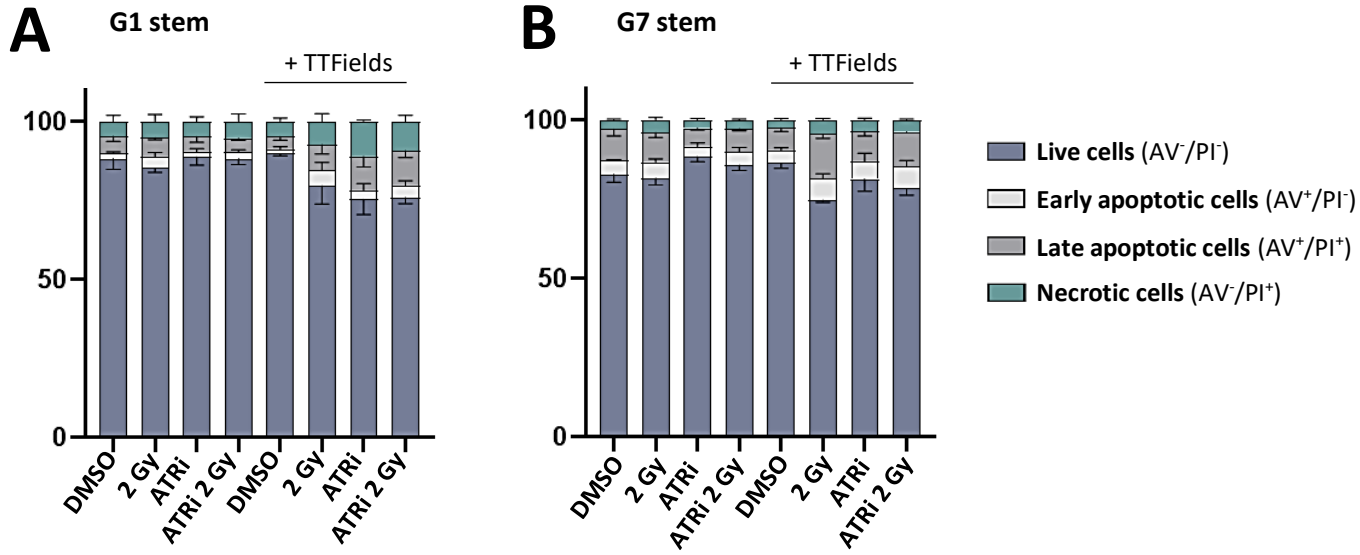

Figure 4.3. Treatment with PARPi, IR and TTFields either alone or in combination does not induce activation of cell death mechanisms.
At the end of TTFields treatment, G1 (**A.**) and G7 (**B.**) stem cells were collected and analysed for Annexin V/PI staining via flow cytometry. Error bars represent the SEM. n=3

4.2.3 The effects of treatment with ATRi, radiation and/or TTFields alone and in combination on signalling of DDR factors and on damage induction.

The effects of treatment on protein expression of key DDR factors, including effectors of ATR and ATM, were investigated via western blot. At the end of treatment, ATR activity was no longer inhibited in GSCs that had been exposed to ATR inhibitor (figure 4.4). In fact, the expression of p-Chk1(Ser345) was augmented in the samples that had been exposed to ATRi treatment compared to those that had not been treated with the inhibitor. Previous studies have shown that other PIKKs, like ATM, can phosphorylate predominately ATR substrates in its absence (535, 536). Additionally, this increase could be explained by reactivation of ATR. The half-life of the inhibitor, AZD6738, which has been reported to be ~6-11 hours (537-539). As previously shown (figure 4.1), AZD6738 does inhibit ATR activity as shown by a reduction in Chk1 phosphorylation via Western Blot. However, in the initial optimisation experiment, the samples were collected 2 hours post-inhibitor treatment, when the inhibitor is still expected to be active. For the combination experiment, the samples were collected ~48 hours after the inhibitor treatment had been administered, therefore it is possible that the inhibitor was no longer active at the time the samples were collected and does not reflect lack of target activity.

The increased Chk1 phosphorylation (figure 4.4) at this later timepoint could therefore be a result of compensatory phosphorylation by ATM and/or reactivation of ATR activity, which may be enhanced

in order to compensate for its lack of activity earlier during the treatment, for example from increased replication stress. This could be because of the damage that may have accumulated during the period of ATR inactivity and this increase in Chk1 phosphorylation may then reflect increased damage, especially given that effectors of the DSB sensor, ATM, are mirroring the increased ATR activity. Indeed, phosphorylation of both Chk2 and Kap1 at Thr68 and Ser824, respectively, are increased in GSCs treated with ATRi (figure 4.4).

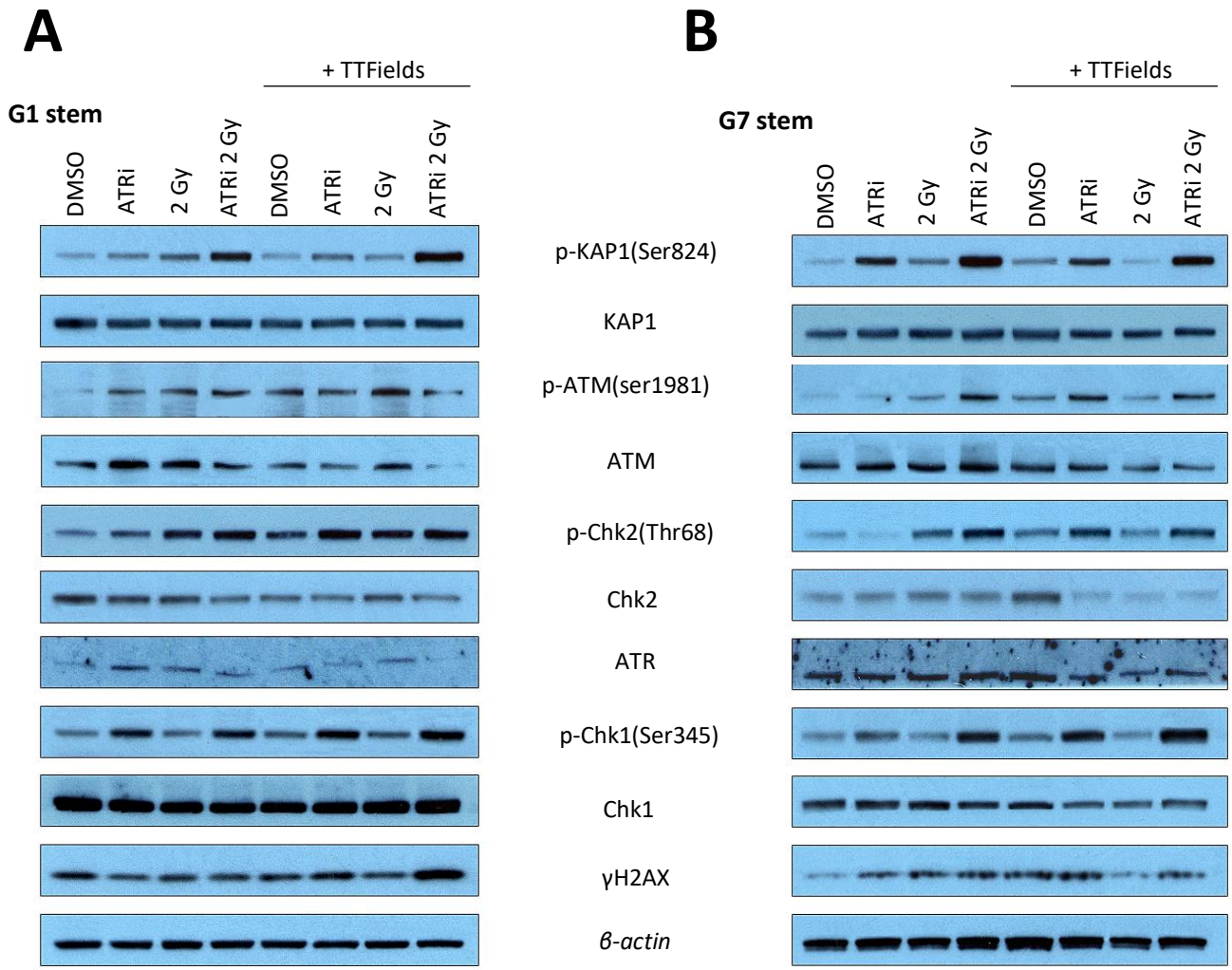

Figure 4.4. The effects of ATRi and/or radiation in combination with TTFields on signalling of DDR proteins.
The effects of treatment on the activity of various DDR factors, such as ATM and ATR, were assessed via Western Blot in G1 (**A.**) and G7 (**B.**) stem cells. Phosphorylation of Chk1, which is a substrate for ATR activity, and phosphorylation of KAP1 and Chk2, which are substrates of ATM activity, were increased by combination treatment with TTFields, ATRi and irradiation in combination in both G1 and G7 stem cells. n=2.

Additionally, as measured by increased induction of γH2AX- and 53BP1-foci formation via immunofluorescence, treatment with ATR inhibitor was shown to increase the signalling of proteins involved in DNA repair, especially when combined with radiation and/or TTFields (figure 4.5). G1 and G7 stem cells experienced a doubling in the percentage of cells stained positively for γH2AX when cells received TTFields treatment in addition to pre-treatment with ATRi and IR in combination compared to cells receiving ATRi and IR in combination only. The mean number of 53BP1 foci per cell was ~1.5 and ~1.3 fold higher in G7 and G1 cells, respectively, when cells were exposed to TTFields following pre-treatment with ATRi and radiation (figure 4.5). As signalling of DDR does not always directly correlate with DNA damage levels, the effects of treatment on DNA damage induction were assessed via alkaline comet assay. There was no difference in DNA damage induction across all TTFields-treated conditions as measured by the alkaline comet assay in G1 stem cells (figure 4.6a). TTFields treatment did not enhance DNA damage induction following pre-treatment with ATRi and radiation in combination in G1 stem cells in contrast to what the signalling data might indicate. On the other hand, DNA damage induction was augmented by TTFields treatment when G7 stem cells were pre-treated with either ATRi and/or radiation, with the biggest induction in DNA damage seen following pre-treatment with the combination of ATRi and radiation (figure 4.6b).

Together this data suggests that treatment combination with all three modalities (TTFields, ATRi and IR) increases signalling of DDR/replication stress factors in GSCs when compared to other treatment permutations, but this increase in signalling does not always correlate with increased levels of DNA damage at the investigated timepoint.

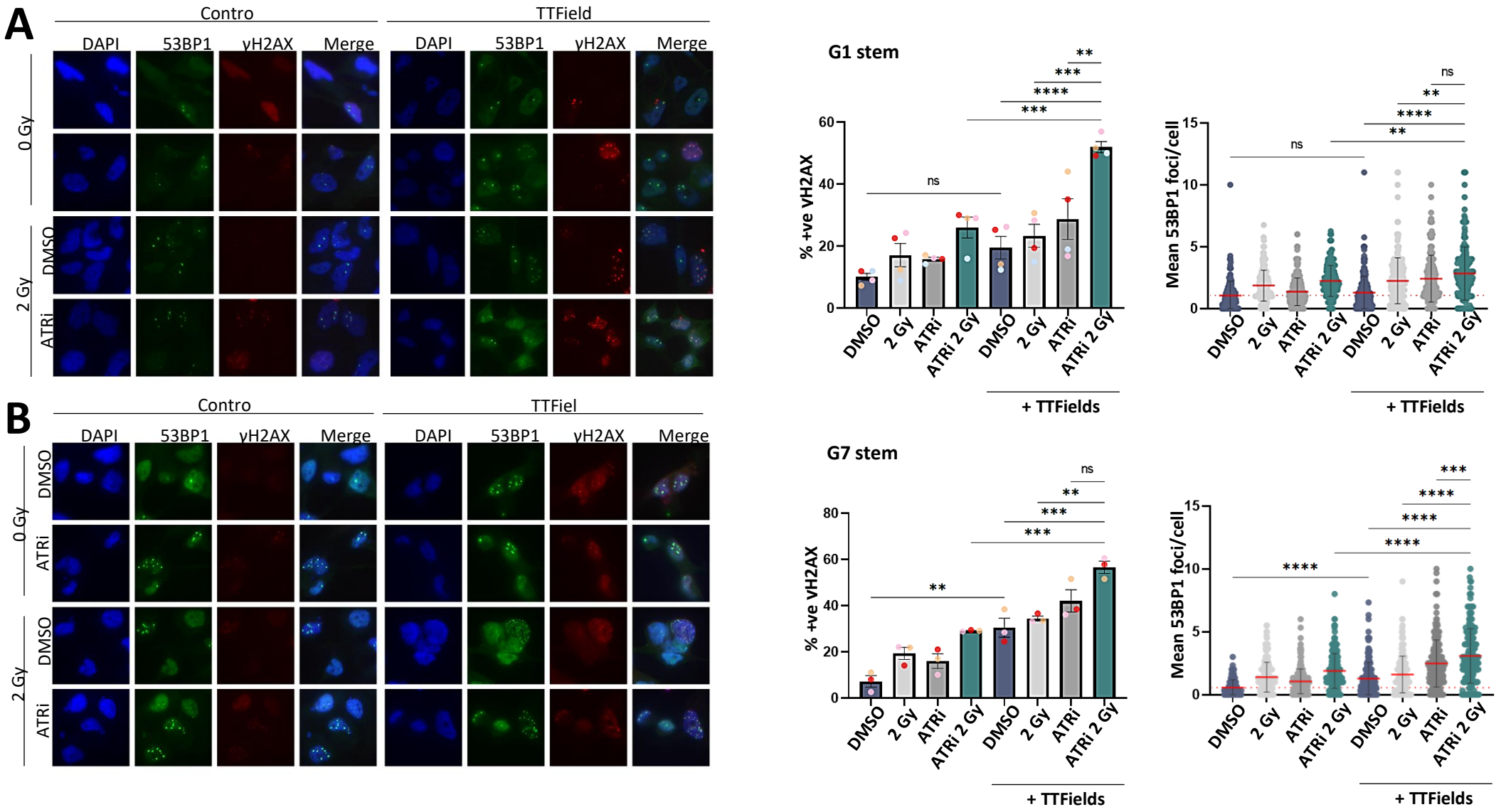

Figure 4.5. The effects of ATRi and/or radiation in combination with TTFields on signalling of DDR proteins.

γH2AX- and 53BP1-foci quantification via immunofluorescence was used to determine the effects of treatment on DNA damage induction in G1 (**A.**) and G7 (**B.**) stem cells. Left – Representative images. Right – Bar charts showing the percentage of cells showing positive γH2AX staining (≥5foci/cell), where graph bars represent the mean of experimental replicates and individual dots representing each replicate. Dot plots demonstrating the number of 53BP1 foci/cell, where each dot represents an individual cell and the red line = mean +- SD. SEM n=3

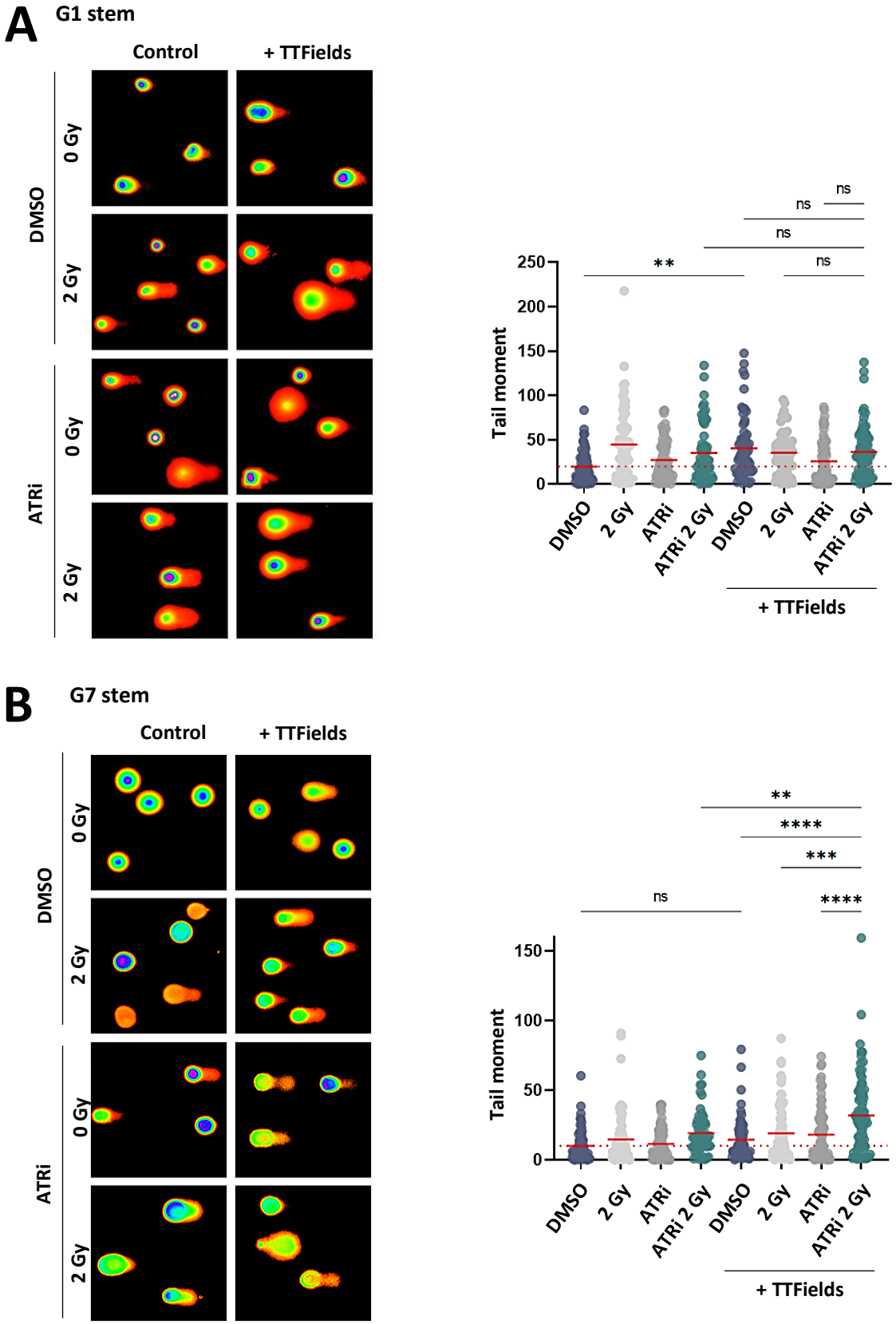

Figure 4.6. The effects of ATRi and/or radiation in combination with TTFields on DNA damage induction and signalling of DDR proteins.

The effects of treatment on DNA damage induction were assessed via alkaline comet assay in both G1 (**A.**) and G7 (**B.**) stem cells. Left – Representative images for the alkaline comet assay. Right – Dot plots showing the tail moment of individual cells, with the red line showing the mean for each condition. n=3

4.2.4 The effects of pre-treatment with ATRi and/or radiation on DNA repair kinetics of TTFields-treated GSCs.

Seeing as ATRi-mediated conversation of stalled replication forks into DSBs is dependent on RPA binding to ssDNA, the effects of treatment on RPA levels were assessed. TTFields alone significantly induced p-RPA foci in both G1 and G7 stem cells, suggesting replication stress is induced by TTFields treatment (figure 4.7). ATR inhibitor alone enhanced radiation-induced p-RPA foci formation in G1 stem cells, this was further augmented by TTFields treatment (figure 4.7a). However, pre-treatment with ATRi and radiation prior to TTFields exposure did not enhance foci formation compared to cells pre-treated with radiation or when cells received TTFields as a monotherapy. Surprisingly, fewer p-RPA foci were formed by pre-treatment with both ATRi and irradiation in combination prior to TTFields exposure compared to cells pre-treated with ATRi alone in G1 stem cells.

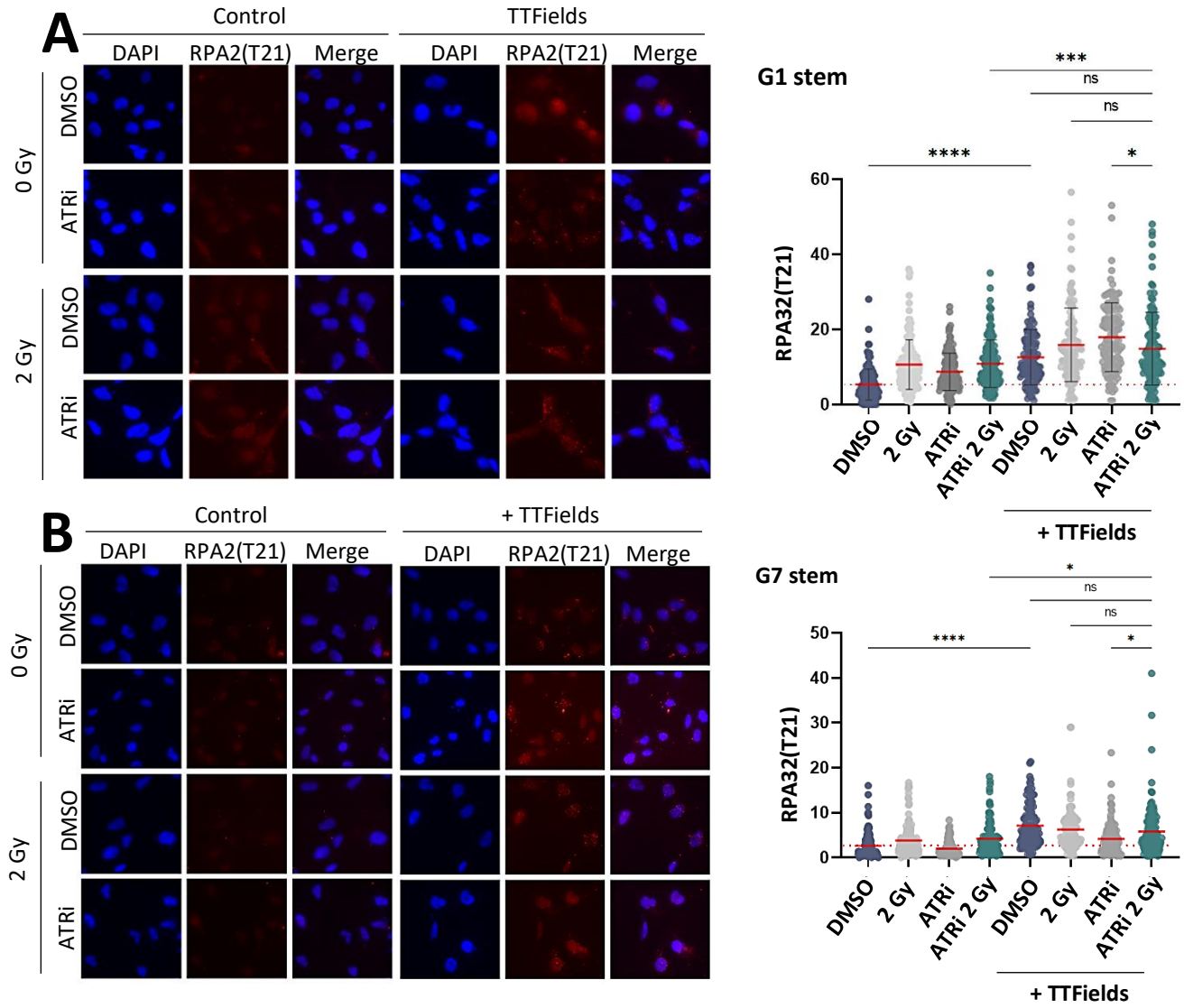

Figure 4.7. The effects of pre-treatment with either ATRi and radiation either alone or in combination prior to TTFields treatment on RPA signalling.

G1 (**A.**) and G7 (**B.**) stem cells were stained for p-RPA32(T21) foci and quantified by immunofluorescence following treatment with TTFields, ATRi and IR , either alone or in combination. Left shows representative images and right shows dot plots demonstrating the number of p-RPA32(T21) foci/cell, where each dot represents an individual cell and the red line = mean +- SD. n=3

ATR-mediated phosphorylation of RPA2 at T21 during replication stress serves as a scaffold for the recruitment of DDR factors to mediate damage repair. Changes in RPA phosphorylation may then indicate changes in repair kinetics and the effects of treatment on the formation and resolution of damage were assessed over time. G1 stem cells treated with ATRi and radiation in combination both with and without TTFields treatment had a high DSB burden (4.8 vs 5.3 mean 53BP1 foci per cell) and a high total DNA damage burden (52% and 45% positive γH2AX cells, respectively). This DNA damage burden was sustained only when cells received TTFields treatment and was in fact increased with a mean of 7.1 53BP1 foci per cell 24-hours after treatment completion and 59.7% of cells exhibiting positive γH2AX staining (figure 4.8a and figure 4.9a). G1 stem cells treated with ATRi and IR but without TTFields had mostly repaired damage by the 24-hour timepoint, with an average of 2.2 53BP1 foci per cell (equal to basal levels of 53BP1 stain) and only 20% of cells stained positively for γH2AX (on average 15% of the population is stained positively for γH2AX in untreated cells). 53BP1 foci formation in G1 stem cells pre-treated with either ATRi or 2 Gy alone prior to exposure to TTFields treatment also returned to basal levels 24 hours following completion treatment, from on average 3.8 and 3.0 53BP1 foci per cell to 2.5 and 2.2 foci per cell, respectively. Treatment with ATRi, irradiation and TTFields in combination resulted in persistent γH2AX- and 53BP1-foci in G1 stem cells, indicative of impaired DNA damage repair (figure 4.8a and figure 4.9a).

For G7 stem cells, whilst 53BP1 was high immediately at the end of treatment with TTFields, ATRi and IR in combination and remained high 24-hours after treatment completion (4.6 53BP1 foci per cell vs 4.9 53BP1 foci per cell, higher than any other condition), H2AX foci staining was initially high immediately at the end of treatment (50% H2AX) but started to subside by 4-hours following treatment completion (21%; figure 4.8b and figure 4.9b), suggesting than the remaining DNA damage could mostly constitute DSBs. The remaining total DNA damage was then sustained for up to 24-hours post-treatment completion (23%), a 2-fold increase in 53BP1 and γH2AX stain compared to untreated cells, with ~10% of cells stained positively for γH2AX in control cells at the same timepoint, indicating that whilst G7 cells receiving the full treatment combination are still able of repairing the damage, they are still subjected to increased levels of damage to what can be considered normal in this cell line. G7 stem cells pre-treated with 2 Gy only prior to TTFields exhibited comparable γH2AX staining with the full combination treatment (23%) but 53BP1 foci staining was significantly lower (3.4 foci per cell). G7 stem cells pre-treated with ATRi alone prior to exposure to TTFields had fully resolved γH2AX signal by the 24-hour timepoint (19% of positive γH2AX cells to ~11%), whereas 53BP1 staining was sustained at ~3.4 53BP1 foci per cell), although this was still significantly lower compared to the full combination. Together this data suggests the combination treatment with TTFields, ATRi and IR perturbs the resolution of DNA damage.

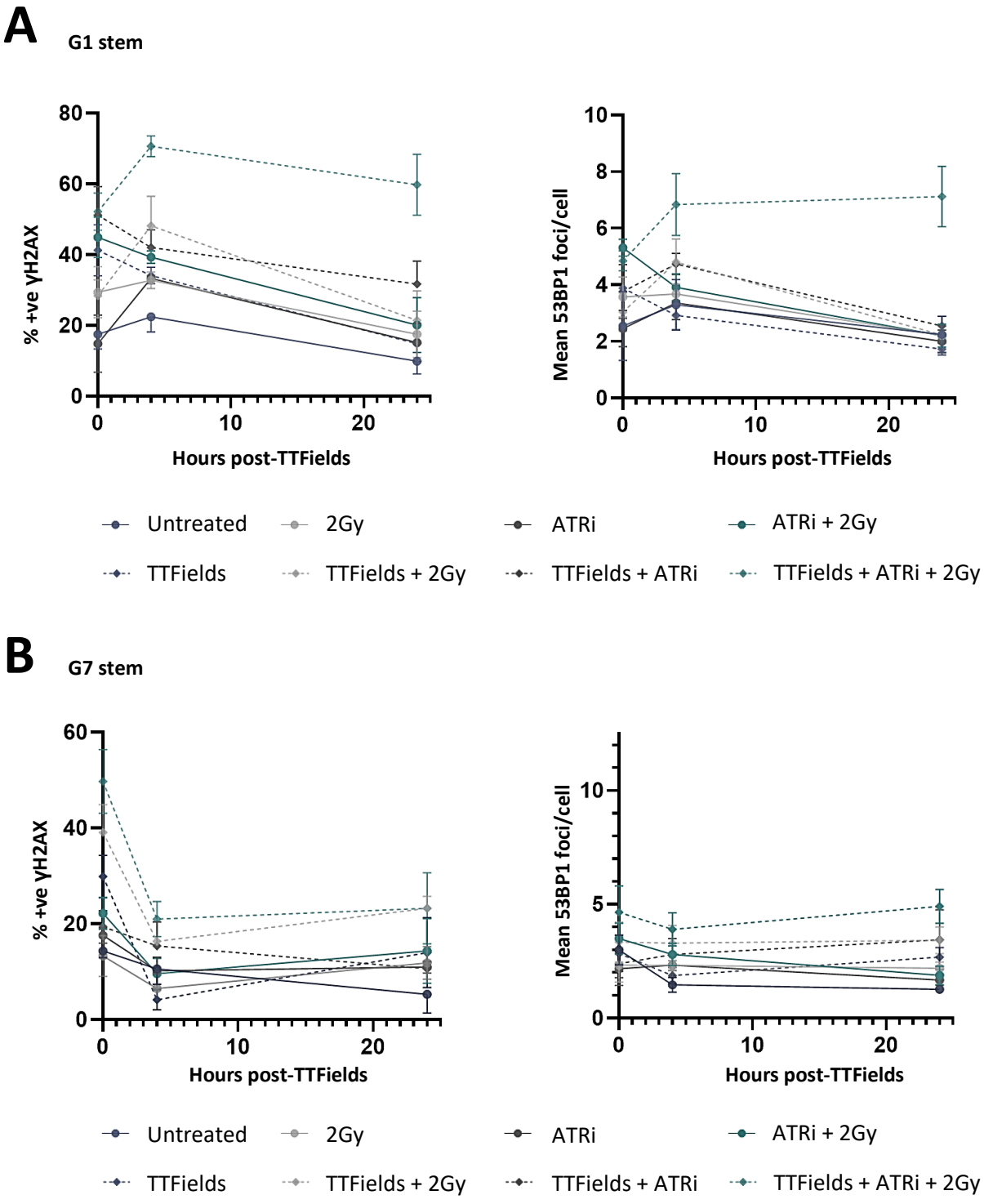

Figure 4.8. The effects of pre-treatment with either ATRi and radiation either alone or in combination prior to TTFields treatment on DNA damage repair.
Time-course summary line graph for γH2AX- and 53BP1-foci formation in G1 (**A.**) and G7 (**B.**) stem cells following treatment with TTFields, ATRi, and irradiation, either alone or in combination.
Time-course experiment in G1 stem cells were produced by Dr. Callum Jones. n=3

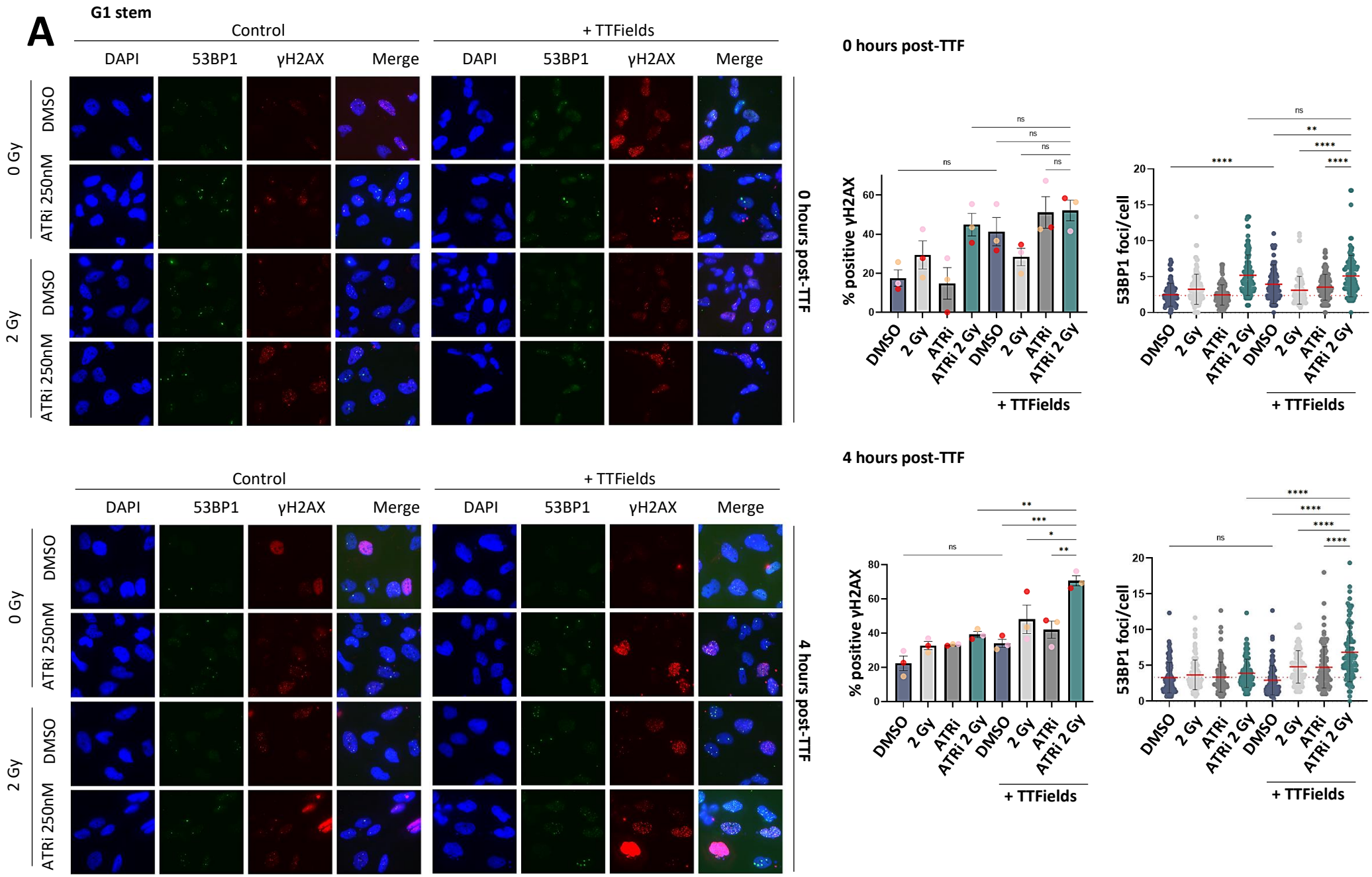
A
G1 stem
Control
+ TTFields
DAPI
53BP1
γH2AX
Merge
0 Gy
2 Gy
DMSO
ATRi 250nM
0 hours post-TTF
4 hours post-TTF
% positive γH2AX
53BP1 foci/cell
DMSO
2 Gy
ATRi
ATRi 2 Gy
+ TTFields
ns

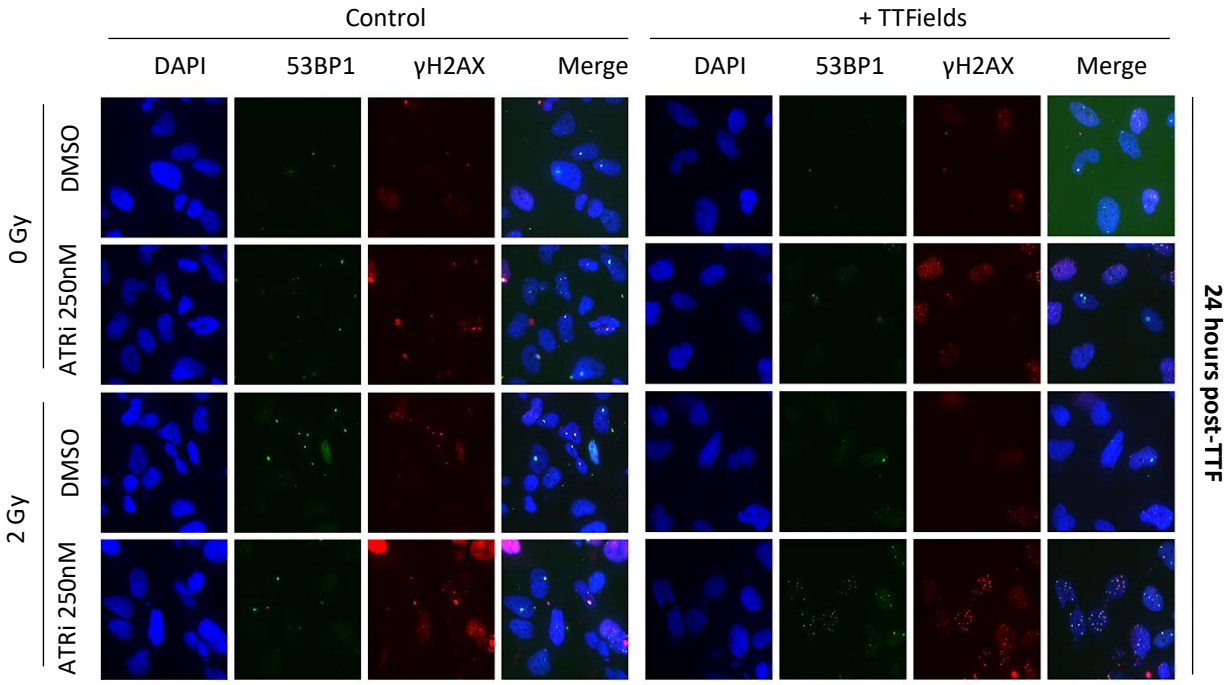
Control
+ TTFields
DAPI
53BP1
γH2AX
Merge
0 Gy
2 Gy
DMSO
ATRi 250nM
24 hours post-TTF

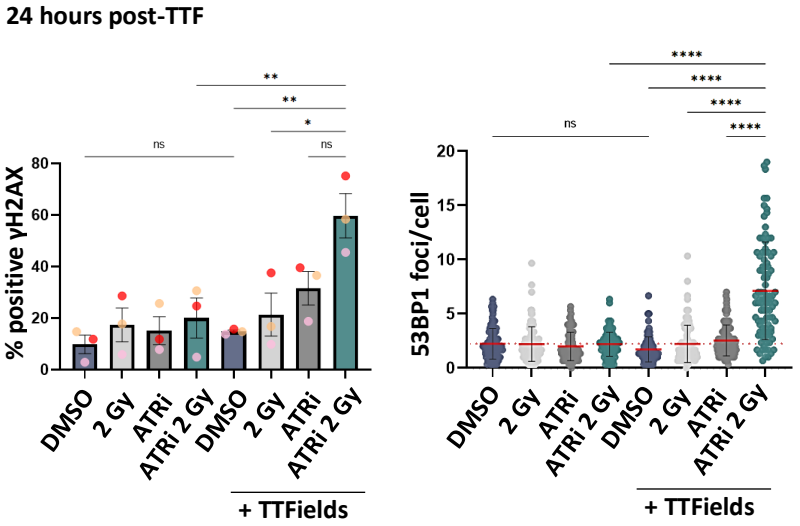
24 hours post-TTF
% positive γH2AX
53BP1 foci/cell
DMSO
2 Gy
ATRi
ATRi 2 Gy
+ TTFields

B **G7 stem**

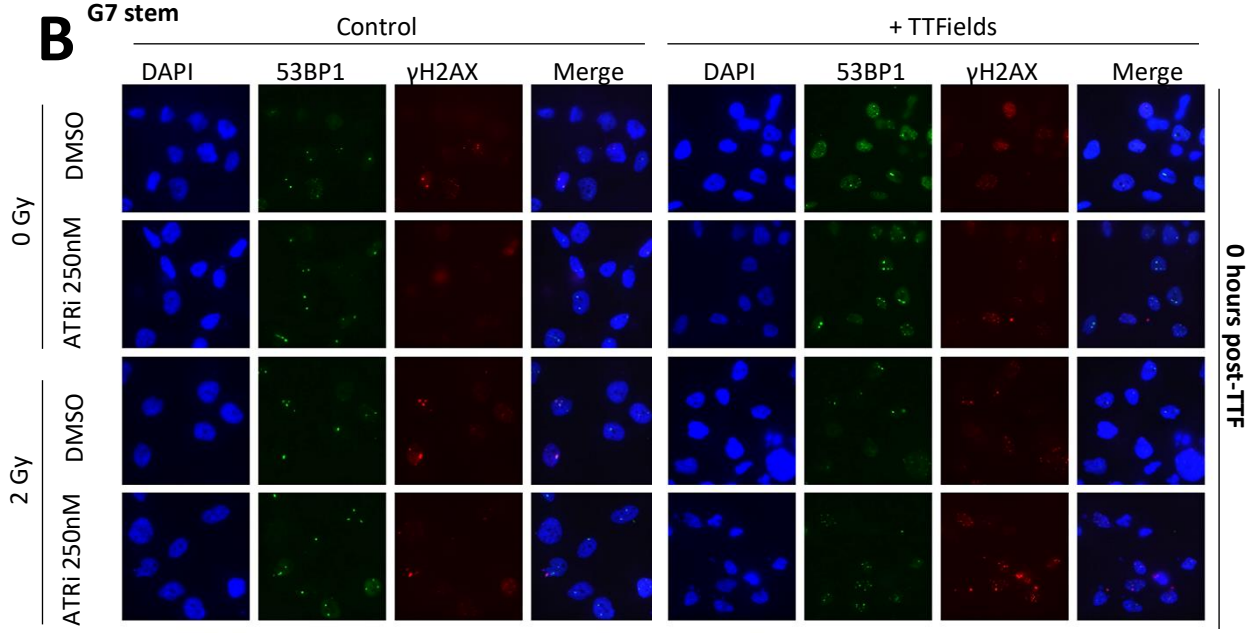
Control
+ TTFields
DAPI
53BP1
γH2AX
Merge
0 Gy
2 Gy
DMSO
ATRi 250nM
0 hours post-TTF

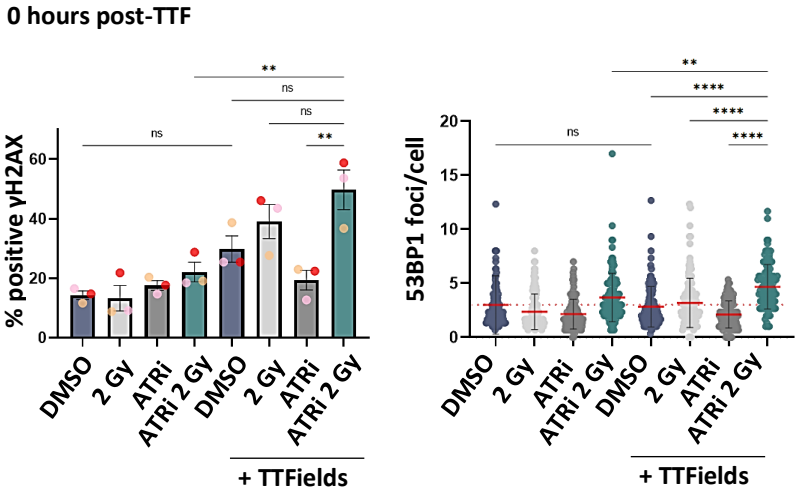
0 hours post-TTF
% positive γH2AX
53BP1 foci/cell
DMSO
2 Gy
ATRi
ATRi 2 Gy
+ TTFields

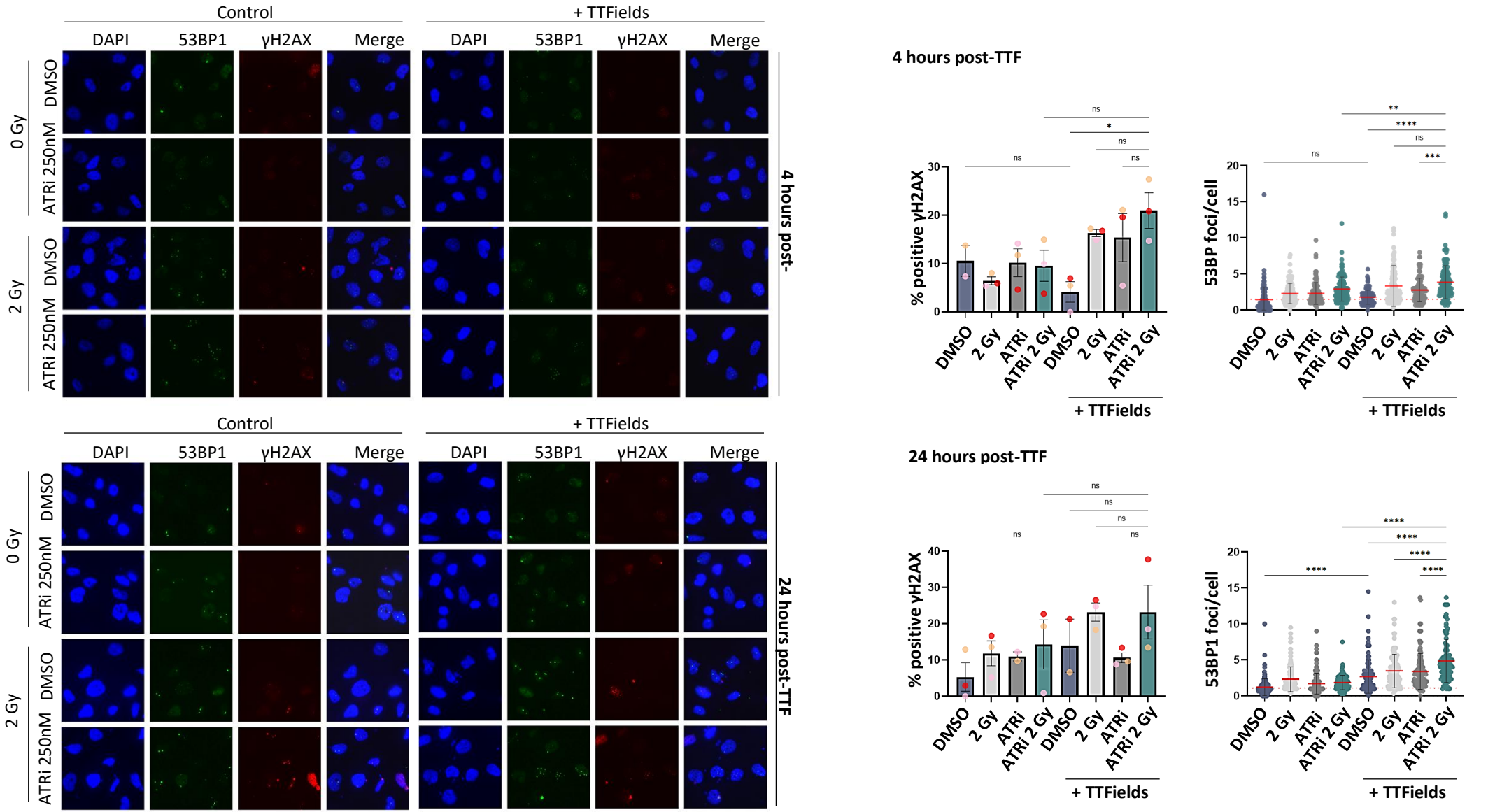

Figure 4.9. The effects of pre-treatment with either ATRi and radiation either alone or in combination prior to TTFields treatment on signalling in DNA damage repair.
The effects of combination treatment with TTFields/ATRi/IR on DNA damage repair were assessed in G1 (**A.**) and G7 (**B.**) stem cells. Cells were fixed at 0-, 4- and 24-hours following completion of TTFields treatment. Cells were subsequently stained for γH2AX and 53BP1. Left – Representative images. Right – Bar charts showing the percentage of cells showing positive γH2AX staining (≥5foci/cell) at 0-, 4- and 24-hours post-TTFields treatment. Graph bars represent the mean of experimental replicates and individual dots representing each repeat. Dot plots showing the number of 53BP1 foci/cell at 0-, 4- and 24-hours post-TTFields treatment. Each dot represents an individual cell and the red line = mean +- SD. n=3

4.3 Discussion

ATR activity in glioma stem cells has been shown to be enhanced relative to bulk counterparts and mediates resistance to standard care DNA damage-inducing treatments (382). ATR is mainly activated by ssDNA during stalled replication forks or during processing of various types of DNA lesions. ATR inhibition has previously been shown to sensitise glioma cells to treatment with radiation and Temozolomide. This sensitivity has been suggested to be mediated through inhibition of G2/M checkpoint activation and increased conversion of replication fork impeding lesions into DSBs. Given that TTFields has been shown to induce replication stress and downregulate proteins involved in the resolution of stalled replication forks, such as BRCA genes and FA repair pathway genes (314, 320), we postulated that inhibition of ATR, a protein that ensures faithful replication, in combination with TTFields may further exacerbate TTFields-induced replication stress in these cells, especially when combined with a DNA damaging treatment such as radiation. Given that unresolved stalled replication forks can be converted to DSBs, the most toxic type of damage, we hypothesised that enhanced DNA damage levels generated by the increased levels of replication stress with combination treatment would correlate with a reduction in survival in glioma stem cell models.

Here, we confirm that ATR inhibition radiosensitises GSCs in line with the literature as measured by a reduction in the surviving fraction via clonogenic survival compared to cells treated with either ATRi or IR alone. TTFields treatment enhanced ATRi-mediated radiosensitisation, reflected by a further 23% and 19% reduction in surviving fraction of G1 and G7 stem cells, respectively. G1 and G7 stem cells pre-treated with ATRi and radiation in combination prior to TTFields exposure experienced a larger reduction in clonogenic capacity compared to GSCs pre-treated with either ATRi or IR alone. To our knowledge, this is the first time that ATR inhibition has been evidenced to enhance TTFields toxicity in glioma stem cells.

RPA associates with ssDNA during replication stress and therefore acts as a surrogate marker for replication stress, and ATR inhibitor sensitivity is dependent on RPA. ATR-mediated phosphorylation of RPA32 at T21 occurs in response to DNA damage, which then acts as a scaffold for the recruitment of downstream DDR factors (540). DDR proteins have been suggested to associate with RPA primarily in its phosphorylated state. As such, phosphorylation of RPA32 at T21 was assessed with the various treatment combinations to determine the effects of treatment on replication stress and DNA repair. Consistent with inducing replication stress, TTFields enhanced p-RPA21(T21)-foci formation in all conditions compared to their respective non-TTFields treated controls. Unexpectedly however, G1 stem cells exhibited reduced levels of p-RPA(T21) when cells were pre-treated with ATRi and 2Gy in combination prior to TTFields treatment compared to cells pre-treated with ATRi alone.

Phosphorylation of RPA32 at T21 has been shown to prevent its association with replication centres, inhibiting DNA replication during replication stress (217, 483) and Toledo *et al*. showed that as RPA levels are artificially reduced, the number of DSBs generated increased (223). Lower levels of p-RPA(T21) may then indicate that replication forks are being converted more rapidly into DSBs which would provide one explanation for why G1 stem cells pre-treated with both ATRi and radiation in combination exhibited increased levels of DSBs compared to cells pre-treated with ATRi alone despite exhibiting lower levels of RPA foci. However, whilst RPA32 phosphorylation promotes checkpoint activation, PP2A-mediated dephosphorylation of RPA in not essential for reactivation of replication (222) and therefore phosphorylation of RPA32 alone is not necessarily indicative of replication state. Phosphorylation at T21 has also been suggested to occur at sites of broken replication forks during replication catastrophe only. However, Toledo *et al.* showed that phosphorylation of RPA32 at T21 takes place in all replication factories, irrespective of DNA damage abundance. RPA can protect ssDNA from nuclease attack even in the absence of ATR activity, as long as there are sufficient RPA stores. Unprotected ssDNA strands are converted to DSBs only upon depletion of RPA (223). Toledo *et al.* also suggested that cells that replicate more rapidly may reach RPA exhaustion sooner than cells that are less replicative, and that in the absence of ATR activity replication fork collapse is S-phase dependent and there may therefore be a delay in the appearance of DSBs following ATR inhibition (223). TTFields has repeatedly been shown to impact the proliferation rate of cells (282, 541-543). Combining TTFields with an inhibitor targeted at a protein that is essential for replication like ATR, may further impact cell proliferation, especially when combined with a DNA damage inducer like radiation which triggers cell cycle checkpoint activation. Indeed, cell counts obtained at the end of the treatment were reduced in the TTFields-treated conditions (supp. figure 4.10), more so in G1 stem cells compared to G7 cells, only achieving significance with the full combination and TTFields monotherapy when compared to the untreated control. Without any evidence of cell death occurring at this timepoint, this might suggest that TTFields reduces cell proliferation in our GSC models. Cells exposed to the full combination treatment may therefore reach RPA exhaustion at a later timepoint compared to less harsh conditions. This may explain why G1 stem cells exhibited even higher levels of damage 4-hours post-completion of treatment as DSBs may take longer to be generated. G7 stem cells have more DSBs immediately after treatment compared to G1 stem cells. Overall phosphorylation of RPA was lower in G7 stem cells. There was no difference in phosphorylation of RPA across TTFields-treated conditions in G7 stem cells. G7 stem cells may convert replication stress more rapidly into DSBs compared to G1 stem cells. This could also explain why a higher DNA damage burden by alkaline comet assay with full combination treatment was detected in G7 stem cells immediately upon treatment completion whereas despite increased signalling of DDR factors (Kap1, Chk1, Chk2 H2AX and 53BP1) in G1 stem

cells, changes in DNA damage levels were not detectable via alkaline comet assay. G1 stem cells may take longer to convert stalled replication forks into DSBs if they have higher RPA stores especially if the cells are replicating more slowly from TTFields exposure. However, because total levels of RPA were not assessed, it cannot be determined whether the differences in phosphorylation levels between cell lines are due to changes in total RPA levels or due to changes in signalling of RPA. RPA signalling is an indirect measure of replication stress and might not be the best marker of replication stress, especially when using inhibitors that mediate RPA signalling such as ATR inhibitors because changes in RPA signalling may not correlate with changes in replication stress levels but rather reflect changes in signalling irrespective of replication stress. However, it is unlikely that at the timepoint investigated, the changes in p-RPA32(T21) levels are due to changes in signalling by ATR because the western blot assay suggested that at that timepoint, ATR activity may no longer be inhibited but is in fact amplified in cells that were previously exposed to ATR inhibitor. However, given the elusiveness of RPA phosphorylation, this data could be interpreted in different ways and using RPA as an isolated marker for replication stress does not depict the full picture.

Irrespective of the exact mechanism of how the damage is generated, the DNA damage burden was higher in cells receiving full combination treatment with TTFields, ATRi and IR in both cell lines. Both G1 and G7 stem cells sustained increased levels of DNA damage, particularly DSBs, 24 hours post treatment (TTFields+ATRi+IR combination) termination, indicating either continual DNA damage formation and/or impaired repair kinetics. G7 stem cells sustained fewer H2AX foci 24-hours after treatment compared to G1 stem cells, suggesting that G7 stem cells may repair damage more efficiently when compared with G1 stem cells, and may reflect differences in activity of DDR proteins. Ahmed *et al*. reported a limited radiosensitisation effect from Chk1 inhibition in GSCs because of increased repair kinetics (vs bulk cells) (382). ATM has been shown to compensate in the absence of ATR through Chk2 phosphorylation (544, 545). However, inhibition of both ATM and ATR simultaneously did not further sensitise glioma cell lines compared to inhibition with ATR inhibitor alone (544). Additionally, cells that are deficient in a G1/S checkpoint, for example through mutations in P53, are more reliant on G2/M checkpoint activation for repair. P53 activity may therefore dictate how cells repair damage following ATR inhibition (546, 547). P53 expression is higher in G7 stem cells compared to G1 stem cells (see supp. Figure 4.12). Additionally, Dueva *et al*. showed that in the absence of RPA, NHEJ is increased by up to 350-fold because spontaneous annealing of ssDNA strands cannot be prevented (548). Differences in RPA levels between cell lines may therefore also alter DNA repair capacity.

γH2AX and 53BP1-foci form almost instantly following irradiation (within 3 minutes) and usually resolve within 24-hours following treatment (549). Persistent γH2AX and 53BP1-foci eventually results in cell death or premature senescence (550, 551). The reduction in clonogenicity observed was not mediated by an increased induction in apoptosis as there was no difference in the fraction of apoptotic cells or necrotic cells across all treatment conditions. However, cells that escape apoptosis can undergo cellular senescence (552). Senescence refers to a commitment to a non-proliferative state, while maintaining metabolic activity and viability (553). Initially, senescence was thought to be an irreversible process, and contrasted with quiescent cells, where proliferation is halted only temporarily (554). However, this is now being contested and several studies have demonstrated that senescent cells can regain the ability to proliferate under certain conditions (555-557). Typically, senescence occurs during telomere shortening, oncogenic activation senescence, or is triggered by DNA damage generated either endogenously or exogenously (558). DNA-damage mediated activation of senescence likely occurs under conditions of sustained DNA damage and is as a result usually accompanied by a persistence of DDR signalling from the unresolved lesions (559). Senescence has number of consequences on tumour growth and dictates treatment response. Senescent cells do not directly contribute to the expansion of tumour cells in the arrested state and have consequentially been associated with a reduction in tumorigenicity (560). However, senescent cells adopt a senescence-associated secretory phenotype (SASP) and can promote tumour growth indirectly through secretion of pro-inflammatory cytokines, such as IL6 and IL8 through NF-κB signalling (561). Reversible activation of senescence also protects them from the toxic effects of treatment, but can mediate tumour recurrence when proliferation is restored, suggesting that the senescent state acts as a survival mechanism and may contribute to treatment resistance (562).

TMZ has previously been shown to induce senescence in glioma cells in an O^6-MeG-dependent way and was triggered by activation of G2/M checkpoint through the ATR-Chk1 axis and p53-p21 axis (520, 546, 563, 564). TMZ-mediated activation of senescence correlated with transcriptional silencing of MMR proteins (MSH2, MSH6, and EXO1) and HRR protein RAD51 and consequently reduced DNA repair activity (546). Senescence is also activated by irradiation, with mitotic catastrophe being suggested to be the main form of cell death mechanism induced by ionising radiation. Mitotic catastrophe is triggered by abnormal mitosis from abnormal chromosome segregation and form non-viable cells associate with several micronuclei. Mitotic catastrophe is not a separate form a cell death per se, rather mitotic catastrophe precedes the induction of various cell fates such as cell death through apoptosis, necrosis and autophagy, but can also trigger activation of senescence (565). Induction of mitotic catastrophe or senescence inhibit cell proliferation and would therefore also be reflected by a failure to form colonies in the clonogenic survival assay. Senescence has been linked to

cellular polyploidy and several studies have previously shown that senescence over apoptosis was activated by treatments that interfere with cell division and induce mitotic catastrophe (566-568). NF-κB activity through activation of SASP has been suggested to suppresses apoptosis in favour of senescence (546). TTFields interferes with cell division and results in abnormal chromosomal segregation, polyploidy and subsequent mitotic catastrophe and cell death (252, 282). Additionally, NF-κB signalling has been suggested to be increased by TTFields (339). Therefore, it is plausible that TTFields may favour activation of senescence at the expense of apoptosis. However, to our knowledge, there have to date been no reports of activation of senescence with TTFields.

There is no single marker for senescence, rather classification of senescent cells relies on a collection of markers, the most established being senescence-associated beta-galactosidase (SA-β-gal) staining (569). Because activation of senescence strongly correlates with persistent DDR signalling and cell cycle checkpoint activation, DDR signalling is usually used in conjunction with SA-β-gal stain to identify senescent cells (559). DDR signalling foci associated with senescence present differently to transient foci that arise from repairable DNA damage and were given the name 'DNA segments with chromatin alterations reinforcing senescence' (DNA-SCARS). DNA-SCARS were not associated with RPA or RAD51 foci staining but did correlate with activated forms of H2AX, ATM, ATR, p53 and 53BP1 (559, 570-573). G1 and G7 stem cells exhibited elevated ATR and ATM activity (p-Chk1, p-Chk2 and p-Kap1) and elevated H2AX and 53BP1 signalling, which was sustained for up to 24 hours following treatment. However, further staining with SA-β-gal would be required to determine whether the cells enter a senescent state with this treatment regimen.

In summary, although the precise mechanism remains to be elucidated, targeting ATR in combination with radiation and TTFields reduces survival of GSCs, potentially through enhanced DNA damage burden and impaired DNA repair kinetics.

4.4 Supplementary figures

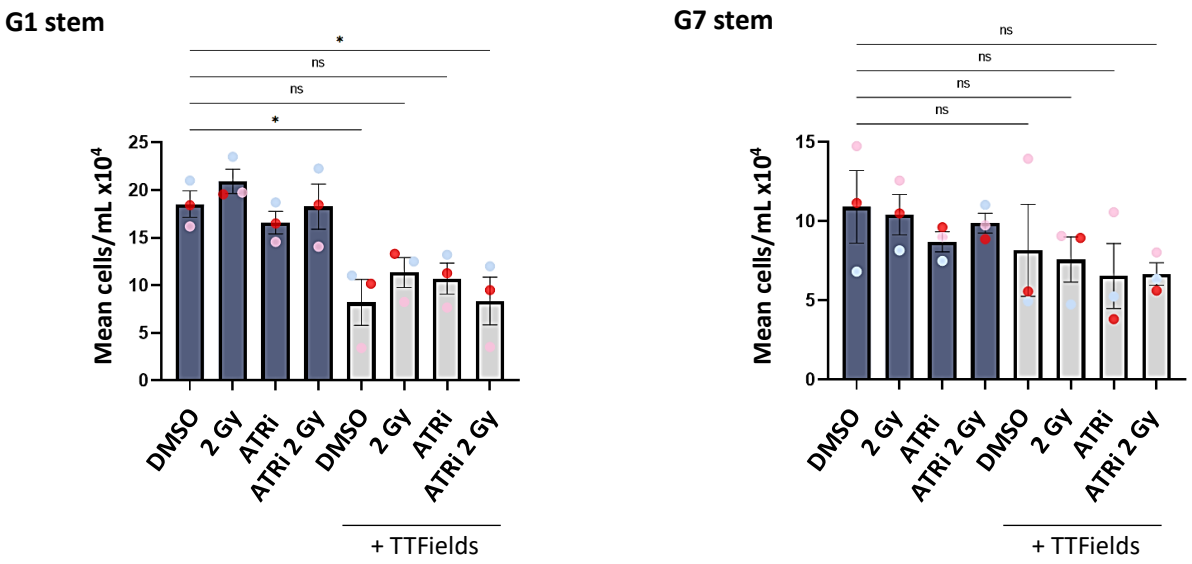

Figure 4.10. Cell counts following treatment with TTFields, ATRi and IR either alone or in combination.
Following treatment with ATRi, IR and/or TTFields, G1 and G7 stem cells were lifted with Accutase. Cells were resuspended in media and counted using a haemocytometer. Error bars represent the standard error of the mean, with individual repeats represented as differently coloured dots. n=3

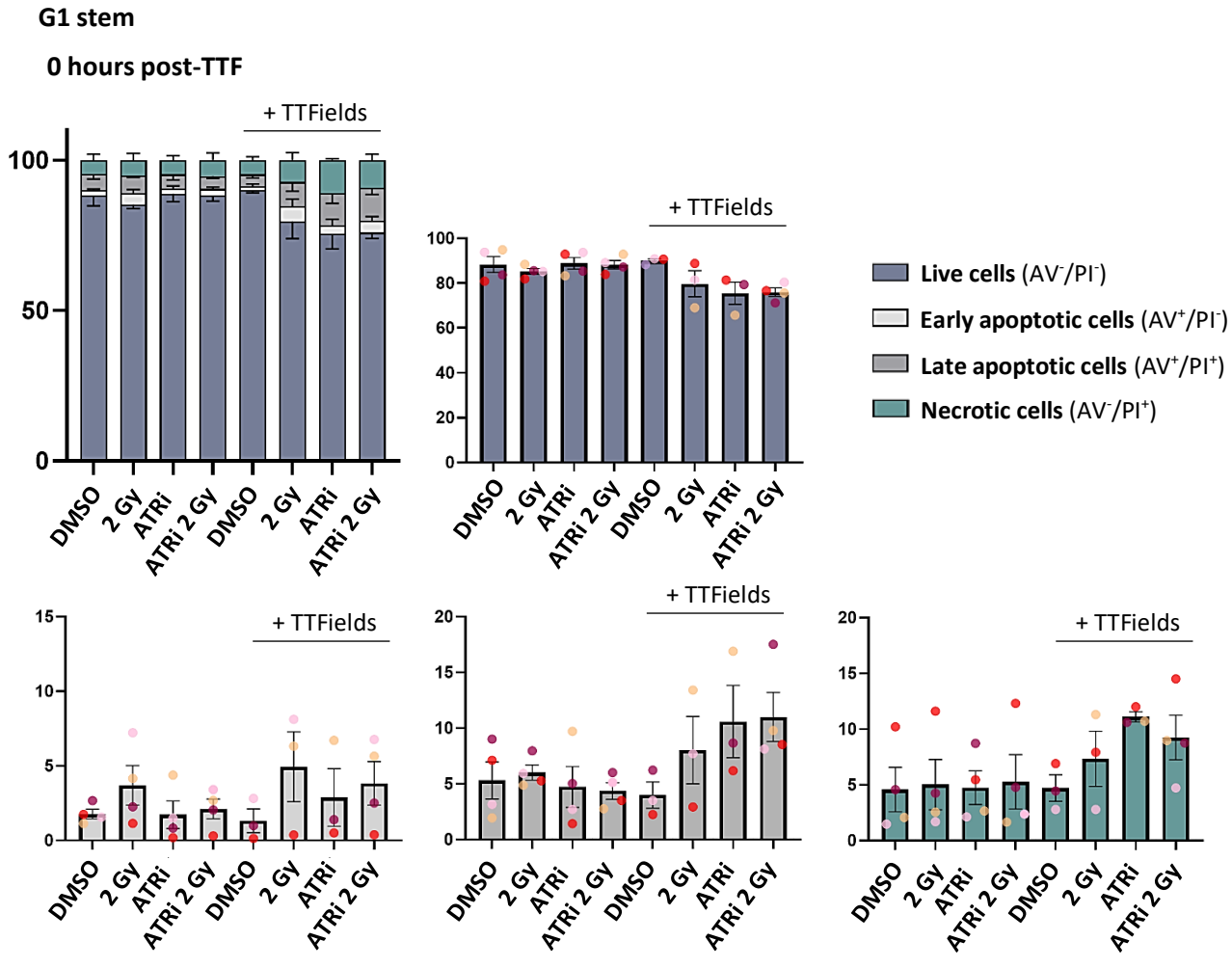

G1 stem

24 hours post-TTF

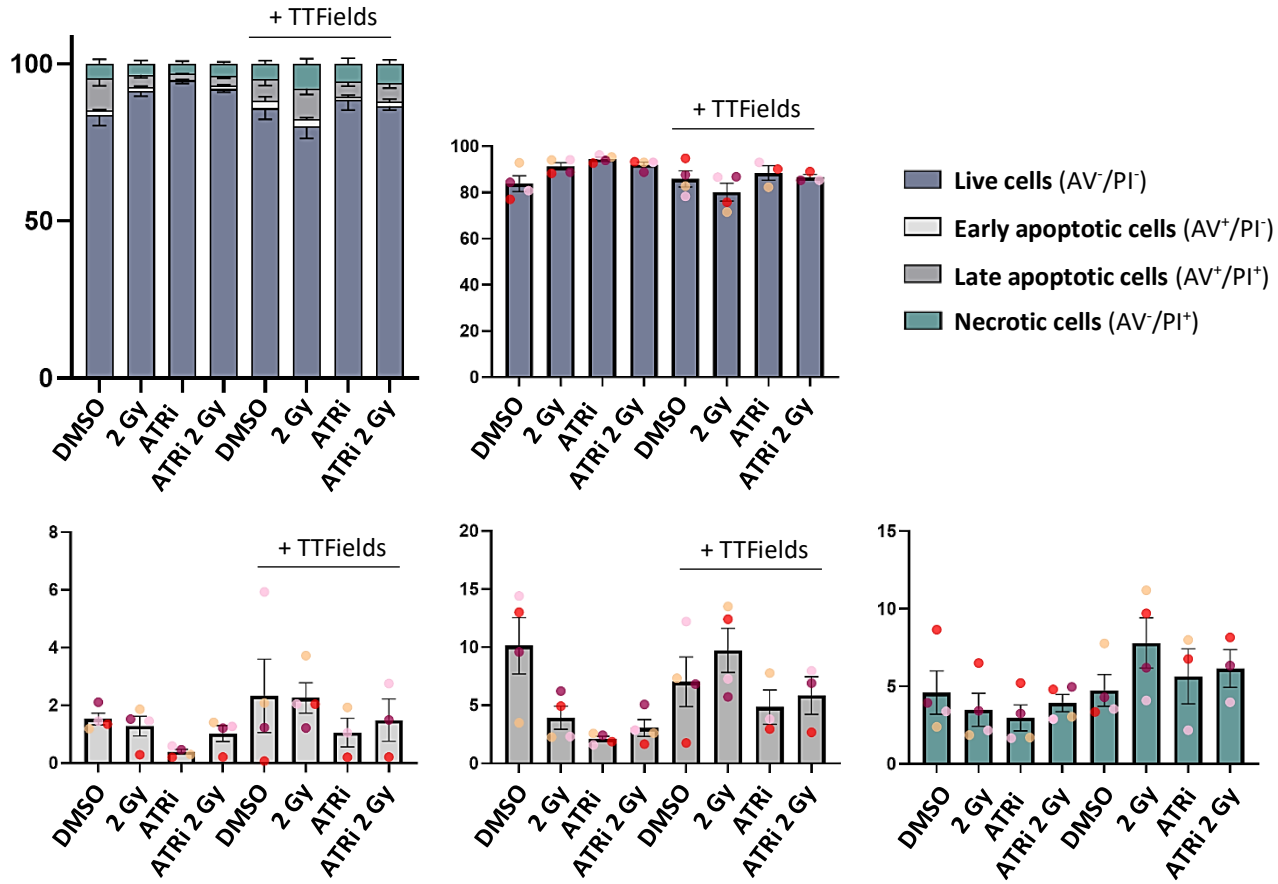

G7 stem

0 hours post-TTF

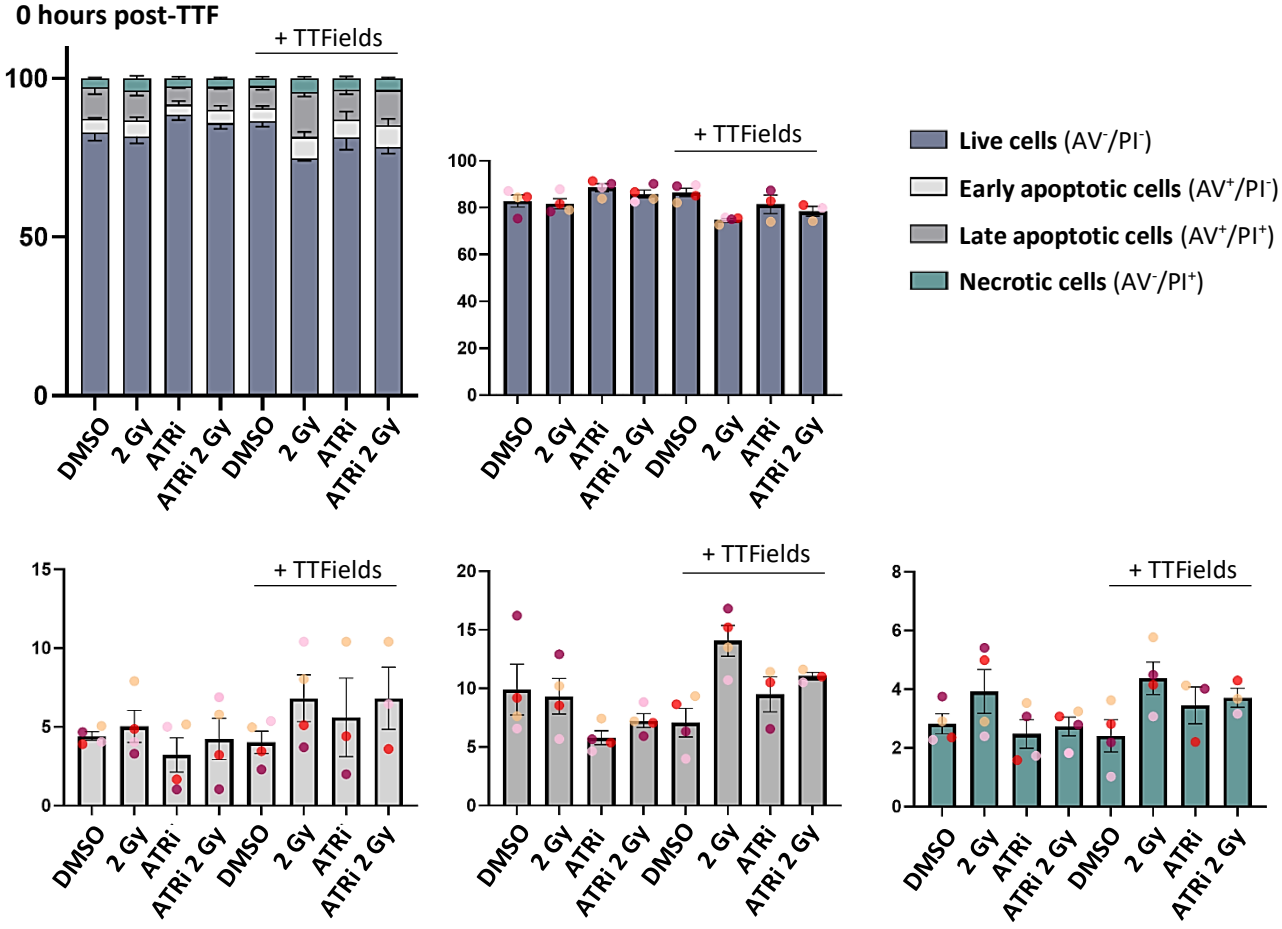

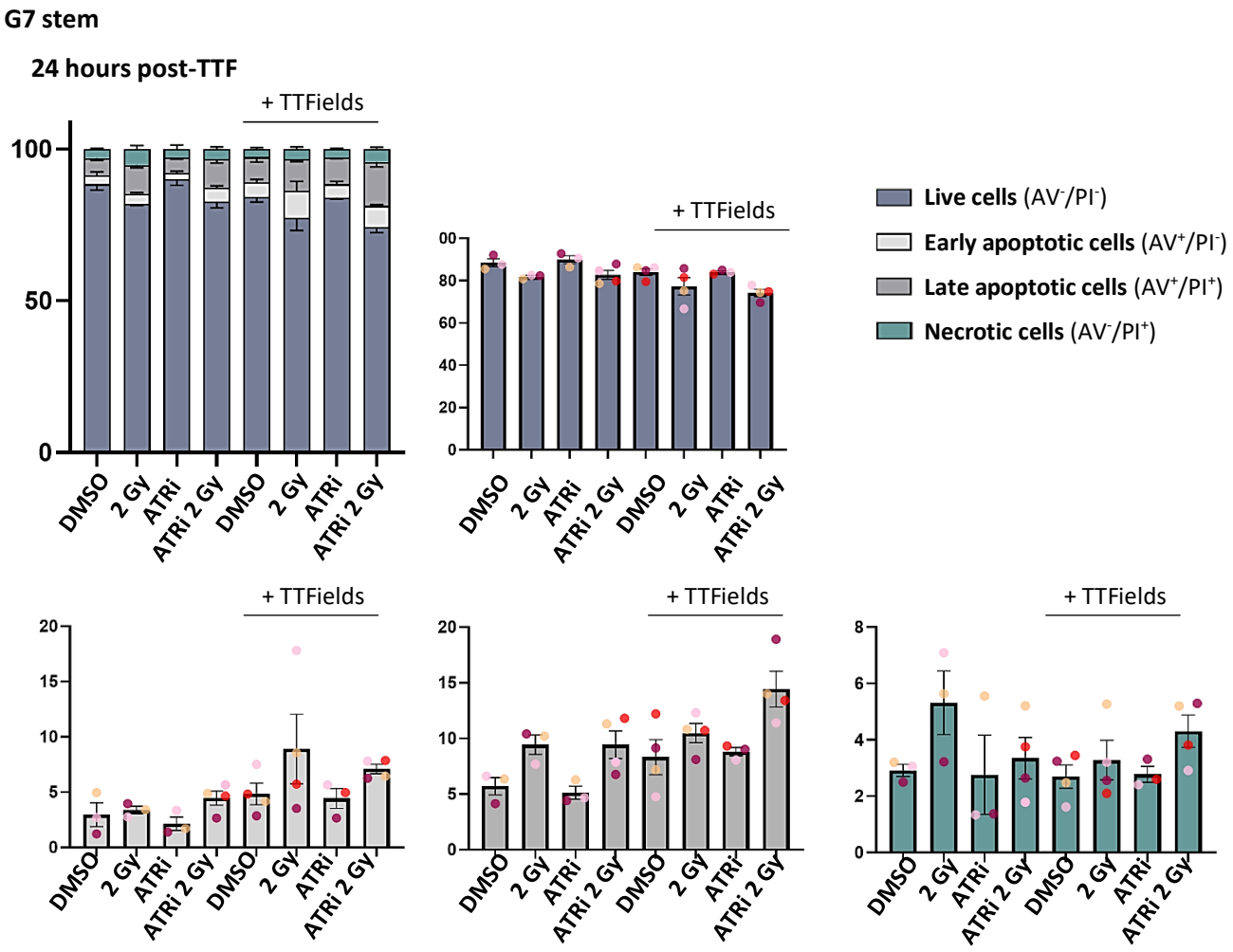

Figure 4.11. Treatment with ATRi, IR and TTFields either alone or in combination does not induce activation of cell death mechanisms.

Following treatment, G1 and G7 stem cells were collected and analysed for Annexin V/PI staining via flow cytometry to assess the effects of treatment on the induction of apoptosis. There was no significant difference in induction of apoptosis across all conditions in both cell lines 0- and 24-hours after treatment completion. Error bars represent the standard error of the mean, with individual repeats represented as differently coloured dots. n=3

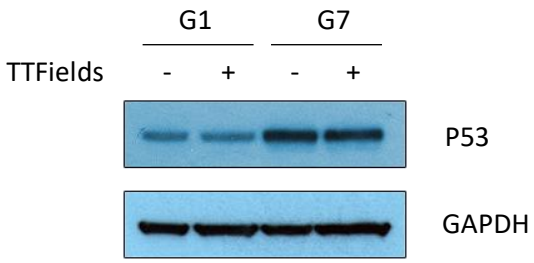

Figure 4.12. P53 protein expression in GSCs.

G7 stem cells express higher levels of P53 compared to G1 stem cells as assessed via Western blot assay. n=1

CHAPTER 5. TARGETING WEE1 OR ATM IN COMBINATION WITH TTFIELDS AND STANDARD-OF-CARE TREATMENT

5.1 Introduction

5.1.1 Role of WEE1 in the DDR

WEE1 is a protein kinase that is activated in response to DNA damage and initiates cell cycle arrest at both the G1 and G2 phase. G1/S and G2/M transitions are initiated by activated cyclin E-Cdk2 and cyclin B-Cdk1 complexes, respectively. WEE1 regulates Cdk2 activity by inhibitory phosphorylation on tyrosine 15 (Tyr15) and prevents transition from G1 to S phase and suppresses replication initiation (see figure 1.5 in section 1.2) (574, 575). Cdk1 activity is mediated by both WEE1 kinase and Cdc25 phosphatase. WEE1 phosphorylates Cdk1 (also known as cycle protein 2 homolog - Cdc2) on residue Tyr15 inactivating Cdk1 and preventing progression through the G2/M checkpoint (576, 577). On the other hand, Cdc25 dephosphorylates Cdk1 on Tyr15, counteracting the inhibitory activity of WEE1 on Cdk1 and promoting entry into mitosis (figure 10) (578, 579).

WEE1 inhibition increases replication origin firing and has been shown to induce replication-dependent DNA damage in cells due to abnormal DNA replication taking place as a result of failure to inhibit G1/S transition (580). In addition, WEE1 inhibition has been shown to aggravate the amount of DNA damage induced by chemotherapeutic agents, leading to increased sensitivity to chemotherapy treatment (581). WEE1 inhibition was also shown to force cells to progress through G2/M and S phase checkpoints with unrepaired DNA damage, resulting in mitotic catastrophe and cell death (582, 583). Additionally, p53 is dysregulated in 87% of glioblastoma patients and cancers cells with dysregulated p53 function lack functional G1 arrest (584) such that they become reliant on arrest at G2 following the induction of DNA damage. WEE1 kinase was shown to be a major driver of G2 arrest in response to DNA damage in glioblastoma and WEE1 inhibition was shown to abolish IR- and TMZ-induced G2 arrest, resulting in mitotic catastrophe and cell death (585). Furthermore, WEE1 inhibition has already been shown to sensitise glioblastoma cells, including GSCs, to radiotherapy and improved survival of tumour-bearing mice. These data highlight the potential for the use of WEE1 inhibition as a therapeutic strategy in the treatment of glioblastoma, especially considering WEE1 expression is increased in glioblastoma and is correlated with poorer survival outcomes (585). The effects of CDK1 inhibition should also be specific to tumour cells seeing as most healthy tissue is not actively replicating (586).

The WEE1 inhibitor, AZD1775, in combination with RT/TMZ has been evaluated in recurrent glioblastoma in a phase I clinical trial (NCT01849146), which concluded that the toxicity profile was acceptable at a dose of 150mg and demonstrated good BBB penetration, despite not crossing the BBB in mice models of glioblastoma (587, 588). Future clinical trials will reveal whether WEE1 inhibition constitutes an attractive therapeutic approach for the treatment of glioblastoma. In the meantime, it will be interesting to see how combining an inhibitor which forces cell to enter mitosis prematurely (like AZD1775) with an anti-mitotic treatment, such as TTFields, affects cancer cell survival.

5.1.2 Role of ATM in the DDR

Ataxia-telangiectasia mutated (ATM) is a serine/threonine protein kinase that belongs to the phosphatidylinositol 3-kinase (PI3K)–related kinase (PIKK) family (168). ATM responds to DNA DSBs and subsequently mediates signalling and repair of those lesions. Germline mutations in the ATM gene result in an autosomal recessive disease known as ataxia-telangiectasia (A-T). A-T is characterised by immunodeficiency, increased susceptibility to cancer development, and a hypersensitivity to IR, which can be accounted for by residual DSBs (589, 590).

In the absence of damage, ATM exists as an inactive dimer. Following the induction of DNA damage, the MRE11-RAD50-NBS1 (MRN) complex localises to DSBs and recruits ATM to DSBs. MRN binds to DSBs with blunt ends and at ssDNA/dsDNA junctions. MRN binding to DSBs results in conformational changes in the complex and recruitment of ATM by DNA end-tethering (591). The MRN complex activates ATM via autophosphorylation of ATM on residue Serine 1981 (Ser1981), which causes dissociation of the inactive dimer into active monomers, which in turn phosphorylate several substrates (592). Activated ATM triggers phosphorylation of chromatin surrounding the break on Ser139 of histone variant H2AX (γH2AX), leading to the recruitment of DDR components to the lesion site in order to aid in the resolution of DSBs via HR or NHEJ (593, 594). Phosphorylation of H2AX recruits 53BP1 and BRCA1 to DSBs. Additionally, ATM is essential for the repair of DSBs within heterochromatic regions through phosphorylation of KAP1 (595). ATM-mediated phosphorylation of KAP1 on S824 during DNA damage results in detachment of the heterochromatin protein HP1-β from H3K9me3 and relaxation of chromatin structure within heterochromatin (596, 597). In addition, ATM activates cell cycle arrest by phosphorylation of Chk2 and p53 on residue threonine 68 (Thr68) and Ser15, respectively (598). P-Chk2(Thr68) mediates degradation of the phosphatase, Cdc25A, whilst p-p53(Ser15) stimulates the CDK2 inhibitor p21, and both therefore act to block entry into S-phase and prevent induction of DNA synthesis by CDK2 (figure 10) (513, 599, 600). Additionally, H2AX phosphorylation recruits Mediator of DNA damage checkpoint protein 1 (MDC1). MDC1 localises to

kinetochores during mitosis and activated the spindle assemble checkpoint to regulate mitotic progression (601). As such, ATM functions to halt the cell cycle in response to DNA damage to allow time for lesion repair before the cell cycle can restart (see figure 1.12 in section 1.3) (602).

ATM signalling has been shown to be elevated in glioma stem cells and correlates with increased resistance to IR (486). GSCs display more efficient DSBR compared to their bulk counterparts making them more resistant to radiation. ATM inhibition reversed this enhanced repair activity of DSBs in GSCs, with ATM inhibited GSCs repairing IR-induced DSBs less efficiently than their bulk counterparts (486). Whilst ATR inhibition has been suggested to sensitise glioma cells more effectively than ATM inhibition, deletion of ATR is non-viable whereas ATM is not and therefore ATM inhibitors are expected to have fewer unwanted toxicities on surrounding healthy cells (603). ATM activity has been shown to be correlate with tumour grade, with increased ATM activity exclusively seen in high grade gliomas and therefore inhibition of ATM has potential applications in the treatment of glioblastoma (604). Small molecule inhibitors of the ATM protein have been shown to replicate some of the characteristics of A-T, such as increased sensitivity to chemotherapy and radiation (605, 606). ATM inhibition is therefore being considered as a sensitising agent to DNA damaging agents for the treatment of cancer and following promising pre-clinical data (607-610), this strategy is being explored in clinical trials in patients with advanced solid cancers (NCT02588105). AZD1390 is a BBB-penetrant ATMi that has been shown to extend survival of orthotopic mice models of lung cancer brain metastases when combined with radiation (607). AZD1390 is undergoing clinical trial investigation in a phase I study assessing the safety and tolerability of AZD1390 combination with radiation for the treatment of both newly diagnosed, recurrent glioblastoma and brain metastases (NCT03423628).

Given the impacts on HRR-mediate DNA repair processes together with the increased DSB burden and reduced DSBR efficiency reported following TTFields treatment (312), which was correlated with increased cell death both in glioma stem and non-stem cells, simultaneously combining TTFields treatment with an inhibitor targeted at a protein that is essential for the response and resolution of DSBs, such as ATM, may potentially enhance TTFields efficacy.

5.2 Results

5.2.1 Optimisation of WEE1 inhibitor for use in glioma stem cells

AZD1775 is a blood-brain barrier penetrant WEE1 oral inhibitor that has already entered clinical trial stages in glioblastoma, where it demonstrated a favourable toxicity profile (611), and was therefore used for WEE1 inhibition in these studies. Western blot was used to investigate the effects of doses between 50nM and 500nM WEE1i (AZD1775) on WEE1 activity in G1 and G7 GSCs. Doses were selected based on the IC50 value of AZD1775 (5.2nM) and data from a previous paper demonstrating inhibition of WEE1 activity in primary glioma cell lines at doses within this range (612). 5 Gy IR was used to stimulate detectable and robust WEE1 activity. WEE1 appears to be activated under basal conditions as WEE1 activity was detected prior to stimulation with DNA-damaging agents and a mild increase in WEE1 activity was detected following IR treatment. As one would predict, increasing doses of WEE1i, phosphorylation levels of Cdk1/Cdc2 on residue Tyrosine 15 decrease (figure 5.1a), with strong inhibition of WEE1 activity achieved at a dose of 200 nM in G1 and G7 stem cells, respectively. As such, this dose was selected for future optimisation studies. To assess the radiosensitising effect of WEE1 inhibition, clonogenic survival assay in GSCs were carried out with increasing doses of irradiation (figure 5.1b-c). 1-hour pre-treatment with 200nM AZD1775 radiosensitises glioma stem cell models, with SER_{2Gy} of 2.82 and 2.50 in G1 and G7 stem cells, respectively. Sensitiser enhancement ratios (SER) are usually defined as the ratio of the radiation dosage that is required to induce a reduction in survival fraction of 50% in the absence of a radiosensitiser (such as a DDRi) to the dose of radiation that is required to achieve the same 50% survival fraction in the presence of a sensitiser. Here, however, SER_{2Gy} was used instead to define the ratio of surviving fractions in the presence and absence of a radiosensitiser at a dose 2Gy because this the fractionation dosage that is used in the clinic and is therefore of clinical relevance.

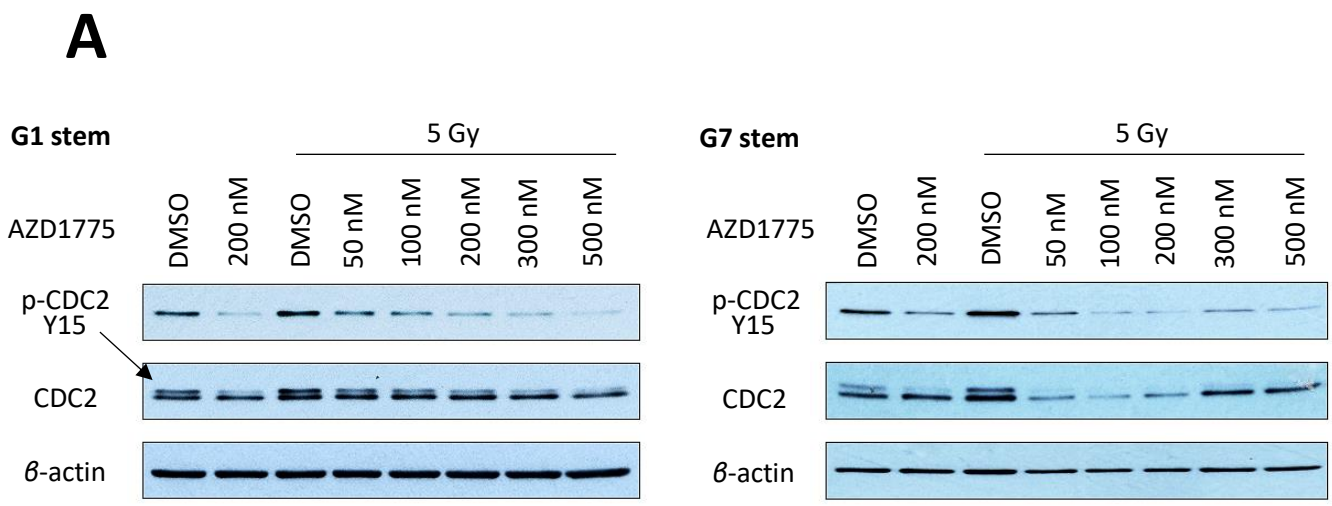

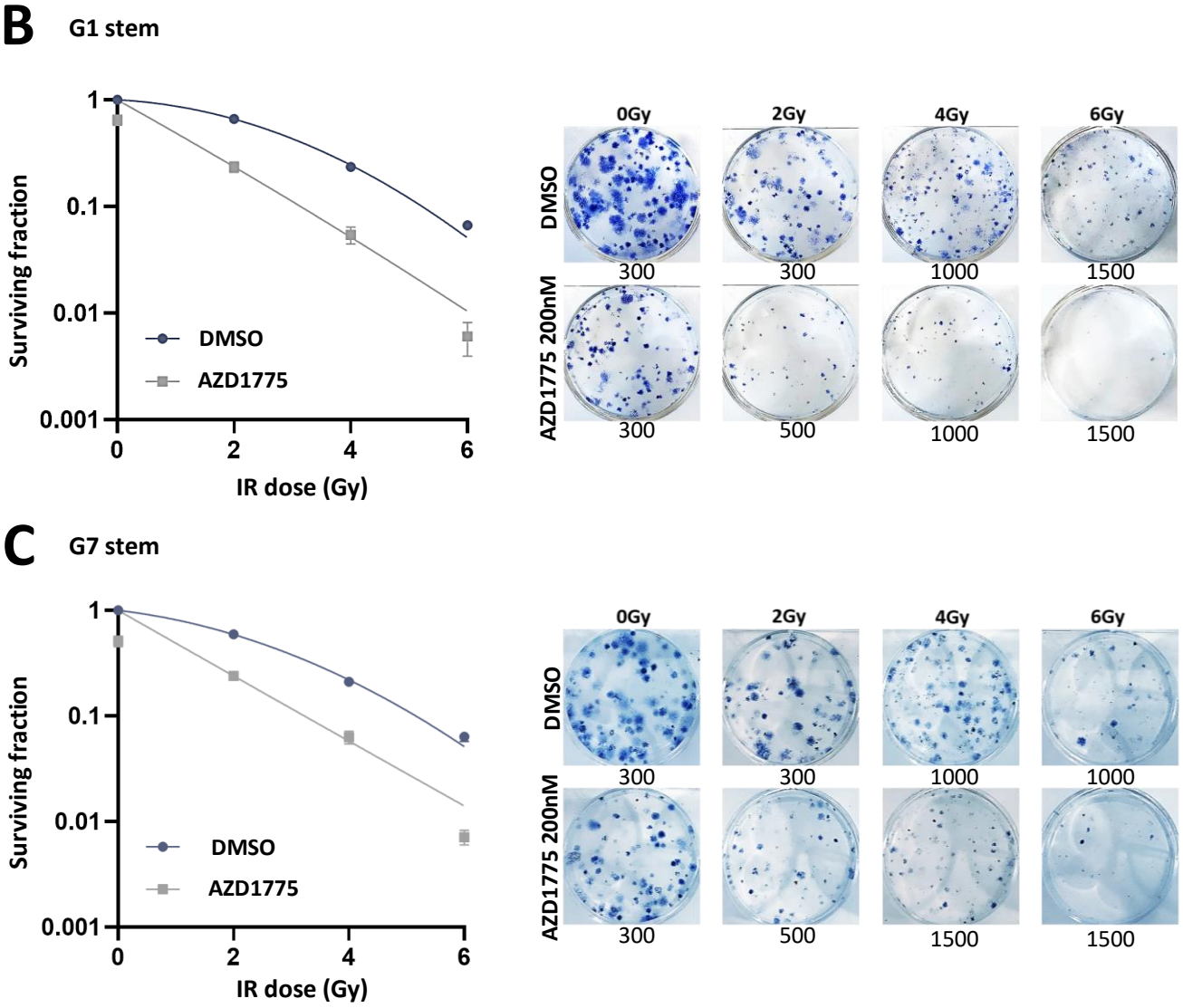

Figure 5.1 WEE1 inhibitor, AZD1775, radiosensitises glioma stem cell models.
A. G1 and G7 GSCs were treated with either DMSO control or WEE1i, AZD1775, at doses ranging between 50nM and 500nM. Cells were treated with 5 Gy IR 1-hour post-inhibitor treatment. 1-hour post-IR treatment, cells were harvested, and protein expression assessed by western blot. AZD1775 demonstrated a dose dependent decrease in phosphorylation of CDC2 on residue Tyrosine 15 in G1 and G7 stem cells with IR. *β*-actin was used as a loading control. n=1. **B.-C.**G1 and G7 glioma stem cells were plated at the indicated densities on 6-well Matrigel-coated plates. The day after seeding, GSCs were pre-treated with either DMSO control or 200nM WEE1i, AZD1775, for 1-hour prior to treatment with increasing doses of radiation (0-6Gy). Clonogenic survival assay was carried out to assess the radiosensitising effect of WEE1 inhibition (n=3). The resulting surviving fractions for both G1 and G7 stem cells are shown on the left in B**.** and **C.** n=3

5.2.2 Optimisation of ATM inhibitor for use in glioma stem cells

Western analyses were used to measure inhibition of ATM activity using a range of doses (0nM-250nM) of the ATM inhibitor (ATMi), AZD1390, in both G1 and G7 glioma stem cells. Because ATM is mainly activated in response to DSBs and IR is a major source of DSBs (613), a dose of 5 Gy IR was used to stimulate robust and detectable ATM activity. ATM is activated via autophosphorylation at Ser1981 briefly following IR treatment and gradually declines over a 24-hour period (592, 607), therefore, samples were harvested 1-hour following treatment with IR. As expected, 5Gy IR resulted in a significant increase in ATM activity compared to DMSO control in both cell lines, as measured by phosphorylation of ATM substrates (p-Chk2(Thr68) and p-ATM(Ser1981)). As seen in figure 5.2, 50nM AZD1390 was able to effectively inhibit irradiation-induced ATM signalling in both G1 and G7 stem cells, as demonstrated by a strong decrease in p-Chk2(Thr68) and p-ATM(Ser1981) levels compared to DMSO control (+IR). Due to its strong ability to inhibit ATM activity, a dose of 50nM AZD1390 was selected for future experiments. 1-hour pre-treatment with 50nM AZD1390 radiosensitises glioma stem cell models, with SER_{2Gy} of 6.89 and 7.88 in G1 and G7 stem cells, respectively (figure 5.3). Initially, a dose of 250nM was used for combination studies but this proved to be too toxic (see supp. figure 5.7).

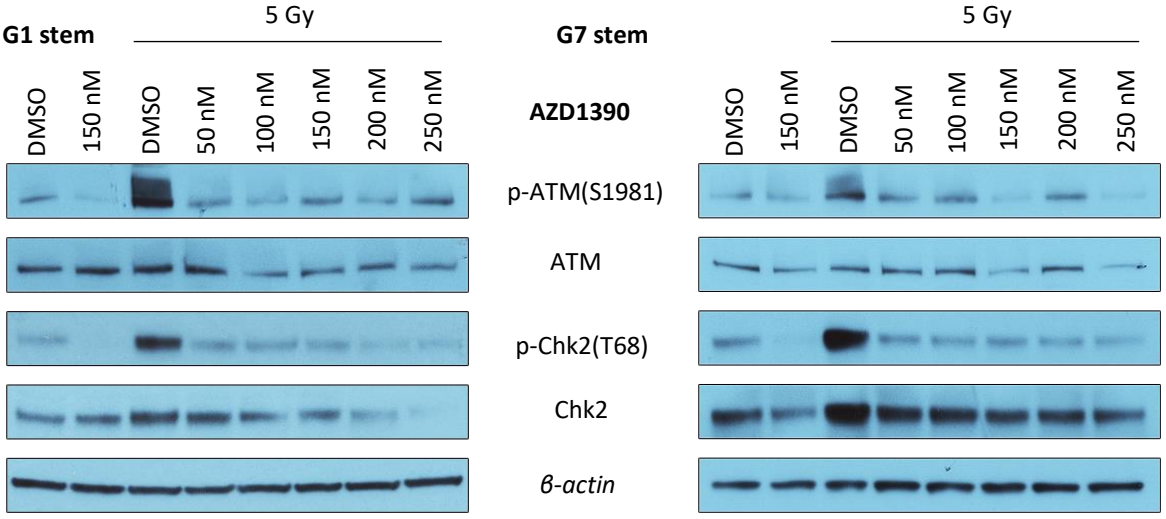

Figure 5.2 Inhibition of ATM activity following treatment with ATMi, AZD1390.
G1 and G7 glioma stem cells were pre-treated either with DMSO control or with ATMi, AZD1390, at concentrations ranging between 50nM and 250nM. One hour following inhibitor treatment, cells were treated with 5 Gy IR to stimulate ATM activity. Cells were harvested 1-hour post-IR treatment and protein expression was assessed via western blot. *β*-actin was used as a loading control. AZD1390 inhibited auto-phosphorylation on residue Ser1981 and phosphorylation of Chk2 on residue Thr68, a substrate of ATM activity, in both G1 and G7 GSCs at all doses tested. n=2

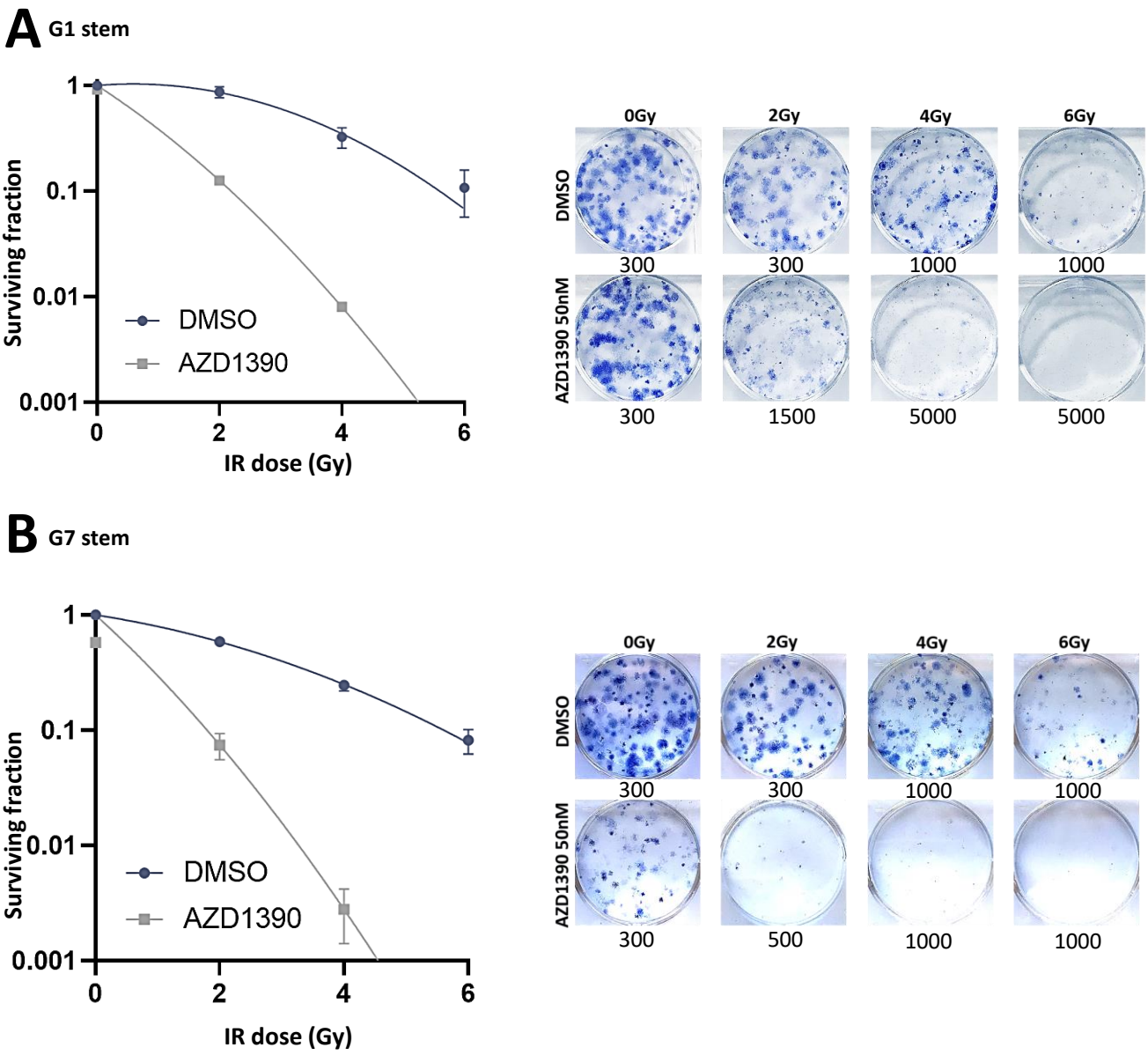

Figure 5.3 ATM inhibitor, AZD1390, potently sensitises glioma stem cells to radiation.
G1 and G7 glioma stem cells were plated at the indicated densities on 6-well Matrigel-coated plates. The day after seeding, GSCs were pre-treated with either DMSO control or 50nM ATMi, AZD13905, for 1-hour prior to treatment with increasing doses of radiation (0-6Gy). Clonogenic survival assay was carried out to assess the radiosensitising effect of ATM inhibition. The resulting surviving fractions for both G1 and G7 stem cells are shown on the left in **A.** and **B.**, respectively, with representative images shown on the right. Numbers below the representative images indicate the number of cells seeded during plating. Error bars show SEM (some error bars are too small to be seen). n=3

5.3 Discussion

Activation of DNA damage checkpoints plays an essential role in the cellular response to DNA damage as it ensures the cell cycle is halted in the presence of DNA lesions to allow time for lesion repair and maintains genetic stability by preventing damaged DNA from being passed onto daughter cells. WEE1 kinase is a major driver of G2 arrest in response to DNA damage in glioblastoma and WEE1 inhibition has been shown to abolish IR- and TMZ-induced G2 arrest, resulting in mitotic catastrophe and cell death (585). Seeing as WEE1 inhibition forces cells to enter mitosis prematurely, even in the presence of unrepaired DNA damage and/or increased replication stress, and TTFields mainly acts on mitotic cells, combining TTFields with a WEE1 inhibitor should make for an interesting combination. Additionally, WEE1 inhibition increases levels of replication stress by increasing replication origin firing by activating cyclin-CDK complexes during cell cycle progression. TTFields has been shown to increase replication stress, therefore, WEE1 inhibition may exacerbate replication stress levels in TTFields-treated cells, exceeding thresholds of tolerable levels of replication stress. Given the reliance on the G2/M arrest when G1 arrest is dysregulated, p53-mutant cancers may particularly benefit from this combination.

AZD1775 is a blood-brain barrier penetrant WEE1 oral inhibitor that has already entered clinical trial stages in glioblastoma, where it demonstrated reasonable tolerability (156) and was therefore selected for WEE1 inhibition in our studies. Strong inhibition of WEE1 activity was achieved at a dose of 200nM in G1 and G7 stem cells. As such, this dose was selected to assess the radiosensitising effect of WEE1 inhibition in these GSCs. Previous groups have reported that the WEE1 radiosensitises and chemosensitises various glioma cell models (612, 614, 615). Here, we show that WEE1 inhibitor, AZD1775, effectively radiosensitised both G1 and G7 stem cell lines, at a clinically relevant dose of irradiation (2Gy), with SERs of 2.82 and 2.50 in G1 and G7 stem cells, respectively, and a surviving fraction of ~24% in both cell lines.

Future studies will need to be carried out to assess the effects of TTFields treatment on the radiosensitising effect of WEE1 inhibition in glioma stem cells. Preliminary data from a published abstract from Slangen *et al*. has suggested that WEE1 inhibition synergistically reduced colony formation by TTFields treatment in established glioma cell lines, however they did not measure a difference in DNA damage induction by the different treatments combinations, suggesting that the sensitising effects of WEE1 inhibition on TTFields may not be from augmented DNA damage levels (616), although this could be dependent on the dose of WEE1 inhibitor used or the timing/scheduling of the combination treatment. WEE1 inhibition has been shown to increase the release of pro-

inflammatory cytokines through activation of the cGAS/STING pathway and enhanced macrophage type I and cytotoxic T cell infiltration in genetically engineered mouse models of small cell lung cancers (617). Given that TTFields has been shown to provoke an anti-inflammatory response, WEE1 inhibition could synergise with TTFields instead by further promoting anti-tumour immunity. Further, Pokorny *et al*. suggested that AZD1775 efficacy could be limited due to inhomogeneous distribution of inhibition across the brain in orthotopic mouse models of glioblastoma (612). TTFields could enhance drug delivery to the brain, improving efficacy of WEE1 inhibitors.

ATM is another cell cycle checkpoint regulator protein and is mainly activated in response to DSBs. Upon binding to DSBs, ATM mediates the recruitment of proteins required for DSBR and mediates phosphorylation of substrates that are required for cell cycle arrest activation. GSCs have been shown to exhibit increased ATM activity under basal conditions, which is further induced following IR treatment, and has been associated with increased resistance to IR treatment (486). Given the increased DSB burden and reduced DSBR efficiency reported following TTFields treatment, which was correlated with increased cell death both in glioma stem and non-stem cells, simultaneously combining TTFields treatment with an inhibitor targeted at a protein that is essential for the response and resolution of DSBs, such as ATM, may potentially enhance TTFields efficacy, especially given that ATM inhibition has already been shown to sensitise glioma cells to radiotherapy, a known DSB inducer.

AZD1390 is a newly developed highly selective, BBB penetrating ATM inhibitor that has recently entered in human trials (NCT03423628) in brain cancers, including primary and recurrent glioblastoma patients, in a phase I study which aims to assess the safety and tolerability of AZD1390 given in combination with radiation therapy. AZD1390 inhibited IR-induced ATM activity in G1 and G7 stem cells at a dose of 50nM, as shown by reduced phosphorylation of ATM substrates, p-Chk2(Thr68) and p-ATM(Ser1981). From the work carried out in this chapter, it was shown that AZD1390 potently radiosensitises glioma stem cell models, with SER_{2Gy} of 6.89 and 7.88 in G1 and G7 stem cells, respectively. There are to date no studies examining the effects of combining an ATM inhibitor with TTFields. Given the potent radiosensitisation effects induced by AZD1390 treatment, it will be interesting to see how AZD1390 affects TTFields response, both alone and in combination with radiotherapy across a range of preclinical glioma models.

Previous work undertaken with PARPi and ATRi in this thesis serves as proof-of-concept for the use of DDRi as a strategy for the sensitisation of GSCs to TTFields treatment. Because tumours display vast intra- and inter-tumoural heterogeneity, the DDRi of choice to elicit the optimal sensitisation effect to TTFields may very between tumours depending on their genetic background. For example, ATRi

sensitised both G1 and G7 GSCs more profoundly to TTFields+IR combinations compared to PARPi and G1 GSCs were more sensitive to combination treatment with TTFields+PARPi+IR compared to G7 GSCs. Therefore, it will be important to determine how GSCs respond to additional TTFields/DDRi combinations and identify genetic markers that might predict how glioblastoma patients respond to these various TTFields/DDRi combinations, which may in future help guide treatment strategies in the clinic based on the genetic profile of tumours from individual patients. Given the roles of ATM and WEE1 within the DDR, as detailed in this section, there is a strong rational for further preclinical evaluation for their potential use in combination with TTFields and standard-of-care treatment to improve the treatment of gliomas.

5.4 Supplementary figures

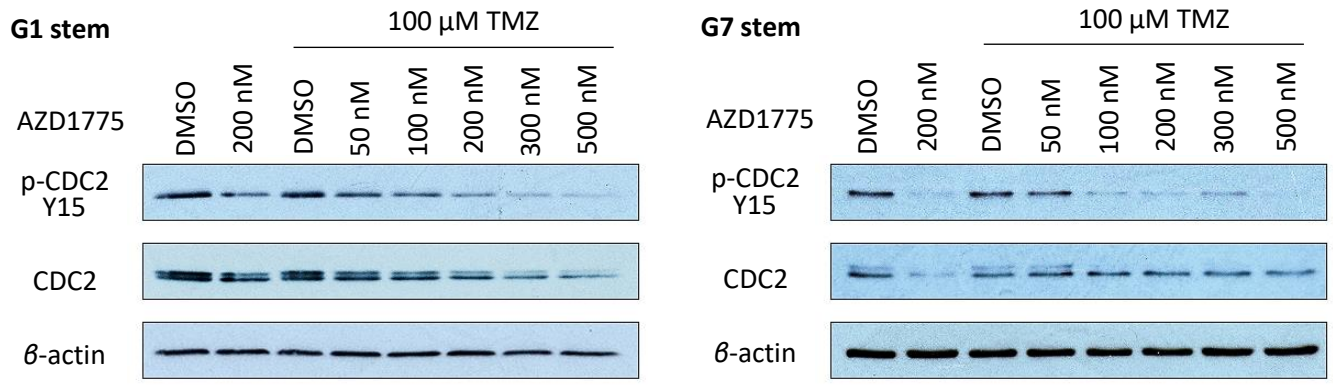

Figure 5.4 WEE1 inhibition in GSCs following treatment with WEE1 inhibitor, AZD1775.
G1 and G7 GSCs were treated with either DMSO control or WEE1i, AZD1775, at doses ranging between 50nM and 500nM. Cells were treated with 100 µM TMZ 1-hour post-inhibitor treatment. Four hours following TMZ treatment, cells were harvested, and samples were ran on a western blot. AZD1775 demonstrated a dose dependent decrease in phosphorylation of CDC2 on residue Tyrosine 15 in G1 and G7 stem cells with TMZ (B). β-actin was used as a loading control. n=1

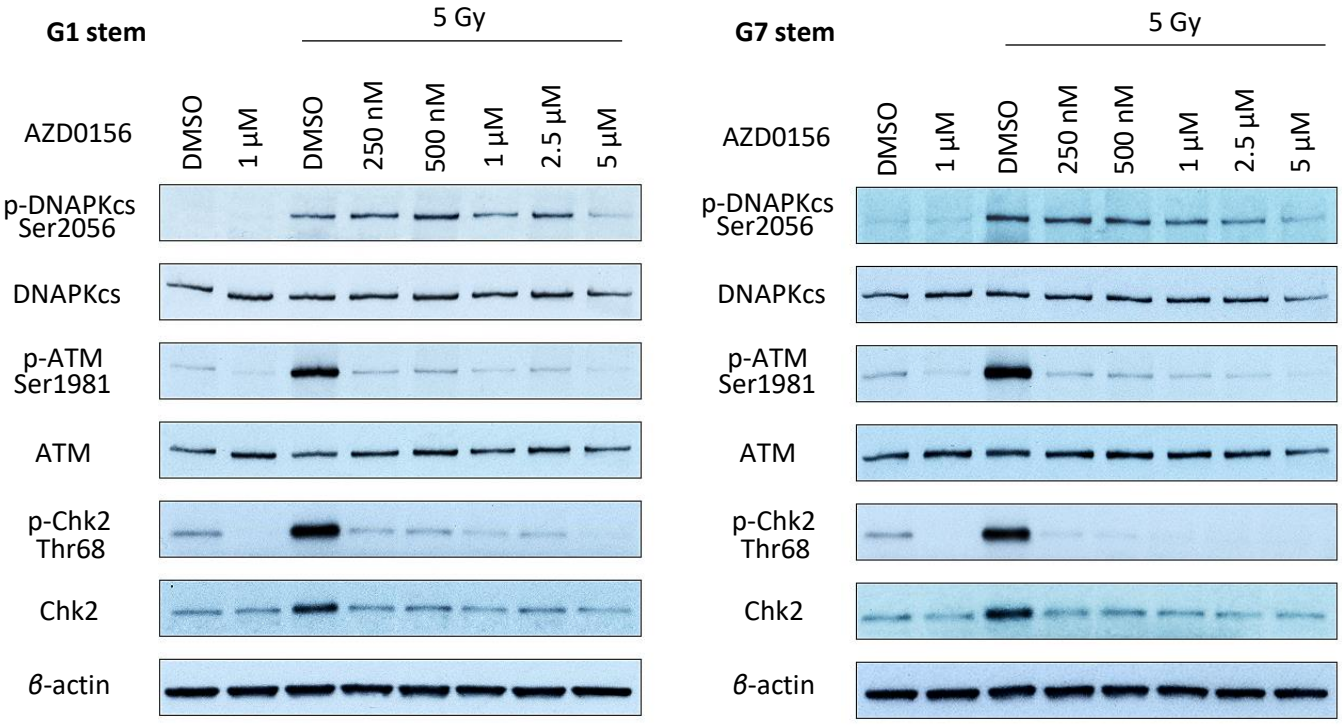

Figure 5.5. Inhibition of ATM activity in GSCs using ATMi.
G1 and G7 glioma stem cells were pre-treated either with DMSO control or with ATMi, AZD0156, at concentrations ranging between 250nM and 5µM. One hour following inhibitor treatment, cells were treated with 5 Gy IR to stimulate ATM activity. Cells were harvested 1-hour post-IR treatment and samples were run on a western blot. β-actin was used as a loading control. AZD0156 was able to inhibit phosphorylation of Chk2 on residue Thr68 and ATM on residue Ser1981, substrates for ATM activity, in both G1 and G7 GSCs at all doses tested. Phosphorylation of DNA-PKcs on residue Ser2056 was inhibited at 5µM and 2.5µM AZD0156 in G1 and G7 GSCs, respectively. n=1

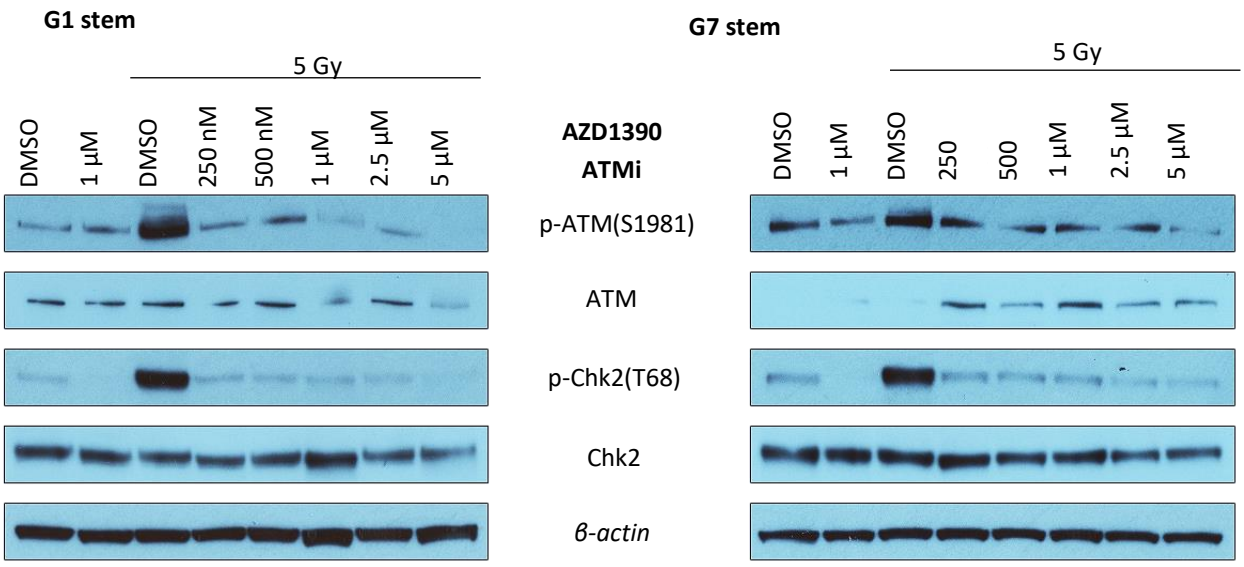

Figure 5.6 ATM inhibitor activity in glioma stem cell models.

G1 and G7 glioma stem cells were pre-treated either with DMSO control or with ATMi, AZD1390, at concentrations ranging between 50nM and 250nM. One hour following inhibitor treatment, cells were treated with 5 Gy IR to stimulate ATM activity. Cells were harvested 1-hour post-IR treatment and samples were run on a western blot. *β*-actin was used as a loading control. AZD1390 inhibited auto-phosphorylation on residue Ser1981 and phosphorylation of Chk2 on residue Thr68, a substrate of ATM activity, in both G1 and G7 GSCs at all doses tested. n=2

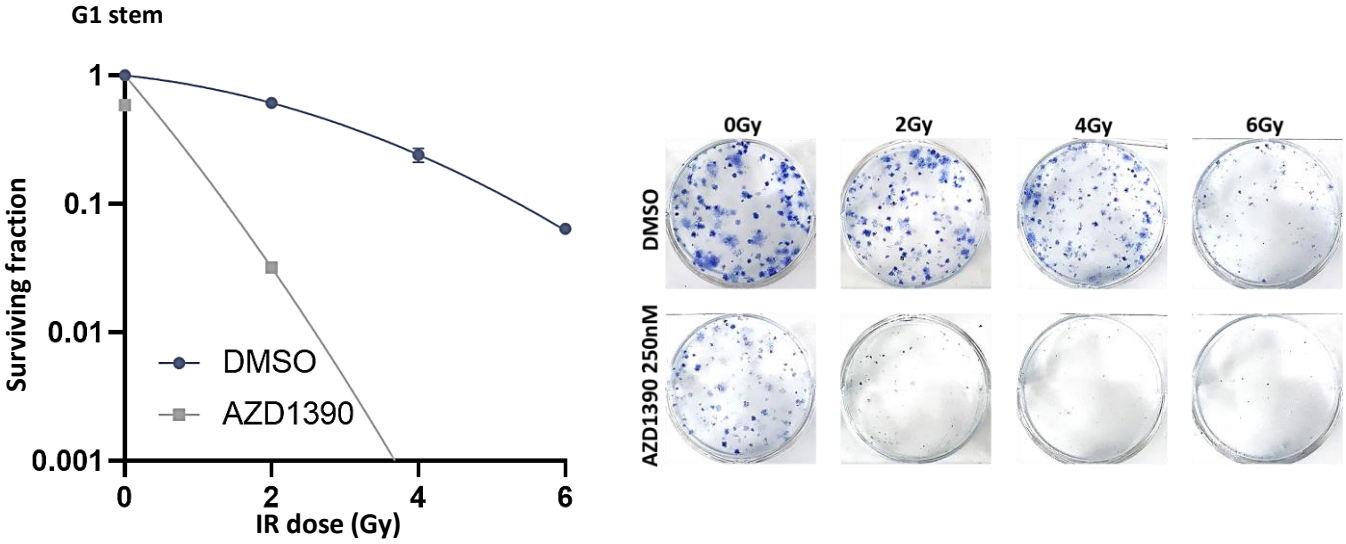

Figure 5.7 ATM inhibitor, AZD1390, radiosensitises glioma stem cell models.

G1 glioma stem cells were plated at the indicated densities on 6-well Matrigel-coated plates. The day after seeding, GSCs were pre-treated with either DMSO control or 250nM ATMi, AZD13905, for 1-hour prior to treatment with increasing doses of radiation (0-6Gy). Clonogenic survival assay was carried out to assess the radiosensitising effect of ATM inhibition. The resulting surviving fractions for G1 stem cells are shown on the left, with representative images shown on the right. Numbers below the representative images indicate the number of cells seeded during plating. n=3

CHAPTER 6. DISCUSSION, LIMITATIONS AND FUTURE STUDIES

6.1 Discussion

Glioblastomas are the most common and the deadliest cancer arising in the brain. Despite aggressive treatment regimens, glioblastomas are currently incurable, which has been attributed to a number of factors. Firstly, these tumours are highly invasive and infiltrate into surrounding healthy tissue, limiting the extent of safe surgical resection possible. Secondly, the extensive intra- and inter-tumoral heterogeneity, which characterises these tumours, and the presence of the BBB limit treatment efficacy and glioblastoma almost always recurs, often in a more treatment resistant form (62). Efforts to extend survival by increasing irradiation/chemotherapy doses results in unacceptable toxicities in healthy tissue (235), and as such, inhibitors targeted at the DDR have been suggested to expand therapeutic efficacy within cancer cells specifically (238). Cancer cells harbour deficiencies in key DDR genes and because of this, cancer cells, in particular glioma stem cells, have adapted to rely on a reduced subset of repair pathways that are hyperactivated in order to compensate from the increased DNA damage burden they are subjected to as a result of increased replicative and oxidative stress (239, 240). This method should spare healthy tissue because, in contrast to cancer cells, healthy cells can recruit the activity of a fully functioning DDR. Functional redundancy across repair pathways limits single agent efficacy. Therefore, targeting multiple DDR processes simultaneously is likely to be required for optimal therapeutic benefit (249, 250, 618). TTFields has been shown to exert its effects via numerous mechanisms, but of interest to this thesis, TTFields was shown to induce DNA damage and replication stress and delay DNA damage repair, which was more specifically suggested to be through impaired HRR activity from downregulation of BRCA genes (312, 314, 315, 320). Both pre-clinical and clinal studies have demonstrated the effects of TTFields to be specific to cancer cells (285, 376, 619-621). This has mainly been suggested to be due to TTFields targeting actively replicating cells whilst healthy brain tissue mostly consists of nonreplicating cells and are therefore protected from the effects of TTFields. Additionally, TTFields crosses the BBB and therefore limitations associated with conventional drugs in terms of delivery to the brain do not need to be considered. In fact, given that TTFields has been suggested to enhance cell membrane and BBB permeability (376), TTFields could be exploited as a tool to enhance drug delivery at the tumour site. For these reasons, TTFields makes the ideal candidate to form the basis of combinational strategies aimed at the DDR, particularly in resistant GSC populations (622).

We hypothesised that combining TTFields with therapeutic DDR inhibitors (PARPi, ATMi, ATRi and WEE1i) could enhance TTFields potency in glioma cells alone or in combination with Temozolomide

and/or IR. We therefore aimed to determine the most effective combination of therapeutic DDRi with TTFields for treating a range of 2D glioma cell models and assess mechanistic basis of interaction.

The electric field frequency of 200kHz was chosen because, not only have previous studies established that this frequency offers optimal inhibition of cell proliferation in glioblastoma cell lines, including GSCs (252), this is also currently the only approved frequency for treatment of both primary and recurrent glioblastoma in the clinic. TTFields as a monotherapy induces a reduction in survival of glioma stem cells by an average of 29% and 16% in G1 and G7 GSCs, respectively. This is a smaller reduction in survival compared to what has previously been measured for GSCs. Clark *et al.* (2018) reported a 33-74% decrease (depending on the cell line) in GSCs survival following monotherapy TTFields (200 kHz, 1 V/cm) compared to untreated control (276). Although they used a smaller field intensity in their studies, their cells were exposed to TTFields for a duration of 8 days (in comparison to 2 days in our experiments), which might explain why they observed a larger reduction in survival. However, preliminary data produced by Mazzanti *et al.* (2019) described a 60% reduction in survival in GSCs following TTFields (200kHz) treatment, even when GSCs were exposed to TTFields for a shorter duration of 72 hours, which is still considerable larger than what we measured. However, it is clear from the wide range of responses (between 33-74% reduction in cell survival following TTFields treatment) that have been described in prior studies that the effects of TTFields on cell proliferation are highly variable between cell lines.

As mentioned previously, cells that are deficient in HRR are particularly vulnerable to PARP inhibition through synthetic lethality mechanisms (623). PARP inhibition therefore constitutes an obvious candidate for TTFields-based DDRi combinations. The data presented in this thesis shows that PARP inhibitor treatment, at a clinically relevant dose significantly sensitises glioma stem cell models to TTFields treatment, especially when combined with the current standard care DNA damaging treatment, radiation and temozolomide. In addition to their role in HRR, BRCA genes cooperate with FA repair proteins to mediate replication fork stabilisation in response to replication stress. Given that TTFields reduces the expression of genes involved in the response to replication stress, drugs that target pathways involved in replication fork stabilisation and replication fork restart, such as ATR inhibitors, may prove to be more effective when combined with TTFields. ATR plays a central role in the response to following genomic stress and, as such, constitutes an alternative promising target for TTFields-based combinations. Here, we show that the BBB penetrant ATRi, AZD6738 sensitised G1 and G7 stem cells to TTFields treatment both with and without irradiation. This is to our knowledge the first time that PARP and ATR inhibition have been shown to increase sensitivity to TTFields treatment in GSCs. ATRi demonstrated more profound sensitisation to TTFields+IR combinations in both G1 and

G7 GSCs compared to PARPi and G1 GSCs were overall more sensitive to TTFields/DDRi-based combination treatment compared to G7 GSCs, highlighting how inter-tumoural heterogeneity may dictate how GSCs respond to treatment. We propose that the increased sensitivity seen with both DDRi in combination with TTFields is mediated by an increased induction in DNA damage, particularly DSBs, and/or delayed DNA damage repair. The increased sensitivity seen by PARP inhibitor could be more specifically regulated by TTFields-mediated downregulation of the HHR pathway. Although, additional studies need to be carried out to confirm that DNA repair via the HRR pathway is in fact inhibited.

Whilst the vast majority of the work carried out in this thesis investigated the effects of TTFields/DDRi combinations with radiation, currently, TTFields is only approved in combination with chemotherapy, requiring the course of radiation therapy and concomitant chemotherapy to be completed before administering TTFields with adjuvant Temozolomide (625). The data presented in this thesis encourages the usage of TTFields in combination with radiotherapy to be explored clinically, however, there are concerns regarding the delivery of TTFields treatment in combination with radiation with respects to skin toxicities from the dosimetric impact of electrodes on the scalp, within the radiation field. Clinical trials have suggested that the presence of transducer-arrays did not significantly impact on dosimetric measurements, both when transducer arrays were removed or left on during RT delivery (626-629), suggesting that TTFields may be feasible and safe when combined with radiotherapy. As such, initiating TTFields treatment earlier following surgery and in combination with radiation may be of huge significance in terms of improving treatment response to TTFields for glioblastoma patients.

Tumour progression inevitably occurs even for patients receiving TTFields and resistance to TTFields treatment has been described in ~ 14% of patients (622). The mechanisms that enable cancer cells to evade the biophysical forces of TTFields will inform on strategies that can be exploited to overcome this resistance Previous studies have shown that the optimal inhibitory frequency of TTFields treatment is inversely correlated to cell size (252). TTFields has been shown to trigger cancer cells to increase in cell size. One case study reported that at recurrence cells had had adopted a ‘giant-cell’ morphology (630), enabling them to escape the effects of TTFields. Changing the frequency of the electric fields applied overcame this resistance. Adjusting the frequency to account for this increase in cell size could therefore target this new population of cells of increased cell size. Schneiderman et al. have proposed that periodically switching the frequency between 150 and 200kHz could prevent the increase in cell size provoked by continuous exposure to TTFields at a single frequency of 200kHz (631).

Additionally, glioblastoma patients do not equally benefit from TTFields, hence, the development of prognostic biomarkers that may help identify patients that will most likely benefit from additional TTFields treatment would be extremely beneficial to future clinical trials (632). A retrospective study carried out by Dono *et al*. identified molecular alterations that corresponded with increased response to TTFields treatment in glioblastoma patients. Glioblastoma patients with IDH or PTEN mutations are more likely to benefit to from current standard treatment and are generally associated with improved survival outcomes. PTEN was additionally identified as a marker for preferential response to TTFields treatment in patients with recurrent isocitrate IDH wild-type glioblastoma (633). PTEN plays a role in mitotic spindle architecture and promotes chromosome alignment and segregation. Loss of PTEN results in improper spindle assembly and chromosome segregation (634, 635). Given that TTFields is also known to interfere with microtubule organisation and chromosome segregation, these effects may be enhanced when TTFields is applied to patients with loss of PTEN. Glioblastoma patients with IDH or PTEN mutations have been proposed to be particularly sensitive to PARP inhibitors because of known defects in HR repair pathways associated in these cancers. TTFields may however extend application of PARP inhibitors to tumours outside of this context (for example for high grade gliomas which tend to be IDH wt) or may delay the establishment of resistance for those cancers harbouring HRR deficiencies. A clinical trial is currently recruiting participants to evaluate the efficacy and safety of PARPi, Niraparib, and TTFields in recurrent glioblastoma (NCT04221503). NF1 alterations, wt PIK3CA and wt EGFR, which extended both PFS and OS of glioblastoma patients receiving TTFields treatment, were also identified as molecular markers associated with improved response to TTFields (632, 636).

Finally, improvements with regards to the delivery of the Optune system may also be considered for improved patient response. The optimal positioning of the four transducers arrays is determined using the NovoTAL™ (Novocure Ltd., Haifa, Israel) simulation software based on tumour location and the size and shape of the patient's head (5) in order to maximise intensity of the fields at the site of the tumour whilst sparing the surrounding healthy tissue. Secondary lesions have been reported at distant sites away from the region of optimal field intensity (630, 637). Adjusting array positioning may be necessary to target these new lesions. Additionally, improvements in the duty cycle, such as changing the duration of time between switching current injection between the two pairs of electrodes or activating both pairs of electrodes simultaneously rather than alternatively but at reduced intensity, could increase the area of the tumour at which an intensity of 1V/cm is achieved (the minimum intensity required for the anti-proliferative effects of TTFields), which could improve the delivery of Optune and enhance TTFields efficacy. The Optune system is designed to switch off automatically when the temperature at the site of attachment of the electrodes rises to 41°C, beyond this

temperature patients are at risk of thermal injury (638). Both electrodes switch off when a temperature rise is detected by one of the electrodes, even though the other electrode might still be within the range of accepted temperatures. If the system was adapted to turn on and off the paired electrodes independently then again, improvements in response to TTFields could be seen (639).

As evident from the preclinical studies undertaken in this thesis, TTFields/DDRi-based combinations have great potential for the treatment of glioblastoma.

6.2 Limitations and future studies

6.2.1 Experimental limitations associated with the Inovitro™ system.

The delivery of electric fields generates heat therefore the temperature of the incubator is set to a value lower than the target temperature in order to compensate for electric field-induced heating of the ceramic dishes and maintain the temperature within the ceramic dishes at 37 degrees. The temperature of the incubator also determines the intensity of the fields that can be achieved within the ceramic dishes. For the data presented here, the temperature of the incubator was set to 18°C, which allows the highest intensity (1.62 V/cm RMS) to be achieved based on current known expected TTFields intensities (385). However, because of the high ambient room temperature that the equipment is set up in (primary TC facilities), a temperature of 18°C could not always be achieved. As such, the incubator temperature varied from experiment to experiment (fluctuating between ~20 and ~25 °C) with changes in room temperature, which would result in different intensities of TTFields treatment applied across experiments. Because the anti-proliferative effects of TTFields are dependent on the intensity of the fields, with higher intensities inducing increased cell death (334), changes in intensities will most likely affect the outcome of the results. Additionally, when inserting the Inovitro™ dishes onto the base plate, the dishes require rotating into place in order to establish the adequate contact between the electrical components on the bottom of the dishes and the electrical springs on the base plate. The computer software gives a readout of the temperature, resistance and current passing through each dish and indicates whether the connection between the dish and the plate has been achieved. The time taken for the dishes to connect to the base plate varied within the same experiment and between experiments. As the dishes began to wear through the duration of this project, these would take longer to connect, sometimes taking over 1-hour to connect, which may have impacted the overall state of cells and may have influenced the results. Finally, the intensity in the dishes is not uniform, with intensities in the centre dishes being higher than the intensity measured at the edge of the dish, therefore not all cells within each dich experience the

same intensity of treatment. Novocure are currently further refining their Inovitro system to try and minimise some of these issues which would be welcome in future work.

6.2.2 TTFields/DDRi combinations treatment scheduling limitations.

Given that the duration of TTFields treatment was determined based on the cell doubling time of the cells and that cells were collected further analysis only after completion of the TTFields treatment, some the mechanistic effects of DDRi treatment on TTFields may have been missed to a certain extent, especially with the ATRi has which has a short life of only approximately 8-hours. Because of this, treated cells may have started to recover from the effects of ATR inhibition during the remainder of the TTFields treatment. Although, given this short half-life, the sensitising effects of ATRi to TTFields and radiation achieved are even more impressive. The work undertaken in this thesis did not look at the effects of treatment throughout the course of TTFields delivery. As such, it may be interesting to track the effects of treatment throughout this period. Additionally, the initial response to ATRi and radiation, either alone or in combination, were not assessed seeing as these conditions were collected at the same time as the TTFields-treated samples, 48-hours after these treatments were administered. In future, it might be worth including controls to measure the baseline response to these treatments and see how this relates to TTFields-based combinations with the scheduling used in these studies. For example, it is known that DNA damage in response to irradiation forms almost instantly following irradiation and usually resolves within 24-hours following treatment (549). It would be therefore interesting to see how the damage induced by the various combinations compares to immediate DNA damage levels induced by radiation treatment.

On the other hand, these studies allowed us to measure the ability of TTFields to sustain the effects induced by DDRi and IR treatment. In future, alternative treatment scheduling may be considered. RT has been shown to enhance TTFields efficacy when administered both prior to and immediately after TTFields treatment (312, 313), therefore, irradiating the cells at the end of the TTFields treatment could be an option. Additionally, Mazzanti *et al.* (640) reported that the effects of TTFields on cell proliferation are reversed 24-hours after cessation of TTFields treatment and showed that once cells had recovered from TTFields treatment they could resume proliferation as normal. Therefore, an alternative scheduling for DDRi treatment could also be considered. Kessler *et al.* (542) showed that continuing DNA damage checkpoint inhibitor treatment up to 72 hours following completion of TTFields treatment produced a much more striking reduction in survival in comparison to discontinuation of the inhibitor treatment at the end of TTFields treatment and compared to either treatment alone. Given that patients are currently advised to wear the Optune device for 18 hours/day, it has therefore been suggested that DDRi treatment could be used to bridge the

interruption in TTFields treatment (542). Additionally, continuing DDRi treatment after completion of TTFields treatment could further delay how quickly cells are able to recover from TTFields treatment.

6.2.3 Model development incorporating the Inovitro™ system.

Although extraordinary advances in glioblastoma research have been achieved in the past decades, most clinical trials investigating strategies to battle glioblastoma fail to show improvements in survival (641). This is in part due to the recurrent and infiltrative nature of the disease, but also reflects the lack of suitable models available to conduct *in vitro* assessment of potential therapeutics (642). Whilst *in vitro* 2D culture of patient-derived glioblastoma stem cells have been of huge significance in terms of understanding glioblastoma biology and identifying promising pharmacological targets, GSCs cultured as adherent 2D monolayers lose their intrinsic heterogeneity and lose the ability to form interconnections with surrounding cells and their environment in a 3-demenional space. 2D models therefore fail to replicate key histological features of glioblastoma which are thought to drive treatment resistance (643, 644) and models that better reflect such features are needed. Berkelmann *et al.* previously measured a reduction in TTFields efficacy with glioma cells grown in a collagen matrix as 3D structures (302). The effects of TTFields on cell division vary depending on the axis of cell division relative to the field, with cells dividing parallel to the field demonstrating more toxic effects and cells dividing perpendicular to the fields being less sensitive to the effects of the electric fields (252). In 3D, the number of potential directions that cells can be dividing in are increased, meaning that a smaller proportion of cells will be diving parallel to field (the direction in which you would expect to see the most pronounced effect of toxicity), therefore cells will somewhat be more protected from the effects of the fields in 3D culture and may explain the difference in sensitivity to TTFields treatment in 3D.

The 3D Alvetex® scaffold (figure 6.1a), which was recently developed by Gomez-Roman *et al.* (2017) and recapitulates key histological features of glioblastoma, was shown to more reliably predict clinical efficacy of various pharmacological agents (including TMZ, bevacizumab and erlotinib), for which adequate clinical trial data has been published, compared to adherent 2D monolayer cultures, validating its use as a valuable model for *in vitro* assessment of potential pharmacological agents for the treatment of glioblastoma (381). An additional benefit to using the 3D Alvetex scaffold over the 2D models used is that it precludes the requirement for counting and replating the cells onto 6-well Matrigel coated plates that is required with the 2D work as the 3D scaffolds can easily be transferred. As such, the third and final aim of this thesis was to incorporate the 3D Alvetex™ within the Inovitro™ system for investigation of our most promising TTFields/DDRi combinations with patient derived GSCs as it will be of translational relevance. Computational data produced by Novocure suggested that

clinically relevant intensities of TTFields can be achieved within cells cultured in the 3D scaffold in the Inovitro™ system (data not shown). Interestingly, whilst the intensities of TTFields delivered across the mouse brain are mostly uniform (data not shown), the intensities of TTFields treatment were non-uniform throughout the scaffold, as is the case across the human brain, and therefore the 3D Alvatex-model may better reflect what takes place in the clinic in terms of delivery of the TTFields treatment in comparison to mouse models. Optimisations surrounding the incorporation of Alvatex scaffold within the Inovitro™ system mainly involved identifying the optimal method to prevent scaffold floatation without compromising TTFields delivery. An initial pilot study confirmed that TTFields reduced viability of GSCs cultured in the 3D Alvetex scaffold (figure 6.1b-c).

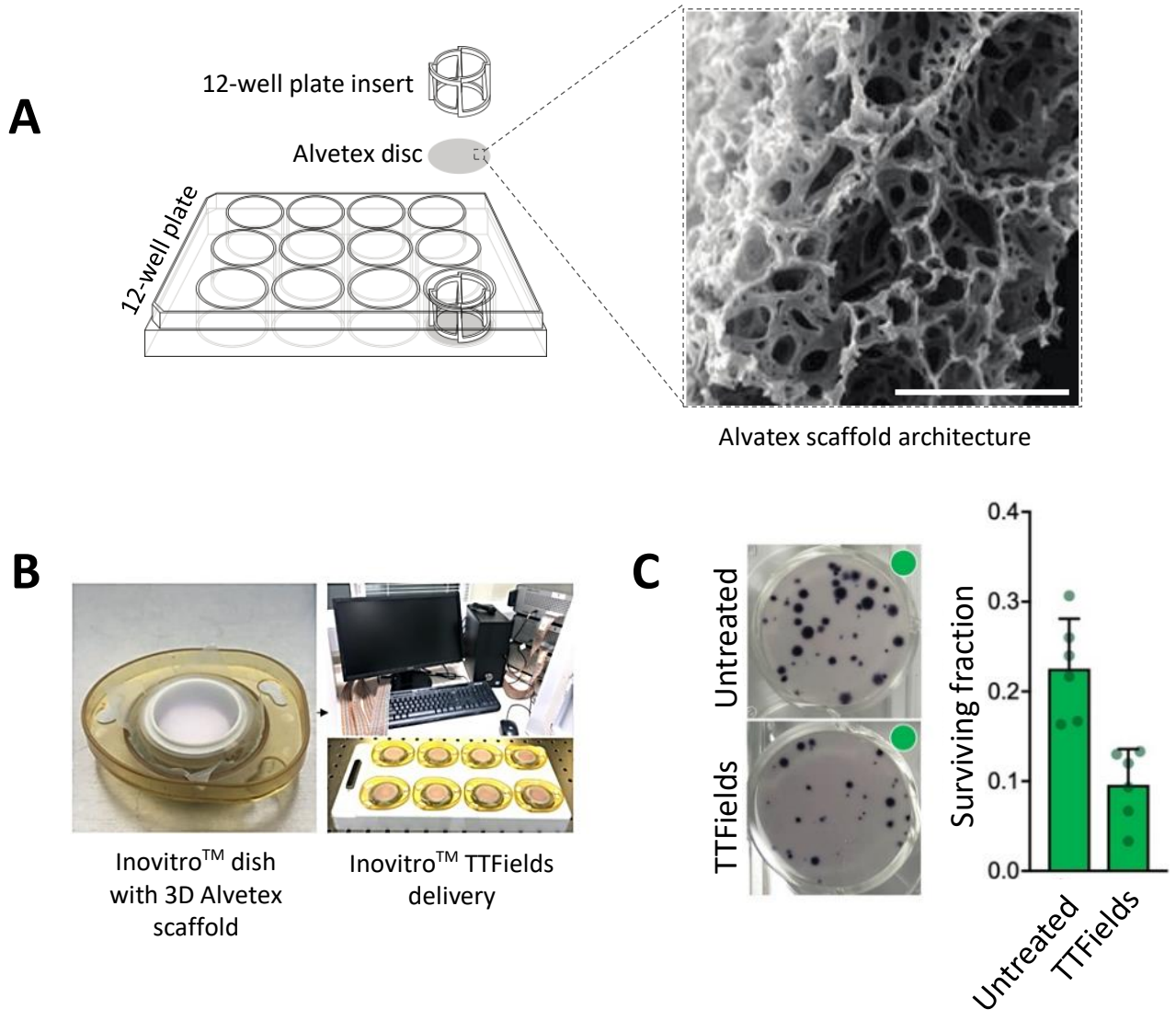

Figure 6.1. TTFields delivery within the 3D Alvetex™ scaffold culture system.
A. Left – Alvetex 12-well plate. Right – Architecture of the porous polystyrene 3D scaffold. **B.** Inovitro dish with the Alvetex scaffold. **C.** Right – Surviving fractions of OX5-edge stem cells cultured in the 3D Alvetex™ system both with and without TTFields. Error bars represent standard error of the mean and replicates are represented by dots. Left – Representative images.

Based on this preliminary data together with some of the early data established in this thesis (Chapter 3 – Section 3.2.2), funding was awarded to our group by AACR (American Association for Cancer Research)- Novocure Tumour-Treating Fields Research Grant for a project entitled: 'TTFields-based DDRi combinations to overcome spatiofunctional heterogeneity.' Further development and application of the aforementioned 3D Alvetex™ scaffold-based TTFields culture and delivery system were proposed as part of this study. As such, the optimisation of this 3D system was finalised by Dr. Callum Jones. While this project aims to compare the effects of TTFields/DDRi combinations across various Sheffield-derived primary glioma cell lines, as described in the methods (see section 2.2.1), these cell lines are not suitable for direct comparison in 2D as they do not form colonies when grown in 2D. Additionally, the studies that are currently under way in 3D have primarily focused on assessing the effects of these combinations on survival with no further investigations into the mechanism driving the effects in 3D or how they may compare to 2D models. Preliminary data comparing the efficacy of TTFields/DDRi based combinations with irradiation in GSCs cultured both in 2D and 3D suggest that these treatments may exert differences in toxicity across the models used (data not shown). As such, investigating the mechanisms driving the differences in sensitivity to these combinations between 2D and 3D models may be of interest in future studies, particularly in terms of the effects on the DNA damage induction and repair.

Although the 3D Alvetex scaffold may constitute a more robust model in terms of dimensionality, this model still fails to recreate the original tumour microenvironment (TME) in other aspects, such as the presence of a vasculature, immune cells, fibroblasts, and other signalling molecules, all of which may modulate how a tumour responds to treatment. Co-culturing tumour cells with various stromal cells, including immune cells, to study how they interact with each other may overcome this limitation. Alternatively, other 3D models may be used. Organoids, for example, represent more accurately patient tumour properties because they preserve the original TME (they retain the 3D structure, some of the genetic heterogeneity of the original tissue and can contain multiple types of immune cells) (646). Such a model is currently being explored by other groups. Nickl *et al*. have optimised the use of patient-derived organoids and tumour slice cultures within the Inovitro system (645). So far, they have shown that these models respond to TTFields therapy, suggesting that these models could potentially be used to screen for drug combinations that may offer maximal clinical benefit (645).

Finally, the Inovivo system is a preclinical laboratory research system that allows the evaluation of the effects of TTFields in animal models. One advantage in using animal models over other models for predicting drug responses is that they allow tumour cells to interact with the host environment (646). Additionally, *in vivo* studies may give some indication of the toxicity profiles of these treatments.

Whilst the Inovivo system is not currently available in the UK, our industrial collaborator (Novocure™, based in Israel) has offered to validate our most promising TTFields/DDRi combinations from our 2D or 3D scaffold-based TTFields culture system against rodent orthotopic xenograft models using the Inovivo system.

6.3 Concluding remarks

Despite efforts to improve the treatment of glioblastoma, resistance (innate and acquired) and tumour regrowth occur in almost all glioblastoma patients leading to stubbornly poor survival rates. As evident from the preclinical and clinical studies highlighted in this review, TTFields has great potential, both in the short-term and long-term, to help treat a multitude of cancers and positively impact on several cancer patient cohorts, particularly those with cancers of unmet need such as brain tumours. As such, increasing our knowledge of the molecular mechanisms that underpin TTFields-based cellular toxicity and tumour-specificity/therapeutic index will hopefully aid in the adoption of this new modality for additional tumours. Glioma stem cells are one of the underlying causes driving resistance to current standard-of-care DNA damaging treatment because of their increased DNA repair capacity. Our studies provide evidence for the use of TTFields-based combinations with inhibitors targeted at the DDR as a strategy for overcoming resistance in glioma stem cell population. Our results show that these combinations achieve this effect through inhibition of DNA repair capacity in GSCs.

Future work will focus on replicating these studies in more clinically relevant 3D models across a wider range of GSC models which recapitulate both intra- and inter-tumoural heterogeneity. In the meantime, a reduction in production costs of the therapeutic TTFields units, through technological advancements will likely facilitate further clinical approval of TTFields based anti-cancer therapies from additional health care regulators, particularly if TTFields efficacy can be enhanced through combination approaches. In addition, there are plenty of opportunities for improvements with regards to the TTFields delivery system, such as adjusting/optimising the intensity and frequency of TTFields or reducing the weight of the device, extending battery life, simpler connectivity of wires, and/or increasing the number of directions from which the alternating electric fields are applied. Finally, the development of prognostic biomarkers that may help identify patients that will most likely benefit from additional TTFields treatment would be extremely beneficial to future clinical trials.

CHAPTER 7. REFERENCES

1. Louis DN, Perry A, Reifenberger G, von Deimling A, Figarella-Branger D, Cavenee WK, et al. The 2016 World Health Organization Classification of Tumors of the Central Nervous System: a summary. Acta Neuropathol. 2016;131(6):803-20.
2. Jäkel S, Dimou L. Glial cells and their function in the adult brain: A journey through the history of their ablation. Front Cell Neurosci. 2017;11:24-.
3. Cheo STT, Lim GH, Lim KHC. Glioblastoma multiforme outcomes of 107 patients treated in two Singapore institutions. Singapore medical journal. 2017;58(1):41-5.
4. Ohgaki H, Kleihues P. The definition of primary and secondary glioblastoma. Clin Cancer Res. 2013;19(4):764-72.
5. Ohgaki H, Kleihues P. Genetic Pathways to Primary and Secondary Glioblastoma. Am J Pathol. 2007;170(5):1445-53.
6. Schäfer N, Gielen GH, Rauschenbach L, Kebir S, Till A, Reinartz R, et al. Longitudinal heterogeneity in glioblastoma: Moving targets in recurrent versus primary tumors. J Transl Med. 2019;17(1):96-.
7. Neilsen BK, Sleightholm R, McComb R, Ramkissoon SH, Ross JS, Corona RJ, et al. Comprehensive genetic alteration profiling in primary and recurrent glioblastoma. J Neurooncol. 2019;142(1):111-8.
8. Cioca A, Olteanu EG, Gisca MD, Morosanu CO, Marin I, Florian IS. Expression of EGFR in paired new and recurrent glioblastomas. Asian Pacific journal of cancer prevention : APJCP. 2016;17(9):4205-8.
9. van den Bent M, Gao Y, Kerkhof M, Kros JM, Gorlia T, van Zwieten K, et al. Changes in the EGFR amplification and EGFRvIII expression between paired primary and recurrent glioblastomas. Neuro Oncol. 2015;17(7):935-41.
10. Li R, Chen X, You Y, Wang X, Liu Y, Hu Q, et al. Comprehensive portrait of recurrent glioblastoma multiforme in molecular and clinical characteristics. Oncotarget. 2015;6(31):30968-74.
11. Homma T, Fukushima T, Vaccarella S, Yonekawa Y, Di Patre PL, Franceschi S, et al. Correlation Among Pathology, Genotype, and Patient Outcomes in Glioblastoma. J Neuropathol Exp Neurol. 2006;65(9):846-54.
12. Marusyk A, Polyak K. Tumor heterogeneity: Causes and consequences. Biochimica et biophysica acta Reviews on cancer. 2010;1805(1):105-17.
13. Szerlip NJ, Pedraza A, Chakravarty D, Azim M, McGuire J, Fang Y, et al. Intratumoral heterogeneity of receptor tyrosine kinases EGFR and PDGFRA amplification in glioblastoma defines subpopulations with distinct growth factor response. Proc Natl Acad Sci U S A. 2012;109(8):3041-6.
14. Holland EC, Huse JT. Targeting brain cancer: advances in the molecular pathology of malignant glioma and medulloblastoma. Nat Rev Cancer. 2010;10(5):319-31.
15. Verhaak RGW, Hoadley KA, Purdom E, Wang V, Qi Y, Wilkerson MD, et al. Integrated Genomic Analysis Identifies Clinically Relevant Subtypes of Glioblastoma Characterized by Abnormalities in PDGFRA, IDH1, EGFR, and NF1. Cancer Cell. 2010;17(1):98-110.
16. Phillips HS, Kharbanda S, Chen R, Forrest WF, Soriano RH, Wu TD, et al. Molecular subclasses of high-grade glioma predict prognosis, delineate a pattern of disease progression, and resemble stages in neurogenesis. Cancer Cell. 2006;9(3):157-73.
17. Louis DN, Perry A, Wesseling P, Brat DJ, Cree IA, Figarella-Branger D, et al. The 2021 WHO classification of tumors of the central nervous system: A summary. Neuro Oncol. 2021;23(8):1231-51.
18. Brennan C, Momota H, Hambardzumyan D, Ozawa T, Tandon A, Pedraza A, et al. Glioblastoma subclasses can be defined by activity among signal transduction pathways and associated genomic alterations. PLoS One. 2009;4(11):e7752-e.
19. Szopa W, Burley TA, Kramer-Marek G, Kaspera W. Diagnostic and Therapeutic Biomarkers in Glioblastoma: Current Status and Future Perspectives. Biomed Res Int. 2017;2017:8013575-13.
20. Nobusawa S, Watanabe T, Kleihues P, Ohgaki H. IDH1 Mutations as Molecular Signature and Predictive Factor of Secondary Glioblastomas. Clin Cancer Res. 2009;15(19):6002-7.
21. Marker DF, Agnihotri S, Amankulor N, Murdoch GH, Pearce TM. The dominant TP53 hotspot mutation in IDH -mutant astrocytoma, R273C, has distinctive pathologic features and sex-specific prognostic implications. Neurooncol Adv. 2022;4(1):vdab182-vdab.
22. Ebrahimi A, Skardelly M, Bonzheim I, Ott I, Mühleisen H, Eckert F, et al. ATRX immunostaining predicts IDH and H3F3A status in gliomas. Acta Neuropathol Commun. 2016;4(1):60.
23. Cohen AL, Holmen SL, Colman H. IDH1 and IDH2 Mutations in Gliomas. Curr Neurol Neurosci Rep. 2013;13(5):345-.

24. Xu W, Yang H, Liu Y, Yang Y, Wang P, Kim S-H, et al. Oncometabolite 2-Hydroxyglutarate Is a Competitive Inhibitor of α-Ketoglutarate-Dependent Dioxygenases. Cancer Cell. 2011;19(1):17-30.
25. Boots-Sprenger SHE, Sijben A, Rijntjes J, Tops BBJ, Idema AJ, Rivera AL, et al. Significance of complete 1p/19q co-deletion, IDH1 mutation and MGMT promoter methylation in gliomas: use with caution. Mod Pathol. 2013;26(7):922-9.
26. Cairncross G, Berkey B, Shaw E, Jenkins R, Scheithauer B, Brachman D, et al. Phase III Trial of Chemotherapy Plus Radiotherapy Compared With Radiotherapy Alone for Pure and Mixed Anaplastic Oligodendroglioma: Intergroup Radiation Therapy Oncology Group Trial 9402. J Clin Oncol. 2006;24(18):2707-14.
27. McNally EJ, Luncsford PJ, Armanios M. Long telomeres and cancer risk: The price of cellular immortality. J Clin Invest. 2019;129(9):3474-81.
28. Clynes D, Jelinska C, Xella B, Ayyub H, Scott C, Mitson M, et al. Suppression of the alternative lengthening of telomere pathway by the chromatin remodelling factor ATRX. Nat Commun. 2015;6(1):7538-.
29. Heaphy CM, de Wilde RF, Jiao Y, Klein AP, Edil BH, Shi C, et al. Altered Telomeres in Tumors with ATRX and DAXX Mutations. Science. 2011;333(6041):425-.
30. Reddel RR, Cesare AJ. Alternative lengthening of telomeres: models, mechanisms and implications. Nat Rev Genet. 2010;11(5):319-30.
31. Wiestler B, Capper D, Holland-Letz T, Korshunov A, von Deimling A, Pfister SM, et al. ATRX loss refines the classification of anaplastic gliomas and identifies a subgroup of IDH mutant astrocytic tumors with better prognosis. Acta Neuropathol. 2013;126(3):443-51.
32. Qin T, Mullan B, Ravindran R, Messinger D, Siada R, Cummings JR, et al. ATRX loss in glioma results in dysregulation of cell-cycle phase transition and ATM inhibitor radio-sensitization. Cell Rep. 2022;38(2):110216-.
33. Chan K-M, Fang D, Gan H, Hashizume R, Yu C, Schroeder M, et al. The histone H3.3K27M mutation in pediatric glioma reprograms H3K27 methylation and gene expression. Genes Dev. 2013;27(9):985-90.
34. Hu XM, Nie Xy, Xu Kl, Wang Y, Tang F, Du Zg, et al. H3K27M Mutation Doesn't Mean Worse Prognosis in Old Patients. Frontiers in oncology. 2022;12:912166-.
35. Bender S, Tang Y, Lindroth Anders M, Hovestadt V, Jones David TW, Kool M, et al. Reduced H3K27me3 and DNA Hypomethylation Are Major Drivers of Gene Expression in K27M Mutant Pediatric High-Grade Gliomas. Cancer Cell. 2013;24(5):660-72.
36. Lewis PW, Müller MM, Koletsky MS, Cordero F, Lin S, Banaszynski LA, et al. Inhibition of PRC2 Activity by a Gain-of-Function H3 Mutation Found in Pediatric Glioblastoma. Science. 2013;340(6134):857-61.
37. Venneti S, Garimella MT, Sullivan LM, Martinez D, Huse JT, Heguy A, et al. Evaluation of Histone 3 Lysine 27 Trimethylation (H3K27me3) and Enhancer of Zest 2 (EZH2) in Pediatric Glial and Glioneuronal Tumors Shows Decreased H3K27me3 in H3F3A K27M Mutant Glioblastomas. Brain Pathology. 2013;23(5):558-64.
38. Funato K, Major T, Lewis PW, Allis CD, Tabar V. Use of human embryonic stem cells to model pediatric gliomas with H3.3K27M histone mutation. Science. 2014;346(6216):1529-33.
39. Killela PJ, Reitman ZJ, Jiao Y, Bettegowda C, Agrawal N, Diaz Jr LA, et al. TERT promoter mutations occur frequently in gliomas and a subset of tumors derived from cells with low rates of self-renewal. Proc Natl Acad Sci U S A. 2013;110(15):6021-6.
40. Nonoguchi N, Ohta T, Oh J-E, Kim Y-H, Kleihues P, Ohgaki H. TERT promoter mutations in primary and secondary glioblastomas. Acta Neuropathol. 2013;126(6):931-7.
41. Kaina B, Christmann M, Naumann S, Roos WP. MGMT: Key node in the battle against genotoxicity, carcinogenicity and apoptosis induced by alkylating agents. DNA Repair (Amst). 2007;6(8):1079-99.
42. Eoli M, Menghi F, Filippini G, Broggi G, Boiardi A, Finocchiaro G, et al. Methylation of O6-Methylguanine DNA Methyltransferase and Loss of Heterozygosity on 19q and/or 17p Are Overlapping Features of Secondary Glioblastomas with Prolonged Survival. Clin Cancer Res. 2007;13(9):2606-13.
43. Nakamura M, Watanabe T, Yonekawa Y, Kleihues P, Ohgaki H. Promoter methylation of the DNA repair gene MGMT in astrocytomas is frequently associated with G:C → A:T mutations of the TP53 tumor suppressor gene. Carcinogenesis. 2001;22(10):1715-9.
44. Jiang Z, Pore N, Cerniglia GJ, Mick R, Georgescu M-M, Bernhard EJ, et al. Phosphatase and tensin homologue deficiency in glioblastoma confers resistance to radiation and temozolomide that is reversed by the protease inhibitor nelfinavir. Cancer Res. 2007;67(9):4467-73.
45. Chakravarti A, Zhai G, Suzuki Y, Sarkesh S, Black PM, Muzikansky A, et al. The Prognostic Significance of Phosphatidylinositol 3-Kinase Pathway Activation in Human Gliomas. J Clin Oncol. 2004;22(10):1926-33.
46. Maehama T, Dixon JE. The Tumor Suppressor, PTEN/MMAC1, Dephosphorylates the Lipid Second Messenger, Phosphatidylinositol 3,4,5-Trisphosphate. J Biol Chem. 1998;273(22):13375-8.

47. Endersby R, Baker SJ. PTEN signaling in brain: neuropathology and tumorigenesis. Oncogene. 2008;27(41):5416-30.
48. Ohgaki H, Dessen P, Jourde B, Horstmann S, Nishikawa T, Di Patre P-L, et al. Genetic pathways to glioblastoma: A population-based study. Cancer Res. 2004;64(19):6892-9.
49. Ekstrand AJ, James CD, Cavenee WK, Seliger B, Pettersson RF, Collins VP. Genes for epidermal growth factor receptor, transforming growth factor α, and epidermal growth factor and their expression in human gliomas in vivo. Cancer Res. 1991;51(8):2164-72.
50. Frederick L, Wang X-Y, Eley G, James CD. Diversity and frequency of epidermal growth factor receptor mutations in human glioblastomas. Cancer Res. 2000;60(5):1383-7.
51. Zhang H, Berezov A, Wang Q, Zhang G, Drebin J, Murali R, et al. ErbB receptors: From oncogenes to targeted cancer therapies. J Clin Invest. 2007;117(8):2051-8.
52. Nishikawa R, Ji XD, Harmon RC, Lazar CS, Gill GN, Cavenee WK, et al. A Mutant Epidermal Growth Factor Receptor Common in Human Glioma Confers Enhanced Tumorigenicity. Proc Natl Acad Sci U S A. 1994;91(16):7727-31.
53. Shinojima N, Tada K, Shiraishi S, Kamiryo T, Kochi M, Nakamura H, et al. Prognostic Value of Epidermal Growth Factor Receptor in Patients with Glioblastoma Multiforme. Cancer Res. 2003;63(20):6962-70.
54. Srividya MR, Thota B, Arivazhagan A, Thennarasu K, Balasubramaniam A, Chandramouli BA, et al. Age-dependent prognostic effects of EGFR/p53 alterations in glioblastoma: study on a prospective cohort of 140 uniformly treated adult patients. J Clin Pathol. 2010;63(8):687-91.
55. Chen JR, Xu HZ, Yao Y, Qin ZY. Prognostic value of epidermal growth factor receptor amplification and EGFRvIII in glioblastoma: meta-analysis. Acta Neurol Scand. 2015;132(5):310-22.
56. Felsberg J, Hentschel B, Kaulich K, Gramatzki D, Zacher A, Malzkorn B, et al. Epidermal growth factor receptor variant III (EGFRvIII) positivity in EGFR-amplified glioblastomas: Prognostic role and comparison between primary and recurrent tumors. Clin Cancer Res. 2017;23(22):6846-55.
57. Stupp R, Mason WP, van den Bent MJ, Weller M, Fisher B, Taphoorn MJB, et al. Radiotherapy plus Concomitant and Adjuvant Temozolomide for Glioblastoma. The New England Journal of Medicine. 2005;352(10):987-96.
58. Hegi ME, Diserens A-C, Gorlia T, Hamou M-F, de Tribolet N, Weller M, et al. MGMT Gene Silencing and Benefit from Temozolomide in Glioblastoma. The New England Journal of Medicine. 2005;352(10):997-1003.
59. Hermisson M, Klumpp A, Wick W, Wischhusen J, Nagel G, Roos W, et al. O6-methylguanine DNA methyltransferase and p53 status predict temozolomide sensitivity in human malignant glioma cells. Journal of neurochemistry. 2006;96(3):766-76.
60. Hegi ME, Diserens A-C, Godard S, Dietrich P-Y, Regli L, Ostermann S, et al. Clinical Trial Substantiates the Predictive Value of O-6-Methylguanine-DNA Methyltransferase Promoter Methylation in Glioblastoma Patients Treated with Temozolomide. Clin Cancer Res. 2004;10(6):1871-4.
61. Seo YJ, Cho WH, Kang DW, Cha SH. Extraneural metastasis of glioblastoma multiforme presenting as an unusual neck mass. J Korean Neurosurg Soc. 2012;51(3):147-50.
62. Seker-Polat F, Degirmenci NP, Solaroglu I, Bagci-Onder T. Tumor Cell Infiltration into the Brain in Glioblastoma: From Mechanisms to Clinical Perspectives. Cancers (Basel). 2022;14(2):443.
63. Stupp R, Taillibert S, Kanner A, Read W, Steinberg DM, Lhermitte B, et al. Effect of Tumor- Treating Fields Plus Maintenance Temozolomide vs Maintenance Temozolomide Alone on Survival in Patients With Glioblastoma: A Randomized Clinical Trial. JAMA. 2017;318(23):2306-16.
64. Stupp R, Taillibert S, Kanner AA, Kesari S, Steinberg DM, Toms SA, et al. Maintenance Therapy With Tumor-Treating Fields Plus Temozolomide vs Temozolomide Alone for Glioblastoma: A Randomized Clinical Trial. JAMA. 2015;314(23):2535-43.
65. Stupp R, Wong ET, Kanner AA, Steinberg D, Engelhard H, Heidecke V, et al. NovoTTF-100A versus physician's choice chemotherapy in recurrent glioblastoma: A randomised phase III trial of a novel treatment modality. European Journal of Cancer. 2012;48(14):2192-202.
66. Stephen PJ, Jiri B. The DNA- damage response in human biology and disease. Nature. 2009;461(7267):1071.
67. Surova O, Zhivotovsky B. Various modes of cell death induced by DNA damage. Oncogene. 2013;32(33):3789.
68. Ciccia A, Elledge SJ. The DNA Damage Response: Making It Safe to Play with Knives. Molecular Cell. 2010;40(2):179-204.
69. Mykyta VS, Lubomir BS, Eric JH, Igor GP, William MB, Olga AS. Ionizing radiation induces DNA double-strand breaks in bystander primary human fibroblasts. Oncogene. 2005;24(49):7257.

70. Rastogi RP, Richa A, Kumar MB, Tyagi RP, Sinha RP. Molecular mechanisms of ultraviolet radiation-induced DNA damage and repair. Journal of nucleic acids. 2010;2010(2010):592980-.
71. Hannah S, Tim B, Rahel F, Katharina S, Markus DS, Georg K-M, et al. Temozolomide and Other Alkylating Agents in Glioblastoma Therapy. Biomedicines. 2019;7(3):69.
72. Weng M-W, Zheng Y, Jasti VP, Champeil E, Tomasz M, Wang Y, et al. Repair of mitomycin C mono- and interstrand cross-linked DNA adducts by UvrABC: a new model. Nucleic acids research. 2010;38(20):6976-84.
73. Hakem R. DNA-damage repair; the good, the bad, and the ugly. EMBO Journal. 2008;27(4):589-605.
74. Jan HJH. Genome maintenance mechanisms for preventing cancer. Nature. 2001;411(6835):366.
75. Wilson S, Beard W, Shock D, Batra V, Cavanaugh N, Prasad R, et al. Base excision repair and design of small molecule inhibitors of human DNA polymerase β. Cellular and Molecular Life Sciences. 2010;67(21):3633-47.
76. Keith WC. Single-strand break repair and genetic disease. Nature Reviews Genetics. 2008;9(8):619.
77. Shibata A, Jeggo PA. DNA Double-strand Break Repair in a Cellular Context. Clinical Oncology. 2014;26(5):243-9.
78. Ceccaldi R, Rondinelli B, D'andrea AD. Repair Pathway Choices and Consequences at the Double-Strand Break. Trends in Cell Biology. 2016;26(1):52-64.
79. Josef J. The multifaceted mismatch-repair system. Nature Reviews Molecular Cell Biology. 2006;7(5):335.
80. Jurgen AM, Hannes L, Wim V, Jan HJH. Understanding nucleotide excision repair and its roles in cancer and ageing. Nature Reviews Molecular Cell Biology. 2014;15(7):465.
81. Kee Y, D'Andrea AD. Expanded roles of the Fanconi anemia pathway in preserving genomic stability. Genes Dev. 2010;24(16):1680-94.
82. Niraj J, Färkkilä A, D'Andrea AD. The Fanconi Anemia Pathway in Cancer. 2019;3(1):457-78.
83. Bi X. Mechanism of DNA damage tolerance. World journal of biological chemistry. 2015;6(3):48-56.
84. Sedgwick B, Bates PA, Paik J, Jacobs SC, Lindahl T. Repair of alkylated DNA: Recent advances. DNA Repair. 2007;6(4):429-42.
85. Elledge SJ. Cell cycle checkpoints: Preventing an identity crisis. Science. 1996;274(5293):1664-72.
86. Hartwell LH, Weinert TA. Checkpoints: Controls that Ensure the Order of Cell Cycle Events. Science. 1989;246(4930):629-34.
87. Rhind N, Russell P. Roles of the Mitotic Inhibitors Wee1 and Mik1 in the G sub(2) DNA Damage and Replication Checkpoints. Molecular and Cellular Biology. 2001;21(5):1499-508.
88. Malumbres M. Cyclin-dependent kinases. Genome biology. 2014;15(6):122-.
89. Visconti R, Della Monica R, Grieco D. Cell cycle checkpoint in cancer: a therapeutically targetable double- edged sword. J Exp Clin Cancer Res. 2016;35(1).
90. Li J, Koczor CA, Saville KM, Hayat F, Beiser A, McClellan S, et al. Overcoming Temozolomide Resistance in Glioblastoma via Enhanced NAD + Bioavailability and Inhibition of Poly-ADP-Ribose Glycohydrolase. Cancers (Basel). 2022;14(15):3572.
91. Yarosh DB, Foote RS, Mitra S, Day RS. Repair of O 6 -methylguanine in DNA by demethylation is lacking in Mer − human tumor cell strains. Carcinogenesis (New York). 1983;4(2):199-205.
92. Sarkaria JN, Kitange GJ, James CD, Plummer R, Calvert H, Weller M, et al. Mechanisms of Chemoresistance to Alkylating Agents in Malignant Glioma. Clin Cancer Res. 2008;14(10):2900-8.
93. Agnihotri S, Burrell K, Buczkowicz P, Remke M, Golbourn B, Chornenkyy Y, et al. ATM regulates 3-methylpurine- DNA glycosylase and promotes therapeutic resistance to alkylating agents. Cancer discovery. 2014;4(10):1198-213.
94. Srivenugopal KS, Yuan X-H, Friedman HS, Ali-Osman F. Ubiquitination-Dependent Proteolysis of O 6-Methylguanine-DNA Methyltransferase in Human and Murine Tumor Cells following Inactivation with O 6-Benzylguanine or 1,3-Bis(2-chloroethyl)-1-nitrosourea. Biochemistry. 1996;35(4):1328-34.
95. Xu-Welliver M, Pegg AE. Degradation of the alkylated form of the DNA repair protein, O(6)-alkylguanine-DNA alkyltransferase. Carcinogenesis. 2002;23(5):823.
96. Wedge SR, Newlands ES. O6-Benzylguanine enhances the sensitivity of a glioma xenograft with low O6-alkylguanine-DNA alkyltransferase activity to temozolomide and BCNU. Br J Cancer. 1996;73(9):1049-52.
97. Bobola MS, Silber JR, Ellenbogen RG, Geyer JR, Blank A, Goff RD. O6-Methylguanine-DNA Methyltransferase, O6-Benzylguanine, and Resistance to Clinical Alkylators in Pediatric Primary Brain Tumor Cell Lines. Clin Cancer Res. 2005;11(7):2747-55.

98. Hirose Y, Kreklau EL, Erickson LC, Berger MS, Pieper RO. Delayed repletion of O6-methylguanine-DNA methyltransferase resulting in failure to protect the human glioblastoma cell line SF767 from temozolomide-induced cytotoxicity. J Neurosurg. 2003;98(3):591-8.
99. Mullapudi SRS, Ali-Osman F, Shou J, Srivenugopal KS. DNA repair protein O6-alkylguanine-DNA alkyltransferase is phosphorylated by two distinct and novel protein kinases in human brain tumour cells. Biochem J. 2000;351(2):393-402.
100. Sibghat U, Day RS. Incision at O6-methylguanine:thymine mispairs in DNA by extracts of human cells. Biochemistry. 1992;31(34):7998-8008.
101. Quiros S, Roos WP, Kaina B. Processing of O6- methylguanine into DNA double- strand breaks requires two rounds of replication whereas apoptosis is also induced in subsequent cell cycles. Cell Cycle. 2010;9(1):168-78.
102. Noonan EM, Shah D, Yaffe MB, Lauffenburger DA, Samson LD. O6-Methylguanine DNA lesions induce an intra-S-phase arrest from which cells exit into apoptosis governed by early and late multi-pathway signaling network activation. Integr Biol (Camb). 2012;4(10):1237-55.
103. Jiricny J. The multifaceted mismatch-repair system. Nat Rev Mol Cell Biol. 2006;7(5):335-46.
104. Fuchs RP, Isogawa A, Paulo JA, Onizuka K, Takahashi T, Amunugama R, et al. Crosstalk between repair pathways elicits double-strand breaks in alkylated dna and implications for the action of temozolomide. eLife. 2021;10.
105. Hunter C, Smith R, Cahill DP, Stephens P, Stevens C, Teague J, et al. A hypermutation phenotype and somatic MSH6 mutations in recurrent human malignant gliomas after alkylator chemotherapy. Cancer research. 2006;66(8):3987-91.
106. Cahill DP, Levine KK, Betensky RA, Codd PJ, Romany CA, Reavie LB, et al. Loss of the Mismatch Repair Protein MSH6 in Human Glioblastomas Is Associated with Tumor Progression during Temozolomide Treatment. Clin Cancer Res. 2007;13(7):2038-45.
107. Gupta T, Tibdewal A, Mohanty S, Pietsch T, Kannan S, Juvekar S, et al. Correlation of conventional magnetic resonance imaging features with O6-methylguanine-DNA-methyltransferase gene promoter methylation status and survival outcomes in patients with newly diagnosed glioblastoma: Single-center correlative imaging substudy from a prospective clinical trial. Glioma (Mumbai, India). 2018;1(2):50-8.
108. The chemical basis of radiation biology. 1987.
109. Kim W, Lee S, Seo D, Kim D, Kim K, Kim E, et al. Cellular Stress Responses in Radiotherapy. Cells. 2019;8(9):1105.
110. Maynard S, Schurman SH, Harboe C, de Souza-Pinto NC, Bohr VA. Base excision repair of oxidative DNA damage and association with cancer and aging. Carcinogenesis. 2008;30(1):2-10.
111. Dungey FABS, Löser DAMS, Chalmers AJFRCRPD. Replication-Dependent Radiosensitization of Human Glioma Cells by Inhibition of Poly(ADP-Ribose) Polymerase: Mechanisms and Therapeutic Potential. Int J Radiat Oncol Biol Phys. 2008;72(4):1188-97.
112. Saleh-Gohari N, Bryant HE, Schultz N, Parker KM, Cassel TN, Helleday T. Spontaneous homologous recombination is induced by collapsed replication forks that are caused by endogenous DNA single- strand breaks. Molecular and cellular biology. 2005;25(16):7158-69.
113. Caldecott KW. Single-strand break repair and genetic disease. Nat Rev Genet. 2008;9(8):619-31.
114. Singer B, Hang B. What Structural Features Determine Repair Enzyme Specificity and Mechanism in Chemically Modified DNA? Chem Res Toxicol. 1997;10(7):713-32.
115. Wood RD. DNA Repair in Eukaryotes. Annu Rev Biochem. 1996;65(1):135-67.
116. Kladova OA, Bazlekowa-Karaban M, Baconnais S, Piétrement O, Ishchenko AA, Matkarimov BT, et al. The role of the N-terminal domain of human apurinic/apyrimidinic endonuclease 1, APE1, in DNA glycosylase stimulation. DNA Repair (Amst). 2018;64:10-25.
117. Matsumoto Y, Kim K. Excision of Deoxyribose Phosphate Residues by DNA Polymerase β During DNA Repair. Science. 1995;269(5224):699-702.
118. Sattler U, Frit P, Salles B, Calsou P. Long-patch DNA repair synthesis during base excision repair in mammalian cells. EMBO Rep. 2003;4(4):363-7.
119. Matsumoto Y, Bogenhagen DF. Repair of a synthetic abasic site involves concerted reactions of DNA synthesis followed by excision and ligation. Mol Cell Biol. 1991;11(9):4441-7.
120. Kitange GJ, Carlson BL, Schroeder MA, Grogan PT, Lamont JD, Decker PA, et al. Induction of MGMT expression is associated with temozolomide resistance in glioblastoma xenografts. Neuro Oncol. 2009;11(3):281-91.

121. Goellner EM, Grimme B, Brown AR, Lin Y-C, Wang X-H, Sugrue KF, et al. Overcoming temozolomide resistance in glioblastoma via dual inhibition of NAD+ biosynthesis and base excision repair. Cancer research. 2011;71(6):2308-17.
122. Caldecott KW. Protein-protein interactions during mammalian DNA single-strand break repair. Biochem Soc Trans. 2003;31(1):247-51.
123. Galia A, Calogero AE, Condorelli R, Fraggetta F, La Corte A, Ridolfo F, et al. PARP- 1 protein expression in glioblastoma multiforme. European journal of histochemistry : EJH. 2012;56(1):e9-e.
124. Horton JK, Stefanick DF, Prasad R, Gassman NR, Kedar PS, Wilson SH. Base excision repair defects invoke hypersensitivity to PARP inhibition. Mol Cancer Res. 2014;12(8):1128-39.
125. Agnihotri S, Gajadhar AS, Ternamian C, Gorlia T, Diefes KL, Mischel PS, et al. Alkylpurine- DNA- N-glycosylase confers resistance to temozolomide in xenograft models of glioblastoma multiforme and is associated with poor survival in patients. The Journal of clinical investigation. 2012;122(1):253-66.
126. Bennett CB, Lewis AL, Baldwin KK, Resnick MA. Lethality Induced by a Single Site-Specific Double-Strand Break in a Dispensable Yeast Plasmid. Proc Natl Acad Sci U S A. 1993;90(12):5613-7.
127. Sandell LL, Zakian VA. Loss of a yeast telomere: Arrest, recovery, and chromosome loss. Cell. 1993;75(4):729-39.
128. Borrego-Soto G, Ortiz-López R, Rojas-Martínez A. Ionizing radiation-induced DNA injury and damage detection in patients with breast cancer. Genet Mol Biol. 2015;38(4):420-32.
129. Roos WP, Batista LFZ, Naumann SC, Wick W, Weller M, Menck CFM, et al. Apoptosis in malignant glioma cells triggered by the temozolomide-induced DNA lesion O6-methylguanine. Oncogene. 2007;26(2):186-97.
130. Roos WP, Kaina B. DNA damage-induced cell death: From specific DNA lesions to the DNA damage response and apoptosis. Cancer Lett. 2012;332(2):237-48.
131. Helleday T. Homologous recombination in cancer development, treatment and development of drug resistance. Carcinogenesis. 2010;31(6):955-60.
132. Eich M, Roos WP, Dianov GL, Digweed M, Kaina B. Nijmegen breakage syndrome protein (NBN) causes resistance to methylating anticancer drugs such as temozolomide. Molecular pharmacology. 2010;78(5):943-51.
133. Quiros S, Roos WP, Kaina B. Rad51 and BRCA2 - new molecular targets for sensitizing glioma cells to alkylating anticancer drugs. PLoS One. 2011;6(11):e27183.
134. Short SC, Giampieri S, Worku M, Alcaide-German M, Sioftanos G, Bourne S, et al. Rad51 inhibition is an effective means of targeting DNA repair in glioma models and CD133+ tumor- derived cells. Neuro-Oncology. 2011;13(5):487-99.
135. Lavin MF. ATM and the Mre11 complex combine to recognize and signal DNA double-strand breaks. Oncogene. 2007;26(56):7749-58.
136. Doil C, Mailand N, Bekker-Jensen S, Menard P, Larsen DH, Pepperkok R, et al. RNF168 Binds and Amplifies Ubiquitin Conjugates on Damaged Chromosomes to Allow Accumulation of Repair Proteins. Cell. 2009;136(3):435-46.
137. Huen MSY, Grant R, Manke I, Minn K, Yu X, Yaffe MB, et al. RNF8 Transduces the DNA-Damage Signal via Histone Ubiquitylation and Checkpoint Protein Assembly. Cell. 2007;131(5):901-14.
138. Mailand N, Bekker-Jensen S, Faustrup H, Melander F, Bartek J, Lukas C, et al. RNF8 Ubiquitylates Histones at DNA Double-Strand Breaks and Promotes Assembly of Repair Proteins. Cell. 2007;131(5):887-900.
139. Thompson LH. Recognition, signaling, and repair of DNA double-strand breaks produced by ionizing radiation in mammalian cells: The molecular choreography. Mutation research Reviews in mutation research. 2012;751(2):158-246.
140. Bothmer A, Robbiani DF, Feldhahn N, Gazumyan A, Nussenzweig A, Nussenzweig MC. 53BP1 regulates DNA resection and the choice between classical and alternative end joining during class switch recombination. J Exp Med. 2010;207(4):855-65.
141. Bunting SF, Callén E, Wong N, Chen H-T, Polato F, Gunn A, et al. 53BP1 Inhibits Homologous Recombination in Brca1-Deficient Cells by Blocking Resection of DNA Breaks. Cell. 2010;141(2):243-54.
142. Helmink BA, Tubbs AT, Dorsett Y, Bednarski JJ, M.walker L, Feng Z, et al. H2AX prevents CtIP-mediated DNA end resection and aberrant repair in G1-phase lymphocytes (Nature 469 (2010) (245-249)). Nature (London). 2011;472(7342):247.
143. Sun J, Lee K-J, Davis AJ, Chen DJ. Human Ku70/80 Protein Blocks Exonuclease 1-mediated DNA Resection in the Presence of Human Mre11 or Mre11/Rad50 Protein Complex. J Biol Chem. 2012;287(7):4936-45.
144. Langerak P, Mejia-Ramirez E, Limbo O, Russell P. Release of Ku and MRN from DNA ends by Mre11 nuclease activity and Ctp1 is required for homologous recombination repair of double-strand breaks. PLoS Genet. 2011;7(9):e1002271-e.

145. McVey M, Lee SE. MMEJ repair of double-strand breaks (director's cut): deleted sequences and alternative endings. Trends Genet. 2008;24(11):529-38.
146. Jasin M, Moynahan ME. Mitotic homologous recombination maintains genomic stability and suppresses tumorigenesis. Nat Rev Mol Cell Biol. 2010;11(3):196-207.
147. Williams RS, Moncalian G, Williams JS, Yamada Y, Limbo O, Shin DS, et al. Mre11 Dimers Coordinate DNA End Bridging and Nuclease Processing in Double-Strand-Break Repair. Cell. 2008;135(1):97-109.
148. Sartori AA, Lukas C, Coates J, Mistrik M, Fu S, Bartek J, et al. Human CtIP promotes DNA end resection. Nature. 2007;450(7169):509-14.
149. Hiom K, Yun MH. CtIP-BRCA1 modulates the choice of DNA double-strand-break repair pathway throughout the cell cycle. Nature. 2009;459(7245):460-3.
150. You Z, Shi LZ, Zhu Q, Wu P, Zhang Y-W, Basilio A, et al. CtIP Links DNA Double-Strand Break Sensing to Resection. Mol Cell. 2009;36(6):954-69.
151. Guirouilh-Barbat J, Rass E, Plo I, Bertrand P, Lopez BS. Defects in XRCC4 and KU80 Differentially Affect the Joining of Distal Nonhomologous Ends. Proc Natl Acad Sci U S A. 2007;104(52):20902-7.
152. Alt FW, Yan CT, Boboila C, Souza EK, Franco S, Hickernell TR, et al. IgH class switching and translocations use a robust non-classical end-joining pathway. Nature. 2007;449(7161):478-82.
153. Bennardo N, Cheng A, Huang N, Stark JM. Alternative-NHEJ is a mechanistically distinct pathway of mammalian chromosome break repair. PLoS Genet. 2008;4(6):e1000110-e.
154. Guirouilh-Barbat J, Huck S, Bertrand P, Pirzio L, Desmaze C, Sabatier L, et al. Impact of the KU80 Pathway on NHEJ-Induced Genome Rearrangements in Mammalian Cells. Mol Cell. 2004;14(5):611-23.
155. Nimonkar AV, Genschel J, Kinoshita E, Polaczek P, Campbell JL, Wyman CL, et al. BLM-DNA2-RPA-MRN and EXO1-BLM-RPA-MRN constitute two DNA end resection machineries for human DNA break repair. Genes Dev. 2011;25(4):350-62.
156. Bouwman P, Aly A, Escandell JM, Pieterse M, Bartkova J, Van Der Gulden H, et al. 53BP1 loss rescues BRCA1 deficiency and is associated with triple-negative and BRCA-mutated breast cancers. Nat Struct Mol Biol. 2010;17(6):688-95.
157. Cao L, Xu X, Bunting SF, Liu J, Wang R-H, Cao LL, et al. A Selective Requirement for 53BP1 in the Biological Response to Genomic Instability Induced by Brca1 Deficiency. Mol Cell. 2009;35(4):534-41.
158. Yang H, Jeffrey PD, Miller J, Kinnucan E, Sun Y, Thomä NH, et al. BRCA2 Function in DNA Binding and Recombination from a BRCA2-DSS1-ssDNA Structure. Science. 2002;297(5588):1837-48.
159. Pavletich NP, Yang H, Li Q, Fan J, Holloman WK. The BRCA2 homologue Brh2 nucleates RAD51 filament formation at a dsDNA-ssDNA junction. Nature. 2005;433(7026):653-7.
160. Davies AA, Masson J-Y, McIlwraith MJ, Stasiak AZ, Stasiak A, Venkitaraman AR, et al. Role of BRCA2 in Control of the RAD51 Recombination and DNA Repair Protein. Molecular Cell. 2001;7(2):273-82.
161. Stauffer ME, Chazin WJ. Physical Interaction between Replication Protein A and Rad51 Promotes Exchange on Single-stranded DNA. J Biol Chem. 2004;279(24):25638-45.
162. Daley JM, Sung P. 53BP1, BRCA1, and the choice between recombination and end joining at DNA double-strand breaks. Mol Cell Biol. 2014;34(8):1380-8.
163. Escribano-Díaz C, Orthwein A, Fradet-Turcotte A, Xing M, Young Jordan TF, Tkáč J, et al. A Cell Cycle-Dependent Regulatory Circuit Composed of 53BP1-RIF1 and BRCA1-CtIP Controls DNA Repair Pathway Choice. Mol Cell. 2013;49(5):872-83.
164. Shibata A, Jeggo PA. Roles for the DNA-PK complex and 53BP1 in protecting ends from resection during DNA double-strand break repair. J Radiat Res. 2020;61(5):718-26.
165. Davis AJ, Chi L, So S, Lee K-J, Mori E, Fattah K, et al. BRCA1 modulates the autophosphorylation status of DNA-PKcs in S phase of the cell cycle. Nucleic Acids Res. 2014;42(18):11487-501.
166. Gorodetska I, Kozeretska I, Dubrovska A. BRCA genes: The role in genome stability, cancer stemness and therapy resistance. J Cancer. 2019;10(9):2109-27.
167. Symington LS, Gautier J. Double-Strand Break End Resection and Repair Pathway Choice. Annu Rev Genet. 2011;45(1):247-71.
168. Maréchal A, Zou L. DNA damage sensing by the ATM and ATR kinases. Cold Spring Harbor perspectives in biology. 2013;5(9).
169. Zhuang W, Li B, Long L, Chen L, Huang Q, Liang Z-Q. Knockdown of the DNA- dependent protein kinase catalytic subunit radiosensitizes glioma- initiating cells by inducing autophagy. Brain Research. 2011;1371:7-15.
170. Mukherjee B, McEllin B, Camacho CV, Tomimatsu N, Sirasanagandala S, Nannepaga S, et al. EGFRvIII and DNA double-strand break repair: A molecular mechanism for radioresistance in glioblastoma. Cancer Res. 2009;69(10):4252-9.

171. Macheret M, Halazonetis TD. DNA Replication Stress as a Hallmark of Cancer. Annu Rev Pathol Mech Dis. 2015;10(1):425-48.
172. Sandie T, Laure C, Chiara C, Hélène T, Heidi H-G, Anna J, et al. Topoisomerase I suppresses genomic instability by preventing interference between replication and transcription. Nature Cell Biology. 2010;12(11):1122.
173. Frédéric L, Gerry PC, Ivan VR, Mark JA, Ketan JP. Fancd2 counteracts the toxic effects of naturally produced aldehydes in mice. Nature. 2011;475(7354):53.
174. Foote KM, Nissink JWM, McGuire T, Turner P, Guichard S, Yates JWT, et al. Discovery and Characterization of AZD6738, a Potent Inhibitor of Ataxia Telangiectasia Mutated and Rad3 Related (ATR) Kinase with Application as an Anticancer Agent. Journal of medicinal chemistry. 2018;61(22):9889-907.
175. da Costa AABA, Chowdhury D, Shapiro GI, D'Andrea AD, Konstantinopoulos PA. Targeting replication stress in cancer therapy. Nat Rev Drug Discov. 2023;22(1):38-58.
176. Zeman MK, Cimprich KA. Causes and consequences of replication stress. Nat Cell Biol. 2014;16(1):2-9.
177. Sale JE, Lehmann AR, Woodgate R. Y-family DNA polymerases and their role in tolerance of cellular DNA damage. Nat Rev Mol Cell Biol. 2012;13(3):141-52.
178. McInerney P, O'Donnell M. Functional uncoupling of twin polymerases: Mechanism of polymerase dissociation from a lagging-strand block. J Biol Chem. 2004;279(20):21543-51.
179. Regairaz M, Zhang Y-W, Fu H, Agama KK, Tata N, Agrawal S, et al. Mus81-mediated DNA cleavage resolves replication forks stalled by topoisomerase I-DNA complexes. J Cell Biol. 2011;195(5):739-49.
180. Thangavel S, Berti M, Levikova M, Pinto C, Gomathinayagam S, Vujanovic M, et al. DNA2 drives processing and restart of reversed replication forks in human cells. J Cell Biol. 2015;208(5):545-62.
181. Lemaçon D, Jackson J, Quinet A, Brickner JR, Li S, Yazinski S, et al. MRE11 and EXO1 nucleases degrade reversed forks and elicit MUS81-dependent fork rescue in BRCA2-deficient cells. Nat Commun. 2017;8(1):860-12.
182. Sun H, Ma L, Tsai Y-F, Abeywardana T, Shen B, Zheng L. Okazaki fragment maturation: DNA flap dynamics for cell proliferation and survival. Trends in cell biology. 2022.
183. Truong LN, Li Y, Shi LZ, Hwang PY-H, He J, Wang H, et al. Microhomology-mediated End Joining and Homologous Recombination share the initial end resection step to repair DNA double-strand breaks in mammalian cells. Proc Natl Acad Sci U S A. 2013;110(19):7720-5.
184. Lundin C, Erixon K, Arnaudeau C, Schultz N, Jenssen D, Meuth M, et al. Different Roles for Nonhomologous End Joining and Homologous Recombination following Replication Arrest in Mammalian Cells. Mol Cell Biol. 2002;22(16):5869-78.
185. Byun TS, Pacek M, Yee M-C, Walter JC, Cimprich KA. Functional uncoupling of MCM helicase and DNA polymerase activities activates the ATR-dependent checkpoint. Genes Dev. 2005;19(9):1040-52.
186. Liao H, Ji F, Helleday T, Ying S. Mechanisms for stalled replication fork stabilization: new targets for synthetic lethality strategies in cancer treatments. EMBO Rep. 2018;19(9):n/a.
187. Bryant HE, Petermann E, Schultz N, Jemth AS, Loseva O, Issaeva N, et al. PARP is activated at stalled forks to mediate Mre11- dependent replication restart and recombination. EMBO Journal. 2009;28(17):2601-15.
188. Schlacher K, Christ N, Siaud N, Egashira A, Wu H, Jasin M. Double-Strand Break Repair-Independent Role for BRCA2 in Blocking Stalled Replication Fork Degradation by MRE11. Cell. 2011;145(4):529-42.
189. Schlacher K, Wu H, Jasin M. A Distinct Replication Fork Protection Pathway Connects Fanconi Anemia Tumor Suppressors to RAD51-BRCA1/2. Cancer Cell. 2012;22(1):106-16.
190. Chaudhuri AR, Callen E, Ding X, Gogola E, Duarte AA, Lee J-E, et al. Replication fork stability confers chemoresistance in BRCA-deficient cells. Nature. 2016;535(7612):382-7.
191. Lovett ST. Template-switching during replication fork repair in bacteria. DNA Repair (Amst). 2017;56:118-28.
192. Costanzo V, Chaudhuri AR, Lopes M, Hashimoto Y. Rad51 protects nascent DNA from Mre11-dependent degradation and promotes continuous DNA synthesis. Nat Struct Mol Biol. 2010;17(11):1305-11.
193. Bugreev DV, Rossi MJ, Mazin AV. Cooperation of RAD51 and RAD54 in regression of a model replication fork. Nucleic Acids Res. 2011;39(6):2153-64.
194. Li X, Heyer W-D. Homologous recombination in DNA repair and DNA damage tolerance. Cell Research. 2008;18(1):99-113.
195. Bochkareva E, Korolev S, Lees-Miller SP, Bochkarev A. Structure of the RPA trimerization core and its role in the multistep DNA-binding mechanism of RPA. EMBO J. 2002;21(7):1855-63.

196. Seo Y-S, Bae S-H, Bae K-H, Kim J-A. RPA governs endonuclease switching during processing of Okazaki fragments in eukaryotes. Nature. 2001;412(6845):456-61.
197. Yuzhakov A, Kelman Z, Hurwitz J, O'Donnell M. Multiple competition reactions for RPA order the assembly of the DNA polymerase δ holoenzyme. EMBO J. 1999;18(21):6189-99.
198. Dornreiter I, Erdile LF, Gilbert IU, Winkler D, Kelly TJ, Fanning E. Interaction of DNA polymerase alpha-primase with cellular replication protein A and SV40 T antigen. EMBO J. 1992;11(2):769-76.
199. Soniat MM, Myler LR, Kuo H-C, Paull TT, Finkelstein IJ. RPA Phosphorylation Inhibits DNA Resection. Mol Cell. 2019;75(1):145-53.e5.
200. Deng SK, Gibb B, De Almeida MJ, Greene EC, Symington LS. RPA antagonizes microhomology-mediated repair of DNA double-strand breaks. Nat Struct Mol Biol. 2014;21(4):405-12.
201. Sugiyama T, New JH, Kowalczykowski SC. DNA Annealing by Rad52 Protein is Stimulated by Specific Interaction with the Complex of Replication Protein A and Single-Stranded DNA. Proc Natl Acad Sci U S A. 1998;95(11):6049-54.
202. Chen H, Lisby M, Symington Lorraine S. RPA Coordinates DNA End Resection and Prevents Formation of DNA Hairpins. Mol Cell. 2013;50(4):589-600.
203. Poole LA, Cortez D. Functions of SMARCAL1, ZRANB3, and HLTF in maintaining genome stability. Crit Rev Biochem Mol Biol. 2017;52(6):696-714.
204. Cortez D, Guntuku S, Qin J, Elledge SJ. ATR and ATRIP: Partners in Checkpoint Signaling. Science. 2001;294(5547):1713-6.
205. Yan S, Michael WM. TopBP1 and DNA polymerase-α directly recruit the 9-1-1 complex to stalled DNA replication forks. J Cell Biol. 2009;184(6):793-804.
206. Kumagai A, Lee J, Yoo HY, Dunphy WG. TopBP1 Activates the ATR-ATRIP Complex. Cell. 2006;124(5):943-55.
207. Delacroix S, Wagner JM, Kobayashi M, Yamamoto K-I, Karnitz LM. The Rad9-Hus1-Rad1 (9-1-1) clamp activates checkpoint signaling via TopBP1. Genes Dev. 2007;21(12):1472-7.
208. Lee J, Kumagai A, Dunphy WG. The Rad9-Hus1-Rad1 Checkpoint Clamp Regulates Interaction of TopBP1 with ATR. J Biol Chem. 2007;282(38):28036-44.
209. Liu Q, Guntuku S, Cui XS, Matsuoka S, Cortez D, Tamai K, et al. Chk1 is an essential kinase that is regulated by Atr and required for the G(2)/M DNA damage checkpoint. Genes & development. 2000;14(12):1448-59.
210. Ge XQ, Blow JJ. Chk1 inhibits replication factory activation but allows dormant origin firing in existing factories. J Cell Biol. 2010;191(7):1285-97.
211. Mihaylov IS, Kondo T, Jones L, Ryzhikov S, Tanaka J, Zheng J, et al. Control of DNA Replication and Chromosome Ploidy by Geminin and Cyclin A. Mol Cell Biol. 2002;22(6):1868-80.
212. Melixetian M, Ballabeni A, Masiero L, Gasparini P, Zamponi R, Bartek J, et al. Loss of Geminin Induces Rereplication in the Presence of Functional p53. J Cell Biol. 2004;165(4):473-82.
213. Finn KJ, Li JJ. Single-Stranded Annealing Induced by Re-Initiation of Replication Origins Provides a Novel and Efficient Mechanism for Generating Copy Number Expansion via Non-Allelic Homologous Recombination. PLoS Genet. 2013;9(1):e1003192.
214. Neelsen KJ, Zanini IMY, Mijic S, Herrador R, Zellweger R, Chaudhuri AR, et al. Deregulated origin licensing leads to chromosomal breaks by rereplication of a gapped DNA template. Genes Dev. 2013;27(23):2537-42.
215. Li JJ, Nguyen VQ, Co C. Cyclin-dependent kinases prevent DNA re-replication through multiple mechanisms. Nature. 2001;411(6841):1068-73.
216. Block WD, Yu Y, Lees-Miller SP. Phosphatidyl inositol 3-kinase-like serine/threonine protein kinases (PIKKs) are required for DNA damage-induced phosphorylation of the 32 kDa subunit of replication protein A at threonine 21. Nucl Acids Res. 2004;32(3):997-1005.
217. Vassin VM, Wold MS, Borowiec JA. Replication Protein A (RPA) Phosphorylation Prevents RPA Association with Replication Centers. Mol Cell Biol. 2004;24(5):1930-43.
218. Haring SJ, Mason AC, Binz SK, Wold MS. Cellular Functions of Human RPA1: MULTIPLE ROLES OF DOMAINS IN REPLICATION, REPAIR, AND CHECKPOINTS. J Biol Chem. 2008;283(27):19095-111.
219. Dutta A, Stillman B. cdc2 family kinases phosphorylate a human cell DNA replication factor, RPA, and activate DNA replication. EMBO J. 1992;11(6):2189-99.
220. Fang F, Newport JW. Distinct roles of cdk2 and cdc2 in RP-A phosphorylation during the cell cycle. J Cell Sci. 1993;106(3):983-94.

221. Anantha RW, Sokolova E, Borowiec JA. RPA phosphorylation facilitates mitotic exit in response to mitotic DNA damage. Proc Natl Acad Sci U S A. 2008;105(35):12903-8.
222. Feng J, Wakeman T, Yong S, Wu X, Kornbluth S, Wang X-F. Protein Phosphatase 2A-Dependent Dephosphorylation of Replication Protein A Is Required for the Repair of DNA Breaks Induced by Replication Stress. Mol Cell Biol. 2009;29(21):5696-709.
223. Toledo Luis I, Altmeyer M, Rask M-B, Lukas C, Larsen Dorthe H, Povlsen Lou K, et al. ATR Prohibits Replication Catastrophe by Preventing Global Exhaustion of RPA. Cell. 2013;155(5):1088-103.
224. Brill SJ, Stillman B. Replication factor-A from Saccharomyces cerevisiae is encoded by three essential genes coordinately expressed at S phase. Genes Dev. 1991;5(9):1589-600.
225. Chen R, Wold MS. Replication protein A: Single-stranded DNA's first responder: Dynamic DNA-interactions allow replication protein A to direct single-strand DNA intermediates into different pathways for synthesis or repair. Bioessays. 2014;36(12):1156-61.
226. Rebecca AB, Nicholas M, Jiri B, Charles S. The causes and consequences of genetic heterogeneity in cancer evolution. Nature. 2013;501(7467):338.
227. Chae Y, Anker J, Carneiro BA, Chandra S, Kaplan J, Kalyan A, et al. Genomic landscape of DNA repair genes in cancer. Oncotarget. 2016;7(17):23312-21.
228. Hanahan D, Weinberg Robert a. Hallmarks of Cancer: The Next Generation. Cell. 2011;144(5):646-74.
229. Broustas CG, Lieberman H. DNA Damage Response Genes and the Development of Cancer Metastasis. Radiat Res. 2014;181(2):111-30.
230. Thomas H, Eva P, Cecilia L, Ben H, Ricky AS. DNA repair pathways as targets for cancer therapy. Nature Reviews Cancer. 2008;8(3):193.
231. Srinivas U, Tan B, Vellayappan BA, Jeyasekharan AD. ROS and the DNA damage response in cancer. Redox Biol. 2019;25.
232. Kotsantis P, Petermann E, Boulton SJ. Mechanisms of Oncogene-Induced Replication Stress: Jigsaw Falling into Place. Cancer Discov. 2018;8(5):537-55.
233. Cheung-Ong K, Giaever G, Nislow C. DNA-Damaging Agents in Cancer Chemotherapy: Serendipity and Chemical Biology. Chemistry & Biology. 2013;20(5):648-59.
234. Brown J, O'Carrigan B, Jackson S, Yap TA. Targeting DNA Repair in Cancer : Beyond PARP Inhibitors. Cancer Discov. 2017;7(1):20-37.
235. O'connor Mark j. Targeting the DNA Damage Response in Cancer. Molecular Cell. 2015;60(4):547-60.
236. Rocha CRR, Silva MM, Quinet A, Cabral-Neto JB, Menck CFM. DNA repair pathways and cisplatin resistance: an intimate relationship. Clinics (Sao Paulo, Brazil). 2018;73(Suppl 1):e478s-es.
237. Palanichamy K, Patel D, Jacob JR, Litzenberg KT, Gordon N, Acus K, et al. Lack of Constitutively Active DNA Repair Sensitizes Glioblastomas to Akt Inhibition and Induces Synthetic Lethality with Radiation Treatment in a p53-Dependent Manner. Molecular cancer therapeutics. 2018;17(2):336-46.
238. Dietlein F, Thelen L, Reinhardt HC. Cancer-specific defects in DNA repair pathways as targets for personalized therapeutic approaches. Trends in Genetics. 2014;30(8):326-39.
239. Shideng B, Qiulian W, Roger EM, Yueling H, Qing S, Anita BH, et al. Glioma stem cells promote radioresistance by preferential activation of the DNA damage response. Nature. 2006;444(7120):756.
240. Fukumoto Y. Radiosensitization of cancer stem cells in glioblastoma by the simultaneous inhibition of parallel DNA damage response pathways. Annals of Translational Medicine. 2017;5(Suppl 1).
241. Chalmers AJ. Science in Focus: Combining Radiotherapy with Inhibitors of the DNA Damage Response. Clinical Oncology. 2016;28(5):279-82.
242. Gong-She G, Feng-Mei Z, Rui-Jie G, Robert D, Zhi-Hui F, Simon NP. DNA repair and synthetic lethality. International Journal of Oral Science. 2011;3(4):176.
243. Adrian CB, Fiona AS, Conchita V. Strategies to improve radiotherapy with targeted drugs. Nature Reviews Cancer. 2011;11(4):239.
244. Prasad C, Prasad S, Yadav S, Pandey L, Singh S, Pradhan S, et al. Olaparib modulates DNA repair efficiency, sensitizes cervical cancer cells to cisplatin and exhibits anti-metastatic property. Sci Rep. 2017;7(1):12876-.
245. Mateo J, Carreira S, Sandhu S, Miranda S, Mossop H, Perez-Lopez R, et al. DNA-Repair Defects and Olaparib in Metastatic Prostate Cancer. 2015.
246. González-Martín A, Pothuri B, Vergote I, Depont Christensen R, Graybill W, Mirza MR, et al. Niraparib in Patients with Newly Diagnosed Advanced Ovarian Cancer. The New England journal of medicine. 2019;381(25):2391-402.

247. Pearl LH, Schierz AC, Ward SE, Al-Lazikani B, Pearl FMG. Therapeutic opportunities within the DNA damage response. Nature reviews Cancer. 2015;15(3):166-80.
248. Paola F, Sven R. Mechanisms of PARP inhibitor resistance in cancer and insights into the DNA damage response. Genome medicine. 2018;10(1):1-3.
249. Bukhari AB, Lewis CW, Pearce JJ, Luong D, Chan GK, Gamper AM. Inhibiting Wee1 and ATR kinases produces tumor-selective synthetic lethality and suppresses metastasis. The Journal of clinical investigation. 2019;129(3):1329-44.
250. Caitriona H, Sandra Van S, Daniel BL, Patrick GJ. Cancer drug resistance: an evolving paradigm. Nature Reviews Cancer. 2013;13(10):714.
251. Chaudhry A, Benson L, Varshaver M, Farber O, Weinberg U, Kirson E, et al. NovoTTF (TM)-100A System (Tumor Treating Fields) transducer array layout planning for glioblastoma: a NovoTAL (TM) system user study. World J Surg Oncol. 2015;13(1).
252. Kirson ED, Gurvich Z, Schneiderman R, Dekel E, Itzhaki A, Wasserman Y, et al. Disruption of cancer cell replication by alternating electric fields. Cancer research. 2004;64(9):3288-95.
253. Lacouture M, Davis ME, Elzinga G, Butowski N, Tran D, Villano J, et al. DERMATOLOGIC EVENT CHARACTERISTICS AND MANAGEMENT WITH THE NOVOTTF-100A SYSTEM, A NOVEL ANTI-MITOTIC DEVICE FOR THE TREATMENT OF RECURRENT GLIOBLASTOMA (rGBM). Neuro-Oncology. 2013;15:229-.
254. Julie AM, Reid A, Proskauer R, D. TDR, Byron R. Form S-1 REGISTRATION STATEMENT UNDER THE SECURITIES ACT OF 1933: Novocure Limited: UNITED STATESSECURITIES AND EXCHANGE COMMISSION; 2015 [Available from: https://www.sec.gov/Archives/edgar/data/1645113/000119312515308245/d940664ds1.htm.
255. Novocure. Patient Information and Operation Manuel: Novocure; 2019 [Available from: https://www.optune.com/content/pdfs/Optune_PIOM_8.5x11.pdf.
256. William W, Yeun Mi Y, Ashley K, Martin C, Marjolaine G-L, Patrick G-S, et al. Assessment of costs associated with adverse events in patients with cancer. PLoS ONE. 2018;13(4):e0196007.
257. Bernard-Arnoux F, Lamure M, Ducray F, Aulagner G, Honnorat J, Armoiry X. The cost-effectiveness of tumor-treating fields therapy in patients with newly diagnosed glioblastoma. Neuro-Oncology. 2016;18(8):1129-36.
258. Connock M, Auguste P, Dussart C, Guyotat J, Armoiry X. Cost-effectiveness of tumor-treating fields added to maintenance temozolomide in patients with glioblastoma: an updated evaluation using a partitioned survival model. J Neurooncol. 2019;143(3):605-11.
259. Guzauskas GF, Pollom EL, Stieber VW, Wang BCM, Garrison Jr LP. Tumor treating fields and maintenance temozolomide for newly-diagnosed glioblastoma: a cost-effectiveness study. Journal of Medical Economics. 2019;22(10):1006-13.
260. Porter KR, McCarthy BJ, Berbaum ML, Davis FG. Conditional Survival of All Primary Brain Tumor Patients by Age, Behavior, and Histology. Neuroepidemiology. 2011;36(4):230-9.
261. Larkin J, Hatswell AJ, Nathan P, Lebmeier M, Lee D. The predicted impact of ipilimumab usage on survival in previously treated advanced or metastatic melanoma in the UK. PLoS One. 2015;10(12):e0145524-e.
262. Excellence. TNIfHaC. Ipilimumab for previously treated advanced (unresectable or metastatic) melanoma: guidance and guidelines (TA268). 2012.
263. McCabe C, Claxton K, Culyer A. The NICE Cost-Effectiveness Threshold. Pharmacoeconomics. 2008;26(9):733-44.
264. Taylor C, Jan S. Economic evaluation of medicines. Australian prescriber. 2017;40(2):76-8.
265. Novocure. Novocure Reports 2015 Operating Statistics and Financial Results: Novocure; 2016 [Available from: https://www.novocure.com/novocure-reports-2015-operating-statistics-and-financial-results/.
266. Novocure. Novocure Reports Fourth Quarter and Full Year 2018 Financial Results and Provides Company Update. Novocure; 2019.
267. Mehta M, Wen P, Nishikawa R, Reardon D, Peters K. Critical review of the addition of tumor treating fields (TTFields) to the existing standard of care for newly diagnosed glioblastoma patients. Critical Reviews in Oncology / Hematology. 2017;111(C):60-5.
268. M MM, H EH, Dinh TD, Yvonne K, Robert C, L VJ, et al. Clinical practice experience with NovoTTF-100A™ system for glioblastoma: The Patient Registry Dataset (PRiDe). Seminars in Oncology; 2014.
269. Wick W. TTFields: where does all the skepticism come from? Neuro-Oncology. 2016;18(3):303-5.
270. The National Institute for Health and Care Excellence. Brain tumours (primary) and brain metastases in adults NICE guideline [NG99]. 2018 [Available from: https://www.nice.org.uk/guidance/ng99.

271. Moghadam M, Firoozabadi S, Janahmadi M. 50 Hz alternating extremely low frequency magnetic fields affect excitability, firing and action potential shape through interaction with ionic channels in snail neurones. The Environmentalist. 2008;28(4):341-7.
272. Cheung AY, Neyzari A. Deep local hyperthermia for cancer therapy: external electromagnetic and ultrasound techniques. Cancer research. 1984;44(10 Suppl):4736s-44s.
273. Davies AM, Weinberg U, Palti Y. Tumor treating fields: a new frontier in cancer therapy. Annals of the New York Academy of Sciences. 2013;1291(1):86-95.
274. Rominiyi O, Vanderlinden A, Clenton SJ, Bridgewater C, Al-Tamimi Y, Collis SJ. Tumour treating fields therapy for glioblastoma: current advances and future directions. Br J Cancer. 2021;124(4):697-709.
275. Eilon DK, Vladimír D, František T, Josef V, Jean FS, Aviran I, et al. Alternating electric fields arrest cell proliferation in animal tumor models and human brain tumors. Proceedings of the National Academy of Sciences. 2007;104(24):10152.
276. Clark PA, Gaal JT, Strebe JK, Pasch CA, Deming DA, Kuo JS, et al. The effects of tumor treating fields and temozolomide in MGMT expressing and non-expressing patient-derived glioblastoma cells. Journal of Clinical Neuroscience. 2017;36:120-4.
277. Fabian D, Guillermo Prieto Eibl MD, Alnahhas I, Sebastian N, Giglio P, Puduvalli V, et al. Treatment of Glioblastoma (GBM) with the Addition of Tumor-Treating Fields (TTF): A Review. Cancers. 2019;11(2).
278. Squatrito M, Brennan CW, Helmy K, Huse JT, Petrini JH, Holland EC. Loss of ATM/Chk2/p53 Pathway Components Accelerates Tumor Development and Contributes to Radiation Resistance in Gliomas. Cancer Cell. 2010;18(6):619-29.
279. Kline-Smith S, Walczak CE. Mitotic spindle assembly and chromosome segregation: Refocusing on microtubule dynamics. Mol Cell. 2004;15(3):317-27.
280. Moshe G, Rosa SS, Tali V, Yaara P, Mijal M, Roni B, et al. Mitotic Spindle Disruption by Alternating Electric Fields Leads to Improper Chromosome Segregation and Mitotic Catastrophe in Cancer Cells. Scientific Reports. 2015;5(1).
281. Joshua JT, Jordane P, Jack AT, Eric TW. Tubulin's response to external electric fields by molecular dynamics simulations. PLoS ONE. 2018;13(9):e0202141.
282. Moshe G, Rosa SS, Tali V, Yaara P, Mijal M, Roni B, et al. Mitotic Spindle Disruption by Alternating Electric Fields Leads to Improper Chromosome Segregation and Mitotic Catastrophe in Cancer Cells. Scientific Reports. 2015;5(1).
283. Andrea M, Kevin HG. The spindle checkpoint: structural insights into dynamic signalling. Nature Reviews Molecular Cell Biology. 2002;3(10):731.
284. Nidhi G, Aaron Y, Talia SH, Sze Xian L, Eric TW, Kenneth DS. Tumor treating fields perturb the localization of septins and cause aberrant mitotic exit. PLoS ONE. 2015;10(5):e0125269.
285. Jo Y, Hwang S-G, Jin YB, Sung J, Jeong YK, Baek JH, et al. Selective toxicity of tumor treating fields to melanoma: an in vitro and in vivo study. Cell Death Discov. 2018;4(1):46-10.
286. Branter J, Estevez-Cebrero M, Diksin M, Griffin M, Castellanos-Uribe M, May S, et al. Genome-Wide Expression and Anti-Proliferative Effects of Electric Field Therapy on Pediatric and Adult Brain Tumors. Int J Mol Sci. 2022;23(4):1982.
287. Field CM, Coughlin M, Doberstein S, Marty T, Sullivan W. Characterization of anillin mutants reveals essential roles in septin localization and plasma membrane integrity. Development (Cambridge, England). 2005;132(12):2849-60.
288. Spiliotis ET, Kinoshita M, Nelson WJ. A mitotic septin scaffold required for Mammalian chromosome congression and segregation. Science (New York, NY). 2005;307(5716):1781-5.
289. Paul F, Eric H, Michael L, Mena K, Paknoosh P, Alisa P. An anillin-Ect2 complex stabilizes central spindle microtubules at the cortex during cytokinesis. PLoS ONE. 2012;7(4):e34888.
290. Goldbach P, Wong R, Beise N, Sarpal R, Trimble WS, Brill JA. Stabilization of the actomyosin ring enables spermatocyte cytokinesis in Drosophila. Molecular biology of the cell. 2010;21(9):1482-93.
291. Mun E, Babiker HM, Weinberg U, Kirson E, Von Hoff DD. Tumor-Treating Fields: A Fourth Modality in Cancer Treatment. Clin Cancer Res. 2018;24(2):266-75.
292. Tuszynski JA, Wenger C, Friesen DE, Preto J. An overview of sub-cellular mechanisms involved in the action of TTFields. Int J Environ Res Public Health. 2016;13(11):1128.
293. Li X, Yang F, Rubinsky B. A Theoretical Study on the Biophysical Mechanisms by Which Tumor Treating Fields Affect Tumor Cells During Mitosis. IEEE Trans Biomed Eng. 2020;67(9):2594-602.

294. Wenger C, Miranda PC, Salvador R, Thielscher A, Bomzon Z, Giladi M, et al. A Review on Tumor-Treating Fields (TTFields): Clinical Implications Inferred From Computational Modeling. IEEE Rev Biomed Eng. 2018;11:195-207.
295. Sun ZL, Wataha JC, Hanks CT. Effects of metal ions on osteoblast-like cell metabolism and differentiation. J Biomed Mater Res. 1997;34(1):29-37.
296. Whitfield JF, MacManus JP, Rixon RH, Boynton AL, Youdale T, Swierenga S. The Positive Control of Cell Proliferation by the Interplay of Calcium Ions and Cyclic Nucleotides. A Review. In Vitro. 1976;12(1):1-18.
297. Bortner CD, Gómez-Angelats M, Cidlowski JA. Plasma Membrane Depolarization without Repolarization Is an Early Molecular Event in Anti-Fas-induced Apoptosis. J Biol Chem. 2001;276(6):4304-14.
298. Yang M, Brackenbury WJ. Membrane potential and cancer progression. Front Physiol. 2013;4:185-.
299. Neuhaus E, Zirjacks L, Ganser K, Klumpp L, Schüler U, Zips D, et al. Alternating electric fields (TTFields) activate Ca v 1.2 channels in human glioblastoma cells. Cancers. 2019;11(1):<xocs:firstpage xmlns:xocs=""/>.
300. van Breemen C, Farinas BR, Casteels R, Gerba P, Wuytack F, Deth R. Factors Controlling Cytoplasmic Ca2+Concentration. Philosophical transactions of the Royal Society of London Series B, Biological sciences. 1973;265(867):57-71.
301. Gal V, Martin S, Bayley P. Fast disassembly of microtubules induced by Mg2+ or Ca2. Biochem Biophys Res Commun. 1988;155(3):1464-70.
302. Berkelmann L, Bader A, Meshksar S, Dierks A, Hatipoglu Majernik G, Krauss JK, et al. Tumour-treating fields (TTFields): Investigations on the mechanism of action by electromagnetic exposure of cells in telophase/cytokinesis. Scientific Reports. 2019;9(1):<xocs:firstpage xmlns:xocs=""/>.
303. Daniels CS, Rubinsky B. Temperature modulation of electric fields in biological matter. PLoS One. 2011;6(6):e20877-e.
304. Racuciu M, Miclaus S, Creanga D. On the thermal effect induced in tissue samples exposed to extremely low-frequency electromagnetic field. J Environ Health Sci Eng. 2015;13(1):85-.
305. Gao C-q, Zhao Y-l, Li H-c, Sui W-g, Yan H-c, Wang X-q. Heat stress inhibits proliferation, promotes growth, and induces apoptosis in cultured Lantang swine skeletal muscle satellite cells. J Zhejiang Univ Sci B. 2015;16(6):549-59.
306. Collins CM, Liu W, Wang J, Gruetter R, Vaughan JT, Ugurbil K, et al. Temperature and SAR calculations for a human head within volume and surface coils at 64 and 300 MHz. J Magn Reson Imaging. 2004;19(5):650-6.
307. Bai L, Pfeifer T, Gross W, De La Torre C, Zhao S, Liu L, et al. Establishment of Tumor Treating Fields Combined With Mild Hyperthermia as Novel Supporting Therapy for Pancreatic Cancer. Front Oncol. 2021;11:738801-.
308. Sreedhar AS, Csermely P. Heat shock proteins in the regulation of apoptosis: New strategies in tumor therapy - A comprehensive review. Pharmacol Ther. 2004;101(3):227-57.
309. Warters RL, Henle KJ. DNA degradation in Chinese hamster ovary cells after exposure to hyperthermia. Cancer Res. 1982;42(11):4427-32.
310. Kampinga HH, Konings AWT. Inhibition of Repair of X-Ray-Induced DNA Damage by Heat: The Role of Hyperthermic Inhibition of DNA Polymerase α Activity. Radiat Res. 1987;112(1):86-98.
311. Makarov SN, Nummenmaa A. Brain and Human Body Modeling 2020 [electronic resource] : Computational Human Models Presented at EMBC 2019 and the BRAIN Initiative® 2019 Meeting. 2021.
312. Giladi M, Munster M, Schneiderman RS, Voloshin T, Porat Y, Blat R, et al. Tumor treating fields (TTFields) delay DNA damage repair following radiation treatment of glioma cells. Radiation oncology (London, England). 2017;12(1):206-.
313. Kim E, Kim Y, Song H, Jeong Y, Lee J, Sung J, et al. Biological effect of an alternating electric field on cell proliferation and synergistic antimitotic effect in combination with ionizing radiation. Oncotarget. 2016;7(38):62267-79.
314. Narasimha K, Kalayarasan S, Lianghao D, Brock S, Debabrata S, D. SM. Tumor-treating fields elicit a conditional vulnerability to ionizing radiation via the downregulation of BRCA1 signaling and reduced DNA double-strand break repair capacity in non-small cell lung cancer cell lines. Cell Death and Disease. 2017;8(3):e2711.
315. Mumblat H, Martinez-Conde A, Braten O, Munster M, Dor-On E, Schneiderman RS, et al. Tumor Treating Fields (TTFields) downregulate the Fanconi Anemia-BRCA pathway and increase the efficacy of chemotherapy in malignant pleural mesothelioma preclinical models. Lung cancer (Amsterdam, Netherlands). 2021;160:99-110.
316. Scully R, Chen J, Plug A, Xiao Y, Weaver D, Feunteun J, et al. Association of BRCA1 with Rad51 in Mitotic and Meiotic Cells. Cell. 1997;88(2):265-75.

317. Venkitaraman AR. Functions of BRCA1 and BRCA2 in the biological response to DNA damage. Journal of Cell Science. 2001;114(20):3591-8.
318. Mason JM, Chan YL, Weichselbaum RW, Bishop DK. Non-enzymatic roles of human RAD51 at stalled replication forks. Nature Communications. 2019;10(1).
319. Kais Z, Rondinelli B, Holmes A, O'leary C, Kozono D, D'andrea Alan d, et al. FANCD2 Maintains Fork Stability in BRCA1/2-Deficient Tumors and Promotes Alternative End-Joining DNA Repair. Cell Reports. 2016;15(11):2488-99.
320. Karanam NK, Ding L, Aroumougame A, Story MD. Tumor treating fields cause replication stress and interfere with DNA replication fork maintenance: Implications for cancer therapy. Translational Research. 2020;217:33-46.
321. Quinet A, Carvajal-Maldonado D, Lemacon D, Vindigni A. DNA Fiber Analysis: Mind the Gap! Methods in enzymology. 2017;591:55-82.
322. Luke AY, Ricardo JA, Nilisha P, Colleen CC, Joshua AK, Rajika LP, et al. A structural and dynamic model for the assembly of Replication Protein A on single-stranded DNA. Nature Communications. 2018;9(1):1-14.
323. Belotserkovskii BP, Tornaletti S, D'souza AD, Hanawalt PC. R-loop generation during transcription: Formation, processing and cellular outcomes. DNA Repair. 2018;71:69-81.
324. Yun CW, Lee SH. The Roles of Autophagy in Cancer. International journal of molecular sciences. 2018;19(11).
325. Shteingauz A, Porat Y, Voloshin T, Schneiderman RS, Munster M, Zeevi E, et al. AMPK-dependent autophagy upregulation serves as a survival mechanism in response to Tumor Treating Fields (TTFields). Cell death & disease. 2018;9(11):1074-.
326. Kim EH, Jo Y, Sai S, Park MJ, Kim JY, Kim JS, et al. Tumor-treating fields induce autophagy by blocking the Akt2/miR29b axis in glioblastoma cells. Oncogene. 2019;38(39):6630-46.
327. Tanida I, Ueno T, Kominami E. LC3 and Autophagy. Methods in molecular biology (Clifton, NJ). 2008;445:77-88.
328. Saori RY, Noboru M. Monitoring and Measuring Autophagy. International Journal of Molecular Sciences. 2017;18(9):1865.
329. Orhon I, Reggiori F. Assays to Monitor Autophagy Progression in Cell Cultures. Cells. 2017;6(3).
330. Mauthe M, Orhon I, Rocchi C, Zhou X, Luhr M, Hijlkema K-J, et al. Chloroquine inhibits autophagic flux by decreasing autophagosome-lysosome fusion. Autophagy. 2018;14(8):1435-55.
331. Inoue T, Nakayama Y, Li Y, Matsumori H, Takahashi H, Kojima H, et al. SIRT 2 knockdown increases basal autophagy and prevents postslippage death by abnormally prolonging the mitotic arrest that is induced by microtubule inhibitors. FEBS Journal. 2014;281(11):2623-37.
332. Paquette M, El-Houjeiri L, Pause A. mTOR Pathways in Cancer and Autophagy. Cancers. 2018;10(1):18.
333. Garcia D, Shaw RJ. AMPK: Mechanisms of Cellular Energy Sensing and Restoration of Metabolic Balance. Molecular Cell. 2017;66(6):789-800.
334. Silginer M, Weller M, Stupp R, Roth P. Biological activity of tumor-treating fields in preclinical glioma models. Cell death & disease. 2017;8(4):e2753-e.
335. Nduom EK, Weller M, Heimberger AB. Immunosuppressive mechanisms in glioblastoma. Neuro Oncol. 2015;17(suppl 7):vii9-vii14.
336. Wang N, Liang H, Zen K. Molecular mechanisms that influence the macrophage m1-m2 polarization balance. Frontiers in immunology. 2014;5:614-.
337. Arango Duque G, Descoteaux A. Macrophage cytokines: involvement in immunity and infectious diseases. Frontiers in immunology. 2014;5(491):491-.
338. Tripathi P, Tripathi P, Kashyap L, Singh V. The role of nitric oxide in inflammatory reactions. Oxford, UK2007. p. 443-52.
339. Park J-I, Song K-H, Jung S-Y, Ahn J, Hwang S-G, Kim J, et al. Tumor-Treating Fields Induce RAW264.7 Macrophage Activation Via NK-κB/MAPK Signaling Pathways. Technology in Cancer Research & Treatment. 2019;18.
340. Diamant G, Goldman HS, Plotnitsky LG, Roitman M, Shiloach T, Globerson-Levin A, et al. T cells retain pivotal antitumoral functions under tumor-treating electric fields. The Journal of immunology (1950). 2021;207(2):709-19.
341. Tan H-Y, Wang N, Li S, Hong M, Wang X, Feng Y. The Reactive Oxygen Species in Macrophage Polarization: Reflecting Its Dual Role in Progression and Treatment of Human Diseases. Oxidative medicine and cellular longevity. 2016;2016:2795090-.

342. Ting L, Lingyun Z, Donghyun J, Shao-Cong S. NF-κB signaling in inflammation. Signal Transduction and Targeted Therapy. 2017;2(1).
343. Chen D, Le SB, Hutchinson TE, Calinescu A-A, Sebastian M, Jin D, et al. Tumor Treating Fields dually activate STING and AIM2 inflammasomes to induce adjuvant immunity in glioblastoma. J Clin Invest. 2022;132(8):1-21.
344. MacKenzie KJ, Carroll P, Martin C-A, Murina O, Fluteau A, Simpson DJ, et al. CGAS surveillance of micronuclei links genome instability to innate immunity. Nature. 2017;548(7668):461-5.
345. Giladi M, Schneiderman R, Porat Y, Munster M, Itzhaki A, Mordechovich D, et al. Mitotic disruption and reduced clonogenicity of pancreatic cancer cells in vitro and in vivo by tumor treating fields. Pancreatology. 2014;14(1):54-63.
346. Wan D, Jiang W, Hao J. Research Advances in How the cGAS-STING Pathway Controls the Cellular Inflammatory Response. Front Immunol. 2020;11:615-.
347. Martinon F, Burns K, Tschopp J. The Inflammasome: A Molecular Platform Triggering Activation of Inflammatory Caspases and Processing of proIL-β. Mol Cell. 2002;10(2):417-26.
348. Fu Z, Schroeder M, Shabanowitz J, Kaldis P, Togawa K, Rustgi A, et al. Activation of a Nuclear Cdc2-Related Kinase within a Mitogen-Activated Protein Kinase-Like TDY Motif by Autophosphorylation and Cyclin-Dependent Protein Kinase-Activating Kinase. Molecular and Cellular Biology. 2005;25(14):6047-64.
349. Kim J-Y, Jo Y, Oh H-K, Kim EH. Sorafenib increases tumor treating fields-induced cell death in glioblastoma by inhibiting STAT3. American journal of cancer research. 2020;10(10):3475-86.
350. Wong ET, Lok E, Gautam S, Swanson KD. Dexamethasone exerts profound immunologic interference on treatment efficacy for recurrent glioblastoma. Br J Cancer. 2015;113(11):1642-.
351. Kirson ED, Giladi M, Gurvich Z, Itzhaki A, Mordechovich D, Schneiderman RS, et al. Alternating electric fields (TTFields) inhibit metastatic spread of solid tumors to the lungs. Clinical & experimental metastasis. 2009;26(7):633-40.
352. O'Donnell JS, Smyth MJ, Teng MWL. PD1 functions by inhibiting CD28-mediated co-stimulation. In: O'Donnell JS, editor. 2017. p. e138-e.
353. Jiang X, Wang J, Deng X, Xiong F, Ge J, Xiang B, et al. Role of the tumor microenvironment in PD-L1/PD-1-mediated tumor immune escape. Molecular Cancer. 2019;18(1).
354. Voloshin T, Yitzhaki OT, Kaynan N, Giladi M, Shteingauz A, Munster M, et al. IMMU-59. ALTERNATING ELECTRIC FIELDS (TTFIELDs) INDUCE IMMUNOGENIC CELL DEATH RESULTING IN ENHANCED ANTITUMOR EFFICACY WHEN COMBINED WITH ANTI-PD-1 THERAPY. 2017. p. vi126-vi.
355. Wolf K, Chen J, Coombes JD, Aghi M, Kumar S. Dissecting and rebuilding the glioblastoma microenvironment with engineered materials. Nat Rev Mater. 2019;4(10):651-68.
356. van Zijl F, Krupitza G, Mikulits W. Initial steps of metastasis: Cell invasion and endothelial transmigration. Mutation Research-Reviews in Mutation Research. 2011;728(1-2):23-34.
357. Kim E, Song H, Yoo S, Yoon M. Tumor treating fields inhibit glioblastoma cell migration, invasion and angiogenesis. Oncotarget. 2016;7(40):65125-36.
358. Yang J, Weinberg RA. Epithelial-Mesenchymal Transition: At the Crossroads of Development and Tumor Metastasis. Developmental Cell. 2008;14(6):818-29.
359. Bram De C, Geert B. Regulatory networks defining EMT during cancer initiation and progression. Nature Reviews Cancer. 2013;13(2):97.
360. Lee WS, Seo S-J, Chung HK, Park JW, Kim J-K, Kim EH. Tumor-treating fields as a proton beam-sensitizer for glioblastoma therapy. American journal of cancer research. 2021;11(9):4582-94.
361. Harburger DS, Calderwood DA. Integrin signalling at a glance. J Cell Sci. 2009;122(2):159-63.
362. Parsons JT, Horwitz AR, Schwartz MA. Cell adhesion: integrating cytoskeletal dynamics and cellular tension. Nat Rev Mol Cell Biol. 2010;11(9):633-43.
363. Kim DH, Wirtz D. Focal adhesion size uniquely predicts cell migration. FASEB J. 2013;27(4):1351-61.
364. Nagano M, Hoshino D, Koshikawa N, Akizawa T, Seiki M. Turnover of Focal Adhesions and Cancer Cell Migration. Int J Cell Biol. 2012;2012:310616-10.
365. Geiger B, Balaban NQ, Schwarz US, Riveline D, Goichberg P, Tzur G, et al. Force and focal adhesion assembly: a close relationship studied using elastic micropatterned substrates. Nat Cell Biol. 2001;3(5):466-72.
366. Voloshin T, Schneiderman RS, Volodin A, Shamir RR, Kaynan N, Zeevi E, et al. Tumor Treating Fields (TTFields) Hinder Cancer Cell Motility through Regulation of Microtubule and Actin Dynamics. Cancers. 2020;12(10):3016.

367. Choi CK, Horwitz AR, Zareno J, Vicente-Manzanares M, Whitmore LA, Mogilner A. Actin and α-actinin orchestrate the assembly and maturation of nascent adhesions in a myosin II motor-independent manner. Nat Cell Biol. 2008;10(9):1039-50.
368. Nishida N, Yano H, Nishida T, Kamura T, Kojiro M. Angiogenesis in cancer. Vascular health and risk management. 2006;2(3):213-9.
369. Haas TL, Milkiewicz M, Davis SJ, Zhou AL, Egginton S, Brown MD, et al. Matrix metalloproteinase activity is required for activity-induced angiogenesis in rat skeletal muscle. American journal of physiology Heart and circulatory physiology. 2000;279(4):H1540-H7.
370. Mikala E, Zena W. New functions for the matrix metalloproteinases in cancer progression. 2002. p. 161.
371. Daneman R, Prat A. The blood-brain barrier. Cold Spring Harbor perspectives in biology. 2015;7(1):a020412-a.
372. Jiao H, Wang Z, Liu Y, Wang P, Xue Y. Specific Role of Tight Junction Proteins Claudin-5, Occludin, and ZO-1 of the Blood–Brain Barrier in a Focal Cerebral Ischemic Insult. Journal of Molecular Neuroscience. 2011;44(2):130-9.
373. Kessler AF, Salvador E, Domröse D, Burek M, Schaeffer C, Tempel Brami C, et al. Blood Brain Barrier (BBB) Integrity Is Affected By Tumor Treating Fields (TTFields) in Vitro and In Vivo. International Journal of Radiation Oncology, Biology, Physics. 2019;105(1):S162-S3.
374. Hayder J, Isaac MA, Vinod L. Optical imaging to map blood-brain barrier leakage. Scientific Reports. 2013;3(1).
375. Salvador E, Kessler AF, Domroese D, Hoermann J, Schaeffer C, Giniunaite A, et al. Tumor Treating Fields (TTFields) Reversibly Permeabilize the Blood-Brain Barrier In Vitro and In Vivo. Biomolecules (Basel, Switzerland). 2022;12(10):1348.
376. Chang E, Patel C, Pohling C, Young C, Song J, Flores TA, et al. Tumor treating fields increases membrane permeability in glioblastoma cells. Cell Death Discov. 2018;4(1).
377. Szachowicz-Petelska B, Figaszewski Z, Lewandowski W. Mechanisms of transport across cell membranes of complexes contained in antitumour drugs. 2001. p. 169-82.
378. Kotnik T, Rems L, Tarek M, Miklav i D. Membrane Electroporation and Electropermeabilization: Mechanisms and Models. Annu Rev Biophys. 2019;48(1):63-91.
379. Gabriel B, Teissié J. Direct observation in the millisecond time range of fluorescent molecule asymmetrical interaction with the electropermeabilized cell membrane. Biophys J. 1997;73(5):2630-7.
380. Tekle E, Astumian RD, Chock PB. Electro-permeabilization of cell membranes: Effect of the resting membrane potential. Biochem Biophys Res Commun. 1990;172(1):282-7.
381. Gomez-Roman N, Stevenson K, Gilmour L, Hamilton G, Chalmers AJ. A novel 3D human glioblastoma cell culture system for modeling drug and radiation responses. Neuro-Oncology. 2017;19(2):229-41.
382. Ahmed SU, Carruthers R, Gilmour L, Yildirim S, Watts C, Chalmers AJ. Selective Inhibition of Parallel DNA Damage Response Pathways Optimizes Radiosensitization of Glioblastoma Stem- like Cells. Cancer research. 2015;75(20):4416-28.
383. Fael Al-Mayhani TM, Ball SLR, Zhao J-W, Fawcett J, Ichimura K, Collins PV, et al. An efficient method for derivation and propagation of glioblastoma cell lines that conserves the molecular profile of their original tumours. Journal of Neuroscience Methods. 2009;176(2):192-9.
384. Roth V. Doubling Time Computing Available from: http://www.doubling-time.com/compute.php2006 [
385. Porat Y, Giladi M, Schneiderman RS, Blat R, Shteingauz A, Zeevi E, et al. Determining the Optimal Inhibitory Frequency for Cancerous Cells Using Tumor Treating Fields (TTFields). Journal of Visualized Experiments. 2017;2017(123).
386. Kamaletdinova T, Fanaei-Kahrani Z, Wang Z. The Enigmatic Function of PARP1: From PARylation Activity to PAR Readers. Cells. 2019;8(12).
387. Barkauskaite E, Jankevicius G, Ahel I. Structures and Mechanisms of Enzymes Employed in the Synthesis and Degradation of PARP-Dependent Protein ADP-Ribosylation. Molecular Cell. 2015;58(6):935-46.
388. Liu C, Vyas A, Kassab MA, Singh AK, Yu X. The role of poly ADP-ribosylation in the first wave of DNA damage response. Nucleic acids research. 2017;45(14):8129-41.
389. Pazzaglia S, Pioli C. Multifaceted Role of PARP-1 in DNA Repair and Inflammation: Pathological and Therapeutic Implications in Cancer and Non-Cancer Diseases. Cells. 2019;9(1).
390. de Murcia G, Ménissier de Murcia J, Ricoul M, Tartier L, Niedergang C, Huber A, et al. Functional interaction between PARP-1 and PARP-2 in chromosome stability and embryonic development in mouse. EMBO J. 2003;22(9):2255-63.

391. Dea S, Mark SD, Eva B, Ria W, Pierre L, Neil D, et al. The structure and catalytic mechanism of a poly(ADP-ribose) glycohydrolase. Nature. 2011;477(7366):616.
392. Bonicalzi ME, Haince J, Droit A, Poirier G. Regulation of poly(ADP-ribose) metabolism by poly(ADP-ribose) glycohydrolase: where and when? CMLS-Cell Mol Life Sci. 2005;62(7-8):739-50.
393. Yu SW, Wang HM, Poitras MF, Coombs C, Bowers WJ, Federoff HJ, et al. Mediation of Poly(ADP-Ribose) Polymerase-1-Dependent Cell Death by Apoptosis-Inducing Factor. Science. 2002;297(5579):259-63.
394. Yu S-W, Andrabi SA, Wang H, No SK, Poirier GG, Dawson TM, et al. Apoptosis-Inducing Factor Mediates Poly(ADP-Ribose) (PAR) Polymer-Induced Cell Death. Proc Natl Acad Sci U S A. 2006;103(48):18314-9.
395. Sukhanova MV, Singatulina AS, Pastré D, Lavrik OI. Fused in sarcoma (FUS) in dna repair: Tango with poly(ADP-ribose) polymerase 1 and compartmentalisation of damaged DNA. Int J Mol Sci. 2020;21(19):1-18.
396. Ammar AEA, Gyula T, Raquel A-B, Marek K, Paul OH, Markus H, et al. The zinc-finger domains of PARP1 cooperate to recognize DNA strand breaks. Nature Structural & Molecular Biology. 2012;19(7):685.
397. Langelier M-F, Planck JL, Roy S, Pascal JM. Structural basis for DNA damage-dependent poly(ADP-ribosyl)ation by human PARP-1. Science (New York, NY). 2012;336(6082):728-32.
398. Lan L, Nakajima S, Oohata Y, Takao M, Okano S, Masutani M, et al. In situ Analysis of Repair Processes for Oxidative DNA Damage in Mammalian Cells. Proc Natl Acad Sci U S A. 2004;101(38):13738-43.
399. Wilson DM, Takeshita M, Grollman AP, Demple B. Incision Activity of Human Apurinic Endonuclease (Ape) at Abasic Site Analogs in DNA (∗). J Biol Chem. 1995;270(27):16002-7.
400. El-Khamisy SF, Masutani M, Suzuki H, Caldecott KW. A requirement for PARP-1 for the assembly or stability of XRCC1 nuclear foci at sites of oxidative DNA damage. Nucl Acids Res. 2003;31(19):5526-33.
401. Caldecott KW, McKeown CK, Tucker JD, Ljungquist S, Thompson LH. An interaction between the mammalian DNA repair protein XRCC1 and DNA ligase III. Mol Cell Biol. 1994;14(1):68-76.
402. Marintchev A, Robertson A, Dimitriadis EK, Prasad R, Wilson SH, Mullen GP. Domain specific interaction in the XRCC1-DNA polymerase β complex. Nucleic Acids Res. 2000;28(10):2049-59.
403. Pines A, Vrouwe MG, Marteijn J, Typas D, Luijsterburg MS, Cansoy M, et al. PARP1 promotes nucleotide excision repair through DDB2 stabilization and recruitment of ALC1. J Cell Biol. 2012;199(2):235-49.
404. Eustermann S, Wu W-F, Langelier M-F, Yang J-C, Easton Laura E, Riccio Amanda A, et al. Structural Basis of Detection and Signaling of DNA Single-Strand Breaks by Human PARP-1. Mol Cell. 2015;60(5):742-54.
405. Ström CE, Johansson F, Uhlen M, Szigyarto CAK, Erixon K, Helleday T. Poly (ADP-ribose) polymerase (PARP) is not involved in base excision repair but PARP inhibition traps a single-strand intermediate. 2011.
406. Godon C, Cordelières FP, Biard D, Giocanti N, Mégnin-Chanet F, Hall J, et al. PARP inhibition versus PARP-1 silencing: different outcomes in terms of single-strand break repair and radiation susceptibility. Nucleic Acids Res. 2008;36(13):4454-64.
407. Wang M, Wu W, Wu W, Rosidi B, Zhang L, Wang H, et al. PARP-1 and Ku compete for repair of DNA double strand breaks by distinct NHEJ pathways. Nucleic acids research. 2006;34(21):6170-82.
408. Mansour WY, Rhein T, Dahm-Daphi J. The alternative end-joining pathway for repair of DNA double-strand breaks requires PARP1 but is not dependent upon microhomologies. Nucleic acids research. 2010;38(18):6065-77.
409. Hochegger H, Dejsuphong D, Fukushima T, Morrison C, Sonoda E, Schreiber V, et al. Parp-1 protects homologous recombination from interference by Ku and Ligase IV in vertebrate cells. EMBO J. 2006;25(6):1305-14.
410. Wu S, Li X, Gao F, De Groot JF, Koul D, Yung WKA. PARP-mediated PARylation of MGMT is critical to promote repair of temozolomide-induced O6-methylguanine DNA damage in glioblastoma. Neuro Oncol. 2021;23(6):920-31.
411. Kurgina TA, Anarbaev RO, Sukhanova MV, Lavrik OI. A rapid fluorescent method for the real-time measurement of poly(ADP-ribose) polymerase 1 activity. Anal Biochem. 2018;545:91-7.
412. Wookee M, Christopher B, Paulius G, Zhong-Wei Z, Fu L, Anja K, et al. Poly(ADP-ribose) binding to Chk1 at stalled replication forks is required for S-phase checkpoint activation. Nature Communications. 2013;4(1).
413. Ronson GE, Piberger AL, Higgs MR, Olsen AL, Stewart GS, McHugh PJ, et al. PARP1 and PARP2 stabilise replication forks at base excision repair intermediates through Fbh1-dependent Rad51 regulation. Nat Commun. 2018;9(1):746-12.
414. Berti M, Chaudhuri AR, Thangavel S, Gomathinayagam S, Kenig S, Vujanovic M, et al. Human RECQ1 promotes restart of replication forks reversed by DNA topoisomerase I inhibition. Nat Struct Mol Biol. 2013;20(3):347-54.
415. Caron M-C, Sharma AK, O'Sullivan J, Myler LR, Ferreira MT, Rodrigue A, et al. Poly(ADP-ribose) polymerase-1 antagonizes DNA resection at double-strand breaks. Nat Commun. 2019;10(1):2954-16.

416. Mijic S, Zellweger R, Chappidi N, Berti M, Jacobs K, Mutreja K, et al. Replication fork reversal triggers fork degradation in BRCA2-defective cells. Nat Commun. 2017;8(1):859-11.
417. Nguyen B, Sokoloski J, Galletto R, Elson EL, Wold MS, Lohman TM. Diffusion of Human Replication Protein A along Single-Stranded DNA. J Mol Biol. 2014;426(19):3246-61.
418. Ma CJ, Gibb B, Kwon Y, Sung P, Greene EC. Protein dynamics of human RPA and RAD51 on ssDNA during assembly and disassembly of the RAD51 filament. Nucleic Acids Res. 2017;45(2):749-61.
419. Gibb B, Ye LF, Gergoudis SC, Kwon Y, Niu H, Sung P, et al. Concentration-dependent exchange of replication protein A on single-stranded DNA revealed by single-molecule imaging. PLoS One. 2014;9(2):e87922-e.
420. Carreira A, Kowalczykowski SC, Jensen RB. Purified human BRCA2 stimulates RAD51-mediated recombination. Nature. 2010;467(7316):678-83.
421. Zellweger R, Dalcher D, Mutreja K, Berti M, Schmid JA, Herrador R, et al. Rad51-mediated replication fork reversal is a global response to genotoxic treatments in human cells. J Cell Biol. 2015;208(5):563-79.
422. Petermann E, Orta ML, Issaeva N, Schultz N, Helleday T. Hydroxyurea-Stalled Replication Forks Become Progressively Inactivated and Require Two Different RAD51-Mediated Pathways for Restart and Repair. Mol Cell. 2010;37(4):492-502.
423. Krishna S, Wagener BM, Liu HP, Lo Y-C, Sterk R, Petrini JHJ, et al. Mre11 and Ku regulation of double-strand break repair by gene conversion and break-induced replication. DNA Repair (Amst). 2007;6(6):797-808.
424. Strumberg D, Pilon AA, Smith M, Hickey R, Malkas L, Pommier Y. Conversion of Topoisomerase I Cleavage Complexes on the Leading Strand of Ribosomal DNA into 5'-Phosphorylated DNA Double-Strand Breaks by Replication Runoff. Mol Cell Biol. 2000;20(11):3977-87.
425. Strzalka W, Ziemienowicz A. Proliferating cell nuclear antigen (PCNA): a key factor in DNA replication and cell cycle regulation. Ann Bot. 2011;107(7):1127-40.
426. Sugimura K, Takebayashi S-I, Taguchi H, Takeda S, Okumura K. PARP-1 ensures regulation of replication fork progression by homologous recombination on damaged DNA. The Journal of cell biology. 2008;183(7):1203-12.
427. Smerdon MJ, Lieberman MW. Nucleosome rearrangement in human chromatin during UV-induced DNA- reapir synthesis. Proc Natl Acad Sci U S A. 1978;75(9):4238-41.
428. Ura K, Araki M, Saeki H, Masutani C, Ito T, Iwai S, et al. ATP-dependent chromatin remodeling facilitates nucleotide excision repair of UV-induced DNA lesions in synthetic dinucleosomes. EMBO J. 2001;20(8):2004-14.
429. Groth A, Corpet A, Cook AJL, Roche D, Bartek J, Lukas J, et al. Regulation of Replication Fork Progression Through Histone Supply and Demand. Science. 2007;318(5858):1928-31.
430. Norton VG, Marvin KW, Yau P, Bradbury EM. Nucleosome linking number change controlled by acetylation of histones H3 and H4. J Biol Chem. 1990;265(32):19848-52.
431. Oliva R, Bazett-Jones DP, Locklear L, Dixon GH. Histone hyperacetylation can induce unfolding of the nucleosome core particle. Nucleic Acids Res. 1990;18(9):2739-47.
432. LeRoy G, Loyola A, Lane WS, Reinberg D. Purification and Characterization of a Human Factor That Assembles and Remodels Chromatin. J Biol Chem. 2000;275(20):14787-90.
433. Mizuguchi G, Wu C, Shen X, Hamiche A. A chromatin remodelling complex involved in transcription and DNA processing. Nature. 2000;406(6795):541-4.
434. Poirier GG, Murcia Gd, Jongstra-Bilen J, Niedergang C, Mandel P. Poly(ADP-ribosyl)ation of polynucleosomes causes relaxation of chromatin structure. Proceedings of the National Academy of Sciences of the United States of America. 1982;79(11):3423.
435. Huletsky A, De Murcia G, Muller S, Hengartner M, Menard L, Lamarre D, et al. The effect of poly(ADP-ribosyl)ation on native and H1-depleted chromatin. A role of poly(ADP-ribosyl)ation on core nucleosome structure. J Biol Chem. 1989;264(15):8878-86.
436. Krishnakumar R, Kraus WL. PARP-1 Regulates Chromatin Structure and Transcription through a KDM5B-Dependent Pathway. Mol Cell. 2010;39(5):736-49.
437. Pekowska A, Benoukraf T, Zacarias-Cabeza J, Belhocine M, Koch F, Holota H, et al. H3K4 tri-methylation provides an epigenetic signature of active enhancers. EMBO J. 2011;30(20):4198-210.
438. Jamieson K, Rountree MR, Lewis ZA, Stajich JE, Selker EU. Regional control of histone H3 lysine 27 methylation in Neurospora. Proc Natl Acad Sci U S A. 2013;110(15):6027-32.
439. Paro R, Beisel C. Silencing chromatin: comparing modes and mechanisms. Nat Rev Genet. 2011;12(2):123-35.

440. Caruso LB, Martin KA, Lauretti E, Hulse M, Siciliano M, Lupey-Green LN, et al. Poly(ADP-ribose) Polymerase 1, PARP1, modifies EZH2 and inhibits EZH2 histone methyltransferase activity after DNA damage. Oncotarget. 2018;9(12):10585-605.
441. Blessing C, Mandemaker IK, Gonzalez-Leal C, Preisser J, Schomburg A, Ladurner AG. The Oncogenic Helicase ALC1 Regulates PARP Inhibitor Potency by Trapping PARP2 at DNA Breaks. Mol Cell. 2020;80(5):862-75.e6.
442. Hewitt G, Borel V, Segura-Bayona S, Takaki T, Ruis P, Bellelli R, et al. Defective ALC1 nucleosome remodeling confers PARPi sensitization and synthetic lethality with HRD. Mol Cell. 2021;81(4):767-83.e11.
443. Adamowicz M, Hailstone R, Demin AA, Komulainen E, Hanzlikova H, Brazina J, et al. XRCC1 protects transcription from toxic PARP1 activity during DNA base excision repair. Nat Cell Biol. 2021;23(12):1287-98.
444. Min A, Im S-A. PARP inhibitors as therapeutics: Beyond modulation of parylation. Cancers (Basel). 2020;12(2):394.
445. Gradwohl G, De Murcia JM, Molinete M, Simonin F, Koken M, Hoeijmakers JHJ, et al. The Second Zinc-Finger Domain of Poly(ADP-Ribose) Polymerase Determines Specificity for Single-Stranded Breaks in DNA. Proc Natl Acad Sci U S A. 1990;87(8):2990-4.
446. Kumar C, P. T. V L, Arunachalam A. A mechanistic approach to understand the allosteric reverse signaling by selective and trapping poly(ADP-ribose) polymerase 1 (PARP-1) inhibitors. J Biomol Struct Dyn. 2020;38(8):2482-92.
447. Murai JJ, Huang S-yNS-yN, Das BBBB, Renaud AA, Zhang YY, Doroshow JHJH, et al. Differential trapping of PARP1 and PARP2 by clinical PARP inhibitors. Cancer research (Chicago, Ill). 2012;72(21):5588-99.
448. Murai J, Huang S-YN, Renaud A, Zhang Y, Ji J, Takeda S, et al. Stereospecific PARP trapping by BMN 673 and comparison with olaparib and rucaparib. Mol Cancer Ther. 2014;13(2):433-43.
449. Vaitsiankova A, Burdova K, Sobol M, Gautam A, Benada O, Hanzlikova H, et al. PARP inhibition impedes the maturation of nascent DNA strands during DNA replication. Nat Struct Mol Biol. 2022;29(4):329-38.
450. McCabe N, Turner N, Lord C, Kluzek K, Bialkowska A, Swift S, et al. Deficiency in the Repair of DNA Damage by Homologous Recombination and Sensitivity to Poly(ADP-Ribose) Polymerase Inhibition. Cancer Research. 2006;66(16):8109-15.
451. Smith GCM, Ashworth A, Farmer H, McCabe N, Lord CJ, Tutt ANJ, et al. Targeting the DNA repair defect in BRCA mutant cells as a therapeutic strategy. Nature. 2005;434(7035):917-21.
452. Lu Y, Kwintkiewicz J, Liu Y, Tech K, Frady LN, Su Y-T, et al. Chemosensitivity of IDH1-mutated gliomas due to an impairment in PARP1-mediated DNA repair. Cancer Res. 2017;77(7):1709-18.
453. Sulkowski PL, Corso CD, Robinson ND, Scanlon SE, Purshouse KR, Bai H, et al. 2- Hydroxyglutarate produced by neomorphic IDH mutations suppresses homologous recombination and induces PARP inhibitor sensitivity. Science translational medicine. 2017;9(375).
454. Mendes-Pereira AM, Martin SA, Brough R, McCarthy A, Taylor JR, Kim JS, et al. Synthetic lethal targeting of PTEN mutant cells with PARP inhibitors. EMBO Molecular Medicine. 2009;1(6-7):315-22.
455. Ducray F, Sanson M, Chinot O, Fontanilles M, Rivoirard R, Thomas-Maisonneuve L, et al. KS02.4.A Olaparib in Recurrent IDH-mutant High-Grade Glioma (OLAGLI). Neuro-oncology (Charlottesville, Va). 2021;23(Supplement_2):ii4-ii.
456. Hopkins TA, Ainsworth WB, Ellis PA, Donawho CK, DiGiammarino EL, Panchal SC, et al. PARP1 Trapping by PARP Inhibitors Drives Cytotoxicity in Both Cancer Cells and Healthy Bone Marrow. Mol Cancer Res. 2019;17(2):409-19.
457. Lesueur P, Chevalier F, El-Habr EA, Junier M-P, Chneiweiss H, Castera L, et al. Radiosensitization Effect of Talazoparib, a Parp Inhibitor, on Glioblastoma Stem Cells Exposed to Low and High Linear Energy Transfer Radiation. Sci Rep. 2018;8(1):3664-12.
458. Weigelt B, Comino-Méndez I, De Bruijn I, Tian L, Meisel JL, García-Murillas I, et al. Diverse BRCA1 and BRCA2 reversion mutations in circulating cell-free DNA of therapy-resistant breast or ovarian cancer. Clin Cancer Res. 2017;23(21):6708-20.
459. Sakai W, Swisher EM, Karlan BY, Agarwal MK, Higgins J, Friedman C, et al. Secondary mutations as a mechanism of cisplatin resistance in BRCA2-mutated cancers. Nature. 2008;451(7182):1116-20.
460. Nacson J, Krais JJ, Bernhardy AJ, Clausen E, Feng W, Wang Y, et al. BRCA1 Mutation-Specific Responses to 53BP1 Loss-Induced Homologous Recombination and PARP Inhibitor Resistance (vol 24, 3513, 2018). Cell Rep. 2018;25(5):1384-.
461. Hong R, Ma F, Zhang W, Yu X, Li Q, Luo Y, et al. 53BP1 depletion causes PARP inhibitor resistance in ATM-deficient breast cancer cells. BMC Cancer. 2016;16(1):725-.

462. Belotserkovskaya R, Raga Gil E, Lawrence N, Butler R, Clifford G, Wilson MD, et al. PALB2 chromatin recruitment restores homologous recombination in BRCA1-deficient cells depleted of 53BP1. Nat Commun. 2020;11(1):819-.
463. Pettitt SJ, Krastev DB, Brandsma I, Dréan A, Song F, Aleksandrov R, et al. Genome-wide and high-density CRISPR-Cas9 screens identify point mutations in PARP1 causing PARP inhibitor resistance. Nat Commun. 2018;9(1):1849-14.
464. Gogola E, Duarte AA, de Ruiter JR, Wiegant WW, Schmid JA, de Bruijn R, et al. Selective Loss of PARG Restores PARylation and Counteracts PARP Inhibitor-Mediated Synthetic Lethality. Cancer Cell. 2019;35(6):950-2.
465. Hanna C, Kurian KM, Williams K, Watts C, Jackson A, Carruthers R, et al. Pharmacokinetics, safety and tolerability of olaparib and temozolomide for recurrent glioblastoma: results of the phase I OPARATIC trial. Neuro-oncology. 2020.
466. Schulz E, Kessler AF, Salvador E, Domröse D, Burek M, Tempel Brami C, et al. EXTH-02. THE BLOOD BRAIN BARRIER (BBB) PERMEABILITY IS ALTERED BY TUMOR TREATING FIELDS (TTFIELDS) IN VIVO. Neuro-oncology (Charlottesville, Va). 2019;21(Supplement_6):vi82-vi.
467. Mulvey B, Martinez-Conde A, Efimov V, Dor-On E, Haber A, Giladi M, et al. Efficacy of combining tumor treating fields (TTFields) with a PARP inhibitor in ovarian cell lines (300.5). Gynecologic oncology. 2022;166:S158.
468. Rundle S, Bradbury A, Drew Y, Curtin N. Targeting the ATR-CHK1 Axis in Cancer Therapy. Cancers. 2017;9(5).
469. Chalmers A, Short S, Watts C, Herbert C, Morris A, Stobo J. Phase I clinical trials evaluating olaparib in combination with radiotherapy (RT) and/or temozolomide (TMZ) in glioblastoma patients: Results of OPARATIC and PARADIGM phase I and early results of PARADIGM- 2. J Clin Oncol. 2018;36(15).
470. Rieger AM, Nelson KL, Konowalchuk JD, Barreda DR. Modified annexin V/propidium iodide apoptosis assay for accurate assessment of cell death. J Vis Exp. 2011(50).
471. Bendall LJ, Green DR. Autopsy of a cell. Leukemia. 2014;28(6):1341-3.
472. Rogakou EP, Pilch DR, Orr AH, Ivanova VS, Bonner WM. DNA Double-stranded Breaks Induce Histone H2AX Phosphorylation on Serine 139. J Biol Chem. 1998;273(10):5858-68.
473. Ward IM, Chen J. Histone H2AX Is Phosphorylated in an ATR-dependent Manner in Response to Replicational Stress. J Biol Chem. 2001;276(51):47759-62.
474. Stiff T, O'Driscoll M, Rief N, Iwabuchi K, Loebrich M, Jeggo P. ATM and DNA-PK Function Redundantly to Phosphorylate H2AX after Exposure to Ionizing Radiation. Cancer Research. 2004;64(7):2390-6.
475. Burma S, Chen BP, Murphy M, Kurimasa A, Chen DJ. ATM Phosphorylates Histone H2AX in Response to DNA Double-strand Breaks. J Biol Chem. 2001;276(45):42462-7.
476. Halazonetis TD, Huyen Y, Zgheib O, DiTullio Jr RA, Gorgoulis VG, Zacharatos P, et al. Methylated lysine 79 of histone H3 targets 53BP1 to DNA double-strand breaks. Nature. 2004;432(7015):406-11.
477. Pesavento JJ, Yang H, Kelleher NL, Mizzen CA. Certain and Progressive Methylation of Histone H4 at Lysine 20 during the Cell Cycle. Mol Cell Biol. 2008;28(1):468-86.
478. Kleiner RE, Verma P, Molloy KR, Chait BT, Kapoor TM. Chemical proteomics reveals a γH2AX-53BP1 interaction in the DNA damage response. Nat Chem Biol. 2015;11(10):807-14.
479. Ward IM, Minn K, van Deursen J, Chen J. p53 Binding Protein 53BP1 Is Required for DNA Damage Responses and Tumor Suppression in Mice. Mol Cell Biol. 2003;23(7):2556-63.
480. Bartek J, Halazonetis TD, DiTullio RA, Mochan TA, Venere M, Bartkova J, et al. 53BP1 functions in an ATM-dependent checkpoint pathway that is constitutively activated in human cancer. Nat Cell Biol. 2002;4(12):998-1002.
481. Fernandez-Capetillo O, Chen H-T, Celeste A, Ward I, Romanienko PJ, Morales JC, et al. DNA damage-induced G2-M checkpoint activation by histone H2AX and 53BP1. Nat Cell Biol. 2002;4(12):993-7.
482. Fairbairn DW, Olive PL, O'Neill KL. The comet assay: a comprehensive review. Mutation research Reviews in genetic toxicology. 1995;339(1):37-59.
483. Olson E, Nievera CJ, Klimovich V, Fanning E, Wu X. RPA2 Is a Direct Downstream Target for ATR to Regulate the S-phase Checkpoint. J Biol Chem. 2006;281(51):39517-33.
484. Portnow J, Badie B, Chen M, Liu A, Blanchard S, Synold TW. The Neuropharmacokinetics of Temozolomide in Patients with Resectable Brain Tumors: Potential Implications for the Current Approach to Chemoradiation. Clin Cancer Res. 2009;15(22):7092-8.
485. Ostermann S, Csajkag C, Buclin T, Leyvraz S, Lejeune F, Decosterd LA, et al. Plasma and Cerebrospinal Fluid Population Pharmacokinetics of Temozolomide in Malignant Glioma Patients. Clin Cancer Res. 2004;10(11):3728-36.

486. Carruthers R, Ahmed SU, Strathdee K, Gomez - Roman N, Amoah - Buahin E, Watts C, et al. Abrogation of radioresistance in glioblastoma stem- like cells by inhibition of ATM kinase. Molecular Oncology. 2015;9(1):192-203.
487. Kessler A, Frombling G, Gross F, Hahn M, Dzokou W, Ernestus R, et al. Tumor-treating fields (TTFields) effects on glioblastoma cells are augmented by mitotic checkpoint inhibition. Cancer Res. 2018;78(13).
488. Jo Y, Han YI, Lee E, Seo J, Oh G, Sung H, et al. The combination of tumor treating fields and hyperthermia has synergistic therapeutic effects in glioblastoma cells by downregulating STAT3. Am J Cancer Res. 2022;12(3):1423-32.
489. Voloshin T, Kaynan N, Davidi S, Porat Y, Shteingauz A, Schneiderman RS, et al. Tumor-treating fields (TTFields) induce immunogenic cell death resulting in enhanced antitumor efficacy when combined with anti-PD-1 therapy. Cancer Immunol Immunother. 2020;69(7):1191-204.
490. Baus F, Gire V, Fisher D, Piette J, Dulić V. Permanent cell cycle exit in G2 phase after DNA damage in normal human fibroblasts. EMBO J. 2003;22(15):3992-4002.
491. Jackson MW, Agarwal MK, Yang J, Bruss P, Uchiumi T, Agarwal ML, et al. p130/p107/p105Rb-dependent transcriptional repression during DNA-damage-induced cell-cycle exit at G2. J Cell Sci. 2005;118(9):1821-32.
492. Noda A. Radiation-induced unrepairable DSBs: their role in the late effects of radiation and possible applications to biodosimetry. J Radiat Res. 2018;59(suppl_2):ii114-ii20.
493. Friskes A, Koob L, Krenning L, Severson TM, Koeleman ES, Vergara X, et al. Double-strand break toxicity is chromatin context independent. Nucleic acids research. 2022;50(17):9930-47.
494. Bhogal N, Jalali F, Bristow RG. Microscopic imaging of DNA repair foci in irradiated normal tissues. Int J Radiat Biol. 2009;85(9):732-46.
495. Liu SK, Olive PL, Bristow RG. Biomarkers for DNA DSB inhibitors and radiotherapy clinical trials. Cancer Metastasis Rev. 2008;27(3):445-58.
496. Kinner A, Wu W, Staudt C, Iliakis G. γ-H2AX in recognition and signaling of DNA double-strand breaks in the context of chromatin. Nucleic Acids Res. 2008;36(17):5678-94.
497. Buis J, Wu Y, Deng Y, Leddon J, Westfield G, Eckersdorff M, et al. Mre11 Nuclease Activity Has Essential Roles in DNA Repair and Genomic Stability Distinct from ATM Activation. Cell. 2008;135(1):85-96.
498. Menolfi D, Zha S. ATM, ATR and DNA-PKcs kinases-the lessons from the mouse models: Inhibition = deletion. Cell Biosci. 2020;10(1):8-.
499. Brown EJ, Baltimore D. ATR disruption leads to chromosomal fragmentation and early embryonic lethality. Genes Dev. 2000;14(4):397-402.
500. Shastri N, Tsai Y-C, Hile S, Jordan D, Powell B, Chen J, et al. Genome-wide Identification of Structure-Forming Repeats as Principal Sites of Fork Collapse upon ATR Inhibition. Mol Cell. 2018;72(2):222-38.e11.
501. Kabeche L, Nguyen HD, Buisson R, Zou L. A mitosis-specific and R loop-driven ATR pathway promotes faithful chromosome segregation. Science. 2018;359(6371):108-14.
502. Pennarun G, Hoffschir F, Revaud D, Granotier C, Gauthier LR, Mailliet P, et al. ATR contributes to telomere maintenance in human cells. Nucleic Acids Res. 2010;38(9):2955-63.
503. Karlene AC, David C. ATR: an essential regulator of genome integrity. Nature Reviews Molecular Cell Biology. 2008;9(8):616.
504. Macdougall CA, Byun TS, Van C, Yee M-C, Cimprich KA. The structural determinants of checkpoint activation. Genes & development. 2007;21(8):898-903.
505. Sundar R, Brown J, Ingles Russo A, Yap TA. Targeting ATR in cancer medicine. Current Problems in Cancer. 2017;41(4):302-15.
506. Ohashi E, Takeishi Y, Ueda S, Tsurimoto T. Interaction between Rad9–Hus1–Rad1 and TopBP1 activates ATR–ATRIP and promotes TopBP1 recruitment to sites of UV-damage. DNA Repair. 2014;21:1-11.
507. Bermudez VP, Lindsey-Boltz LA, Cesare AJ, Maniwa Y, Griffith JD, Hurwitz J, et al. Loading of the Human 9-1-1 Checkpoint Complex onto DNA by the Checkpoint Clamp Loader hRad17-Replication Factor C Complex in vitro. Proc Natl Acad Sci U S A. 2003;100(4):1633-8.
508. Rappas M, Oliver AW, Pearl LH. Structure and function of the Rad9-binding region of the DNA-damage checkpoint adaptor TopBP1. Nucleic acids research. 2013;41(8):4741-.
509. Menolfi D, Jiang W, Lee BJ, Moiseeva T, Shao Z, Estes V, et al. Kinase-dead ATR differs from ATR loss by limiting the dynamic exchange of ATR and RPA. Nat Commun. 2018;9(1):5351-16.
510. Walworth NC, Bernards R. rad-Dependent Response of the chk1-Encoded Protein Kinase at the DNA Damage Checkpoint. Science. 1996;271(5247):353-6.
511. Liu S, Bekker-Jensen S, Mailand N, Lukas C, Bartek J, Lukas J. Claspin operates downstream of TopBP1 to direct ATR signaling towards Chk1 activation. Molecular and cellular biology. 2006;26(16):6056-64.

512. Kumagai A, Dunphy WG. Claspin, a Novel Protein Required for the Activation of Chk1 during a DNA Replication Checkpoint Response in Xenopus Egg Extracts. Molecular Cell. 2000;6(4):839-49.
513. Xiao Z, Chen Z, Gunasekera A, Sowin T, Rosenberg S, Fesik S, et al. Chk1 Mediates S and G sub(2) Arrests through Cdc25A Degradation in Response to DNA-damaging Agents. Journal of Biological Chemistry. 2003;278(24):21767-73.
514. Saini P, Li Y, Dobbelstein M. Wee1 is required to sustain ATR/Chk1 signaling upon replicative stress. Oncotarget. 2015;6(15):13072-87.
515. Moiseeva TN, Yin Y, Calderon MJ, Qian C, Schamus-Haynes S, Sugitani N, et al. An ATR and CHK1 kinase signaling mechanism that limits origin firing during unperturbed DNA replication. Proceedings of the National Academy of Sciences of the United States of America. 2019;116(27):13374-83.
516. Chen Y-H, Jones MJK, Yin Y, Crist SB, Colnaghi L, Sims RJ, et al. ATR-Mediated Phosphorylation of FANCI Regulates Dormant Origin Firing in Response to Replication Stress. Mol Cell. 2015;58(2):323-38.
517. Shigechi T, Tomida J, Sato K, Kobayashi M, Eykelenboom JK, Pessina F, et al. ATR-ATRIP kinase complex triggers activation of the Fanconi anemia DNA repair pathway. Cancer research. 2012;72(5):1149-56.
518. Shell SM, Li Z, Shkriabai N, Kvaratskhelia M, Brossey C, Serrano MA, et al. Checkpoint kinase ATR promotes nucleotide excision repair of UV-induced DNA damage via physical interaction withxeroderma pigmentosum group A. Journal of Biological Chemistry. 2009;284(36):24213-22.
519. Claus Storgaard S, Lasse Tengbjerg H, Jaroslaw D, Randi GS, Cecilia L, Jiri B, et al. The cell-cycle checkpoint kinase Chk1 is required for mammalian homologous recombination repair. Nature Cell Biology. 2005;7(2):195.
520. Hirose Y, Berger R, Pieper Y. Abrogation of the Chk1- mediated G sub(2) Checkpoint Pathway Potentiates Temozolomide- induced Toxicity in a p53- independent Manner in Human Glioblastoma Cells. Cancer Research. 2001;61(15):5843-9.
521. Wang Y, Qin J. MSH2 and ATR Form a Signaling Module and Regulate Two Branches of the Damage Response to DNA Methylation. Proc Natl Acad Sci U S A. 2003;100(26):15387-92.
522. Ganesa S, Sule A, Sundaram RK, Bindra RS. Mismatch repair proteins play a role in ATR activation upon temozolomide treatment in MGMT-methylated glioblastoma. Sci Rep. 2022;12(1):5827-.
523. Jackson CB, Noorbakhsh SI, Sundaram RK, Kalathil AN, Ganesa S, Jia L, et al. Temozolomide Sensitizes MGMT-Deficient Tumor Cells to ATR Inhibitors. Cancer Res. 2019;79(17):4331-8.
524. Sidi S, Sanda T, Kennedy RD, Hagen AT, Jette CA, Hoffmans R, et al. Chk1 Suppresses a Caspase-2 Apoptotic Response to DNA Damage that Bypasses p53, Bcl-2, and Caspase-3. Cell. 2008;133(5):864-77.
525. Rafiei S, Fitzpatrick K, Liu D, Cai M-Y, Elmarakeby HA, Park J, et al. ATM loss confers greater sensitivity to ATR inhibition than PARP inhibition in prostate cancer. Cancer Res. 2020;80(11):2094-100.
526. Reaper PM, Griffiths MR, Long JM, Charrier J-D, MacCormick S, Charlton PA, et al. Selective killing of ATM- or p53-deficient cancer cells through inhibition of ATR. Nat Chem Biol. 2011;7(7):428-30.
527. Min A, Im S-A, Jang H, Kim S, Lee M, Kim DK, et al. AZD6738, A novel oral inhibitor of ATR, induces synthetic lethality with ATM deficiency in gastric cancer cells. Mol Cancer Ther. 2017;16(4):566-77.
528. Mohni KN, Kavanaugh GM, Cortez D. ATR pathway inhibition is synthetically lethal in cancer cells with ercc1 deficiency. Cancer Res. 2014;74(10):2835-45.
529. Sultana R, Abdel-Fatah T, Perry C, Moseley P, Albarakti N, Mohan V, et al. Ataxia Telangiectasia Mutated and Rad3 Related (ATR) Protein Kinase Inhibition Is Synthetically Lethal in XRCC1 Deficient Ovarian Cancer Cells. PLoS One. 2013;8(2):e57098-e.
530. Nazareth D, Jones M, Gabrielli B. Everything in Moderation: Lessons Learned by Exploiting Moderate Replication Stress in Cancer. Cancers. 2019;11(9).
531. Ubhi T, Brown G. Exploiting DNA Replication Stress for Cancer Treatment. Cancer Res. 2019;79(8):1730-9.
532. Fròsina G, Profumo A, Marubbi D, Marcello D, Ravetti JL, Daga A. ATR kinase inhibitors NVP-BEZ235 and AZD6738 effectively penetrate the brain after systemic administration. Radiation oncology (London, England). 2018;13(1):76-.
533. Kim ST, Smith SA, Mortimer P, Loembé A-B, Cho H, Hkim K-M, et al. Phase i study of ceralasertib (AZD6738), a novel DNA damage repair agent, in combination with weekly paclitaxel in refractory cancer. Clin Cancer Res. 2021;27(17):4700-9.
534. Dillon M, Guevara J, Mohammed K, Smith SA, Dean E, McLellan L, et al. A phase I study of ATR inhibitor, AZD6738, as monotherapy in advanced solid tumours (PATRIOT part A, B). Annals of oncology. 2019;30:v165-v6.

535. Jackson SP, Jazayeri A, Falck J, Lukas C, Bartek J, Smith GCM, et al. ATM- and cell cycle-dependent regulation of ATR in response to DNA double-strand breaks. Nat Cell Biol. 2006;8(1):37-45.
536. Gatei M, Sloper K, Sörensen C, Syljuäsen R, Falck J, Hobson K, et al. Ataxia-telangiectasia-mutated (ATM) and NBS1-dependent Phosphorylation of Chk1 on Ser-317 in Response to Ionizing Radiation. J Biol Chem. 2003;278(17):14806-11.
537. Krebs MG, Lopez J, El-Khoueiry A, Bang Y-J, Postel-Vinay S, Abida W, et al. Abstract CT026: Phase I study of AZD6738, an inhibitor of ataxia telangiectasia Rad3-related (ATR), in combination with olaparib or durvalumab in patients (pts) with advanced solid cancers. Cancer research (Chicago, Ill). 2018;78(13_Supplement):CT026-CT.
538. Vendetti FP, Lau A, Schamus S, Conrads TP, O'Connor MJ, Bakkenist CJ. The orally active and bioavailable ATR kinase inhibitor AZD6738 potentiates the anti-tumor effects of cisplatin to resolve ATM-deficient non-small cell lung cancer in vivo. Oncotarget. 2015;6(42):44289-305.
539. Yap TA, Krebs MG, Postel-Vinay S, El-Khouiery A, Soria J-C, Lopez J, et al. Ceralasertib (AZD6738), an oral ATR kinase inhibitor, in combination with carboplatin in patients with advanced solid tumors: A phase I study. Clin Cancer Res. 2021;27(19):5213-24.
540. Anantha RW, Vassin VM, Borowiec JA. Sequential and Synergistic Modification of Human RPA Stimulates Chromosomal DNA Repair. J Biol Chem. 2007;282(49):35910-23.
541. Kirson ED, Dbalý V, Tovaryš F, Vymazal J, Soustiel JF, Itzhaki A, et al. Alternating electric fields arrest cell proliferation in animal tumor models and human brain tumors. Proc Natl Acad Sci U S A. 2007;104(24):10152-7.
542. Kessler AF, Frömbling GE, Gross F, Hahn M, Dzokou W, Ernestus R-I, et al. Effects of tumor treating fields (TTFields) on glioblastoma cells are augmented by mitotic checkpoint inhibition. Cell death discovery. 2018;4(1):12-.
543. Mannarino L, Mirimao F, Panini N, Paracchini L, Marchini S, Beltrame L, et al. Tumor treating fields affect mesothelioma cell proliferation by exerting histotype-dependent cell cycle checkpoint activations and transcriptional modulations. Cell death & disease. 2022;13(7):612-.
544. Eich M, Roos WP, Nikolova T, Kaina B. Contribution of ATM and ATR to the resistance of glioblastoma and malignant melanoma cells to the methylating anticancer drug temozolomide. Mol Cancer Ther. 2013;12(11):2529-40.
545. Kaur E, Ketkar M, Dutt S. Glioblastoma recurrent cells switch between ATM and ATR pathway as an alternative strategy to survive radiation stress. Med Oncol. 2022;39(5):50-.
546. Aasland D, Götzinger L, Hauck L, Berte N, Meyer J, Effenberger M, et al. Temozolomide Induces Senescence and Repression of DNA Repair Pathways in Glioblastoma Cells via Activation of ATR-CHK1, p21, and NF-κB. Cancer Res. 2019;79(1):99-113.
547. Kwok M, Davies N, Agathanggelou A, Smith E, Oldreive C, Petermann E, et al. ATR inhibition induces synthetic lethality and overcomes chemoresistance in TP53- or ATM-defective chronic lymphocytic leukemia cells. Blood. 2016;127(5):582-95.
548. Dueva R, Iliakis G. Replication protein A: a multifunctional protein with roles in DNA replication, repair and beyond. NAR cancer. 2020;2(3):zcaa022-zcaa.
549. Sedelnikova OA, Pilch DR, Redon C, Bonner WM. Histone H2AX in DNA damage and repair. Cancer Biol Ther. 2003;2(3):233-5.
550. Fumagalli M, Rossiello F, Clerici M, Barozzi S, Cittaro D, Kaplunov JM, et al. Telomeric DNA damage is irreparable and causes persistent DNA-damage-response activation. Nat Cell Biol. 2012;14(4):355-65.
551. Noda A, Hirai Y, Hamasaki K, Mitani H, Nakamura N, Kodama Y. Unrepairable DNA double-strand breaks that are generated by ionising radiation determine the fate of normal human cells. J Cell Sci. 2012;125(22):5280-7.
552. Hu L, Li H, Zi M, Li W, Liu J, Yang Y, et al. Why Senescent Cells Are Resistant to Apoptosis: An Insight for Senolytic Development. Front Cell Dev Biol. 2022;10:822816-.
553. Deursen JMAv. The role of senescent cells in ageing. Nature. 2014;509(7501):439-46.
554. Hayflick L. The limited in vitro lifetime of human diploid cell strains. Exp Cell Res. 1965;37(3):614-36.
555. Campisi J, Beauséjour CM, Krtolica A, Galimi F, Narita M, Lowe SW, et al. Reversal of human cellular senescence: roles of the p53 and p16 pathways. EMBO J. 2003;22(16):4212-22.
556. Michishita E, Nakabayashi K, Ogino H, Suzuki T, Fujii M, Ayusawa D. DNA Topoisomerase Inhibitors Induce Reversible Senescence in Normal Human Fibroblasts. Biochem Biophys Res Commun. 1998;253(3):667-71.
557. Chitikova ZV, Gordeev SA, Bykova TV, Zubova SG, Pospelov VA, Pospelova TV. Sustained activation of DNA damage response in irradiated apoptosis-resistant cells induces reversible senescence associated with mTOR downregulation and expression of stem cell markers. Cell Cycle. 2014;13(9):1424-39.

558. Di Micco R, Krizhanovsky V, Baker D, d'Adda di Fagagna F. Cellular senescence in ageing: from mechanisms to therapeutic opportunities. Nat Rev Mol Cell Biol. 2021;22(2):75-95.
559. Rodier F, Muñoz DP, Teachenor R, Chu V, Le O, Bhaumik D, et al. DNA-SCARS: distinct nuclear structures that sustain damage-induced senescence growth arrest and inflammatory cytokine secretion. J Cell Sci. 2011;124(1):68-81.
560. Zeng S, Shen W, Liu L. Senescence and Cancer. Cancer translational medicine. 2018;4(3):70-4.
561. Campisi J, Davalos AR, Hoeijmakers WAM, Muñoz DP, Campeau E, Raza SR, et al. Persistent DNA damage signalling triggers senescence-associated inflammatory cytokine secretion. Nat Cell Biol. 2009;11(8):973-9.
562. Wang B, Kohli J, Demaria M. Senescent Cells in Cancer Therapy: Friends or Foes? Trends Cancer. 2020;6(10):838-57.
563. Hirose Y, Berger MS, Pieper RO. p53 effects both the duration of G2/M arrest and the fate of temozolomide-treated human glioblastoma cells. Cancer Res. 2001;61(5):1957-63.
564. Knizhnik AV, Roos WP, Nikolova T, Quiros S, Tomaszowski K-H, Christmann M, et al. Survival and Death Strategies in Glioma Cells: Autophagy, Senescence and Apoptosis Triggered by a Single Type of Temozolomide-Induced DNA Damage. PLoS One. 2013;8(1):e55665.
565. Sazonova EV, Petrichuk SV, Kopeina GS, Zhivotovsky B. A link between mitotic defects and mitotic catastrophe: detection and cell fate. Biol Direct. 2021;16(1):25-.
566. Mannino M, Gomez-Roman N, Hochegger H, Chalmers AJ. Differential sensitivity of Glioma stem cells to Aurora kinase A inhibitors: Implications for stem cell mitosis and centrosome dynamics. Stem Cell Research. 2014;13(1):135-43.
567. Huck JJ, Zhang M, McDonald A, Bowman D, Hoar KM, Stringer B, et al. MLN8054, an inhibitor of Aurora A kinase, induces senescence in human tumor cells both in vitro and in vivo. Mol Cancer Res. 2010;8(3):373-84.
568. Liu Y, Hawkins OE, Su Y, Vilgelm AE, Sobolik T, Thu YM, et al. Targeting aurora kinases limits tumour growth through DNA damage-mediated senescence and blockade of NF-κB impairs this drug-induced senescence. EMBO Mol Med. 2013;5(1):149-66.
569. Dimri GP, Lee X, Basile G, Acosta M, Scott G, Roskelley C, et al. A Biomarker that Identifies Senescent Human Cells in Culture and in Aging Skin in vivo. Proc Natl Acad Sci U S A. 1995;92(20):9363-7.
570. Fugger K, Ørntoft T, Lukas J, Karakaidos P, Halazonetis TD, Liontos M, et al. Oncogene-induced senescence is part of the tumorigenesis barrier imposed by DNA damage checkpoints. Nature. 2006;444(7119):633-7.
571. d'Adda di Fagagna F, Di Micco R, Fumagalli M, Cicalese A, Piccinin S, Gasparini P, et al. Oncogene-induced senescence is a DNA damage response triggered by DNA hyper-replication. Nature. 2006;444(7119):638-42.
572. Bonner WM, Sedelnikova OA, Horikawa I, Zimonjic DB, Popescu NC, Barrett JC. Senescing human cells and ageing mice accumulate DNA lesions with unrepairable double-strand breaks. Nat Cell Biol. 2004;6(2):168-70.
573. Mallette FA, Gaumont-Leclerc M-F, Ferbeyre G. The DNA damage signaling pathway is a critical mediator of oncogene-induced senescence. Genes Dev. 2007;21(1):43-8.
574. Wu CL, Kirley SD, Xiao H, Chuang Y, Chung DC, Zukerberg LR. Cables enhances cdk2 tyrosine 15 phosphorylation by Wee1, inhibits cell growth, and is lost in many human colon and squamous cancers. Cancer research. 2001;61(19):7325-32.
575. Moiseeva TN, Qian C, Sugitani N, Osmanbeyoglu HU, Bakkenist CJ. WEE1 kinase inhibitor AZD1775 induces CDK1 kinase-dependent origin firing in unperturbed G1- and S-phase cells. Proceedings of the National Academy of Sciences of the United States of America. 2019;116(48):23891-3.
576. Kathleen LG, Paul N. Tyrosine phosphorylation of the fission yeast cdc2+ protein kinase regulates entry into mitosis. Nature. 1989;342(6245):39.
577. Lundgren K, Walworth N, Booher R, Dembski M, Kirschner M, Beach D. mik1 and wee1 cooperate in the inhibitory tyrosine phosphorylation of cdc2. Cell. 1991;64(6):1111-22.
578. Dunphy WG, Kumagai A. The cdc25 protein contains an intrinsic phosphatase activity. Cell. 1991;67(1):189-96.
579. Millar JB, Blevitt J, Gerace L, Sadhu K, Featherstone C, Russell P. p55CDC25 is a nuclear protein required for the initiation of mitosis in human cells. Proceedings of the National Academy of Sciences of the United States of America. 1991;88(23):10500.
580. Guertin AD, Li J, Liu Y, Hurd MS, Schuller AG, Long B, et al. Preclinical evaluation of the WEE1 inhibitor MK-1775 as single-agent anticancer therapy. Molecular cancer therapeutics. 2013;12(8):1442-52.

581. Chen D, Lin X, Gao J, Shen L, Li Z, Dong B, et al. Weel Inhibitor AZD1775 Combined with Cisplatin Potentiates Anticancer Activity against Gastric Cancer by Increasing DNA Damage and Cell Apoptosis. Biomed Res Int. 2018;2018.
582. Indovina P, Marcelli E, Di Marzo D, Casini N, Forte IM, Giorgi F, et al. Abrogating G2/M checkpoint through WEE1 inhibition in combination with chemotherapy as a promising therapeutic approach for mesothelioma. Cancer Biology & Therapy. 2014;15(4):380-8.
583. Aarts M, Sharpe R, Garcia-Murillas I, Gevensleben H, Hurd MS, Shumway SD, et al. Forced mitotic entry of S-phase cells as a therapeutic strategy induced by inhibition of WEE1. Cancer discovery. 2012;2(6):524-39.
584. Slebos RJ, Lee MH, Plunkett BS, Kessis TD, Williams BO, Jacks T, et al. p53-dependent G1 arrest involves pRB-related proteins and is disrupted by the human papillomavirus 16 E7 oncoprotein. Proceedings of the National Academy of Sciences of the United States of America. 1994;91(12):5320.
585. Mir SE, De Witt Hamer PC, Krawczyk PM, Balaj L, Claes A, Niers JM, et al. In Silico Analysis of Kinase Expression Identifies WEE1 as a Gatekeeper against Mitotic Catastrophe in Glioblastoma. Cancer Cell. 2010;18(3):244-57.
586. Prevo R, Pirovano G, Puliyadi R, Herbert KJ, Rodriguez-Berriguete G, O'Docherty A, et al. CDK1 inhibition sensitizes normal cells to DNA damage in a cell cycle dependent manner. Cell Cycle. 2018;17(12):1513-23.
587. Alexander B, Supko J, Agar N, Ahluwalia M, Desai A, Dietrich J, et al. PHASE I STUDY OF AZD1775 WITH RADIATION THERAPY (RT) AND TEMOZOLOMIDE (TMZ) IN PATIENTS WITH NEWLY DIAGNOSED GLIOBLASTOMA (GBM) AND EVALUATION OF INTRATUMORAL DRUG DISTRIBUTION (IDD) IN PATIENTS WITH RECURRENT GBM. Neuro-Oncology. 2018;20(s6):13-4.
588. Pokorny JL, Calligaris D, Gupta SK, Iyekegbe DO, Mueller D, Bakken KK, et al. The efficacy of the wee1 inhibitor MK-1775 combined with temozolomide is limited by heterogeneous distribution across the blood-brain barrier in glioblastoma. Clin Cancer Res. 2015;21(8):1916-24.
589. Gosink EC, Chong M, McKinnon P. Ataxia telangiectasia mutated deficiency affects astrocyte growth but not radiosensitivity. Cancer Res. 1999;59(20):5294-8.
590. Banin S, Moyal L, Shieh SY, Taya Y. Enhanced phosphorylation of p53 by ATM in response to DNA damage. Science (Washington). 1998;281(5383):1674-7.
591. Gautier J, Dupré A, Boyer-Chatenet L. Two-step activation of ATM by DNA and the Mre11-Rad50-Nbs1 complex. Nat Struct Mol Biol. 2006;13(5):451-7.
592. Christopher JB, Michael BK. DNA damage activates ATM through intermolecular autophosphorylation and dimer dissociation. Nature. 2003;421(6922):499.
593. Durant ST, Nickoloff JA. Good Timing in the Cell Cycle for Precise DNA Repair by BRCA1. 2005. p. 1216-22.
594. Durant S, Karran P. Vanillins--a novel family of DNA-PK inhibitors. Nucleic acids research. 2003;31(19):5501-12.
595. Goodarzi AA, Noon AT, Deckbar D, Ziv Y, Shiloh Y, Löbrich M, et al. ATM Signaling Facilitates Repair of DNA Double-Strand Breaks Associated with Heterochromatin. Mol Cell. 2008;31(2):167-77.
596. Bolderson E, Savage KI, Mahen R, Pisupati V, Graham ME, Richard DJ, et al. Krüppel-associated Box (KRAB)-associated Co-repressor (KAP-1) Ser-473 Phosphorylation Regulates Heterochromatin Protein 1β (HP1-β) Mobilization and DNA Repair in Heterochromatin. J Biol Chem. 2012;287(33):28122-31.
597. Ayoub N, Jeyasekharan AD, Bernal JA, Venkitaraman AR. HP1-β mobilization promotes chromatin changes that initiate the DNA damage response. Nature. 2008;453(7195):682-6.
598. Matsuoka S, Huang M, Elledge SJ. Linkage of ATM to Cell Cycle Regulation by the Chk2 Protein Kinase. Science. 1998;282(5395):1893-7.
599. Jacob F, Niels M, Randi GS, Jiri B, Jiri L. The ATM–Chk2–Cdc25A checkpoint pathway guards against radioresistant DNA synthesis. Nature. 2001;410(6830):842.
600. Pizarro JG, Folch J, De La Torre AV, Junyent F, Verdaguer E, Jordan J, et al. ATM is involved in cell-cycle control through the regulation of retinoblastoma protein phosphorylation. Journal of Cellular Biochemistry. 2010;110(1):210-8.
601. Eliezer Y, Argaman L, Kornowski M, Roniger M, Goldberg M. Interplay between the DNA Damage Proteins MDC1 and ATM in the Regulation of the Spindle Assembly Checkpoint. J Biol Chem. 2014;289(12):8182-93.
602. Kastan M, Bartek J. Cell-cycle checkpoints and cancer. Nature. 2004;432(7015):316-23.
603. Majd NK, Yap TA, Koul D, Balasubramaniyan V, Li X, Khan S, et al. The promise of DNA damage response inhibitors for the treatment of glioblastoma. Neurooncol Adv. 2021;3(1):vdab015-vdab.

604. Bartkova J, Hamerlik P, Stockhausen MT, Ehrmann J, Hlobilkova A, Laursen H, et al. Replication stress and oxidative damage contribute to aberrant constitutive activation of DNA damage signalling in human gliomas. Oncogene. 2010;29(36):5095-102.
605. White JS, Choi S, Bakkenist CJ. Transient ATM kinase inhibition disrupts DNA damage-induced sister chromatid exchange. Science signaling. 2010;3(124):ra44-ra.
606. Choi S, Gamper AM, White JS, Bakkenist CJ. Inhibition of ATM kinase activity does not phenocopy ATM protein disruption: Implications for the clinical utility of ATM kinase inhibitors. Cell Cycle. 2010;9(20):4052-7.
607. Durant ST, Zheng L, Wang Y, Chen K, Zhang L, Zhang T, et al. The brain- penetrant clinical ATM inhibitor AZD1390 radiosensitizes and improves survival of preclinical brain tumor models. Science advances. 2018;4(6):eaat1719-eaat.
608. Riches LC, Trinidad AG, Hughes G, Jones GN, Hughes AM, Thomason AG, et al. Pharmacology of the ATM Inhibitor AZD0156: Potentiation of Irradiation and Olaparib Responses Preclinically. Molecular cancer therapeutics. 2020;19(1):13-25.
609. Batey MA, Zhao Y, Kyle S, Richardson C, Slade A, Martin NMB, et al. Preclinical evaluation of a novel ATM inhibitor, KU59403, in vitro and in vivo in p53 functional and dysfunctional models of human cancer. Molecular cancer therapeutics. 2013;12(6):959-67.
610. Hickson I, Zhao Y, Richardson CJ, Green SJ, Martin NMB, Orr AI, et al. Identification and characterization of a novel and specific inhibitor of the ataxia-telangiectasia mutated kinase ATM. Cancer research. 2004;64(24):9152-9.
611. Sanai N, Li J, Boerner J, Stark K, Wu J, Kim S, et al. Phase 0 Trial of AZD1775 in First-Recurrence Glioblastoma Patients. Clinical cancer research : an official journal of the American Association for Cancer Research. 2018;24(16):3820-8.
612. Pokorny JL, Calligaris D, Gupta SK, Iyekegbe DO, Mueller D, Bakken KK, et al. The Efficacy of the Wee1 Inhibitor MK-1775 Combined with Temozolomide Is Limited by Heterogeneous Distribution across the Blood-Brain Barrier in Glioblastoma. Clinical cancer research : an official journal of the American Association for Cancer Research. 2015;21(8):1916-24.
613. Yoshimoto K, Mizoguchi M, Hata N, Murata H, Hatae R, Amano T, et al. Complex DNA repair pathways as possible therapeutic targets to overcome temozolomide resistance in glioblastoma. Frontiers in oncology. 2012;2(4):186-.
614. Caretti V, Hiddingh L, Lagerweij T, Schellen P, Koken PW, Hulleman E, et al. WEE1 kinase inhibition enhances the radiation response of diffuse intrinsic pontine gliomas. Mol Cancer Ther. 2013;12(2):141-50.
615. Cetin MH, Rieckmann T, Hoffer K, Riepen B, Christiansen S, Gatzemeier F, et al. G2 checkpoint targeting via Wee1 inhibition radiosensitizes EGFRvIII-positive glioblastoma cells. Radiat Oncol. 2023;18(1):19-0.
616. Slangen PLG, de Gooijer MC, van Geldorp M, van Tellingen O, Borst GR. EXTH-31. INCREASING TUMOR TREATING FIELDS (TTFIELDS) EFFICACY BY TARGETING THE G2 CELL CYCLE CHECKPOINT WITH WEE1 OR CHK1 INHIBITORS IN GLIOBLASTOMA CELL LINES. Neuro-oncology (Charlottesville, Va). 2020;22(Supplement_2):ii93-ii.
617. Taniguchi H, Caeser R, Chavan SS, Zhan YA, Chow A, Manoj P, et al. WEE1 inhibition enhances the antitumor immune response to PD-L1 blockade by the concomitant activation of STING and STAT1 pathways in SCLC. Cell Rep. 2022;39(7):110814-.
618. Golder A, Nelson L, Tighe A, Barnes B, Coulson-Gilmer C, Morgan Robert D, et al. Multiple-low-dose therapy: effective killing of high-grade serous ovarian cancer cells with ATR and CHK1 inhibitors. NAR cancer. 2022;4(4):zcac036-zcac.
619. Le HT, Staelens M, Lazzari D, Chan G, Tuszyński JA. Real-Time Monitoring of the Effect of Tumour-Treating Fields on Cell Division Using Live-Cell Imaging. Cells (Basel, Switzerland). 2022;11(17):2712.
620. Blatt R, Davidi S, Munster M, Shteingauz A, Cahal S, Zeidan A, et al. In Vivo Safety of Tumor Treating Fields (TTFields) Applied to the Torso. Front Oncol. 2021;11:670809-.
621. Shi W, Blumenthal DT, Oberheim Bush NA, Kebir S, Lukas RV, Muragaki Y, et al. Global post-marketing safety surveillance of Tumor Treating Fields (TTFields) in patients with high-grade glioma in clinical practice. J Neurooncol. 2020;148(3):489-500.
622. Chen B, Zhou X, Yang L, Zhou H, Meng M, Wu H, et al. Glioma stem cell signature predicts the prognosis and the response to tumor treating fields treatment. CNS neuroscience & therapeutics. 2022;28(12):2148-62.
623. Helleday T. The underlying mechanism for the PARP and BRCA synthetic lethality: Clearing up the misunderstandings. 2011. p. 387-93.
624. Chen C, Taniguchi T, D'Andrea A. The Fanconi anemia (FA) pathway confers glioma resistance to DNA alkylating agents. Journal of Molecular Medicine. 2007;85(5):497-509.

625. Administration TUSFaD. Premarket Approval (PMA): Optune: The U.S. Food and Drug Administration; 2015 [updated 01/27/2020. Available from: https://www.accessdata.fda.gov/scripts/cdrh/cfdocs/cfpma/pma.cfm?id=P100034S013.
626. Li T, Shukla G, Peng C, Lockamy V, Liu H, Shi W. Dosimetric impact of a tumor treating fields device for glioblastoma patients undergoing simultaneous radiation therapy. Front Oncol. 2018;8:51-.
627. Bokstein F, Blumenthal D, Limon D, Harosh CB, Ram Z, Grossman R. Concurrent Tumor Treating Fields (TTFields) and Radiation Therapy for Newly Diagnosed Glioblastoma: A Prospective Safety and Feasibility Study. Front Oncol. 2020;10:411-.
628. Grossman R, Bokstein F, Blumenthal D, Harush CB, Limon D, Ram Z. INNV-30. TUMOR TREATING FIELDS AND RADIOTHERAPY FOR NEWLY DIAGNOSED GLIOBLASTOMA: SAFETY AND EFFICACY RESULTS FROM A PILOT STUDY. Neuro-oncology (Charlottesville, Va). 2018;20(suppl_6):vi144-vi.
629. Guberina N, Pöttgen C, Kebir S, Lazaridis L, Scharmberg C, Lübcke W, et al. Combined radiotherapy and concurrent tumor treating fields (TTFields) for glioblastoma: Dosimetric consequences on non-coplanar IMRT as initial results from a phase I trial. Radiat Oncol. 2020;15(1):83-11.
630. Turner S, Gergel T, Wu H, Lacroix M, Toms S. The effect of field strength on glioblastoma multiforme response in patients treated with the NovoTTF(TM)-100A system. World Journal of Surgical Oncology. 2014;12(1).
631. S. SR, Moshe G, Yaara P, Mijal M, Uri W, David KE, et al., editors. Overcoming cell size escape from tumor treating fields using a varying frequency treatment paradigm in vitro. ASCO Annual Meeting I; 2013.
632. Pandey M, Xiu J, Mittal S, Zeng J, Saul M, Kesari S, et al. Molecular alterations associated with improved outcome in patients with glioblastoma treated with Tumor-Treating Fields. Neuro-oncology advances. 2022;4(1):vdac096-vdac.
633. Dono A, Mitra S, Shah M, Takayasu T, Zhu J-J, Tandon N, et al. PTEN mutations predict benefit from tumor treating fields (TTFields) therapy in patients with recurrent glioblastoma. J Neurooncol. 2021;153(1):153-60.
634. He J, Zhang Z, Ouyang M, Yang F, Hao H, Lamb KL, et al. PTEN regulates EG5 to control spindle architecture and chromosome congression during mitosis. Nat Commun. 2016;7(1):12355-.
635. Zhang Z, Hou S-Q, He J, Gu T, Yin Y, Shen WH. PTEN regulates PLK1 and controls chromosomal stability during cell division. Cell Cycle. 2016;15(18):2476-85.
636. Lin Y, Chen B. Case report: tumor-treating fields prolongs IDH-mutant anaplastic astrocytoma progression-free survival and pathological evolution to glioblastoma. Ann Transl Med. 2021;9(24):1804-.
637. Kebir S, Ballo MT, Jeyapalan S, Toms SA, Hottinger A, Pollom E, et al. P14.66 TTFields dose distribution and tumor growth patterns confirm clinical activity of TTFields: MRI analysis of the randomized phase 3 EF-14 trial. Neuro-oncology (Charlottesville, Va). 2019;21(Supplement_3):iii82-iii3.
638. NovoTTF™-100L System -H180002: The U.S. Food and Drug Administration; 2019 [Available from: https://www.accessdata.fda.gov/cdrh_docs/pdf18/H180002C.pdf.
639. Gentilal N, Salvador R, Miranda PC, editors. A Thermal Study of Tumor-Treating Fields for Glioblastoma Therapy. EMBC 2019 and the BRAIN Initiative® 2019 Meeting; 2019.
640. Mazzanti M, Verduci I, Cannavale G, Pyromali I, Poloni R, Rampini D. GLIOBLASTOMA CANCER STEM CELLS PROLIFERATION AND CELL CYCLE ARREST UNDER TTFIELDS INFLUENCE. Neuro-Oncology. 2019;21(s3):46-.
641. Anthony P, McArdle S, McHugh M. Tumor Treating Fields: Adjuvant Treatment for High-grade Gliomas. Seminars in Oncology Nursing. 2018;34(5):454-64.
642. Aldape K, Brindle KM, Chesler L, Chopra R, Gajjar A, Gilbert MR, et al. Challenges to curing primary brain tumours. Nat Rev Clin Oncol. 2019;16(8):509-20.
643. Osswald M, Jung E, Sahm F, Solecki G, Venkataramani V, Blaes J, et al. Brain tumour cells interconnect to a functional and resistant network. Nature. 2015;528(7580):93-8.
644. Azzarelli R. Organoid Models of Glioblastoma to Study Brain Tumor Stem Cells. Frontiers in cell and developmental biology. 2020;8:220-.
645. Nickl V, Schulz E, Salvador E, Trautmann L, Diener L, Kessler AF, et al. Glioblastoma-Derived Three-Dimensional Ex Vivo Models to Evaluate Effects and Efficacy of Tumor Treating Fields (TTFields). Cancers. 2022;14(21):5177.
646. Huang Y, Huang Z, Tang Z, Chen Y, Huang M, Liu H, et al. Research Progress, Challenges, and Breakthroughs of Organoids as Disease Models. Frontiers in cell and developmental biology. 2021;9:740574-.

CHAPTER 8. APPENDICES

8.1 Appendix A

DNA damage response inhibitor combinations enhance Tumour Treating Fields potency in glioma stem-like cells

Aurelie Vanderlinden[1], Callum G. Jones[1], Katie N Myers[1], Ola Rominiyi[1, 2*] & Spencer J Collis[1*].

[1]Department of Oncology & Metabolism, The University of Sheffield Medical School, Sheffield, UK.

[2]Department of Neuroscience, The University of Sheffield Medical School, Sheffield, UK.

[3]Department of Neurosurgery, Royal Hallamshire Hospital, Sheffield Teaching Hospitals NHS Foundation Trust, Sheffield, UK.

*co-corresponding authors:

s.collis@sheffield.ac.uk

o.rominiyi@sheffield.ac.uk

Running tittle: TTFields efficacy in glioma stem cells is potentiated by DDRi

Abstract

Brain tumours account for around 200,000 deaths/year globally, with high-grade gliomas being the most common and aggressive type of primary brain cancer. Despite maximal surgical resection, followed by chemotherapy and radiotherapy, there has been limited improvement in survival rates over the last 40 years and overall survival for these patients remains only 10-16 months. These dire survival rates highlight an urgent unmet clinical need to develop more effective therapeutic interventions for these devastating and incurable tumours. More recently, Tumour-Treating Fields (TTFields) therapy has been approved in several countries to treat both newly diagnosed and recurrent gliomas. Whilst TTFields are primarily thought to mediate their anti-cancer effects by disrupting mitotic spindles due to the high levels of mitosis in cancer cells, recent data suggests that TTFields may also attenuate DNA damage repair efficiency and replication fork dynamics. We therefore set out to determine if combining TTFields with therapeutic and pre-clinical DNA damage response inhibitors (DDRi) could enhance TTFields potency in typically resistant glioma stem-like cells (GSCs). We show that combining TTFields with clinically approved PARP1 inhibitor treatment leads to significantly reduced GSC clonogenic survival, which is further enhanced by radiation treatment. Mechanistically, we show that this is associated with increased amounts of DNA damage due to retarded DNA damage resolution. Furthermore, we observe similar impressive potency and associated enhance levels of persistent DNA damage when TTFields treatments are combined with a pre-clinical ATR inhibitor and/or radiation treatments. To our knowledge, these data represent the first report of TTFields combined with therapeutically relevant DDRi in GSCs and provide encouraging data for further preclinical evaluation of such approaches. Overall, our findings support such a combinatorial therapeutic approach as part of a next generation multimodal TTFields-based therapy regimes for patients with these currently incurable tumours.

Introduction

Brain tumours kill more children and adults under 40 than any other cancer, with high-grade glioblastomas being the most common tumours arising within the brain, contributing to around 200,000 deaths/year globally(1, 2). The current standard-of-care therapy for these currently incurable tumours is de-bulking surgical resection followed by a therapeutic regimen of radio-/chemotherapy, utilising the DNA alkylating agent Temozolomide (TMZ)(3, 4). Interestingly, even though around half of glioblastomas exhibit promoter methylation of the dealkylating enzyme MGMT that specifically and directly removes alkylation lesions induced by TMZ and is therefore an established biomarker of TMZ effectiveness/clinical response, MGMT promoter methylation status does not affect overall survival rates which remain poor at around 12-15 months post-diagnosis. In addition to large amounts of inter- and intra-tumoural genetic and transcriptomic heterogeneity(5-17), one of the main reasons ascribed to the high levels of treatment resistance and recurrence exhibited by glioblastomas is the presence of difficult-to-treat glioblastoma stem-like cell (GSC) subpopulations(18, 19), which possess unlimited regenerative potential and exhibit enhanced DNA repair pathway activity(20-24). As such, mean disease recurrence is only around 7 months, resulting in less than 10% of glioblastoma patients surviving more than 5 years post-diagnosis, which unfortunately have not improved in the last 40-50 years(5, 25).

Tumour Treating Fields (TTFields) is a non-invasive therapy which delivers low-intensity (1–3 V/cm) intermediate-frequency (100–300 kHz) alternating electric fields to localised tumour sites(26). Importantly, TTFields represents an exciting new clinically-approved ‘fourth modality’ for the treatment of glioblastomas in over 10 years(26), as confirmed by the extension of overall survival by ~5 months in patients with newly diagnosed glioblastoma within randomised clinical trials(27). Molecular evidence suggests that TTFields, through the exertion of physical forces on dipolar macromolecules, can exert a plethora of biological effects within cells(26) including: targeting of cell cycle proteins, enhancement of cell membrane permeability, and induction of immunogenic cell death(28-30). However, since DNA fragments are negatively charged and DNA-damaging chemoradiotherapy is the standard-of-care for post-surgical management of glioblastoma, the discovery of TTFields modulatory effects on DNA damage and highly-coordinated cellular DNA damage response (DDR) processes(31-33) presents a critical opportunity to develop more effective, rationally-designed TTFields-based therapeutic strategies(26, 34, 35). Therefore, using clinically-relevant GSC models(23, 24), we investigated combining established therapeutic and preclinical DDR inhibitors (DDRi(35, 36)) with TTFields and radiation as part of important

preclinical evaluation studies to determine if such strategies could be developed clinically to enhance TTFields potency in the treatment of currently incurable glioblastoma.

Materials and Methods

Cell culture

G1 and G7 patient-derived primary glioblastoma stem-like cells (GSCs) were kindly gifted by Professor Colin Watts (University of Birmingham, Brain Cancer Programme Chair) and Professor Anthony Chalmers (University of Glasgow, Chair of Clinical Oncology), which were initially derived from freshly resected anonymised glioblastoma specimens by Professor Watts' former laboratory in Cambridge(23, 24, 37). All GSCs were propagated as adherent monolayers on matrigel-coated T75 flasks. Cells were grown in advanced DMEM supplemented with L-glutamine (Invitrogen, 25030081), B27 (Invitrogen, 17504-044), N2 (Invitrogen, 17502-048), Penicillin-Streptomycin (Invitrogen, 15140122), Heparin (Sigma, H3393-10KU), amphotericin B (Gibco, 15290), EGF (100µg/ml, Invitrogen, PHG0313) and FGF (100µg/ml, Invitrogen, PHG0263), in a humidified incubator at: 37°C, 5% CO_2 and 21% O_2.

Inhibitor and irradiation treatments

DDRi drugs AZD6738 (Selleckchem; S7693) and Olaparib/Lynparza/AZD2281 (Adooq Bioscience; A10111) were diluted with DMSO to make 10mM stocks and were stored at -20°C. Cells were treated with the DDRi at the indicated concentrations or with vehicle control only (DMSO). DMSO and all DDRi were diluted in stem media to the final intended concentrations and 2mL of the drug/DMSO dilutions was added to the desired wells. DMSO at concentrations equivalent to the drug solutions (<2%) were used as the vehicle control in all experiments. One hour following DDRi treatment, cells were treated with either TTFields and/or ionising radiation. Cells were irradiated in a Caesium-137 (^{137}Cs) Irradiator (CIS IBL437c). A dose of either 2 or 5 Gy was used as indicated. In all experiments, irradiation was administered 1 hour following the DDRi treatment. Unirradiated control plates were taken out of the incubator for the same duration as the treatment plates to minimise experimental variation and act as a 'sham' radiation control such that control plates were subjected to comparable environmental changes as experienced by cells during the irradiation process.

TTFields treatments

The Inovitro system (NovoCure Ltd; Haifa, Israel) was used to generate TTFields. G1 and G7 stem cells were seeded onto sterile, matrigel-coated glass coverslips in 12-well plates at a density of 3-5 x 10^4 cells/well. Following seeding, cells were incubated overnight to allow for cell adhesion to the coverslips. The following day, the matrigel-coated coverslips with attached cells were transferred into Inovitro ceramic dishes (one coverslip/dish), which contained two pairs of electrodes positioned at a 90°angle relative to each other. Dishes to receive TTFields treatment were slotted onto an Inovitro base plate, which were then connected through transducer arrays to a generator (generates electric fields at the desired frequency, 200kHz) and the electric fields treatment was applied. The orientation of the TTFields alternated 90^o every 1 second. The base plate with the dishes were placed in a refrigerated incubator (set at a temperature of 22°C, with 5% CO_2 and 21% O_2) to maintain the temperature of each dish at 37°C, as the delivery of electric fields generates micro heating within the dish. The temperature was detected by 2 thermistors located within the walls of the ceramic dish. The temperature of the refrigerated incubator also helps determine the intensity at which the electric fields can be delivered, with a temperature of 22°C equating to an intensity of 1.33 V/cm RMS. Control dishes were placed in a humidified incubator at: 37°C, 5% CO_2 and 21% O_2 for the duration of the treatment. Cells were treated for a duration of 48 hours (based on calculated cell doubling times as determined by cell growth assays (supplementary Figure S1A). As such, all subsequent TTFields treatments were at 200kHz, ~1.33 V/cm RMS for 48 hours.

Clonogenic survival assays

Following treatment with RT, DDRi and/or TTFields, cells were harvested and re-seeded in matrigel-coated 6-well tissue culture plates at varying densities (300 and 500 cells/well) (specified in the results). Cells were incubated for 21 days, then stained with methylene blue, and the resulting colonies (cluster of 50 cells or more) were counted. The plating efficiency (PE) was determined for untreated control populations and the surviving fraction (SF) for each experimental condition was calculated relative to the untreated control; number counted / (number plated x PE).

Western blotting

Between 25-50μg of protein and 4x NuPage LDS Loading Buffer mix were loaded into each lane of a NuPAGE 4-12% Bis-Tris gradient gel and electrophoresed for ~75mins at 150V.

Proteins were then transferred to nitrocellulose membranes at 100V for 120 minutes in Mini PROTEAN Tetra Cells, using 1x NuPAGE transfer buffer (20X stock) diluted with pure methanol and ddH_2O. Membranes were blocked for 60 minutes in 5% milk with phosphate-buffered saline (Thermo Fisher Scientific, BR0014) with 5% Tween-20 (Sigma, P1379) (PBS-T) or 5% bovine serum albumin (BSA) (Sigma, A2153) with TBS-T, when blotting for pChk1 Ser345. Membranes were incubated with primary antibodies overnight at 4°C with anti β-actin (Santa Cruz, sc-47778; 1:5000), anti-pChk1 Ser345 (Cell signalling, #2341; 1:500), anti-Chk1 (Cell signalling, #2360; 1:1000), anti-ATR (R&D Systems, #AF4717; 1:250), anti-PARP1 (Santa Cruz, sc-8007; 1:1000), anti-αPAR (Millipore, MABE1016; 1:1000), or anti-γH2AX Ser139 (Santa Cruz, sc517348; 1:1000). Primary antibodies were made up in 5% milk with PBS-T or 3% BSA with TBS-T, again when blotting for pChk1. Membranes were washed 3x with PBS-T, each wash lasting 10 minutes. Membranes were then incubated with secondary antibodies conjugated to HRP all at 1:1000 in 5% milk with PBS-T for 1hr: anti-rabbit (DAKO, P0399), anti-goat (DAKO, P0449) or anti-mouse (DAKO, P0447). Membranes were washed 3 times in PBS-T and protein bands visualised using Pierce ECL western blotting substrate and developed using medical x-ray film and a Konica SRX 101A Processor.

Immunofluorescence

Cells were seeded onto sterile Matrigel-coated coverslips in 12-well plates at a density of 3 x 10^4 cells/well. At the end of TTF/IR/DDRi treatment, cells were fixed with 4% Paraformaldehyde (PFA; Santa Cruz Biotechnology, SC-281692) for ten minutes and subsequently washed twice with PBS. Cells were permeabilised with 0.5% Triton X-100 (Thermo Fisher Scientific, A16046) in PBS for ten minutes. Once permeabilised, cells were washed three times with PBS and blocked for 1 hour with 3% BSA in PBS. Cells were then incubated overnight at 4°C with primary antibodies; phospho-histone ser139 (γH2AX) antibody (Millipore, JBW301; 1:500) and p53-binding protein 1 (53BP1) antibody (Abcam, ab36823; 1:500) in 1% BSA PBS. Following incubation with primary antibodies, cells were washed three times with PBS. Cells were then incubated with the secondary antibodies Alexa Fluor 488-conjugated anti-rabbit antibody (Life Technologies, A-11034; 1:500) and Alexa Fluor 555-conjugated anti-mouse antibody (Life Technologies, A11005; 1:500) made up in PBS with 1% BSA at room temperature for 1-hour in the dark (wrapped in foil). Finally, coverslips were washed three times in PBS, including a final wash in PBS containing 2μg/ml DAPI before being mounted onto microscope slides using Shandon Immu-Mount medium (Thermo Fisher Scientific, 9990402). Slides were left to dry overnight at room temperature in the dark. Microscopy was performed on a Nikon Eclipse T200 inverted microscope (Melville), using a

100x objective lens. Individual 53BP1 foci in each cell nucleus were counted and cells were scored as either positive (≥5 foci) or negative (<5 foci) for γH2AX stain. A minimum of 100 cells were analysed for each experimental condition per slide.

Comet assays

The comet assay kit (Trevigen; 4250-050-K) was used to process samples. At the end of treatment, cells were collected and resuspended in warm PBS, and then pelleted at ~180rcf for 3mins and washed twice with warm PBS. Cell pellets were then resuspended in 1mL warm PBS and cells were counted using a haemocytometer. A final cell suspension of 1 x 10^5 cells/mL in PBS for each sample was produced. 12.5μL of cell suspension was then mixed with 112.5μl L-Magarose (4250-050-02; 1:10 dilution) and 100μLof the L-Magarose/cell mix was pipetted onto the sample area of a comet slide (Trevigen; 4250-050-03). Cells were stored flat at 4°C in the dark for 30 mins to promote adherence, and then lysed with COMET Lysis Solution (4250-050-01) at 4°C for 30 mins in the dark. Following lysis, cells were exposed to Alkaline Unwinding Buffer (200 mM NaOH (Sigma; S5881), 1 mM EDTA (Trevigen; 4250-050-04) for 20 mins at room temperature. Electrophoresis was carried out at ~21V, with a constant current of 300mA (achieved by adjusting the volume of Alkaline Electrophoresis Buffer (200 mM NaOH, 1 mM EDTA (Sigma; 1233508)) for 30 mins at 4°C. Slides were rinsed twice with H_2O and were then immersed in 70% ethanol for 5 minutes. Samples were dried overnight at room temperature. To stain cells, 100μl 10,000X SYBR Gold Solution (Invitrogen; S11494) made up at 1:30,000 in TE buffer (10 mM Tris-HCl, Sigma; 10812846001) pH 7.5, 1 mM EDTA (Sigma; 1233508) was pipetted onto each sample area and left to stain for 30 mins in the dark. Excess SYBR Gold solution was removed by gently tapping the slides and dipping them in H_2O. Slides were allowed to dry before imaging. A least 50 cells per condition were imaged using the FITC channel and 20x lens on a Nikon Eclipse TE200 Fluorescent Microscope. Images were analysed using TriTek COMET Score software (AMSBiotechnology, 2010) to determine the tail moment which was used as a direct measure of DNA damage.

Flow Cytometry

The Biosciences kit (#556547) was used to process samples as described in the manufacturer's protocol. At various time points following treatment (as specified in the results), media from each dish was collected and transferred to a labelled centrifuge tube. Cells were lifted and washed twice with cold PBS and resuspended in 100μL 1X Binding Buffer (10X Binding Buffer - 0.1 M HEPES, pH 7.4; 1.4 M NaCl; 25 mM $CaCl_2$; diluted to 1X in ddH_2O,

Biosciences, 556454). 5μL Annexin V (27μg/mL, Biosciences; 556419) and 5μL Propidium Iodide (PI, Biosciences; 556463) were added to each sample and cells were incubated at room temp for 15mins in the dark. A further 200μL Binding Buffer was added to each tube and the cell suspension was then transferred into labelled FACS tube and analysed by BD LSR II Flow Cytometer. 10,000 cells/sample were counted on the LSRII and the resulting data was analysed using FlowJo software.

Statistical analyses

Statistical significance was calculated using the nonparametric Mann–Whitney U-test comparing the indicated treatment to DMSO controls or to another indicated treatment cell population, and represented as follows: ns = not significant, * = $p < 0.05$, ** = $p < 0.01$, *** = $p < 0.001$, and **** = $p < 0.0001$.

Results

PARP1i enhances TTFields-mediated cell death in GSCs

TTFields have previously been shown to elicit DNA damage and replication stress in human cells and interfere with the efficient repair of radiation-induced DNA lesions(26, 32, 33). Consistent with this, exposure of primary glioma stem-like cultures (GSCs) with optimised therapeutically relevant doses of TTFields caused DNA damage and activated both PARP1 and ATR signalling pathways (supplementary Figure S1B), and recent work using established lung cancer cell lines has also shown that combinations of TTFields with radiation and/or PARP1 inhibitors (PARPi) impart enhanced cell killing effects(32). Furthermore, PARPi have been shown to successfully cross the blood-brain barrier (BBB) to deliver therapeutic doses at glioma tumour sites(38). We therefore assessed if combining PARPi with or without additional therapeutically relevant ionising radiation (IR) doses in primary GSCs could augment TTFields potency. Indeed, combination of PARP1 inhibition with the therapeutic compound Olaparib (Lynparza™) augmented TTFields potency, which was further and dramatically enhanced when combined with 2Gy IR (Figure 1A). Importantly, a similar enhanced cytotoxic effect on clonogenic capacity was also independently observed in the G7 GSC model (Figure 1B), which was not due to large amounts of early induced apoptosis (Figure 1C). It is interesting to note that decreased clonogenic survival was more pronounced

in G1 GSCs compared with G7 GSCs, which could be linked to the enhanced basal levels of PARP1 present in the G7 GSC model compared with G1 GSCs (supplementary Figure S1C) conferring a greater inherent IR and PARPi resistance.

TTFields-PARP1i combinations yield elevated and prolonged DNA damage in GSCs

Consistent with the clonogenic survival data, we determined that both G1 and G7 GSCs treated with PARP1i-TTFields combinations exhibited elevated levels of DNA damage that was further and dramatically enhanced when combined with 2Gy IR (Figures 2A and 2B respectively). Furthermore, direct assessment of DNA damage by Comet assays confirmed enhanced levels of DNA damage in both G1 and G7 populations treated with PARP1-TTFields and PARP1i-IR-TTFields combinations compared with those treated with either modality alone (Figures 3A and 3B). In keeping with the differential clonogenic survival and apoptotic index between combination treated G1 and G7 GSCs (Figure 1), the increased levels of DNA damage were consistently more elevated in G1 GSCs compared with G7 GSCs (Figure 2 and 3), which is important as inter-tumoural inherent treatment sensitivity/resistances heterogeneity is common across gliomas.

Given that TTFields have been shown to enhance replication stress by downregulation of BRCA/FA repair pathway genes, and that PARP1 is important for replication fork stabilisation during replication stress(26), we assessed the effects of the combination treatments on replication stress. Consistent with data derived from other cells, PARPi, IR and TTFields all individually led to modest increased replication stress, which was again more enhanced in G1 compared to G7 GSC (Figures 3C and 3D). Consistent with this data, the various combinations of PARPi, IR and TTFields led to further significant increases in replication stress in G1 but not in G7 GSCs (Figure 3C and 3D). These data suggest that although some of the DNA damage induced by the combination treatments may be a consequence of elevated replication stress leading to fork collapse, other mechanisms may be involved.

Therefore, in order to investigate the resolution of the DNA damage induced by the various combination treatments, we assessed the levels of DNA damage at both early (4hrs) and late timepoint (24hrs) post-treatment using immunofluorescent quantification of the respective DNA damage and double-strand break markers γH2AX and 53BP1. Similar to that observed immediately following TTFields dosing (Figure 2), PARPi-IR-TTFields combination treated G1

GSCs exhibited significantly higher levels of DNA damage (~2-fold) compared with either PAPP1i-TTFields or IR-TTFields treatments, with elevated levels of DNA damage still remaining 24hrs post-treatment (Figures 4A-C and supplementary Figure S1D). Encouragingly, although overall, less DNA damage was induced in G7 GSCs compared with G1 GSCs (Figure 2) comparable effects on efficient damage resolution were observed in G7 GSCs (Figures 4D-F and supplementary Figure S1E). Collectively, these data suggest that such therapeutic combinations are worth investigating in a larger panel of primary GSC models that represent more inherently IR and PARPi sensitive tumour cells, as well as those that are indicative or inherently treatment resistant tumours.

Preclinical assessment of ATRi in combination with IR and TTFields in GSCs

Given the key role of the ATR-mediated signalling pathway in cellular response to DNA damage and replication stress, the ATR kinase is an established oncology drug target in a range of tumours, including gliomas(35, 36). For these studies, we focused on the use of the BBB-penetrant ATR inhibitor AZD6738 (ATRi), which is currently undergoing investigation in several clinical trials, including in combination with Olaparib, but also in combination with radiotherapy(35, 36, 39). Even more pronounced that what we observed for PARPi, combinations of relatively non-toxic doses of ATRi with IR and TTFields led to significant reduced clonogenic survival in both G1 and G7 GSCs, which was unexpectedly not associated with significantly enhanced apoptosis (Figure 5). As with the PARPi combinations, the ATRi-IR-TTFields combination was particularly potent in G1 GSCs compared with G7 GSCs (Figure 5). Encouragingly, the increased cytotoxicity in both GSC models was accompanied by elevated levels of DNA damage as assessed using the immunofluorescent markers γH2AX and 53BP1 (Figure 6). Unexpectedly however, this only correlated with a significant increase in DNA damage as measured by Comet assay in G7 GSCs (Figures 7A and 7B), and neither G1 or G7 combination-treated cell populations exhibited elevated levels of replication stress as measured using pRPA2 foci formation (Figure 7C and 7D). This is particular intriguing given that both TTFields alone and ATRi treatment prior to IR enhanced radiation-induced pRPA2 foci formation in both G1 and G7 GSCs (Figures 7C and 7D), which suggests that this may simply reflect stalled forks being converted into DNA breaks which releases RPA from ssDNA. Additionally, previous work from others has shown that GSCs have a greater capacity to repair DNA damage after ATRi-IR combination treatments than their bulk (non-stem) counterparts(23).

Therefore, in order to assess to DNA damage levels in more detailed, we carried out time-courses analyses of G1 and G7 GSCs treated with either ATRi, IR or TTFields alone, or in various combinations. Akin to the results for PARPi (Figure 4) pre-treatment of both G1 and G7 GSCs prior to combination IR-TTFields treatment led to elevated and persistent levels of DNA damage (Figure 8 and supplementary Figure S2), although consistent with our other findings, this was significantly more pronounced in G1 GSCs compared with G7 GSCs (Figures 8A-C and 8D-F respectively), which exhibited nearly 4-fold increased DNA damage over basal levels even at 24hrs post-treatment (figure 8C). However, even in the inherently more resistant G7 GSCs, combining ATRi with IR and TTFields led to significantly elevated levels of DNA damage and DNA breaks 24hrs post-treatment, where the single agent or dual combination treated cells had returned to basal levels of DNA damage (Figure 8F). Collectively, these encouraging data together with our data for PARPi in these GSC models, highlight the potential for DDRi combinations to enhance the efficacy and potency of TTFields therapeutics in the treatment of high-grade gliomas.

Discussion

To our knowledge, we present here the first report of combining TTFields with DNA repair inhibitors in glioma stem cells and the first reported use of combining ATRi with TTFields. Encouragingly, our data are consistent with recent work by others showing the effectiveness of combining TTFields with PARPi and IR in non–small-cell lung cancer cell lines(32). The profound increased sensitivity to TTFields that we observe in primary GSCs by pre-treatment with either PARPi or ATRi is particular exciting given that both PARPi and ATRi have been shown to exhibit good safety profiles in human trials and are able to reach the glioma tumour site through the BBB. As such, both are currently being assessed in a range of glioma-focused clinical trials as part of both monotherapy approaches and in combination with current standard-of-care TMZ or IR therapies(38-45). This is particularly interesting given that TTFields have previously been shown to enhance BBB permeability(26), which could further improve the effective dose of such compounds at the tumour site. With regards to this, it is interesting and important to note that in addition to the use of clinically relevant 2Gy IR doses throughout our study, the 0.5μM dose of Olaparib that we used is in line with the median drug dose observed at orthotopic tumour sites and clinically effective doses used in recent clinical trials(38). Our data therefore provides further important preclinical evaluation of the potential to combine these compounds as well as other DDRi with current standard-of-care therapies

for gliomas(35), including TTFields, which has been clinically approved in numerous countries for both newly diagnosed and recurrent gliomas(26).

A major current limitation to our current work is that these data have been generated in 2D GSCs that are several passages away from their primary tumour resection(23, 24), and have been shown to be amenable to 3D culture that yield more clinically-relevant drug responses(37, 46). The main reason for this is that although there are preclinical TTFields devices available and still in development for *in vivo* studies(26, 47), presently no defined protocols for the delivery of TTFields in such 3D culture models(47). However, very recent work has started to explore the possibility of delivering effective doses of TTFields within *ex vivo* 3D glioma models(48), and we have also recently been able to develop effective and robust delivery of TTFields within 3D GSC cultures (unpublished data). As such, under our current ethics approval, we are now carrying out subsequent evaluation of PARPi, ATRi and other DDRi in combination with TTFields within primary *ex vivo* 3D GSC models which we hope to publish in the near future.

Other aspects worth considering when taking our findings presented here forward into further preclinical models is the often ‘left behind’ post-surgical residual disease and the inherent inter- and intra-tumour heterogeneity that exists within these tumours, and how these traits can impact responses to radio-chemotherapy treatments and overall patient survival(5, 9). In order to address this, we have developed an ongoing living biobank of over 110 3D GSCs models derived from over 50 individual patients that have undergone surgical resection of their gliomas, which incorporates multiple models that recapitulate both intra-tumoural heterogeneity (multi-region sampling) and typically post-surgical residual disease using adjacent, invaded brain within *en-bloc* partial lobectomy specimens (manuscript in preparation). We therefore plan to harness these models together with our recently developed 3D GSC TTFields protocols to provide further preclinical evaluation of PARPi, ATRi and other DDRi combinations to augment the efficacy of TTFields alone and in combination with current standard-of-care TMZ and IR therapies, and to also assess the potential pan-tumour efficacy of such approaches.

Figure Legends

Figure 1. Olaparib potentiates TTFields cytotoxicity in glioma stem cells.

A: Upper panel; western blots showing effective PARP inhibition (reduction in PARylation) in G1 GSCs with the indicated doses of Olaparib. Middle panel; representative images of colony formation of G1 GSC treated as indicated. Lower panel; clonogenic survival of G1 GSCs treated as indicated. **B:** Same as in A:, but for G7 GSCs. C: Measurements of apoptosis and necrosis in G1 (upper panel) and G7 (lower panel) GSCs treated as indicated. Data shown represents the means derived from at least three independent biological repeat experiments along with their respective standard errors. Bars above the data highlight statistical significance calculations between the two indicated cell populations.

Figure 2. PARPi elevates DNA damage levels induced by TTFields-IR combinations.

A: Left panel; Representative immunofluorescent images of the indicated G1 GSC population stained for either 53BP1 (green) or γH2AX (red) after the indicated treatment combinations. DAPI DNA stain (blue) was used to identify cell nuclei for scoring purposes. Right panel; quantification of γH2AX positive cells (%) or mean 53BP foci/nucleus in the indicated G1 GSC cell populations. **B:** Same as in A:, but for G7 GSCs. Red dashed line indicates the mean in DMSO treated population. Data shown on the graphs represents the either means derived from at least three independent biological repeat experiments along with their respective standard errors or collated data from at least three independent biological repeat experiments along with their respective standard deviations. Bars above the data highlight statistical significance calculations between the two indicated cell populations.

Figure 3. Further assessment of DNA damage and replication stress induced by combining PARPi with TTFields and IR treatments.

A: Representative Comet images of the indicated G1 GSC population with quantification of tail moment from at least three independent biological repeat experiments shown to the right. **B:** Same as in A:, but for G7 GSCs. **C:** Upper panel; Representative immunofluorescence images of the indicated G1 GSC cell population stained for pRPA2 (red) and DAPI (blue) used to identify nuclei. Lower panel; quantification of pRPA2 positive cells in the indicated G1 GSC populations. **D:** Same as in C:, but for G7 GSCs. Red dashed line indicates the mean in DMSO treated population. Data shown on the graphs represents collated data derived from at least three independent biological repeat experiments along with their respective standard

deviations. Bars above the data highlight statistical significance calculations between the two indicated cell populations.

Figure 4. PARPi impedes the efficient resolution of TTFields-IR induced DNA damage.

A: and **B:** Respective quantification of γH2AX positive cells (%) or mean 53BP foci/nucleus in the indicated G1 GSC cell populations at 4hrs and 24hrs post-treatment (see Supplementary Figure S1D). Note: the 0hr timepoint data isn't shown for space purposes and is a further three independent repeats of the data shown in Figure 2 but it is shown on the line graph below. **C:** Line graphs showing the data above together with the 0hr time point data for this set of experiments for the indicated DNA damage marker and treated G1 GSC population. D-E: same as for A-C, but for G7 GSCs. Note: representative 4hr and 24hr images for γH2AX and 53BP are shown in Supplementary Figure S1E. Red dashed line indicates the mean in DMSO treated population. Data shown on the graphs represents the either means derived from at least three independent biological repeat experiments along with their respective standard errors or collated data from at least three independent biological repeat experiments along with their respective standard deviations with calculated statistical significance values shown as outlined in the material and methods section. Bars above the data highlight statistical significance calculations between the two indicated cell populations.

Figure 5. The ATRi AZD6738 potentiates TTFields cytotoxicity in glioma stem cells.

A: Upper panel; western blots showing effective ATR kinase inhibition (reduction in IR-induced CHK1 phosphorylation on Ser345) in G1 GSCs with the indicated doses of ATRi. Middle panel; representative images of colony formation of G1 GSC treated as indicated. Lower panel; clonogenic survival of G1 GSCs treated as indicated. **B:** Same as in A:, but for G7 GSCs. C: Measurements of apoptosis and necrosis in G1 (upper panel) and G7 (lower panel) GSCs treated as indicated. Data shown represents the means derived from at least three independent biological repeat experiments along with their respective standard errors. Bars above the data highlight statistical significance calculations between the two indicated cell populations.

Figure 6. ATRi elevates DNA damage levels induced by TTFields-IR combinations.

A: Left panel; Representative immunofluorescent images of the indicated G1 GSC population stained for either 53BP1 (green) or γH2AX (red) after the indicated treatment combinations. DAPI DNA stain (blue) was used to identify cell nuclei for scoring purposes. Right panel; quantification of γH2AX positive cells (%) or mean 53BP foci/nucleus in the indicated G1 GSC cell populations. **B:** Same as in A:, but for G7 GSCs. Red dashed line indicates the mean in DMSO treated population. Data shown on the graphs represents the either means derived from at least three independent biological repeat experiments along with their respective standard errors or collated data from at least three independent biological repeat experiments along with their respective standard deviations. Bars above the data highlight statistical significance calculations between the two indicated cell populations.

Figure 7. Further assessment of DNA damage and replication stress induced by combining ATRi with TTFields and IR treatments.

A: Representative Comet images of the indicated G1 GSC population with quantification of tail moment from at least three independent biological repeat experiments shown to the right. **B:** Same as in A:, but for G7 GSCs. **C:** Upper panel; Representative immunofluorescence images of the indicated G1 GSC cell population stained for pRPA2 (red) and DAPI (blue) used to identify nuclei. Lower panel; quantification of pRPA2 positive cells in the indicated G1 GSC populations. **D:** Same as in C:, but for G7 GSCs. Red dashed line indicates the mean in DMSO treated population. Data shown on the graphs represents collated data derived from at least three independent biological repeat experiments along with their respective standard deviations. Bars above the data highlight statistical significance calculations between the two indicated cell populations.

Figure 8. ATRi impedes the efficient resolution of TTFields-IR induced DNA damage.

A: and **B:** Respective quantification of γH2AX positive cells (%) or mean 53BP foci/nucleus in the indicated G1 GSC cell populations at 4hrs and 24hrs post-treatment (see Supplementary Figure S2A). Note: the 0hr timepoint data isn't shown for space purposes and is a further three independent repeats of the data shown in Figure 6 but it is shown on the line graph below. **C:** Line graphs showing the data above together with the 0hr time point data for this set of experiments for the indicated DNA damage marker and treated G1 GSC population. D-E: same as for A-C, but for G7 GSCs. Note: representative 4hr and 24hr images for γH2AX and 53BP are shown in Supplementary Figure S2B. Red dashed line indicates the mean in DMSO treated population. Data shown on the graphs represents the either means derived from at

least three independent biological repeat experiments along with their respective standard errors or collated data from at least three independent biological repeat experiments along with their respective standard deviations with calculated statistical significance values shown as outlined in the material and methods section. Bars above the data highlight statistical significance calculations between the two indicated cell populations.

Supplementary Figure S1.

A: Growth curves for G1 and G7 stem cells. The cell doubling time was calculated from the growth phase of the curves as detailed in the materials and methods section. G7 stem cells were calculated to have a doubling time of 1.6 days and G1 stem cells of 1.3 days. **B:** and **C:** Western blots of GSCs probed for the indicated proteins. **D:** and **E:** representative immunofluorescence images of G1 and G7 GSC stained respectively for γH2AX or 53BP1 at the indicated time post singular or PARPi-IR-TTFields combination treatment. The collated data associated with these images from three independent repeat experiments are shown in Figure 4.

Supplementary Figure S2.

A: and **B:** representative immunofluorescence images of G1 and G7 GSC stained respectively for γH2AX or 53BP1 at the indicated time post singular or ATRi-IR-TTFields combination treatment. The collated data associated with these images from three independent repeat experiments are shown in Figure 8. Data shown on the graphs represents collated data derived from at least three independent biological repeat experiments along with their respective standard deviations. Bars above the data highlight statistical significance calculations between the two indicated cell populations.

Acknowledgments

We wish to thank Novocure for the loan of the Inovitro TTFields system, Prof. Anthony Chalmers, Dr. Natividad Gomez-Roman and Colin Watts for supply of the G1 and G7 GSCs, and Dr. Helen Bryant, Dr. Yaara Porat and Dr. Moshe Giladi for helpful advice and discussions throughout the course of this research.

Funding

AVL is a recipient of a Faculty PGT to PGR PhD Scholarship, with additional consumable funding provided by the Sheffield Neuroscience Biomedical Research Centre, Faculty HEIF/KE funds and Novocure, who also kindly provided our laboratory with the Inovitro TTFields system and associated equipment.

Author contributions

AVL, OR and SJC conceived and planed the experiments which were carried out by AVL with assistance from CGJ and KNM. SJC, OR and AVL wrote the manuscript with additional input from CGJ and KNM.

References

1. Alexander BM, Ba S, Berger MS, Berry DA, Cavenee WK, Chang SM, et al. Adaptive Global Innovative Learning Environment for Glioblastoma: GBM AGILE. Clin Cancer Res. 2018;24(4):737-43.
2. Brain GBD, Other CNSCC. Global, regional, and national burden of brain and other CNS cancer, 1990-2016: a systematic analysis for the Global Burden of Disease Study 2016. Lancet Neurol. 2019;18(4):376-93.
3. Stupp R, Mason WP, van den Bent MJ, Weller M, Fisher B, Taphoorn MJ, et al. Radiotherapy plus concomitant and adjuvant temozolomide for glioblastoma. N Engl J Med. 2005;352(10):987-96.
4. Stupp R, Hegi ME, Mason WP, van den Bent MJ, Taphoorn MJ, Janzer RC, et al. Effects of radiotherapy with concomitant and adjuvant temozolomide versus radiotherapy alone on survival in glioblastoma in a randomised phase III study: 5-year analysis of the EORTC-NCIC trial. Lancet Oncol. 2009;10(5):459-66.
5. Aldape K, Brindle KM, Chesler L, Chopra R, Gajjar A, Gilbert MR, et al. Challenges to curing primary brain tumours. Nat Rev Clin Oncol. 2019;16(8):509-20.
6. Bergmann N, Delbridge C, Gempt J, Feuchtinger A, Walch A, Schirmer L, et al. The Intratumoral Heterogeneity Reflects the Intertumoral Subtypes of Glioblastoma Multiforme: A Regional Immunohistochemistry Analysis. Front Oncol. 2020;10:494.
7. Piccirillo SGM, Colman S, Potter NE, van Delft FW, Lillis S, Carnicer MJ, et al. Genetic and functional diversity of propagating cells in glioblastoma. Stem Cell Reports. 2015;4(1):7-15.
8. Sottoriva A, Spiteri I, Piccirillo SG, Touloumis A, Collins VP, Marioni JC, et al. Intratumor heterogeneity in human glioblastoma reflects cancer evolutionary dynamics. Proc Natl Acad Sci U S A. 2013;110(10):4009-14.

9. Rominiyi O, Al-Tamimi Y, Collis SJ. The 'Ins and Outs' of Early Preclinical Models for Brain Tumor Research: Are They Valuable and Have We Been Doing It Wrong? Cancers (Basel). 2019;11(3).
10. Patel AP, Tirosh I, Trombetta JJ, Shalek AK, Gillespie SM, Wakimoto H, et al. Single-cell RNA-seq highlights intratumoral heterogeneity in primary glioblastoma. Science. 2014;344(6190):1396-401.
11. Varn FS, Johnson KC, Martinek J, Huse JT, Nasrallah MP, Wesseling P, et al. Glioma progression is shaped by genetic evolution and microenvironment interactions. Cell. 2022;185(12):2184-99 e16.
12. Barthel FP, Johnson KC, Varn FS, Moskalik AD, Tanner G, Kocakavuk E, et al. Longitudinal molecular trajectories of diffuse glioma in adults. Nature. 2019;576(7785):112-20.
13. Brennan CW, Verhaak RG, McKenna A, Campos B, Noushmehr H, Salama SR, et al. The somatic genomic landscape of glioblastoma. Cell. 2013;155(2):462-77.
14. Cancer Genome Atlas Research N. Comprehensive genomic characterization defines human glioblastoma genes and core pathways. Nature. 2008;455(7216):1061-8.
15. Spiteri I, Caravagna G, Cresswell GD, Vatsiou A, Nichol D, Acar A, et al. Evolutionary dynamics of residual disease in human glioblastoma. Ann Oncol. 2019;30(3):456-63.
16. Stupp R, Lukas RV, Hegi ME. Improving survival in molecularly selected glioblastoma. Lancet. 2019;393(10172):615-7.
17. Verhaak RG, Hoadley KA, Purdom E, Wang V, Qi Y, Wilkerson MD, et al. Integrated genomic analysis identifies clinically relevant subtypes of glioblastoma characterized by abnormalities in PDGFRA, IDH1, EGFR, and NF1. Cancer Cell. 2010;17(1):98-110.
18. Prager BC, Bhargava S, Mahadev V, Hubert CG, Rich JN. Glioblastoma Stem Cells: Driving Resilience through Chaos. Trends Cancer. 2020;6(3):223-35.
19. Singh SK, Hawkins C, Clarke ID, Squire JA, Bayani J, Hide T, et al. Identification of human brain tumour initiating cells. Nature. 2004;432(7015):396-401.
20. Bao S, Wu Q, McLendon RE, Hao Y, Shi Q, Hjelmeland AB, et al. Glioma stem cells promote radioresistance by preferential activation of the DNA damage response. Nature. 2006;444(7120):756-60.
21. Chen J, Li Y, Yu TS, McKay RM, Burns DK, Kernie SG, et al. A restricted cell population propagates glioblastoma growth after chemotherapy. Nature. 2012;488(7412):522-6.
22. Neftel C, Laffy J, Filbin MG, Hara T, Shore ME, Rahme GJ, et al. An Integrative Model of Cellular States, Plasticity, and Genetics for Glioblastoma. Cell. 2019;178(4):835-49 e21.
23. Ahmed SU, Carruthers R, Gilmour L, Yildirim S, Watts C, Chalmers AJ. Selective Inhibition of Parallel DNA Damage Response Pathways Optimizes Radiosensitization of Glioblastoma Stem-like Cells. Cancer Res. 2015;75(20):4416-28.
24. Fael Al-Mayhani TM, Ball SL, Zhao JW, Fawcett J, Ichimura K, Collins PV, et al. An efficient method for derivation and propagation of glioblastoma cell lines that conserves the molecular profile of their original tumours. J Neurosci Methods. 2009;176(2):192-9.
25. Ostrom QT, Cote DJ, Ascha M, Kruchko C, Barnholtz-Sloan JS. Adult Glioma Incidence and Survival by Race or Ethnicity in the United States From 2000 to 2014. JAMA Oncol. 2018;4(9):1254-62.
26. Rominiyi O, Vanderlinden A, Clenton SJ, Bridgewater C, Al-Tamimi Y, Collis SJ. Tumour treating fields therapy for glioblastoma: current advances and future directions. Br J Cancer. 2021;124(4):697-709.

27. Stupp R, Taillibert S, Kanner A, Read W, Steinberg D, Lhermitte B, et al. Effect of Tumor-Treating Fields Plus Maintenance Temozolomide vs Maintenance Temozolomide Alone on Survival in Patients With Glioblastoma: A Randomized Clinical Trial. JAMA. 2017;318(23):2306-16.
28. Chang E, Patel CB, Pohling C, Young C, Song J, Flores TA, et al. Tumor treating fields increases membrane permeability in glioblastoma cells. Cell Death Discov. 2018;4:113.
29. Mun EJ, Babiker HM, Weinberg U, Kirson ED, Von Hoff DD. Tumor-Treating Fields: A Fourth Modality in Cancer Treatment. Clin Cancer Res. 2018;24(2):266-75.
30. Voloshin T, Kaynan N, Davidi S, Porat Y, Shteingauz A, Schneiderman RS, et al. Tumor-treating fields (TTFields) induce immunogenic cell death resulting in enhanced antitumor efficacy when combined with anti-PD-1 therapy. Cancer Immunol Immunother. 2020;69(7):1191-204.
31. Giladi M, Munster M, Schneiderman RS, Voloshin T, Porat Y, Blat R, et al. Tumor treating fields (TTFields) delay DNA damage repair following radiation treatment of glioma cells. Radiat Oncol. 2017;12(1):206.
32. Karanam NK, Ding L, Aroumougame A, Story MD. Tumor treating fields cause replication stress and interfere with DNA replication fork maintenance: Implications for cancer therapy. Transl Res. 2020;217:33-46.
33. Karanam NK, Srinivasan K, Ding L, Sishc B, Saha D, Story MD. Tumor-treating fields elicit a conditional vulnerability to ionizing radiation via the downregulation of BRCA1 signaling and reduced DNA double-strand break repair capacity in non-small cell lung cancer cell lines. Cell Death Dis. 2017;8(3):e2711.
34. Elmore KB, Schaff LR. DNA Repair Mechanisms and Therapeutic Targets in Glioma. Curr Oncol Rep. 2021;23(8):87.
35. Rominiyi O, Collis SJ. DDRugging glioblastoma: understanding and targeting the DNA damage response to improve future therapies. Mol Oncol. 2022;16(1):11-41.
36. Curtin NJ. Targeting the DNA damage response for cancer therapy. Biochem Soc Trans. 2023.
37. Gomez-Roman N, Stevenson K, Gilmour L, Hamilton G, Chalmers AJ. A novel 3D human glioblastoma cell culture system for modeling drug and radiation responses. Neuro Oncol. 2017;19(2):229-41.
38. Hanna C, Kurian KM, Williams K, Watts C, Jackson A, Carruthers R, et al. Pharmacokinetics, safety, and tolerability of olaparib and temozolomide for recurrent glioblastoma: results of the phase I OPARATIC trial. Neuro Oncol. 2020;22(12):1840-50.
39. Frosina G, Profumo A, Marubbi D, Marcello D, Ravetti JL, Daga A. ATR kinase inhibitors NVP-BEZ235 and AZD6738 effectively penetrate the brain after systemic administration. Radiat Oncol. 2018;13(1):76.
40. Derby SJ, Chalmers AJ, Carruthers RD. Radiotherapy-Poly(ADP-ribose) Polymerase Inhibitor Combinations: Progress to Date. Semin Radiat Oncol. 2022;32(1):15-28.
41. Lesueur P, Lequesne J, Grellard JM, Dugue A, Coquan E, Brachet PE, et al. Phase I/IIa study of concomitant radiotherapy with olaparib and temozolomide in unresectable or partially resectable glioblastoma: OLA-TMZ-RTE-01 trial protocol. BMC Cancer. 2019;19(1):198.
42. She L, Su L, Shen L, Liu C. Retrospective Study of the Safety and Efficacy of Anlotinib Combined With Dose-Dense Temozolomide in Patients With Recurrent Glioblastoma. Front Oncol. 2021;11:687564.

43. Bradbury A, Hall S, Curtin N, Drew Y. Targeting ATR as Cancer Therapy: A new era for synthetic lethality and synergistic combinations? Pharmacol Ther. 2020;207:107450.
44. Karnitz LM, Zou L. Molecular Pathways: Targeting ATR in Cancer Therapy. Clin Cancer Res. 2015;21(21):4780-5.
45. Dillon MT, Boylan Z, Smith D, Guevara J, Mohammed K, Peckitt C, et al. PATRIOT: A phase I study to assess the tolerability, safety and biological effects of a specific ataxia telangiectasia and Rad3-related (ATR) inhibitor (AZD6738) as a single agent and in combination with palliative radiation therapy in patients with solid tumours. Clin Transl Radiat Oncol. 2018;12:16-20.
46. Gomez-Roman N, Chong MY, Chahal SK, Caragher SP, Jackson MR, Stevenson KH, et al. Radiation Responses of 2D and 3D Glioblastoma Cells: A Novel, 3D-specific Radioprotective Role of VEGF/Akt Signaling through Functional Activation of NHEJ. Mol Cancer Ther. 2020;19(2):575-89.
47. Pohling C, Nguyen H, Chang E, Schubert KE, Nie Y, Bashkirov V, et al. Current status of the preclinical evaluation of alternating electric fields as a form of cancer therapy. Bioelectrochemistry. 2023;149:108287.
48. Nickl V, Schulz E, Salvador E, Trautmann L, Diener L, Kessler AF, et al. Glioblastoma-Derived Three-Dimensional Ex Vivo Models to Evaluate Effects and Efficacy of Tumor Treating Fields (TTFields). Cancers (Basel). 2022;14(21).

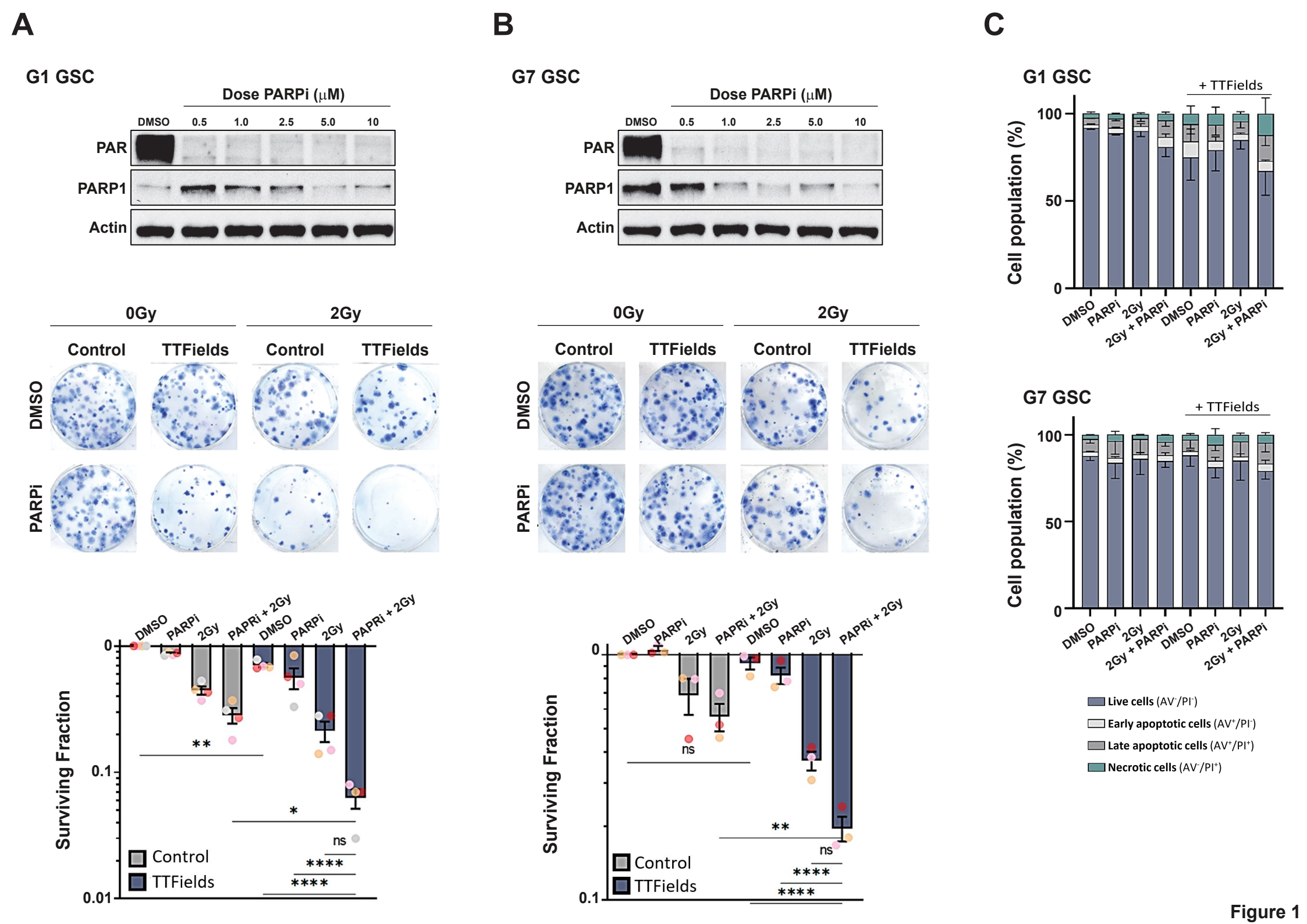
A
G1 GSC
Dose PARPi (μM)
DMSO
0.5
1.0
2.5
5.0
10
PAR
PARP1
Actin
0Gy
2Gy
Control
TTFields
Control
TTFields
DMSO
PARPi
DMSO
PARPi
2Gy
PARPi + 2Gy
Surviving Fraction
0
0.1
0.01
**
*
ns
****
****
Control
TTFields
B
G7 GSC
Dose PARPi (μM)
DMSO
0.5
1.0
2.5
5.0
10
PAR
PARP1
Actin
0Gy
2Gy
Control
TTFields
Control
TTFields
DMSO
PARPi
DMSO
PARPi
2Gy
PARPi + 2Gy
Surviving Fraction
0
0.1
ns
**
ns
****
****
Control
TTFields
C
G1 GSC
+ TTFields
Cell population (%)
100
50
0
DMSO
PARPi
2Gy
2Gy + PARPi
DMSO
PARPi
2Gy
2Gy + PARPi
G7 GSC
+ TTFields
Cell population (%)
100
50
0
DMSO
PARPi
2Gy
2Gy + PARPi
DMSO
PARPi
2Gy
2Gy + PARPi
Live cells (AV-/PI-)
Early apoptotic cells (AV+/PI-)
Late apoptotic cells (AV+/PI+)
Necrotic cells (AV-/PI+)

Figure 1

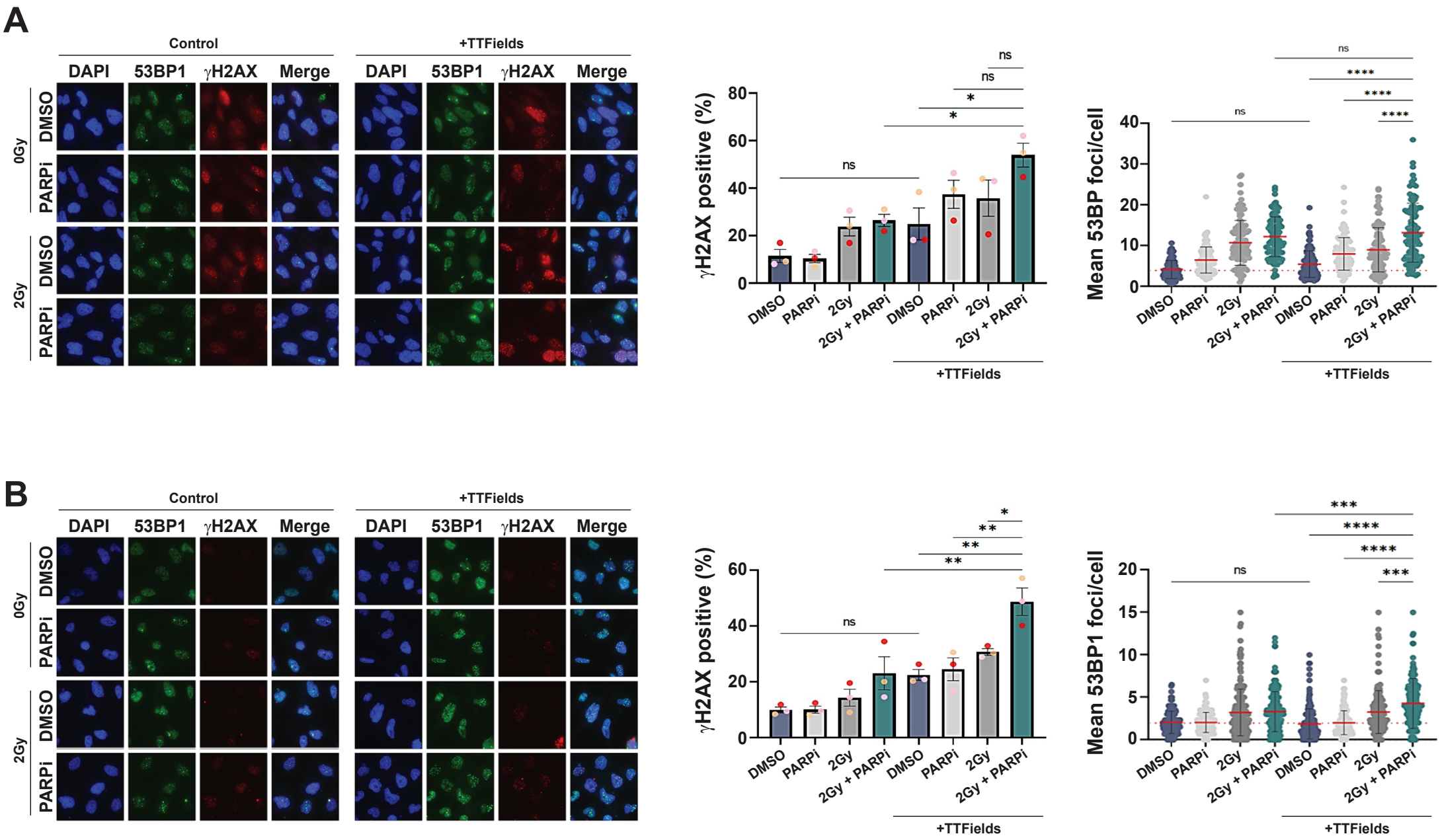
A
Control
+TTFields
DAPI
53BP1
γH2AX
Merge
0Gy
2Gy
DMSO
PARPi
γH2AX positive (%)
Mean 53BP foci/cell
ns
*
**
***
****
2Gy + PARPi
+TTFields
B
Mean 53BP1 foci/cell

Figure 2

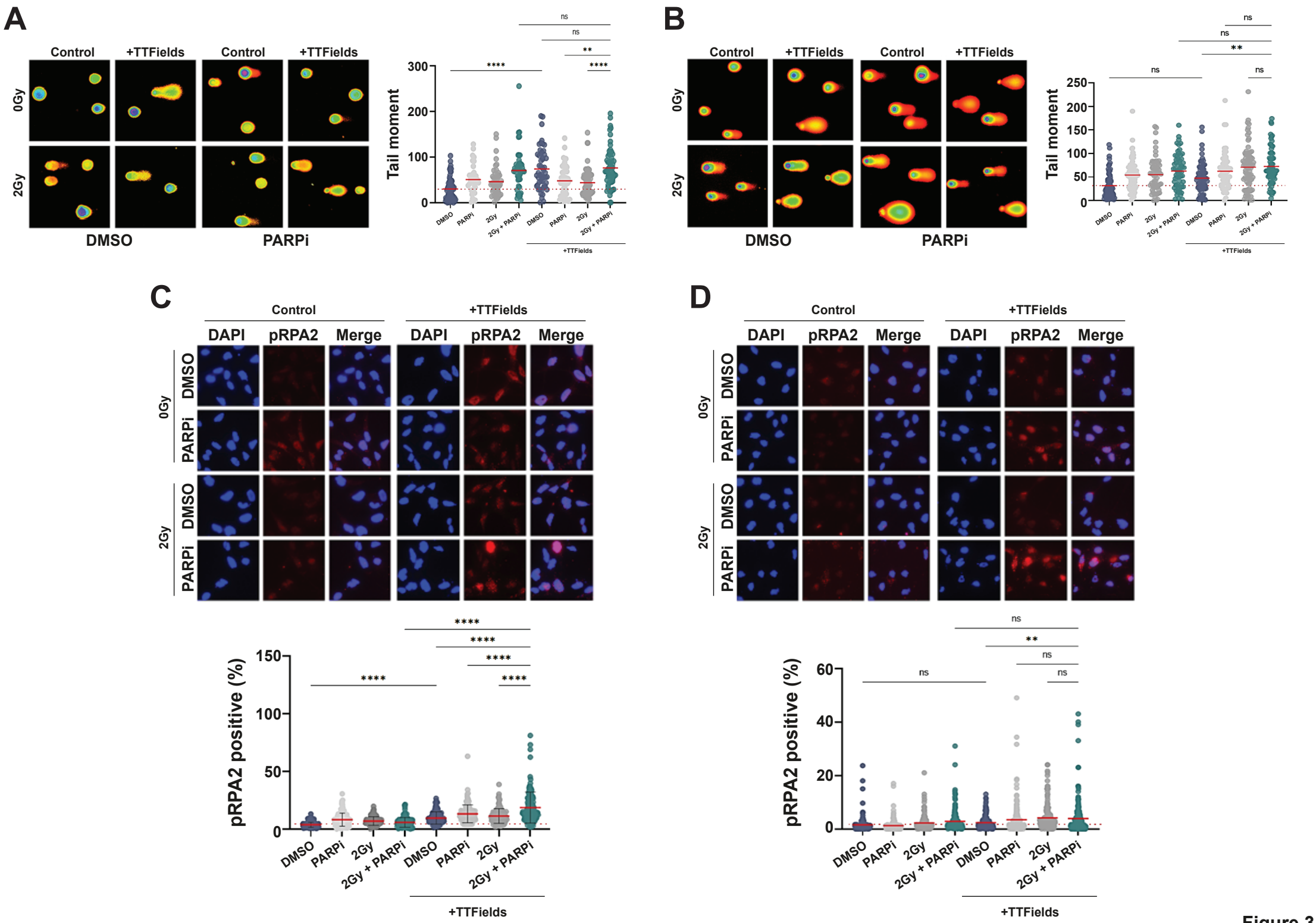
A
Control
+TTFields
Control
+TTFields
0Gy
2Gy
DMSO
PARPi
Tail moment
300
200
100
0
ns
ns
**
****
****
DMSO
PARPi
2Gy
2Gy + PARPi
DMSO
PARPi
2Gy
2Gy + PARPi
+TTFields
B
Control
+TTFields
Control
+TTFields
0Gy
2Gy
DMSO
PARPi
Tail moment
250
200
150
100
50
0
ns
ns
**
ns
ns
DMSO
PARPi
2Gy
2Gy + PARPi
DMSO
PARPi
2Gy
2Gy + PARPi
+TTFields
C
Control
+TTFields
DAPI
pRPA2
Merge
DAPI
pRPA2
Merge
0Gy
2Gy
DMSO
PARPi
DMSO
PARPi
pRPA2 positive (%)
150
100
50
0
****
****
****
****
****
DMSO
PARPi
2Gy
2Gy + PARPi
DMSO
PARPi
2Gy
2Gy + PARPi
+TTFields
D
Control
+TTFields
DAPI
pRPA2
Merge
DAPI
pRPA2
Merge
0Gy
2Gy
DMSO
PARPi
DMSO
PARPi
pRPA2 positive (%)
60
40
20
0
ns
**
ns
ns
ns
DMSO
PARPi
2Gy
2Gy + PARPi
DMSO
PARPi
2Gy
2Gy + PARPi
+TTFields

Figure 3

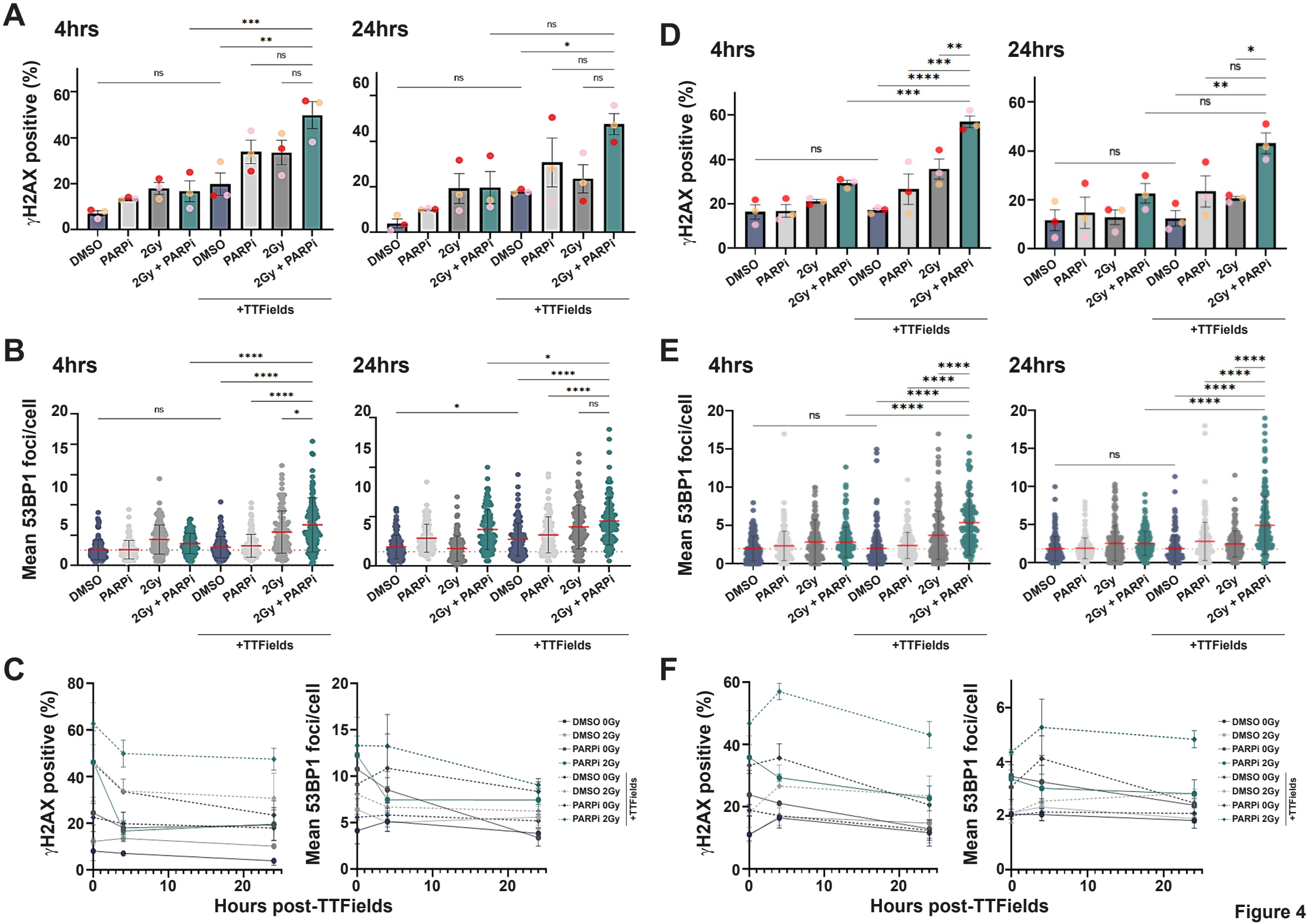
A
4hrs
24hrs
γH2AX positive (%)
DMSO
PARPi
2Gy
2Gy + PARPi
+TTFields
B
Mean 53BP1 foci/cell
D
E
C
F
Hours post-TTFields
DMSO 0Gy
DMSO 2Gy
PARPi 0Gy
PARPi 2Gy
+TTFields

Figure 4

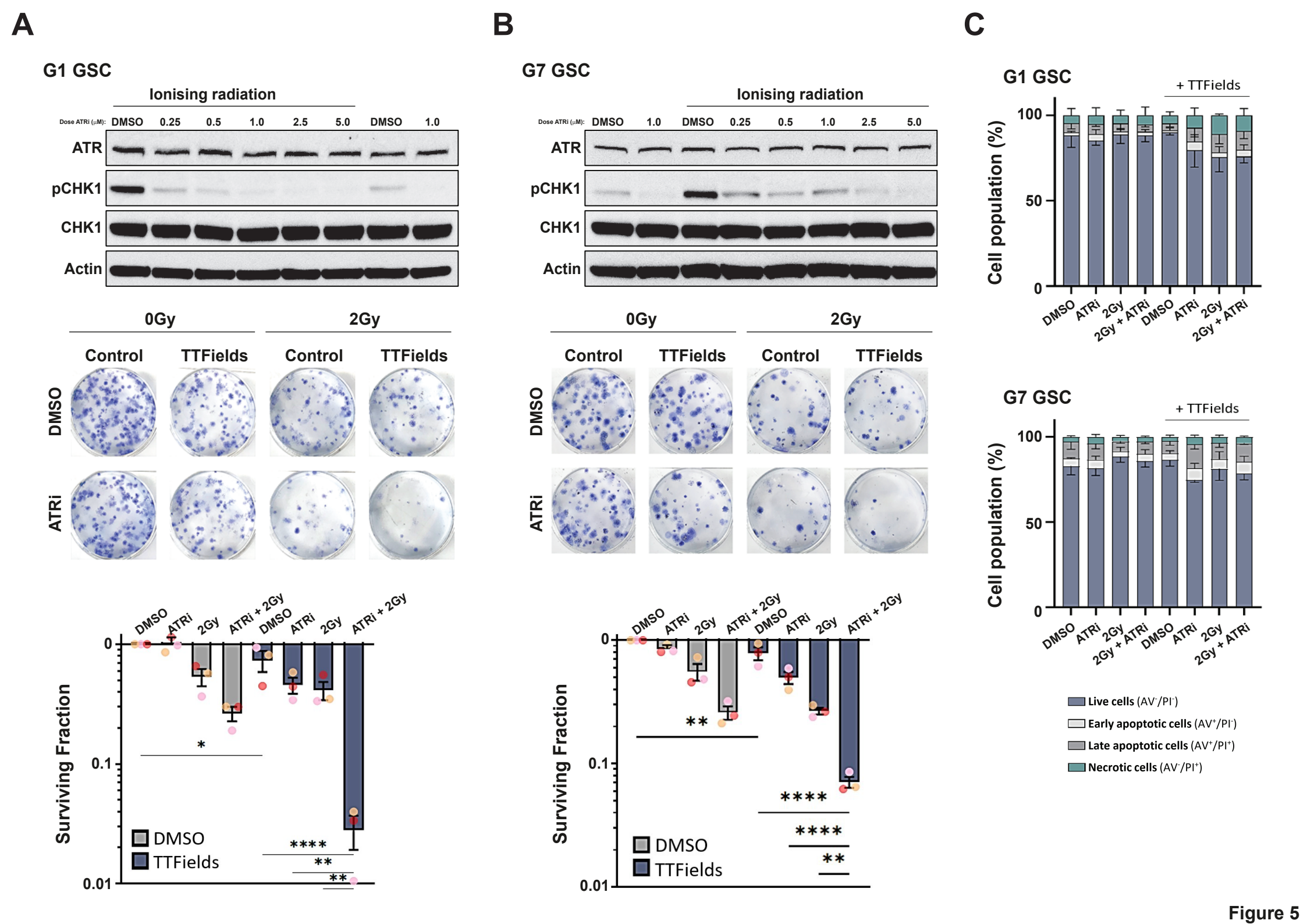
A
G1 GSC
Ionising radiation
Dose ATRi (μM): DMSO 0.25 0.5 1.0 2.5 5.0 DMSO 1.0
ATR
pCHK1
CHK1
Actin
0Gy
2Gy
Control
TTFields
DMSO
ATRi
Surviving Fraction
DMSO
ATRi
2Gy
ATRi + 2Gy
TTFields
B
G7 GSC
C
G1 GSC
+ TTFields
Cell population (%)
G7 GSC
Live cells (AV-/PI-)
Early apoptotic cells (AV+/PI-)
Late apoptotic cells (AV+/PI+)
Necrotic cells (AV-/PI+)

Figure 5

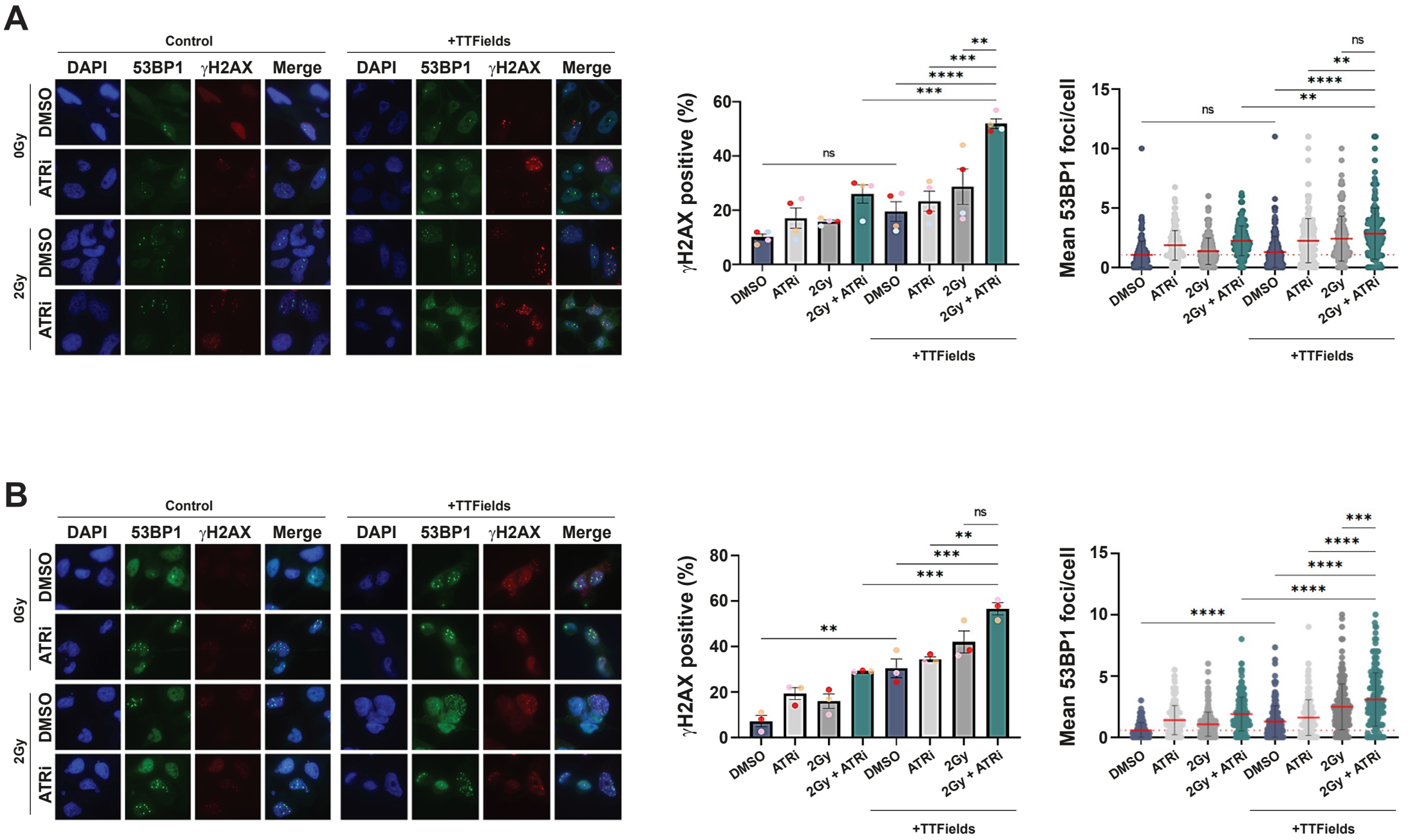
A
Control
+TTFields
DAPI
53BP1
γH2AX
Merge
0Gy
2Gy
DMSO
ATRi
γH2AX positive (%)
Mean 53BP1 foci/cell
ns
**
***
****
DMSO
ATRi
2Gy
2Gy + ATRi
+TTFields
B
Control
+TTFields
DAPI
53BP1
γH2AX
Merge
0Gy
2Gy
DMSO
ATRi
γH2AX positive (%)
Mean 53BP1 foci/cell
ns
**
***
****
DMSO
ATRi
2Gy
2Gy + ATRi
+TTFields

Figure 6

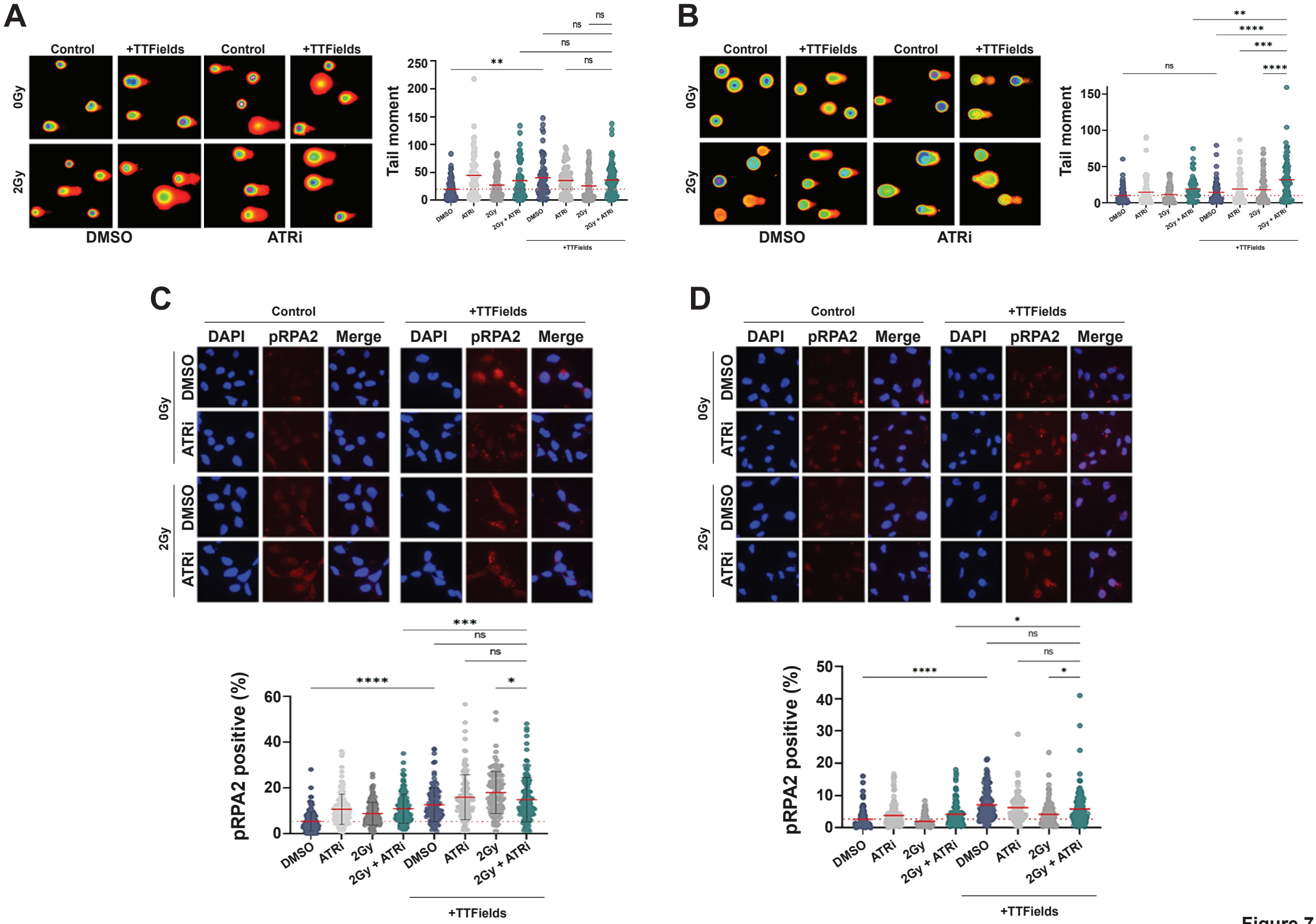
A
Control
+TTFields
Control
+TTFields
0Gy
2Gy
DMSO
ATRi
Tail moment
ns
**
ns
ns
ns
DMSO
ATRi
2Gy
2Gy + ATRi
+TTFields
B
Control
+TTFields
Control
+TTFields
0Gy
2Gy
DMSO
ATRi
Tail moment
**
****
***
ns
****
C
Control
+TTFields
DAPI
pRPA2
Merge
DAPI
pRPA2
Merge
0Gy
2Gy
DMSO
ATRi
pRPA2 positive (%)
***
ns
ns
****
*
+TTFields
D
Control
+TTFields
DAPI
pRPA2
Merge
DAPI
pRPA2
Merge
0Gy
2Gy
DMSO
ATRi
pRPA2 positive (%)
*
ns
ns
****
*
+TTFields

Figure 7

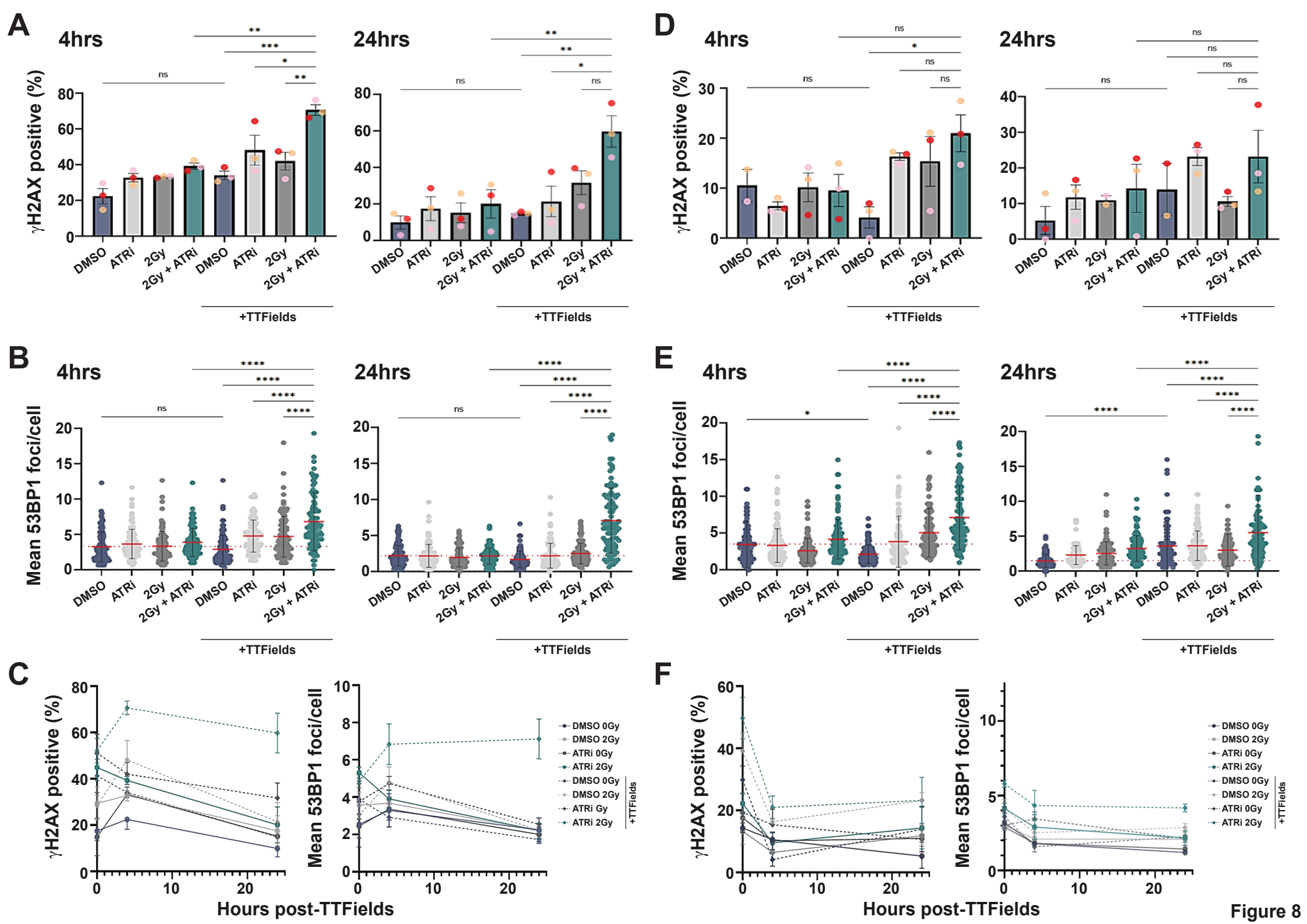
A
4hrs
24hrs
γH2AX positive (%)
DMSO
ATRi
2Gy
2Gy + ATRi
+TTFields
B
Mean 53BP1 foci/cell
C
Hours post-TTFields
DMSO 0Gy
DMSO 2Gy
ATRi 0Gy
ATRi 2Gy
ATRi Gy
D
E
F
Figure 8

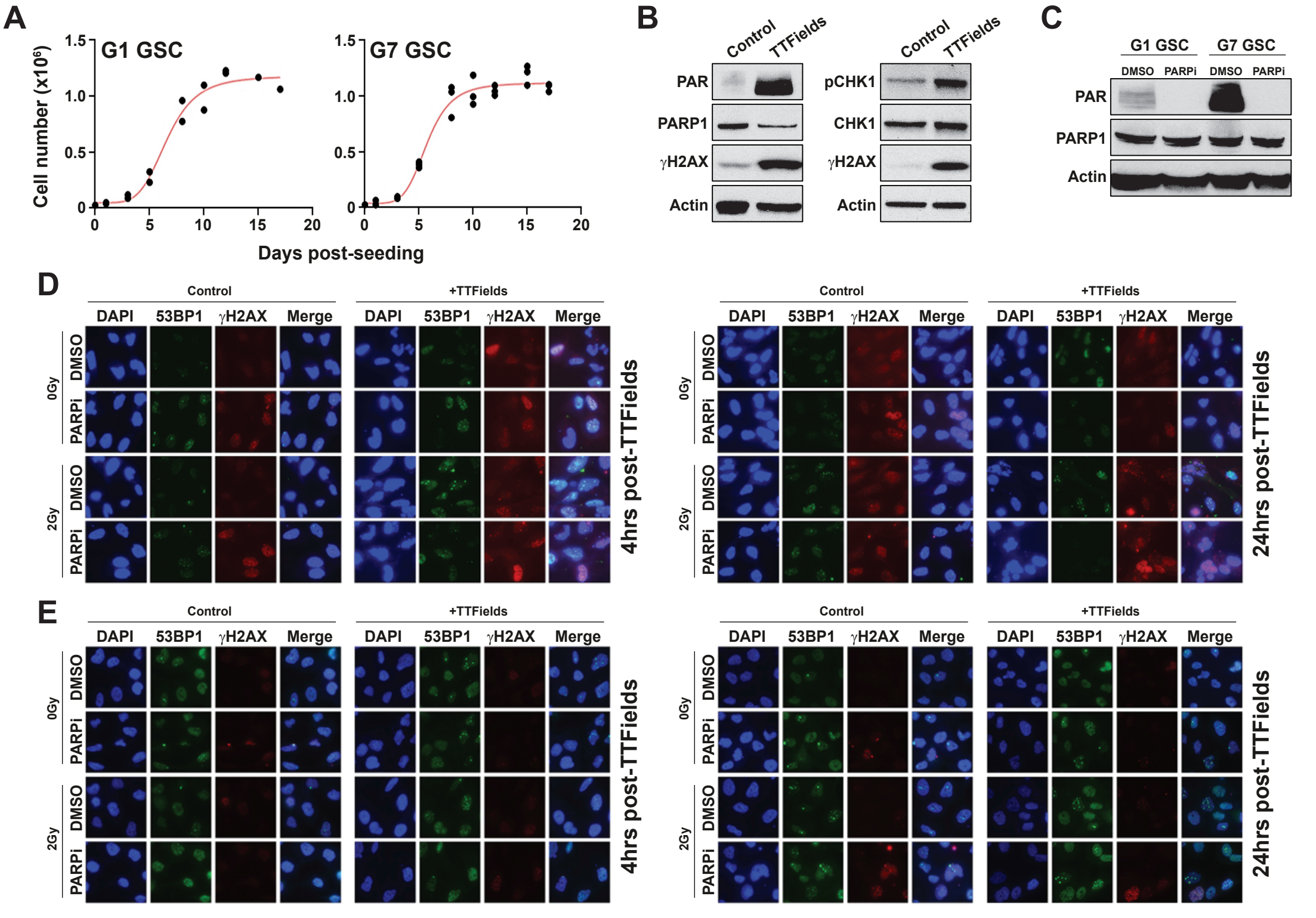

Supplementary Figure S1

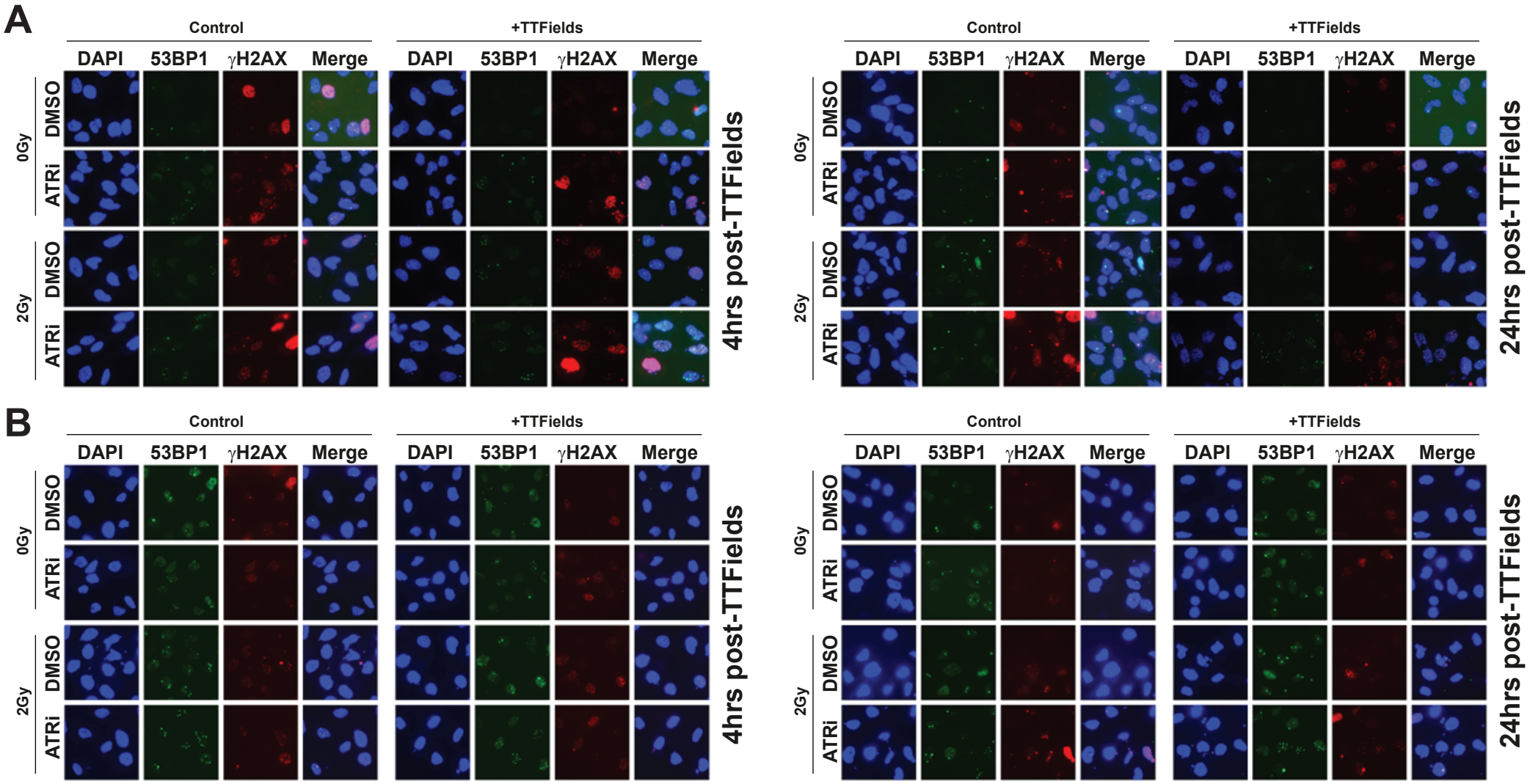

Supplementary Figure S2

8.2 Appendix B

BJC British Journal of Cancer

www.nature.com/bjc

REVIEW ARTICLE

Tumour treating fields therapy for glioblastoma: current advances and future directions

Ola Rominiyi[1,2], Aurelie Vanderlinden[1], Susan Jane Clenton[3], Caroline Bridgewater[3], Yahia Al-Tamimi[2] and Spencer James Collis[1]

Glioblastoma multiforme (GBM) is the most common primary brain tumour in adults and continues to portend poor survival, despite multimodal treatment using surgery and chemoradiotherapy. The addition of tumour-treating fields (TTFields)—an approach in which alternating electrical fields exert biophysical force on charged and polarisable molecules known as dipoles—to standard therapy, has been shown to extend survival for patients with newly diagnosed GBM, recurrent GBM and mesothelioma, leading to the clinical approval of this approach by the FDA. TTFields represent a non-invasive anticancer modality consisting of low-intensity (1–3 V/cm), intermediate-frequency (100–300 kHz), alternating electric fields delivered via cutaneous transducer arrays configured to provide optimal tumour-site coverage. Although TTFields were initially demonstrated to inhibit cancer cell proliferation by interfering with mitotic apparatus, it is becoming increasingly clear that TTFields show a broad mechanism of action by disrupting a multitude of biological processes, including DNA repair, cell permeability and immunological responses, to elicit therapeutic effects. This review describes advances in our current understanding of the mechanisms by which TTFields mediate anticancer effects. Additionally, we summarise the landscape of TTFields clinical trials across various cancers and consider how emerging preclinical data might inform future clinical applications for TTFields.

British Journal of Cancer (2020) 124:697–709; https://doi.org/10.1038/s41416-020-01136-5

BACKGROUND

Glioblastoma (GBM) is the most common and aggressive type of primary brain tumour, causing roughly 2500 deaths each year in the United Kingdom[1] and the majority of ~200,000 deaths related to tumours of the central nervous system worldwide each year.[2,3] The current standard of care for patients with GBM consists of maximal surgical resection followed by radiotherapy and chemotherapy with temozolomide (TMZ). However, even with this combination of treatment, the median overall survival (OS) is around 10–16 months, with fewer than 10% of patients surviving for 5 years or more from the time of diagnosis,[4,5] and this scenario has improved very little over the past four decades.[6] There is, therefore, a critical need for more effective treatment strategies to improve outcomes for patients faced with this devastating diagnosis.

Tumour-treating fields (TTFields) represent an emerging non-invasive anticancer therapeutic modality that involves the transcutaneous delivery of low-intensity (1–3 V/cm), intermediate-frequency (100–300 kHz), alternating electric fields (the approach is also known as alternating electric field therapy) that exert biophysical force on charged and polarisable molecules known as dipoles. The beneficial effects of TTFields therapy are influenced by treatment duration (with evidence that application >18 h/day improves survival[7]), electrical field intensity (where increased intensity confers greater reduction in cell proliferation) and electrical field frequency,[8] which varies between cancer types—in the case of glioma cells, TTFields are clinically delivered at an optimum frequency of 200 kHz.[9]

The frequency of the alternating field has also been shown to provide different biological effects. Low-frequency electric fields (<1 kHz) influence cell membrane polarisation and can alter the behaviour of excitable tissue, such as action potential firing in neuronal cells.[10] On the other hand, high-frequency fields (>500 kHz) cause charged and/or polar molecules inside cells to vibrate, creating friction and causing kinetic energy to transfer between molecules, which can be radiated out as thermal energy, leading to tissue heating.[11] Intermediate-frequency alternating electric fields (100–500 kHz) do not generate enough thermal energy to cause significant tissue heating and alternate too quickly to trigger action potential firing, and were consequently originally thought to lack any beneficial effects.[12] However, Kirson et al. demonstrated that low-intensity alternating electric fields delivered at 100–300 kHz successfully inhibited cancer cell growth, both in vitro (using cell lines derived from melanoma, glioma, lung, prostate and breast cancer) and in vivo, by interfering with microtubule polymerisation during mitosis.[9] These findings led to the first pilot study (EF-07) in GBM patients launched in 2004[13] and, eventually, to the development of TTFields as a strategy for treating cancer (Fig. 1).

It has subsequently emerged that, in addition to its antimitotic effects, TTFields can influence a spectrum of biological processes, including autophagy, DNA repair, antitumour immunity and tumour cell migration, in addition to altering cell membrane, and potentially blood–brain barrier (BBB) permeability. This review examines the emergence of TTFields as a therapeutic modality to

[1]Weston Park Cancer Centre, Department of Oncology & Metabolism, The University of Sheffield Medical School, Sheffield, UK; [2]Department of Neurosurgery, Royal Hallamshire Hospital, Sheffield Teaching Hospitals NHS Foundation Trust, Sheffield, UK and [3]Department of Clinical Oncology, Weston Park Hospital, Sheffield Teaching Hospitals NHS Foundation Trust, Sheffield, UK

Correspondence: Ola Rominiyi (o.rominiyi@sheffield.ac.uk) or Spencer James Collis (s.collis@sheffield.ac.uk)

These authors contributed equally: Ola Rominiyi, Aurelie Vanderlinden

Received: 2 April 2020 Revised: 16 September 2020 Accepted: 5 October 2020
Published online: 4 November 2020

Published by Springer Nature on behalf of Cancer Research UK

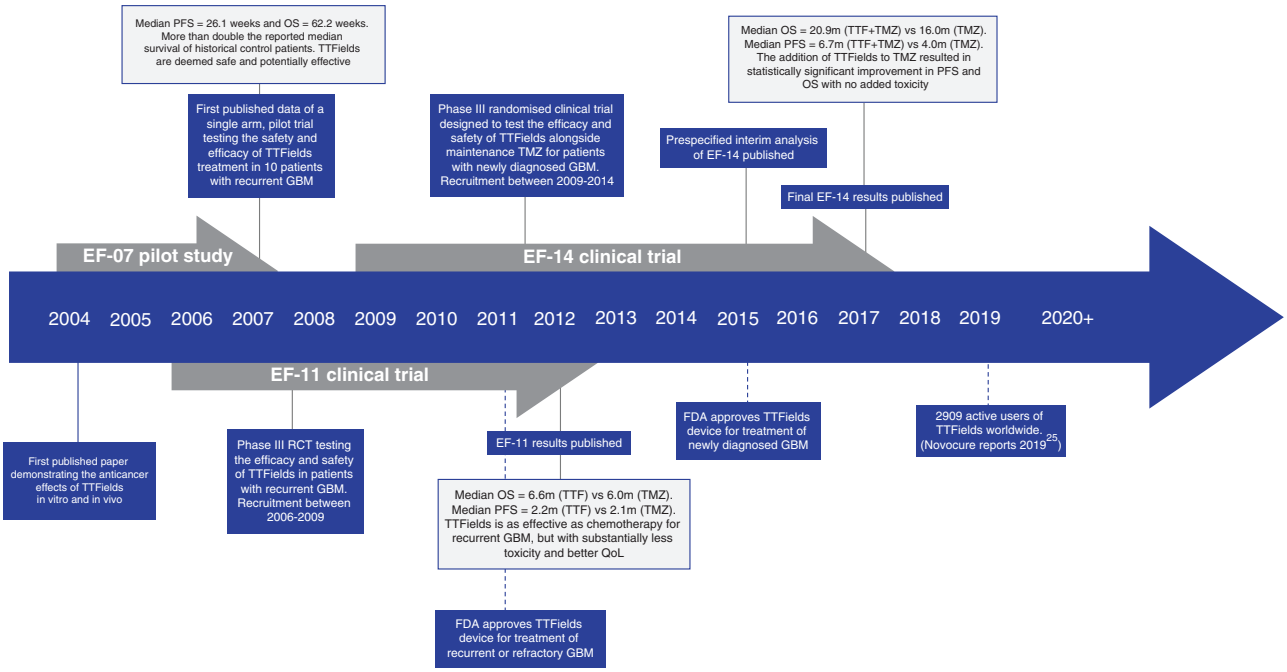

Fig. 1 Historical timeline of the emergence of TTFields as novel therapy for GBM patients. In 2004, the first paper demonstrating the anticancer effects of TTFields in vitro and in vivo was published.[9] Following these promising preclinical data, a number of clinical trials investigating the safety and efficacy of TTFields for the treatment of GBM were completed (details described at each relevant date), leading to the approval in 2011 and 2015 of TTFields for the treatment of recurrent and newly diagnosed GBM, respectively.

treat GBM and highlights molecular mechanisms that are likely to contribute to its anticancer efficacy. We also summarise the current landscape of TTFields clinical trials across various cancer types and consider how emerging preclinical data might inform future applications for TTFields in the clinic.

TTFIELDS AS AN EMERGING THERAPEUTIC MODALITY

The EF-14 trial represents a landmark study, as it was the first trial in a decade to show an increase in OS for patients with newly diagnosed GBM since the addition of temozolomide (TMZ) chemotherapy to standard care.[14–17] Following randomisation at the end of chemoradiotherapy, the addition of TTFields to maintenance of TMZ chemotherapy significantly increased median OS by 4.9 months (20.9 vs 16.0 months with TMZ alone).[16,17] Importantly, the addition of TTFields was not associated with any significant increase in rates of systemic adverse events (48% vs 44% with TMZ alone, $P = 0.58$), and the continuous usage of TTFields appears to be associated with maintained or enhanced quality of life.[18–20] Data from the EF-14 trial led to the approval of TTFields by the FDA in 2015 for newly diagnosed GBM.[21]

TTFields delivery

The most widely used clinical TTFields delivery system, Optune (Novocure™), consists of four transducer arrays, a field generator and a power source (shown in Fig. 2). For GBM, the four transducer arrays are attached in pairs, orthogonally to the patient's scalp. The patient's head must be shaved consistently to allow optimal contact of the transducer arrays with the scalp, and optimal array positioning is determined using NovoTAL™ (Novocure Ltd., Haifa, Israel) simulation software based on the location of the tumour and the size and shape of the patient's head.[22] Each transducer array is made up of nine ceramic discs, each with a superficial hydrogel coating to improve conductivity with the skin. The field generator delivers alternating electric fields through the transducer arrays across the brain and to the tumour site.

The main adverse event of TTFields is irritant or allergic contact dermatitis at the site of transducer array attachment resulting from prolonged exposure to sweat, hydrogel, adhesive or a combination of these factors. However, skin complications are usually of low grade (grade 1–2 adverse events) and can easily be managed by topical corticosteroids, modification of array positioning and/or protecting the skin with sterile dressing pads.[23]

The cost-effectiveness of TTFields

Important financial considerations are associated with incorporating TTFields therapy into the standard of care for GBM patients. Presently, Novocure, the sole producer of the therapeutic TTFields delivery systems, rents Optune to patients for a total monthly cost of around $21,000 (subject to discounts negotiated by healthcare providers/payers).[24] This cost covers the TTFields delivery system, and includes transducer arrays, array layout planning, patient/physician training and 24-h technical support.[25] Additional expenses associated with implementing TTFields might include additional staff and training,[22] and costs associated with managing treatment-related morbidities.[26]

There have been three major studies estimating the costs associated with adding TTFields to the standard-of-care therapy for GBM, all of which use EF-14 trial data. Bernard-Arnoux et al.[27] used interim EF-14 data, while Connock et al.[28] and Guzauskas et al.[29] used the trial's final results. During economical modelling, the assumptions made by Bernard-Arnoux et al. and Connock et al. were based on a French National Health Insurance perspective, while analyses by Guzauskas et al. were based on the US healthcare perspective. All three studies relied on the full list price of TTFields therapy and therefore do not incorporate potential discounts negotiated by healthcare payers.

Bernard-Arnoux et al. estimated 0.34 life years gained (LYG) from the addition of TTFields to maintenance of TMZ, with an added cost of €185,476, while Connock et al. estimated 0.604 LYG with an added cost of €453,848. These two studies then estimated the incremental cost-effectiveness ratio (ICER, a summary measure that compares the economic value of a particular intervention

Fig. 2 The Optune system. Left: the Optune TTFields delivery system consists of four transducer arrays, a field generator and a power source. Right: a patient wearing the Optune system. Images taken from Novocure, 2020.[36]

with another expressed as cost per LYG) to be €549,909 and €510,273, respectively. Both studies analysed survival using statistical models that were unable to account for changing (decreasing) hazard rates as patients live longer. This is an important limitation since epidemiological data suggest that as a patient survives longer, the ongoing probability of death reduces. For example, analysis of the US SEER database demonstrated patients alive 5 years after diagnosis had a 70.4% probability of surviving to 10 years post diagnosis.[30] Therefore, although data from the EF-14 trial suggest that addition of TTFields may increase 5-year OS from 5% to 13%, the studies by Bernard-Arnoux et al. and Connock et al. did not fully account for the impact of long-term survivors beyond the trial period. This resulted in reported incremental lifetime survival benefits (the LYG) close to the median OS benefit observed within the trial period. By contrast, Guzauskas et al. integrated EF-14 data with external GBM epidemiology data and US life expectancy data to estimate long-term conditional survival (similar integration of oncology trial and epidemiological data to model long-term survival has previously been considered by NICE in its decision to licence ipilimumab for metastatic melanoma[31,32]). Consequently, the Guzauskas model estimates 1.25 LYG from adding TTFields to TMZ and estimates a corresponding ICER of $150,452.

As such, Japan, Israel and Sweden have included TTFields within their national reimbursement systems following cost-effectiveness evaluations, whilst Germany has approved TTFields for national reimbursement based on a clinical comparative effectiveness review without respect to costs. As noted above, the method of estimating future survival beyond the time observed in the trial is a critical assumption within any model. Healthcare payers that prefer the extrapolated constant hazard rate models of Bernard-Arnoux and Connock might not be willing to adopt the therapy. Adoption by healthcare systems that include considerations of cost-effectiveness as a major driver of decision-making, such as the NHS in the United Kingdom or the Australian and Canadian systems,[33,34] is likely to depend on how those systems choose to model long-term survival.

Clinical availability of TTFields

Although the number of patients receiving TTFields has increased since this approach was first approved for use in GBM patients (2909 patients worldwide in 2019 compared with 605 patients in 2015),[35,36] it is thought that many more patients with approved indications could benefit from TTFields treatment (on average, 30% of eligible GBM patients currently receive TTFields in countries where the therapy is available).[29,37] Substantial geographic variation in TTFields availability exists in the clinical usage of Optune, with the majority of patients who receive TTFields residing in the United States (roughly twice as many patients receive TTFields in the United States compared with the rest of the world).[37] As highlighted above, high treatment costs and differences in long-term survival modelling represent major drivers of geographical variation in the usage of TTFields worldwide. Notably, some reluctance to adopt TTFields within the neuro-oncology community also exists; this might be fuelled by a range of factors. Firstly, the high cost of TTFields therapy (discussed above) may represent a barrier to adoption at an individual or national level. Secondly, valid concerns have been raised that patients in the control group of the EF-14 trial did not receive any placebo treatment,[16] such as via a sham TTFields device. However, requiring patients to wear a sham device (ideally > 18 h per day) with no potential for benefit would likely present its own ethical challenges,[38] and objective endpoints such as OS (which demonstrated survival benefit with TTFields in the EF-14 trial) are unlikely to be influenced substantially by the lack of placebo or blinding. Thirdly, a perceived burden of patients having to carry and wear the device with high compliance may contribute to reluctance to adopt or prescribe TTFields; nevertheless, objective data suggest that quality of life in these patients is not reduced.[19,20] Critically, much reluctance to adopt TTFields may stem from the fact that the mechanisms of action for TTFields are currently less well-defined relative to more established therapeutic modalities.[39] It can be expected that, as technologies continue to evolve and as competing products enter the market, TTFields might become increasingly affordable. Additionally, any enhancement of the therapeutic efficacy of TTFields might also improve the ICER and facilitate TTFields uptake by healthcare systems that currently do not deem the technology to be cost-effective, including the NHS (NICE[40]). To improve the efficacy of TTFields, an improved understanding of the diverse mechanistic effects of this therapy and how these effects can be exploited to increase the therapeutic index of TTFields-based regimens is required.

MOLECULAR MECHANISMS FOR THE ANTICANCER EFFECTS OF TTFIELDS

Increasing evidence suggests the therapeutic effects of TTFields may be associated with a diverse range of intracellular mechanisms. This is perhaps unsurprising considering the abundance of a broad range of charged and polarisable molecules within cells upon which TTFields could exert biophysical forces. Although the spectrum of effects elicited remains incompletely understood, emerging data suggest that in addition to the antimitotic effects of TTFields, a multitude of biological processes, including DNA repair, autophagy, cell migration, permeability and immunological responses, are perturbed by TTFields to elicit anticancer effects. A summary of the reported molecular

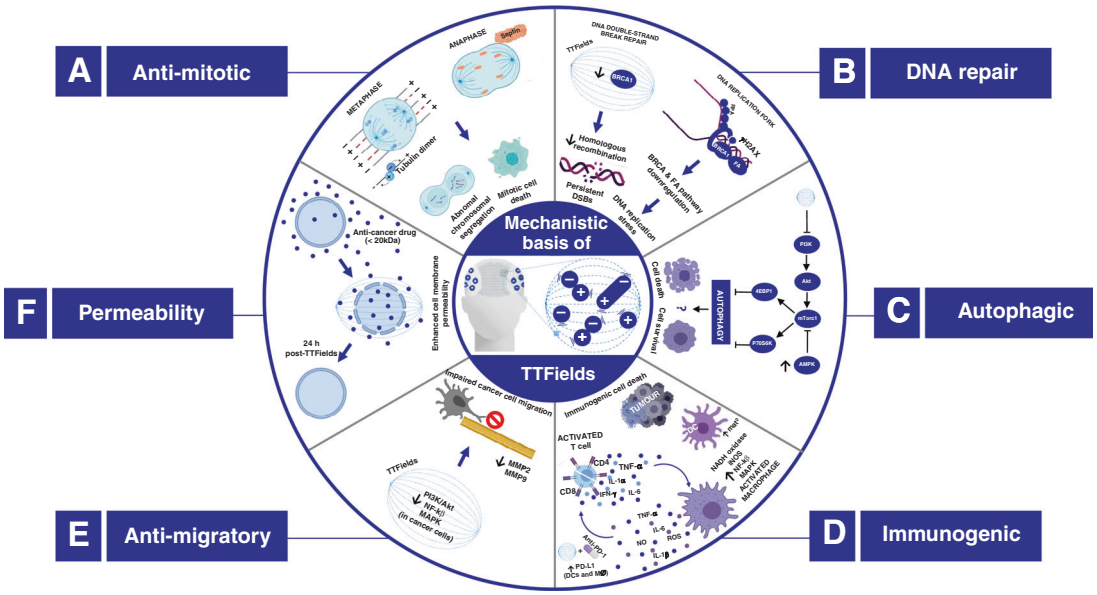

Fig. 3 Summary of the mechanisms of action of TTFields. Low-intensity, intermediate-frequency, alternating electrical fields exert biophysical forces on a variety of charged and polarisable molecules to elicit a spectrum of biological effects. **A** Antimitotic effects: during metaphase, the electric fields are uniform, causing dipolar molecules, such as tubulin, to align with the field. TTFields therefore interfere with tubulin polymerisation and depolymerisation during metaphase. At anaphase, TTFields prevent localisation of septin proteins to the mitotic spindle and inhibit assembly of the septin complex into a ring structure at the cleavage furrow. During cytokinesis, the electric fields are non-uniform, with the fields converging on the cleavage furrow, where the field intensity is the highest. As a result, strong dielectric force is applied on polarisable objects, pushing them towards the high-intensity region. Together, these effects result in abnormal chromosome segregation and/or cell death. **B** DNA repair. TTFields have been shown to downregulate BRCA and Fanconi anaemia (FA) pathway genes, which have been associated with increased replication stress and increased double-strand break (DSB) formation. Additionally, homologous recombination repair (HRR) is impaired by TTFields, resulting in reduced efficiency of DSB repair. **C** Autophagy. TTFields have been suggested to prevent the inhibitory effects of the PI3K/Akt/mTORC1 signalling pathway on autophagy, resulting in increased activation of autophagy with TTFields therapy. Further studies are needed to ascertain whether autophagy is activated as a cell survival or cell death signal in response to TTFields. **D** Antitumour immunity. TTFields stimulates macrophages (Mø) to secrete reactive oxygen species (ROS), nitric oxide (NO) and proinflammatory cytokines such as interleukin (IL)-1β, tumour necrosis factor (TNF)-α and IL-6. Additionally, TTFields promote immunogenic cell death via dendritic cell (DC) recruitment and maturation (mat), ultimately leading to an increase in the accumulation of CD4 + and CD8 + T cells at the tumour site. The combination of TTFields with anti-PD-1 therapy might enhance PD-L1 expression in infiltrating DCs and macrophages to further enhance antitumour immunity. **E** Anti-migratory. TTFields reduce the capacity of cancer cells for migration and invasion through nuclear factor (NF)-κB-, mitogen-activated protein kinase (MAPK)- and phosphatidylinositol 3-kinase (PI3K)/Akt-dependent mechanisms. **F** Cell membrane permeability. TTFields increase cell membrane permeability by increasing the number and size of holes in the cell membrane, thereby potentially enhancing sensitivity to chemotherapeutic drugs.

mechanisms by which TTFields impacts tumour cell toxicity is shown in Fig. 3.

Antimitotic effects of TTFields

The principle mechanisms of action through which TTFields application is thought to mediate its therapeutic effects are antimitotic. The rapidly dividing nature of cancer cells, relative to normal tissue, underlies their specific sensitivity to TTFields. Furthermore, comparison of TTFields susceptibility between various cancer cell lines demonstrates an inverse correlation between the typical doubling time of cell lines and TTFields-induced cell death.[41] However, the effects of TTFields are also dependent on the specific frequency of alternating electric fields applied;[9] therefore, calibration of an optimal frequency to exert cytotoxic effects on a specific cancer cell type within the intermediate range (100–300 kHz) is also postulated to facilitate the cancer-specific effects of TTFields on mitosis. During chromosome segregation, chromosomes align at the metaphase plate, and sister chromatids are separated and pulled to opposite poles of the cell by the mitotic spindle. The mitotic spindle is formed from an array of microtubules, comprising tubulin polymers, with each tubulin subunit possessing a relatively high dipole moment.[42] When TTFields are applied, tubulin dimers align with the electric field, which interferes with the normal microtubule polymerisation–depolymerisation process during mitosis. This, in turn, results in abnormal spindle formation, which can lead to cellular arrest in mitosis for several hours, eventually leading to mitotic cell death. In other cases, failure of the spindle assembly checkpoint (SAC),[43,44] a mitotic checkpoint ensuring that all chromosomes are properly attached to the mitotic spindle before proceeding through to anaphase to enable correct chromosome segregation,[45] might lead to aberrant metaphase exit, abnormal chromosome segregation, multinucleation and consequently cell death.[43,46] Interestingly, pharmacological inhibition of the SAC key regulator monopolar spindle 1 (MPS1) kinase using the inhibitor IN-3 in combination with TTFields has been demonstrated to increase nuclear abnormalities, G2/M cell-cycle arrest and apoptotic cell death relative to either treatment used as a single therapy in glioblastoma cell lines.[47] Furthermore, use of this combination (TTFields + IN-3) in cultured GBM cells provided a durable therapeutic response for 72 h following the cessation of TTFields, highlighting the potential clinical utility of such combinatorial strategies to resist tumour regrowth during breaks in the delivery of TTFields therapy to patients (e.g., breaks in therapy due to TTFields-associated skin toxicity).[47] A Phase 1 clinical trial of the potent MPS1 inhibitor BAY1217389[48] (NCT02366949) has recently been completed; therefore, future clinical studies assessing the use of SAC inhibition to enhance the effectiveness of TTFields would be feasible.

With TTFields, although the electric field is uniform in non-replicating cells, it is non-uniform in dividing cells because of the ‘hourglass’ structure adopted by dividing cells after anaphase.

Non-uniform electric fields generate forces that cause dielectrophoresis, in which the field intensity is increased at the furrow during cytokinesis, causing charged and/or dipolar molecules to accumulate here.[13] During cytokinesis, the mitotic septin complex (comprising septins 2, 6 and 7) is normally recruited to the spindle midline and cleavage furrow at anaphase, and assembles into a ring structure, where it positions the cleavage furrow to limit contraction to the equatorial plane and restricts determinants to separate cortical domains.[49,50] The septin complex is also involved in cross-linking actin, non-muscle myosin II and RhoA, facilitating actin-based myosin contraction, which directs cleavage furrow ingression and provides the contractile forces required to physically separate the forming daughter cells from each other.[50–52] TTFields therapy has been shown to prevent the localisation of the mitotic septin complex to the spindle midline and cleavage furrow at anaphase due to TTFields-induced dielectrophoresis. Failure to localise the septin complex appropriately also leads to abnormal chromosomal segregation, extended duration in mitosis and morphological changes in the membrane of cells that are characteristic of post-mitotic apoptotic cell death, such as cell membrane blebbing and rupture[46] (Fig. 3A).

Effects of TTFields on the DNA-damage response

Several studies have reported that TTFields sensitise glioma cell lines to radiotherapy. Exposure to TTFields prior to radiotherapy was shown to delay the repair of radiation-induced DNA damage, enhance mitotic catastrophe and reduce glioma cell line survival.[53,54] Additionally, cell survival was decreased in non-small-cell lung carcinoma (NSCLC) cells treated with TTFields prior to or after radiotherapy treatment compared with either treatment alone; however, exposing cells to TTFields before radiotherapy was more toxic.[55] These findings could have implications for the timing of TTFields application in future preclinical and clinical studies, with TTFields application prior to, or immediately after, radiotherapy likely to optimise therapeutic efficacy. TTFields therapy has also been suggested to interfere with the efficiency of DNA repair. Giladi et al. found more numerous γH2AX foci (an established marker of DNA damage) in glioma cells 24 h post radiotherapy in the combination group compared with either treatment alone. These results suggest that the increased sensitivity to radiotherapy observed with TTFields could be mediated through both an increase in DNA damage and reduced repair capacity following TTFields treatments.[53]

Consistent with these findings, differential gene expression analysis revealed that the expression of genes encoding the DNA-repair proteins BRCA1, ATRIP, MLH1, MRE11A, FANCM and FANCD2, was significantly downregulated in TTFields-treated NSCLC cell lines compared with baseline expression, and that this downregulation was more pronounced in cell lines that were more sensitive to TTFields relative to cell lines that are more resistant to TTFields.[55] BRCA1 plays a central role in homologous recombination DNA repair (HRR), recruiting, along with BRCA2, RAD51 filaments to sites of DNA damage.[56–58] During homologous recombination, RAD51 mediates sequence homology search and strand invasion into the sister chromatid, and prevents nucleolytic degradation of stalled replication forks.[59] RAD51 foci can therefore be used to monitor HRR efficiency, with cells that retain RAD51 foci for 24 h following radiotherapy being associated with persistent DNA double-strand breaks (DSBs) and eventually cell death. Giladi et al. showed an increase in persistent RAD51 foci 24 h following combination treatment (radiotherapy plus TTFields) compared with either treatment alone, suggesting that the reduced repair efficiency seen with TTFields could be the result of impaired HRR following TTFields application. Notably, non-homologous end-joining repair kinetics were not affected by TTFields treatment.[53]

In addition to their role in HRR, BRCA genes cooperate with Fanconi anaemia pathway proteins to maintain DNA replication fork stability.[60] Karanam et al. showed that replication stress was increased with TTFields, and that replication fork dynamics were impaired.[61] Measuring the incorporation of labelled nucleotides into newly synthesised DNA strands during DNA replication serves as a robust readout for replication stress and replication fork dynamics.[62] Karanam et al. showed that DNA fibre length was shorter in H157 and H1299 cells treated with TTFields compared with DNA fibre length in untreated cells, and the difference in DNA fibre length between groups increased over time, indicating that TTFields interfere with replication fork progression and induce replication stress. In addition, the authors demonstrated the presence of other replication-stress markers following TTFields treatments,[61] such as increased replication protein A (RPA) foci (RPA is recruited to single-stranded DNA (ssDNA) intermediates during DNA replication, where it protects exposed ssDNA from nucleases and prevents ssDNA from reannealing[63]) and increased R-loop formation (regions of 3-stranded nucleic acid that form when a replication fork collides with the transcription machinery; these are produced at a higher rate during replication stress).[64] Finally, the authors demonstrated reduced expression of the mini-chromosome maintenance (MCM) complex genes MCM6 and MCM10[61] (the MCM complex functions as a DNA helicase that is crucial for replication initiation and replication fork assembly). Collectively, these data suggest that downregulation of BRCA/Fanconi anaemia pathway genes by TTFields results in an increase in replication-stress-induced DSBs and reduced DSB-repair efficiency due to impaired HRR kinetics (Fig. 3B). As cancerous cells often demonstrate overreliance on a reduced repertoire of DNA-damage response processes,[65,66] future combinatorial strategies that exploit these TTFields-induced vulnerabilities might be particularly effective.

Effects of TTFields on autophagy

The roles of autophagy in cancer are diverse. During the early phases of cancer initiation, the upregulation of autophagy exhibits tumour-suppressive functions, whereas autophagy can be activated to promote cancer cell survival and treatment resistance during the later stages of cancer development.[67] Previous studies have demonstrated that TTFields-treated cells display features that are characteristic of autophagy, such as increased cell volume and granularity and the formation of double-membraned autophagosomes.[46,68–70] When cells undergo autophagy, microtubule-associated protein light-chain 3 (LC3-I) is converted into LC3-II through lipidation by autophagy-related protein 7 (ATG7), enabling its recruitment to the autophagic vesicle membrane, where it activates ATG5, a key component in autophagic vesicle formation.[71] As such, LC3 is often used as a marker for monitoring autophagy.[72] Shteingauz et al. observed an increase in the LC3-II protein in cancer cells following the application of TTFields.[68] However, increased levels of LC3-II do not always correlate with increased autophagy, and can also signify the reduced turnover of autophagosomes owing to defects in autophagosome transport and fusion of the autophagosome with the lysosome.[73] Consequently, autophagic flux, which describes the entire process of autophagy (autophagosome formation, maturation, fusion with lysosomes and lysosomal degradation of cytoplasmic constituents) must be measured to determine the degree of autophagy. Measuring the difference in LC3-II levels in the presence and absence of a lysosome inhibitor, such as chloroquine (which inhibits autophagosome–lysosome fusion), allows the determination of how much LC3-II is degraded in a lysosome-dependent manner because it stops autophagic flux before lysosomal degradation can take place, and therefore indicates the extent of degradation that would have taken place during the treatment, reflecting the degree of autophagy.[74] Combining chloroquine with TTFields was shown to significantly increase LC3-II levels in cells relative to control and relative to TTFields-treated cells in the absence of chloroquine, indicating that TTFields increase autophagic flux and activate autophagy.[68]

TTFields therapy has also been shown to induce abnormal chromosomal segregation,[43] and aberrant mitotic events have been linked to the increased activation of autophagy.[75] TTFields-treated cells that underwent aberrant mitosis (identified as cells displaying abnormal numbers of chromosomes or abnormal cell morphology) were shown to be more likely to activate autophagy in comparison with cells that had not divided over the course of the experiment or cells that underwent normal cell division,[68] suggesting that TTFields-induced aberrant mitotic events could be driving activation of autophagy. The phenomenon of 'doryphagy' describes the specific autophagy-mediated turnover of centrosomal satellites that leads to chromosome-segregation errors and chromosomal instability.[76] Given the data described above, it would be interesting to determine if TTFields impact on centrosomal proteins through autophagy-mediated degradation.

The phosphatidylinositol 3-kinase (PI3K)/protein kinase B (Akt)/mammalian target of rapamycin (TOR) signalling pathway is known to suppress the activation of autophagy.[77] Kim et al. found that the expression of Akt2 and the downstream targets of mTOR complex (mTORC)1, 4E-binding protein 1 (4EBP1) and 70-kDa ribosomal protein S6 kinase (p70S6K), was downregulated in glioma cells upon TTFields therapy, and that phosphorylation of mTOR at Ser2448 was reduced. Re-expressing Akt2 prevented the TTFields-mediated induction of autophagy, indicating that Akt2 pathway signalling regulates autophagy in TTFields-treated cells, and that TTFields activate autophagy by suppressing the inhibitory action of PI3K/Akt/mTOR pathway on autophagy.[69] Additionally, the function of mTORC1 is inhibited by various types of stress within the cell. For example, AMP-dependent kinase (AMPK), which phosphorylates and inhibits mTORC1, thereby suppressing the inhibitory effects of mTORC1 on autophagy,[78] is activated by low-energy (ATP) levels. Shteingauz et al. demonstrated that intracellular levels of ATP were reduced in surviving cells after TTFields application, and that knockdown of AMPK prevented TTFields-mediated upregulation of autophagy, suggesting that activation of AMPK was required for increased activation of autophagy in TTFields-treated cells.[68] Together, these data suggest that activation of autophagy in TTFields-treated GBM cells might be mediated via regulation of the PI3K/Akt/mTOR signalling pathway (Fig. 3C).

Whether activation of autophagy by TTFields serves as a cell survival or a cell death signal is still unclear. Some studies have shown that inhibition of autophagy enhances the killing of cancer cells with TTFields, suggesting that upregulation of autophagy might act as a mechanism of resistance to TTFields, and thus highlighting the potential use of autophagy inhibition as a strategy to enhance the therapeutic efficacy.[68] Others, however, have reported that autophagy inhibition reduces the killing of cancer cells with TTFields.[69] For example, Silginer et al. reported that TTFields-mediated cell death took place in a caspase-independent manner, and that autophagy played an important role in TTFields-mediated cell death.[70] However, TTFields-mediated cell death has been shown to occur through both caspase-dependent (characteristic of apoptotic cell death) and caspase-independent pathways,[43,46,70] suggesting that the type of cell death activated upon TTFields application might be conditional, influenced, for example, by cancer type and genetic context.[70,79] The regulatory mechanisms that direct autophagy to act as a pro-survival or pro-death signal following TTFields warrant further study, but could facilitate the identification of defined populations of patients that are most likely to benefit from concomitant inhibition of autophagy.

TTFields and innate immunity

Macrophages play a central role in governing the nature of immune responses, and represent the dominant infiltrating immune cell population in GBM, constituting ~30–40% of the tumour mass.[80] Macrophages can assume one of two phenotypes: M1 macrophages are considered proinflammatory and secrete proinflammatory cytokines, such as interleukin-1β (IL-1β), IL-12 and tumour necrosis factor-α (TNF-α),[81] to initiate an immune response; M2 macrophages are involved in the resolution of inflammation and release anti-inflammatory cytokines, including IL-10 and transforming growth factor-β (TGF-β). In addition, macrophages are themselves stimulated by cytokines.[81,82] Inflammatory cytokines stimulate macrophages to produce nitric oxide (NO), which induces toxic reactions against invading pathogens and regulates the function of host immune cells, such as T cells, antigen-presenting cells, mast cells, neutrophils and natural killer cells. NO is converted from L-arginine by the inducible NO synthase (iNOS) during inflammation. The proinflammatory cytokines TNF-α, IL-1β and IL-6 mediate the upregulation of iNOS in macrophages by activating the nuclear factor κB (NF-κB) transcription factor and the mitogen-activated protein kinase (MAPK) protein p38, extracellular signal-regulated kinase (Erk)1/2 and c-Jun-activated kinase (JNK). Additionally, when macrophages are first activated by cytokines, the low concentrations of NO can stimulate the NF-κB signalling pathway to upregulate iNOS expression in a positive-feedback loop.[83] Park et al.[84] showed that the mRNA expression levels of IL-1β and TNF-α were significantly increased in RAW 264.7 murine macrophage cells following TTFields treatment. TTFields therapy also upregulated iNOS at both the mRNA and protein levels, consistent with the increased production of NO in these cells. Additionally, an increase in IL-1β, TNF-α and IL-6 secreted into the medium of TTFields-treated RAW 264.7 cells co-cultured with 4T1 cancer cells was detected. These data indicate that TTFields promote phenotype skewing of macrophages towards a proinflammatory phenotype. Furthermore, 4T1 cells that were exposed to the culture medium from TTFields-treated RAW 264.7 cells displayed a reduction in cell viability compared with 4T1 cells that were exposed to the culture medium of untreated RAW 264.7 cells, suggesting that TTFields-mediated activation of macrophages promotes antitumour immunity.[84]

Reactive oxygen species (ROS), which are also produced by macrophages, function as secondary messengers that activate both NF-κB and MAPK signalling pathways within these cells.[85] Under normal circumstances, the inhibitor of NF-κB (IκB-α) protein is bound to, and inhibits, NF-κB, sequestering it in the cytoplasm. Both ROS and TNF-α can mediate the activation of MAPK signalling[85] and IκB kinase (IKK), which phosphorylates IκB-α, resulting in its polyubiquitination and subsequent proteasomal degradation. This process releases the p65 transcriptional subunit from the NF-κB complex, which can then translocate to the nucleus and regulate the transcription of target genes, including those encoding proinflammatory cytokines.[86] Interestingly, ROS secretion was increased in RAW 264.7 cells following TTFields treatment. Additionally, TTFields-treated RAW 264.7 cells displayed increased phosphorylation of IκB-α, the NF-κB p65 subunit and p38 MAPK.[84] These data suggest that TTFields therapy mediates its antitumour immunity effects via the regulation of NF-κB and MAPK signalling pathways in RAW 264.7 macrophages, and raises the potential that TTFields could provide a way to overcome the mechanisms of immune escape typically associated with glioblastoma.[87]

TTFields enhance immunogenic cell death

Using a rabbit model of metastatic cancer, Kirson et al.[88] showed that applying TTFields therapy to VX-2 cell (squamous cell carcinomas) implanted within the kidney capsule significantly reduced distant metastases in the lungs. As the lungs were not directly treated, the observed abscopal effect was most likely mediated by the immune system. Indeed, there was a significant increase in the infiltration of CD45+ T cells, CD4+ T helper cells and CD8+ cytotoxic T cells to the lungs of the treated rabbits, confirming that TTFields can stimulate antitumour immunity in vivo.[88]

Voloshin et al.[89] showed that TTFields induce the membrane translocation and subsequent exposure of the chaperone calreticulin, as well as secretion of the damage-associated molecular pattern ATP and high-mobility group box protein 1 (HMGB1), both of which lead to immunogenic death in cancer cells. Furthermore, dendritic cells, when co-cultured with TTFields-treated cells, demonstrated enhanced phagocytic activity and upregulation of the major histocompatibility complex (MHC) class II and the activation markers CD40 and CD80, indicative of enhanced dendritic cell maturation and immunogenic cell death. Notably, combining TTFields with an inhibitor of programmed cell death protein 1 (PD-1) reduced the tumour volume in lung- and colon-tumour-bearing mice compared with sham control and compared with mice treated with TTFields or the inhibitor alone,[89] suggesting that PD-1 inhibition might further promote the antitumour immune response elicited by TTFields treatment. PD-1 normally functions by disrupting T-cell activation, thereby preventing activation of the immune response; this immune checkpoint, and others, is essential to prevent hyperactivation of the immune system, which can result in autoimmune disorders (e.g., rheumatoid arthritis and multiple sclerosis), but cancer cells can exploit this mechanism in order to evade immune-response-mediated cell death.[90] Immune checkpoint inhibitors such as anti-PD-1 thus enable T cells to kill cancer cells again and further enhance the anticancer immune response induced by TTFields therapy (Fig. 3D). Several clinical trials assessing the use of immune checkpoint inhibitors in glioblastoma are ongoing, whilst the combination of TTFields with anti-PD-1 therapy is currently being assessed in patients with NSCLC (NCT02973789),[91] potentially providing an important platform for future clinical studies assessing a similar combination to treat patients with a glioblastoma.

TTFields suppress cancer cell migration

GBMs are locally invasive tumours. As the extensive migration and infiltration of glioma cells into healthy brain tissue contribute to therapeutic resistance and poor outcomes, restraining these properties represents an appealing therapeutic strategy.[92] Studies by both Kim et al. and Silginer et al. demonstrated that the application of TTFields therapy to established GBM cells significantly reduced cancer cell migration and invasion, as determined through the use of scratch wound-healing and Transwell systems.[54,70] Silginer et al. also identified similar anti-migratory effects of TTFields on glioma-initiating cells, which can undergo self-renewal and initiate tumorigenesis; this is an important finding given the key role played by glioma-initiating cells in mediating therapeutic resistance and recapitulating the tumour cell hierarchy following treatment.[93–95] Interestingly, the results indicated that the anti-infiltrative effects of TTFields were mediated by downregulation of the NF-κB, MAPK and PI3K/AKT signalling pathways in glioma cells, which modulate the transcriptional regulation of matrix metalloproteinase (MMP)2 and MMP9 (Fig. 3E).[54] Additionally, TTFields were found to reduce the expression of vascular endothelial growth factor (VEGF) and hypoxia-inducible factor (HIF)-1α, and to suppress vascular development using human umbilical vein endothelial cells within an in vitro Matrigel™-based endothelial tube-formation assay.[54] The ability of glioma-initiating cells to remodel the tumour microenvironment, including via complex interplay with endothelial cells, has been implicated in their aggressive nature.[95] These findings therefore suggest that TTFields may restrain the invasiveness of GBM by reducing MMP-mediated cleavage through ECM proteins in the surrounding brain by glioma cells and potentially reducing nutrient supply by limiting neovascularisation through reduced VEGF and HIF-1α production in glioma cells.

TTFields enhance cell membrane permeability and intracellular drug concentrations

Whereas integral membrane proteins mediate the transport of large molecules across the cell membrane by passive or active transport, small molecules and ions can simply diffuse across the cell membrane through small holes that punctuate the surface of the cell membrane.[96] Chang et al.[97] used scanning electron microscopy to reveal that TTFields increased both the number and the size of holes in the membrane of glioma cells, with an average hole size of $240.6 \pm 91.7\ nm^2$ in TTFields-treated cells compared with $129.8 \pm 31.9\ nm^2$ in untreated cells. Importantly, these changes appear to be cancer-specific, as no changes in the membrane structure of healthy human fibroblast cells were observed. Additionally, the authors observed a significant increase in the uptake of membrane-associating reagents with a size of 20 kDa, and no larger than 50 kDa, into glioma cells with TTFields. These changes were reversible and returned to normal within 24 h of ceasing TTFields treatment[97] (Fig. 3F). Emerging data also suggest that the application of TTFields therapy might interfere with the integrity of the blood–brain barrier by transiently disrupting the localisation of tight-junction proteins such as claudin 5 and ZO-1.[98] Additional studies and their results will be highly informative.

These findings suggest that TTFields therapy has the potential to increase intracellular/intratumoral concentrations of chemotherapy, and therefore provides a rational explanation for the reported increase in sensitivity to chemotherapeutic drugs observed following TTFields therapy—perhaps even explaining the significant improvement in patient survival observed in the EF-14 trial when TTFields was combined with TMZ.[16] Therefore, in theory, TTFields might enhance the clinical efficacy of many pharmacotherapies, independent of drug mechanism, by increasing the drug concentration selectively within neoplastic cells. These studies also highlight important implications for the rational design of TTFields–chemotherapy combinations and drug scheduling, since ensuring TTFields delivered prior to drug administration could help optimise therapeutic response (e.g., exit may be beneficial to delay drug doses until a few hours after scheduled breaks in TTFields therapy).

AN OVERVIEW AND UPDATE ON TTFIELDS CLINICAL TRIALS

The emerging landscape of clinical trials assessing TTFields therapy to treat intracranial and extracranial tumours has to date supported FDA approvals (and a European CE mark for Optune) for the indications of recurrent and newly diagnosed glioblastoma and mesothelioma (discussed below). Additionally, over 25 registered clinical trials assessing TTFields are currently active.[99]

Recurrent GBM

From 2006 until 2009, 237 patients with recurrent GBM were enrolled in a randomised Phase 3 clinical trial (EF-11, the first Phase 3 trial to investigate the efficacy of TTFields as a monotherapy in humans) and treated with either TTFields (120 patients) or chemotherapy alone (117 patients). The primary endpoint was OS, and secondary endpoints included progression-free survival (PFS), 1-year survival, quality of life (QoL) and safety/toxicity. Although there was no significant difference in OS or PFS in TTFields-treated patients compared with the chemotherapy control group (6.6 vs 6.0 months and 2.2 vs 2.1 months, respectively), TTFields therapy was concluded to be just as effective as physician's choice chemotherapy in treating recurrent GBM, with the added benefits of fewer severe adverse events and overall improvement in QoL.[20] The results of the EF-11 trial led to the FDA approval of TTFields as a treatment for GBM recurrence following standard-of-care chemotherapy.[21]

Newly diagnosed GBM

Between 2009 and 2014, a randomised, Phase 3 clinical trial (EF-14) enrolled patients to receive either TTFields plus adjuvant TMZ (466 patients) or TMZ alone (229 patients). All patients had completed initial radiotherapy with concomitant TMZ prior to randomisation. The study primary endpoint was PFS. The

secondary endpoint was OS, with further exploratory endpoints, including PFS at 6 months, QoL and cognitive function. TTFields with TMZ significantly increased both the PFS and OS of newly diagnosed GBM patients by 2.7 months (6.7 vs 4.0 months, $P < 0.001$) and 4.9 months (20.9 vs 16.0 months, $P = 0.004$), respectively, compared with treatment with TMZ alone. Two years into the trial, 43% of patients randomised to receive TTFields plus TMZ treatment were still alive, compared with 29% in the TMZ-only group. The addition of TTFields to TMZ did not compromise QoL or increase the rate of serious adverse events.[16] Following the results of the EF-14 trial, the FDA approved TTFields together with concomitant TMZ for the treatment of newly diagnosed GBM after maximal resection and completion of standard-of-care radiotherapy and chemotherapy.[21]

Brain metastases and extracranial tumours

Clinical trials assessing the impact of TTFields to treat brain metastases from NSCLC and a range of other extracranial malignancies (including mesothelioma, NSCLC and pancreatic, ovarian, hepatic and gastric cancer) are actively progressing. These trials are summarised in Table 1. Although it is not possible to provide a detailed commentary on each trial within this review, the results of the STELLAR trial, completed in 2019, should be highlighted.[100] This single-arm Phase 2 clinical trial examined the safety and efficacy of continuous TTFields delivery (>18 h per day) at 150 kHz in combination with standard-of-care chemotherapy to treat patients with unresectable treatment-naive malignant pleural mesothelioma. The trial demonstrated encouraging median OS and PFS of 18.2 and 7.6 months, respectively, which are considered to represent a major advance compared with OS and PFS of 12.1 and 5.7 months for historical controls receiving standard-of-care chemotherapy only.[101] In light of the STELLAR trial, TTFields received FDA approval for use in combination with chemotherapy to treat malignant pleural mesothelioma under humanitarian device exemption[102] (a regulatory framework which helps facilitate device approval for rare diseases; this recognises the challenge of generating clinical evidence with a limited patient population, and whilst stringent safety criteria must be maintained, the device can be exempt from some effectiveness requirements, subject to certain profit and use restrictions). This approval established TTFields therapy as the first FDA-approved mesothelioma treatment in over 15 years. A summary of key completed and ongoing TTFields clinical trials is detailed in Table 1.

CONCLUSIONS AND FUTURE OPPORTUNITIES

Further potential applications for TTFields include expanding the population of patients receiving this therapy through additional trials for which existing and emerging preclinical data support clinical studies (e.g., colorectal, renal and breast). In addition, investigation of cancers that have not yet been studied in the context of TTFields—haematological cancers, for example—could be considered. Several key ongoing clinical trials (see Table 1) evaluating the efficacy of combining TTFields with existing anticancer agents in a range of cancer types together with increasing mechanistic data derived from preclinical studies will help to clarify the role of TTFields in treatment regimens and establish the feasibility of making TTFields more readily available across a wider range of cancer types in the years to come. As cancers from different anatomical regions gain attention, transducer array redesigns might be required to ensure optimal TTFields delivery in new anatomical regions whilst maintaining QoL.

Solid paediatric malignancies, including brain tumours, represent a clear indication in need of less harmful anticancer therapies.[103] Ongoing preclinical research suggests that TTFields might demonstrate efficacy in paediatric GBM, medulloblastoma and ependymoma,[104] whilst limited case reports/series suggest that TTFields treatment in children is likely to be safe.[105,106] One of these studies indicated that TTFields was tolerable in five paediatric patients with high-grade glioma, aged between 10 and 20, three of whom showed partial responses when they received TTFields alongside chemotherapy and/or radiation.[106] The study of the use of TTFields to improve outcomes and avoid the substantial morbidity associated with use of chemotherapy and radiotherapy in children is an area of investigation that should be prioritised. To this end, an investigator-initiated study (NCT03033992) testing the feasibility of TTFields for children with recurrent or progressive supratentorial high-grade glioma and ependymoma is ongoing; additional studies and long-term follow-up data would, however, be desirable.

Regarding the treatment of adult patients with newly diagnosed GBM, even with improvements in outcome following the addition of TTFields, survival for most patients remains under 2 years,[16] highlighting an ongoing need to further enhance the efficacy of TTFields and current chemoradiotherapy. The EF-14 trial concluded that compliance with TTFields therapy correlated with improved OS in GBM patients. Patients with a compliance of over 90% (≥ 18 h of daily TTFields) had a median OS of 28.7 months from diagnosis and a 5-year survival rate of 29.3%,[7] and simulation-based analysis of the EF-14 Phase 3 data suggests that the overall dose of TTFields delivered at the tumour site strongly correlates with OS.[107] Considering these findings, it is clear that any method that could effectively increase TTFields usage time (such as improved portability of the clinical device[108]) or increase intensity at target regions should support improvements in therapeutic efficacy.

Emerging preclinical data outlined in this review suggest a strong mechanistic rationale for the use of TTFields in combination with a number of molecularly targeted therapies to improve efficacy. Preclinical data have shown that PD-1 inhibitors can increase antitumour immunity with TTFields[89] and underpin a currently ongoing clinical trial investigating the efficacy of combining PD-1 inhibitors with TTFields for the treatment of patients with NSCLC (LUNAR NCT02973789—see Table 1). A state of 'BRCAness' (deficiency in BRCA or related HRR function) following TTFields-mediated downregulation of BRCA genes (discussed above) has been described.[53,55] BRCA-deficient cancers are characterised by an inherent vulnerability to DNA single-strand break repair inhibitors, such as PARP inhibitors,[109,110] under the concept of synthetic lethality due to impaired HRR efficiency.[111] Preclinical data have shown TTFields and olaparib, a PARP1 inhibitor, synergised to increase cell killing compared with either treatment alone.[61] Future trials combining TTFields with PARP inhibition, including an active trial (recruitment commenced in early 2020) using niraparib and TTFields in GBM (NCT04221503), will be highly informative. The combination of TTFields with other DNA-damage response processes should also be considered. In this respect, our team are actively investigating TTFields combinations that incorporate inhibition of the Fanconi anaemia pathway, as this pathway has been implicated in therapeutic resistance to TMZ[112–114] and also demonstrates synthetic lethality with loss of BRCA.[60]

TTFields-induced 'BRCAness' could also enhance the response to radiotherapy. This effect has been demonstrated in a number of preclinical research projects.[55,115,116] It could, therefore, be hypothesised that the simultaneous delivery of TTFields with chemoradiotherapy in the clinic should maximise the DNA-damage-response-modulating influence of TTFields and might lead to a synergistic effect. Encouragingly, a pilot study of TTFields concomitant with radiotherapy and TMZ in ten newly diagnosed GBM patients demonstrated that this regimen does not increase toxicity.[117] This study is being expanded in a Phase 2 clinical trial (NCT03869242), and a similar Phase 3 trial is currently in registration (TRIDENT—see Table 1). Finally, future studies should also aim to identify and characterise predictive biomarkers that could help to identify which patients most likely benefit from TTFields treatment.

Table 1. Key TTFields clinical trials—completed and ongoing.

Intracranial tumours

Indication & trial [ref.]	Status & design	*n* (rec dates)	Treatment(s)	1° Endpoint	2° Endpoint(s)	Remarks/conclusions
rGBM EF-11[20] *NCT00379470*	COMPLETE Phase 3 Randomised	237 patients (2006–2009)	(A) TTFields alone (120) (B) Chemo alone (117)	OS: 6.6 m (TTFields) vs 6.0 m N/S	(A) PFS: 2.2 m (TTFields) vs 2.1 m N/S. (B) OS at 1 year: 20% in both groups. (C) Toxicity: 6% (TTFields) vs 16% (chemo) AEs$^{(G3-4)}$ ($P = 0.022$). Confirmed TTFields-related AEs = 2% (Grade 2 skin AEs). (D) QoL: ↑ cognitive & emotional, slight ↓ physical functioning.	• TTFields as effective (OS/PFS) as physician's choice chemotherapy. • ↓ Severe AEs and overall ↑ QoL. • Led to FDA approval of TTFields for rGBM.[21]
nGBM EF-14[16] *NCT00916409*	COMPLETE Phase 3 Randomised	695 patients (2009–2014)	(A) TTFields + TMZ (466) (B) TMZ alone (229)	PFS: 6.7 m (TTFields + TMZ) vs 4.0 m ($P < 0.2006$)	(A) OS: 20.9 m (TTFields + TMZ) vs 16 m ($P < 0.001$). (B) Toxicity: 48% (TTFields + TMZ) vs 44% AEs$^{(G3-4)}$—TTFields-related = 2% (all grade 3 skin). (C) Tolerability: sig. delay in 6-pt MMSE decline and 10-pt KPS decline.	• Randomisation after initial radiochemotherapy. • Patients alive at 5 y post randomisation = 13% (TTFields + TMZ) vs 5% ($P = 0.004$). • TTFields improved survival with no added toxicity or compromise in QoL. • Led to FDA approval for TTFields with TMZ for nGBM following maximal surgical debulking and SoC RT with concomitant TMZ.[21]
nGBM TRIDENT *NCT# pending*	In registration Phase 3 Randomised	950 patients—planned (2020 +)	(A) Concomitant TTFields + RT + TMZ (B) RT + TMZ	OS	(A) PFS (median and at 2, 6 and 12 m). (B) OS at 1 and 2 years. (C) Radiological response (ORR, RANO). (D) Toxicity (AEs). (E) QoL (EORTC QLQ C30). (F) Pathological Δ in resected rGBM post treatment.	• Study to establish the efficacy and safety of 200-kHz TTFields in combination with RT (and TMZ) in patients with nGBM. • Builds on preclinical work suggesting synergy between TTFields and RT.[55,115,116] • RT delivered through the TTFields arrays to maximise device usage and the putative radiosensitising effects of TTFields.
Brain metastases (1–10 from NSCLC origin) METIS[118] *NCT02831959*	Ongoing (recruiting) Phase 3 Randomised	260 patients—planned (2016–2020)	(A) TTFields after SRS (130 planned) (B) SRS only (130 planned)	Time to first intracranial progression	(A) OS. (B) Toxicity (AEs). (C) QoL. (D) Radiological response (RANO-BM & RECIST V1.1). (E) Neurocognitive failure.	• Study to establish the efficacy and safety of 150-kHz TTFields in patients with brain metastases from NSCLC. • Builds on Phase 1/2 trial of TTFields for primary lesion in advanced NSCLC.[119] • Estimated study completion: Dec 2020.

Extracranial tumours

Indication & trial [ref.]	Status & design	*n* (rec dates)	Treatment(s)	1° Endpoint	2° Endpoint(s)	Remarks/conclusions
Mesothelioma STELLAR[100,120] *NCT02397928*	COMPLETE Phase 2 Single arm	80 patients (2015–2017)	TTFields + chemo (pemetrexed with cisplatin or carboplatin)	OS: 18.2 m	(A) PFS: 7.6 m (B) Toxicity: 36% AEs$^{(G3-4)}$ + 3 (4%) chemotherapy-related deaths—TTFields-related = 5% (all grade 3 skin). (C) Radiological response (mRECIST): 40% partial response, 57% stable disease at first F/U scan (6 weeks).	• Study aimed to identify a signal for the activity of 150 kHz TTFields with chemotherapy in patients with unresectable malignant pleural mesothelioma. • Encouraging survival data compared with historical OS of 12.1m.[101] • Led to first FDA-approved mesothelioma treatment in over 15 years.[102]
NSCLC [119] *NCT00749346*	COMPLETE Phase 1/2 Single arm	42 patients (2008–2009)	TTFields + chemo (pemetrexed)	Time to local ('in-field') progression: 28w	(A) (Systemic) PFS: 22 weeks. (B) OS: 13.8 m (57% survival at 1 year) (C) Radiological response: 15% partial response, 49% stable disease. (D) Toxicity: no TTFields-related SAEs.	• Study to establish the safety and potential efficacy of TTFields in patients with NSCLC with advanced disease following first-line therapy and eligible for second line pemetrexed. • Encouraging survival relative to historical control for pemetrexed only[121] (2.9 m historic vs 5 m+ with TTFields). • TTFields + pemetrexed is safe and potentially effective—led to Phase 3 LUNAR trial (below).
NSCLC LUNAR[91] *NCT02973789*	Ongoing (recruiting) Phase 3 Randomised	534 patients—planned (2016–2021)	(A) TTFields + ICI or DOCE (B) ICI or DOCE	OS (TTFields + ICI/DOCE vs ICI/DOCE alone)	(A) OS (TTFields + ICI vs ICI) and OS (TTFields + DOCE vs DOCE). (B) PFS. (C) Toxicity (AEs). (D) Radiological response. (E) QoL (EORTC QLQ C30 questionnaire). (F) Exploratory non-inferiority analysis of TTFields+DOCE vs ICI.	Study to establish whether the addition of TTFields to ICI or docetaxel with improve OS in stage IV NSCLC following platinum doublet failure. • Estimated study completion: December 2021.

Table 1. continued

Extracranial tumours

Indication & trial [ref.]	Status & design	*n* (rec dates)	Treatment(s)	1° Endpoint	2° Endpoint(s)	Remarks/conclusions
Pancreatic cancer PANOVA [122] *NCT01971281*	COMPLETE Phase 2 Non-randomised	40 patients (2013–2017)s	(A) TTFields + GEM (B) TTFields + GEM & nab-P* *Arm added to reflect new SoC established while trial was ongoing.*[123]	Toxicity (SAEs): TTFields+GEM = 85% TTFields+GEM + nab-P = 85% (individual rates similar to historic non-TTFields control[123]) G3 TTFields-related skin toxicities = 18%	(A) OS: 14.9 m (TTFields + GEM) & median OS not reached (>15 m) (TTFields + GEM + nab-P). (B) PFS: 8.3 m (TTFields + GEM) & 12.7 m (TTFields + GEM + nab-P)	• Study to establish the safety and preliminary efficacy of TTFields with chemotherapy in patients with pancreatic ductal adenocarcinoma. • One-year OS rates of 55% (TTFields + GEM) & 72% (TTFields + GEM + nab-P)—encouraging relative to historic control 22% (GEM) & 35% (GEM + nab-P).[123] • TTFields+GEM + /-nab-P represents a safe, potentially effective combination—led to Phase 3 PANOVA-3 trial (below).
Pancreatic cancer PANOVA-3[124] *NCT03377491*	Ongoing (recruiting) Phase 3 Randomised	556 patients—planned (2017–2022)	(A) TTFields + GEM & nab-P (B) GEM & nab-P	OS	(A) PFS. (B) Toxicity (AEs). (C) Radiological response. (D) Resectability rate. (E) QoL.	• Study to establish efficacy of TTFields with standard-of-care GEM & nab-P to treat patients with unresectable, locally advanced pancreatic adenocarcinoma. • Estimated study completion: December 2022.
Ovarian cancer INNOVATE (EF-22)[125] *NCT02244502*	COMPLETE Phase 2 Single arm	31 patients (2014–2016)	TTFields + PAC	Toxicity: G3–4 AEs 55% patients – no increase relative to historic non-TTFields control. G3 TTFields-related skin toxicities = 6%.	(A) OS: median not reached (>21 m). (B) PFS: 8.9 m. (C) Response rate: 25% partial response, 46% stable disease.	• Study to establish the safety and preliminary efficacy of TTFields (200 kHz) with PAC to treat patients with recurrent, platinum-resistant ovarian carcinoma. • Heavily pre-treated patient cohort— median 4 prior chemotherapy lines and 2 lines on/after platinum at enrolment. • Encouraging median OS relative to previous studies inc. 17.6 m, 11.3 m and 6.2 m after first, second and fourth relapse by Hanker et al.[126] • Led to Phase 3 INNOVATE-3 trial (below).
Ovarian cancer INNOVATE-3[127] *NCT03940196*	Ongoing (recruiting) Phase 3 Randomised	540 patients—planned (2019–2024)	(A) TTFields + PAC (B) PAC	OS	(A) PFS. (B) Toxicity (AEs). (C) Radiological response rate. (D) QoL (EORTC QLQ C30).	• Study to establish efficacy of TTFields with standard-of-care PAC to treat patients with platinum-resistant ovarian cancer within 6 months of last platinum therapy with ≤2 previous lines following diagnosis of PROC and maximum total of 5 prior lines of systemic therapy. • Estimated study completion: December 2024.
Hepatocellular carcinoma HEPANOVA[128] *NCT03606590*	Ongoing (recruiting) Phase 2 Single arm	25 patients – planned (2019–2020)	TTFields + sorafenib	Overall response rate (patients with CR or PR as per RECIST criteria)	(A) OS. (B) PFS. (C) In-field control rate at 1 year. (D) Distant metastases-free survival at 1 year.	• Study to establish the safety and preliminary efficacy of adding TTFields (150 kHz) to sorafenib in patients with unresectable HCC. • Estimated study completion: December 2020.
Gastric cancer *NCT04281576*	Ongoing (recruiting) Phase 2 Single arm	28 patients – planned (2019–2022)	TTFields + XELOX (+ Trastuzumab if HER-2 positive)	Overall response rate	(A) OS. (B) PFS. (C) Disease control rate. (D) Time to progression. (E) Duration of response. (F) 12-month OS rate. (G) Toxicity (AEs).	• Study to establish the safety and preliminary efficacy of TTFields (150 kHz) with SoC chemotherapy as first-line treatment for patients with unresectable, locally advanced or metastatic gastroesophageal junction or gastric adenocarcinoma. • Estimated study completion: December 2022.

rGBM recurrent GBM, *nGBM* newly diagnosed GBM, *NSCLC* non-small-cell lung cancer, *TTFields* tumour-treating fields, *TMZ* temozolomide, *SoC* standard of care, *DOCE* docetaxel, *GEM* gemcitabine, *nab-P* nab-paclitaxel, *PAC* paclitaxel, *ICI* immune checkpoint inhibitors, *XELOX* capecitabine (Xeloda) + oxaliplatin (Eloxatin), *RT* radiotherapy, *SRS* stereotactic radiosurgery, *OS* (median) overall survival, *PFS* (median) progression-free survival, *CR* complete response, *PR* partial response, *ORR* overall response rate (proportion of patients with a PR or CR), *F/U* follow-up, *QoL* quality of life, *AEs* adverse events, $AEs^{(G3-4)}$ grade 3–4 adverse events, *SAEs* severe adverse events, *MMSE* mini-mental-state examination, *KPS* Karnofsky performance score, *N/S* no significant difference.

As evident from the preclinical and clinical studies highlighted in this review, TTFields has great potential, both in the short- and long term, to improve outcomes for many patients diagnosed with a range of cancers. Continuing to enhance our knowledge of the molecular mechanisms that underpin TTFields-based cellular toxicity and tumour specificity/therapeutic index will hopefully aid further adoption of this new modality and integration into existing and novel treatment strategies to improve outcomes for a wide range of cancer patient cohorts.

AUTHOR CONTRIBUTIONS

O.R. and S.p.J.C. conceptualised the review. A.V., O.R. and S.p.J.C. contributed to writing early drafts of the paper. All authors contributed to writing–review and editing the paper.

ADDITIONAL INFORMATION

Ethics approval and consent to participate Not applicable.

Consent to publish Not applicable.

Data availability Not applicable.

Competing interests O.R. and S.p.J.C. are recipients of an Inovitro™ system (on loan from Novocure) and take part in the annual Inovitro™ Users Meeting hosted by Novocure. The remaining authors declare no competing interests.

Funding information O.R. and S.p.J.C. acknowledge funding support from the Royal College of Surgeons, Neurocare, Yorkshire's Brain Tumour Charity (formerly BTRS) and The Brain Tumour Charity. O.R., S.p.J.C. and C.B. acknowledge funding support from Sheffield Hospitals Charity. O.R., A.V., Y.A.T. and S.p.J.C. are supported by the NIHR Sheffield Biomedical Research Centre/NIHR Sheffield Clinical Research Facility, and all the authors wish to acknowledge kind funding support to cover the costs of publication provided by the NIHR Sheffield Biomedical Research Centre. The views expressed are those of the authors and not necessarily those of the NHS, the NIHR or the Department of Health and Social Care.

REFERENCES

1. Philips, A., Henshaw, D. L., Lamburn, G. & O'Carroll, M. J. Brain tumours: rise in glioblastoma multiforme incidence in England 1995-2015 suggests an adverse environmental or lifestyle factor. *J. Environ. Public Health v.* **2018**, 7910754 (2018).
2. Patel, A. P., Fisher, J. L., Nichols, E., Abd-Allah, F., Abdela, J., Abdelalim, A., Abraha, H. N., Agius, D., Alahdab, F., Alam, T. & Allen, C.A. Global, regional, and national burden of brain and other CNS cancer, 1990-2016: a systematic analysis for the Global Burden of Disease Study 2016. *Lancet Neurol.* **18**, 376–393 (2019).
3. Alexander, B. M., Ba, S., Berger, M. S., Berry, D. A., Cavenee, W. K., Chang, S. M. et al. Adaptive global innovative learning environment for glioblastoma: GBM AGILE. *Clin. Cancer Res.* **24**, 737–743 (2018).
4. Ostrom, Q. T., Cote, D. J., Ascha, M., Kruchko, C. & Barnholtz-Sloan, J. S. Adult glioma incidence and survival by race or ethnicity in the United States From 2000 to 2014. *JAMA Oncol.* **4**, 1254–1262 (2018).
5. Stupp, R., Hegi, M. E., Mason, W. P., van den Bent, M. J., Taphoorn, M. J., Janzer, R. C. et al. Effects of radiotherapy with concomitant and adjuvant temozolomide versus radiotherapy alone on survival in glioblastoma in a randomised phase III study: 5-year analysis of the EORTC-NCIC trial. *Lancet Oncol.* **10**, 459–466 (2009).
6. Cancer Research UK. Tackle cancers with substantial unmet need: our research strategy. http://www.cancerresearchuk.org/funding-for-researchers/our-research-strategy/tackle-cancers-with-substantial-unmet-need (2017).
7. Toms, S., Kim, C., Nicholas, G. & Ram, Z. Increased compliance with tumor treating fields therapy is prognostic for improved survival in the treatment of glioblastoma: a subgroup analysis of the EF-14 phase III trial. *J. Neuro-Oncol.* **141**, 467–473 (2019).
8. Kirson, E. D., Dbalý, V., Tovarys, F., Vymazal, J., Soustiel, J. F., Itzhaki, A. et al. Alternating electric fields arrest cell proliferation in animal tumor models and human brain tumors. *Proc. Natl Acad. Sci. USA* **104**, 10152–10157 (2007).
9. Kirson, E. D., Gurvich, Z., Schneiderman, R., Dekel, E., Itzhaki, A., Wasserman, Y. et al. Disruption of cancer cell replication by alternating electric fields. *Cancer Res.* **64**, 3288–3295 (2004).
10. Moghadam, M., Firoozabadi, S. & Janahmadi, M. 50 Hz alternating extremely low frequency magnetic fields affect excitability, firing and action potential shape through interaction with ionic channels in snail neurones. *Environmentalist* **28**, 341–347 (2008).
11. Cheung, A. Y. & Neyzari, A. Deep local hyperthermia for cancer therapy: external electromagnetic and ultrasound techniques. *Cancer Res.* **44**, 4736s–4744s (1984).
12. Davies, A. M., Weinberg, U. & Palti, Y. Tumor treating fields: a new frontier in cancer therapy. *Ann. N. Y. Acad. Sci.* **1291**, 86–95 (2013).
13. Eilon, D. K., Vladimír, D., František, T., Josef, V., Jean, F. S., Aviran, I. et al. Alternating electric fields arrest cell proliferation in animal tumor models and human brain tumors. *Proc. Natl Acad. Sci. USA* **104**, 10152 (2007).
14. Cohen, M. H., Johnson, J. R. & Pazdur, R. Food and drug administration drug approval summary: temozolomide plus radiation therapy for the treatment of newly diagnosed glioblastoma multiforme. *Clin. Cancer Res.* **11**, 6767–6771 (2005).
15. Kesari, S. & Ram, Z. Tumor-treating fields plus chemotherapy versus chemotherapy alone for glioblastoma at first recurrence: a post hoc analysis of the EF-14 trial. *CNS Oncol.* **6**, 185–193 (2017).
16. Stupp, R., Taillibert, S., Kanner, A., Read, W., Steinberg, D. M., Lhermitte, B. et al. Effect of tumor-treating fields plus maintenance temozolomide vs maintenance temozolomide alone on survival in patients with glioblastoma: a randomized clinical trial. *J. Am. Med. Asooc.* **318**, 2306–2316 (2017).
17. Stupp, R., Taillibert, S., Kanner, A. A., Kesari, S., Steinberg, D. M., Toms, S. A. et al. Maintenance therapy with tumor-treating fields plus temozolomide vs temozolomide alone for glioblastoma: a randomized clinical trial. *J. Am. Med. Assoc.* **314**, 2535–2543 (2015).
18. Zhu, J. J., Demireva, P., Kanner, A. A., Pannullo, S., Mehdorn, M., Avgeropoulos, N. et al. Health-related quality of life, cognitive screening, and functional status in a randomized phase III trial (EF-14) of tumor treating fields with temozolomide compared to temozolomide alone in newly diagnosed glioblastoma. *J. Neuro-Oncol.* **135**, 545–552 (2017).
19. Mrugala, M. M., Engelhard, H. H., Dinh Tran, D., Kew, Y., Cavaliere, R., Villano, J. L. et al. Clinical practice experience with NovoTTF-100A system for glioblastoma: The Patient Registry Dataset (PRiDe). *Semin. Oncol.* **42**, e33–e43 (2015).
20. Stupp, R., Wong, E. T., Kanner, A. A., Steinberg, D., Engelhard, H., Heidecke, V. et al. NovoTTF-100A versus physician's choice chemotherapy in recurrent glioblastoma: a randomised phase III trial of a novel treatment modality. *Eur. J. Cancer* **48**, 2192–2202 (2012).
21. US Food and Drug Administration. Premarket Approval (PMA): Optune. https://www.accessdata.fda.gov/scripts/cdrh/cfdocs/cfpma/pma.cfm?id=P100034S013 (2020).
22. Chaudhry, A., Benson, L., Varshaver, M., Farber, O., Weinberg, U., Kirson, E. et al. NovoTTF (TM)-100A system (tumor treating fields) transducer array layout planning for glioblastoma: a NovoTAL (TM) system user study. *World J. Surg. Oncol.* **13**, 316 (2015).
23. Lacouture, M., Davis, M. E., Elzinga, G., Butowski, N., Tran, D., Villano, J. et al. Dermatologic event characteristics and management with the novoTTF-100A system, a novel anti-mitotic device for the treatment of recurrent glioblastoma (rGBM). *Neuro. Oncol.* **15**, 229–229 (2013).
24. Novocure. Form S-1 registration statement under the Securities Act of 1933: Novocure Limited: United States Securities and Exchange Commission. https://www.sec.gov/Archives/edgar/data/1645113/000119312515308245/d940664ds1.htm (2015).
25. Novocure. Patient Information and Operation Manuel. https://www.optune.com/content/pdfs/Optune_PIOM_8.5x11.pdf (2019).
26. William, W., Yeun, Mi. Y., Ashley, K., Martin, C., Marjolaine, G.-L., Patrick, G.-S. et al. Assessment of costs associated with adverse events in patients with cancer. *PLoS ONE* **13**, e0196007 (2018).
27. Bernard-Arnoux, F., Lamure, M., Ducray, F., Aulagner, G., Honnorat, J. & Armoiry, X. The cost-effectiveness of tumor-treating fields therapy in patients with newly diagnosed glioblastoma. *Neuro. Oncol.* **18**, 1129–1136 (2016).
28. Connock, M., Auguste, P., Dussart, C., Guyotat, J. & Armoiry, X. Cost-effectiveness of tumor-treating fields added to maintenance temozolomide in patients with glioblastoma: an updated evaluation using a partitioned survival model. *J. Neuro-Oncol.* **143**, 605–611 (2019).
29. Guzauskas, G. F., Pollom, E. L., Stieber, V. W., Wang, B. C. M. & Garrison, L. P. Jr Tumor treating fields and maintenance temozolomide for newly-diagnosed glioblastoma: a cost-effectiveness study. *J. Med. Econ.* **22**, 1006–1013 (2019).
30. Porter, K. R., McCarthy, B. J., Berbaum, M. L. & Davis, F. G. Conditional survival of all primary brain tumor patients by age, behavior, and histology. *Neuroepidemiology* **36**, 230–239 (2011).
31. Larkin, J., Hatswell, A. J., Nathan, P., Lebmeier, M. & Lee, D. The predicted impact of ipilimumab usage on survival in previously treated advanced or metastatic melanoma in the UK. *PLoS ONE* **10**, e0145524 (2015).

32. The National Institute for Health and Care Excellence. Ipilimumab for previously treated advanced (unresectable or metastatic) melanoma: guidance and guidelines (TA268). https://www.nice.org.uk/guidance/ta268 (2012).
33. McCabe, C., Claxton, K. & Culyer, A. The NICE cost-effectiveness threshold. *Pharmacoeconomics* **26**, 733–744 (2008).
34. Taylor, C. & Jan, S. Economic evaluation of medicines. *Aust. Prescr.* **40**, 76–78 (2017).
35. Novocure. Novocure reports 2015 operating statistics and financial results. https://www.novocure.com/novocure-reports-2015-operating-statistics-and-financial-results/ (2016).
36. Novocure. Novocure reports fourth quarter and full year 2019 financial results and provides company update. https://www.novocure.com/novocure-reports-fourth-quarter-and-full-year-2019-financial-results-and-provides-company-update/ (2020).
37. Novocure. Novocure reports fourth quarter and full year 2018 financial results and provides company update. https://www.novocure.com/novocure-reports-fourth-quarter-and-full-year-2018-financial-results-and-provides-company-update/ (2019).
38. Mehta, M., Wen, P., Nishikawa, R., Reardon, D. & Peters, K. Critical review of the addition of tumor treating fields (TTFields) to the existing standard of care for newly diagnosed glioblastoma patients. *Crit. Rev. Oncol. Hemat.* **111**, 60–65 (2017).
39. Wick, W. TTFields: where does all the skepticism come from? *Neuro. Oncol.* **18**, 303–305 (2016).
40. The National Institute for Health and Care Excellence. Brain tumours (primary) and brain metastases in adults NICE guideline [NG99]. https://www.nice.org.uk/guidance/ng99 (2018).
41. Lavy Shahaf, G., Giladi, M., Schneiderman, R., Kinzel, A., Weinberg, U., Kirson, E. et al. P04.17 cancer cell lines response to tumor treating fields: results of a meta-analysis. *Neuro. Oncol.* **20**, iii282–iii282 (2018).
42. Kline-Smith, S. & Walczak, C. E. Mitotic spindle assembly and chromosome segregation: Refocusing on microtubule dynamics. *Mol. Cell.* **15**, 317–327 (2004).
43. Moshe, G., Rosa, S. S., Tali, V., Yaara, P., Mijal, M., Roni, B. et al. Mitotic spindle disruption by alternating electric fields leads to improper chromosome segregation and mitotic catastrophe in cancer cells. *Sci. Rep.* **5**, 18046 (2015).
44. Joshua, J. T., Jordane, P., Jack, A. T. & Eric, T. W. Tubulin's response to external electric fields by molecular dynamics simulations. *PLoS ONE* **13**, e0202141 (2018).
45. Andrea, M. & Kevin, H. G. The spindle checkpoint: structural insights into dynamic signalling. *Nat. Rev. Mol. Cell Biol.* **3**, 731 (2002).
46. Nidhi, G., Aaron, Y., Talia, S. H., Sze Xian, L., Eric, T. W. & Kenneth, D. S. Tumor treating fields perturb the localization of septins and cause aberrant mitotic exit. *PLoS ONE* **10**, e0125269 (2015).
47. Kessler, A. F., Frömbling, G. E., Gross, F., Hahn, M., Dzokou, W., Ernestus, R.-I. et al. Effects of tumor treating fields (TTFields) on glioblastoma cells are augmented by mitotic checkpoint inhibition. *Cell Death Dis.* **4**, 77 (2018).
48. Schulze, V. K., Klar, U., Kosemund, D., Wengner, A. M., Siemeister, G., Stöckigt, D. et al. Treating cancer by spindle assembly checkpoint abrogation: discovery of two clinical candidates, BAY 1161909 and BAY 1217389, targeting MPS1 kinase. *J. Med. Chem.* **63**, 8025–8042 (2020).
49. Field, C. M., Coughlin, M., Doberstein, S., Marty, T. & Sullivan, W. Characterization of anillin mutants reveals essential roles in septin localization and plasma membrane integrity. *Development* **132**, 2849–2860 (2005).
50. Spiliotis, E. T., Kinoshita, M. & Nelson, W. J. A mitotic septin scaffold required for mammalian chromosome congression and segregation. *Science* **307**, 1781–1785 (2005).
51. Paul, F., Eric, H., Michael, L., Mena, K., Paknoosh, P. & Alisa, P. An anillin-Ect2 complex stabilizes central spindle microtubules at the cortex during cytokinesis. *PLoS ONE* **7**, e34888 (2012).
52. Goldbach, P., Wong, R., Beise, N., Sarpal, R., Trimble, W. S. & Brill, J. A. Stabilization of the actomyosin ring enables spermatocyte cytokinesis in Drosophila. *Mol. Biol. Cell* **21**, 1482–1493 (2010).
53. Giladi, M., Munster, M., Schneiderman, R. S., Voloshin, T., Porat, Y., Blat, R. et al. Tumor treating fields (TTFields) delay DNA damage repair following radiation treatment of glioma cells. *Radiat. Oncol.* **12**, 206 (2017).
54. Kim, E., Song, H., Yoo, S. & Yoon, M. Tumor treating fields inhibit glioblastoma cell migration, invasion and angiogenesis. *Oncotarget* **7**, 65125–65136 (2016).
55. Karanam, N. K., Srinivasan, K., Ding, L., Sishc, B., Saha, D. & Story, M. D. Tumor-treating fields elicit a conditional vulnerability to ionizing radiation via the downregulation of BRCA1 signaling and reduced DNA double-strand break repair capacity in non-small cell lung cancer cell lines. *Cell Death Dis.* **8**, e2711 (2017).
56. Davies, A. A., Masson, J.-Y., McIlwraith, M. J., Stasiak, A. Z., Stasiak, A., Venkitaraman, A. R. et al. Role of BRCA2 in control of the RAD51 recombination and DNA repair protein. *Mol. Cell* **7**, 273–282 (2001).
57. Scully, R., Chen, J., Plug, A., Xiao, Y., Weaver, D., Feunteun, J. et al. Association of BRCA1 with Rad51 in mitotic and meiotic cells. *Cell* **88**, 265–275 (1997).
58. Venkitaraman, A. R. Functions of BRCA1 and BRCA2 in the biological response to DNA damage. *J. Cell Sci.* **114**, 3591–3598 (2001).
59. Mason, J. M., Chan, Y. L., Weichselbaum, R. W. & Bishop, D. K. Non-enzymatic roles of human RAD51 at stalled replication forks. *Nat. Commun.* **10**, 4410 (2019).
60. Kais, Z., Rondinelli, B., Holmes, A., O'leary, C., Kozono, D, D'andrea Alan d. et al. FANCD2 maintains fork stability in BRCA1/2-deficient tumors and promotes alternative end-joining DNA repair. *Cell Rep.* **15**, 2488–2499 (2016).
61. Karanam, N. K., Hao-Ding, L., Aroumougame, A. & Story, M. D. Tumor treating fields cause replication stress and interfere with DNA replication fork maintenance: implications for cancer therapy. *Transl. Res.* **217**, 33–46 (2020).
62. Quinet, A., Carvajal-Maldonado, D., Lemacon, D. & Vindigni, A. DNA fiber analysis: mind the gap! *Method. Enzymol.* **591**, 55–82 (2017).
63. Luke, A. Y., Ricardo, J. A., Nilisha, P., Colleen, C. C., Joshua, A. K., Rajika, L. P. et al. A structural and dynamic model for the assembly of replication protein A on single-stranded DNA. *Nat. Commun.* **9**, 1–14 (2018).
64. Belotserkovskii, B. P., Tornaletti, S., D'souza, A. D. & Hanawalt, P. C. R-loop generation during transcription: formation, processing and cellular outcomes. *DNA Repair* **71**, 69–81 (2018).
65. Pearl, L. H., Schierz, A. C., Ward, S. E., Al-Lazikani, B. & Pearl, F. M. Therapeutic opportunities within the DNA damage response. *Nat. Rev. Cancer* **15**, 166–180 (2015).
66. Rominiyi, O., Gomez-Roman, N., Lad, N., Al-Tamimi, Y., Jellinek, D., Chalmers, A. et al. Preclinical evaluation of combinations targeting the DNA damage response in 2D and 3D models of glioblastoma stem cells [abstract]. *Neuro. Oncol.* **20**, iii297 (2018).
67. Yun, C. W. & Lee, S. H. The roles of autophagy in cancer. *Int. J. Mol. Sci.* **19**, 3466 (2018).
68. Shteingauz, A., Porat, Y., Voloshin, T., Schneiderman, R. S., Munster, M., Zeevi, E. et al. AMPK-dependent autophagy upregulation serves as a survival mechanism in response to tumor treating fields (TTFields). *Cell Death Dis.* **9**, 1074 (2018).
69. Kim, E. H., Jo, Y., Sai, S., Park, M. J., Kim, J. Y., Kim, J. S. et al. Tumor-treating fields induce autophagy by blocking the Akt2/miR29b axis in glioblastoma cells. *Oncogene* **38**, 6630–6646 (2019).
70. Silginer, M., Weller, M., Stupp, R. & Roth, P. Biological activity of tumor-treating fields in preclinical glioma models. *Cell Death Dis.* **8**, e2753 (2017).
71. Tanida, I., Ueno, T. & Kominami, E. LC3 and autophagy. *Methods Mol. Biol.* **445**, 77–88 (2008).
72. Saori, R. Y. & Noboru, M. Monitoring and measuring autophagy. *Int. J. Mol. Sci.* **18**, 1865 (2017).
73. Orhon, I. & Reggiori, F. Assays to monitor autophagy progression in cell cultures. *Cells*. **6**, 20 (2017).
74. Mauthe, M., Orhon, I., Rocchi, C., Zhou, X., Luhr, M., Hijlkema, K.-J. et al. Chloroquine inhibits autophagic flux by decreasing autophagosome-lysosome fusion. *Autophagy* **14**, 1435–1455 (2018).
75. Inoue, T., Nakayama, Y., Li, Y., Matsumori, H., Takahashi, H., Kojima, H. et al. SIRT 2 knockdown increases basal autophagy and prevents postslippage death by abnormally prolonging the mitotic arrest that is induced by microtubule inhibitors. *FEBS J.* **281**, 2623–2637 (2014).
76. Holdgaard, S. G., Cianfanelli, V., Pupo, E., Lambrughi, M., Lubas, M., Nielsen, J. C. et al. Selective autophagy maintains centrosome integrity and accurate mitosis by turnover of centriolar satellites. *Nat. Commun.* **10**, 4176 (2019).
77. Paquette, M., El-Houjeiri, L. & Pause, A. mTOR pathways in cancer and autophagy. *Cancers* **10**, 18 (2018).
78. Garcia, D. & Shaw, R. J. AMPK: mechanisms of cellular energy sensing and restoration of metabolic balance. *Mol. Cell* **66**, 789–800 (2017).
79. Gera, N., Yang, A., Holtzman, T. S., Lee, S. X., Wong, E. T. & Swanson, K. D. Tumor treating fields perturb the localization of septins and cause aberrant mitotic exit. *PLoS ONE* **10**, e0125269 (2015).
80. Chen, Z. & Hambardzumyan, D. Immune microenvironment in glioblastoma subtypes. *Front. Immunol.* **9**, 1004 (2018).
81. Wang, N., Liang, H. & Zen, K. Molecular mechanisms that influence the macrophage m1-m2 polarization balance. *Front. Immunol.* **5**, 614–614 (2014).
82. Arango Duque, G. & Descoteaux, A. Macrophage cytokines: involvement in immunity and infectious diseases. *Front. Immunol.* **5**, 491–491 (2014).
83. Tripathi, P., Tripathi, P., Kashyap, L. & Singh, V. The role of nitric oxide in inflammatory reactions. *FEMS Immunol. Med. Microbiol.* **51**, 443-452 (2007).
84. Park, J.-I., Song, K.-H., Jung, S.-Y., Ahn, J., Hwang, S.-G., Kim, J. et al. Tumor-treating fields induce RAW264.7 macrophage activation via NK-κB/MAPK signaling pathways. *Technol. Cancer Res. T* https://doi.org/10.1177/1533033819868225 (2019).
85. Tan, H.-Y., Wang, N., Li, S., Hong, M., Wang, X. & Feng, Y. The reactive oxygen species in macrophage polarization: reflecting its dual role in progression and treatment of human. *Dis. Oxid. Med.* **2016**, 2795090 (2016).
86. Ting, L., Lingyun, Z., Donghyun, J. & Shao-Cong, S. NF-κB signaling in inflammation. *Signal Transduct. Tar.* **2**, 17023 (2017).
87. Brown, N. F., Carter, T. J., Ottaviani, D. & Mulholland, P. Harnessing the immune system in glioblastoma. *Br. J. Cancer* **119**, 1171–1181 (2018).

88. Kirson, E. D., Giladi, M., Gurvich, Z., Itzhaki, A., Mordechovich, D., Schneiderman, R. S. et al. Alternating electric fields (TTFields) inhibit metastatic spread of solid tumors to the lungs. *Clin. Exp. Metastasis* **26**, 633–640 (2009).
89. Voloshin, T., Kaynan, N., Davidi, S., Porat, Y., Shteingauz, A., Schneiderman, R. S. et al. Tumor-treating fields (TTFields) induce immunogenic cell death resulting in enhanced antitumor efficacy when combined with anti-PD-1 therapy. *Cancer Immunol. Immun.* **69**, 1191–1204 (2020).
90. Jiang, X., Wang, J., Deng, X., Xiong, F., Ge, J., Xiang, B. et al. Role of the tumor microenvironment in PD-L1/PD-1-mediated tumor immune escape. *Mol. Cancer* **18**, 10 (2019).
91. Weinberg, U., Farber, O., Giladi, M., Bomzon, Z. & Kirson, E. Tumor treating fields (150 kHz) concurrent with standard of care treatment for stage 4 non-small cell lung cancer (NSCLC) following platinum failure: the phase III LUNAR study [Abstract CT173]. *Cancer Res.* **79** (2019).
92. Birch, J. L., Strathdee, K., Gilmour, L., Vallatos, A., McDonald, L., Kouzeli, A. et al. A novel small-molecule inhibitor of MRCK prevents radiation-driven invasion in glioblastoma. *Cancer Res.* **78**, 6509–6522 (2018).
93. Singh, S. K., Hawkins, C., Clarke, I. D., Squire, J. A., Bayani, J., Hide, T. et al. Identification of human brain tumour initiating cells. *Nature* **432**, 396–401 (2004).
94. Bao, S., Wu, Q., McLendon, R. E., Hao, Y., Shi, Q., Hjelmeland, A. B. et al. Glioma stem cells promote radioresistance by preferential activation of the DNA damage response. *Nature* **444**, 756–760 (2006).
95. Prager, B. C., Bhargava, S., Mahadev, V., Hubert, C. G. & Rich, J. N. Glioblastoma stem cells: driving resilience through chaos. *Trends Cancer* **6**, 223–235 (2020).
96. Szachowicz-Petelska, B., Figaszewski, Z. & Lewandowski, W. Mechanisms of transport across cell membranes of complexes contained in antitumour drugs. *Int. J. Pharm.* **222**, 169–182 (2001).
97. Chang, E., Patel, C. B., Pohling, C., Young, C., Song, J., Flores, T. A. et al. Tumor treating fields increases membrane permeability in glioblastoma cells. *Cell Death Discov.* **4**, 113 (2018).
98. Kessler, A. F., Salvador, E., Domröse, D., Burek, M., Schaeffer, C., Tempel Brami, C. et al. Blood brain barrier (BBB) integrity is affected by tumor treating fields (TTFields) in vitro and in vivo. *Int. J. Radiat. Oncol.* **105**, S162–S163 (2019).
99. NIH US National Library of Medicine. ClinicalTrials.gov. https://clinicaltrials.gov (2020).
100. Ceresoli, G. L., Aerts, J. G., Dziadziuszko, R., Ramlau, R., Cedres, S., van Meerbeeck, J. P. et al. Tumour treating fields in combination with pemetrexed and cisplatin or carboplatin as first-line treatment for unresectable malignant pleural mesothelioma (STELLAR): a multicentre, single-arm phase 2 trial. *Lancet Oncol.* **20**, 1702–1709 (2019).
101. Vogelzang, N. J., Rusthoven, J. J., Symanowski, J., Denham, C., Kaukel, E., Ruffie, P. et al. Phase III study of pemetrexed in combination with cisplatin versus cisplatin alone in patients with malignant pleural mesothelioma. *J. Clin. Oncol.* **21**, 2636–2644 (2003).
102. US Food and Drug Administration. NovoTTF™-100L System -H180002. https://www.fda.gov/medical-devices/recently-approved-devices/novottftm-100l-system-h180002 (2019).
103. Adamson, P. C. Improving the outcome for children with cancer: Development of targeted new agents. *CA Cancer J. Clin.* **65**, 212–220 (2015).
104. Branter, J., Estevez-Cebrero, M., Grundy, R., Basu, S. & Smith, S. Tumor treating fields (TTFields) have antiproliferative effects on high-grade pediatric brain tumor cell lines [Abstract 4637]. *Cancer Res.* **78**, 4637 (2018).
105. O'Connell, D., Shen, V., Loudon, W. & Bota, D. A. First report of tumor treating fields use in combination with bevacizumab in a pediatric patient: a case report. *CNS Oncol.* **6**, 11–18 (2017).
106. Green, A. L., Mulcahy Levy, J. M., Vibhakar, R., Hemenway, M., Madden, J., Foreman, N. et al. Tumor treating fields in pediatric high-grade glioma. *Child. Nerv. Syst.* **33**, 1043–1045 (2017).
107. Ballo, M. T., Urman, N., Lavy-Shahaf, G., Grewal, J., Bomzon, Z. & Toms, S. Correlation of tumor treating fields dosimetry to survival outcomes in newly diagnosed glioblastoma: a large-scale numerical simulation-based analysis of data from the phase 3 EF-14 randomized trial. *Int. J. Radiat. Oncol.* **104**, 1106–1113 (2019).
108. Kinzel, A., Ambrogi, M., Varshaver, M. & Kirson, E. D. Tumor treating fields for glioblastoma treatment: patient satisfaction and compliance with the second-generation Optune® system. *Clin. Med. Insights: Oncol.* **13**, 1–7 (2019).
109. Bryant, H. E., Schultz, N., Thomas, H. D., Parker, K. M., Flower, D., Lopez, E. et al. Specific killing of BRCA2-deficient tumours with inhibitors of poly(ADP-ribose) polymerase. *Nature* **434**, 913–917 (2005).
110. Farmer, H., McCabe, N., Lord, C. J., Tutt, A. N., Johnson, D. A., Richardson, T. B. et al. Targeting the DNA repair defect in BRCA mutant cells as a therapeutic strategy. *Nature* **434**, 917–921 (2005).
111. Helleday, T. The underlying mechanism for the PARP and BRCA synthetic lethality: clearing up the misunderstandings. *Mol. Oncol.* **5**, 387–393 (2011).
112. Patil, A. A., Sayal, P., Depondt, M.-L., Beveridge, R. D., Roylance, A., Kriplani, D. H. et al. FANCD2 re-expression is associated with glioma grade and chemical inhibition of the Fanconi Anaemia pathway sensitises gliomas to chemotherapeutic agents. *Oncotarget* **5**, 6414 (2014).
113. Rominiyi, O., Myers, K., Gomez-Roman, N., Lad, N., Dar, D., Jellinek, D. et al. RDNA-12. The Fanconi anaemia (FA) pathway and glioblastoma: a new foundation for DNA damage response targeted combinations [Abstract RNDA-12]. *Neuro. Oncol.* **21**, vi209–vi209 (2019).
114. MacLeod, G., Bozek, D. A., Rajakulendran, N., Monteiro, V., Ahmadi, M., Steinhart, Z. et al. Genome-wide CRISPR-Cas9 screens expose genetic vulnerabilities and mechanisms of temozolomide sensitivity in glioblastoma stem cells. *Cell Rep.* **27**, 971–986.e979 (2019).
115. Li, T., Shukla, G., Peng, C., Lockamy, V., Liu, H. & Shi, W. Dosimetric impact of a tumor treating fields device for glioblastoma patients undergoing simultaneous radiation therapy. *Front. Oncol.* **8**, 51 (2018).
116. Straube, C., Oechsner, M., Kampfer, S., Scharl, S., Schmidt-Graf, F., Wilkens, J. J. et al. Dosimetric impact of tumor treating field (TTField) transducer arrays onto treatment plans for glioblastomas—a planning study. *Radiat. Oncol.* **13**, 31 (2018).
117. Grossman, R., Limon, D., Bokstein, F., Harosh, C. B. & Ram, Z. Randomized phase II trial of tumor treating fields plus radiation therapy plus temozolamide compared to radiation therapy plus temozolomide in patients with newly diagnosed glioblastoma [Abstract]. *Cancer Res.* **79**, CT203 (2019).
118. Mehta, M., Gondi, V., Ahluwalia, M. & Brown, P. Radiosurgery followed by tumour treating fields (TTFields) for brain metastases (1-10) from NSCLC in the phase III METIS trial. *Ann. Oncol.* **30**, v659 (2019).
119. Pless, M., Droege, C., Von Moos, R., Salzberg, M. & Betticher, D. A phase I/II trial of tumor treating fields (TTFields) therapy in combination with pemetrexed for advanced non-small cell lung cancer. *Lung Cancer* **81**, 445–450 (2013).
120. Ceresoli, G., Aerts, J., Madrzak, J., Dziadziuszko, R., Ramlau, R., Cedres, S. et al. STELLAR—final results of a phase 2 trial of TTFields with chemotherapy for first-line treatment of malignant pleural mesothelioma. *J. Thorac. Oncol.* **13**, S397–S398 (2018).
121. Hanna, N., Shepherd, F. A., Fossella, F. V., Pereira, J. R., De Marinis, F., von Pawel, J. et al. Randomized phase III trial of pemetrexed versus docetaxel in patients with non-small-cell lung cancer previously treated with chemotherapy. *J. Clin. Oncol.* **22**, 1589–1597 (2004).
122. Rivera, F., Benavides, M., Gallego, J., Guillen-Ponce, C., Lopez-Martin, J. & Kung, M. Tumor treating fields in combination with gemcitabine or gemcitabine plus nab-paclitaxel in pancreatic cancer: results of the PANOVA phase 2 study. *Pancreatology* **19**, 64–72 (2019).
123. Von Hoff, D. D., Ervin, T., Arena, F. P., Chiorean, E. G., Infante, J., Moore, M. et al. Increased survival in pancreatic cancer with nab-paclitaxel plus gemcitabine. *N. Engl. J. Med.* **369**, 1691–1703 (2013).
124. Picozzi, V., Weinberg, U., Giladi, M., Bomzon, Z. & Kirson E. PANOVA-3: a phase 3 study of tumor treating fields with nab-paclitaxel and gemcitabine for front-line treatment of locally advanced pancreatic adenocarcinoma (LAPC) [Abstract P-260]. *Ann. Oncol.* **30**, mdz155-259 (2019).
125. Vergote, I., von Moos, R., Manso, L., Van Nieuwenhuysen, E., Concin, N. & Sessa, C. Tumor treating fields in combination with paclitaxel in recurrent ovarian carcinoma: results of the INNOVATE pilot study. *Gynecol. Oncol.* **150**, 471–477 (2018).
126. Hanker, L. C., Loibl, S., Burchardi, N., Pfisterer, J., Meier, W., Pujade-Lauraine, E. et al. The impact of second to sixth line therapy on survival of relapsed ovarian cancer after primary taxane/platinum-based therapy. *Ann. Oncol.* **23**, 2605–2612 (2012).
127. Kirson, E. D., Giladi, M., Bomzon, Z., Weinberg, U. & Farber, O. INNOVATE-3: phase 3 randomized, international study of tumor treating fields (200 kHz) concomitant with weekly paclitaxel for the treatment of platinum-resistant ovarian cancer [Abstract]. *J. Clin. Oncol.* **36**, TPS5614 (2018).
128. Grosu, A., Gkika, E., Brunner, T. B., Thimme, R. & Weinberg, U. Phase II HEPANOVA trial of tumor treating fields concomitant with sorafenib for advanced hepatocellular carcinoma [Abstract]. *J. Clin. Oncol.* **37**, TPS470 (2019).